Micro-managing fibroblast senescence:

The role of small non-coding RNAs in

senescence-associated secretory phenotype (SASP)

Tasnuva D. Kabir

Submitted for

Degree for Doctor of Philosophy (Ph.D)

University of Sheffield, School of Clinical Dentistry

February, 2015

Names of supervisors:

Dr. Daniel W. Lambert

Professor Paul M. Speight

Acknowledgements

I would like to thank **Dr. Daniel W. Lambert** and **Professor Paul M. Speight** for giving me this splendid opportunity to pursue my career in research. I am especially grateful to **Dr. Daniel W. Lambert** for his constant supervision and motivation that enabled me to become a self-competent and independent researcher.

I am also very grateful to **Dr. Graham P. Stafford** for his support and guidance, which helped me to learn cloning in a very short time. I also want to thank **Dr. Craig Murdoch** and **Dr. Stuart Hunt** for helping me with several sophisticated laboratory techniques, making lab work easier.

I highly appreciate the support I received from **Brenka McCabe** who always made sure I had every reagent available on time to carry out my work on schedule.

I would also like to thank all my friends in the laboratory and post-graduate office especially **Genevieve Melling**, **Lucie Hadly**, **Kate Nylor**, **Andrew Frey**, **Charlotte Green**, **Priyanka Prajapati**, **Hanan Niaz**, **Mark Ofield**, **Dr. Raghu Radhakrishnan**, **Pris Cila** and **Dr. Fahad Hakami**, who made this entire duration of PhD very enjoyable and memorable for me. I am also thankful to **Ross Leigh** (student from Sheffield Undergraduate Research Experience) who helped me carryout a short fruitful summer project that gave an entire new perspective to my ongoing research.

I also owe my humble gratitude to the **University of Sheffield** for funding my project.

Nevertheless I am very grateful to the Almighty, my parents (**Commodore (RTD) M. S**. **Kabir** and **Mrs. Dilshad Kabir**), my brother (**Mr. Mishel Kabir**) and my husband (**Dr. Ranjan Kumer Roy**) for having patience and supporting me during every little struggle I suffered throughout my PhD.

Tasnuva D. Kabir

DECLARATION

I certify that this thesis is a presentation of my original research work and contains no material that has been accepted for award of any other degree or diploma in my name, in any other University or tertiary institution. I also certify that this thesis does not duplicate any materials that had been previously published or written up by another author. Wherever contributions of other research groups or colleagues are involved, every effort is made to indicate this clearly, with due reference to the literatures and acknowledgement of collaborators and discussion. I certify no work from this thesis will be used in submission in my name, for any other degree or diploma in any other University or tertiary institution.

I give consent to the University of Sheffield Library to display a copy of my thesis and make it publicly accessible for loan and where applicable, online, subject to the provisions of the Copyright Designs and Patent Act 1988 (UK) and Copyright Regulations 2003 (European Directive).

This research project was carried out under supervision of Dr. Daniel W. Lambert and Professor Paul M. Speight, at the School of Clinical Dentistry, University of Sheffield, UK.

Tasnuva D. Kabir

In my capacity as the principal supervisor of the candidate's thesis, I certify that the above statements are true to the best of my knowledge.

Dr. Daniel W. Lambert

LIST OF PUBLICATIONS

UNPUBLISHED:

1. Hunt S, Lambert LA, Hinsley EE, Kabir TD, Mo YY, Turner AJ, Lambert DW. microRNA-145 attenuates GPCR agonist-induced cancer cell motility by suppressing ADAM17. (submission to Scientific reports).

2. Mellone M, Hanley C, Mellows T, Tod J, Frampton S, Jenei V, Moutassim KA, Kabir TD, Lim KP, Brennan PA, Bullock M, Herranz N, Lambert DW, Noble F, Elicein K, Szyndralewiez C, Prime SS, Mimezamu AH, Underwood T, King EV, Gil J, Ottensmeier CH, Thomas GJ (2014). Induction of fibroblast senescence generates a myofibroblastic phenotype through NOX4 generation of reactive oxygen species. Submitted to Nature Medicine.

PUBLISHED:

3. Pal A, Melling G, Hinsley EE, Kabir TD, Colley HE, Murdoch C, Lambert DW (2013). Cigarette smoke condensate promotes pro-tumourigenic stromal-epithelial interactions by suppressing miR-145. J Oral Pathol Med; 42 (4), 309-14.

Abstract

Introduction: The molecular pathways that dictate the acquisition of senescence-associated secretory phenotype (SASP) by stromal fibroblast during ageing or in response to genotoxic insult have yet to be elucidated. In this thesis the ability of cisplatin-induced SASP of oral fibroblasts to stimulate pro-tumourigenic stromal tumour cross-talk in oral cancer has been studied. Moreover the miRNA expression profile associated with development of SASP in stress-induced premature senescent oral fibroblasts and senescent-CAFs of genetically unstable oral squamous cell carcinoma (GU OSCC) had been thoroughly investigated.

Materials and methods: Oral fibroblasts were treated with sub-cyotoxic doses of H_2O_2 and cisplatin or allowed to undergo replicative exhaustion to induce senescence. Senescence was confirmed by measurement of SA-β-gal activity, cyclin dependent kinase inhibitors (CDKI): p21 and p16, and secreted cytokines and MMP-2 by human cytokine array, ELISA and zymography. MiRNA expression profile was determined by TaqMan miRNA TLDA and candidate miRNAs were validated by qRT-PCR. Transfection was used to study the functional effects of candidate miRNAs. Paracrine effects were assessed by proliferation, migration and invasion assays. pmiR-Reporter vector was used to identify novel functional gene target of miRNAs.

Results: Senescent oral fibroblasts showed increased SA-β-Gal activity and higher levels of p21 and p16. They secreted more MMP-2, IL-6, MCP-1, Endothelin-1, PGE2. Inhibiting COX-2 activity and blockade of secreted MCP-1 diminished the stimulatory effect of senescent fibroblasts on oral cancer cells. Both senescent-normal oral fibroblasts and senescent-CAFs demonstrated differential expression of miRNAs. miR-335 and miR-148b were significantly elevated in senescent fibroblasts and was found

to target PTEN. A COX-2 mediated inflammatory loop was identified in senescent oral fibroblasts that could be rescued by celecoxib treatment (selective COX-2 inhibitor) via up-regulation of PTEN.

Conclusion: In this thesis a SASP-associated miRNA signature had been identified in oral fibroblasts, which may provide insight into the molecular pathways associated with chemotherapy resistance and cancer recurrences in elderly patients.

Table of Contents

List of Abbreviations

911: RAD9-HUS1-RAD1

3' UTR: 3' untranslated region

AER: Apical ectodermal ridge

AKT: v-akt murine thymoma viral oncogene homolog 1

ARF: Alternate reading frame

ATM: Ataxia telangiectasia mutated

ATR: ATM and RAD 3 related

α-SMA: Alpha smooth muscle actin (ACTA2)

B2M: β-2-microglobulin

BGN: Biglycan

BPH: Benign prostatic hyperplasia

CAFs: Carcinoma associated fibroblasts

CADPS: Ca^{++} -dependent secretion activator

CDK: Cyclin dependent kinase

CDKI: Cyclin dependent kinase inhibitor

c/EBP-β : CCAAT/enhancer binding protein β

CHK1: Checkpoint kinase 1

CHK2: Checkpoint kinase2

COPZ1: Coatomer protein complex, subunit zeta 1

COQ7: Coenzyme Q7 homolog

COX-2: Cyclooxygenase 2

Ct: Cycle threshold

CTGF: Connective tissue growth factor

CXCL12: Chemokine (C-X-C motif) ligand 12

CXCR4: Chemokine receptor type 4

DDF: DNA damage foci

dd H_2O: Deionized distilled water

DDR: DNA damage response

DDSB: DNA double stranded breaks

DGCR8: Digeorge critical region 8

DMEM: Dulbeco's Modified Eagle Medium

DNA: Deoxyribonucleic acid

ECM: Extracellular matrix

EED: Embryonic ectoderm development

EMT: Epithelial to messenchymal transition

ERK: Extracellular signal regulated kinase

EZH2: Enhancer of zeste homologue 2

FAP: Fibroblast activating protein

FGF-1: Fibroblast growth factor 2

FOXO: Forkheadbox, subgroup O

FSP-1: Fibroblast specific protein-1

GRO: Growth related oncogene

GS: Genetically stable

GU: Genetically unstable

h: Hour

H_2O_2: Hydrogen peroxide

H3K27me3: Tri-methylation of histone H3 and lysine residue 27

HCC: Hepatocellular carcinoma

HDAC1: Histone deacetylase 1

HGF: Hepatocyte growth factor

HMGA: High mobility group A protien

HNSCC: Head and neck squamous cell carcinoma

HPV: Human papilloma virus

HSCs: Hepatic stellate cells

hTERT: Human telomerase

IGF-1: Insulin like growth factor-1

IGFBP7: Insulin like growth factor binding protein 7

IL-1: Interleukin 1

IL-1α: Interleukin 1 alpha

IL-1R: Interleukin 1 receptor

IL-1β: Interleukin 1 beta

IL-6: Interleukin 6

IL-8: Interleukin 8

ITGA6: Integrin α6

LOH: Loss of heterozygosity

m: Minutes

MCP-1: Monocyte chemotactic protein 1

MDC1: Mediator DNA damage checkpoint protein 1

MEST: Mesoderm specific transcript

miRNA: microRNA

miRISC: miRNA induced silencing complex

MMP: Matrix metalloproteinase

MRN: MRE11-RAD50-NBS1

mRNA: Messenger RNA

MSR1: Macrophage scavenger receptor

mTOR: mammalian target of rapamycin

NFκB: Nuclear factor kappa B

NHOF: Normal human oral fibroblasts

NG2: Neuron-Glial 2

NOX: NAPDH oxidase

NRF-1: Nuclear respiratory factor 1

OSCC: Oral squamous cell carcinoma

PAI-1: Plasminogen activator inhibitor 1

PBS: Phosphate buffer saline

PcG: Polycomb group of repressor

PCR: Polymerase chain reaction

PDK: Phosphatidylinositol dependent kinases

PDGF: Platelet derived growth factor

PDGFRβ: Platelet derived growth factor receptor beta

PECAM1: platelet endothelial cell adhesion molecule 1

PEMPA1: Prostrate transmembrane protein, androgen induced 1

PGE2: Prostaglandin 2

PI-3-K: Phosphoinositide-3-kinase

PLK1: Polo-like kinase-1

PPARδ: Peroxisome proliferator activated receptor δ

pRB: Retinoblastoma protein

PRC-2: Polycomb repressive complex

PTEN: Phosphatase and tensin homolog deleted on chromosome 10

qRT-PCR: quantitative real time PCR

RFC: Replication factor C

RPA: Replication protein A

RNA: Ribonucleic acid

ROS: Reactive oxygen species

s: Seconds

SA-β-Gal: Senescence-associated β-galactosidase

SAHF: Senescence-associated heterochromatic foci

SASP: Senescence-associated secretory phenotype

SDF-1: Stromal derived factor-1

SGK: Serum/glucocorticoid regulated kinase

SMCs: Smooth muscle cells

SMC-1: Structural maintenance of chromosome protein 1

SIRT1: Sirtuin 1

SOCS: Suppressor of cytokine signaling

STAT3: Signal transducer and activator of transcription 3

SUZ12: Suppressor of zeste homologue 12

TGF-β: Transforming growth factor beta

TRBP: Tar RNA binding protein

TLDA: Tiling low density array

TP53: Tumour protein p53

VEGFA: Vascular endothelial derived factor A

VEGFC: Vascular endothelial derived factor C

LIST OF CHAPTERS

List of Figures

List of Tables

1.0: Introduction

1.1: Head and Neck Cancer Statistics

Head and neck squamous cell carcinoma (HNSCC) is the 6th most common cancer in the world (Wu *et al.*, 2011). In 2014, it was estimated that there was going to be an annual incidence of 42,440 cases of head and neck cancer including that of the oral cavity in USA with 8,390 deaths (Cancer facts and figures, ACS, 2014). According to Cancer Research UK, 6,767 patients suffered oral cancer in 2011 among which 2,119 patients (approximately one third) died by 2012 (Oral Cancer Statistics, November, 2014). Males suffer twice as much from oral cancer than females with white males being more prone to develop cancer of the oropharynx associated with human papilloma virus (HPV) infection (Cancer facts and figures, ACS, 2014; Cancer Research UK, 2014).

Oral squamous cell carcinoma (OSCC) contributes to 96% of all tumours occurring in oral cavity (Ramos *et al.*, 1997). In the UK the major risk factor for developing oral cancer is maintenance of unhealthy lifestyle that includes tobacco smoking (65% cases), alcohol consumption (30% cases) and infection (13% cases) (Cancer Research UK, September, 2014). Prolonged chewing of tobacco and betel nuts are other predisposing factors for development of premalignant lesions of the oral cavity such as leukoplakia and erythroplakia which subsequently leads into development of more severe diseases such as verrucous carcinoma and invasive OSCC (Chaudhary *et al.*, 2012).

In UK, the incidence of oral cancer had risen by one third while the mortality rate had increased by 10% since the last decade (Cancer Research UK, November, 2014). Despite development of neo-adjuvant therapy the percentage survival rate after 5 years remains around 60% (Wutzl *et al.*, 2007) and for 10 years is about 51% (Cancer facts

and figures, ACS, 2014). Patients usually succumb from locoregional recurrences, peri-operative complications related to co-morbidity and from development of new secondary tumours of either head and neck or other areas of the body such as oesophagus and lungs that share common predisposing factors for cancer such as previous exposure to tobacco smoke (Wutzl *et al.*, 2007).

Cancer is responsible for 28% of deaths in the UK (approximately 1 in 4 deaths) and more than half of these deaths usually occur in patients aged 75 years and older (Cancer Research UK, Cancer Statistics, September, 2014).

Ageing is therefore the most important predisposing factor for cancer. Only 1% patients are likely to suffer from cancer between 0 and 25 years, while incidence increases to 1 in 35 in men and 1 in 20 in women by 50 years of age, contributing to 53% of diagnosed cases, and peaks with further increase in age contributing to 36% (this percentage is apparently lower and depends on the average life expectancy of people) of diagnosed cases in patients of 75 years and older. Among patients the most common age group for developing oral cancer is between 50 and 74 years wherein approximately three quarters of deaths occur in those aged 60 years and above (Cancer Research UK, Oral cancer statistics, November, 2014). As a result there is a close association between ageing and risk of developing oral cancer. Moreover most anti-cancer therapies act by either killing or accelerating the ageing process of cancer cells but it is poorly understood if these drugs exert similar effects on neighbouring non-cancerous tissues, which may further predispose patients to develop new tumours or even provoke cancer relapses. It is therefore essential to understand the mechanisms involved in age-associated changes in body physiology that may promote development of late-life cancer in older patients and this will aid in innovating novel anti-cancer regimens to improve health of cancer patients.

1.2: Molecular pathways linked to ageing

The genetic pathways that regulate ageing are reported to remain conserved across species (Smith-Vikos and Slack, 2012). Insulin and insulin like growth factor-1 (IGF-1) signalling cascade is the most well established pathway that is associated with ageing and longevity. This pathway was first studied in *C. elegans* (Friedman and Johnson, 1988). When either insulin or IGF-1 binds to insulin or IGF-1 receptor, phospoinositide-3-kinase (PI-3-K) becomes active (Tissenbaum and Ruvkun, 1998) and phosphorylates its downstream signalling molecules phosphatidylinositol dependent kinases (PDK), v-AKT murine thymoma viral oncogene homolog 1 (AKT) and serum/glucocorticoid regulated kinases (SGK). This in turn phosphorylates DAF16 or its human orthologue: FOXO (forkhead box, subgroup O) and prevents its translocation into the nucleus (Murphy *et al.*, 2003). DAF18 or its human homologue: tumor suppressor *PTEN* (phosphatase and tensin homolog deleted on chromosome 10) can inhibit PI-3-K and cause FOXO to remain in unphosphorylated state. Under this circumstances DAF16 or FOXO translocates into the nucleus where it can regulate transcription of genes that promote longevity (Kenyon, 2010)

Some reports suggest that dietary restriction to certain level can also promote longevity (Bishop and Guarente, 2007). This is achieved via either activation of sirtuin 1 (SIRT1) or inhibition of mammalian target of rapamycin (mTOR). When mTOR is inhibited there is an increase in autophagy accompanied by a decrease in translation of proteins. This is thought to promote survival. Other transcription factors linked to dietary restrictions that contribute to longevity include nuclear respiratory factor 1 (*NRF-1*) and *FOXO A* (reviewed by Smith-Vikos and Slack, 2012).

Recent work demonstrates that polymorphisms in *FOXO3* and *IGF-1* are associated with extended longevity in humans. Cell cycle checkpoint proteins like *CHK1* (checkpoint kinase 1) are also thought to be important in cell survival (reviewed by Smith-Vikos and Slack, 2012). Moreover contemporary studies by other groups found

an association between "loss of function" mutation of *COQ7* (coenzyme Q7 homolog), which is required for the synthesis of coenzyme Q in mitochondrial respiration and longevity (Lakowski and Hekimi, 1996).

For many years it was thought that accumulation of somatic mutations alone in epithelial cells initiated cancer in older patients. However recent discoveries suggest cancer behaves more like a dysfunctional tissue in which interactions between both stroma and the mutated epithelia are required for cancer initiation and its subsequent malignant progression (reviewed by Kalluri and Zeisberg, 2006).

1.3: Role of tumour microenvironment in cancer

For a while scientists struggled to grow tumour cells in animal models while the same transformed cell lines could be easily cultured *in vitro* demonstrating all features of cancer (Picard *et al.*, 1986). Initially inadequate dampening of host's defence system was considered to incapacitate transformed cells to form tumour masses *in vivo*. Much later the notion of a possible role of tissue microenvironment to permeate and maintain tumour growth emerged. In agreement with this theory it was discovered that fibroblasts and endothelial cells but not macrophages, which are chief cells of tumour microenvironment accelerated growth of tumour cells *in vivo* (Picard *et al.*, 1986; Camps *et al.*, 1990). This effect was more pronounced when tumour cells were co-inoculated with fibroblasts than endothelial cells and was independent of their self-tumourigenic potential and lack of proliferative capacity because both non-tumourigenic fibroblast cell lines and those which had been irradiated as well as their conditioned media remarkably stimulated cancer formation in animal models (Picard *et al.*, 1986; Camps *et al.*, 1990). Conversely killing of fibroblasts or heat mediated inactivation of proteins in conditioned media repressed their growth stimulatory effect on cancer cells (Picard *et al.*, 1986) suggesting that fibroblasts exerted pro-tumourigenic effect on cancer cells by secreting soluble factors, extracellular matrix proteins and possibly

mesenchymal-epithelial interaction. Fibroblasts could also promote invasiveness and metastasizing capacity of less metastatic cancer cells underscoring their importance in cancer dissemination and progression (Picard *et al.*, 1986). But to serve this purpose fibroblasts need to be first activated by signals from either adjacent cancer cells or tissue microenvironment in absence of which cancer may not be even initiated (reviewed by Kalluri and Zeisberg, 2006). Moreover emerging evidence showed that genetic abnormalities alone in the cancer cells fail to elicit tumour development in presence of a normal stroma, while a stroma bearing somatic mutation, for instance activated H-Ras, could instigate tumour formation by stimulating both normal and initiated epithelia *in vivo* (Maffini *et al.*, 2003). This implied the possibility of existence of functional cross-talk between stroma and cancer cells.

1.3.1: Stromal-tumour cross-talk

During tumourigenesis cancer cells send cues to the surrounding tissue of the tumour microenvironment comprising primarily of fibroblasts which become activated and remodel the connective tissue components constituting the stromal response or desmoplasia (reviewed by Elenbaas and Weinberg, 2001).

Normal fibroblasts are thought to have a growth inhibitory effect on cancer cell proliferation (Olumi *et al.*, 1999; Orimo *et al.*, 2005; Peng *et al.*, 2013). Even those derived from non-reactive stroma adjoining reactive stroma of the same tumour exert less stimulatory effects on cancer cell growth and migration than their counterpart activated fibroblasts, however their effects were more pronounced when compared to normal fibroblasts of healthy donors (Giannoni *et al.*, 2010; Orimo *et al.*, 2005). Moreover dermal fibroblasts obtained from patients suffering cancer of breast, colon, kidney or even retina tend to have an altered and activated phenotype compared to normal fibroblasts derived from healthy individuals (reviewed by Kalluri and Zeisberg, 2006). This suggested that in cancer fibroblasts have a sustained activated state,

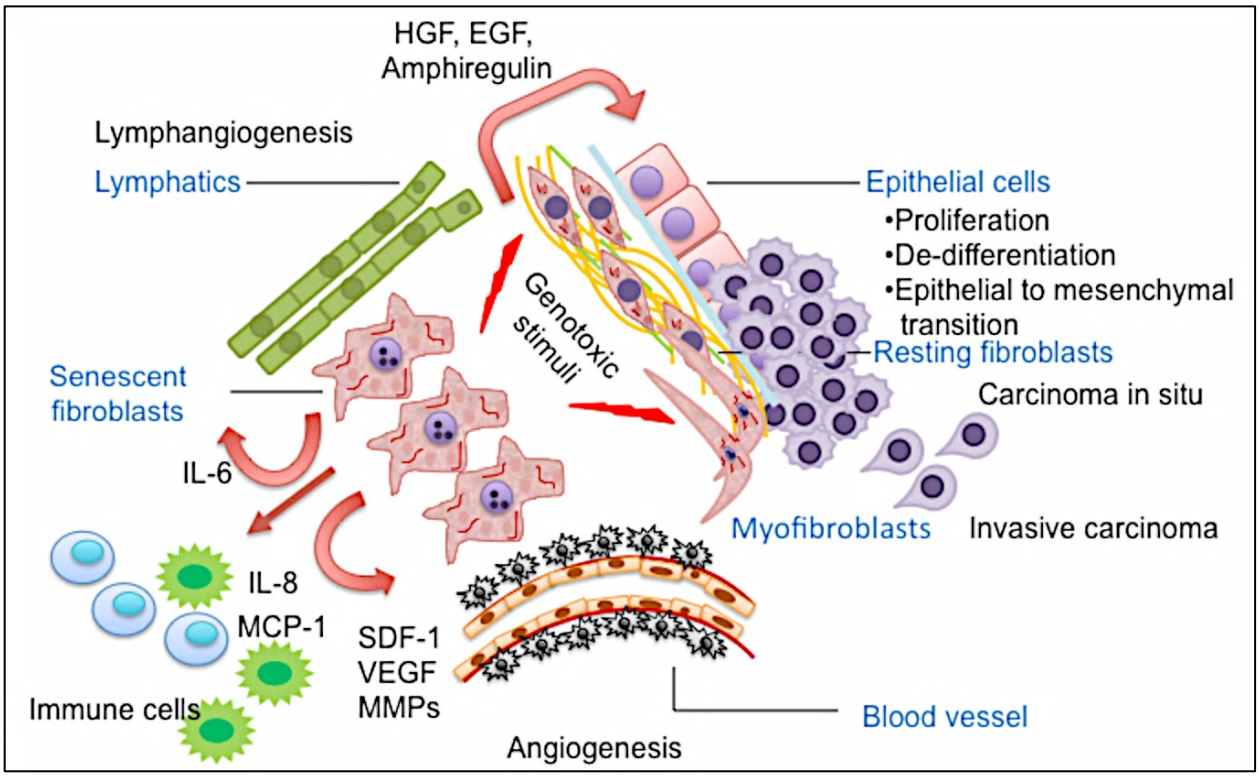

Figure 1.1: Stromal-tumour cross-talk in ageing. Cancer cells are surrounded by the basement membrane, extracellular matrix, immune cells, nerves, blood vessels, lymphatics, progenitor cells and predominantly of fibroblasts which constitute the stroma. Cancer cells secrete factors which stimulate transdifferentiation of resident fibroblasts into myofibroblasts. Persistent signalling from cancer cells or stimulation with genotoxic stimuli causes some of the myofibroblasts or resting fibroblasts to undergo premature ageing called senescence. The senesced fibroblasts develop a distinct secretome secreting diverse growth factors, cytokines and proteases that can remodel the tissue microenvironment to produce a permissive niche to allow tumour growth, invasion, dissemination and metastasis to distant site.

which may contribute to tumour progression.

Fibroblasts that are recruited in the tumour stroma have augmented proliferative and synthetic capacity (reviewed by Elenbaas and Weinberg, 2001). These cells display enhanced motility and invasive potentials, resembling behaviours of either activated fibroblasts existing at sites of wound healing called myofibroblasts or foetal fibroblasts during embryogenesis (Peng *et al.*, 2013; Ehrlich, 1988; Schor *et al.*, 1988). In addition they secrete vast amount of extracellular matrix (ECM) proteins, growth factors, cytokines, proteases to initially suppress tumour growth until they become reprogrammed by signals from cancer cells to support their progression (reviewed by Elenbaas and Weinberg, 2001). This phenomenon is called stromal-tumour cross-talk (reviewed by Elenbaas and Weinberg, 2001; figure 1.1) and is essential for tumour growth, vascularization, progression, dissemination, colonization to distant sites and in acquisition of stemness by premalignant cells (Togo *et al.*, 2013). These activated fibroblasts occurring at sites of reactive stroma in cancer are called carcinoma-associated fibroblasts (CAFs) or peri-tumoural fibroblasts (Togo *et al.*, 2013).

In a recent study it was stated that in cancers including OSCC, CAFs constitute a population of both highly active, synthetic and less migratory cell types that show diverse gene expression compared to normal fibroblasts designated as CAF-D and the less synthetic but highly migratory cell types which show similar gene expression profile as that of normal fibroblasts designated as CAF-N (Costea *et al.*, 2013). This study suggested that cooperation between both these phenotypes is essential in establishment of invasive OSCC (Costea *et al.*, 2013).

To demarcate the myofibroblast population from normal fibroblasts different markers have been identified among which α-smooth muscle actin (α-SMA) and fibroblast activating protein (FAP) are the most accepted (Orimo and Weinberg, 2007). Fibroblast specific protein-1 (FSP-1) has emerged as another very specific marker for a certain

subset of CAFs and its expression was discovered to be critical for tumour formation and metastasis (Sugimoto *et al.*, 2006; Orimo and Weinberg, 2007). Some of the other nonspecific biomarkers of myofibroblasts include those denoting mesenchymal origin; vimentin, collagen I, fibronectin and prolyl-4-hydroxylase (Togo *et al.*, 2013). The Neuron-Glial 2 (NG2) chondroitin sulphate proteoglycan and platelet derived growth factor receptor-β (PDGFRβ) are two more myofibroblastic markers the expression of which are remarkably correlated with that of α-SMA (Sugimoto *et al.*, 2006).

Functionally CAFs may be further classified by their synthetic capacity and responsiveness to transforming growth factor β (TGF-β). For instance, CAF-D secrete profuse amounts of TGF-β, without exerting any significant autocrine effect on its activation but stimulate epithelial to mesenchymal transition (EMT) in OSCC cells in paracrine manner to facilitate their invasion. Again, CAF-N secrete vast amounts of hyaluronic acids and are highly responsive to paracrine activation by TGF-β which enhances their motility and assists formation of deep invasive tumours (Costea *et al.*, 2013). Lastly persistent stimulation of normal fibroblasts with TGF-β derived from cancer cells stimulates their myofibroblastic transdifferentiation with subsequent development of senescence that further assists in formation of an aggressive tumour (Hassona *et al.*, 2013; figure 1.1).

CAFs do not purely originate from transdifferentiation of resident fibroblasts but can be derived from transdifferentiation of various other cell types such as pericytes, preadipocytes, EMT, bone marrow derived cells such as fibrocytes and mesenchymal stem cells and very rarely from genetic modification for instance loss of TP53 (Kurose *et al.*, 2002; Togo *et al.*, 2013). As a result CAFs comprise a diverse cell population of different origin and this contribute to the development of heterogeneity in reactive stroma, a major determinant for developing chemotherapy resistance.

Once fibroblasts transdifferentiate into CAFs this trait persists and is manifested by cells for several passages during subsequent culture *in vitro* (Schor *et al.*, 1988; Orimo *et al.*, 2005; Hassona *et al.*, 2013; Kojima *et al.*, 2010). This suggested that either CAFs harbour some kind of activated autocrine positive feedback loop or a modified transcriptome profile or even both, which are responsible for ensuing their persistent activation. Recent work showed that cancer cell derived TGF-β induces transdifferentiation of resident fibroblasts into myofibroblasts which then instigate an autocrine activation loop within myofibroblasts in CXCL-12/SDF-1 (stromal derived factor-1) and CXCR-4 dependent manner (Kojima *et al.*, 2010).

Some of the signalling pathways that are chronically activated in CAFs include sonic hedgehog pathway, TGFβ pathway, CXCL-12/CCR4 signalling, PDGF/PDGFRβ signalling, IL-1/NFκB signalling, PI-3-K/AKT pathway, Wnt pathway, ATM pathway and lastly PTEN-Ets2 (Togo *et al.*, 2013; Costea *et al.*, 2013; Elenbaas and Weinberg, 2001; Peng *et al.*, 2013). In addition CAFs express more oncogenic genes such as regulators of cell proliferation (CDK1; cyclin dependent kinase-1, PLK1; polo-like kinase-1), secrete chemokines and proteolytic enzymes (CCL-18, MMP-9; matrix-metallo proteinase 9), growth factors (FGF-2; fibroblast growth factor-2, VEGFC; vascular endothelial growth factor C), adhesion molecules (PECAM1; platelet endothelial cell adhesion molecule 1), transcriptional regulators (RUNX2, FOXM1) and molecules of Wnt signaling pathway (WNT5A) (Peng *et al.*, 2013).

1.3.2: Myofibroblasts as a biomarker for diagnosis and prognosis of premalignant and malignant lesions of oral cavity

Fibroblasts occurring in normal oral mucosa and in lesions with low grade dysplasia do not express α-SMA whereas those occurring at sites of moderate to severe dysplasia, verrucous carcinoma and invasive OSCC strongly express α-SMA and the number of positive cells increase as disease progresses, implying that fibroblasts became hyperactive in these lesions and may functionally contributed to their malignant transition (Chaudhary *et al.*, 2012). Highly invasive OSCC with predilection for metastasis to lymph nodes showed increased accumulation of myofibroblasts expressing α-SMA than less invasive cancer (de-Assis *et al.*, 2012; Kawashiri *et al*, 2009). Further an increase in the number of α-SMA positive myofibroblasts were identified with advancement of disease stage, for instance: stage IV cancer has more α-SMA positive cells than stage III or stage II, suggesting that occurrence of myofibroblasts may be associated with worsening of OSCC and shortening of disease free survival rate (Chaudhary *et al.*, 2012; Kawashiri *et al.*, 2009; Marsh *et al.*, 2011). CAFs involved in TGF-β pathway express genes that were associated with reduced disease free survival in HNSCC patients wherein lower levels of PMEPA1, BGN and CADPS modulators of cellular responses to TGF-β and regulators of fibroblast secretory function were associated with best outcome in these patients (Costea *et al.*, 2013).

Emerging evidence imply that fibroblasts originating in genetically stable (GS) tumours which arise from diploid dysplasia with minimum loss of heterozygosity (LOH) and copy number variation are functionally distinct from those derived from genetically unstable (GU) tumours which show frequent LOH with copy number variation in addition to TP53 and p16 inactivation (Lim *et al.*, 2011). These fibroblasts are slow growing and resembled morphology of senescent or aged fibroblasts (Hassona *et al.*, 2013).

Moreover like senescent human dermal fibroblasts these cells also have increased expression of *IGFBP-7* and *CDKN1A* (p21) (Lim *et al.*, 2011; Wajapeyee *et al.*, 2008). Furthermore, fibroblasts arising from GU tumours are more tumour promoting than those derived from GS tumours and this is linked to increased expression of α-SMA (*ACTA2*) and integrin α6 (*ITGA6*) and poor patient prognosis in patients suffering from OSCC (Lim *et al.*, 2011).

1.4: Cellular and structural differences between young and aged stroma

Stromal ageing causes smooth muscle cells (SMCs) and fibroblasts to express comparatively less collagen: Col1a1, Col2a1 and Col4a1, than their younger counterparts while secreting more inflammatory molecules that attract immune cells chiefly macrophages and T-lymphocytes to tissue microenvironment generating a pro-inflammatory milieu characteristic of old age (Bianchi-Frias *et al.*, 2010). This modifies the arrangement of collagen fibres in aged stroma characterised by a meshwork of discontinuous, coarse, adherent but less firm fibrils interspersed with rounded SMCs. In contrast the collagen fibres of young stroma are highly organized, loosely woven sharp fibrils with abundant spindle shaped SMCs distributed in parallel (Bianchi-Frias *et al.*, 2010). As a result ageing distorts the normal tissue architecture and this may interfere with normal tissue functions.

1.4.1: Differences and similarities between aged and tumour/carcinoma associated fibroblasts

Aged or senescent fibroblasts like CAFs show increased expression of stress fibres, a marker of fibroblast activation (Hassona *et al.*, 2013). Both senescent fibroblasts and CAFs have a sustained modified gene expression profile, which imparts them a pro-tumourigenic phenotype (Lim *et al.*, 2011; Hassona *et al.*, 2013.). Despite sharing a common secretome the molecular switches that govern such distinct gene expressions

are highly different (Begley *et al.*, 2005; Orimo *et al.*, 2005). For instance, most senescence associated growth arrest are strongly linked to increased level of p16INK4a (p16), which is regulated by the RNA binding protein AUF1 (Guo *et al.* 2010). Apart from secretion of VEGF most reports state that p16 does not affect the secretome of senescent fibroblasts (Coppe *et al.*, 2006; Rodier *et al.*, 2009). In contrast it was found that CAFs derived from breast cancer patients expressed more AUF1 and less p16 by means of which they stimulated cancer cell proliferation, de-differentiation, migration and invasion (Al-Ansari *et al.*, 2013). In CAFs p16 was found to regulate expressions of α-SMA, MMP-2 & -9, COX-2 (cyclooxygenase 2) and SDF-1, dependent on phosphorylation of AKT and NFκB pathway (Al-Ansari *et al.*, 2013).

It is still uncertain if senescent fibroblasts arise from myofibroblasts or from a distinct population of resident fibroblasts subjected to genotoxic stimuli. Certain reports confirmed that at sites of chronic non-healing and healing wounds such as oral submucosal fibrosis (OSMF), keloids and other cutaneous wounds, and liver cirrhosis excessive inflammatory signals, reactive oxygen species (ROS), matricellular proteins: CCN1 and persistent hyperactivation of myofibroblasts accelerated the capacity of young fibroblasts to senesce (Pitiyage *et al.,* 2011; Varmeh *et al*., 2012; Krizhanovsky *et al.,* 2008; Jun and Lau, 2010). It is therefore important to understand the process by which fibroblasts including CAFs age in diseased state particularly in cancer and then determine pathways that are commonly deregulated in both senescent fibroblasts and CAFs which may offer identifications of putative drug targets to improve current anti-cancer treatments.

1.5: What is senescence?

The human body adapted different tumour suppressive mechanisms to preclude neoplastic growth and resist their malignant transformation. The key mechanisms include the interplay of the intricate machinery involved in DNA repair, elimination of transformed cells by apoptosis and induction of irreversible growth arrest known as senescence (figure 1.2). Beside attainment of irreversible growth arrest senescent cells also evade apoptosis, display altered expression of genes and secrete diverse range of pro-inflammatory cytokines and soluble factors that contribute to the senescence associated secretory phenotype or SASP (Campisi and d'Adda di Fagagna, 2007).

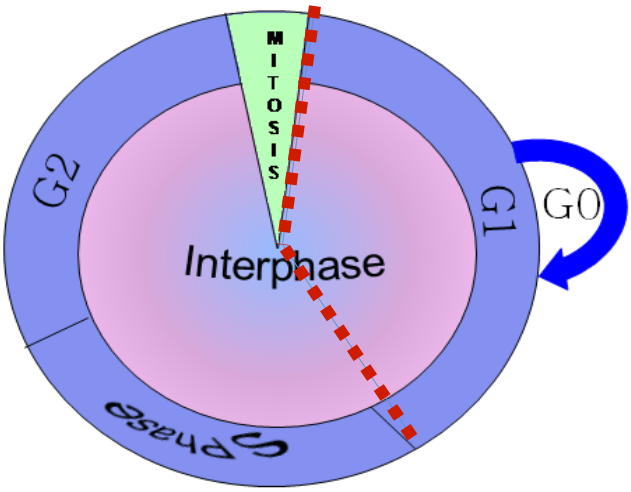

Figure 1.2 Stages in a cell cycle. The cell cycle comprises of quiescent or G_0 stage followed by G_1, S and G_2 phase during which the cell grows and synthesises DNA and the M phase or mitotic stage during which cell divides. Senescence is characterized by irreversible growth arrest usually at G1 and sometimes at G2 phase of the cell cycle.

Abbreviation: G, growth; S, synthetic.

All these defensive mechanisms are not flawless because despite adequate DNA repair some cells still escape which harbour the mutation that gives them additional advantage to evade both apoptosis and senescence. Intriguingly, whatever the stimuli and pathways activated in the mutated cell, all these anti-tumour defence mechanisms converge to stimulate the two most conventional tumour suppressive pathways regulated by TP53 and retinoblastoma protein (pRB) – p16INK4a. What is more, these tumour suppressor proteins are also occasionally mutated in cancer. Therefore it is extremely important to understand and unmask the pathways which participate either upstream or downstream of these effector proteins that may trigger formation of initiated cancer cells *in vivo* (Campisi and d'Adda di Fagagna, 2007).

Among these, cellular senescence appears to be the most critical tumour suppressive mechanism. Senescence was initially discovered as the terminal replicative stage in mitotic cells and was linked to loss of telomeres during cell division (Hayflick, 1965). Afterwards it was discovered that genotoxic stimuli such as oxidative stress (Chen *et al.*, 1995), ionizing radiation including ultraviolet rays (Kang *et al.*, 2008) and chemotherapeutic reagents (Coppe *et al.*, 2008b, Bavik *et al.*, 2006), activation of oncogenes; *H-Ras* (Coppe *et al.*, 2008b) and inactivation of tumour suppressor genes; *PTEN* (Kim *et al*., 2011; Lee *et al.*, 2011), all of which cause cellular stress can provoke senescence. This led into the notion that senescence emerged as a tumour suppressor mechanism to prevent accumulation of somatic mutation in the mitotic cells to mitigate neoplastic growth (Campisi and d'Adda di Fagagna, 2007). Some common genotoxic substances are tobacco (Coppe *et al.*, 2008a, Pitiyage *et al.,* 2011), areca nut (Pitiyage *et al.,* 2011), angiotensin II (Kim *et al.*, 2011), chemotherapeutic agents such as etoposide (Krizhanovsky *et al.,* 2008, te Poele *et al.*, 2002), bleomycin (Bavik *et al.,* 2006, Liu and Hornsby, 2007b), cisplatin (Zhao *et al.,* 2004), doxorubicin, aphidicolin (Chang *et al.*, 1999), cell differentiating agents such as retinoic acid derivatives (Cheng *et al.*, 1999) and many more (figure 1.3).

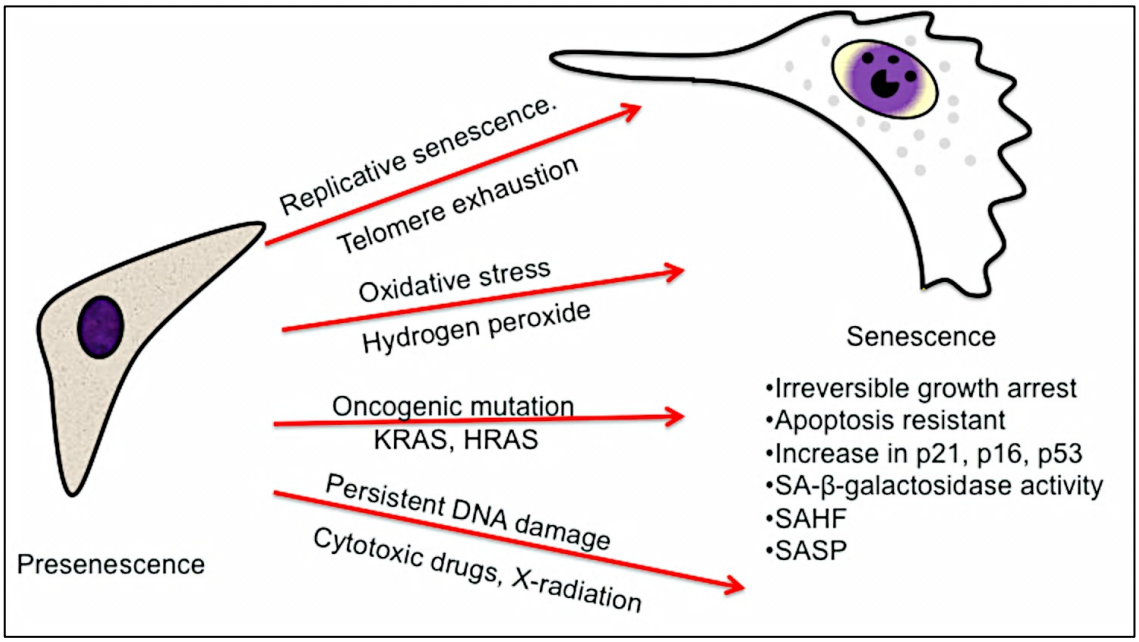

Figure 1.3: Stimuli triggering senescence. Mitotic cells can be stimulated by various genotoxic stimuli to induce senescence fate. The senescence response causes these cells to develop an enlarged morphology with extensive granular cytoplasm and cytoplasmic processes. These cells show SA-β-Gal activity, SAHF and elevated SASP factors. Cell cycle inhibitors: p21/cip1 and p16INK4a and tumor suppressor TP53 also show elevated expression.

1.5.1: Mechanisms of senescence

Most genotoxic substances generate ROS either by triggering mitochondrial damage (Pitiyage *et al.,* 2011) or increasing the activity of NADPH oxidase (NOX) and Rac I (Jun and Lau, 2010; Kim *et al.*, 2011) with subsequent oxidative damage to DNA and induction of DNA damage response (DDR). A DDR may be transient or persistent determined by the strength of the genotoxic stimuli and accordingly a mitotic cell can either reach a reversible growth arrest phase during which the checkpoint proteins repair the DNA or enter a phase of irreversible growth arrest when the DNA damage is irreparable (Rodier *et al.*, 2009).

Similarly cells can senesce at diseased sites by loss of telomeres (Wiemann *et al.*, 2002), which is recognized as double stranded DNA breaks by the DNA repair machinery. It was reported that the number of DNA damage foci; DDF, increases with the severity of disease and is accompanied by a rise in senescent cell population (Pitiyage *et al.,* 2011). Under certain circumstances, despite presence of persistent genotoxic signal or worsening of diseased state, the accumulation of oxidative DDF declines over time implying that senescent cells still harbour anti-oxidant defence mechanisms and try to attenuate the effect of the damaging stimuli by maintaining growth arrest (Coppe *et al.,* 2008a; Pitiyage *et al.,* 2011). Senescence also results from increased deposition of ECM protein CCN1 by activated fibroblast as observed in sites of cutaneous wounds which interacts with α6β1 integrin and cell surface heparin sulphate proteoglycans to induce growth arrest (Jun and Lau, 2010). This evidence supports the idea that it is the natural tendency of the body to prevent excessive scarring and perhaps senescence has evolved to capacitate efficient tissue remodelling. Disruption of extracellular matrix proteins can also initiate senescence. For instance, abnormally deposited versican can release hyaluronans into tissue microenvironment, which can trigger senescence in fibroblasts and other neighbouring cells via CD44 mediated signalling (Suwan *et al.*, 2009).

Senescence may also result independent of activation of TP53 and pRB-p16INK4a pathway and DDR. In early embryonic life, developing and maturing organs such as embryonic kidney (mesoneohros) and the endolymphatic sac of the inner ear display senescence at times of involution or selective expansion of a particular cell (Munoz-Espin *et al.,* 2013). Embryonic senescent cells were chiefly confined to the parenchyma and expressed predominantly p21 accompanied by heterochromatin formation; one of the hallmarks of senescence. These cells were genetically distinct from previous models of damage induced or ageing induced senescent fibroblasts (Munoz-Espin *et al.* 2013). Activation of TGFβ, Wnt and Hedgehog pathways, important during embryogenesis, were enhanced during normal development leading into senescence. Lack of p21 completely abrogated senescence in early embryonic life (Munoz-Espin *et al.,* 2013). It was reported that TGFβ mediated phosphorylation of SMAD2 and subsequent interactions with FOXO were critical in p21 activation in senescent epithelia in embryonic life (Munoz-Espin *et al.,* 2013). Moreover increased inhibitory activity of PTEN on PI-3-K pathway was found to be necessary in keeping FOXO in its active state to stimulate senescence in embryonic life (Munoz-Espin *et al.,* 2013).

PTEN also has anti-oxidant properties. Studies showed angiotensin II which predisposes atherosclerotic plaques in large vessels stimulated premature senescence in vascular SMCs by activating NOX to generate ROS via PI-3-K/AKT pathway. This effect was abrogated by peroxisome proliferator activated receptor δ (PPAR-δ) agonist; a new drug target for treating vascular disease, which induced PTEN expression (Kim *et al.*, 2011).

Recent work by our collaborators showed that generation of ROS is a critical event in transdifferentiation of oral fibroblasts into CAFs or senescent oral fibroblasts and required activation of NOX-4 (Mellone *et al*., submitted). In this study it was found that increased accumulation of ROS in both TGFβ stimulated myofibroblasts and irradiated senescent fibroblasts contributed to their pro-tumourigenic properties and were

associated with lower level of PTEN (Mellone *et al*., submitted). The relevance of PTEN in senescence and in tumour microenvironment is further described in the later sections.

1.5.2: DNA damage response (DDR)

All proliferating cells exhibit endpoint replication problems because the DNA polymerase fails to efficiently replicate the DNA terminals. Thus, at every synthetic phase in the cell cycle, 50-200 base pairs of telomere is lost from its original length of 10-15 kilobase pairs. This short or dysfunctional telomere then induces a DDR, which is sensed by the cells as double stranded DNA breaks. Oncogenes can also initiate DDR via initiating abnormal DNA replication and activating cyclin dependent kinase inhibitors (CDKI): p16. If DDR is acute, growth arrest occurs but if it is persistent then cellular senescence is initiated. Certain anti-proliferative cytokines such as interferon-β can induce senescence by generating ROS via TP53 dependent pathway whereas others such as TGF-β can induce senescence via pRB-p16INK4a dependent pathway. Cellular senescence that occurs during cell culture stress (also known as culture shock) is usually telomerase independent and is mediated via p16INK4a dependent pathway. The pathway to be activated during senescence is also determined by the cell type. For instance, cellular senescence in epithelial cells occurs predominately via activation of pRB-p16INK4a pathway (reviewed in Campisi and d'Adda di Fagagna, 2007).

In cells DDR is recognised by replication protein A (RPA) and replication factor C (RFC) like proteins. These proteins form complexes with RAD17 which is a cell cycle checkpoint protein. RAD17 then recruits the 911 complex; RAD9-HUS1-RAD1. DDR can also be recognised by MRN complex (MRE11-RAD50-NBS1). These proteins then activate its upstream kinases: ataxia telangiectasia mutated (ATM) and ATM and RAD 3 related (ATR). These then phosphorylate histone; H2AX, causing chromatin reorganisation. Subsequently more proteins are recruited which include adapter

proteins like 53BP1, BRCA1, claspin, mediator DNA damage checkpoint protein 1 (MDC1) and downstream kinases such as checkpoint proteins; CHK1 and CHK2.

These proteins then propagate signals to effector molecules TP53, CDC25 and structural maintenance chromosome protein 1 (SMC-1) (reviewed in Campisi and d'Adda di Fagagna, 2007). This is summarized in figure 1.4.

When the TP53 dependent pathway is activated, there is an increase in transcription of CDKI; p21/cip1 (p21). This inhibits cyclin dependent kinases (CDKs): CDK2, CDK6 and CDK4. TP53 can be negatively regulated by E3 ubiquitin protein ligase or HDM2, which in turn is inhibited by alternate reading frame (ARF) protein (reviewed in Campisi and d'Adda di Fagagna, 2007).

There are different stimuli that up-regulate p21 in cells in a TP53 dependent and independent manner. Stimuli like cytotoxic drugs, ionizing radiation and oncogenic Ras mutation cause TP53 mediated induction of p21 whereas TGF-β and drugs affecting DNA replication such as Mimosine cause a TP53 independent rise in p21 levels (Roninson *et al.,* 2002). Conversely reduced expression of polycomb INK4a group of repressors like BMI1 and CBX7 can induce p16INK4a (p16), which also inhibits CDKs.

Both p21 and p16 cause the retinoblastoma protein (pRB) to remain in its active hypophosphorylated state. This suppresses the transcriptional activity of E2F and thereby prevents cell proliferation (Alcorta *et al.,* 1996). E2F can also stimulate ARF expression. These events then trigger different cell cycle fates such as growth arrest, cellular senescence or apoptosis (reviewed in Campisi and d'Adda di Fagagna, 2007).

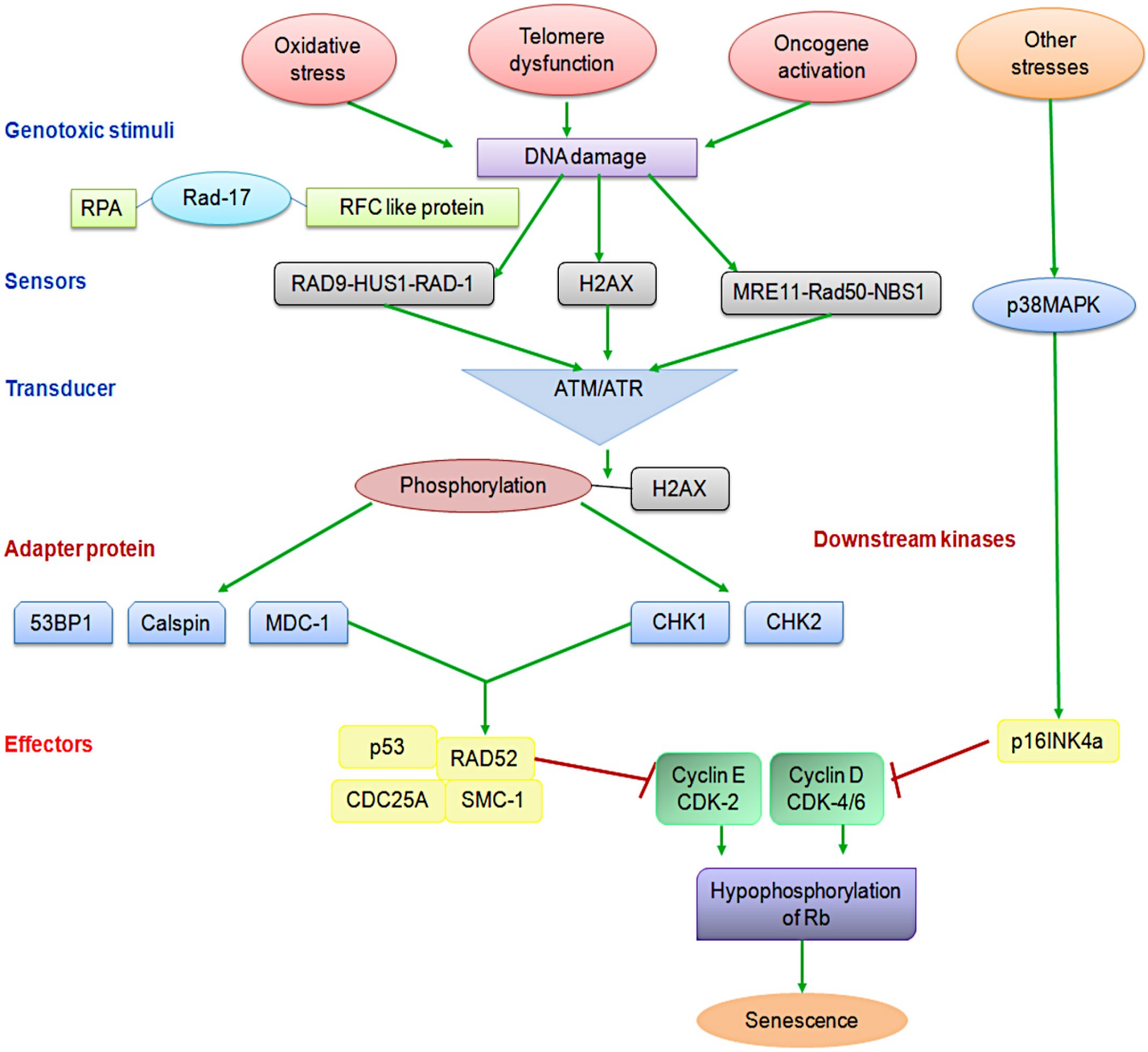

Figure 1.4: Mechanism of cellular senescence. Sensors such as 911-complex (RAD-9, HUS-1, RAD-1) and MRN complex (MRE11, RAD50, NBS1) perceives genotoxic stress and transduces a double stranded DNA damage response via ATM/ATR kinases. These then recruit downstream adapter molecules and kinases to activate TP53 and pRB tumor suppressor pathway. Senescence can also be activated independent of DNA damage response, via p38MAPK and p16INK4a-pRB pathway.

Abbreviations: RFC; replication factor C, **RPA**; replication protein A, **CDK**; cyclin dependent kinases, **pRB**; retinoblastoma protein.

1.5.3: Markers of senescence

To date senescence-associated β-galactosidase activity is regarded as the most sensitive biomarker of senescence (Dimri *et al.,* 1995). β-galactosidase is a hydrolytic enzyme that is encoded by *GLB-1* (Lee *et al.*, 2006). It cleaves compounds containing β-D-galactosyl residues such as glycoproteins, gangliosides, glycosaminoglycans into β-D-galactoside and derivatives (Kurz *et al.*, 2000). The optimum pH for this enzyme activity in young cells is between 3 and 5 and thus it is sometimes called acid β-galactosidase (Krishna *et al.*, 1999; Kurz *et al.*, 2000). In the laboratory, β-galactosidase activity is often measured using a chromogenic indole substrate called X-gal or 5-bromo-4-chloro-3-indolyl-galactopyranoside which is hydrolyzed to form a turquoise blue precipitate around nucleus both at pH=4.0 and pH=6.0 (Dimri *et al.*, 1995). In aged tissues there is an increase in β-galactosidase activity at pH=6.0 called senescence-associated β-galactosidase (SA-β-Gal) activity and hence it is used as a marker to detect senescence (Dimri *et al.*, 1995; Campisi and d'Adda di Fagagna, 2007). It is assumed that this difference in catalytic activity of β-galactosidase may result from translation of two distinct alternative spliced variant of β-galactosidase mRNA which act at different pH or because of residual enzyme activity at sub-optimal pH owing to its increased synthesis by accumulating lysosomes upon ageing (Morreau *et al.*, 1989; Kruz *et al.*, 2000; Dimri *et al.*, 1995). The later is most reasonably the cause of SA-β-Gal activity because the alternative spliced variant was found to lack enzymatic activity (Morreau *et al.*, 1989). It was also confirmed that this activity was not associated with other forms of growth arrest like state such as quiescence and in post-mitotic cells but rather associated with replicative age of cells. It was seen that patients suffering from premature ageing such as Werner syndrome or in elderly individual there was an increase in the number of SA-β-Gal positive cells implying an association between ageing and cellular senescence (Dimri *et al.,* 1995). Later senescent cells were also discovered in other age related pathologies such as benign prostatic

hyperplasia (BPH) (Castro *et al.,* 2003), cancer (Paradis *et al.,* 2001), atherosclerosis and osteoarthritis (reviewed by Campisi and d'Adda di Fagagna, 2007). Since then cellular senescence has been studied as a marker to understand age-related disease processes. Sometimes GLB-1 gene can be mutated, for example, in lysosomal storage diseases such as G_{M1} gangliosidoses, or may be conditionally deleted, causing senescent cells to be deprived of SA-β-galactosidase activity (Lee *et al.*, 2006). This implied the necessity of use of additional biomarkers to detect senescence. Examples of some of these biomarkers that are routinely used to characterise senescence in laboratory are described in table 1.1 (reviewed by Davalos *et al.,* 2010).

1.5.4: Benefits of senescence

1.5.4.1: Significance of senescence on maturing embryo

Emerging evidence suggests that similar to apoptosis a specific programmed pathway gives rise to senescent cells during organogenesis and is conserved across species (Munoz-Espin *et al.*, 2013; Storer *et al.*, 2013). Like apoptosis senescence also helps in involution and remodelling of remnant tissues. Once the organs are mature macrophages eliminate both senescent and apoptotic cells from the developing foetus (Munoz-Espin *et al.*, 2013; Storer *et al.*, 2013). Embryos that had defective senescence pathway were found to be borned with congenital anomalies (Storer *et al.*, 2013). Therefore senescence is important during early embryonic life for formation of functionally mature organs.

1.5.4.2: Preservation of tissue architecture and function during wound healing

Normal human keratinocytes are one of the most stringent cells to culture because they tend to differentiate instantaneously *in vitro* (Bisson *et al*., 2013). Supplementation of

Pros and Cons of senescence markers	
1. Marker of Cell proliferation	5-bromodeoxyuridine or ^{3}H-thymidine incorporation / immunostaining for PCNA (proliferating cell nuclear antigen) or Ki67 are used to detect DNA replication. However this marker fails to demarcate among senesced cells from quiescent and differentiated cells.
2. SA-β-Gal activity	This test fails to demarcate between senescence and stress like prolong confluence in culture.
3. Measurement of cyclin dependent kinase inhibitors	p21/cip1, p16INK4a, etc. However they also increase upon quiescence.
4. Visualization of senescence associated heterochromatic foci (SAHF)	This is detected by binding of DNA binding DAPI dye (4'6-diamidino-2-phenylindole) and presence of heterochromatin protein 1 (HCP-1) and heterochromatin associated histone modifications (H3-lys9 modification). The only disadvantage of this marker is that murine pericentromeric foci may mimic SAHF.
5. Visualization of senescence associated DNA damage foci (SADDF)	This is determined by measuring either phosphorylated gamma histone H2AX or TP53 binding protein 1 (53BP1) recruited to sites of double stranded DNA breaks. But this is detectable in any type of acute and chronic DDR independent of senesence.
6. Measurement of senescence associated secretory phenotype (SASP)	This detects factors that are secreted by the senesced cells. Again CAFs also have similar secretory features.

Table 1.1: Senescence markers. Routine biomarkers commonly used in the laboratory to determine cellular senescence.

these cultures with a feeder layer comprising of irradiated murine embryonic (3T3) or human dermal fibroblasts helps them to grow for prolong period in culture until the keratinocytes differentiate and senesce with time (Bisson *et al.*, 2013). These irradiated human dermal fibroblasts survived for weeks when co-cultured with human keratinocytes and facilitated their survival and proliferation by down regulating genes that modulated keratinocyte differentiation (Bisson *et al.*, 2013). Therefore it may be presumed that because irradiation induces senescence in human diploid fibroblasts (Coppe *et al.*, 2008b), the feeder layer perhaps regulated keratinocyte differentiation via release of SASP factors. This is one of the first lines of evidence which portrayed that SASP may regulate normal epithelial cell survival and differentiation and this may contribute to their role in promoting wound closures by stimulating epithelial regeneration in areas of widely gapped wounds and ulcers.

On the other hand at sites of chronic wounds senescent cells were found to express less genes for ECM proteins such as fibronectin, collagen I and IV, and many others which constitute the fibrotic scar (Krizhanovsky *et al.*, 2011; Bavik *et al.,* 2006). Rather these cells secreted more matrix remodelling enzymes such as MMP-1, -2, -3 and -9 and lesser amount of tissue inhibitor of matrix metalloproteinase (West *et al.*, 1989; Liu and Hornsby, 2007b; Coppe *et al.,* 2008b; Pitiyage *et al.,* 2011; Jun and Lau, 2010), which breaks down ECM and reduces the extent of fibrosis. In addition senescent cells also secreted cytokines and immune cell specific ligands that can recruit immune cells to the affected site, facilitating clearance of not only senescent cells but also the neighbouring ECM depositing activated cells (Krizhanovsky *et al.,* 2011). It is also reported that non-senescent fibroblasts occurring in non-diseased tissue carrying inflammatory stimuli have shortened replicative life span which suggests that in these tissues fibrosis is being delayed by the onset of senescence (Pitiyage *et al.,* 2011). Therefore accumulation of senescent cells at sites of chronic wounds and diseases are beneficial because they limit proliferation of abnormal cells, breakdown excessive

tissue scar and aid in elimination of abnormally activated cells such as myofibroblast-like cells, infected cells, damaged tissues and cancer cells, by stimulating immunosurveillance. As a result the immunosuppressive effect of steroids may be useful in treating chronic wounds by aiming to prevent elimination of senescent fibroblasts by immune cells to retain a pool of secreted MMPs and cytokines from senescent cells which can reduce the extent of fibrosis by degrading ECM proteins and reinforcing senescence of bystander activated cells (Acosta *et al.,* 2008; Wajapeyee *et al.,* 2008; Pitiyage *et al.,* 2011). Topical administration of CCN1 (senescence inducers) was also found promising in reducing cutaneous scarring in mice models (Jun and Lau, 2010). Hence development of senescence-based therapies is a promising approach to treat non-healing or severely fibrosed wounds to retain normal tissue architecture and preserve normal tissue homeostasis.

1.5.4.3: Role of senescence in tumour suppression

Apart from accumulating oncogenic mutations, somatic cells can also undergo malignant transformation by either functional mutation or loss of tumour suppressor genes like *TP53*, *CDKN1A* (encodes p21) and *CDKN2A* (encodes p16) (Campisi and d'Adda di Fagagna, 2007). P21 expression usually increases during the early stages of senescence whereas p16 expression rises gradually over time to maintain senescence (Alcorta *et al.*, 1996). In fact these changes in gene expression were recently identified as a critical step to prevent neoplastic growth and its subsequent malignant transition (Takeuchi *et al.*, 2010). Studies from two step chemical carcinogenesis mice models showed that elevated levels of p21 was necessary to minimize growth of benign papilloma whereas elevated levels of p16 was necessary to prevent development of highly aggressive squamous cell carcinoma (Takeuchi *et al.*, 2010). Mice lacking both genes bypassed senescence and developed multiple benign papillomas accompanied by invasive squamous cell carcinoma (Takeuchi *et al.*, 2010). This is the first *in vivo*

study, which revealed that cellular senescence is beneficial against development of both benign and malignant tumours.

Certain cytokines such as IL-6, IL-8, CXCR-2 ligands, IGFBP-7, IL-1α, IL-β, TGF-β family, WNT16B *etc.* secreted by senescent cells are able to reinforce senescence in other neighbouring non-senescent cells in both an autocrine and paracrine manner (Kuilman *et al.,* 2008; Acosta *et al.*, 2008; Wajapeyee *et al.,* 2008; Acosta *et al.,* 2013; Binet *et al.*, 2009). It was found that expressions of some of these cytokines like IL-β, IL-8 and IGFBP-7 are markedly accentuated in benign tumours but reduced in cancer tissues (Acosta *et al.*, 2013; Wajapeyee *et al.*, 2008) signifying their importance in preventing malignant transition. Furthermore this reinforcement of senescence by cytokines was restricted to only transformed but not normal cells (Kuilman *et al.*, 2008).

In benign conditions such as melanocytic nevi activation of BRAF oncogene were also found to induce senescence in rapidly proliferating neoplastic cells to mitigate their malignant transition as means of tumour suppression. In contrast, cancer cells carrying activated BRAF oncogene demonstrated functional inactivation of CXCR-2 receptors and hypermethylation of IGFBP-7 promoter region, both of which are required to maintain senescence, implying that evasion of senescence pathway is utilized by cancer cells to undergo malignant transformation (Acosta *et al.*, 2008; Wajapeyee *et al.,* 2008).

Recently more emphasis is given to the paracrine transmission of senescence to immune cells because unlike embryonic life senescent cells tend to accumulate at sites of tumours contributing to their enlarged size (Choi *et al.,* 2000; Munoz-Espin *et al*., 2013). It is therefore thought that transmission of senescence to immune cells particularly lymphocytes and plasma cells (Acosta *et al.*, 2013; Hassona *et al*., 2013) could impede their function in recognizing and eliminating not only senescent cells but

also other cell types from tumour microenvironment that will eventually facilitate progression of an indolent disease into highly aggressive cancer.

1.5.4.4: Mediator of immunosurveillance

Elimination of senescent cells by macrophages was proven to be essential from early life which otherwise caused birth defects in animal models including infertility (Munoz-Espin *et al.,* 2013). Similarly, in mice models of liver fibrosis, there is an increased infiltration of immune cells such as macrophages, lymphocytes particularly natural killer cells (NK-cells) and neutrophils within the vicinity of occurrence of senescent hepatic stellate cells (HSCs) (Krizhanovsky *et al.,* 2011). Human senescent fibroblasts show enhanced expression of ligands such as MICA, which adheres to receptor NKG2D on surface of NK-cells for being eliminated (Krizhanovsky *et al.,* 2011). Another study had shown that senescent stroma occurring at sites of papilloma secretes osteopontin to recruit immune cells and favour tumour growth (Pazolli *et al.*, 2009). Recent work also suggests that hypoxic senescent stroma recruited macrophages to the tumour microenvironment and induced their polarization to tumour promoting phenotype; M2 (Taddei *et al.*, 2014). Therefore senescent cells synthesize and secrete various pro-inflammatory factors, which can recruit immune cells to injured tissue sites including the tumour microenvironment and play an important role in establishing and maintaining immunosurveillance.

1.5.5: Senescence associated secretory phenotype (SASP)

Senescent cells secrete over forty different types of soluble and insoluble factors that participate in both intercellular and intracellular communications, contributing to the senescence associated secretory phenotype or SASP; one of the most distinctive hallmarks of senescence. Some of these soluble factors are cytokines and chemokines (IL-6, IL-8, MCP-1, -2 & -4, GRO-α and –β), growth factors (FGF-7, HGF, IGFBPs) and

proteases (tissue type plasminogen activator, urokinase type plasminogen activator, MMP etc). (Davalos *et al.*, 2010; Coppe *et al.*, 2008b; Bavik *et al.*, 2006; Krizhanovsky *et al.*, 2011). The insoluble factors include ECM proteins (fibronectin) and others such as ROS (Davalos *et al.*, 2010). Although senescence can be provoked by diverse range of stimuli, the composition of SASP is inordinately variable among tissues (Coppe *et al.*, 2008b). For instance, lung fibroblasts display a more potent SASP than those derived from foreskin and mammary gland (Coppe *et al.*, 2008b). This is probably because pulmonary fibroblasts are constantly exposed to ROS in contrast to fibroblasts originating in skin and breasts and are possibly sensitized to insults from ROS generated by continuous oxidative phosphorylation and other types of aerobic metabolic processes occurring within the lung microenvironment. As a result lung fibroblasts are plausibly very sensitive to oxidative DNA damage and by the virtue of tumour suppressive mechanism senesce and develop a more robust SASP even under physiological oxygen saturation in comparison to other fibroblasts as had been reported (Coppe *et al.*, 2008b). SASP factors induced by irradiation and replicative exhaustion were reported to be highly similar and the levels of these secreted factors were severely exaggerated when senescence was induced by either oncogene activation or TP53 inactivation (Coppe *et al.*, 2008a; Coppe *et al.*, 2008b). Moreover development of SASP is not restricted to only fibroblasts. Reports show that both normal and transformed prostatic epithelial cells also developed SASP in response to treatment with anti-cancer drugs and irradiation (Coppe *et al.*, 2008b).

1.6: Paracrine effects of SASP

Cellular senescence had evolved in an environment exposed to infection, starvation and predation. This suggests that during the evolution of senescence fate the lifespan of organism was very short and this tumour suppressive mechanism needed to be effective for a brief period. As a result gradual accumulation of senescent cells over time generated little selection pressure to eliminate them. This hypothesis piloted

development of a second concept called “The antagonistic pleiotropy”, which states that senescence, whilst beneficial to young organism, could be detrimental at older age (reviewed by Davalos *et al.,* 2010; Coppe *et al.,* 2010).

The pro-tumourigenic effect of SASP was first observed when lethally irradiated fibroblasts and prostate cancer cells were found to stimulate growth of other non-irradiated cellular components and lower the tumourigenic threshold and latency period required for tumour formation in animal models (Picard *et al.*, 1986; Camps *et al.*, 1990). This cross-talk was mutual and occurred in a cell specific manner; that is irradiated prostatic epithelial cells induced formation of fibrosarcoma but not carcinoma when co-inoculated with tumourigenic strains of fibroblasts and homologous cells, respectively (Camps *et al.*, 1990). Likewise irradiated fibroblasts stimulated formation of carcinoma in human breast, prostate, colon, Ewing’s sarcoma and bladder cancer derived cell lines but not fibrosarcoma even when co-injected with highly tumourigenic fibroblast cell line (Picard *et al.*, 1986; Camps *et al.*, 1990). Since both these reports did not provide information about the viability of irradiated cells, it can therefore be presumed that these cells were plausibly senesced in response to high dose radiation. Later other groups showed that irradiation of the tissue microenvironment altered the composition of ECM and generated a niche which could foster tumour growth (Barcellos-Hoff and Ravani, 2000; Ohuchida *et al*., 2004). Below are some examples of the paracrine effects of SASP important for normal homeostasis and tumorigenesis.

1.6.1: Effect on developing embryo

SASP mediated cross-talk between ectodermal and mesodermal tissues are essential in early life for growth, development and patterning of various organs (Storer *et al.*, 2013). This study reported that during the early phases of limb development stimulatory signals from mesenchymal tissues induced senescence in signalling tissues; the apical ectodermal ridge (AER), and these senescent embryonic cells then released factors

such as Fgf8 and Fgf4 to direct proliferation and migration of mesenchymal tissues to form functionally mature organs. Once the organs are developed the senescent cells are rapidly removed by tissue remodeler macrophages (Storer *et al.*, 2013).

1.6.2: Effect on de-differentiation and epithelial to mesenchymal transition (EMT)

Accumulation of senescent fibroblasts was found to disrupt normal mammary gland morphogenesis and interfere with differentiation of murine mammary epithelial cells into mature milk-secreting alveoli by releasing MMP-3 (Parrinello *et al.*, 2005). Human senescent fibroblasts were found to irreversibly reprogram and transform immortalized but non-malignant murine breast cancer cell line SCp2 into an invasive cancer cell line *in vivo*, partly by stimulating EMT (Parrinello *et al.*, 2005). Conditioned media from senescent fibroblasts also conferred malignant properties to less invasive breast cancer cell lines by stimulating EMT (Coppe *et al.,* 2008b). In addition senescent fibroblasts also increased motility of neighbouring cells by reducing expression of tight junction proteins, for example: claudin-I in breast cancer cells and zona occludens protein-I in immortalized keratinocytes (Coppe *et al.,* 2008a; Coppe *et al.*, 2008b).

1.6.3: Effect on proliferation and tumour growth

Senescent fibroblasts secrete different types of soluble factors and extracellular matrix proteins by means of which they reduce the latency period required by premalignant and malignant cells to produce tumours (Krotolica *et al.*, 2001; Bavik *et al.*, 2006; Lawrenson *et al.*, 2010; Coppe *et al.*, 2008a, Pazolli *et al.*, 2009). In contrast presenescent fibroblasts were reported to inhibit growth of both transformed and cancer cells (Lawrenson *et al.*, 2010; Begley *et al.*, 2005; Dilley *et al.*, 2003). This was presumed to result from contact mediated growth inhibition that is lost in senescent cells (Dilley *et al.*, 2003). However others showed that direct cell contact between

senescent fibroblasts and premalignant or malignant epithelial cells stimulated a more pronounced growth of cancer cells than presenescent fibroblasts (Krotolica *et al.*, 2001). Converesly senescent and presenescent fibroblasts have similar growth stimulatory effects on normal epithelial cells (Krotolica *et al.*, 2001; Lawrenson *et al.*, 2010; Coppe *et al.*, 2008a).

The direct effect of aged stroma on promoting growth of neighbouring tumour cells in humans was first demonstrated in studies carried out in BPH (Begley *et al.*, 2005). The incidence of BPH increases dramatically with ageing (Choi *et al.*, 2002). It was observed that stromal fibroblasts derived from older patients with benign disease showed increased secretion of SDF-1 compared to those derived from younger patients and this stimulated proliferation of immortalized normal prostatic epithelial cells *in vitro* by inducing phosphorylation of ERK-1/2 and NFκB (Begley *et al.*, 2005).

Other reports show senescent stroma induces formation of well capsulated, keratinized and regressing non-malignant tumours by premalignant epithelial cells but poorly differentiated non-regressing malignant tumours by cancer cells *in vivo* (Krotolica *et al.*, 2001). This is possibly due to residual tumour suppressive mechanisms persisting in preneoplastic cells and is probably lost upon acquisition of malignant trait (Wajapeyee *et al.*, 2008). Interestingly there were no major histological differences in tumours produced by senescent and presenescent fibroblasts co-inoculated with highly aggressive human breast cancer cell line MDA231 in mice models, however the same senescent fibroblasts stimulated a highly malignant anaplastic tumour when co-inoculated with mouse non-tumourigenic immortalized mammary epithelial cell line SCp2 (Krotolica *et al.*, 2001). This implied that either the human cancer cell lines failed to reproduce the complete malignant picture in mice models that is usually observed in patients, or the human cancer cells harbour a more complex tumour suppressive mechanism that persists to function during cancer advancement and delays their growth in animal models.

Deposition of ECM proteins by senescent fibroblasts also drives the tumourigenic growth potentials of the surrounding cancer cells (Krotolica *et al.*, 2001; Kang *et al.*, 2008). It was reported that these secreted matrix proteins activate focal adhesion kinases, ERK signalling and to a lesser extent PI-3-K/AKT pathway in transformed cells to stimulate their proliferation (Kang *et al.*, 2008). Senescent fibroblast also stimulated growth of tumours by secreting MMPs (MMP-1, MMP-2, MMP-3 and HGF) in mouse xenograft models (Liu and Hornsby, 2007a & 2007b). MMPs are essential for hyperpermeability of blood vessels and cleavage of growth factors from matrix proteins.

Intriguingly the growth promoting effect of senescent fibroblasts were only favoured when these cells were co-injected with cancer cells either subcutaneously or intra-muscularly in animal models, where blood flow was slow and steady. Transplanting the tumour-fibroblast mass into sub-renal capsular space having profuse blood flow produced no difference in tumour size in presence of young and senescent fibroblasts indicating that senescent fibroblasts stimulated tumour growth by causing sustained release of secreted factors which need to endure at the niche to create a favourable tumourigenic microenvironment (Liu and Hornsby, 2007a & 2007b).

Even under hypoxic conditions the senescent stroma were found to upregulate expression of enzymes and transporters involved in anaerobic metabolism and increase secretion of ketone and lactate rich metabolites for direct uptake by cancer cells to stimulate and support their growth *in vitro* (Taddei *et al.*, 2014). Some other SASP factors that stimulate growth of cancer cells are amphireguin, HGF, WNT16B, IL-8 and osteopontin (OPN) (Bavik *et al.*, 2006; Liu and Hornsby, 2007b; Sun *et al.*, 2012; Begley *et al.*, 2005; Castro *et al.*, 2004; Pazolli *et al.*, 2009).

The growth stimulatory effect of SASP is not only confined to stroma. Past work showed that senescent prostatic epithelial cells accumulating in BPH patients stimulated growth of neighbouring young epithelial cells by secreting IL-1α and IL-8

(Castro *et al.*, 2003; Castro *et al.*, 2004). It was suggested that IL-8 from senescent prostatic epithelial cells may additionally provoke FGF-2 expression in the adjoining stromal fibroblasts and thus set up a cross-talk to further stimulate epithelial hyperplasia leading into worsening of BPH.

Therefore age dependent accumulation of epithelial cells carrying somatic mutation and senescent stroma may synergize to promote cancer development in late-life.

1.6.4: Effect on apoptosis

To date there is only one report which showed that extracellular matrix proteins derived from senescent dermal fibroblasts induced a greater degree of apoptosis in transformed keratinocytes than their younger counterparts (Kang *et al*., 2008). This may be associated with SASP induced by UV light that may slightly differ in function than SASP induced by other types of genotoxic stress.

1.6.5: Effect on invasion

Conditioned media from senescent fibroblasts stimulated invasiveness of transformed, precancerous and cancerous mammary, ovarian and prostate epithelial cells partly by secreting IL-6, IL-8, WNT16B and MMPs (Lawrenson *et al.*, 2010; Coppe *et al.*, 2008a; Taddei *et al.* 2014; Sun *et al.*, 2012).

1.6.6: Effect on angiogenesis

Senescent human fibroblasts have differential effects on angiogenesis. It was found that senescent human fibroblasts derived from neonatal foreskin, HCA2, enhanced endothelial tubulogenesis in 2D models but produced fragile and less stable vessels than that of young fibroblasts (Liu and Hornsby, 2007b). Conversely senescent human foetal pulmonary fibroblasts, WI-38, secreted more VEGF independent of hypoxia inducible factor 1 (HIF-1) than their counterpart young fibroblasts and stimulated

invasion of endothelial cells *in vitro* and produced large highly vascularized tumours in mice models (Coppe *et al.*, 2006). This is probably due to the regulatory effect of p16 on VEGF secretion described in section 1.9.2. HCA2 cells lack p16-dependent senescence response and showed no change in VEGF secretion. In contrast WI-38 cells show p16-dependent senescence response and secreted more VEGF (Coppe *et al.*, 2006). However senescent fibroblasts secrete many more factors that can also modulate angiogenesis in tumour microenvironment (Coppe *et al.*, 2006) but VEGF is probably necessary to maintain the stability of newly formed vessels. Recently, hypoxic senescent stroma was also found to promote capillary tube formation in 2D assay (Taddei *et al.*, 2014) to support prostate tumour growth *in vivo*. Some senescent cells also secrete factors that inhibit angiogenesis. For instance, senescent keratinocytes secrete maspin which inhibits recruitment of vascular endothelial cells (Laberge *et al.*, 2011). Therefore depending on tissue context and diseased environment senescent stroma or epithelial cells may either promote or inhibit angiogenesis.

1.6.7: Perspectives on chemotherapy resistance

Until now there are only few reports associating use of chemotherapy to the emergence of tumour recurrences and treatment failure. Senescence plays an essential role in determining sensitivity and resistance of cancer cells to chemotherapy. However the exact mechanism of how this occurs is poorly understood. In animal models of lymphoma and hepatocellular carcinoma bypass of senescence due to NFκB and TP53 inactivation were observed to produce highly metastatic tumours, which failed to regress in response to chemotherapy (Chien *et al.*, 2011). Conversely SASP factors from senescent fibroblasts populating the tumour microenvironment can also create a receptive niche for cancer cell survival and growth. SASP factors such as osteopontin, and WNT16B were found to reduce the rate of apoptosis while increased the rate of survival and proliferation of preneoplastic and neoplastic cells *in vivo* and *in*

vitro (Pazolli *et al.*, 2009; Sun *et al*., 2012). Further it was found that in post-chemotherapy patients increased expression of WNT16B in periglandular region of the prostate gland was associated with higher rates of cancer recurrences (Sun *et al.*, 2012). Anti-cancer drugs such as cyclophosphamide, commonly used in treatment of prostate cancer, also created a permissive bone microenvironment partly by disrupting bone vasculature and partly by releasing MCP-1 which favoured colonization of prostate tumours within bones (Park *et al.*, 2012). Recently it was reported that SASP developing in plasma cells obtained from multiple myeloma patients selects for a surviving population of cancer stem cells which retain the capacity to grow, differentiate and produce tumours in animal models and this may contribute to relapsed cases in patients treated with irradiation and chemotherapy (Cahu *et al.*, 2012). This evidence suggested certain SASP factors may support development of chemotherapy resistance.

1.7: *In vivo* senescence in human and association with pathology

Senescent cells are frequently found at sites of hyperproliferative disorders such as benign melanocytic nevi (Bennett and Medrano, 2002; Wajapeyee *et al.,* 2008), BPH (Choi *et al.*,2000), colorectal adenoma including sessile serrated adenoma (Kuilman *et al.*, 2008; Acosta *et al.,* 2013, Sohn *et al.*, 2012), at sites of chronic inflammatory and degenerative diseases such as ulcerative colitis, Crohn's disease, fibrotic liver disease (Wiemann *et al.,* 2002; Sohn *et al.*, 2012), arthritis, atherosclerosis (Campisi and D'Adda di Fagagna, 2007), hepatocellular carcinoma; HCC (Paradis *et al.*, 2000) and oral submucosal fibrosis (Pitiyage *et al.,* 2011). Senescent cells are also identified in malignant tissues derived from post-chemotherapy and post-radiotherapy patients (te Poele *et al*., 2002; Roberson *et al*., 2005).

In benign proliferative disorders such as BPH (Choi *et al.*, 2000; Castro *et al.*, 2003) and fibrotic disease such as liver cirrhosis (Wiemann *et al.*, 2002, Paradis *et al.*, 2000) the appearance of senescent cells is restricted chiefly to the epithelial compartment

supporting their role in tumour suppression (Choi *et al.,* 2000). It is assumed that with ageing the body gradually accumulates senescent cells that give rise to an emerging population of cancer initiating cells. This notion is supported by report from Paradis *et al.* (2000) who showed that upon ageing the number of replicative senescent cells increases from normal liver to cirrhotic liver to HCC alluding an association between replicative senescence and cancer initiation (Paradis *et al.*, 2000). Moreover the enlarged size of the prostate gland observed in BPH patients directly correlates with the number of SA-β-Gal positive cell and expression of SASP factors (IL-1α and IL-8) in tissue sections (Castro *et al.*, 2003; Castro *et al.*, 2004; Choi *et al.*, 2002). Interestingly in tissue sections of cirrhotic liver diseases of diverse etiology senescent hepatocytes were found to accumulate at the edge of regenerative nodules, which is the source for clonal expansion of liver parenchyma for healing (Wiemann *et al.,* 2002).

Conversely in mice models of fibrotic liver disease senescent cells chiefly constituted hepatic stellate cells; HSCs (Krizhanovsky *et al.,* 2011). Consistent with this, another study showed senescent cells occurring in oral submucosal fibrosis were predominantly fibroblasts (Pitiyage *et al.,* 2011).

Some evidence suggests that presence of senescent cells in diseased tissue can be also used as prognostic marker. For instance, in human patients of liver cirrhosis and oral submucosal fibrosis accumulation of senescent hepatocytes and oral fibroblasts, respectively, was associated with advanced disease (Wiemann *et al.*, 2002, Pitiyage *et al.*, 2011). Moreover it was observed that appearance of senescent fibroblasts in oral submucosal fibrosis was associated with existence of disease because in tissue sections of non-diseased paan users that had been insulted with both areca nut and tobacco, and presented with signs of inflammation were deprived of senescent cells. This study suggested that senescence is therefore an effect of the disease process rather than the cause of the disease (Pitiyage *et al.,* 2011).

1.8: Differences in SASP between senescent cancer cells and senescent fibroblasts

Ewald *et al.* (2008) demonstrated for the first time that replicative senescent fibroblasts derived from prostatic tissue had twice as much stimulatory effect on proliferation of bystander non-senescent prostate cancer cell lines than senescent prostate cancer cell lines *in vitro* and *in vivo*. This effect was achieved via secretion of soluble factors from the senescent fibroblasts rather than direct cell-cell contact. There was minimum overlap in gene expression profiles between senescent cancer cells and senescent fibroblasts highlighting the activation of different molecular pathways in different kinds of senescent cells (Ewald *et al.,* 2008) that is possibly associated with their role in either promoting or inhibiting tumour formation.

Similar effects were also observed with breast cancer cells. Co-transplant of senescent and non-senescent breast cancer cells in murine xenograft model did not produce massive changes in tumour size whereas co-transplant of non-senescent breast cancer cells with senescent fibroblasts produced remarkably large tumours (Liu and Hornsby, 2007b).

Based on above evidence it can be therefore concluded that both the beneficial and deleterious effects of senescent cells are dependent on the secretion of SASP factors. The complexity and assorted nature of SASP in senescent fibroblasts suggests development of SASP must involve activation and interaction of multiple molecular pathways that synchronize to produce the characteristic features of SASP and yet it is poorly understood. Some pathways that had been associated with SASP development are described below.

1.9: Regulation of SASP

1.9.1: Role of telomerase

Loss of telomeres in proliferating cells at late passage is associated with development of persistent DDF with concomitant rise in expression of SASP factors such as IL-6, MMP-3 (Rodier *et al.*, 2009). Introduction of hTERT (human telomerase) into these cells prolonged their doubling time and reduced the secretory levels of some of these SASP factors implying that progressive loss of telomere mediates persistent DNA damage which is necessary to develop SASP in these cells (Rodier *et al.*, 2009). This also suggested proteins initiating and acting in the DDR pathway may be involved in regulating SASP.

1.9.2: Role of *TP53* and CDKIs

The two most common tumour suppressor proteins involved in mediating the growth arrest effect of DDR are tumour suppressor: TP53 and CDKI: p16, both of which activate retinoblastoma protein (pRB) (Campisi and d'Adda di Fagagna, 2007).

Reports show prior to induction of senescence inactivation of *TP53*, which acts as a potent downstream effector kinase of DDR pathway, caused early accumulation of persistent DDF accompanied by development of an amplified SASP in senescent cells (Rodier *et al.*, 2009; Coppe *et al.*, 2008b). Moreover *TP53* deficient senescent prostatic cancer cells secreted more SASP factors than normal senescent prostatic epithelial cells and senescent fibroblasts both of which harbour wildtype *TP53* (Coppe *et al.*, 2008b). Furthermore over-expression of *Ras* oncogene or inactivation of *TP53* in human diploid fibroblasts shortened the latency period for SASP development to between 2 and 4 days in comparison to their usual lag period of 4 to 7 days post-induction of senescence (Coppe *et al.*, 2008b). Simultaneous activation and

inactivation of Ras oncogene and TP53, respectively, produced the most amplified SASP observed in the senescent cells (Coppe *et al.*, 2008b). In contrast inactivation of *TP53* and *RB* gene in senescent fibroblasts only reversed their growth arrest state and stimulated these cells to reach mitotic catastrophe (Rodier *et al.*, 2009) without impairing release of SASP factors.

Similarly, inactivation of TP53 in fibroblasts expressing p16 (such as WI-38 and IMR-90) neither reversed senescence nor affected SASP. Inactivation of p16 in these cells before reaching replicative senescence also did not modify SASP (Coppe *et al.*, 2011). However in fibroblasts expressing lower levels of p16 (such as BJ and HCA2) TP53 inactivation after senescence induction reversed growth arrest but failed to alter SASP (Coppe *et al.*, 2008b). Likewise in absence of DNA damage, overexpression of p16 in BJ and HCA2 cells induced senescence but not SASP (Coppe *et al.*, 2011). However depletion of p16 in replicative senescent cells was associated with increase in the number of DDF, therefore p16 may indirectly negatively regulate SASP via protecting cells from DNA damage (Coppe *et al.*, 2011).

Emerging evidence shows CDKI, p21, may regulate certain SASP components both dependent and independent of DDR (Storer *et al.*, 2013; Chang *et al.*, 2000). These include certain proteases, matricellular proteins, mitogenic and anti-apoptotic genes such as plasminogen activator inhibitor I (PAI-1), fibronectin 1, connective tissue growth factor (CTGF), activin A, galectin-3, and prosaposin, all of which contribute to SASP. Transcription of all these genes was found to depend on p21 transactivation. It was reported that p21-induced senescent fibrosarcoma cells secreted these factors to stimulate survival and reduce apoptosis of other slow growing fibrosarcoma derived cell lines and murine embryonic fibroblasts, respectively, *in vitro* (Chang *et al.*, 2000). However later it was reported that modulation of p21 in DNA damage induced senescent cells had no effect on SASP development (Coppe *et al.*, 2011). Contrary to this, recent work now shows that p21 is critical for development of senescence in

embryonic tissue independent of DDR and its deficiency abrogates both senescence and release of SASP factors such as Fgf8, Fgf4, Bmp-4 and many other components that are required for normal organogenesis (Storer *et al.*, 2013). This implies in mammalian cells under circumstances where TP53 or p16INK4a is lost, p21 may take the upper hand to complement the loss of function of other tumour suppressors as a defence measure against neoplastic growth.

From above evidence it can therefore be concluded that TP53 can modulate both the magnitude and the latency period for SASP at an early stage of senescence development but has no definite role once it is fully established. Further both TP53 and p16 restrain SASP phenotype probably by minimizing the spread of DNA damage across senescent cells whereas p21 besides inducing senescence may indirectly control release of certain SASP factors. Lastly p16 may be dispensable for SASP but p16-mediated cellular senescence is an irreversible process whereas that induced by p21 or TP53 or pRB overexpression is reversible (Coppe *et al.*, 2011, Coppe *et al.*, 2008b; Chang *et al*., 2000).

1.9.3: Role of DDR Kinases

Since inactivation of TP53 and introduction of p16 or p21 (Coppe *et al.*, 2008b, Coppe *et al.*, 2011) in senescent fibroblasts did not affect SASP while TP53 inactivation during induction of senescence precipitated DDR and amplified SASP, this indicated that there must be other pathways which may be regulating SASP.

In vivo studies showed presence of persistent DDF in precancerous and cancerous lesions of breast (Rodier *et al.*, 2009), lung, colon and bladder (Bartkova *et al.*, 2005, Gorgoulis *et al.*, 2005). Further it was observed that in breast cancer tissue presence of DDF was associated with increased levels of IL-6 and phosphorylated ATM/ATR (Rodier *et al.*, 2009). This therefore suggested that upstream kinases of the DDR are critical in regulating some, but not all, SASP factors. It was shown that depletion of

phosphatidylinositol 3-kinase like proteins, ATM; checkpoint protein, CHK2; and upstream adaptor protein, NBS1 of 911-complex; of DDR pathway in senescent fibroblasts were associated with reduced secretion of IL-6 and IL-8 (Rodier *et al.*, 2009). Further IL-6 secretion in oncogene induced senescent fibroblasts also depended on phosphorylated ATM levels. Therefore both IL-6 and IL-8 are DDR dependent SASP factors (Rodier *et al.*, 2009). Recently it was demonstrated that ECM protein CCN1 induced senescence in human fibroblasts by phosphorylating ATM, CHK1 and CHK2 to activate TP53 dependent senescence while phosphorylating ERK (extracellular signal regulated kinase) and p38MAPK described later (Jun and Lau, 2010) to activate p16-dependent senescence pathways.

1.9.4: Role of stress kinase

DDR is initiated in cells in response to any types of genotoxic stress independent of the nature and strength of the stimuli. Therefore DDR can be both acute and chronic depending on the magnitude of the stimuli. It was observed that SASP develops only upon activation of chronic DDR (Rodier *et al.*, 2009) with only a fraction of it being regulated by DDR kinases. This meant there are other cell-signalling pathways involved in regulation of SASP. Stress kinases such as p38MAPK were identified as another probable regulators of SASP (Freund *et al.*, 2011). It was observed upon induction of senescence, phosphorylated p38MAPK and its downstream target Hsp27 were slowly increased in parallel to the development of SASP (Freund *et al.*, 2011). Further it was shown that transient inhibition of p38MAPK (primarily α-isoform) activity in senescent fibroblasts was associated with decreased secretion of IL-6, IL-8 and GM-CSF and a large fraction of SASP components and it is independent but act co-ordinately and synergistically with DDR and is partly mediated by enhanced transcriptional activity of NFκB (Freund *et al.*, 2011). It was reported that TP53 restrained p38MAPK activation noticeable, as enhanced p38MAPK phosphorylation in

TP53 deficient senescent fibroblasts and possibly this is a mechanism by which TP53 restrains SASP. Further inhibition of p38MAPK activity in *TP53* deficient senescent fibroblasts remarkably mitigated expression of amplified SASP (Freund *et al.*, 2011).

1.9.5: Paracrine senescence

New lines of evidence from studies investigating paracrine transmission of senescence to normal bystander proliferating cells suggested that some of the SASP factors released by senescent cells may induce senescence and establish SASP in the neighbouring cells (Acosta *et al.,* 2013). Among them the interleukin 1 family of cytokines: IL1-α and -β, were observed to have the most profound effect because inhibition of its receptor; interleukin 1 receptor (IL-1R) bypassed both autocrine and paracrine senescence in human diploid fibroblasts (Acosta *et al.,* 2013) while other cytokines such as IL-8, IGFBP-7, CXCR-2 ligands and TGFβ were found to predominately regulate paracrine senescence (Acosta *et al.*, 2008; Wajapeyee *et al.*, 2008; Kuilman *et al.*, 2008). Some of these secretory cytokines were also regulated at transcriptional levels. For instance, expression of transcription factor c/EBP-β is increased upon oncogene induced senescence, which then facilitates transcription of several inflammatory cytokines of SASP such as IL-6 and IL-8 (Acosta *et al.*, 2008; Kuilman *et al.*, 2008). IL-6 in turn induces more transcription of c/EBP-β (CCAAT/enhancer binding protein β) by a positive feedback loop and thus reinforces senescence (Kuilman *et al.,* 2008). Alternatively, cytokine-mediated reinforcement of senescence in cells may also depend on tissue context because while IL-6 induced senescence in transformed cell lines in autocrine manner, it stimulated proliferation of normal cells in paracrine manner (Kuilman *et al.,* 2008). Another line of evidence suggests that persistent activation of cytokine signalling possibly via oncogenic mutations may lead to continuous activation of Janus kinases such as JAK2. Phosphorylated JAK2 then undergoes conformational changes to recruit STAT

signalling molecules like STAT5A. The STATs then translocate into the nucleus and transcribe multiple genes including SOCS1; suppressor of cytokine signalling, to sustain tissue homeostasis. SOCS1, besides negatively regulating JAK2, can also form a ternary complex with TP53-ATM to reinforce senescence (Mallette *et al.*, 2010). Therefore this report further corroborates the notion that SASP is regulated at multiple levels by different mechanisms possibly to ensure adequate tumour suppression.

1.9.6: Role of ERK

In early embryonic life mesenchymal messaging via phosphorylated ERK is critical to reinforce senescence and SASP in signalling tissues of AER and roof plate, which guide development and patterning of the forelimb and nervous system, respectively (Storer *et al.*, 2013). These SASP factors overlap with those of oncogene-induced senescence but are different from those produced by DDR. Some of these SASP factors include members of MMP family, IGFBP5, WNT5a, VEGFA, SOX family, chemotactic signals for macrophage recruitment and so forth (Storer *et al.*, 2013).

1.9.7: Role of chromatin reorganization

SASP can be also regulated at chromatin levels (Davalos *et al.*, 2010). Most of cytokines and growth factors elevated in SASP were found to mechanically cluster in the genome of senescent cells indicating its possible regulation at epigenetic levels (Davalos *et al.*, 2010). In support of this recently it was found that cells developed SASP without undergoing senescence by chromatin rearrangement (Pazolli *et al.*, 2012).

Senescent cells have reduced levels of chromatin remodelling enzyme histone deactelyase 1 (HDAC1), which favour histone acetylation and open up multiple active sites in chromatin to facilitate active transcription of genes involved in SASP. Osteopontin is one such SASP factor, which is predominately regulated via chromatin

remodelling (Pazolli *et al.*, 2012). Other SASP factors like IL-6 and IL-8 can be also actively transcribed in cells by treatment with HDAC1 inhibitors in absence of senescence, however these factors still required phosphorylation of ATM kinases and NFκB activity in addition to chromatin reorganization (Pazolli *et al.*, 2012; Chien *et al.*, 2011). In addition high mobility group A proteins: HMGA1 and HMGA2, transcription factor c/EBP-β and promyelocytic leukaemia proteins (PML) were reported to be enriched in the senescent cell chromatin (Chien *et al.*, 2011).

1.9.8: Emerging roles of microRNAs

Senescence is a complex multistep process tightly controlled by the interplay of tumour suppressor genes TP53 and p16, involving cellular stress, initiation of DDR, growth arrest, formation of nuclear heterochromatin, aberrant gene expression and evasion of apoptosis (Campisi and d'Adda di Fagagna, 2007). MicroRNAs (miRNAs) are a class of small non-coding RNAs about 20 to 22 nucleotides long that regulate post-transcriptional gene expression by recognizing complementary seed sequences primarily at the 3' UTR of mRNAs and inducing either mRNA decay or repressing protein translation (Bartel, 2009; figure 1.6). Emerging evidence indicates miRNA-mediated regulatory networks are critical for diverse biological processes under both physiological and pathological conditions including cancer (Bartel, 2009). miRNAs have both tumour suppressive and oncogenic functions based on the nature of their gene target (Bartel, 2009) and are reported to be differentially expressed with ageing and cancer (Hackl *et al.*, 2010; Wang *et al.*, 2011a). Therefore miRNAs may contribute to the altered expression of genes observed in senescent cells and thus modulate their growth static, tumour suppressive and pro-inflammatory tumourigenic functions in age-related diseased states.

Among these miR-146a is the most well characterised miRNA that had been reported to negatively regulate SASP in senescent cells (Bhaumik *et al.*, 2009). It is thought that

once SASP is fully established IL-1α activates its downstream signalling kinase IRAK1 to activate NFκB. NFκB then induces transcription of miR-146a and -146b wherein miR-146a silences IRAK1 in senescent cells to reduce their pro-inflammatory phenotype by a negative feedback loop mechanism (Bhaumik *et al.*, 2009). Another miRNA whose regulatory function on SASP has recently emerged is miR-210, reported to be critical in hypoxic microenvironment of prostate cancer (Taddei *et al.* 2014). miR-210 does not only induce senescence via instigating DDR but also induces myofibroblastic transdifferentiation and is associated with up-regulation of SASP factors such as IL-6, IL-8, MMP-2 and -3 and VEGFA (Taddei *et al.*, 2014). It is still unknown how this miRNA is exerting its regulatory effect on SASP but previous evidence suggests it might be associated with impairment of mitochondrial function (Taddei *et al.*, 2014).

All these regulatory mechanisms controlling SASP are summarized in figure 1.5.

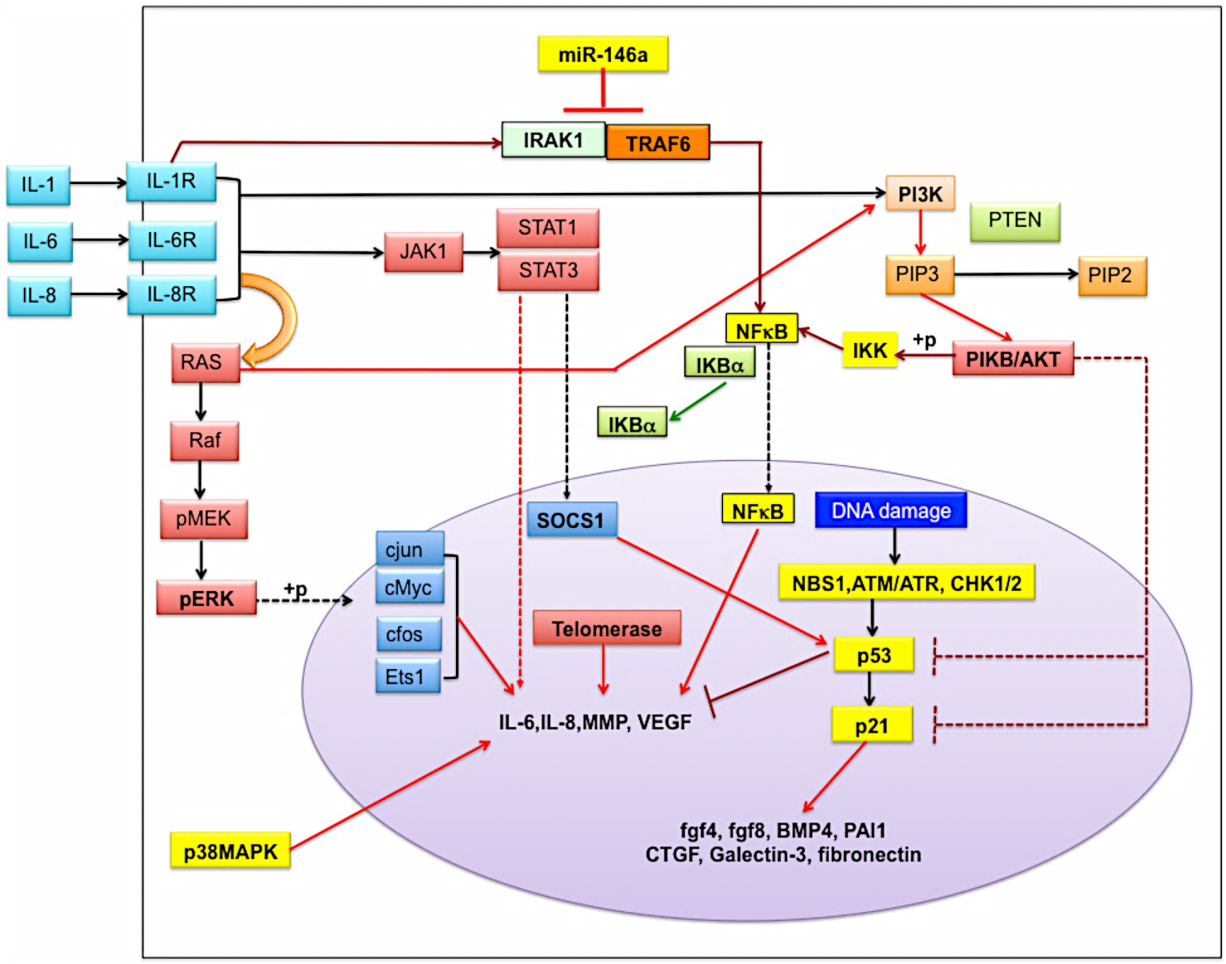

Figure 1.5: Summary of pathways regulating SASP in senescent cells. The DNA damage signal is transduced by cell using sensors like NBS1, kinases like ATM/ATR and checkpoint proteins CHK1 and CHK2 to activate p53 (TP53) and its downstream effector p21. This induces senescence and activates transcription of genes involved in SASP. Certain SASP factors like IL-6, IL-8 and IL-1 then initiates a vicious cycle that activates PI-3K pathway, RAS-MEK-ERK signalling cascade and NFκB to further amplify the senescence fate and provoke release of more SASP factors. Stress that triggers DNA damage can also activate p38MAPK that further stimulates secretion of growth factors and cytokines by synergizing with DDR. Lastly hyperactivation of these pathways also induce transcription of negative regulators such as miR-146a. This establishes a negative feedback regulatory mechanism to control SASP.

1.10: Mechanism of action of miRNA

RNA polymerase II or III enzymes transcribe microRNAs in the nucleus to form stem-loop shaped primary miRNA transcripts or pri-miRNAs (Kim *et al.*, 2009). These pri-miRNAs are then sliced by Drosha-DGCR8/Digeorge critical region 8 (Pasha) of RNase III family to form a shorter hairpin precursor miRNA (pre-miRNA) intermediates, roughly 60 to 70 nucleotides long (Bartel, 2009). Afterwards these pre-miRNAs are then exported out of nucleus via exportin 5-Ran-GTP transporter molecule into cytoplasm where they are further cropped by Dicer and TRBP (Tar RNA binding protein) complex to form miRNA duplex that carrys the mature miRNA strand containing roughly 22 nucleotide bases and a passenger strand. AGO-2 initiates unwinding of miRNA duplex. Usually the mature strand comprises of thermodynamically unstable bases at its 5'terminal and so becomes incorporated into the microRNA induced silencing complex (miRISC) whereas the passenger strand becomes decayed (Kim *et al.*, 2009; figure 1.6).

MiRNA and AGO-2 proteins exhibit cell and tissue specificity and hence the extent of translational repression and mRNA degradation varies in different tissues (Fabian *et al.*, 2010). Evidence delineates that miRISC suppresses protein translation via destabilizing cap function (Humphreys *et al.*, 2005). Deadenylation at 3'terminal is considered to be the chief event in initiating mRNA decay (Wu *et al.*, 2006). The deadenylase machinery is recruited by GW182, poly-A-specific ribonucleases and poly-A-ribonucleases (Fabian *et al.*, 2010). These enzymes trim the poly-A-tails until they are 20 to 30 nucleotides long and expose the 3'terminal to the degradative action of 3'→5' exonucleases (Wu *et al.*, 2006). Dissociation of EIF4E from 5'capped region induces the cis-elements at 3'UTR of mRNA to recruit decapping enzymes that catalyzes formation of 5'monophosphorylated mRNA body which are vulnerable to 5'→3' exonucleases; XRN-1 (Franks and Lykke-Andersen, 2008). Both these events

induce formation of P-bodies in which mRNA can be temporarily stored or degraded (Eulalio *et al.*, 2007).

1.10.1: Role of miRNA in ageing

The functions of microRNAs are highly tissue specific but are conserved across species (Bartel, 2009). Owing to their tissue specificity it is difficult to obtain an age-specific miRNA signature. Moreover the stimuli for ageing are also very diverse which is an additional drawback to acquire a list of candidate miRNAs that may be linked to the ageing process. To minimize these problems more emphasis had been given to the molecular pathways that are associated with ageing or involved in development of age-related diseases including cancer. Using this method miR-34 family (miR-34a, -34b and -34c) had emerged as the single most probable candidate miRNA that increases upon ageing (He *et al.*, 2007). This miRNA has a TP53 binding motif in its promoter region and is therefore actively transcribed in senescent cells upon activation of TP53 pathway or DDR (He *et al.*, 2007). Some examples of miRNAs, which are deregulated in different kinds of senescent cells, are described below.

Down-regulation of oncogenic miRNA miR-17 family (miR-17-5p, miR-20a, miR-93, miR-106a) is a common phenomenon in different types of human replicative senescent cells and in human aged tissues of different origin (Hackl *et al.*, 2010). Some other miRNAs which are aberrantly expressed in human aged tissues include miR-146a, miR-15a/b, let-7 family, miR-101, miR-16, miR-199a-3p/b-3p, miR-193b, miR-125a-5p, miR-335, miR-519d, miR-222, miR-212, miR-221, miR-424, miR-19a, miR-20b and many more (Hackl *et al.*, 2010). Moreover study of microRNA expression profiles of old rat kidney tissues compared to young ones showed elevated expressions of miR-335, miR-184, miR-132, miR-34a, miR-34c and many other miRNAs (Bai *et al.*, 2011). The overlap in expressions of some of these miRNAs upon aging across species suggests that their functions are conserved and is critical in modulation of ageing process in

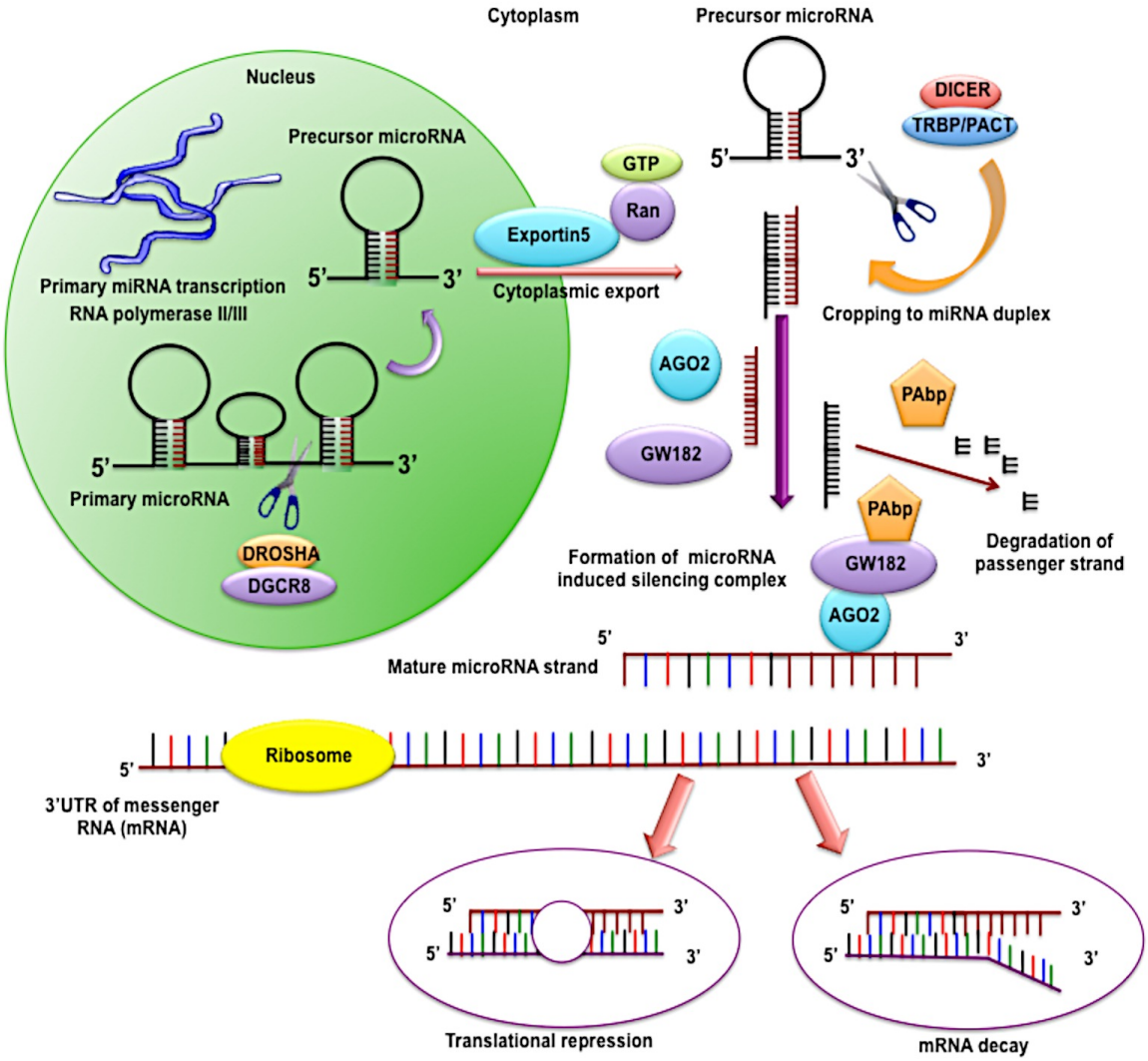

Figure 1.6: Biogenesis of miRNA and its mechanism of action. MicroRNAs are transcribed with in the nucleus by RNA polymerase II or III to form primary miRNA transcripts which are then processed by DROSHA and DGCR8 complex to form precursor miRNAs. This is exported out of the nucleus via Exportin 5. In cytoplasm precursor miRNAs are sliced by DICER and TRBP complex to form 20-22 nucleotides long miRNA duplex. The thermodynamically less stable strand of miRNA duplex incorporates into the miRNA induced silencing complex (miRISC) and the passenger strand is degraded. miRISC recognizes complementary seed sequence at 3'UTR of mRNA and induce wither translational repression or mRNA decay.

humans. In addition to miR-17-92 cluster replicative senescent human pulmonary fibroblasts also shows down-regulation of two other oncogenic miRNAs, miR-15b and miR-25, and up-regulation of several tumour suppressive miRNAs such as miR-127-3p, miR-329, miR-409-3p, miR-487b, miR-495 and miR-493*, which corroborate with the tumour suppressive role of senescence in cancer (Wang *et al.*, 2011a). In another study miR-22 (Hackl *et al.*, 2010) along with miR-24-2*, miR-125-5p, miR-34a and miR-152 were found up-regulated in human senescent mammary fibroblasts (Xu *et al.*, 2011). Some miRNAs which are up-regulated in replicative senescent dermal fibroblasts are miR-10b, miR-23a and miR-34a which had been previously reported to regulate cancer cell motility, apoptosis and senescence, respectively (Bonifacio *et al.*, 2010). These therefore suggest although it is extremely difficult to obtain the same miRNA signature in different kinds of senescent cells, however certain miRNAs do retain their expression in different tissues during the process of ageing and perhaps these are the miRNAs that regulate key events in senescence development.

Furthermore, using more up-to-date technology such as deep sequencing, similar miRNA expression profiles were obtained in replicative senescent fibroblasts (Dhahbi *et al.*, 2011). Deep sequencing also showed up-regulation of miRNAs that had not been reported before which included miR-432, miR-1246, miR-584 and miR-323b-3p (Dhahbi *et al.*, 2011).

Another study carried out in ionizing radiation-induced senescent fibroblasts demonstrated that they display similar miRNA expression profiles to that of replicative senescent cells (Wang *et al.*, 2011b). Moreover, previously it had been reported that ionizing radiation induced and replicative senescent cells have similar gene expression profile and phenotype corroborating the existence of a similar miRNA mediated gene regulatory mechanism in these cells (Coppe *et al.*, 2008b).

Senescence-associated miRNAs may be also classified based on presence and absence of p16 or by dependency on TP53. For example: miR-197 and miR-155 are down-regulated and miR-373* and miR-663 are up-regulated in both BJ (p16 negative) and WI-38 (p16 positive) cells and are therefore independent of p16-driven senescence and are likely to be induced by TP53 activation (Bonifacio *et al.*, 2010). Alternatively miR-34 and let-7 family were reported as positive modulators of p16 as their up-regulation in senescent mammary epithelial cells and fibroblasts correlated with up-regulation of p16 (Overhoff *et al.*, 2013). P16 expression in senescent cells are regulated by polycomb group of repressors (PcG) constituting polycomb repressive complex-2 (PRC-2) and its core subunits EED (embryonic ectoderm development), enhancer and suppressor of zeste homologue 2 and 12 (EZH2 and SUZ12) which induce tri-methylation of histone H3 and lysine residue 27 (H3K27me3) to inhibit p16 expression and delay senescence (Overhoff *et al.*, 2013). Other miRNAs that were positively associated with p16 expressions are miR-26b, -181a, -424 and -210 all of which targeted both PRC-1 and PRC-2 components of the PcG complex and relieved repression of INK/ARF loci encoding p16 in senescent cells (Overhoff *et al.*, 2013). In presenescent cells the loci encoding each of these miRNAs were enriched for H3K27me3, indicating that these sites become demethylated upon attainment of senescence (Overhoff *et al.*, 2013).

Since senescence and quiescence are both a state of growth arrest there is a possibility for these two cell cycle fates to be regulated by similar genetic pathways. It was found that certain miRNAs like miR-155, miR-365 and miR-512-5p are down-regulated whereas miR-26a, miR-10b, miR-624, miR-663, miR-638, miR-377, miR-373* and miR-199-3p are up-regulated in both senescence and quiescent state (Bonifacio *et al.*, 2010; Maes *et al.*, 2009).

To distinguish further miRNAs expressed during senescence from miRNAs associated with late-passage hTERT was used to immortalize human fibroblasts. It was found that

tumour suppressor miRNAs miR-145/143 cluster which is usually up-regulated in replicative senescent cells were down-regulated in late-passage fibroblasts upon hTERT expression. Moreover hTERT expression mitigated the growth arrest inducing effect of miR-143 on fibroblasts implying that this miRNA is an important determinant of cell cycle fate and upon increase in life span the genes regulated by miR-143 are deranged. Again, proto-oncogenic miRNA miR-155, which is down-regulated in senescence is up-regulated by hTERT (Bonifacio *et al.*, 2010). hTERT also increased the basal levels of miR-146a in BJ fibroblasts (Bonifacio *et al.*, 2010). Polycistronic miRNAs: miR-424-503 cluster, previously reported to induce G1 arrest in THP-1 cells, was up-regulated in both late-passage and replicative senescent BJ fibroblasts.

Senescence-associated miRNAs may be also classified according to the causative stimuli. For instance: hydrogen peroxide-induced senescent cells express more of miR-34a and let-7f while replicative senescent cells express more of miR-191, miR-152, miR-181a, miR-638 and miR-663 (Maes *et al.,* 2009; Mancini *et al.*, 2012). Inflammation associated miRNAs like miR-21, -146a, -221, -223, -17 and -126 are up-regulated in nitric oxide-induced senescent fibroblasts (Sohn *et al.*, 2012). Certain miRNAs may be commonly deregulated in different types of senescence response triggered by oxidative stress, DNA damaging agents or even telomere exhaustion. Some of these include up-regulation of miR-486-5p, -210, -376*, 126*, -23b-, 485-5p and down-regulation of miR-17 family, miR-155, miR-15b and miR-199b-5p (Faraonio *et al.*, 2012).

Deletion of miRNA processing enzyme Dicer in murine embryonic fibroblasts was also found to induce premature senescence by initiating DDR and inducing expression of TP53, p21 and p19ARF along with PAI-1; an inducer of replicative senescence (Kortlever *et al*., 2006; Mudhasani *et al.*, 2008). Similarly knock down of canonical miRNA processing enzymes DGCR8 and Drosha as well as Dicer in human primary fibroblasts were also found to induce premature senescence by stimulating p21

expression (Gomez-Cabello *et al.*, 2013). It was found that DGCR8 deficiency was associated with down-regulation of *CDKN1A* targeting miRNAs: miR-106a, -93 and -20a, with concomitant rise in p21 expression in these cells (Gomez-Cabello *et al.*, 2013).

All these evidence further substantiated the importance of miRNAs and their biogenesis as a key determinant of senescence fate, together with their protective role against cancer formation. Moreover manipulation of senescence-associated miRNAs as well as DGCR8 in cancer cells was found to induce growth arrest, apoptosis and improve their sensitivity to chemotherapy (Jin *et al.*, 2013, Gomez-Cabello *et al.*, 2013). Therefore miRNA based targeted therapy may be a promising approach to develop novel anti-cancer therapies.

1.10.2: Functional effects of miRNAs in induction of senescence

miR-210, miR-376*, miR-486-5p, miR-494 and miR-542-5p were found to generate ROS to initiate DDR and induce senescence in human fibroblasts (Faraonio *et al.*, 2012). Higher levels of miR-17-5p and miR-20a were previously reported in breast, prostrate and pancreatic carcinoma (Wang *et al.*, 2011a). Inhibition of these miRNAs in young proliferating fibroblasts induced senescence-mediated growth arrest at G1 phase via up-regulation of their target gene E2F1 of the pRB-p16INK4a pathway (Wang *et al.,* 2011a) showing that miRNAs can regulate senescence via controlling cell cycle progression. Conversely introduction of tumour suppressor miRNA miR-22, down-regulated in human cervical and breast cancer, induced senescence at G1 phase via repressing cyclin dependent kinase 6 (CDK6), Sirtuin1 (SIRT1): NAD^+ dependent deacetylase and transcriptional factor Sp1 in both young fibroblasts and cancer cell lines (Xu *et al.*, 2011). Inhibition of miR-22 by anti-miR-22 prolonged life span in young fibroblasts (Xu *et al.*, 2011). SIRT1 is also a target of miR-181a, miR-181b and miR-138 all of which are up-regulated during keratinocyte senescence in humans (di Val

Cervo *et al.*, 2012). miR-499 and miR-34a are other senescence-associated miRNAs which target CDK6 and prevent cells to enter S phase (Dhahbi *et al.*, 2011; Sun *et al.,* 2008). In addition miR-34a also targets ROS scavenger enzyme thioredoxin reductase in murine aged kidney tissues, important for ROS mediated development of senescence in different tissues (Bai *et al.*, 2011). Again miR-17-92 family, which is frequently down-regulated with age, targets p21 (Hackl *et al.*, 2010; Gomez-Cabello *et al.*, 2013). miR-217 increased in senescent endothelial cells also targets SIRT1 (Dhahbi *et al.*, 2011). miR-155 acts downstream of TP53 and p38MAPK pathway and its up-regulation inhibits ionizing radiation induced senescence via repression of tumour protein 53 induced nuclear protein (Wang *et al.*, 2011b). miR-335 can induce TP53 mediated growth arrest by repressing retinoblastoma protein (RB1) in human and murine cancer cell lines and therefore play a critical role in preventing malignant transformation in such cells (Scarola *et al.*, 2010).

miR-152 up-regulated in senescent fibroblasts targets cell adhesion molecule integrin α5 (*ITGA5*) that reduces their communication with ECM components like fibronectin to hinder their activation by focal adhesion kinases (Mancini *et al.*, 2012). This acts as an effective tumour suppressive mechanism because this can mitigate cross-talk between cancer cells and stroma. Furthermore senescence-associated miRNAs can also alter the composition of ECM components, for example miR-181a, which is frequently up-regulated in senescent fibroblasts represses collagen VI A1 synthesis which reduce the strength of the anchoring fibrils that hold the basement membrane and support the neighbouring epithelial cells (Mancini *et al.*, 2012). This may modify the structural complexity of the basement membrane and thereby create a surrounding favourable for invasion or even reinforcement of senescence.

Alternatively DDR induced by cisplatin causes aberrant expression of miRNAs in head and neck cancer cell lines via ATM kinase mediated phosphorylation and subsequent activation of transcriptional factor ΔNp63α and Dicer (Huang *et al.*, 2011). Both

phosphorylated ΔNp63α and Dicer can work in concert or independently to either increase or decrease expression of effector miRNAs (Huang *et al*., 2011). During normal keratinocyte senescence expression of ΔNp63α appears to be inhibited by miR-130a implying that senescence may be an alternative cell fate in absence of apoptosis that is selected by cells to sustain tissue homeostasis (di Val Cervo *et al.*, 2012).

1.10.3: Role of miRNAs in tumour microenvironment

Genomic instabilities are rare in CAFs. However these cells still maintain a stable tumourigenic phenotype when cultured *in vitro*. Similar to CAFs senescent cells also have a very stable phenotype both *in vitro* and *in vivo*. Therefore it is thought that CAFs and senescent fibroblasts may exhibit some kind of epigenetic mechanism or miRNA mediated gene regulation that enables these cells to sustain their pro-tumourigenic phenotype.

Expression of miR-212/132 family in stromal fibroblasts was found to be essential for development and differentiation of normal mammary gland (Ucar *et al.*, 2010). In absence of miR-212/132 there is an increase in proteolytic activity of its target gene MMP-9 causing excess release and hyper-activation of TGF-β, which subsequently suppress amphiregulin mediated mammary epithelial cell proliferation and gland development in mice models (Ucar *et al.*, 2010). In colorectal carcinoma expression of miR-21 in CAFs correlates with stage of the disease from precancerous lesions to advanced adenocarcinoma and is correlated with decreased survival rate (reviewed by Li *et al*., 2012; Nielsen *et al*., 2011). In endometrial carcinoma down-regulation of miR-31 in CAFs is associated with enhanced expression of SATB2 homeobox gene known to encode nuclear matrix attachment protein (Aprelikova *et al.,* 2010). In prostate cancer miR-15 and miR-16 are down-regulated in CAFs accompanied by an increase in FGF-2 and FGFR1 which facilitates proliferation and migration of prostate cancer

cells (Musumeci *et al.,* 2011). miR-126 is downregulated in various cancers including breast and targets proangiogenic factors IGFBP2, MERTK and PITPNC1 and suppress recruitment of endothelial cells in non-cell autonomous manner (reviewed by Li *et al*., 2012).

Emerging evidence shows that microRNAs are also critical in inducing transdifferentiation of fibroblasts into myofibroblasts in response to TGF-β. Two such miRNAs are miR-146a (Liu *et al.,* 2012) and miR-21 (Yao *et al.,* 2010). It was found that miR-146a negatively regulated SMAD4 in dermal fibroblasts which is a downstream protein in TGF-β signalling pathway and hence impedes the transdifferentiation of fibroblasts (Liu *et al.,* 2012). In contrast miR-21 was observed to cause translational repression of PDCD-4 (programmed cell death 4) which is known to down-regulate genes controlling the contractile phenotype of smooth muscles (Yao *et al.,* 2010). Thus miR-21 and miR-146a acts as a positive and negative regulator of fibroblast transdifferentiation into myofibroblasts and hence exerts a regulatory response in wound healing and protects against formation of fibrotic scars.

The definite mechanism of acquisition of an activated or pro-tumourigenic phenotype by CAFs and senescent fibroblasts is poorly understood. Recently the tumour suppressor protein PTEN has emerged as an important determinant of secretory function in myofibroblasts (Trimboli *et al.*, 2009). It had been reported that loss of PTEN in CAFs derived from breast cancer patients was associated with loss of tumour suppressor miRNA miR-320, which was found to negatively regulate transcription factor Ets2 at post-transcriptional level (Bronsiz *et al.*, 2011). Some important currently known biological functions of PTEN are described below with possible implications of its role in inflammation and cancer.

1.11: PTEN

PTEN (phosphatase and tensin homolog deleted from chromosome 10 or MMAC1/TEP1) is a dual phosphatase, considered to act as a tumour suppressor protein owing to its inhibitory effect on kinases (Li *et al.*, 2002). It inhibits the activity of phosphatidylinositol-3,4,5-triphosphate and bypasses transduction of various oncogenic signals such as EGF/EGFR signaling, HER2 signaling, IGF/IGFR signaling that phosphorylates AKT (Li *et al.*, 2002; Snietura *et al.*, 2012). Under physiological conditions activation of AKT is essential for cell survival, proliferation and migration and its hyper-activation is restrained by PTEN. Mutation or LOH in human chromosomal loci 10q23 leads into functional inactivation of PTEN causing withdrawal of its inhibitory effect on PI-3-K/AKT pathway leading into development of cancer (Li *et al.*, 2002). PTEN may be also epigenetically silenced by DNA methylation (Bian *et al.*, 2012b). PTEN can be also regulated by miRNAs at post-transcriptional levels (He *et al*., 2014b).

PTEN is found to be down-regulated in fibroproliferative disorders such as keloids and systemic sclerosis (Liu *et al.*, 2013; Parapuram *et al.*, 2011). Mutation of PTEN has been reported in various kinds of sporadic cancers of breast (Li *et al.*, 2002), lung (Yanagi *et al.*, 2007), HNSCC and is associated with poor prognosis (da Costa *et al.*, 2014). In HNSCC, 40% patients demonstrate PTEN heterozygosity and 47% patients demonstrate abnormalities in PI-3-K/AKT pathway (Bian *et al.*, 2012a). PTEN expression is also lost in 29% of patients suffering from tongue SCC (Bian *et al.*, 2012a).

1.11.1: Effect of PTEN in epithelial cells

Past reports showed that deletion of Pten in murine mammary epithelial cells cause precocious morphogenesis of mammary gland with prominent milk secreting lobuloalveolar buds characteristic of early pregnancy in virgin mice, mammary gland

hyperplasia in pregnant mice and delayed atrophy of lactating mammary gland at post-weaning period accompanied by an increased incidence of tumour formation (Li *et al.*, 2002).

Pten had been also reported to maintain the turnover of organ specific stem cells, such as in adult prostate gland, haematopoetic cells, brain and lung (Yanagi *et al.*, 2007). Pten deficiency in HNSCC cell lines was found to resist apoptosis and senescence, and acquire stemness (Bian *et al.*, 2012a). During lung development in mice models, embryonic bronchoalveolar epithelial cells expressed less Pten which increased their self-renewal potentials and attenuated differentiation capacity (Yanagi *et al.*, 2007). Furthermore, persistent Pten deficiency in bronchoalveolar epithelia both during embryonic and adult life increased the incidence of adenocarcinoma in mice models (Yanagi *et al.*, 2007).

Again, PTEN inactivation accompanied by mutation of either KRAS oncogene or TGF-β receptor, activates the NFκB pathway and stimulates expression of pro-inflammatory cytokines that eventually creates an immunosuppressive tumour microenvironment in pancreatic ductal adenocarcinoma and HNSCC, respectively (Ying *et al.*, 2011; Bian *et al.*, 2012a).

Therefore PTEN ensures controlled proliferation, apoptosis and differentiation of epithelial cells, prevents emergence of cancer stem cells and suppresses outburst of inflammatory signals at times of oncogenic mutations forming a repressive niche unfavourable for tumour growth. Furthermore, increased expression of PTEN in tumour cells compared to normal tissue after neoadjuvant radiotherapy was found to be associated with better outcome and reduced rate of recurrence in head and neck cancer patients (Snietura *et al.*, 2012). In addition these patients were found less prone to develop radioresistance (Snietura *et al.*, 2012).

1.11.2: Role of PTEN in generation of stem cells

PTEN suppresses development of stemness in normal human adult cells (Yanagi *et al.*, 2007). It is poorly understood how PTEN contributes to the emergence of stem cells in normal tissues, however, recent work showed that Yamanaka's factors (Oct4, cMyc, Klf4 and Sox2) up-regulate miR-17-92 cluster in human adult fibroblasts, among these miR-19a and miR-19b silence PTEN to induce pluripotency in these cells (He *et al.*, 2014b). This effect was predominately mediated by cMyc, however in absence of cMyc over-expression of either miR-19a or miR-19b could induce stemness in fibroblasts by silencing PTEN (He *et al.*, 2014b).

1.11.3: Role of PTEN in stroma

PTEN-regulated differentiation is not only restricted to the epithelial compartment. Ongoing works suggest PTEN also regulates transdifferentiation of fibroblasts into myofibroblasts in fibrotic diseases (White *et al.*, 2006; Parapuram *et al.*, 2011) and cancer (Wallace *et al.*, 2011).

1.11.3.1: Effect of stromal PTEN on fibrosis

Fibroblasts extracted from patients suffering fibroproliferative disorders like idiopathic pulmonary fibrosis, keloids, arthritis, systemic sclerosis, and liver cirrhosis expressed less PTEN (Liu *et al.*, 2013; White *et al.*, 2006; Parapuram *et al.*, 2011; Zheng *et al.*, 2012). Furthermore, expression of PTEN in myofibroblasts was inversely associated with their proliferative capacity, expression of α-SMA and collagen secretion (White *et al*, 2006; Parapuram *et al.*, 2011; Zheng *et al.*, 2012). In fibroblasts derived from patients of diffuse cutaneous systemic sclerosis PTEN was found to exert anti-fibrotic effect by inhibiting PI-3-K/AKT pathway and reducing expression of CCN2 and synthesis of type I collagen (Parapuram *et al.*, 2011). Pten over-expression in Pten null fibroblasts was also found to suppress their myofibroblastic phenotype (White *et al.*,

2006). Although TGF-β is a transcriptional repressor of PTEN, transdifferentiation of myofibroblast in Pten null fibroblast is independent of autocrine activation by TGF-β (White *et al.*, 2006). In animal models of liver fibrosis PTEN expression in activated HSCs was found to reappear upon withdrawal of the injurious stimuli and was found to promote their apoptosis that led to healing with less scar formation (Zheng *et al.*, 2012). Therefore the anti-fibrotic role of PTEN is promising in designing drugs to reduce fibrosis.

1.11.3.2: Effect of stromal PTEN in cancer

Loss of PTEN in the stroma of mammary glands was found to be a poor prognostic marker in breast cancer patients (Wallace *et al.*, 2011). Conditional deletion of *PTEN* in murine fibroblasts failed to transform normal epithelial cells to yield tumours but resulted in formation of multiple tumours in animal models bearing initiated epithelial cells accompanied by an infiltrating population of macrophages (Trimboli *et al.*, 2009; Trimboli *et al.*, 2008). Deficiency of *PTEN* in resident fibroblasts was enough to stimulate tumour growth in transplant models and both tumourous and non-tumourous tissues had increased collagen content reminiscing the anti-fibrotic property of PTEN (Trimboli *et al.*, 2009; Parapuram *et al.*, 2011). PTEN deicient fibroblasts were found to express increased amount of transcription factor Ets2 (Trimboli *et al.*, 2009). Ets2 was reported to regulate secretion of ECM remodeler; Mmp-9 and chemokine Ccl-3 involved in chronic inflammation and Mmp-9 driven release of pro-angiogenic factor VEGF in murine fibroblasts fostering a niche advantageous to tumour growth (Trimboli *et al.*, 2009). Moreover simultaneous deletion of both Pten and Ets2 in murine fibroblasts produced remarkably small tumours with lesser influx of macrophages and poor vasculature compared to only Pten deletion models (Trimboli *et al.*, 2009). Later it was found that PTEN suppressed Ets2 activity via inducing miR-320 in stromal fibroblasts (Bronsiz *et al.*, 2011). In stroma of human invasive carcinoma of breast

PTEN expression was dramatically decreased and inversely correlated with Ets2 and phosphorylated AKT levels, and was associated with development of recurrence (Trimboli *et al.*, 2009). Human oropharyngeal cancer tissues have elevated AKT and AKT2 activity in stroma. It was found that PTEN inactivation in stromal fibroblasts stimulated AKT2 phosphorylation and enabled these cells to secrete more FGF-7, which stimulated invasiveness of premalignant keratinocytes. Depletion of AKT2 in PTEN null fibroblasts stimulated IL-1β secretion, which inhibited expression of FGF-7 binding receptors; FGFR2B, in transformed keratinocytes in paracrine manner and attenuated their invasive behaviour (Cichon *et al.*, 2013). Further enhanced expression of IL-1β level in stromal fibroblasts were found to correlate with improved overall survival (Cichon *et al.*, 2013).

1.11.4: Role of miRNA in regulation of PTEN

The notion that regulation of PTEN may occur at epigenetic level first arose from the functional study carried out in breast cancer patients to determine the association between loss of PTEN and breast cancer (Perren *et al.*, 1999). It was found nearly 40% sporadic cases of primary breast cancer patients displayed LOH and rarely had any mutation in the intragenic region of PTEN (Oerren *et al.*, 1999). Sequencing revealed the loss as mainly hemizygous deletion manifested as reduced staining for PTEN protein in immunohistochemistry and suggested PTEN functioned as a haplosufficient gene (Perren *et al.*, 1999; Ying *et al.*, 2011). However, five samples of breast cancer patients having hemizygous deletion of PTEN, expressed no protein, indicating somehow PTEN translation is either suppressed or its mRNA is rapidly degraded in these cells (Perren *et al.*, 1999). Therefore apart from promoter methylation, microRNAs were also proposed as critical regulators of PTEN expression in cancer.

miRNA-21 is a proto-oncogenic and pro-fibrotic miRNA that is frequently up-regulated in cancer and fibroproliferative disorders and is associated with poor prognosis in

tongue SCC (Liu *et al.*, 2013; Hedback *et al.*, 2014) and chemotherapy resistance (Bullock *et al.*, 2013; Kadera *et al.*, 2013). It is also a biomarker of disease progression from leukoplakia to OSCC and is increased in stroma of relapsed cases of OSCC (Hedback *et al.*, 2014). This oncomiR was reported to target PTEN in myofibroblasts in STAT3, PDGF-BB and TGF-β dependent manner (Liu *et al.*, 2013; Iliopoulos *et al.*, 2010; Wei *et al.*, 2013; Yao *et al.*, 2011). In mice models of mammary carcinoma, miR-205, was found to target PTEN and was found to be over-expressed in mammary cancer stem cells (Greene *et al.*, 2010). miR-29 is another miRNA which targets PTEN in breast cancer cell line to promote their survival and motility (Wang *et al.*, 2011c). In diabetic nephropathy TGF-β induces transcription of miR-216a and miR-217 in mesangial cells which also target PTEN (Kato *et al.*, 2009).

1.12: Hypothesis

The consequence of differential expression of microRNAs in senescent fibroblasts is determined by the nature of microenvironment and the composition of the neighbouring tissue. As a result the deranged microRNAs can function as either oncogenic miRNAs or as tumour suppressors. Most available studies on senescent fibroblast indicate their tumour promoting behaviour is superimposed by their tumour suppressive function that is achieved by development of SASP. Sometimes tumours can remain asymptomatic for many years even after metastasizing to distant sites. Therefore at the time of treatment these cancers have already reached advanced stage. This is frequently observed in head and neck cancer patients. Administration of low doses of chemotherapies or irradiation therapies to treat these patients may provoke senescence in the neighbouring tumour stroma in addition to cancer cells. What remains uncertain are the effects of this accumulating senescent stroma. Does it favour tumour progression or does it favour tumour regression, is yet to be elucidated. Effects of senescent stroma in progression of breast and prostate cancer have been well characterized (Bavik *et al.*, 2006; Parrinello *et al.*, 2005). However their role in OSCC is only emerging. Very recently it was reported that patients suffering from genetically unstable tumours of head and neck showed increased accumulation of senescent fibroblasts and this was associated with poor disease outcome (Lim *et al.*, 2011). The current use of stromal fibroblast marker in predicting cancer outcome emphasizes the importance of understanding stroma-tumour interactions during every step of carcinogenesis. MicroRNAs have been identified as post-transcriptional gene regulators (Bartel, 2009) and as mentioned in section 1.10 numerous of these microRNAs show altered expression in senescent fibroblasts.

Therefore it was hypothesised that induction of SASP in oral fibroblast is associated with changes in expression of miRNAs, which regulate stromal-tumour interactions and contribute to tumour progression.

1.13: Aims and objectives

- To characterise oral fibroblast senescence *in vitro*.
- To analyse the secretome of SASP of oral fibroblasts and determine their paracrine effects on oral dysplastic and cancer cell phenotype.
- To determine if *in vitro* induction of fibroblast senescence is associated with changes in miRNA expression and investigate if any of these miRNAs target any genes involved with regulation of the secretome of senescent fibroblasts.
- To determine if similar trends are mirrored in cancer associated fibroblasts derived from head and neck cancer patients.

2.0: Materials and Methods

2.1: Cell culture

Primary human oral fibroblasts, oral squamous cell carcinoma derived cell lines, oral dysplastic cell lines and acute monocytic leukaemia derived cell lines were routinely cultured as described below.

2.1.1: Fibroblasts

Primary human diploid fibroblasts DENF008, OF20, OF26, OF320 and OFUN (School of Clinical Dentistry, Charles Clifford Dental Hospital and Royal Hallamshire hospital, Sheffield) were obtained from healthy oral mucosa of the gingiva, collagen digested, selectively trypsinized and grown in DMEM (Sigma) supplemented with 10% (v/v) fetal calf serum; FCS, (Sigma) and 2mM L-glutamine (Sigma). Both DENF008 and OF320 were obtained from gingiva of non-smoker female donors aged 17 and 49, respectively. All other oral fibroblasts used in this study were extracted from gingiva of healthy volunteers before 2011 during the initial attainment of ethical approval and therefore specific information related to age and gender of the patients were not obtained. Cancer associated fibroblasts (CAFs) extracted from genetically stable; GS (BICR69 and BICR70) and unstable; GU (BICR3, BICR63, BICR31, BICR18) oral squamous cell carcinoma (OSCC) were kindly gifted by Professor Stephen Prime and Professor Eric Parkinson from the Blizard Institute, QMUL. These cells were also maintained in DMEM supplemented with 10% FCS and 2mM L-glutamine. This study was approved by the University of Sheffield Ethics Committee (ref:07/H1309/105).

2.1.2: Keratinocytes

Oral squamous cell carcinoma derived cell lines (SCC4 and H357) and oral dysplastic cell lines (D20) were used in the study. SCC4 cells were cultured in DMEM

supplemented with F12 medium (Sigma) in 1:1 ratio, 10% FCS, 2mM L-glutamine and 400 ng/mL of hydrocortisone (Sigma). H357 and D20 cells were cultured in modified DMEM as described in section 2.1.1.

2.1.3: Monocytes

Human acute monocytic leukaemia derived cell lines; THP-1, were kindly provided by Dr. Craig Murdoch. These cells were non-adherent and routinely maintained in RPMI-1640 containing either 10% (v/v) FCS or 2% (v/v) human serum further supplemented with penicillin; 10,000 units, and streptomycin; 10 mg/mL (both Sigma).

All the cultures were incubated at 37^{o}C, 20% oxygen and 5% (v/v) CO_2.

2.2: Induction of senescence using genotoxic stimuli and via replicative exhaustion

Two DNA damaging agents were chosen to provoke stress induced premature senescence in fibroblast cultures; hydrogen peroxide, H_2O_2 (Fisher scientific) and the platinum based cytotoxic drug, Cisplatin (Sigma).

Initially doses of H_2O_2 and cisplatin that could induce senescence *in vitro* were optimized. For treatment with H_2O_2, primary human oral fibroblasts were seeded at 5,000 per well in 96-well plates and incubated overnight at 37^{o} C and 20% O_2 saturation. Next day these cells were pulsed with different concentrations of H_2O_2 ranging from 50 μM to 1000 μM for 2 h. This range was chosen because some authors had previously used 200 μM H_2O_2 (Chen *et al*., 1994) to induce senescence in fibroblasts (of different origin) while others used 1 mM concentration (Bavik *et al*., 2006). Therefore to determine the optimum concentration of H_2O_2 that could trigger senescence in oral fibroblasts with minimal cell death a range of concentrations was used to treat oral fibroblasts. To date no reports are available on the use of cisplatin for

induction of senescence in human oral fibroblasts. As a result a range of concentrations of cisplatin was also chosen to treat oral fibroblasts commencing from 2.0 μM to 100 μM for 24 h. After treatment the cells were washed twice with Dulbecco's phosphate buffered saline (PBS, Sigma) and fresh serum enriched medium was added. A cell viability assay (CellTiter 96 AQueous non-radioactive Cell proliferation kit; Promega) was performed according to manufacturer's instructions to determine the sub-cytotoxic range of both H_2O_2 (adapted from Chen *et al*., 1994 and Bavik *et al*., 2006) and cisplatin at 2 h and 24 h post-treatment, respectively. To further evaluate if the selected range of concentrations of both H_2O_2 and cisplatin remained sub-cytotoxic at later time-points, proliferation assay was carried out beginning from the time of treatment to day 7 post-treatment using CyQuant NF cell proliferation kit (Invitrogen). The optimal doses of H_2O_2 and cisplatin were selected as the concentration that caused minimum cytotoxicity after treatment and gradually reduced the rate of cell proliferation over time-points. Based on this 500 μM and 10 μM were selected as the maximum dose of H_2O_2 and cisplatin for treatment of fibroblasts, respectively. Since the principal goal of this project is to determine the regulatory mechanism of SASP in human senescent oral fibroblasts, the duration for sub-culturing oral fibroblasts was extended to until day 17 post-treatment. To determine if both H_2O_2 (500 μM) and cisplatin (10 μM) induced irreversible growth arrest in oral fibroblasts over extended time-points the viability and proliferation assays were repeated using MTS assay (CellTiter 96 AQueous non-radioactive Cell proliferation kit; Promega). Oral fibroblasts were seeded down at a density of 2,000 cells per well of 96-well plate in triplicate and incubated overnight. The cells were washed once with PBS and treated with either H_2O_2 (500 μM) or cisplatin (10 μM) for 2 h and 24 h, respectively. Untreated fibroblasts were used as control. After treatment, each well was washed twice with PBS and fresh medium was added. The cells were then grown for a period of 17 days with regular change of media every 72 h.

MTS assay was performed at the following time-points after treatment with genotoxic stimuli: day 1, 3, 5, 7, 9, 11, 13, 15 and 17. Senescence was induced in 6-well plates, T25, T75 and T175 flasks with a fibroblast seeding density of 100,000, 200,000, 500,000 and 750,000 to 1,000,000 respectively such that the cells were 60% to 80% confluent overnight. All cells were treated with either H_2O_2 (500 μM) for 2 h or cisplatin (10 μM) for 24 h. Cells were then continuously sub-cultured until day 15. Medium was changed every 72 h. At day 15, cells were harvested for RNA extraction and protein analysis.

All experiments for stress induced premature senescence were carried out using fibroblasts cultured at lower passage between passage 3 and 7 during which these cells were proliferating.

To induce replicative senescence fibroblasts at passage 2 were seeded down at 350,000 in T175 flask and grown until they were 90% confluent. Then cells were harvested and total yield density was calculated manually using a conventional haemocytometer (Assistant, Bright-Line, Superior, Germany). Time between seeding and harvest was recorded. Cumulative population doubling was measured as follows:

Population doubling (PD) = Logarithm_{10} (yield density/seeding density) / $\text{Logarithm}_{10}2$

Therefore,

Cumulative PD = Length of time in h after seeding / PD

The procedure was repeated until the population doubling time of fibroblasts exceeded 2 weeks.

SA-β-Gal staining (Abcam) was performed to visualize senescence, as described in section 2.2.2. Cultures were considered to contain stress induced premature senescent and replicative senescent fibroblasts when each culture contained more than 80% SA-

β-Gal positive cells. Unstained presenescent or proliferating fibroblasts were used as controls.

CAFs derived from GS and GU OSCC were also treated with cisplatin to determine if chemotherapy could induce senescence using the same protocol as above.

2.2.1: Preparation of conditioned medium

After completing 14 days of treatment with H_2O_2 (500 μM) or cisplatin (10 μM), fibroblasts were washed twice with PBS and incubated in serum free DMEM supplemented with L-glutamine for 24 h. Conditioned medium derived from untreated proliferating or presenescent fibroblasts were used as controls. The conditioned media was collected, filter sterilized and stored at -20^{o}C for carrying out functional assays. Occasionally serum free RPMI and DMEM plus F12 mixed in 1:1 ratio were used to prepare conditioned media.

The different seeding densities of fibroblasts that were used for senescence induction in different sized flasks and the amount of media that was used to prepare conditioned media are summarized in table 2.1. CAFs were also used at the same density as normal oral fibroblasts for both induction of senescence and preparation of conditioned media.

Flask Size	Fibroblasts seeding density	Volume of serum free media used to prepare conditioned media
6-well	100,000	600 μL
T25	200,000	1 mL
T75	500,000	2.5 mL
T175	750,000-1,000,000	3.5-4.0 mL

Table 2.1: Summary of fibroblasts seeding density used for senescence induction and of volume of media used for preparation of conditioned media.

2.2.2: Senescence associated β-galactosidase assay

Dimri *et al.* (1995) first reported that both presenescent and senescent cells express lysosomal β-galactosidase that is optimally active at pH 4. However only the senesced cells exhibited lysosomal β-galactosidase activity at pH 6. This is referred to as the senescence associated β-galactosidase activity wherein the lysosomal β-galactosidase converted X-gal containing a galactose plus indole compound to a turquoise blue precipitate.

To determine the extent of senescence in human oral fibroblasts at day 15 post-treatment cells treated with either H_2O_2 or cisplatin and the control cells were harvested and seeded down at a density of 20,000 per well of a 12-well plate overnight. The cells were then washed once with 1X PBS and fixed in 1X fixative solution supplied with senescence detection kit (Abcam, #ab65351) for 15 m at room temperature. After fixation the cells were washed thoroughly with 1X PBS and incubated in the dark overnight at 37^{o}C containing staining solution supplemented with 100X staining supplement and 20 μg/μL of X-Gal (5-bromo-4-chloro=3-indolyl-β-D-galactopyranoside). Staining was visualized at 20X magnification using a light microscope (Olympus; CKX41). Images were captured using Nikon Coolpix camera (P5100; 12.1 megapixels). The total number of stained and unstained cells were counted using ImageJ 1.45s software approved by NIH.

Table 2.2 summarizes the volumes of the ingredients used to make up the staining solution for a 12-well plate. The volume was reduced by a factor of 10 when SA-β-Gal assay was performed in 96-well microplates.

Ingredients	Volumes (in μL) per well of 12-well plate
1 X Staining solution	470
100 X Staining supplement	5
X-Gal (20 mg dissolved in 1 mL of DMF: Dimethylformamide)	25
Total volume	500

Table 2.2: Composition of staining solution of SA-β-galactosidase assay.

2. 3: Immunofluorescence immunocytochemistry

2.3.1: Indirect immunofluorescence immunocytochemistry to detect DNA damage foci in oral fibroblasts following genotoxic stress using human anti-53BP1

Human primary oral fibroblasts were seeded down at a density of 50,000 per well of 12-well plate containing sterilized glass cover slips and allowed to settle overnight. On the following day the cells were treated with either H_2O_2 (500 μM) or cisplatin (10 μM) as described in section 2.2. Untreated fibroblasts were used as controls. Before fixation the fibroblasts were washed twice with 1X PBS. To distinguish and determine persistent DNA damage from transient DNA damage both treated and untreated control fibroblasts were fixed at 30 m and at 24 h post-treatment using 4% (v/v) paraformaldehyde (Sigma) for 15 m. Usually in response to DNA damage cells start repairing within 15 to 30 m and repair is usually completed with in 1 to 2 h. Therefore any damage persisting beyond this time-point was defined as chronic or persistent DNA damage response (Rodier *et al.*, 2009).

Immediately after fixation the cells were rinsed repeatedly in 1X PBS and blocked in blocking buffer (1X PBS, 5% (v/v) normal goat serum; Sigma, 0.3% (v/v) Triton X-100; Sigma) for 1 h. The cells were then incubated with diluted (1 in 100; 16 μg/mL) human anti-53BP1-antibody (subtype IgG, Cell Signalling Technology, #4937S) in antibody dilution buffer containing 1X PBS supplemented with 1% (v/v) bovine serum albumin; BSA (Fisher Scientific) and 0.3% (v/v) Triton X-100 (Sigma) for 2 h. The cells were then repeatedly washed for 5 m in 1X PBS and re-incubated with diluted (1 in 200) Alexa Fluor 488 conjugated anti-rabbit IgG, in the same antibody dilution buffer for 1 h. The cells were rewashed in PBS for 5 m and the coverslips were then transferred to glass slides and mounted with DAPI (nuclear stain) containing prolong Gold anti-fade reagent (Invitrogen) and allowed to dry overnight at room temperature in the dark. Anti-mouse IgG_1 (Sigma; 1 in 100) was used as a negative control. Fluorescence was observed using inverted fluorescence microscope (Zeiss; #Axiovert 200M) under 100X oil immersion lens. Images were captured using AxioVision (release 4.6.3) software.

2.2.3.2: Direct immunofluorescence to detect α–SMA expression in senescent oral fibroblasts

At day 15 post-treatment oral fibroblasts induced to senesce with genotoxic stimuli, replicative senescent oral fibroblasts and control cells were seeded down at a density of 50,000 per well of a 12-well plate carrying sterilized glass cover slips. The cells were incubated overnight. The following day all cells were washed once with 1X PBS and fixed with 100% methanol for 20 m. After fixation each well was washed thoroughly twice with 1X PBS and once with 0.4 mM sodium deoxycholate solution (Sigma). The cells were then permeabilized for 10 m in 0.4 mM sodium deoxycholate solution and blocked in 5% BSA for 60 m. Subsequently diluted antibody solution containing FITC conjugated anti-mouse monoclonal α-smooth muscle actin (1 in 100, 2.6 mg/mL) (subtype IgG, Sigma, # F3777) in 5% BSA were added onto the coverslips bearing

fixed cells and incubated in dark overnight at 4^{o} C in humidified chamber. No primary antibody was added to the negative control wells. Next day the coverslips were rinsed repeatedly with 1X PBS and mounted with DAPI containing prolong Gold anti-fade reagent. Fluorescence was observed and captured using fluorescence Zeiss microscope (Axioplan 2 imaging) using image-pro-plus software version 7.0.1 with magnification set at 40X.

2.4: MMP Zymography

To perform MMP zymography, fresh conditioned media was prepared as described in section 2.2.1, collected and concentrated using vivaspin-500 (Sartorius, #VS0101) spin columns having molecular cut-off point of 5,000 Dalton by centrifugation at 10,000 rpm for 15 m. The supernatant was collected and stored at -20^{o}C for later use.

The conditioned media (10 μL) from senescent and presenescent fibroblasts were mixed with 2X non-reducing zymography sample loading buffer (10 μL; table 2.3) and incubated for 30 m at 37^{o}C. The samples (20 μL) were then transferred into the wells of modified polyacrylamide gels containing gelatin substrate (10% PAGE gelatin; Fisher Scientific and Sigma, table 2.4) and separated by electrophoresis at 150 V for 70 m in 1X Tris Glycine gel running buffer [25 mM Tris Base (Fisher scientific), 250 mM glycine (Fisher scientific), 0.1% SDS w/v (Sigma)].

Once the electrophoresis was complete the gels were allowed to renature in 2.5% (v/v) Triton X-100 in 1X PBS (Fisher Chemicals) for 1 h and maintained in zymogram developing buffer; 0.5 M Tris (Fisher Bioreagent), 2 M NaCl (BDH GPR), 50 mM $CaCl_2$ (Sigma), 50 μM $ZnCl_2$ (Sigma), 1% (v/v) Triton X-100, pH=7.5; at 37^{o}C for 24 h on gentle shaker (30 rpm). The gels were then stained with Coomasie brilliant blue R-250 for 30 m and destained with 40% (v/v) methanol (Fisher scientific) and 10% (v/v) glacial acetic acid (Fisher Chemicals) until distinct faint bands became visible. Fisher

Scientific's EZ-Run pre-stained Rec protein ladder was used as a marker to determine the molecular weight of MMPs. The ladder contained proteins with molecular weight ranging between 10 KDa and 170 KDa; with an orange reference protein band at 72 KDa. Band densitometry were determined using BioRad's Quantity One 1D gel software (version 4.5.0) and the intensity of bands were divided by the total number of fibroblasts present in each sample of conditioned medium to normalize the data to cell density.

Ingredients	Concentrations	Amount
Tris Base	1 M (pH=6.8)	500 μL
SDS (Sodium dodecyl sulphate)	2% (w/v)	200 mg
Bromophenol blue	0.1% (w/v)	10 mg
Glycerol	20% (v/v)	2 mL
Total volume of buffer	2X	10 mL

Table 2.3: Composition of non-reducing zymography sample loading buffer.

Ingredients	Stacking	Ingredients	Separating
Gel Percentage	**4%,**	**Gel Percentage**	**10%**
40%Polyacrylamide	1.0 mL	40% Polyacrylamide	5.0 mL
Stacking gel buffer 1 M Tris pH=6.8	2.5 mL	Separating gel buffer 1.5 M Tris pH=8.8	5.0 mL
10% Ammonium persulfate	120 μL	10% Ammonium persulfate	400 μL
TEMED	26 μL	TEMED	8.0 μL
dd H_2O	3.90 mL	dd H2O	3.30 mL
50% Sucrose solution	2.5 mL	50% Sucrose solution	4.30 mL
		1% Gelatin substrate	2.0 mL (Final conc. 0.2%)
Total Volume	10.0 mL	**Total Volume**	20.0 mL

Table 2.4: Composition of gels for gelatin zymography.

2.5: Cloning of 3'UTR of PTEN into pmiR-Reporter vector

At first the entire length of 3'UTR of human PTEN mRNA (6,458 bp) was screened for miR-335 and miR-148b complementary seed sequences both manually and by using online available target prediction tools including miRwalk (version 2.0) and Target Scan (version 5.0 – 5.2). According to Target Scan, the seed sequences of both miR-335 and miR-148b were found poorly conserved in mammalian species. miR-335 had one predicted 7'meric complementary seed sequence (CTCTTGA) extending from position 2688 to 2694 bp (figure 2.1, highlighted in green and figure 3.3.18.B, upper panel) whereas miR-148b had two putative complementary seed sequences: a 8'meric seed sequence (TGCACTGT) extending from position 2254-2260 bp and a 7'meric seed sequence (TGCACTG) extending from 3154-3158 bp downstream to the stop codon of the 3' UTR of PTEN mRNA (figure 2.1, highlighted in black and figure 3.3.18.B, lower panel). As a result a fragment of 1,323 bp was selected extending from 1884 bp downstream of stop codon bearing the putative seed sequences of both miR-335 and miR-148b to amplify to generate a reporter construct.

The forward primer was designed by selecting the first 23 bp of the 1,323 fragment of 3'UTR of PTEN mRNA highlighted in grey in figure 2.1. The reverse complementary primer was designed by reverse complementing the last 24 bp in the 1,323 fragment in the 3'UTR region of PTEN, also highlighted in grey in figure 2.1. The sequences of primers are demonstrated in table 2.5.

Primers	Sequences
Forward primer	5' TGTTGACACGTTTTCCATACCTT 3'
Reverse complement sequence	5' GTGTACAGGATAATGCCTCATCCC3'
Reverse primer	5' GGGATGAGGCATTATCCTGTACAC 3'

Table 2.5: Sequences of forward and reverse primers of 3'UTR fragment of PTEN

5′TGTTGACACGTTTTCCATACCTTGTCAGTTTCATTCAACAATTTTTAAATTTTTAACAAAGCTCTTAG
GATTTACACATTTATATTTAAACATTGATATATAGAGTATTGATTGATTGCTCATAAGTTAAATTGGTAA
AGTTAGAGACAACTATTCTAACACCTCACCATTGAAATTTATATGCCACCTTGTCTTTCATAAAAGCTGA
AAATTGTTACCTAAAATGAAAATCAACTTCATGTTTTGAAGATAGTTATAAATATTGTTCTTTGTTACAA
TTTCGGGCACCGCATATTAAAACGTAACTTTATTGTTCCAATATGTAACATGGAGGGCCAGGTCATAAAT
AATGACATTATAATGGGCTTTTGCACTGTTATTATTTTTCCTTTGGAATGTGAAGGTCTGAATGAGGGTT
TTGATTTTGAATGTTTCAATGTTTTTGAGAAGCCTTGCTTACATTTTATGGTGTAGTCATTGGAAATGGA
AAAATGGCATTATATATATTATATATATAAATATATATTATACATACTCTCCTTACTTTATTTCAGTTAC
CATCCCCATAGAATTTGACAAGAATTGCTATGACTGAAAGGTTTTCGAGTCCTAATTAAAACTTTATTTA
TGGCAGTATTCATAATTAGCCTGAAATGCATTCTGTAGGTAATCTCTGAGTTTCTGGAATATTTTCTTAG
ACTTTTTGGATGTGCAGCAGCTTACATGTCTGAAGTTACTTGAAGGCATCACTTTTAAGAAAGCTTACAG
TTGGGCCCTGTACCATCCCAAGTCCTTTGTAGCTCCTCTTGAACATGTTTGCCATACTTTTAAAAGGGTA
GTTGAATAAATAGCATCACCATTCTTTGCTGTGGCACAGGTTATAAACTTAAGTGGAGTTTACCGGCAGC
ATCAAATGTTTCAGCTTTAAAAAATAAAAGTAGGGTACAAGTTTAATGTTTAGTTCTAGAAATTTTGTGC
AATATGTTCATAACGATGGCTGTGGTTGCCACAAAGTGCCTCGTTTACCTTTAAATACTGTTAATGTGTC
ATGCATGCAGATGGAAGGGGTGGAACTGTGCACTAAAGTGGGGGCTTTAACTGTAGTATTTGGCAGAGTT
GCCTTCTACCTGCCAGTTCAAAAGTTCAACCTGTTTTCATATAGAATATATATACTAAAAAATTTCAGTC
TGTTAAACAGCCTTACTCTGATTCAGCCTCTTCAGATACTCTTGTGCTGTGCAGCAGTGGCTCTGTGTGT
AAATGCTATGCACTGAGGATACACAAAAATACCAATATGATGTGTACAGGATAATGCCTCATCCC3′

Figure 2.1: Fragment of 3'UTR of PTEN, extending 1884 bp downstream of stop codon of PTEN mRNA up to a region of 1323 bp. This region carries the putative complementary seed sequences for miR-335 (highlighted in green) and miR-148b (highlighted in black).

The designed primers were then checked against all known human mRNA sequences available online using NCBI primer blast tool to ensure that the designed primers were specific for the 1,323 bp fragmented region of the 3'UTR of human PTEN mRNA (figure 2.2, upper panel). Further, this 1,323 bp region of the 3'UTR fragment was also screened for restriction sites using NEBcutter tool version 2.0 to select specific restriction enzymes for inserting the 3'UTR fragment into pmiR-reporter vector to ensure that these enzymes lacked binding motifs within the insert (figure 2.2, lower panel). Based on this two restriction enzymes: Spe I and Sac I were chosen for insertion into the pmiR-Reporter vector as illustrated in figure 2.12 and figure 2.2.

Table 2.6 shows the sequences of restriction sites added to the designed primers of PTEN 3'UTR.

Name of restriction enzyme	Restriction site
Spe I	5' A^CTAGT 3'
Sac I	5'GAGCT^C 3'

Table 2.6: Restriction sites of Spe I and Sac I. I. Sites of cleavage are indicated by ^.

The Spe I restriction site was added to the forward primer which is preceded by addition of 5 bases of junk nucleotides, ACTGA (figure 2.3). This allows space for sufficient cutting of the restriction sites during restriction digestion necessary for linearizing DNA before ligation. The Sac I restriction site was added to the reverse primer succeeded by addition of another 5 bases of junk nucleotides, AATAA (figure 2.3). The primer sequences are summarized in table 2.7.

Before using these primers for DNA amplification in-silico analysis was performed to ensure that the newly designed forward and reverse primers carrying the specified restriction sites amplified only the region of interest of PTEN 3'UTR (figure 2.4).

Primer pair 1

	Sequence (5'->3')	Length	Tm	GC%	Self complementarity	Self 3' complementarity
Forward primer	TGTTGACACGTTTTCCATACCTT	23	58.80	39.13	4.00	0.00
Reverse primer	GGGATGAGGCATTATCCTGTACAC	24	60.80	50.00	8.00	4.00

Products on target templates

>XM_006717926.1 PREDICTED: Homo sapiens phosphatase and tensin homolog (PTEN), transcript variant X1, mRNA

```
product length = 1323
Forward primer  1     TGTTGACACGTTTTCCATACCTT  23
Template        3824  ......................  3846

Reverse primer  1     GGGATGAGGCATTATCCTGTACAC  24
Template        5146  ........................  5123
```

>NM_000314.4 Homo sapiens phosphatase and tensin homolog (PTEN), mRNA

```
product length = 1323
Forward primer  1     TGTTGACACGTTTTCCATACCTT  23
Template        4128  ......................  4150

Reverse primer  1     GGGATGAGGCATTATCCTGTACAC  24
Template        5450  ........................  5427
```

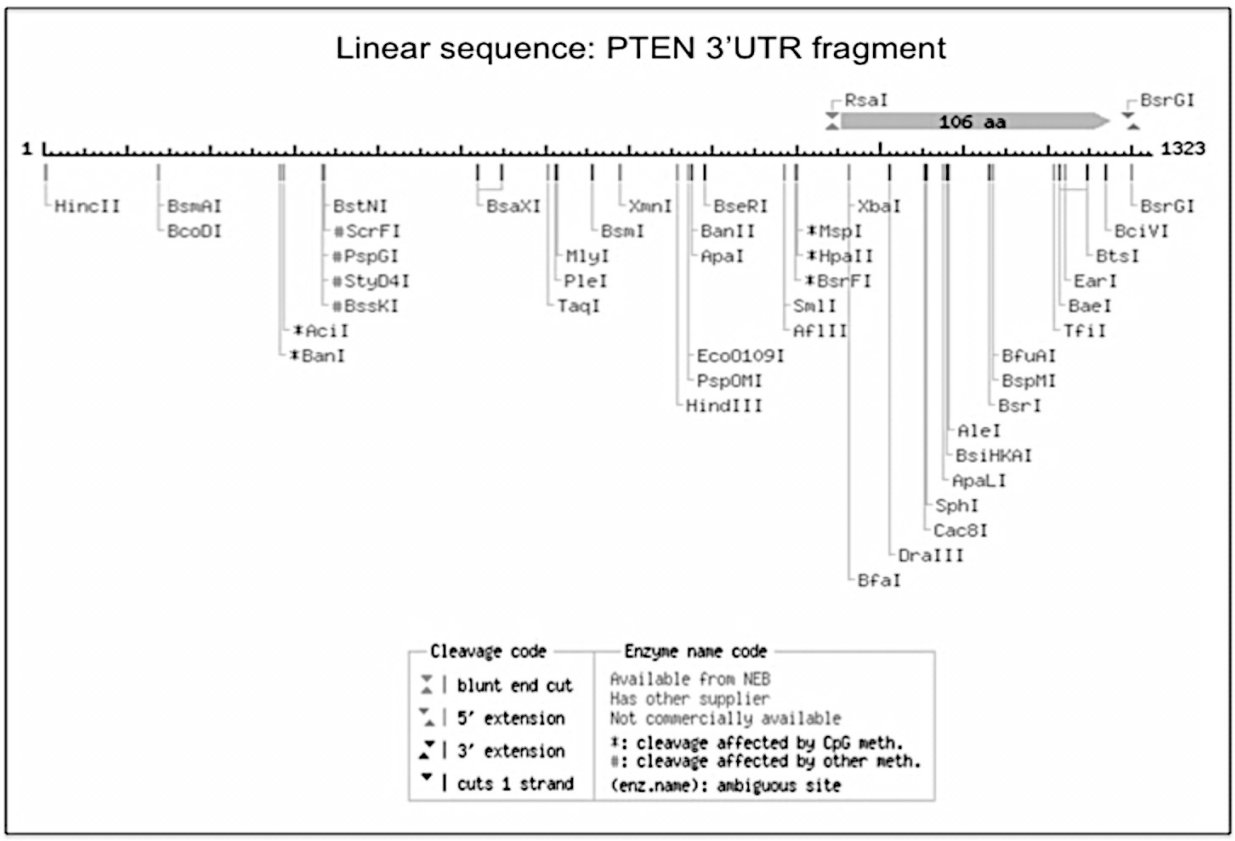

Figure 2.2: In-silico validation of 3'UTR PCR product and its screen for restriction sites. In silico analysis was carried out using designed forward and reverse primers to detect PTEN 3'UTR fragment (upper panel) and screening of the 3'UTR region for restriction sites using NEBcutter tool (lower panel).

5’ACTGAACTAGTTGTTGACACGTTTTCCATACCTTGTCAGTTTCATTCAACAATTTTTAAATTTTTAAC
AAAGCTCTTAGGATTTACACATTTATATTTAAACATTGATATATAGAGTATTGATTGATTGCTCATAAGT
TAAATTGGTAAAGTTAGAGACAACTATTCTAACACCTCACCATTGAAATTTATATGCCACCTTGTCTTTC
ATAAAAGCTGAAAATTGTTACCTAAAATGAAAATCAACTTCATGTTTTGAAGATAGTTATAAATATTGTT
CTTTGTTACAATTTCGGGCACCGCATATTAAAACGTAACTTTATTGTTCCAATATGTAACATGGAGGGCC
AGGTCATAAATAATGACATTATAATGGGCTTTTGCACTGTTATTATTTTTCCTTTGGAATGTGAAGGTCT
GAATGAGGGTTTTGATTTTGAATGTTTCAATGTTTTTGAGAAGCCTTGCTTACATTTTATGGTGTAGTCA
TTGGAAATGGAAAAATGGCATTATATATATTATATATATAAATATATATTATACATACTCTCCTTACTTT
ATTTCAGTTACCATCCCCATAGAATTTGACAAGAATTGCTATGACTGAAAGGTTTTCGAGTCCTAATTAA
AACTTTATTTATGGCAGTATTCATAATTAGCCTGAAATGCATTCTGTAGGTAATCTCTGAGTTTCTGGAA
TATTTTCTTAGACTTTTTGGATGTGCAGCAGCTTACATGTCTGAAGTTACTTGAAGGCATCACTTTTAAG
AAAGCTTACAGTTGGGCCCTGTACCATCCCAAGTCCTTTGTAGCTCCTCTTGAACATGTTTGCCATACTT
TTAAAAGGGTAGTTGAATAAATAGCATCACCATTCTTTGCTGTGGCACAGGTTATAAACTTAAGTGGAGT
TTACCGGCAGCATCAAATGTTTCAGCTTTAAAAAATAAAAGTAGGGTACAAGTTTAATGTTTAGTTCTAG
AAATTTTGTGCAATATGTTCATAACGATGGCTGTGGTTGCCACAAAGTGCCTCGTTTACCTTTAAATACT
GTTAATGTGTCATGCATGCAGATGGAAGGGGTGGAACTGTGCACTAAAGTGGGGGCTTTAACTGTAGTAT
TTGGCAGAGTTGCCTTCTACCTGCCAGTTCAAAAGTTCAACCTGTTTTCATATAGAATATATATACTAAA
AAATTTCAGTCTGTTAAACAGCCTTACTCTGATTCAGCCTCTTCAGATACTCTTGTGCTGTGCAGCAGTG
GCTCTGTGTGTAAATGCTATGCACTGAGGATACACAAAAATACCAATATGATGTGTACAGGATAATGCCT
CATCCCGAGCTCAATAA3’

Figure 2.3: Addition of restriction sites to PTEN 3’UTR fragment. The Spe I and Sac I restriction sites are highlighted in cyan and green respectively. The junk nucleotides are highlighted in yellow.

Primers	Sequences	T_m/°C
Forward	5' ACTGAACTAGTTGTTGACACGTTTTCCATACCTT 3'	71.2
Reverse	5' TTATTGAGCTCGGGATGAGGCATTATCCTGTACAC 3'	76.4

Table 2.7: Final sequences for 3'UTR PTEN for cloning into pmiR-reporter vector.

T_m/°C = predicted melting temperature (Sigma).

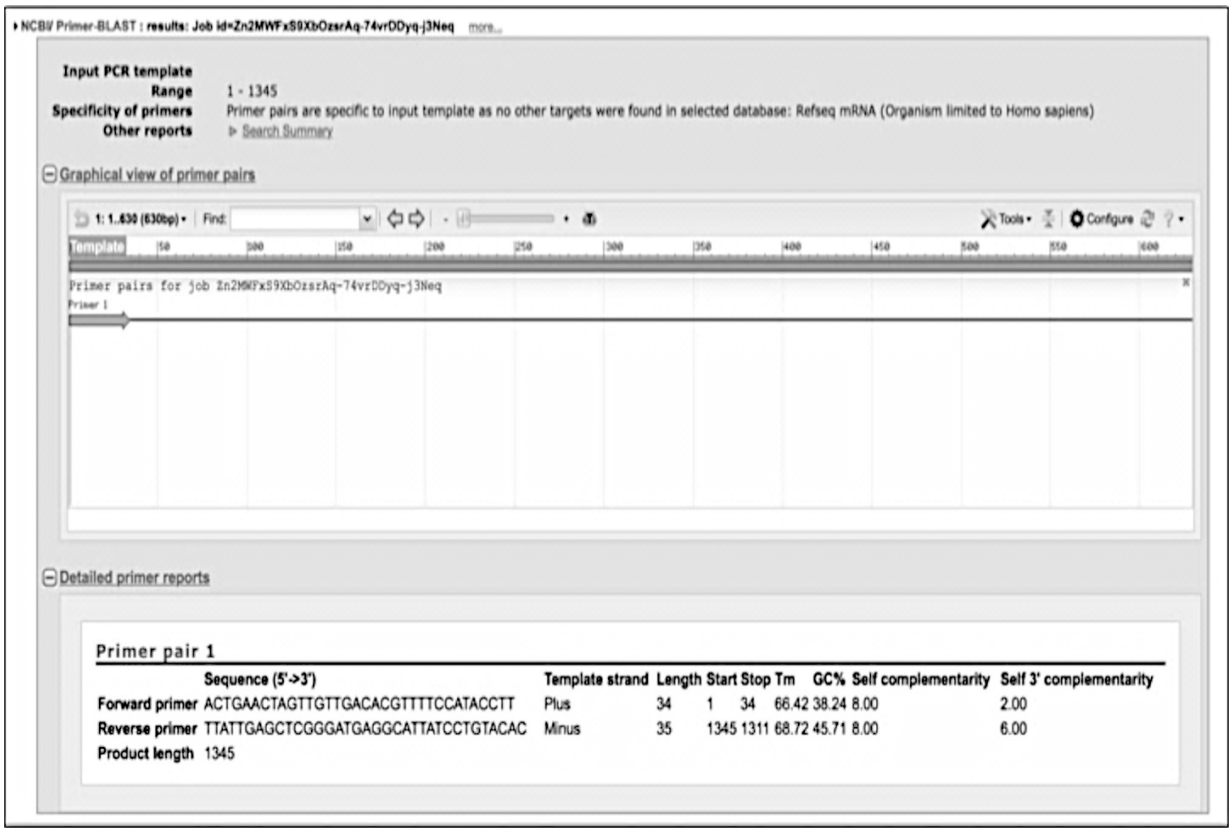

Figure 2.4: In-silico analysis of PTEN 3'UTR insert for cloning into pmiR-reporter vector.

2.5.1: PCR amplification

RNA derived from young normal human oral fibroblasts (passage 6; 1 μg) was reverse transcribed to freshly synthesize cDNA. This cDNA was then amplified with simultaneous introduction of Spe I and Sac I restriction sites at the 5' and 3' end of the PTEN 3'UTR fragment, respectively, by using high fidelity Phusion DNA polymerase enzyme and PTEN 3'UTR specific forward and reverse primers shown in table 2.7. The composition of the PCR master mix and the parameters for DNA amplification are summarized in table 2.8 and table 2.9, respectively.

Briefly, the PCR master mix was prepared (table 2.8). Phusion DNA polymerase was added last to avoid degradation of primers and cDNA by its 3' exonuclease activity. As the primers had high G/C contents: forward (38%) and reverse (46%), both phusion HF buffer and GC buffer were tried in separate master mixes to ensure optimum conditions for polymerase chain reaction (PCR). Further a temperature gradient was set up ranging from 55^{o} C to 72^{o} C to determine the optimum annealing temperature for DNA amplification. Four annealing temperatures were selected based on instructions of the manufacturer (Thermo Scientific). It was suggested to use an annealing temperature 3^{o} C higher than the predicted lowest melting temperature of the designed primers. According to Sigma, the forward primer had the lowest melting temperature of 71.2^{o} C. As this temperature was near the extension temperature instead of setting up 2 step cycle (annealing temperature=extension temperature =72^{o}C), the conventional 3 stage cycle was run at annealing temperatures of 55.5^{o} C, 67.5^{o}C, 71^{o} C and 72^{o}C for both buffers for PCR optimization (figure 2.5).

A total reaction volume of 50 μL was used for DNA amplification in thermal cycler set according to the parameters in table 2.9 (DNA engine; DYAD). Extra duration was chosen for initial denaturation and extension as precautions to provide enough time for efficient DNA disintegration and product amplification by phusion DNA polymerase.

Ingredients	Volume (μL)	Final Concentration
5X Phusion HF buffer or GC buffer plus 7.5 mM $MgCl_2$	10	1X (1.5mM $MgCl_2$)
dNTPs (10 mM)	1.0	200 μM
Forward primer (5 μM)	5.0	0.5 μM
Reverse primer (5 μM)	5.0	0.5 μM
Phusion DNA polymerase (2 U/μL)	0.5	0.02 U/μL
Nuclease free water	26.5	-
cDNA	2.0	-
Total reaction volume	**50.0**	

Table 2.8: Composition of PCR master mix for cDNA amplification using phusion DNA polymerase.

Cycle	Stages	Temperature/°C	Duration	No. of cycles
Cycle 1	Initial denaturation	98°	4 m	1
Cycle 2	Denaturation	98°	10 s	35
	Annealing (gradient)	55°-72°	30 s	
	Extension	72°	5 m	
Cycle	Final extension	72°	10 m	1
	Hold	4°	Forever	-

Table 2.9: Parameters of thermal cycler for amplification of PTEN 3'UTR fragment for cloning.

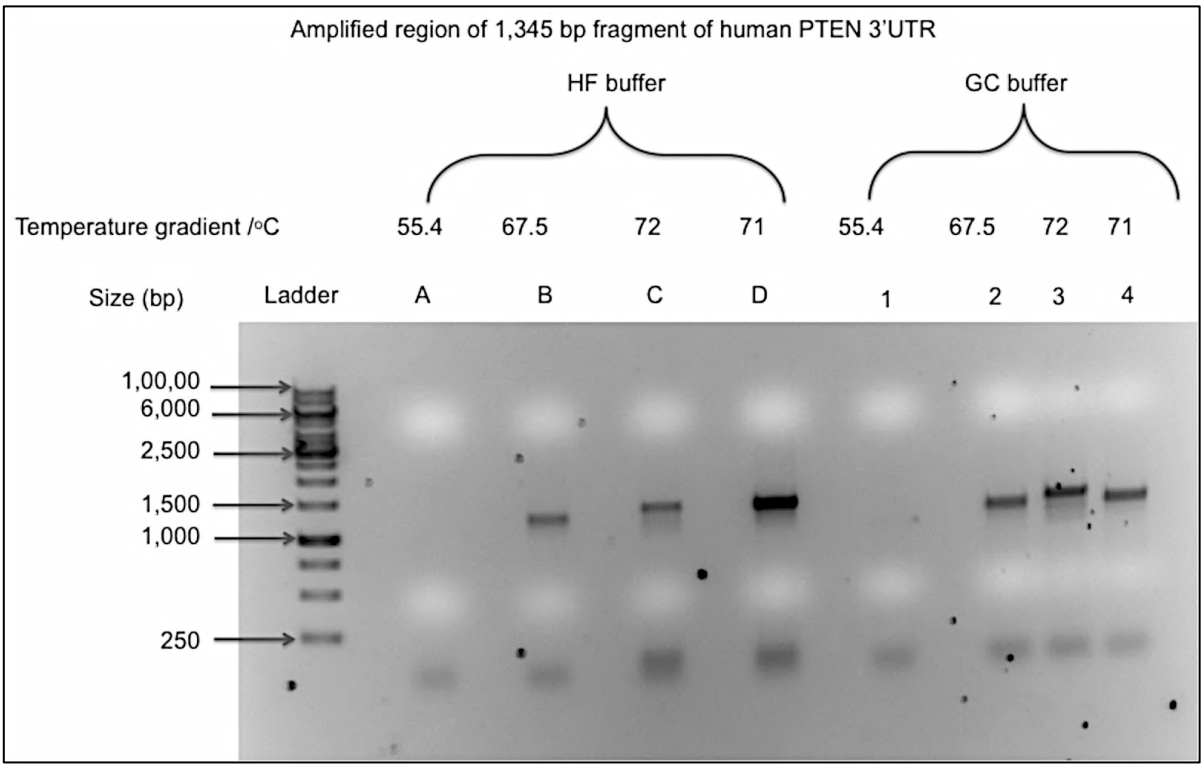

Figure 2.5: Amplified PCR product separated by DNA gel electrophoresis.

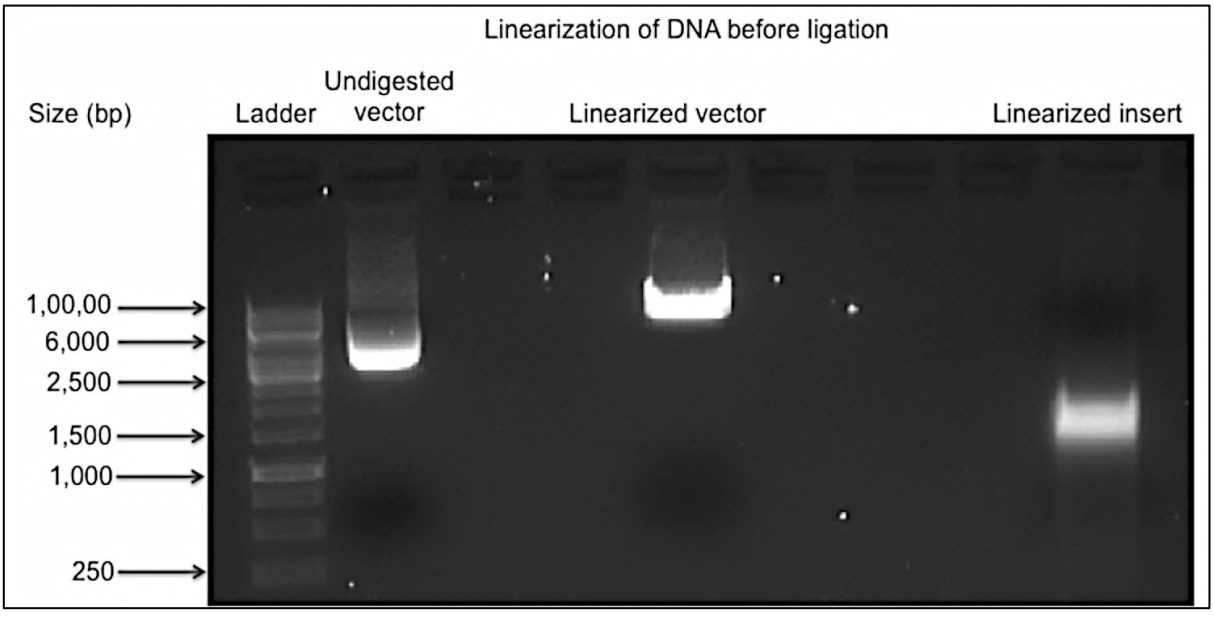

Figure 2.6: Visualization of linearized DNA after restriction digestion with specific endonucleases.

After completing the reaction, 5 μL of PCR product from each tubes were run in 1% agarose gel. Figure 2.5 illustrates the amplified product in presence of Phusion HF and GC buffers and under different annealing conditions.

Although both buffers worked equally to amplify the DNA product, however, HF buffer produced the most distinct band at an annealing temperature of 71^{o} C (sample D; figure 2.8). This sample was selected for PCR clean up for DNA purification.

2.5.2: Purification of PCR product

Isolate II PCR and Gel kit (Bioline) was used for purification of PCR product. Briefly the remains of the PCR product (45 μL) was admixed with double the volume of binding buffer CB (90 μL). The sample was then transferred onto isolate II PCR columns and centrifuged for 30 s at 11,000 X g. The flow through was discarded. About 700 μL of wash buffer CW was added to the column and it was re-centrifuged at 11,000 X g for 30 s. The flow through was discarded. The column was then dried by additional spinning at 11,000 X g for a minute to remove residual ethanol and finally the DNA was eluted in 25 μL of nuclease free water in fresh collection tube.

2.5.3: Restriction digestion of pmiR-Reporter vector and PTEN 3′UTR fragment

Before carrying out restriction digestion, 0.5 μL of the PCR cleaned up DNA was measured using a NanoDrop (ND-1000) Ultra-violet visible spectrophotometer (Thermoscientific) at wavelength 260nm/280nm and using ND-1000, version 3.7.0 software, to determine the concentration of DNA present in the sample after purification; this revealed that the purified product had 82.0 ng/μL of DNA. The amount of DNA in empty pmiR-reporter vector was also quantitated before endonuclease digestion and was 1024.5 ng/μL. Restriction digestions were carried out simultaneously using both

Spe I and Sac I endonucleases in cutSmart buffer because both these restriction enzymes demonstrated 100% catalytic activity in this buffer as instructed by the manufacturer (New England, Biolabs). Roughly equal concentrations (around 2 μg) of the PCR product and empty pmiR-reporter vector were restriction digested. The entire volume of PCR product, 24 μL, and 2 μL of pmiR-reporter vectors were separately digested using restriction endonucleases according to table 2.10 below. The restriction digestion was carried out in a thermal cycler (DNA engine, DYAD) at 37^{o} C for 1 h. After incubation, Sac I and Spe I, were heat inactivated by sequentially incubating the tubes at 65^{o}C and 80^{o}C for 20 m, respectively.

The entire volume (50 μL) of the digested product was then run in 1% agarose gel to observe linearization of vector and insert after endonuclease digestion (figure 2.6).

Ingredients	Volumes for digestion of pmiR-reporter vector	Volume for digestion of PTEN 3'UTR fragment
DNA	2 μL (≈2048 ng)	24 μL (≈1968 ng)
10X CutSmart buffer	5 μL	5 μL
Spe I	2 μL	2 μL
Sac I	1 μL	1 μL
Nuclease free water	40 μL	18 μL
Total reaction volume	50 μL	50 μL

Table 2.10: Protocol for restriction digestion

2.5.4: Gel purification of linearized DNA

After confirming linearization of DNA using image analyzer of G-box (Syngene) the DNA bands corresponding to digested product and empty vector were quickly excised under UV-light and transferred to freshly labelled and weighed collection tubes. The tubes containing gels were reweighed and the extra weight was deducted to calculate the weight of the gel containing DNA. Binding buffer CB (400 μL) was added to each

tube containing either the empty vector or the amplified product. The tubes were then incubated at 50°C for 10 m with regular vortexing every 3 m to allow complete dissolution of gel. The gel solutions were then transferred into separate isolate II gel columns (Bioline) and spun at 11,000 X g for 30 s. The flow through was discarded. The columns were then washed with 700 μL of wash buffer CW for 30 s at 11,000 X g. The membranes were then dried by centrifuging the spin columns for a minute at 11,000 X g. Finally, the DNA was eluted in 25 μL of nuclease free water in fresh collection tubes.

Quantitation of DNA by spectrophotometry revealed the purified linearized empty pmiR-reporter vector contained 57.6 ng/μL of DNA whereas the PTEN 3'UTR insert contained 24.5 ng/μL of DNA.

2.5.5: DNA ligation

Different molar ratios of vector to insert were tried: 1:2, 1:3 and 1:4 and the amount of DNA required were calculated by using the formula below:

$$\frac{\text{ng of vector} \times \text{kb size of insert}}{\text{kb size of vector}} \times \text{molar ratio of } \frac{\text{insert}}{\text{vector}} = \text{ng of insert}$$

Accordingly the following amounts of DNA were added in the ligation mixture as demonstrated in table 2.11.

After addition of all components the tubes were incubated in thermal cycler at 25° C for 1 h followed by heat inactivation of T4 ligase at 70°C for 10 m.

Ingredients	1:2	1:3	1:4
Quantity of vector (ng/μL)	50 (ng/μL) or 0.87 μL	90 (ng/μL) or 1.6μL	45 (ng/μL) or 0.8 μL
Quantity of insert (ng/μL)	20.8 (ng/μL) or 0.85 μL	56.1(ng/μL) or 2.3 μL	37.4 (ng/μL) or 1.5 μL
2X rapid ligation buffer (μL)	5.0 μL	5.0 μL	5.0 μL
T4 DNA ligase (Weiss unit)	1.0 μL (3U)	1.0 μL (3U)	1.0 μL
Nuclease free water (μL)	2.28 μL	0.1 μL	1.7 μL
Final volume (μL)	**10.0 μL**	**10.0 μL**	**10.0 μL**

Table 2.11: Protocol for DNA ligation

2.5.6: Transformation of high efficiency chemically competent NEB 5-alpha competent *E. coli*

At first the chemically competent NEB-5-alpha *E. coli* were thawed on ice for 10 m. The *E. coli* were divided equally into three separate tubes for transformation using different molar ratio of ligated DNA (table 2.11). About 5 μL of the ligated DNA product was added to 16 μL of tubes containing chemocompetent *E. coli.* The tubes were flicked gently to mix the DNA with bacteria and incubated on ice for 30 m. After ice incubation tubes were briefly heat shocked at 42^{o} C for exactly 30 s and replaced on ice for additional 5 m. Then under sterile condition about 950 μL of SOC media was added to each tubes and was incubated at 37^{o} C for 60 m with vigorous shaking (250 rpm). Amplates (Lauria Bertani or LB agar plates containing 100 μg/mL of ampicillin) were pre-warmed at 37^{o} C. The transformed chemocompetent *E. coli* were then mixed thoroughly in SOC media and diluted 1 in 10 and 1 in 100 before they were streaked onto individual amplates. The amplates were incubated at 37^{o}C for 24 h. Un-ligated, digested empty vector was used as a negative control.

2.5.7: Screening of transformed chemocompetent *E. coli* for PTEN 3'UTR insert

After 24 h, it was observed that all plates carrying different combination of ligated vector-insert ratio produced colonies whereas the negative control plate had no colonies. From them ten colonies were selected for mini-prep and PCR screening for the presence of insert.

2.5.7.1: Preparation of mini-prep

Briefly ten colonies were picked up from amplates using autoclaved toothpicks and were quickly dipped into PCR tubes containing mastermix for GoTaq DNA polymerase (section 2.5.7.2) (Promega). The toothpicks carrying the rest of the colonies were then dipped into sterile round bottomed falcon tubes containing 2 mL of media: Lauria Bertani (LB) broth and ampicillin (100 μg/mL). The tubes were then incubated at 37^{o} C overnight with vigorous shaking (300 rpm) to culture bacteria for plasmid extraction by mini-prep.

2.5.7.2: PCR screening of colonies by GoTaq DNA polymerase

Master mix containing GoTaq DNA polymerase was prepared as shown in table 2.12. *E. coli* colonies were picked using sterile toothpicks and dipped into the PCR mastermix. PCR was carried out according to the parameters in table 2.13. After PCR completion when the products were electrophoretically separated in 1% agarose gel no DNA bands were observed suggesting that either the quantity of DNA were too little for GoTaq DNA polymerase to amplify the product or there were hardly any DNA inoculated into the PCR tubes while dipping colonies from toothpicks. Therefore before doing anything further the cell cultures were allowed to grow in LB broth plus ampicillin to yield sufficient DNA for insert screening.

Ingredients	Volume (μL)	Final Concentration
5X green GoTaq reaction buffer	10	1X
dNTPs (10 mM)	1.0	200 μM
Forward primer (5 μM)	5.0	0.5 μM
Reverse primer (5 μM)	5.0	0.5 μM
GoTaq DNA polymerase (5 U/μL)	0.25	1.25 U
Nuclease free water	28.75	-
DNA	colonies	-
Total reaction volume	**50.0**	

Table 2.12: Composition of PCR master mix for cDNA amplification using GoTaq DNA polymerase.

Cycle	Stages	Temperature/^{o}C	Duration	No. of cycles
Cycle 1	Initial denaturation	95^{o}	2 m	1
Cycle 2	Denaturation	95^{o}	30 s	35
	Annealing (gradient)	71^{o}	30 s	
	Extension	72^{o}	2 m	
Cycle 3	Final extension	72^{o}	5 m	1
	Hold	4^{o}	Forever	-

Table 2.13: Parameters of thermal cycler for PCR screening of cloned PTEN 3'UTR insert in *E. coli* colonies.

2.5.8: Mini-prep plasmid extraction of E. *coli* colonies

Bacterial cultures were pelleted by centrifugation at 6,800 X g for 3 m at room temperature. The pellets were then re-suspended in buffer P1 (250 μL) and transferred into 1.5 mL sized microcentrifuge tubes. Equal volume of buffer P2 was added and mixed thoroughly until formation of clear blue solution indicating completion of alkaline lysis of bacteria. The lysates were then neutralized using buffer N3 (350 μL) until the solution becomes colourless and centrifuged at 13,000 rpm for 10 m. The high salt concentration of the buffers precipitates proteins, cellular debris and chromosomal DNA. The supernatants carrying the small plasmid DNA were collected into QIAprep spin columns and spun for 60 s at 13,000 rpm. The DNA becomes selectively adsorbed into the silica membrane of the spin columns by the high salt concentration present in the buffers. The spin columns were then successively washed first with buffer PB (500 μL) to remove endonucleases followed by buffer PE (750 μL) to remove the excess salt concentrations. The spin columns were then dried by centrifugation at 13,000 rpm for a minute to remove any residual ethanol and wash buffers. Lastly the DNAs were eluted in 30 μL of nuclease free water.

The amount of isolated plasmid DNA from bacterial colonies was then quantitated by Nanodrop spectrophotometry. It was observed that all colonies contained between 40 and 50 ng/μL of DNA.

2.5.9: Screening of colonies for PTEN 3'UTR insert by restriction digestion

Plasmid DNA (5 μL) was digested using Spe I and Sac I endonucleases in CutSmart buffer as described in table 2.10 to a final volume of 50 μL at 37^{o} C for 1 h. After heat inactivation of both Sac I and Spe I, the digested plasmids were separated by DNA gel electrophoresis as shown in figure 2.7. It was observed that all the colonies contained a partially digested vector showing a band above 6,000 bp region and a faint linearized

insert showing band slightly below 1,500 bp region in the agarose gel suggesting that the insert was cloned into the pmiR-reporter vector. Further the undigested vector produced a band near 8,000 bp region which is roughly the same size as expected of pmiR-reporter vector carrying the cloned PTEN 3'UTR insert (7,815 bp).

Thus instead of repeating PCR screening using GoTaq DNA polymerase sample 5 and sample 10 were sent for sequencing using insert specific forward and reverse primer.

2.5.10: Sequencing of PTEN 3'UTR

Sequencing was carried out at the core genome facility of University of Sheffield using automated sequencing method by 3730 DNA analyser (Applied Biosysytem), BigDye terminator v3.1 cycle sequencing kit (Applied Biosysytem) and 7900 HT real time PCR system (Applied Biosysytem). The concentration of DNA template used was 100 ng/μL. Sequencing using both PTEN 3' UTR specific forward primer and vector specific reverse primer revealed that the insert had 97% identical sequence as human PTEN 3'UTR and and pmiR reporter expression vector suggesting the insert had been correctly cloned into the 3'UTR region of pmiR-reporter vector (figure 2.8 and figure 2.9). This is because the sequenced result had few Ns near the end of the sequencing, proved to be sequencing errors by sequencing in the opposite direction. Uploading the sequenced data in Finch TV software showed that the missing nucleotides (Ns) showed peaks corresponding to the actual nucleotide base pair present in human PTEN mRNA sequence.

Sequence reverse primer of pmiR-reporter vector: 5' AGGCGATTAAGTTGGGTA 3'

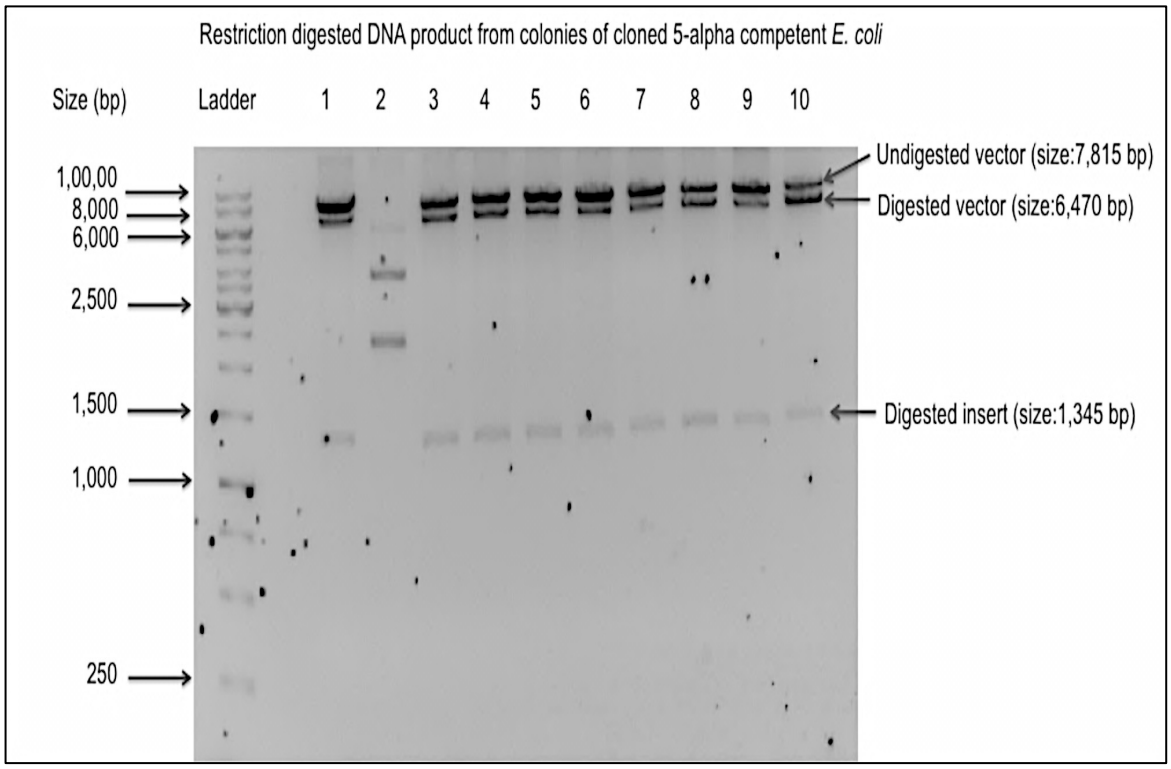

Figure 2.7: DNA gel image of restriction digested cloned PTEN 3'UTR insert in pmiR-reporter vector. The cloned product was digested with restriction endonucleases Spe I and Sac I for 1 h at 37^{o} C in thermal cycler and run in 1% agarose gel to validate insertion of PTEN 3'UTR fragment into pmiR-reporter vector.

```
pMIR-report
Sequence ID: lcl|1097Length: 6470Number of Matches: 1
Related Information
<pre> <@aln_gene_info@> </pre>
Range 1: 1981 to 2867Graphics
Next Match
Previous Match
Alignment statistics for match #1
Score  Expect Identities   Gaps   Strand
1517 bits(821)   0.0 855/887(96%) 1/887(0%) Plus/Minus
Query  14    CGACTCNCTATAGGgagagagagagaATTACCCTCACTAAAGGGAGGAGAAGCATGAATT  73
             |||||| ||||||||||||||||||||||||||||||||||||||||||||||||||||
Sbjct  2867  CGACTCACTATAGGGAGAGAGAGAGAATTACCCTCACTAAAGGGAGGAGAAGCATGAATT  2808

Query  74    CAAGGTACCAGATCTTAGTTATTAATAGTAATCAATTACGGGGTCATTAGTTCATAGCCC  133
             ||||||||||||||||||||||||||||||||||||||||||||||||||||||||||||
Sbjct  2807  CAAGGTACCAGATCTTAGTTATTAATAGTAATCAATTACGGGGTCATTAGTTCATAGCCC  2748

Query  134   ATATATGGAGTTCCGCGTTACATAACTTACGGTAAATGGCCCGCCTGGCTGACCGCCCAA  193
             ||||||||||||||||||||||||||||||||||||||||||||||||||||||||||||
Sbjct  2747  ATATATGGAGTTCCGCGTTACATAACTTACGGTAAATGGCCCGCCTGGCTGACCGCCCAA  2688

Query  194   CGACCCCCGCCCATTGACGTCAATAATGACGTATGTTCCCATAGTAACGCCAATAGGGAC  253
             ||||||||||||||||||||||||||||||||||||||||||||||||||||||||||||
Sbjct  2687  CGACCCCCGCCCATTGACGTCAATAATGACGTATGTTCCCATAGTAACGCCAATAGGGAC  2628

Query  254   TTTCCATTGACGTCAATGGGTGGAGTATTTACGGTAAACTGCCCACTTGGCAGTACATCA  313
             ||||||||||||||||||||||||||||||||||||||||||||||||||||||||||||
Sbjct  2627  TTTCCATTGACGTCAATGGGTGGAGTATTTACGGTAAACTGCCCACTTGGCAGTACATCA  2568

Query  314   AGTGTATCATATGCCAAGTACGCCCCCTATTGACGTCAATGACGGTAAATGGCCCGCCTG  373
             ||||||||||||||||||||||||||||||||||||||||||||||||||||||||||||
Sbjct  2567  AGTGTATCATATGCCAAGTACGCCCCCTATTGACGTCAATGACGGTAAATGGCCCGCCTG  2508

Query  374   GCATTATGCCCAGTACATGACCTTATGGGACTTTCCTACTTGGCAGTACATCTACGTATT  433
             ||||||||||||||||||||||||||||||||||||||||||||||||||||||||||||
Sbjct  2507  GCATTATGCCCAGTACATGACCTTATGGGACTTTCCTACTTGGCAGTACATCTACGTATT  2448

Query  434   AGTCATCGCTATTACCATGGTGATGCGGTTTTGGCAGTACATCAATGGGCGTGGATAGCG  493
             ||||||||||||||||||||||||||||||||||||||||||||||||||||||||||||
Sbjct  2447  AGTCATCGCTATTACCATGGTGATGCGGTTTTGGCAGTACATCAATGGGCGTGGATAGCG  2388

Query  494   GTTTGACTCACGGGGATTTCCAAGTCTCCACCCCATTGACGTCAATGGGAGTTTGTTTTG  553
             ||||||||||||||||||||||||||||||||||||||||||||||||||||||||||||
Sbjct  2387  GTTTGACTCACGGGGATTTCCAAGTCTCCACCCCATTGACGTCAATGGGAGTTTGTTTTG  2328

Query  554   GCACCAAAATCAACGGGACTTTCCAAAATGTCGTAACAACTCCGCCCCATTGACGCAAAT  613
             ||||||||||||||||||||||||||||||||||||||||||||||||||||||||||||
Sbjct  2327  GCACCAAAATCAACGGGACTTTCCAAAATGTCGTAACAACTCCGCCCCATTGACGCAAAT  2268

Query  614   GGGCGGTAGGCGTGTACGGTGGGAGGTCTATATAAGCAGAGCTGGNTTAGTGAACCGTGG  673
             |||||||||||||||||||||||||||||||||||||||||||||| ||||||||||||||
Sbjct  2267  GGGCGGTAGGCGTGTACGGTGGGAGGTCTATATAAGCAGAGCTGGTTTAGTGAACCGTGG  2208

Query  674   ATCCACCATGGAANACGCCAAAAACATAAAGAAAGGCCCGGCGCCATTCTATCCTCTANA  733
             |||||||||||||| |||||||||||||||||||||||||||||||||||||||||||| |
Sbjct  2207  ATCCACCATGGAAGACGCCAAAAACATAAAGAAAGGCCCGGCGCCATTCTATCCTCTAGA  2148

Query  734   GGANGGAACCGCTGGANAGCAACTGCATANNGNTATGAANAGATACNCCCTNNNTCCNGG  793
             ||| |||||||||||| ||||||||||   | |||||| |||||| ||||    ||| ||
Sbjct  2147  GGATGGAACCGCTGGAGAGCAACTGCATAAGGCTATGAAGAGATACGCCCTGGTTCCTGG  2088

Query  794   NACNATTGCTTTTACAGATGCACATATCGAGGTGAANATCACGTACGCNNAATACTTCNA  853
              || ||||||||||||||||||||||||||||||| ||||||||||  |||||||| |
Sbjct  2087  AACAATTGCTTTTACAGATGCACATATCGAGGTGAACATCACGTACGCGGAATACTTCGA  2028

Query  854   AATGNCCGTTCGGNNGGNNNAANCTATNANN-GATATGGGCtgaata  899
             |||| ||||||||   ||    || |||| |    ||||||||||||||
Sbjct  2027  AATGTCCGTTCGGTTGGCAGAAGCTATGAAACGATATGGGCTGAATA  1981
```

Figure 2.8: Sequence alignment using pmiR-reporter specific reverse primer with pmiR-Reporter vector.

Homo sapiens phosphatase and tensin homolog (PTEN), mRNA
Sequence ID: ref|NM_000314.4|**Length:** 5572**Number of Matches:** 1
Related Information
Gene-associated gene details
UniGene-clustered expressed sequence tags
GEO Profiles-microarray expression data
Map Viewer-aligned genomic context
<pre> <@aln_gene_info@> </pre>
Range 1: 4720 to 5450 GenBankGraphics
Next Match
Previous Match
Alignment statistics for match #1

Score	**Expect**	**Identities**	**Gaps**	**Strand**
1271 bits(688)	0.0	711/731(97%)	1/731(0%)	Plus/Minus

```
Query  158   GGGATGAGGCATTATCCTGTACACATCATATTGGTATTTTTGTGTATCCTCAGTGCATAG  217
              ||||||||||||||||||||||||||||||||||||||||||||||||||||||||||||
Sbjct  5450  GGGATGAGGCATTATCCTGTACACATCATATTGGTATTTTTGTGTATCCTCAGTGCATAG  5391

Query  218   CATTTACACACAGAGCCACTGCTGCACAGCACAAGAGTATCTGAAGAGGCTGAATCAGAG  277
              ||||||||||||||||||||||||||||||||||||||||||||||||||||||||||||
Sbjct  5390  CATTTACACACAGAGCCACTGCTGCACAGCACAAGAGTATCTGAAGAGGCTGAATCAGAG  5331

Query  278   TAAGGCTGTTTAACAGACTGAAATTTTTTAGTATATATATTCTATATGAAAACAGGTTGA  337
              ||||||||||||||||||||||||||||||||||||||||||||||||||||||||||||
Sbjct  5330  TAAGGCTGTTTAACAGACTGAAATTTTTTAGTATATATATTCTATATGAAAACAGGTTGA  5271

Query  338   ACTTTTGAACTGGCAGGTAGAAGGCAACTCTGCCAAATACTACAGTTAAAGCCCCCACTT  397
              ||||||||||||||||||||||||||||||||||||||||||||||||||||||||||||
Sbjct  5270  ACTTTTGAACTGGCAGGTAGAAGGCAACTCTGCCAAATACTACAGTTAAAGCCCCCACTT  5211

Query  398   TAGTGCACAGTTCCACCCCTTCCATCTGCATGCATGACACATTAACAGTATTTAAAGGTA  457
              ||||||||||||||||||||||||||||||||||||||||||||||||||||||||||||
Sbjct  5210  TAGTGCACAGTTCCACCCCTTCCATCTGCATGCATGACACATTAACAGTATTTAAAGGTA  5151

Query  458   AACGAGGCACTTTGTGGCAACCACAGCCATCGTTATGAACATATTGCACAAAATTTCTAG  517
              ||||||||||||||||||||||||||||||||||||||||||||||||||||||||||||
Sbjct  5150  AACGAGGCACTTTGTGGCAACCACAGCCATCGTTATGAACATATTGCACAAAATTTCTAG  5091

Query  518   AACTAAACATTAAACTTGTACCCTACTTTTATTTTTTAAAGCTGAAACATTTGATGCTGC  577
              ||||||||||||||||||||||||||||||||||||||||||||||||||||||||||||
Sbjct  5090  AACTAAACATTAAACTTGTACCCTACTTTTATTTTTTAAAGCTGAAACATTTGATGCTGC  5031

Query  578   CGGTAAACTCCACTTAAGTTTATAACCTGTGCCACAGCAAAGAATGGTGATGCTATTTAT  637
              ||||||||||||||||||||||||||||||||||||||||||||||||||||||||||||
Sbjct  5030  CGGTAAACTCCACTTAAGTTTATAACCTGTGCCACAGCAAAGAATGGTGATGCTATTTAT  4971

Query  638   TCAACTACCCTTTTAAAAGTATGGCAAACATGTTCAAGANGAGCTACAAAGGACTTGGGA  697
              |||||||||||||||||||||||||||||||||||| ||||||||||||||||||||||
Sbjct  4970  TCAACTACCCTTTTAAAAGTATGGCAAACATGTTCAAGAGGAGCTACAAAGGACTTGGGA  4911

Query  698   TGGTACAGGGCCCAACTGTAAGCTTTCTTAAAAGTGNNGCCTTCAAGTAACTTCANACAT  757
              |||||||||||||||||||||||||||||||||||  |||||||||||||||||| ||||
Sbjct  4910  TGGTACAGGGCCCAACTGTAAGCTTTCTTAAAAGTGATGCCTTCAAGTAACTTCAGACAT  4851

Query  758   GTAAGCTGCTGCACATCCNAAAAGTCTAAGAAAATATTCCNNANN-TCANANATTACCTA  816
              |||||||||||||||||| ||||||||||||||||||||  |   ||| | ||||||||
Sbjct  4850  GTAAGCTGCTGCACATCCAAAAAGTCTAAGAAAATATTCCAGAAACTCAGAGATTACCTA  4791

Query  817   CAGAATGCATTTCNGNNTAANTATGAATACTGCCATAAATAAAGTTTTAATTNGNACTTG  876
              |||||||||||||  |  ||| ||||||||||||||||||||||||||||| | ||| |
Sbjct  4790  CAGAATGCATTTCAGGCTAATTATGAATACTGCCATAAATAAAGTTTTAATTAGGACTCG  4731

Query  877   aaaanctttca  887
              |||| ||||||
Sbjct  4730  AAAACCTTTCA  4720
```

Figure 2.9: Sequence alignment using PTEN 3'UTR specific forward primer with human 3' UTR of PTEN mRNA.

2.5.11: Transformation of *E. coli* with pmiR-Reporter vector carrying sequenced PTEN 3'UTR insert

The protocol in section 2.5.6 was followed to freshly transform chemically competent NEB 5-alpha competent *E. coli* with pmiR-reporter expression vector carrying sequenced PTEN 3'UTR insert.

Amplates were streaked with bacterial suspension in SOC media and incubated at 37^{o} C for 24 h.

A single colony was selected from the amplate using sterile toothpick and inoculated into 3 mL of freshly prepared LB broth plus ampicillin (100 μg/mL) in sterile round-bottomed falcon tubes. The falcons were then incubated with vigorous shaking at 37 ^{o} C for 8 h.

After 8 h, the falcons were checked for turbidity ensuing from bacterial growth. Then about 1.5 mL of the bacterial culture broth was pipetted into 200 mL of LB broth plus ampicillin (100 μg/mL) in Erlenmeyer flask and incubated at 37^{o} C with vigorous shaking (250 rpm) for 16 h to 18 h.

These cultures were used to harvest *E. coli* pellets by spinning at 6,000 X g for 15 m at 4^{o} C for plasmid extraction using maxi-prep kit (Qiagen).

2.5.12: Plasmid purification of pmiR-reporter carrying PTEN 3'UTR insert by maxi-prep

Similar to mini-prep extraction, alkaline lysis of bacterial pellets were carried out by re-suspending the pellet in equal volumes (10 mL) of buffer P1 and P2 and incubation at room temperature for 5 m. Precipitation of cellular debris, genomic DNA and protein were encouraged by addition of neutralizing buffer P3 (10 mL). The precipitates were then removed by centrifugation at 20,000 X g for 30 m at 4^{o} C. The supernatants were

collected and re-centrifuged for an additional 15 m to completely clear it of any particulate materials. Qiagen-tip 500 was equilibrated using buffer QBT (10 mL) and the supernatants were added to it and allowed to clear through the resin under gravity. The Qiagen-tips were then washed twice with buffer QC (10 mL) to remove any contaminant or residual carbohydrates. The DNA was then eluted in buffer QF. DNA was precipitated by addition of 0.7 volumes of iso-propanol and centrifuged at 15,000 X g for 30 m at 4^{o} C. The supernatant was carefully decanted. The DNA precipitate was re-washed with 70% ethanol (5 mL) and spun at 15,000 X g for 10 m. The supernatant was discarded and the DNA pellets were air dried for 15 m. The pellets were then dissolved in nuclease free water (400 μL) at 4^{o} C overnight.

Plasmid DNA was quantitated using ND-1000 spectrophotometer. The purified plasmids were now ready for transfection.

2.6: DNA gel electrophoresis

1% agarose gel was prepared by dissolving 200 mg of agarose powder (Sigma) in 200 ml of distilled deionized (dd) water and warming in microwave. To the agarose gel solution 7 μL of DNA binding dye, ethidium bromide (25.4 mM; Sigma) was added in fume hood to a final concentration of 1.8 μM. The gel was then poured into the DNA gel cassette, comb inserted and allowed to cool down and solidify. Gene Ruler 1 Kb DNA ladder was used to determine DNA band size.

2.7: Transfection of primary human oral fibroblasts

2.7.1: Transient transfection of oral fibroblasts using human pre-miR miRNA precursors

Transfections were performed in either 6-well plates or T25 flasks. Commercially available double stranded synthetic human pre-miR miRNA precursors were used (Ambion, Life technology): miR-335 (PM10063) and miR-148b (PM10264), to study the functional effects of individual miRNAs in human oral fibroblasts (figure 2.10). These are precursor miRNAs, which are distinct from hairpin RNAs and comprises short miRNA duplexes carrying the mature miRNA and anti-sense strand.

The pre-miR miRNA precursors were initially diluted in nuclease free water (100 μL) to prepare 50 μM stocks. During transfection the concentration of pre-miRs were further diluted to a final concentration of 50 nM. The cationic lipid agent Oligofectamine (Life technology) was used to introduce pre-miR precursors into human primary oral fibroblasts. The positively charged Oligofectamine forms complexes with the negatively charged phosphate backbone of the oligonucleotides and facilitate its uptake by endocytosis into cells (Chesnoy and Huang, 2000, figure 2.10). Within cytoplasm the synthetic pre-miR precursors then separate into mature miRNA strands and directly incorporate into the miRNA induced silencing complex (miRISC) and repress target genes (figure 2.10). Negative control pre-miRs bearing random sequences (pre-miR-negative control 2; Life technology) that do not mimic the functional effects of known human miRNAs in human cells and tissues were used as controls for the experiment and in determination of transfection efficiency.

Before transfection human primary oral fibroblasts (between passage 4 and 6) were seeded down at a density of 5,00,000 in T25 flasks in normal growth media and incubated overnight. The flasks were examined under the microscope the following day to ensure that cells were nearly 70% to 80% confluent prior to transfection.

For a T25 flask the final volume of transfection mixture used was 2 mL. Transfection mixtures were prepared as shown in table 2.14.

Briefly, human pre-miR miRNA precursors and Oligofectamine were diluted in reduced serum medium Opti-MEM (Gibco) according to table 2.14. The diluted miRNA precursors and Oligofectamine were then mixed and incubated at room temperature for 25 m to allow formation of lipid-oligonucleotide complexes (Chesnoy and Huang, 2000).

Dilution of pre-miR miRNA precursors		Dilution of Oligofectamine	
Ingredients	Volume (μL)	Ingredients	Volume (μL)
Pre-miR miRNA precursor (50 μM) or pre-miR negative control 2 (50μM)	2	Oligofectamine	20
Opti-MEM	98	Opti-MEM	80
Total volume	100	Total volume	100

Table 2.14: Composition of the transfection mixture for T25 flask.

Following incubation the transfection cocktails were re-diluted in equal volume of Opti-MEM (200 μL) such that the final volume reached 400 μL.

Before addition of the transfection cocktail, the fibroblasts were washed twice with 1X PBS and subsequently 600 μL of Opti-MEM (Gibco) was added to each flask. Then 400 μL of the transfection cocktail was added to each flask reaching a volume of 1 mL. The flasks were incubated for 4 h at 37^{o} C and 5% CO_2. After 4 h, 1 mL of DMEM supplemented with 20% FCS was added to each flask. Transfection was carried out for 24 h. After 24 h, the transfection mixture containing media were replaced with normal growth media.

Conditioned media from transfected oral fibroblasts was prepared after 24 h post-transfection. After decanting the transfection mixture rich media the transfected fibroblasts were washed twice with 1X PBS and serum free medium was added to each

flask for 24 h. The media were collected, filter sterilized and used directly to carry out functional assays.

Cells were harvested at 72 h post-transfection for RNA extraction, miRNA and gene expression assays and western blot.

For transfection in 6-well plates both the seeding density and the volumes were scaled down to half of the volume used in T25 flasks.

2.7.2: Transient knockdown of PTEN in human oral fibroblasts using RNA interference approach

Short interfering RNA (siRNA) against exon 5 of human *PTEN* gene was used to transiently knock down *PTEN* in human primary oral fibroblasts. Silencer Cy3 labelled negative control 1 siRNA (Life technology, AM4621) was used as the negative control. The PTEN siRNA duplexes (Life technology, AM51331) dissociate into sense and anti-sense strands when introduced into cells, incorporate into the RNA induced silencing complex and the anti-sense strand then recognizes complementary bases on mRNA to inhibit protein translation (Elbashir *et al*., 2001, figure 2.10). The Cy3 labelling at the 5' terminal of the sense strand of the negative control allows visualization and localization of the siRNAs in fibroblasts.

Transfection was carried out in either T25 flasks or 6-well plates. At first both PTEN and silencer Cy3 labelled negative control siRNAs were reconstituted in nuclease free water to prepare 50 μM stocks, aliquoted and stored at -20^{o} C. The negative control siRNAs were stored in dark as they are light sensitive.

In T25 flasks, oral fibroblasts were seeded down at a density of 500,000 and incubated in normal growth medium overnight. SiRNAs were diluted in reduced serum containing media Opti-MEM (Gibco) to a final concentration of 50 nM. Diluted siRNAs were then

Dilution of siRNAs		Dilution of Oligofectamine	
Ingredients	Volume (μL)	Ingredients	Volume (μL)
PTEN siRNA or silencer Cy3 labelled negative control 1 siRNA	2	Oligofectamine	20
Opti-MEM	98	Opti-MEM	80
Total volume	100	Total volume	100

Table 2.15: Composition of transfection mixture to knock down PTEN gene in fibroblasts

mixed with diluted Oligofectamine and incubated at room temperature for 25 m to allow formation of Oligofecatmine-siRNA complex (table 2.15). After 25 m, the transfection cocktail was further diluted in equal volume of Opti-MEM (200 μL) to a final volume of 400 μL. T25 flasks containing 70% to 80% confluent fibroblasts were washed twice with 1X PBS and fed with 600 μL of Opti-MEM. About 400 μL of the transfection mixture was added to each flask containing either the PTEN siRNA or the negative control siRNA. The flasks were then incubated at 37^{o} C for 4 h. After incubation time to each flask 1 mL of DMEM supplemented with 20% FCS was added.

Transfections were carried out for 24 h. After 24 h, the transfection mixtures were decanted and fresh serum free media were added to prepare conditioned media for functional studies. Conditioned media were prepared over 24 h, collected, filter sterilized and directly used to carry out either migration assay or ELISA. Serum was restored into each flask after preparation of conditioned media by addition of normal growth media. The cells were harvested at 72 h for RNA isolation and protein assay. Both the cell seeding density and the volumes of transfection mixtures were halved when carrying out transfections in 6-well plates.

.

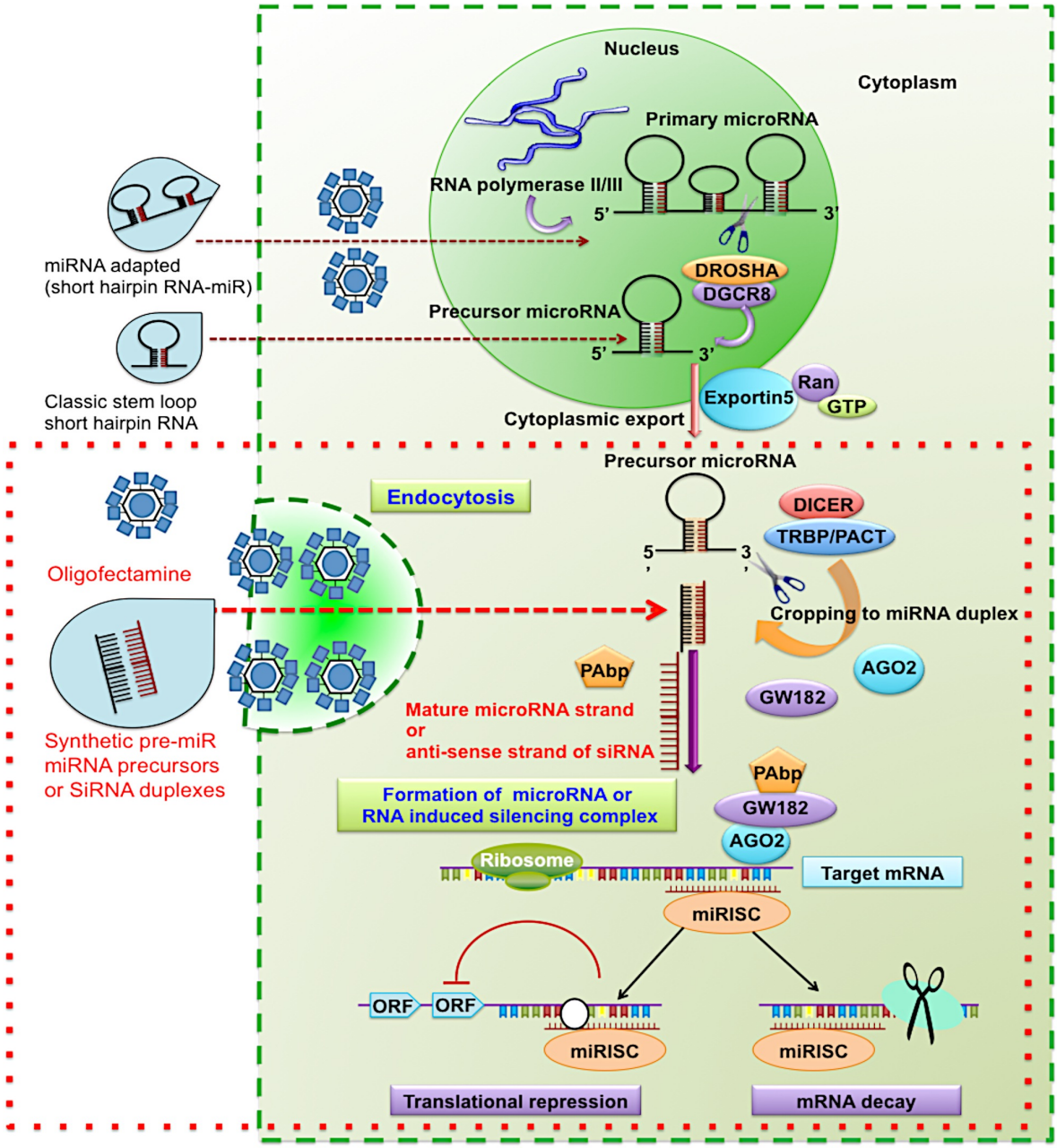

Figure 2.10: Mechanism of action of Oligofectamine, pre-miR miRNA precursors and short interfering RNAs in transfected oral fibroblasts. The green dotted box represents cell boundary. The red dotted box highlights the difference between synthetic pre-miRs and naturally occurring hairpin precursor miRNAs. The synthetic premiRs are miRNA duplexes introduced into the cells by cationic lipid reagent (Oligofectamine) by endocytosis.

2.7.3: Cell transfection for reporter assay

2.7.3.A: NFκB reporter assay

NFκB reporter activity was measured in both aged and miRNA transfected oral fibroblasts. To investigate NFκB activity in aged fibroblasts: presenescent, quiescent, H_2O_2-induced premature senescent and late-passage oral fibroblasts were seeded at 100,000 per well of 12-well plates and incubated overnight in normal culture media at 37^oC and 20% O_2 saturation. Oral fibroblasts were made quiescent by prolonged serum starvation for 72 h. These fibroblasts were seeded down 72 h prior to other conditioned fibroblasts such that all cells were ready to carry out experiments simultaneously. For 12-well plates, transfection cocktail was prepared by diluting 1 μg of plasmid DNA in 100 μL of Opti-MEM. The plasmids comprised of pGL4.32 (Promega) vector carrying NFκB response element driven firefly luciferase and pRL-TK (Promega) control vector carrying Renilla luciferase mixed in a ratio of 12:1, to avoid trans effects between promoter elements of experimental and control reporter vectors that can affect the expression of reporter gene (Farr and Roman, 1992, figure 2.11). Transfection was carried out using FuGENE HD reagent (Promega). To correct for transfection efficiency 3 μL of FuGENE HD was added to 1 μg of vector DNA in a ratio of 3:1. The transfection cocktail was then incubated at room temperature for 15 m to allow formation of lipid-DNA complex.

Before addition of the transfection cocktail the fibroblasts: young, quiescent and aged, were washed twice with 1X PBS and 900 μL of Opti-MEM was added to each well. To this 103 μL of the lipid-vector complex mixture was added. The fibroblasts were allowed to transfect for 48 h at 37^oC.

To determine NFκB activity in miRNA transfected oral fibroblasts, in addition to pGL4.32 vector and pTK-RL, the fibroblasts were also co-transfected with human pre-miR miRNA precursors to a final concentration of 50 nM. Table 2.16 summarizes the compositions of the transfection cocktail for measuring NFκB activity in miRNA over-expressing fibroblasts.

After preparation of the transfection cocktail (table 2.16), it was incubated at room temperature for 15 m to allow complex formation. During this time the fibroblasts were washed twice with 1X PBS and 396 μL of Opti-MEM was added to each well. Then 104 μL of transfection mixture was added to each well. The cells were incubated in serum-deprived state for 4 h at 37^{o}C. After 4 h, 500 μL of DMEM containing 20% FCS was added to each well such that the final volume was 1 mL. Transfection was carried out for 48 h.

Ingredients	Amount	Final amount
pGL4.32 carrying NFκB response element	916.7 ng	1000 ng
pTK-RL	83.3 ng	
Pre-miR-335 (50 μM)or Pre-miR-148b (50 μM) or Pre-miR-negative control 2 (50 μM).	1.0 μL	50 nM
FuGENE HD	3.0 μL	-
Opti-MEM	100.0 μL	-
Total volume of transfection cocktail		104.0 μL

Table 2.16: Composition of the transfection mixture to measure NFκB activity in miRNA transfected oral fibroblasts.

Luciferase activity was measured using Dual Luciferase Reporter Assay system (Promega). Briefly once transfection was completed, the media was removed and the transfected cells were washed with 1X PBS and lysed with 1X passive lysis buffer; 250 μL per well (Promega) for 30 m at room temperature. The luminometer (Glomax 96 microplate luminometer, Promega) was set up such that injector 1 and 2 could

sequentially dispense 100 μL of LAR II and Stop & Glo (Promega) into each well of 96-well microplate. 20 μL of cell lysate was then transferred into each well of a white 96-well microplate in triplicate. Luciferase activity was measured using Glomax 96 microplate luminometer (Promega).

Transcriptional activity was measured as the relative activity between NFκB driven synthetically derived firefly luciferase to Renilla luciferase. Fold induction was calculated from the ratio of average luminescence between senescent and presenescent control cells. The data were normalized to cell density.

2.7.3.B: pmiR-Reporter assay

Briefly 1,345 bp of the 3'UTR of human *PTEN* was cloned into the multiple cloning sites (MCS) of 3'UTR region of firefly luciferase in pmiR-Reporter vector, between restriction sites Spe I and Sac I (figure 2.12). pSV-β-galactosidase control vector was used as the control to normalize luminescence of firefly luciferase and monitor transfection efficiency. Huh-7 cells, derived from hepatocellular carcinoma, were used for reporter assays as they are well characterised for this purpose in the laboratory.

Huh-7 cell lines were seeded at a density of 100,000 per well of 12-well plates and incubated overnight at 37^{o}C and 20% O_2 saturation in DMEM plus 10% FCS and 2 mM L-glutamine.

The following day the cells were co-transfected with pmiR-reporter vector carrying 3'UTR of PTEN (1 μg), pSV-β-galactosidase control vector (0.6 μg) and either individual miRNA mimics of miR-335, or miR-148b, or both, or negative control miRNA precursors (50 μM) using FuGene HD reagent. The composition of the transfection cocktail is summarized in table 2.17.

Briefly the DNA and the pre-miRNA precursors were diluted in 100 μL of Opti-MEM. Since the total concentration of DNA reached 1.6 μg (pmiR report + pSV-β-galactosidase), 4.8 μL of FuGene HD were added to the diluted DNA to maintain the ratio of 1:3 of DNA to transfection reagent. The transfection cocktails were incubated at room temperature for 15 m to allow formation of lipid-DNA or lipid:pre-miR complex.

After 15 m, Huh-7 cells were washed twice with 1X PBS and 394.2 μL of Opti-MEM was added to each well. Subsequently transfection cocktails (105.8 μL) were added to each well and the flasks were incubated at 37° C for 4 h. After 4 h, about 500 μL of DMEM supplemented with 20% FCS and 2 mM L-glutamine were added to each well. The transfection was carried out for 48 h.

Ingredients	Amount	Final amount
pmiR-Reporter carrying 3'UTR of *PTEN*	1000 ng	1600 ng
pSV-β-galactosidase control vector	600 ng	
Pre-miR-335 (50 μM) or Pre-miR-148b (50 μM) or Pre-miR-negative control 2 (50 μM).	1.0 μL	50 nM
FuGENE HD	4.8 μL	-
Opti-MEM	100.0 μL	-
Total volume of transfection cocktail		105.8 μL

Table 2.17: Composition of the transfection mixture to measure luciferase activity of pmiR-Reporter in miRNA transfected Huh-7 cells.

After transfection the cells were washed twice in 1X PBS. The transfected cells were then scraped and lysed in 250 μL of 1X reporter lysis buffer per well. The cell lysates were then collected and microcentrifuged for 2 m at 4000 rpm at 4° C. The supernatants were collected in fresh eppendorfs.

Assay buffer (2X) was made up by combining 200 mM sodium phosphate buffer at pH 7.3 (1 M Na_2HPO_4, 38.7 mL plus 1 M NaH_2PO_4, 11.3 mL) with 2 mM magnesium chloride, 100 mM β-mercaptoethanol and 1.33 mg/mL of ONPG (o-nitrophenyl-β-D-

galactopyranoside). Transfected Huh-7 cells over-expressing β-galactosidase should hydrolyse the colourless ONPG into a yellow product of o-nitrophenol and its absorbance can be recorded by spectrophotometry.

Firstly, luciferase activity was recorded. Supernatants (20 μL) were pipetted into each well of a white 96-well plate in triplicate. To this 150 μL of luciferase assay substance were added. The Glomax 96 microplate luminometer (Promega) were used to determine luciferase activity in transfected HuH-7 lysates.

To measure β-galactosidase activity, 30 μL lysates were pipetted into each well of a transparent 96-well plate. To this 50 μL of assay 2X buffer was added and the plate was incubated for 45 minutes at 37^{o} C until the solution turns pale yellow. The reaction is stopped by addition of 1 M sodium bicarbonate, 150 μL per well. Absorbance was recorded at 420 nM with spectrophotometer.

Luciferase activity was normalized for transfection efficiency to β-galactosidase activity.

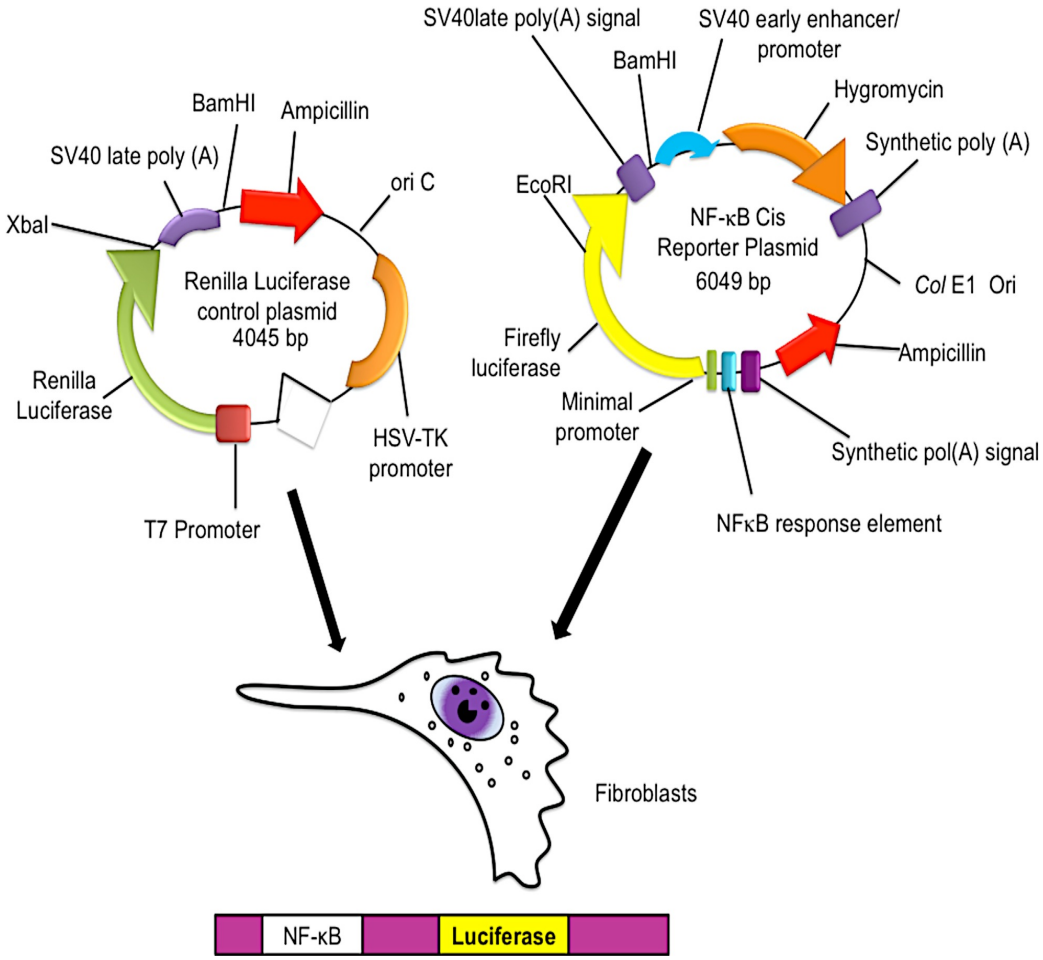

Figure 2.11: Schematic representation of NFκB reporter plasmid and pTK-RL control vector. The pRL-TK vector has herpes simplex virus thymidine kinase (HSV-TK) promoter driven Renilla luciferase acitivity whereas PGL4.32 [*luc2P*-NFκB-Hygro] vector has NFκB response element mediated firefly luciferase activity. Both the vectors have ampicillin as the bacterial selectable marker. The origin of replication is derived from E. coli in pTK-RL and from ColE1 for pGL4.32 vector.

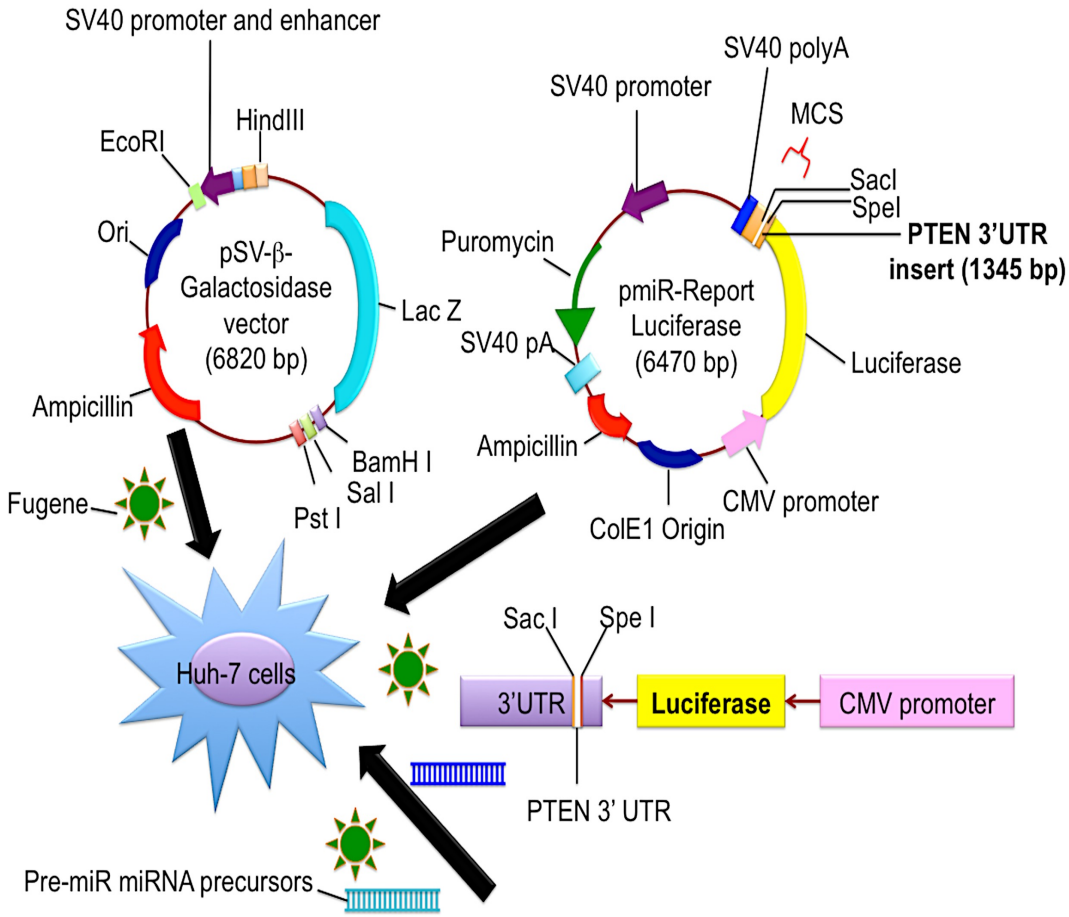

Figure 2.12: Schematic representation of determination of pmiR-Reporter activity to β-galactosidase control miRNA transfected Huh-7 cell lines. The pmiR-Reporter vector has CMV promoter driven firefly luciferase activity and bears multiple cloning sites at the 3'UTR of *luc2P* region for insertion of miRNA targeted genes. The pSV-β-galactosidase control vector shows SV40 early promoter and enhancer driven transcription of *lacZ* gene. Both vectors have ampicillin as the bacterial selection marker.

2.8: Cell harvest

Before harvesting adherent cells the culture media was decanted. The cells were washed twice with PBS and were detached in 1X trypsin and EDTA (Sigma) by incubation at 37^{o} C for 3-5 m. Trypsin was neutralized by double the volume of serum enriched media. The cell suspensions were collected into sterile falcon tubes, centrifuged at 1000 X g for 5 m and the supernatant discarded. The pellets were then washed once with 1X PBS and re-pelleted by centrifugation. The pellets were then directly used for RNA extraction or protein assay or stored at -80^{o} C for future use.

2.9: RNA extraction

Total RNA was extracted using mirVana miRNA isolation kit (Ambion) using manufacturer's protocol. Briefly, the cell pellets were denatured in chaotropic lysis buffer comprising guanidine thiocyanate and β-mercaptoehtanol and allowed to homogenise. The samples were then subjected to acid-phenol: chloroform (APC) solution (pH=4.5). The acidic pH assists in precipitation of proteins and neutralization of negative charges of DNA and simultaneously dissolves carbohydrates and lipids. The APC-nucleic acid mixtures were then centrifuged at 13,000 rpm for 5 m until the mixture separated into an upper RNA rich aqueous phase and lower viscous organic phase rich in DNA, protein and lipid. The aqueous phase was isolated into fresh nuclease free microcentrifuge tubes and mixed with 100% ethanol to precipitate RNA. The RNA was then immobilized on glass fibre filters present within spin column and washed thoroughly to remove salt contaminants. RNA was eluted in nuclease free water preheated to 95^{o}C. The concentration of RNA was measured by NanoDrop (ND-1000) spectrophotometer. RNA integrity was verified using bioanalyzer (Agilent technology, Appendix 11).

2.10: Reverse transcription

cDNA was synthesized by reverse transcription using 500 ng of total RNA template according to protocol in table 2.18. The reaction mixtures were then incubated in the thermal cycler (DNA Engine, DYAD) at 25^{o} C for 10 m, 37^{o}C for 2 h, 85^{o}C for 5 m and 4^{o}C forever.

2.11: Quantitative real time polymerase chain reaction (qRT-PCR)

Expression of specific transcripts was determined by amplifying the cDNA using specific SYBR Green forward and reverse primers listed in table 2.19. Small nucleolar RNA U6 (TaqMan probe) was used as the internal control. qRT-PCR was carried out by adding cDNA (0.5μL) to qRT-PCR master mix containing either 1X SYBR Green

Ingredients	Volume per reaction
10X reverse transcription buffer	2.0 μL
Multiscribe reverse transcriptase (50U/μL)	1.0 μL
25X dNTPs (100 mM)	0.8 μL
10X Random primers	2.0 μL
Nuclease free water	4.20 μL
RNA template	500 ng in 10.0 μL volume
Total volume	20 μL

Table 2.18: Protocol for reverse transcription (Applied Biosystem)

mixture (Applied Biosystem) with 0.50 μM gene specific primers or 1X TaqMan universal PCR master mix II with 1X TaqMan real time probes/primers listed in table 2.19. Assays were performed in triplicate in a 7900 HT Fast real time PCR machine (Applied Biosystems). SDS version 2.4 was used to program the real time device (95^{o}C for 15 s, 60^{o}C for 60 s and 95^{o}C for 15 s) for 40 cycles and RQ manager version 1.2.1 was used to record the Ct (cycle threshold) values. The ΔCt value was calculated from the difference in Ct values between the target gene and internal control. ΔΔCt values

were obtained by normalizing the ΔCt values to presenescent control.

The internal control was selected by carrying out qRT-PCR for three different house keeping genes B2M (β-2-microgloubulin), RNU48 and U6 snRNA using cDNA from both senescent and presenescent fibroblasts. The standard deviation of Ct values for each control was calculated to identify a control that showed deviation of 1 or less than 1 in all samples. The Ct values of both RNU48 and U6 demonstrated the least deviation, standard deviation of less than 1 (Appendix 10). However qRT-PCR for RNU48 required two step PCR reaction (Section 2.13) and use of a RNA concentration different to that used in routine gene expression assay. As a result to keep the RNA template constant throughout reactions U6 was chosen as the best internal control for qRT-PCR.

(Melt curves of all SYBR Green primers are shown in appendix 7)

Gene	Forward	Reverse	Primer efficiency
p21	5' AATAATGCCGCCGCC TCTTC 3'	5' TTATTGTTCCATCGCTC ACG 3'	106.25%
TP53	5'CCTCCATTTGGATGAC AGAAACAC 3'	5' AATAAAGTGGATGGTG GTACAGTCAG 3'	87.69%
p16	5'AATAACCTTCGGCTGA CTGGCTG 3'	5'TTATTCGCCTCCAGCAG CGCCCG 3'	110.72%
MMP2	5'AATAATTCCGCTTCCA GGGCACATCC 3'	5'TTATTGCGGTCGTAGTC CTCAGTGGT 3'	113.15%
MCP-1	5'AATAACGCGAGCTATA GAAGAA 3'	5'TTATTGTCAGCACAGAT CTCCTT 3'	80.05%
PTEN	5'ACTCACATCGGGGCA AATTTTTAAAG 3'	5'TTATTTCTCTGGTCCTT ACTTCCCCA 3'	102.75%
COX-2	5'AATAAGTGTTGACATC CAGATCAC 3'	5'CAATTGGCTCTAGTATA ATAGGAGA 3'	128.96%
STAT3	5'AATAAACAAAGACTCT GGGGACGTTGC 3'	5'AATTCTTGGATTCTTCC ATGTTCATCACTT 3'	111.72%
Pri-miR-335	5'GTTTTGAGCGGGGGT CAAGAG 3'	5'CAAATGAGAGGAGGTC AGGAGC 3'	98.10%
Pri-miR-148b	5'AAGCACGATTAGCATT TGAGGTG 3'	5'ATGCACTGACTTTCAGA GAGC 3'	86.54%
α-SMA	5'GAAGAAGAGGACAGC ACTG 3'	5'TCCCATTCCCACCATCA A 3'	99.70%
FGF-2	5'AATAATTGCCCGAGG ATGGCG 3'	5'TTATTTTTGCAGTACAG CCGCTT 3'	105.20%
IL-6	5'AATAAAACAACCTGAA CCTTCCA 3'	5'TTATTGATTTTCACCAG GCAAGT 3'	98.66%
IL-8	5'TGTGTGAAATTATTGT AAAGCTT 3'	5'TAAATCTTCTCCACAAC CCTCTG 3'	80.06%
IL-1β	5'CCTCCAACAAGTGGT GTTCTCCATG 3'	5'CCTCCTTTCCTTGAGGC CCAAGG 3'	79.77%
MSR-1	5'CCGCCCACTTTAATTC AAGGTCC 3'	5'CCTCAATTGGACCTGGA AATCCTC 3'	134.99%
U6 snRNA	GTGCTCGCTTCGGCAGCACATATACTAAAATTGGAACGATACAGAGA AGATTAGCATGGCCCCTGCGCAAGGATGACACGCAAATTCGTGAAG CGTTCCATATTTT (Life technology, #001973)		

Table 2.19 SYBR Green and TaqMan primers to determine senescence specific gene expression

2.12: TaqMan microRNA tiling low density array (TLDA)

From normal oral fibroblasts about 250 ng of total RNA was measured per 3 µL volume to synthesize cDNA by megaplex reverse transcription (RT) reaction using predefined stem-loop reverse transcription primers (Applied Biosystems) from human Pool A and Pool B mature microRNAs as shown in table 2.20 below. Each pool contains 384 human mature miRNA probes wherein pool A panel comprises mostly of well characterized miRNAs with defined functions and pool B panel comprises of newly identified miRNAs of undetermined functions. Megaplex reverse transcription was carried out by adding 3 µL of the RNA template to 4.5 µL of mastermix in PCR tubes and incubation in DNA engine DYAD thermal cycler using the parameters in table 2.21.

Thereafter 2.5 µL of synthesized miRNA cDNA were pre-amplified using miRNA pool A and pool B specific forward and reverse primers by following the protocol shown in table 2.22. The thermal cycler was programmed according to the parameters in table 2.23. The pre-amplified cDNA (25 µL) was then diluted 4-fold in 0.1X TE buffer at pH 8.0. The diluted pre-amplified product (9 µL) was then further amplified by real time PCR by hybridizing them against 384 miRNA TaqMan primers and probe used to label human pool A and pool B microfluidic cards by combining it with 2X TaqMan universal PCR master mix without AmpErase and UNG (450 µL, Applied Biosystems) and nuclease free water (441 µL). Thermal cycling was carried out in 7900 HT real time PCR machine using the parameters in table 2.24.

RQ manager version 1.2.1 was used to obtain the raw Ct values. The data were analysed by Data Assist software from Life Technologies (version 3.0). Briefly the raw files were converted into tab delimited format in excel and loaded into the software. Each file represented a sample with microRNA array data and thus all files derived from the same conditions (for example either cisplatin treated or presenescent

Megaplex RT reaction	Volume per reaction(µL)
10 X Megaplex RT Primers; Pool A & B	0.8
dNTPs with dTTP (100mM)	0.2
Multiscribe reverse transcriptase (50U/L)	1.5
10X RT buffer	0.8
$MgCl_2$ (25mM)	0.9
RNase inhibitor (20 U/µL)	0.1
Nuclease free water	0.2
Total volume	4.5

Table 2.20: Protocol for preparing megaplex reverse transcription master mix.

Stages	Temperature / °C	Time in seconds
Cycle (40 cycles)	16°C	120
	42°C	60
	50°C	1
Hold	85°C	300
Hold	4°C	Forever

Table 2.21: Parameters for megaplex reverse transcription reaction.

PreAmp reaction mix components	Volume per reaction (µL)
2X TaqMan Pre-Amp Master Mix	12.5
Megaplex Pre-Amp Primers (Pool A & B)	2.5
Nuclease free water	7.5
Total volume	22.5

Table 2.22: Protocol for pre-amplification reaction.

Stages	Temperature / °C	Time in minutes
Hold	95°C	10
Hold	55°C	2
Hold	72°C	2
Cycle (12 cycles)	95°C	0.15
	60°C	4
Hold	99.9°C	10
Hold	4°C	Forever

Table 2.23: Parameters for pre-amplification reaction.

Stages	Temperature / °C	Time in minutes
Cycle (40 cycles)	50°C	2
	94.5°C	10
	97.0°C	0.5
Hold	59.7°C	1

Table 2.24: Parameters for qRT-PCR using TaqMan microfluidic array.

fibroblasts) were grouped as one allowing the software to understand the differences between different conditions and experimental repeats. Endogenous control was selected by the program as the transcript that fluctuated least in cells under different conditions. A cut-off value of 34 was selected as the maximum threshold of cycle at which DNA amplification was detectable. Fold change was calculated from ΔΔCt values as before but by using the software. MicroRNAs were considered to be up-regulated in TLDA when they demonstrated an increase in fold change by 2 or more and down-regulated when they demonstrated a decrease in fold change by 0.5 or less compared to control fibroblasts.

2.13: TaqMan microRNA assay

Two-step PCR was carried out to reverse transcribe microRNA specific cDNA from 10 ng of RNA template using miRNA specific looped reverse transcription primers. Initially TaqMan miRNA reverse transcription master mix was prepared in presence of RNAse inhibitor following the protocol in table 2.25. To 7 μL of master mix, 3 μL of 5X miRNA reverse transcription primers and 10 ng of RNA template were added. Reverse transcription was carried out by setting up the thermal cycler according to the program in table 2.26.

Ingredients	Volume per reaction
10X reverse transcription buffer	1.5 μL
Multiscribe reverse transcriptase (50U/μL)	1.0 μL
25X dNTPs (100 mM)	0.15 μL
RNAse inhibitor (20 U)	0.19 μL
Nuclease free water	4.16 μL
Total volume	7.0 μL

Table 2.25: Protocol for miRNA reverse transcription (Applied Biosystem)

Cycle	Temperature/ ^{o}C	Duration (minutes)
Annealing	16^{o} C	30
Extension	42^{o} C	30
Denaturation	85^{o} C	5
Hold	4^{o} C	Forever

Table 2.26: Program for miRNA reverse transcription.

The miRNA specific cDNA was then amplified by qRT-PCR using specific miRNA real time TaqMan probes (20X) and TaqMan Universal PCR master mix without UNG (2X) similarly to section 2.11.

2.14: Western blot

2.14.1: Preparation of cell lysate

Cell pellets were washed twice in 1X PBS and centrifuged at 13,000 rpm for 5 m to remove excess of wash buffer. The pellets were then solubilized in RIPA buffer (sodium chloride: 150 mM, Nonidet P-40: 1.0%, Tris hydrochloride: 50 mM at pH 8.0, sodium deoxycholate: 0.5% and sodium dodecyl sulphate: 0.1%) supplemented with 1X protease inhibitor cocktail (Complete, mini, EDTA free tablets; Roche), phosphatase inhibitor: 1X phosphostop (Roche) and benzonase nuclease: 1 in 100 dilution (Sigma). The buffer was thoroughly mixed with the cell pellets and incubated on ice for 30 m. After this the cell lysates were cleared of debris and particulate substances by centrifugation at 13,000 rpm for 5 m at 4^{o} C. The protein rich supernatants from the total cell extract was collected into fresh tubes and stored at -80 ^{o} C for future use.

2.14.2: Measurement of protein concentration by Pierce BCA assay

Protein concentration was determined by Pierce BCA assay kit (Thermoscientific). The kit constitutes reagent A containing bicinchoninic acid in sodium hydroxide and reagent B containing 4% cupric sulphate. The kit was developed based on Biuret's reaction in which protein in alkaline solution reduces Cu^{2+} to Cu^{+}, the reduced copper ion then forms a purple complex with 2 molecules of bicinchoninic acid that can be measured by spectrophotometry at 562 nm wavelength.

The cell lysates were diluted 1 in 10 with dd H_2O and pipetted into each well of a clear 96-well plate in triplicate. Reagent A (49 parts) was mixed with reagent B (1 part); the mixtures were then immediately pipetted into each well using a multichannel pipette to a final volume of 200 μL. The plate was incubated in dark at 37^{o} C for 30 m until development of purple colour. The absorbance was recorded at 562 nm using a spectrophotometer (Tecan). Bovine serum albumin (2mg/mL stock) was diluted to

prepare standards. Protein concentrations were determined from the equation obtained by plotting a standard curve in Excel wherein the y-axis indicates the amount of absorbance and the X-axis indicates the concentration of proteins (μg/mL) from albumin standards and subsequent multiplication by the dilution factor.

2.14.3: SDS-Polyacrylamide Gel Electrophoresis and transfer on nitrocellulose membrane

Protein gels were prepared according to table 2.27, a 12% resolving gel was used to separate proteins according to molecular weight because most of the proteins studied in this thesis had apparent molecular weights of between 37 and 60 kDa. About 30 μg of protein samples were denatured in 1X Laemmli buffer (Tris hydrochloride: 62.5 mM at pH=6.8, sodium dodecyl sulphate; SDS: 2%, glycerol: 10%, Dithiothreitol; DTT: 50 mM, bromophenol blue: 0.01%) by heating at 95^{o} C for 5 m. Sterile gel loading tips were used to load protein samples into each well of the protein gel. The denatured proteins were separated electrophorectically by running the gel at 150 V for 70 m in 1X Tris-glycine buffer (25 mM Tris Base, 190 mM glycine and 0.1% SDS). After completion of gel electrophoresis the proteins were transferred onto a nitrocellulose membrane using iBlot (Invitrogen), a semidry transfer method. Briefly, copper containing cathode and anode stacks were used to stimulate negatively charged proteins to migrate towards nitrocellulose membrane positioned near the anode in the following order: sponge, copper cathode, moist filter paper, protein gel, nitrocellulose membrane and copper anode. Transfer was completed by running iBlot program 2, set at 23 V for 6 m.

The nitrocellulose membrane was immediately placed in blocking buffer (1X TBS, Tween-20: 0.1% and semi-skimmed milk: 5%) at room temperature for 1 h. The membranes were then washed thrice for 5 m in 1X TBST buffer (1X TBS plus Tween 20: 0.1%). The washed membranes were then incubated with the primary antibody

solution diluted at 1 in 1000, in 1X TBST buffer containing either 5% BSA (bovine serum albumin) or 5% semi-skimmed milk powder, overnight on shaker at 4^{o} C. The membranes were re-washed thrice for 5 m using 1X TBST buffer and blocked with the secondary antibody conjugated with horseradish peroxidase at a dilution of 1 in 2500, in 1X TBST buffer containing 5% semi-skimmed milk, for 90 m at room temperature. Finally the membranes were washed again thrice for 5 m in 1X TBST buffer and incubated with Pierce ECL (enhanced chemiluminescent) western blotting substrate reagent A and reagent B in a ratio of 1:1 for 2 m. The excess substrates were then drained and the membrane were wrapped in cling film and exposed to X-ray film in a sealed metallic cassette in dark room.

Stacking Gel			Resolving Gel
Gel percentage	5%	Gel percentage	12%
40% Polyacrylamide	1.25 mL	40% Polyacrylamide	6 .0 mL
1 M Tris hydrochloride	1.25 mL (pH=6.8)	1.5 M Tris hydrochloride	5 mL (pH=8.8)
10% APS	100.0 μL	10% APS	400.0 μL
TEMED	17.0 μL	TEMED	8.0 μL
dd H_2O	7.3 mL	dd H_2O	8.6 mL
Total volume	10.0 mL	Total volume	20.0 mL

Table 2.27: Protocol for SDS-PAGE (SDS-polyacrylamide gel electrophoresis. TEMED: tetramethylethylenediamine. APS: Ammonium per sulphate.

The films were then developed in dark using a compact X4 automatic X-ray film processor (Xograph imaging systems). EZ-run pre-stained recombinant protein ladder (Fisher BioReagents) was used to determine the size of the individual protein band.

The different primary and secondary antibodies used are enlisted in table 2.28.

Both GAPDH and β-actin antibodies were used as the loading control, as indicated in individual figure legends The blots were scanned and analysed using 1D BioRad's gel analysis software. Relative band densitometry were measured by calculating the differences in band intensity between either GAPDH or β-actin and the target protein. The data were then normalized to experimental control.

Primary antibody	Molecular Weight & Concentation	Manufacturer	Source of monoclonal antibody	Secondary antibody
Total PTEN	54 kDa (11 μg/mL)	Cell Signalling #9559	Rabbit IgG	Anti-rabbit IgG, HRP-linked antibody
Phospho-AKT (Ser473) (D9E) XP	60 kDa (250 μg/mL)	Cell Signalling #4060	Rabbit IgG	
Phospho-AKT (thr308)	60 kDa (290 μg/mL)	Cell signalling #2965	Rabbit IgG	
AKT (Pan)	60 kDa (35 μg/mL)	Cell signalling #4691	Rabbit IgG	
GAPDH	37 kDa (1.2 mg/mL)	Sigma #G9545	Rabbit IgG	
α-SMA	42 kDa (2.0 mg/mL)	Sigma # A5228	Mouse IgG	Anti-mouse IgG HRP linked antibody
β-actin	42 kDa (2.0 mg/mL)	Sigma #A2228	Mouse IgG	

Table 2.28: List of primary and secondary antibodies used in western blotting.

2.15: Human cytokine antibody array

Conditioned medium from day 15 cisplatin (10 μM) induced premature senescent and presenescent oral fibroblasts were incubated with human cytokine antibody array membrane 6 (RayBio) at 4^{o}C overnight on shaker. The membrane was then repeatedly washed using 1X wash buffer I and II (RayBio) and re-incubated with biotin conjugated

anti-cytokines antibody (Ray Bio) at 4^{o}C overnight on shaker followed by incubation with 1X HRP-conjugated streptavidin (RayBio) for 2 h at room temperature. The membrane was then coated with detection buffer C and D (RayBio) in a ratio of 1:1 and the relative expression levels of different cytokines were detected on X-ray film (Thermo scientific) using the same film developer used in western blot. The signal intensities were quantified using Quantity One 1D Gel analysis software (Biorad).

2.16: Enzyme linked immunosorbent assay (ELISA)

Secreted MCP-1 and IL-6 were quantitated by sandwich ELISA using human MCP-1 and IL-6 ELISA development kit (Peprotech) whereas secreted PGE2 were quantitated by performing competitive ELISA (R&D system; KGE004B). In sandwich ELISA capture and enzyme linked detection antibodies are used to specifically bind to antigen particles in suspensions and the amount of antigen present in solution is directly proportional to the absorbance of the chromogenic product formed by the conjugated enzyme (figure 2.13). In competitive ELISA usually enzyme labelled antigens compete with antigens in suspension to bind to unlabelled primary antibody and therefore the concentration of the antigen is inversely proportional to the absorbance of the chromogenic product (figure 2.13).

2.16.1: Sandwich ELISA

Briefly the captured antibody was diluted in 1X sterile PBS to a final concentration between 0.5 and 1.0 μg/mL and were used to coat wells of 96-well ELISA microplates (Corning). The coated plates were then sealed with adhesive plastics and incubated at room temperature overnight. The coating buffer was then discarded and the wells were thoroughly rinsed four to five times with wash buffer (1X PBS plus 0.05% Tween-20). The plates were dried and blocked with 1% BSA in PBS for 1 h at room temperature. Following a second wash step the wells are then incubated for 2 h with either

recombinant human MCP-1 or IL-6 standards and diluted conditioned media from fibroblasts to immobilize the secreted proteins at room temperature. The wells were washed again and incubated with biotinylated detection antibody (0.5 μg/mL) for 2 h at room temperature. After incubation period excess detection antibody was removed by repetitive washing. Then the plates were incubated for 30 m with avidin-horseradish peroxidase (1 in 2000). Finally the plates were re-washed and incubated with ABTS (2,2'-azino-di-[3-ethyl-benzothiazoline-6 sulfonic acid]-diammonium salt) and incubated in dark until development of a green end product. Absorbance was recorded at 405 nm with correction set to 650 nm.

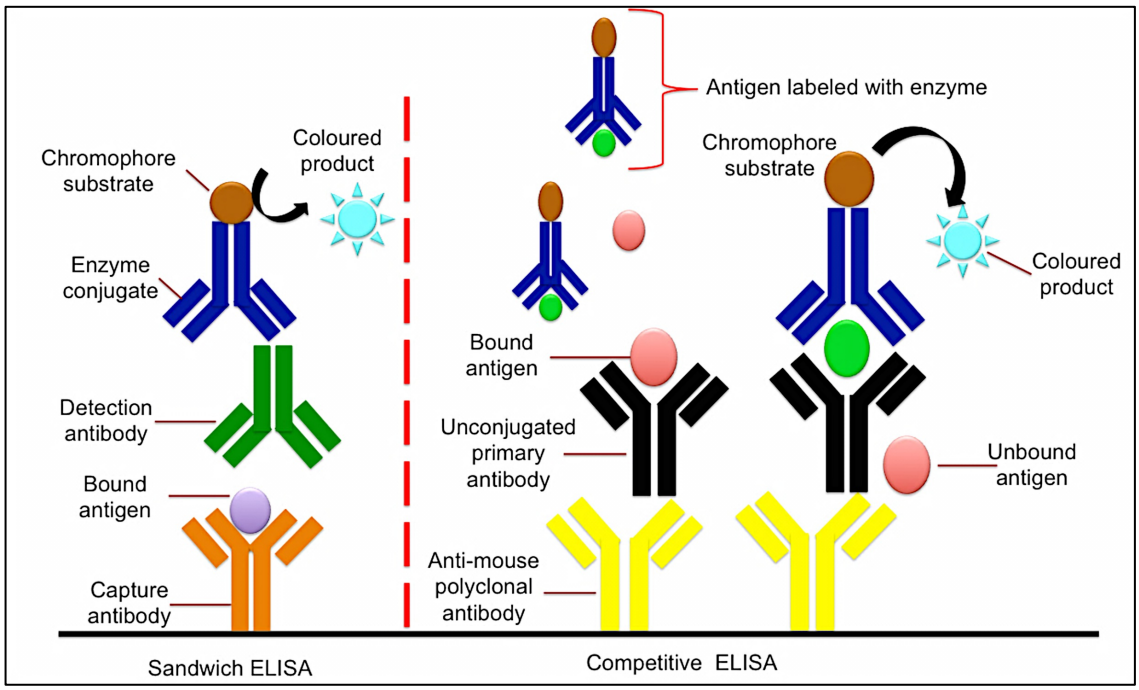

Figure 2.13: Differences between Sandwich and Competitive ELISA

2.16.1.A: Human MCP-1 ELISA

The conditioned media derived from senescent and presenescent fibroblasts were assessed for secreted MCP-1 using human MCP-1 ELISA development kit (Peprotech, 900-K31). Capture and detection antibodies consisted of non-biotinylated and biotinylated antigen affinity purified rabbit anti-human MCP-1 antibody, respectively.

Human MCP-1 standards were prepared by diluting recombinant human MCP-1 in antibody diluent (1X PBS plus 0.1% BSA plus 0..05% Tween-20) from 0-2 ng/mL.

2.16.1.B: Human IL-6 ELISA

IL-6 secretions in conditioned media of young and senescent oral fibroblasts were determined by using human IL-6 ELISA development kit (Peprotech, 900-K16). The capture and detection antibody consisted of non-biotinylated and biotinylated antigen affinity purified goat anti-human IL-6 antibody. Human IL-6 standards were prepared by diluting human recombinant IL-6 in antibody diluent as above from 0-1.5 ng/ mL.

2.16.2: Competitive ELISA for human PGE2

ELISA plates pre-coated with goat anti-mouse monoclonal antibodies were used to immobilize either PGE2 standards or secreted PGE2 present in fibroblast conditioned media and mouse anti-PGE2 monoclonal antibody for 1 h at room temperature on shaker according to manufacture's protocol. To this horseradish peroxidase conjugated recombinant PGE2 were added to compete with fibroblast derived PGE2 and bind to unbound anti-PGE2 antibodies immobilized by mouse IgG present in the microplate for 2 h at room temperature. The ELISA plates were then washed using wash buffer as described in section 2.16.1 followed by addition of substrate solution (hydrogen peroxide plus chromogenic tetramethylbenzidine) until colour development. The reaction was stopped by addition of 2N sulphuric acid. Absorbance was recorded at 450 nM and corrected at 570 nM using a spectrophotometer (Tecan). PGE2 standards were prepared by dilution 25000 pg of lyophilized recombinant PGE2 to 2500 pg/mL concentration with calibrator diluent down to 0 pg/mL.

All reactions were performed in triplicate on three individual days. The data were analysed by preparing a standard curve similar to BCA assay in section 2.14.2.

2.17: Immunohistochemistry

Immunohistochemistry was performed on paraffin embedded tissue sections derived from both 3D organotypic models and post-chemotherapy OSCC patients. The slides were deparaffinised by sequential treatment in xylene followed by hydration in 100% ethanol, twice each lasting for 5 m. Internal peroxidase activity was blocked by incubating the slides in 30% H_2O_2 in methanol for 20 m at room temperature under fume hood. The slides were then rinsed once in 1X PBS. Antigen retrieval was carried out by microwave heating in 0.01M sodium citrate buffer at pH=6.0. The duration of antigen retrieval for 3D models was reduced than those of archival tissue sections derived from patients due to lack of tissue compactness. In 3D models antigen retrieval was done by heating the tissue sections at high temperature for 4 m and at medium temperature for 2 m in microwave. Antigen retrieval of archival tissues was done by heating the tissue sections at the highest temperature for 8 m in microwave. The slides were then washed in 1X PBS and blocked with either normal goat serum (for primary antibodies raised in rabbits) or normal horse serum (for primary antibodies raised in mouse) for 90 m at room temperature in humidified chambers.

Primary antibodies were prepared in the relevant blocking buffers at a dilution of 1 in 100 and were used to incubate the slides overnight at 4^{o} C. The primary antibodies used in the study are enlisted in table 2.29.

Primary antibody	Manufacturer	Catalogue no.	Source and subtype	Conc.
Total PTEN	Cell signalling	9559	Rabbit monoclonal IgG	11 μg/mL
P16 (JC8)	Santa Crutz	Sc-56330	Mouse monoclonal IgG	200 μg/mL
Slug	Abcam	Ab27568	Rabbit polyclonal IgG	1 mg/mL
Twist1	Abcam	Ab50887	Mouse monoclonal IgG	0.1 mg/mL
GLB1	Abcam	Ab96239	Rabbit polyclonal IgG	1 mg/mL
α-SMA	Sigma	A5228	Mouse monoclonal IgG	2.0 mg/mL

Table 2.29: List of primary antibodies used in immunohistochemistry

After incubation period the slides were washed twice for 5 m in 1X PBS and incubated with secondary biotinylated antibody derived from either mouse or rabbit, depending on the source of primary antibody, for 30 m at room temperature. The secondary antibody blocking solution was prepared by mixing 3 drops of blocking sera to 10 mL of 1X PBS with 1 drop of conjugated antibody. Excess biotinylated antibody was removed by thoroughly washing the slides in 1X PBS for 10 m. The slides were then incubated with Vectastain (Vector Laboratories) for 30 m at room temperature, prepared 20 m in advance by mixing 2 drops of reagent A to 5 mL of 1X PBS and 2 drops of reagent B. The slides were then stained by incubation with Novared for 15 m until colour development according to manufacturer's protocol (Vector Laboratories). The reaction was stopped by addition of dd H_2O followed by counterstaining in haematoxylin as shown in flowchart below.

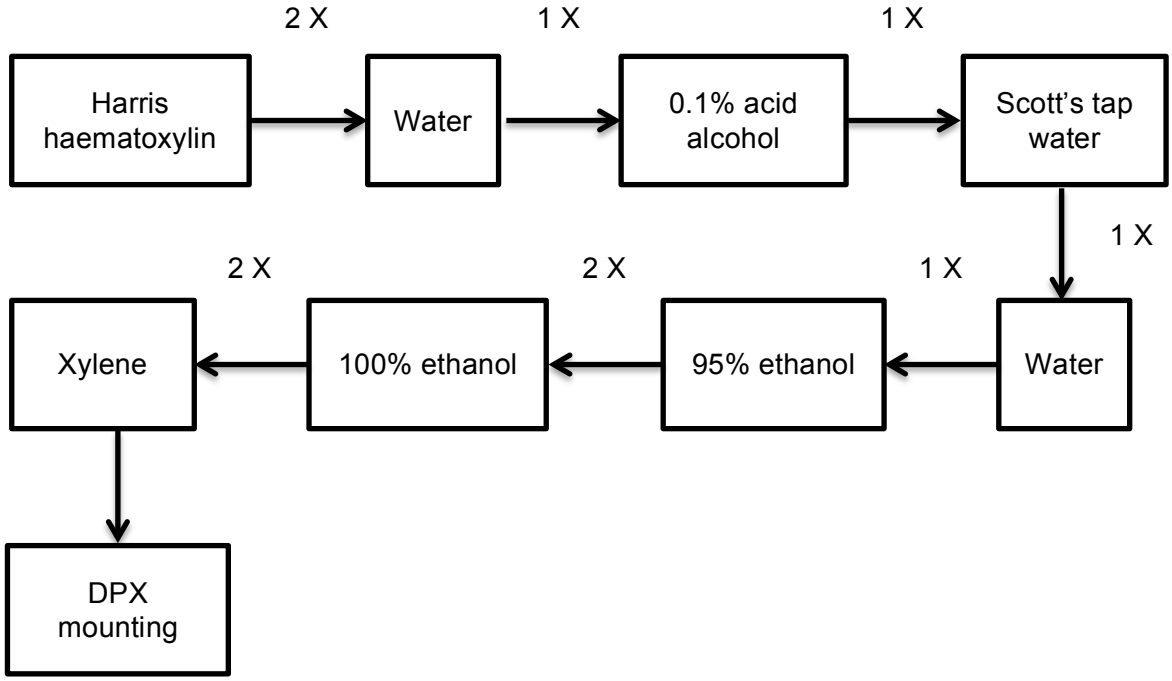

The slides were dipped into each solution for 30 s. Acid alcohol (0.1%) was prepared by combining 0.05 N hydrochloric acid: 100 μL, with isopropanol: 70 mL, and dd H_2O:

30 mL. Scott's tap water was used for blueing of the haematoxylin stain and was prepared by adding magnesium sulphate: 20 g and sodium bicarbonate: 3.5 g to 1 L of tap water. The slides were left in xylene until mounting stage to avoid drying.

2.18: Functional assays

2.18.1: Viability and proliferation assay

In this thesis two different approaches had been used to determine cellular viability and proliferation, which includes measurement of mitochondrial dehydrogenase activity and total amount of cellular DNA.

2.18.1.A: Measurement of viability and proliferation of fibroblasts

As described in section 2.2, viability of fibroblasts was determined at 2 h and 24 h post-treatment with H_2O_2 and cisplatin, respectively, in 96-well plate using Promega's CellTiter 96 AQueous non-radioactive cell proliferation assay kit. Untreated fibroblasts were used as controls. The kit consists of a pre-mixed solution of yellow tetrazolium salt (MTS) that can be reduced by mitochondrial dehydrogenase of viable cells into purple formazan compound whose absorbance is recorded by spectrophotometry at 490 nM. The amount of absorbance is directly proportional to the total number of viable cells. Briefly to 100 μL of culture media of of adherent cells in each well of a 96-well plate, 20 μL of MTS reagent was added and the microplate was incubated in dark at 37^{o}C for 1 h. Absorbance was measured at 490 nM using an ELISA plate reader and Magellan 6, version 6.4 (Tecan).

To determine cell proliferation, fibroblasts were seeded down in triplicate into different wells of 96-well microplate for senescence induction with different concentrations of either H_2O_2 or cisplatin and to measure their subsequent growth before and after treatment at different time-points. Basal proliferation rate were determined by addition

of 20 μL MTS reagent to 100 μL of culture media before initiating treatment in other wells. After treatment, the MTS reagent was then added to individual wells of microplate at respective time-points described in section 2.2 to determine the effect of genotoxic drugs on cell proliferation.

As this kit is optimized for measurement of only dehydrogenase activity and is likely to vary with alteration of cellular metabolism and contact inhibition during cell culture stress a second approach was utilized to effectively measure cell proliferation capacity using a fluorescent DNA binding dye called CyQUANT NF cell proliferation assay kit (Invitrogen, #C35006). This method is an alternative method to thymidine incorporation assay and is more practical being non-radioactive. Briefly, under sterile conditions 1X CyQUANT NF dye reagent (500X) was reconstituted in 1X HBSS buffer (Hank's balanced salt solution). The culture media were then removed from each well of microplate, replaced with the dye solution and incubated at 37^{o} C for 1 h. Fluorescence was recorded at excitation of 485 nM and emission detection at 530 nM using a microplate reader (Tecan). Proliferation was measured at specific time-points described in section 2.2.

2.18.1.B: Measurement of proliferation of oral dysplastic and OSCC cell lines

The oral dysplastic cell line: D20 and OSCC derived cells lines: SCC4 and H357 were seeded down in triplicate into each well of 96-well microplate on three independent days for treatment with conditioned media of presenescent, stress induced senescent and replicative senescent oral fibroblasts prepared according to section 2.2.2. Both SCC4 and D20 cells were seeded down at a density of 5,000 cells per well of 96-well microplate whereas H357 cells were seeded at a density of 2,500 cells per well. The media used to prepare conditioned media for treatment of D20 and H357 cell lines contained serum free DMEM plus 2 mM L-glutamine and for SCC4 the media contained serum and hydrocortisone free DMEM plus F12 media in a ratio of 1:1. Cell

proliferations were determined at time-point 0 h to 72 h for SCC4, 0 h to 96 h for D20 and 0 h to 120 h for H357 cells at 24 h interval. The cells were serum starved for 24 h before addition of conditioned media. Time-point 0 h included wells that were serum starved and not treated with conditioned media or growth factors. Cell survival and proliferation were determined using CyQUANT NF cell proliferation assay (Invitrogen, #C35006) kit in 96-well plates using the protocol described in section 2.18.1.A.

The same protocol was followed when these cells were treated with conditioned media from CAFs. Briefly conditioned media were collected from CAFs of GS OSCC (BICR69 and BICR70) induced to senesce with cisplatin as described in section 2.2.2. Conditioned media from untreated CAFs, normal oral fibroblasts and serum free media were used as experimental controls. Freshly prepared conditioned media were then used to treat D20, SCC4 and H357 cells in 96-well microplate as described before and effect on cell proliferation was measured by CyQUANT NF cell proliferation assay kit.

2.18.2: Migration assay

2.18.2.1: Migration of oral dysplastic and OSCC cell lines

SCC4, D20 and H357 cells were serum starved overnight prior to migration assay. SCC4 and H357 cells (100,000 cells) and D20 cells (35,000) were suspended in 200 μL DMEM (Sigma) plus 0.1% BSA (Fisher Scientific) in the upper chamber of a 24-well transwell (Corning Inc. Costar) with 8.0 μM pore PET (polyethylene terephthalate) membrane. Mitomycin (2μL; 1μg/mL by Sigma) was added to negate any effects of proliferation during the course of the assay. The lower chamber of the transwell was loaded with 500 μL of conditioned medium derived from either senescent or presenescent fibroblasts, miRNA transfected fibroblasts, siRNA transfected fibroblasts or CAFs and normal control fibroblasts from different patients (figure 2.14).

For SCC4 and D20 cells migrations were carried out for 24 h and for H357 cells migration was carried out for 40 h at 37°C. After specific time-points the cells that failed to migrate through the pores of the transwell membrane were scrapped off with cotton swabs. The inserts were then washed once with 1X PBS and fixed in 100% (v/v) methanol (Fisher Scientific) for 15 m at room temperature. The migrated cells were then visualized by staining with 0.1% crystal violet (w/v) (BDH) for 30 m at room temperature. Images of migrated cells in three random fields per well were captured using Nikon Coolpix camera (P5100; 12.1 megapixels) under 20X lens of light microscope (Olympus; CKX41). The total number of cells was counted using ImageJ 1.45s software. The relative number of migrated cells under each condition was calculated by averaging the total number of migrated cells in three random fields as representative of the number of migrated cells. The absolute number of migrated cells was calculated by normalizing the cell number to fibroblast density from which conditioned media were prepared. All experiments were carried out on three independent days in triplicate.

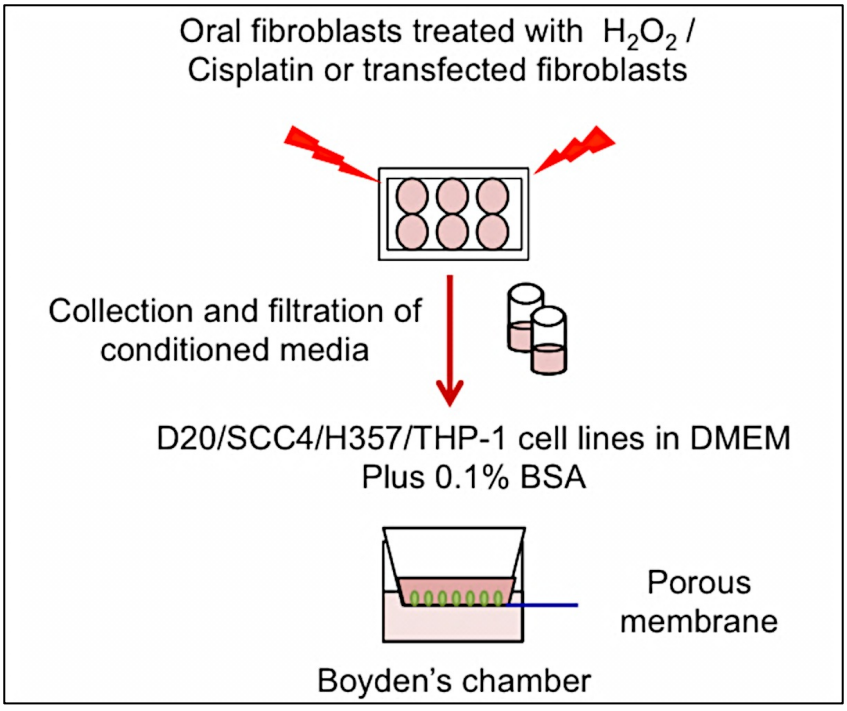

Figure 2.14: 2D transwell assay to determine migration of cancer cells.

2.18.2.2: THP-1 migration assay

THP-1 cell lines were washed twice with 1X PBS and suspended in only RPMI media to serum starve overnight at 37^{o} C. THP-1 cells (100,000) were resuspended in 200 μL volume of RPMI plus 0.1% BSA and inoculated to the upper chamber of transwell assay having 5 μM sized pores in polycarbonate membranes (Corning, #3421). Then 500 μL of conditioned media were pipetted into the lower chambers (figure 2.14). The migration chambers were left in incubator for 4 h at 37^{o} C. After incubation period the unmigrated THP-1 cells were scrapped off from transwell inserts using cotton buds, washed once in 1X PBS and fixed for 10 m in commercially produced fixative (90% methanol plus 3.7% formaldehyde) provided in Differential-Quik stain kit (Polysciences). The migrated THP-1 cells attached to the transwell inserts were then stained by sequentially dipping each inserts into solution B containing blue Azure dye and solution C containing orange Eosin Y dye each for 10 m. The inserts were then rinsed in running tap water and the total number of migrated THP-1 cells were determined by taking pictures in three random fields per well under 20X magnification using light microscope (Olympus; CKX41) fitted to Nikon Coolpix camera (p5100; 12.1 megapixels). The total number of stained cells was counted using ImageJ software (version 1.45s) in each field and averaging the number in three random fields as representative numbers of migrated THP-1 cells. The absolute number of migrated THP-1 was determined by normalizing the data to fibroblast density from which conditioned media were collected.

2.18.3: Invasion assay

2.18.3.1: 2D invasion assay

BD BioCoat matrigel invasion chambers (BD Biosciences, #354480) were used to perform 2D invasion assay. These invasion chambers comprised of tissue culture companion plate and cell culture inserts with PET membrane having 8 μM sized pores.

The PET membranes of these inserts are precoated with a thin layer of matrigel basement membrane matrix (laminin, collagen IV, heparin sulphate proteoglycans and entactin).

The frozen invasion chambers (at -20^{o} C) were allowed to reach room temperature inside class II tissue culture hoods. The inserts were then rehydrated with serum free DMEM at 37^{o} C for 2 h. The media were gently removed. The bottom chambers were immediately filled with 500 μL of conditioned media derived from fibroblasts. Without delay H357 cells (100,000) suspended in 500 μL of DMEM plus 0.1% BSA were loaded to the top chamber. Mitomycin C was added at a concentration of 1.0 μg/ mL of media. The invasion chambers were then incubated at 37^{o} C for 72 h.

After 72 h, the non-invading cancer cells were scraped off from the insert using a cotton bud and the staining protocol in section 2.18.2 followed to determine and compare the total number of invaded cancer cells under each condition. Invasion index was measured using the following formula:

$$\text{Invasive index} = \frac{\text{(Total number of invading cells/Total number of migrated cells) * 100 — At different condition}}{\text{(Total number of invading cells/Total number of migrated cells) * 100 — Of Control}}$$

2.18.3.2: 3D invasion assay using de-epithelialized dermis models

To better understand the process of invasion of OSCC cells in presence of senescent oral fibroblasts a 3D organotypic model was used (as previously described, Colley *et al.* 2011). Human dermis was de-epithelialized by incubation in 1M sodium chloride solution at room temperature on shaker. The de-epithelialized dermis (DD) was then thoroughly washed with 1X PBS for 48 h on shaker to remove excessive glycerol in which it was preserved. The DD was screened for contaminants by incubation in antibiotic free DMEM plus 10% FCS at 37^{o} C for 24 h. The DD was then ready for cell inoculation to grow 3D organotypic models.

The DD was sectioned into 1.5 cm X 1.5 cm squares using a sterile scalpel in cell culture hood and placed inside a well of a 6-well plate. A sterile stainless steel ring (1 cm X 1 cm) was forced on top of the DD to seal any gaps. About 500 μL of media was pipetted into the DD enclosed ring and incubated for 15 m at room temperature to check for leakage. During this time human oral fibroblasts (between passage 4-6) were harvested and suspended in 400 μL of media to a density of 500,000. After ensuring adequate seal the medium was carefully removed and replaced with fibroblast suspension. The fibroblasts were allowed to settle and invade into the dermis by overnight incubation at 37^{o} C. The next day the fibroblasts were treated with cisplatin (10 μM) for 24 h for induction of senescence. Untreated fibroblasts were used as controls. After 24 h the cisplatin containing media were removed and DD carrying cisplatin treated fibroblasts were washed thoroughly with 1X PBS. Fresh media were added to both control and cisplatin treated fibroblasts. The fibroblasts were then cultured in DD for 72 h with regular feeding every 24 h. At day 4 post-treatment OSCC derived cell line H357 cells were harvested, suspended into 400 μL of culture media to a density of 2,50,000 and inoculated onto DD carrying either control or cisplatin treated fibroblasts. The cells were cultured in DD enclosed rings for another 72 h with regular feeding in between. After 72 h, the DDs were then transferred into air-liquid interface by

gently removing the media and the metallic ring and positioning the DD on to a sterile surgical grid in 6-well plates (figure 2.15). The wells were filled with media to a point such that the lower meniscus of the media aligned with the top surface of the surgical grid. Media was changed every 72 h and the models were grown for a period of 21 days. After 21 days, the DD models were fixed in 10% buffered formalin, paraffin embedded and sectioned by microtome to a 5 μM thickness. The models were then used to determine invasion of OSCC cells by routine haematoxylin and eosin staining and assessed for senescence and EMT markers by immunohistochemistry.

The stages of growing 3D models are summarized in figure 2.15.

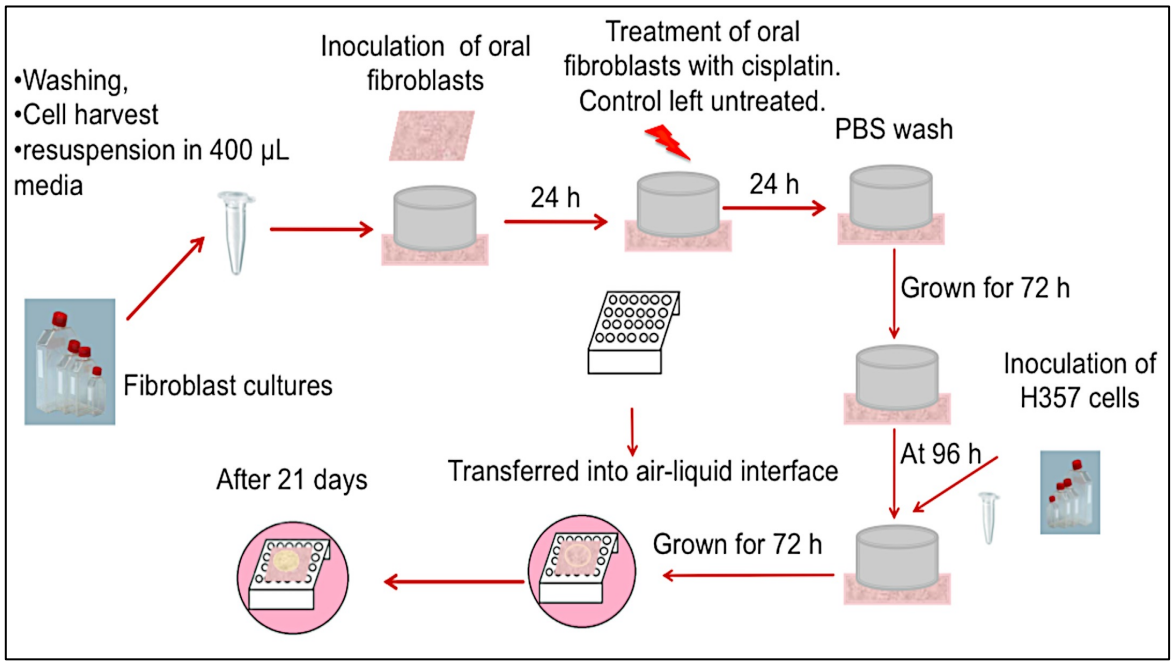

Figure 2.15: Growing 3D models to study cancer cell invasion in presence of senescent fibroblasts

2.18.4: Determination of functional effect of secreted MCP-1

Human anti-MCP-1 antibody (subtype IgG, 500 μg/mL, from R&D: MAB679) was used to block the activity of secreted MCP-1 in conditioned media derived from fibroblasts. Mouse IgG1 and IgG2 isotype control were used as negative controls (Serotec: #MCA1209, Invitrogen; #MG2b00). Anti-MCP-1 antibodies were added at a

concentration of 20 μg/mL to the conditioned media derived from both senescent and presenescent fibroblasts to determine and compare the consequences of impeding MCP-1 activity on chemotaxis of THP-1 cell lines and on both chemotaxis and invasion of H357 cell lines in 2D transwell migration and invasion assay. MCP-1 activity was also blocked in conditioned media derived from miRNA transfected oral fibroblasts. In 3D organotypic models effect of blockade of MCP-1 on senescent and presenescent fibroblast function and cancer cell migration and invasion were determined by adding anti-MCP-1 antibody to the culture media every 72 h for 21 days after the models were transferred to air-liquid interface. Equal volumes of negative control antibodies were added to culture media in control models.

2.18.5: Apoptosis assay

Primary human oral fibroblasts were treated with either H_2O_2 (500 μM) or cisplatin (10 μM) in 96-well microplates as described in section 2.2. Presenescent fibroblasts were used as negative controls. The cells were incubated at 37^{o}C for 24 h and the microplate centrifuged at 200 X g for 10 m. The supernatant was collected for necrosis assay and temporarily thawed on ice. Lysis buffer (200 μL; Cell death detection ELISA^{plus}, Roche, #11774425001, Version 11.0) was added to each well of the microplate and incubated for 30 m at room temperature. The lysates were then centrifuged at 200 X g for 10 m. The supernatants were collected and 20 μL of it was transferred into streptavidin coated microplate followed by addition of 80μL of immunoreagent (incubation buffer; 72μL, anti-histone biotin; 4μL, anti-DNA-POD; 4μL). This was incubated at room temperature for 2 h accompanied with gentle shaking at 300 rpm. Each well was then emptied by gentle tapping followed by thorough rinsing with 300 μL of incubation buffer (thrice). ABST solution (100 μL) was pipetted into each well and incubated on a plate shaker at 250 rpm until colour development (approximately 10 - 20 minutes) for spectrophotometric analysis. ABTS stop solution

(100 μL) was added to stop the reaction. The absorbance was measured at 405 nm using spectrophotometer (Tecan). The data were normalized to background. Apoptosis was determined as a measure of the enrichment factor as calculated below:

Enrichment factor = Absorbance of sample (dying/dead cells)/Absorbance of the negative control; expressed in mU = absorbance [10^3].

2.18.6: Polarization of macrophages

THP-1 cell lines were suspended in 3 mL of RPMI-1640 media containing 10% FCS at a density of 5,00,000 per well of 6-well plate. The cells were centrifuged at 1000 X g for 5 m to remove the media and re-suspended into 3 mL of fresh media containing 200 nM of PMA (phorbol 12-myristate 13-acetate; Sigma). The cells were then incubated with PMA in 6-well plates for 72 h at 37^o C and 5% CO_2. After 72 h PMA containing media was removed and replaced with fresh media. The media was changed every 48 h for a period of 5 days (as described previously, Daigneault *et al*., 2010).

The cells were assessed under microscope for differentiation. THP-1 cells are considered differentiated into macrophages when most of the non-adherent THP-1 monocytes become attached to the surface of 6-well plate.

The differentiated macrophages were then serum starved overnight. The cells were then incubated with conditioned media from senescent and presenescent oral fibroblasts for 72 h. Polarization of macrophages were determined by qRT-PCR for interleukin-1β (IL-1β) and macrophage scavenger receptor-1 (MSR-1) as described before by Lujambio and group (2013) using the protocol described in section 2.11.

2.18.7: Determination of effects of conditioned media derived from OSCC and oral dysplastic cell lines on activation of senescent oral fibroblasts

Oral dysplastic cell line D20 and OSCC derived cell lines H357 cells were seeded down at a density of 4,000,000 per T75 flask in 10 mL of culture media. The cells were incubated at 37^{o} C and 5% CO_2 for 48 h to 72 h until the flasks were 80% confluent. Then the flasks were washed twice with 1X PBS and about 3.5 mL of serum free DMEM containing 2mM L-glutamine was added into each flask to prepare conditioned media for 24 h at 37^{o} C. The conditioned media were collected the next day, filter sterilized and diluted into a volume such that the media were derived from 2,000,000 cells of either D20 or H357 cells per mL. D20 and H357 cell derived conditioned media (500 μL) was then used to treat serum starved senescent and presenescent oral fibroblasts that had been seeded down (50,000) on sterile glass cover slips in a 12-well plates for a duration of 48 h. Fibroblast activation was determined by monitoring expression of α–SMA by immunofluorescence immunocytochemistry (described in section 2.3.2).

2.18.8: Blockade of COX-2 activity

For determination of COX-2 and prostaglandin E2 (PGE2) activity in presenescent, and senescent fibroblasts and in normal human oral fibroblasts (NHOF) and CAFs DMEM supplemented with 20 mM glucose was used because PGE2 requires high glucose concentration to maintain its autocrine intracellular activity by means of lactate transporter (Martien *et al*., 2013). Blockade of cyclooxygenase 2 was achieved by treating the fibroblasts with selective COX-2 inhibitor; celecoxib, 1 μM (Cayman chemical, #10008672) for 48 h after confirmation of senescence, as described by Kim *et al*. (2008), either in serum rich state or serum depleted state under circumstances of preparing conditioned media. Celecoxib treated oral fibroblasts were assessed for changes in both senescence by SA-β-Gal activity (section 2.2.2) and fibroblast

activation by detecting α-SMA by immunofluorescence (section 2.3.2). Untreated presenescent and senescent oral fibroblasts and untreated NHOFs and CAFs were used as experimental controls. The conditioned media derived from celecoxib treated and untreated oral fibroblasts were assessed for role of COX-2 in senescent fibroblasts and in CAFs in mediating cancer cell motility by performing 2D transwell assay. The conditioned media from celecoxib treated and untreated oral fibroblasts were also used for determination of changes in the secreted levels of PGE2 and IL-6; in senescent versus presenescent oral fibroblasts and CAFS versus NHOF, by performing ELISA for IL-6 and PGE2 as described in section 2.16.1 and 2.16.2. Lastly the cell pellets of celecoxib treated and untreated oral fibroblasts were used for RNA and protein extraction to evaluate changes in PTEN mRNA by qRT-PCR (section 2.11) and proteins by western blot (section 2.14) as well as miRNA expression profile (section 2.13). The fibroblasts used in these experiments are shown in table 2.30.

NHOF	CAFs of GS OSCC	CAFs of GU OSCC
DENF008	BICR69	BICR31
OF320	BICR70	BICR63
OF20		BICR18
OF23		
OF18		

Table 2.30: List of fibroblasts used in investigation of COX-2 function.

2.19: Statistical analysis

Sigma Plot (version 12.0) was used to determine statistical significance. One-way ANOVA, ANOVA on repetitive measures, two-way ANOVA and paired student's t-test were used to analyse data. Anova on repetitive measures were used to analyse data from time-point experiments as in proliferation assay and gene expression assay. Two-way repetitive measure ANOVA was used when two conditions were compared at different time-points. Mann Whitney U-test was performed when the data were not normally distributed. P-value <0.05 was considered as statistically significant.

3.0: Results

3.1: Characterisation of senescence and senescence-associated secretory phenotype in human primary oral fibroblasts

Hypothesis:

Genotoxic stimuli and replicative exhaustion induce senescence in human primary oral fibroblasts associated with development of SASP.

Aims and objectives:

- To determine the subcytotoxic doses of H_2O_2 and cisplatin for inducing senescence in primary human oral fibroblasts.
- To determine if H_2O_2 and cisplatin induce premature senescence in human primary oral fibroblasts.
- To determine if replicative exhaustion induce senescence in human primary oral fibroblasts.
- To investigate if cisplatin induces premature senescent oral fibroblasts to develop SASP and
- To validate SASP factors in senescent oral fibroblasts at both mRNA and protein level by qRT-PCR and ELISA.

3.1.1: Genotoxic stress induces premature senescence in human primary oral fibroblasts

Senescence, or programmed cellular ageing, evolved as a tumour suppressive mechanism from embryonic life to adulthood and is conserved among all species (Coppe *et al*., 2010; Storer *et al*., 2013). The most distinguishing feature of a senesced cell is primarily irreversible growth arrest in response to physiological stimuli (Campisi and d'Adda di Fagagna, 2007). In addition these cells also develop a discrete secretory character wherein they release various factors such as pro-inflammatory cytokines, ECM degrading proteases and growth factors, which contribute to the SASP (Davalos *et al*. 2010). It is this SASP which, due to lack of selection pressure, provokes age-associated remodelling of the tissue microenvironment and is critical for development and progression of various diseases including late-life cancer (Campisi and d'Adda di Fagagna, 2007).

Human diploid fibroblasts can senesce naturally with time by replicative exhaustion or may be stimulated to undergo premature senescence by different agents that trigger oxidative stress or DNA damage (Bavik *et al*., 2006, Ewald *et al*., 2010). In this study two genotoxic drugs; H_2O_2 (Hassona *et al*. 2013, Chen *et al*. 1994) and cisplatin; a platinum based chemotherapeutic agent (Zhao *et al*. 2004), were used to stimulate premature senescence in human primary oral fibroblasts. Primary human oral fibroblasts were treated with escalating concentrations of both H_2O_2 (ranging from 50 µM to 1000 µM) for 2 h and cisplatin (ranging from 2.5 µM to 100 µM) for 24 h to determine their sub-lethal dose (figure 3.1.1.1.A & B). Cell viability was measured at 2 h and 24 h post-treatment with H_2O_2 and cisplatin, respectively, by MTS assay described in methods (section 2.18.1.A). It was observed that fibroblasts pulse treated with H_2O_2 concentrations above 700 µM showed diminished mitochondrial dehydrogenase activity, assumed to be a result of toxicity (figure 3.1.1.1.A). Likewise fibroblasts treated with cisplatin concentrations above 20 µM showed less

mitochondrial activity (figure 3.1.1.1.B). To further optimize the dose of H_2O_2 and cisplatin, their effects on cell proliferation were quantified using CyQuant NF cell proliferation assay for duration of 7 days (168 h), described in methods (section 2.18.1.A). It was observed, immediately post-treatment until the first 48 h, both control fibroblasts and those treated with low doses of H_2O_2 (≤ 350 μM) demonstrated an initial diminished proliferation capacity whereas fibroblasts treated with medium to high doses of H_2O_2 (between 400 μM and 1000 μM) demonstrated an initial stimulation of cell proliferation. Thereafter fibroblasts pulse treated with H_2O_2 concentration above 700 μM demonstrated declining rate of proliferation with time, whereas those treated with concentration below 500 μM resumed normal rate of proliferation as the untreated control (figure 3.1.1.2.A). Fibroblasts treated with H_2O_2 concentration between 500 μM and 600 μM showed restoration of cell proliferation at day 7, however the rate of proliferation were reduced compared to untreated control fibroblasts.

Fibroblasts treated with escalating concentrations of cisplatin displayed an initial decrease in cell proliferation capacity immediately post-treatment in comparison to untreated control (figure 3.1.1.2.B). After 24 h, fibroblasts treated with lower concentrations of cisplatin (between 2.0 and 2.5 μM) continued to proliferate gradually over time but at a much slower pace than the control cells (figure 3.1.1.2.B). In contrast, fibroblasts treated with moderate concentrations of cisplatin (between 5.0 and 10.0 μM) displayed no visible variation in cell proliferation capacity with time and the level of fluorescence remained similar to that observed at 24 h post-treatment relative to control, implying attainment of irreversible growth arrest in these samples (figure 3.1.1.2.B). Finally fibroblasts treated with higher concentrations of cisplatin (between 20.0 and 100.0 μM) demonstrated a declining rate of cell proliferation over time indicating that these doses are lethal and the cells fail to recover from DNA damage and possibly undergo apoptosis (figure 3.1.1.2.B). From these experiments concentrations of 500 μM and 10 μM were chosen as the highest dose of H_2O_2 and

cisplatin, respectively, for treatment of primary oral fibroblasts as at these two doses fibroblasts showed reduced rate of proliferation accompanied by effective growth arrest over time compared to the untreated control fibroblasts.

To confirm that both H_2O_2 and cisplatin induced irreversible cell cycle arrest over an extended time period human primary oral fibroblasts were either pulsed with H_2O_2 (500 μM) for 2 h or treated with cisplatin (10 μM) for 24 h in normal culture media (10% FCS plus DMEM). Untreated or presenescent fibroblasts were used as control. After treatment the cells were washed twice with PBS and were allowed to grow for a period of 17 days in normal media with regular feeding every 72 h. MTS assay was performed to monitor cell viability and proliferation post-treatment with the indicated doses of H_2O_2 and cisplatin. It was observed that fibroblasts treated with both H_2O_2 and cisplatin showed an uniform reduction in absorbance compared to normally proliferating control cells and these values did not alter for the entire period of 17 days indicating these cells had reached a state of permanent growth arrest (figure 3.1.1.3.A). To ensure that the steady absorbance observed in fibroblasts treated with H_2O_2 and cisplatin was not due to apoptosis and necrosis, cell death detection ELISA was performed. This is an ELISA-based apoptosis assay, which detects oligonucleosomal DNA fragments; a hallmark of programmed cell death. It was observed that 24 h after treatment of fibroblasts with H_2O_2 and cisplatin similar levels of absorbance were observed as that in presenescent control cells and were significantly lower than the positive control (lyophilized DNA-histone complex) supplied by the manufacturer (figure 3.1.1.3.B). Further, the level of necrosis was within the same range as the presenescent control (figure 3.1.1.3.C).

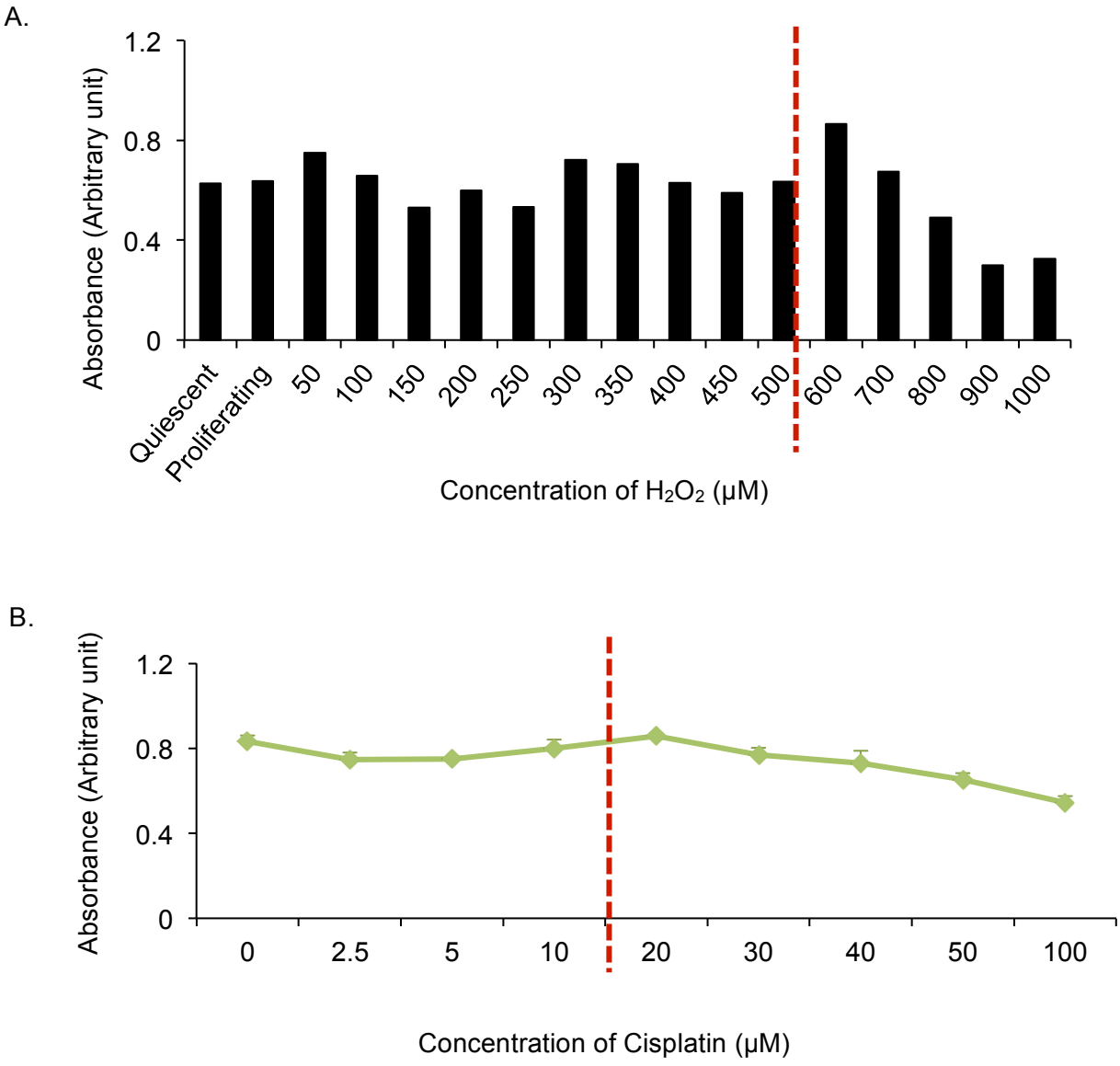

Figure 3.1.1.1: Determination of viability of human primary oral fibroblasts after treatment with H_2O_2 and cisplatin. Primary human oral fibroblasts (5,000 cells/well) were seeded in 96-well plates in triplicate and treated with escalating concentrations of either H_2O_2 for 2 h or cisplatin for 24 h. MTS assay was performed to determine cell viability at 2 h post-pulsation or 24 h post-treatment with H_2O_2 (A) and cisplatin (B), respectively. Red dashed line represents cut-off point. N=1, in triplicate.

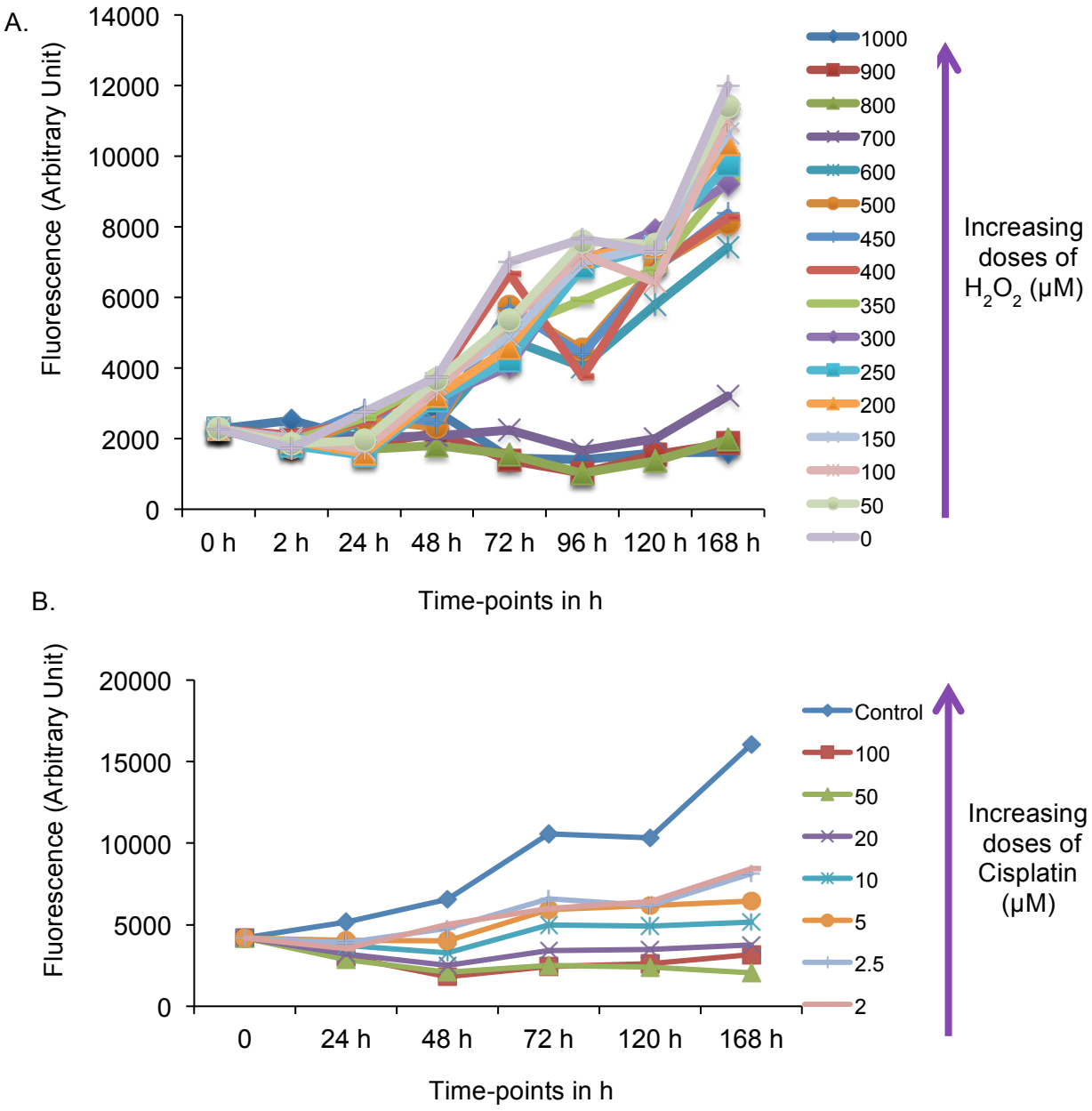

Figure 3.1.1.2: Effect of escalating doses of H_2O_2 and cisplatin on rate of proliferation of fibroblasts. Fibroblasts were seeded down at 5,000 per well of 96-well plate in triplicate and were treated with increasing concentrations of either H_2O_2 for 2 h (A) or cisplatin for 24 h (B). The cells were then washed and cultured in normal media. The rate of cell proliferation was determined by using CyQuant NF cell proliferation assay. N=1, in triplicate.

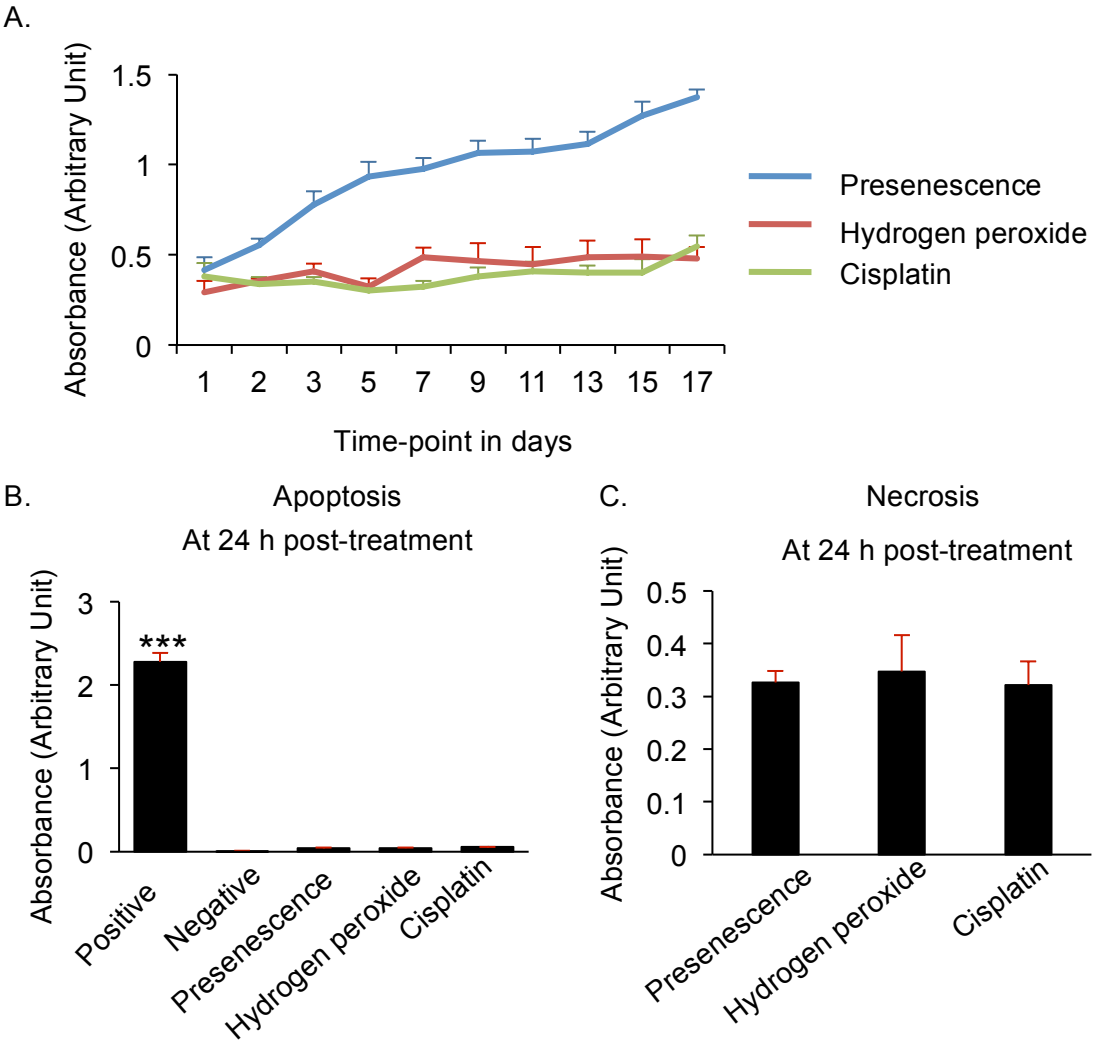

Figure 3.1.1.3: Sub-lethal doses of genotoxic stimuli provoke irreversible growth arrest in human primary oral fibroblasts. Fibroblasts were seeded at 2,000 per well of 96-well plate and were either treated with H_2O_2 (500 μM) for 2 h or cisplatin (10 μM) for 24 h. The cells were washed and then sub-cultured in normal growth media for 17 days. MTS assay was used to determine cell viability and proliferation (A). To exclude that the reduction in cell proliferation was not due to accumulation of dead cells, cell death detection ELISA was performed to determine and compare the level of apoptosis (A) and necrosis (B) between H_2O_2 and cisplatin treated oral fibroblasts with presenescent control fibroblasts and a positive control supplied by manufacturer. Data are presented as +SEM, N=3, in triplicate. ***p<0.001, One-way ANOVA with post-hoc Tukey corrections.

To date senescence associated β-galactosidase (SA-β-Gal) activity (Dimri *et al*., 1995) is considered to be the most well-characterised biomarker of cellular senescence, monitored as development of turquoise blue coloured precipitate in the perinuclear area of senesced cells due to augmented lysosomal β-galactosidase activity at pH 6.0. H_2O_2-induced premature senescence of human diploid fibroblasts, including those derived from oral mucosa, is already characterized by various groups (Chen *et al*. 1994 and Hassona *et al*. 2013). Conversely most chemotherapeutic reagents are known to induce senescence in cancer cells (Chang *et al*., 1999; te Poele *et al*., 2002; Ewald *et al*., 2008; Liu and Hornsby, 2007b) but their effects on the neighbouring stroma are just emerging. The ability of cisplatin to induce senescence of primary human oral fibroblasts is yet to be elucidated.

To address this, escalating doses of cisplatin (between 2.0 μM and 10 μM) were used to treat oral fibroblasts for 24 h. At day 5 post-treatment the cells were fixed and stained for SA-β-Gal activity. All four concentrations of cisplatin showed between 45% (2 μM and 2.5 μM) and 51% (5 μM and 10 μM) positivity for SA-β-Gal activity visualized by increased number of blue cells whereas only 4% cells stained blue in the untreated control (figure 3.1.1.4). Based on previous evidence (figure 3.1.1.2.B) and current observations 10 μM of cisplatin was decided as the optimum concentration for induction of senescence in human oral fibroblasts for further work because it appeared that at this concentration the cells showed maximum achievement of irreversible growth arrest and SA-β-Gal activity. Although 5 μM concentration of cisplatin produced similar result to 10 μM concentration but at this dose a minor percentage of fibroblasts resumed cell proliferation at later time-points as illustrated by the upward inclination from baseline in the graph of figure 3.1.1.2.B.

Development of senescence is not an instantaneous process but rather a slow set of events, which agglomerate to initiate and maintain it (Rodier *et al*., 2009, Freund *et al*.,

2011). As a result a time course study was carried out after treating oral fibroblasts with cisplatin (10 μM) for 24 h and the extent of senescence was monitored using SA-β-Gal activity until day 14. Cisplatin treated oral fibroblasts showed gradual accumulation of SA-β-Gal positive cells over time (figure 3.1.1.5.A), reaching about 41% at day 5, followed by further inclination to 92.5% at day 10 and reaching 95% at day 14 (figure 3.1.1.5.B). In contrast, the untreated presenescent control fibroblasts showed only 4.7% blue stained cells on day 5, which increased slightly to 5.7% on day 10 (figure 3.1.1.5.B). At day 14, an increase in SA-β-Gal activity was observed in the control wells reaching 54%, however the intensity of blue stain was relatively less in these wells and may be explained by cell culture stress resulting from over confluent wells (figure 3.1.1.5 A & B). Furthermore when these cells were re-plated at a lower density and measurement of SA-β-Gal activity was repeated these cells demonstrated almost no β-Gal activity whereas those treated with cisplatin maintained their blue staining even after 14 days post-treatment indicating an influence of cell seeding density on the enzymatic activity of SA-β-Gal. This suggested that treatment of oral fibroblasts with cisplatin induced and maintained senescence whereas SA-β-Gal activity associated with culture stress is a reversible event. From these observations day 15 was then selected as the time-point following either treatment at which senescence would be established and maintained.

To support this, the extent of senescence was assessed in presenescent untreated control and those fibroblasts either pulsed with H_2O_2 or treated with cisplatin at day 15 post-treatment. Oral fibroblasts from the same patient were allowed to undergo replicative exhaustion to generate replicative senescent cells as described in methods (section 2.2) and were used as a positive control. At day 15 post-treatment, both H_2O_2 and cisplatin induced primary human oral fibroblasts became flattened, increased in size, having granular and vacuolated cytoplasm with inconspicuous cellular margin sometimes bearing double or multiple nuclei, occasionally referred to as micronuclei,

and conspicuous chromatin (Chang *et al*., 1999), suggestive of failed capacity to undergo mitotic division, and their morphology closely resembled that of replicative senescent cells (figure 3.1.1.6.A and figure 3.1.1.7). SA-β-Gal activity was observed to be dramatically intensified and increased upon attainment of senescence in both H_2O_2 and cisplatin induced premature senescent cells at day 15 post-treatment and replicative senescent cells compared to presenescent control (figure 3.1.1.6.B). There was a significant increase in the number of blue cells and percentage SA-β-activity in replicative senescent oral fibroblasts; 89.0% ($n=4$, $p<0.05$), H_2O_2-induced; 78.0% ($n=4$, $p<0.05$), cisplatin-induced; 80.0% ($n=4$, $p<0.05$) compared to presenescent control; 2.5%. As it was observed that SA-β-Gal activity becomes positive upon cell culture stress, further corroboration of the acquisition of senescence was sought by analysing mRNA levels of two well-characterised biomarkers of senescence; cyclin dependent kinase inhibitors, p21/cip-1 (p21) and p16INK4a (p16) (Alcorta *et al*., 1996) by qRT-PCR. H_2O_2-induced premature senescent oral fibroblasts showed 4-fold ($n=5$, $p<0.05$) and 2-fold ($n=4$, $p<0.05$) higher levels of p21 and p16, respectively, than control (figure 3.1.1.8). Cisplatin-induced premature senescence oral fibroblasts showed 5-fold ($n=5$, $p<0.05$) and 2-fold ($n=4$, $p<0.05$) higher levels of p21 and p16, respectively (figure 3.1.1.8). Likewise, replicative senescent oral fibroblasts showed 2.8-fold ($n=5$, $p<0.05$) and 1.6 fold ($n=4$, $p<0.05$) higher levels of p21 and p16, respectively, compared to presenescent control (figure 3.1.1.8).

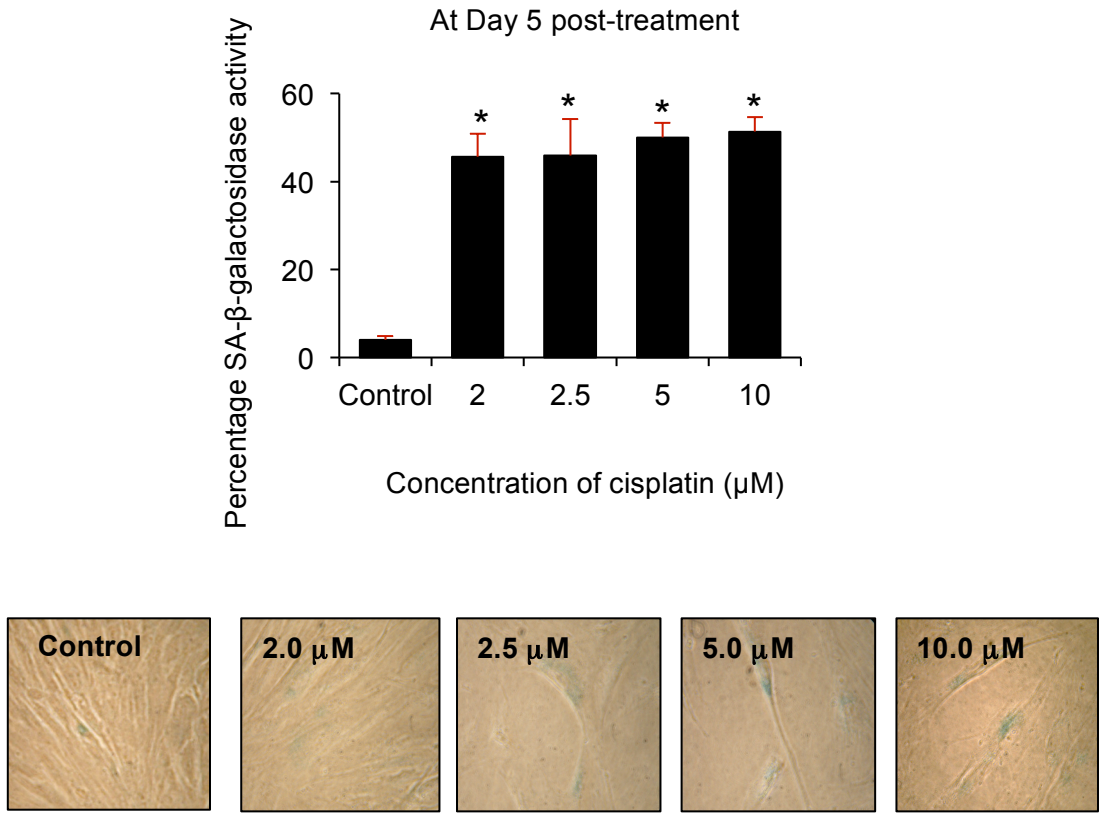

Figure 3.1.1.4: Cisplatin induces premature senescence of primary human oral fibroblasts. Both low and high doses of cisplatin induce premature senescence of primary oral fibroblasts observed as early as day 5 post-treatment by increased percentage of senescence associated β-galactosidase (SA-β-Gal) activity. All images were taken at either 20X or 40X magnifications using light microscope. N=1, in triplicate, *p<0.05, paired student t-test.

A.i. Presenescent control ii. Cisplatin induced

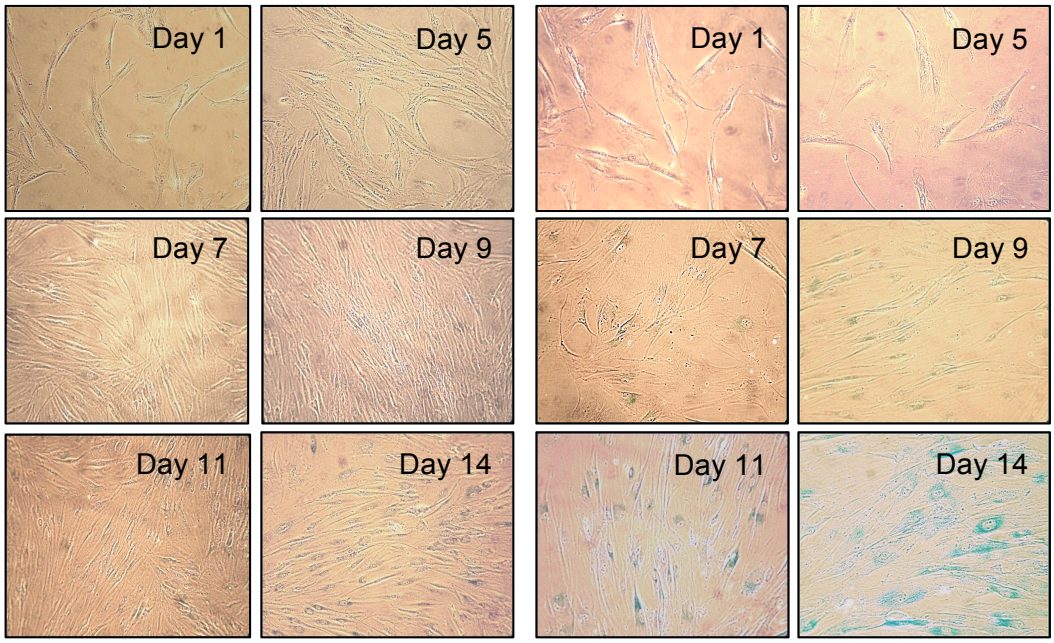

B.

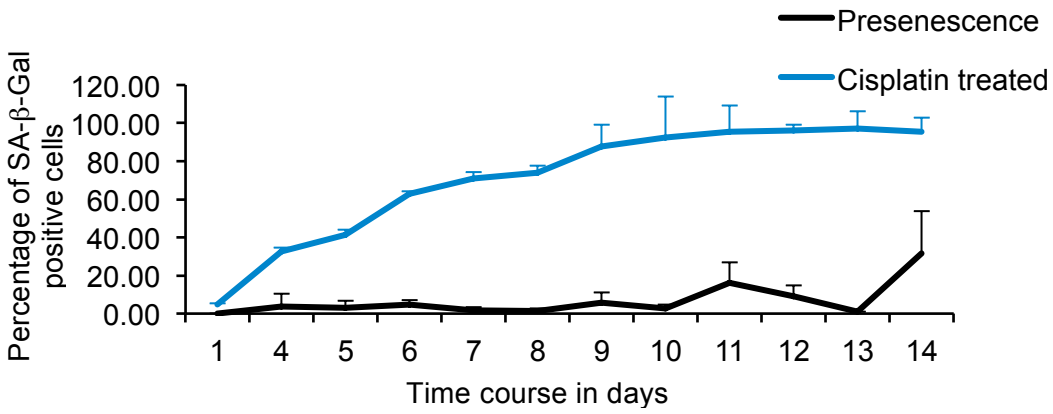

Figure 3.1.1.5: Cisplatin causes progressive development of premature senescence in human primary oral fibroblasts. Treatment of primary human oral fibroblasts with cisplatin causes them to senesce gradually with time compared to untreated presenescent control manifested as gradual accumulating blue cells (A & B). All images were taken at 20X magnifications using light microscope. N=1, in triplicate.

A.

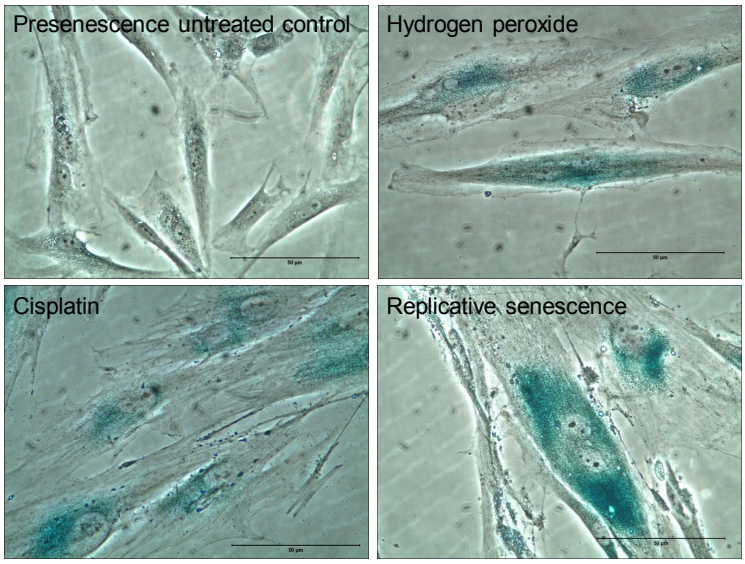

B.

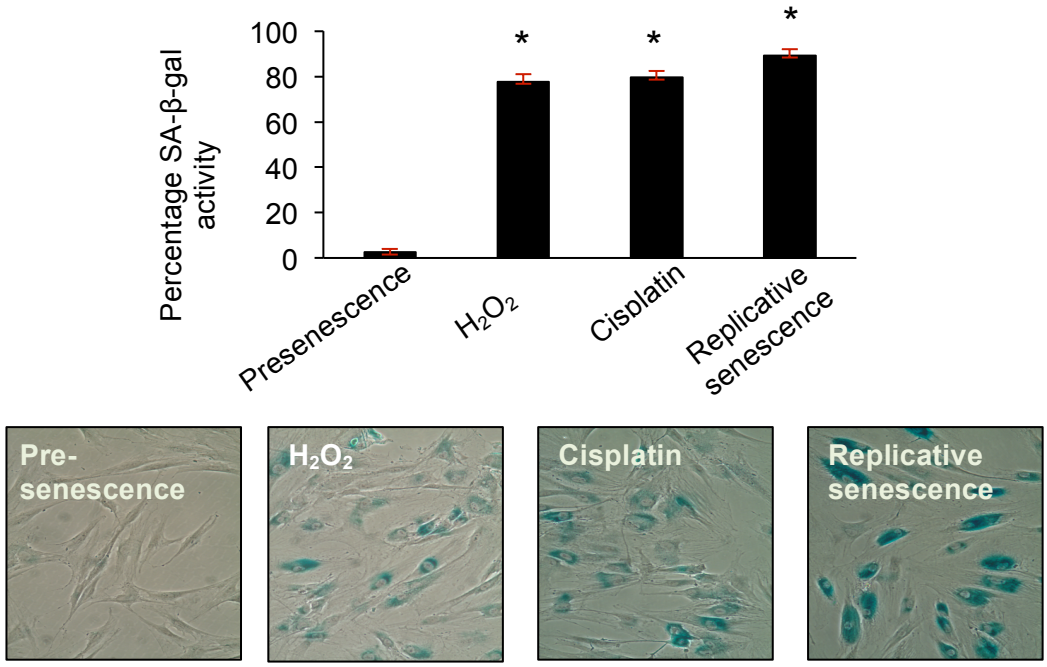

Figure 3.1.1.6: Senescent human primary oral fibroblasts demonstrate increased SA-β-Gal activity. H_2O_2 and cisplatin induce premature senescence in human primary oral fibroblasts and like replicative senescent cells they exhibit an enlarged flattened morphology with granular cytoplasm and micronuclei (A). The presenescent controls appear smaller and unstained (A). The graph illustrates a quantitative measure of percentage SA-β-Gal activity as mean + SEM (B). N=4, in triplicate, *p<0.05, One-way ANOVA with post-hoc Holm-Sidak corrections.

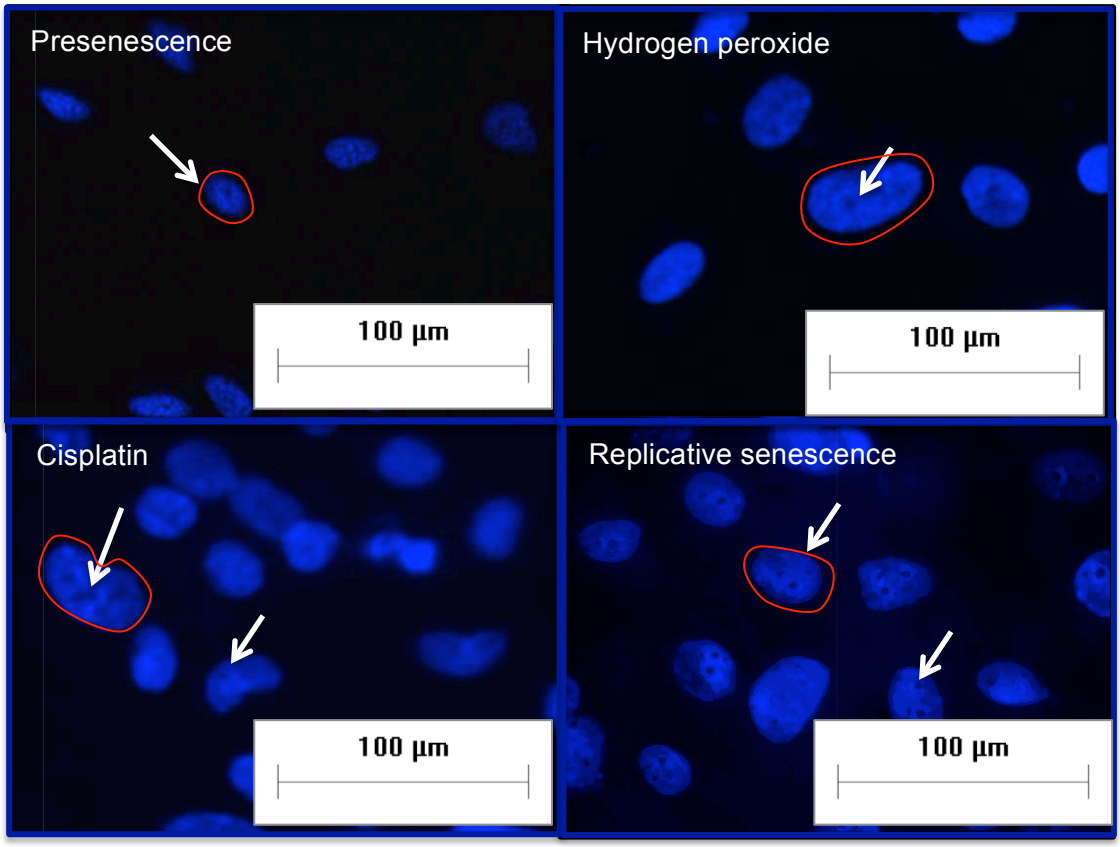

Figure 3.1.1.7: Senescent oral fibroblasts display heterochromatin formation. DAPI was used to stain nuclei of both senescent and presenescent control oral fibroblasts. The nuclei of control fibroblasts are smaller than senescent cells (encircled in red). Heterochromatin formation is observed in senescent oral fibroblasts as visible nuclear clumps surrounding darker active area of euchromatin (indicated by white arrow). The images were captured at 100X magnification using fluorescence microscope. Scale bar = 100 µM.

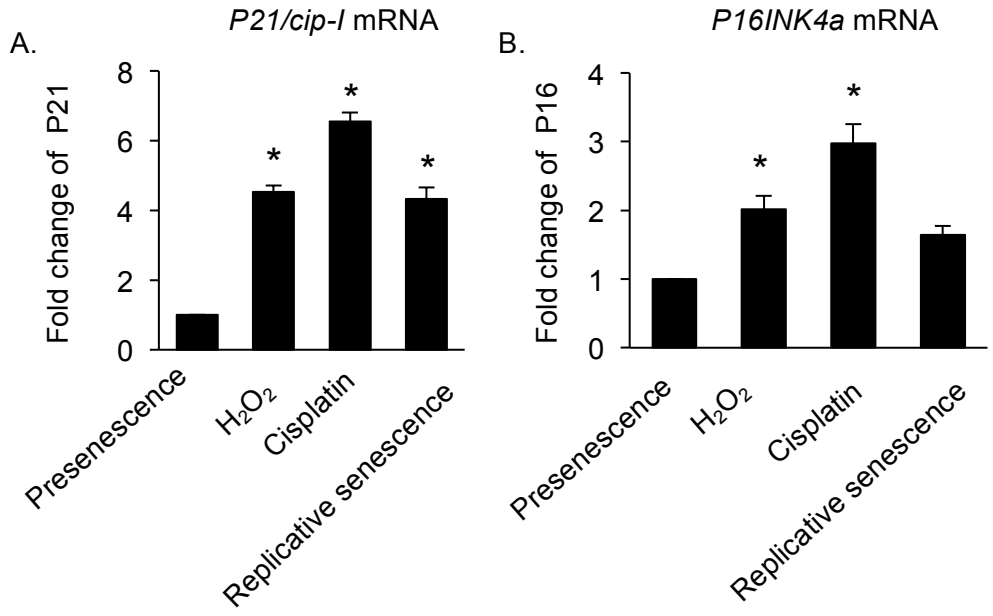

Figure 3.1.1.8: Determination of expression of cyclin dependent kinase inhibitors p21 and p16 in senescent oral fibroblasts by qRT PCR. Increased expression of cyclin dependent kinase inhibitors; p21, n=5 (A) and p16, n=4 (B) mRNA were observed in senescent oral fibroblasts compared presenescent control. ΔΔCt values were normalized to U6 internal control. Data is presented as mean + SEM. All experiments were done in triplicate. *$p<0.05$, one-way ANOVA with post-hoc correction by Dunn's method.

3.1.2: H_2O_2 and cisplatin induced premature senescent oral fibroblasts display a pro-inflammatory SASP

H_2O_2 and cisplatin induce growth arrest in cells primarily by instigating a persistent DDR through either generation of ROS or formation of inter-strand or intra-strand DNA-DNA or DNA-protein crosslinks, respectively (Chen *et al*., 1995; Siddik, 2003). A transient DNA damage lasting about 10 h is reversible wherein cells usually remain quiescent until DNA damage is repaired and these cells re-enter the cell cycle (Rodier *et al*., 2009). A persistent DNA damage lasts for more than 24 h, which may extend to several days and even months. This is physiologically irreversible and the cells exit cell cycle reaching a state of permanent growth arrest described as senescence (Rodier *et al*., 2009).

Severe form of irreversible DNA damage constitutes DNA double stranded breaks (DDSBs) (Campisi and d'Adda di Fagagna, 2007). Once a DDSB is perceived by sensors, the upstream kinases of DDR pathway such as ATM become activated which subsequently phosphorylates γH2AX and adapter molecule 53BP1, which then localize in DDSBs that can be visualized as microscopic foci in nuclei (Campisi and d'Adda di Fagagna, 2007). Further development of SASP correlates with the type of genotoxic stress and is associated with the magnitude and duration of DDR (Coppe *et al*., 2008a; Rodier *et al*., 2009). Therefore before characterising SASP it was necessary to determine if H_2O_2 and cisplatin induced premature senescence in oral fibroblasts by stimulating a persistent DDR. To address this, immunofluorescence cytochemistry for human 53BP1 was done to observe development of senescence associated DNA damage foci in the nuclei of senescent cells at 30 m and 24 h post-treatment. Both H_2O_2 and cisplatin induced several 53BP1 foci (>20 DNA damage foci; DDF) in the nuclei of fibroblasts as early as 30 m post-treatment visible as multiple fluorescent green specks (figure 3.1.2.1.B & C). The nuclei of presenescent control cells did not display immunoreactivity (figure 3.1.2.1.A). The 53BP1 foci (>2 persistent DDF)

persisted as long as 24 h after treatment (figure 3.1.2.1.D & E), suggestive of irreparable DDSB and persisting DDR signal (Rodier *et al*., 2009) while the nuclei of presenescent control remained negative as before (figure 3.1.2.1.D). This observation confirmed that both H_2O_2 and cisplatin induced senescence of human oral fibroblasts partly by triggering a persistent DDR signal. 53BP1 is known to recruit check-point proteins and TP53; a downstream effector kinases of DDR pathway (Campisi and d'Adda di Fagagna, 2007). P21 is a downstream product of activated TP53. Therefore this finding further substantiated the previous observation of elevated levels of p21 mRNA in senescent oral fibroblasts. The reduction of DDF at 24 h in H_2O_2 and cisplatin treated fibroblasts in comparison to 30 m specifies that a significant amount of DNA damage had been repaired since the time of treatment to 24 h. However previous assessment of cell proliferation capacity and development of senescence as illustrated in figure 3.1.1.3.A and 3.1.1.6 demonstrated attainment of both permanent growth arrest and senescence in these cells. Recent evidence suggests that factors secreted by senescent cells can also reinforce senescence in neighbouring cells by both paracrine and autocrine mechanisms (Acosta *et al*., 2013; Wajapeyee *et al*., 2008; Kuilman *et al*., 2008) and secretion of some of these factors may not necessarily require presence of persistent DDR (Pazolli *et al*., 2012).

This observation and that reported by others confirmed that DDR signal is initiated immediately upon genotoxic stress, however, SASP develops at a much slower pace requiring about 4 to 7 days to develop post-treatment (Coppe *et al*., 2008b; Rodier *et al*., 2009; Freund *et al*., 2011). Gelatinase or matrix-metalloproteinase-2; MMP-2, is a well characterized protease among SASP factors which is known to promote invasiveness of various cancer cell lines *in vivo* and *in vitro* (Davalos *et al*., 2010). The proteolytic activity of secreted MMP-2 can be easily visualized and quantified using a modified protein gel electrophoresis containing gelatin as substrate (described in

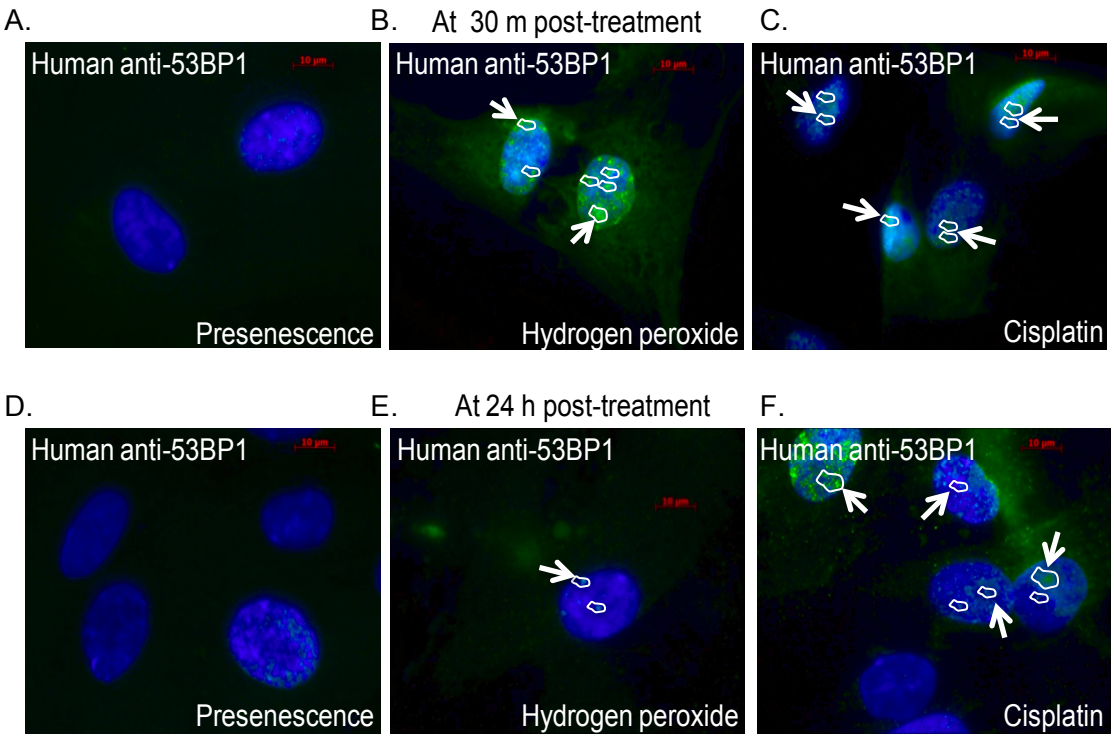

Figure 3.1.2.1: H_2O_2 and cisplatin induce persistent DNA damage in human primary oral fibroblasts. 50,000 cells were seeded on sterile glass coverslips into each well of a 12-well flask. The cells were then treated with either H_2O_2 or cisplatin as described in methods and fixed with 4% paraformaldehyde at 30 m and 24 h post-treatment. Immunofluorescence immunocytochemistry using human anti-53BP-1 antibody demonstrated accumulation of multiple fluorescent green foci within nuclei of H_2O_2 (B & E) and cisplatin (C & F) treated human oral fibroblasts as soon as 30 m after treatment (B & C) and continued to last until 24 h post-treatment (E & F) indicated by white arrows and circles. The nuclei of presenescent control cells demonstrated no such defined foci (A & D).

method, section 2.4). To understand the duration required for SASP development in human oral fibroblasts conditioned media were collected from both H_2O_2 and cisplatin induced premature senescent oral fibroblasts at different time-points commencing from day 1 until day 15 post-treatment. Conditioned media from presenescent oral fibroblasts was used as control.

It was observed that normal human oral fibroblasts secreted MMP-2 at basal level producing a faint gelatinolytic band of 72 kDa in control samples (figure 3.1.2.2). In contrast both cisplatin and H_2O_2 induced senescent oral fibroblasts demonstrated gradual increase in secretion of MMP-2 over time (figure 3.1.2.2.A, B & C). The 72 kDa band corresponds to pro-forms of secreted MMP-2 levels, which retain its catalytic properties. In addition the senescent samples also produced a gelatinolytic band of 130 kDa that became visible on day 7 and persisted until day 11 after which it disappeared. This band may correspond to either MMP-2 dimers or a neutrophil lipocalin complexed pro-MMP-9 (NLP-MMP-9) reported to have a molecular weight of 130 kDa (Hartog *et al*., 2003). Occasionally sometimes another gelatinolytic band became visible at 60 kDa, which is likely to represent the mature form of MMP-2 in the senescent samples. Since the experiment was carried out in 6-well plates and the number of cells in presenescent control wells continued to proliferate with time, conditioned media from only day 5 presenescent samples were used as control.

To quantify the secreted MMP-2 protein levels relative band densitometry was performed and the band density was normalized to the cell number per sample. It was observed that similar to SA-β-Gal activity secreted levels of MMP-2 began to peak at day 5, which correlated with development of senescence (figure 3.1.2.2.D & figure 3.1.1.5.C). The graph had a sinusoidal distribution implying that secretion of MMP-2 is modulated at different time-points and therefore it is not a stable phenotype. At day 5 after treatment both H_2O_2 and cisplatin induced senescent oral fibroblasts secreted

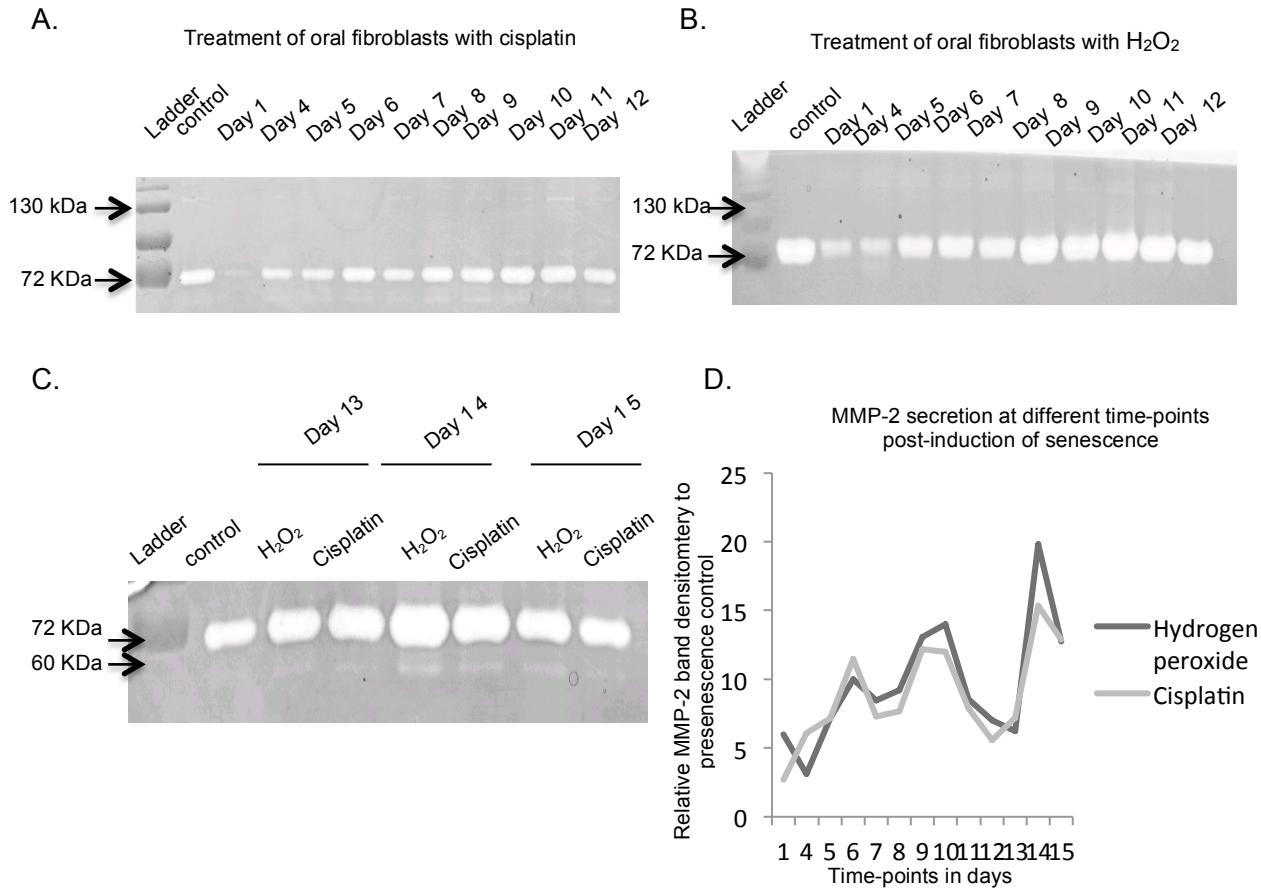

Figure 3.1.2.2: Prematurely senescent human primary oral fibroblasts demonstrate a progressive increase in secreted level of MMP-2 over time which runs in parallel to development of senescence and SASP. Gelatin zymogram showed that both cisplatin (A & C) and hydrogen peroxide (B & C) treated primary human oral fibroblasts displayed a gradual development of senescence associated secretory phenotype (SASP) measured by increase in secretion of MMP-2 over time and quantification of this using relative band densitometry illustrates that this enhancement of MMP-2 secretion lines in parallel to the development of SA-β-Gal activity (D) as observed before.

7-times more MMP-2 than control. At day 10, a second peak was observed during which secretion of MMP-2 was increased by 14-times in H_2O_2 and 12-times in cisplatin induced senescent oral fibroblasts than control cells. A third peak of secreted MMP-2 was noted at day 14 which were 20-fold and 15-fold higher in H_2O_2 and cisplatin induced senescent oral fibroblasts, respectively, compared to control (figure 3.1.2.2.D). These findings confirmed that both H_2O_2 and cisplatin induced gradual development of senescence and SASP in human primary oral fibroblasts.

To rule out the possibility that the elevation of secreted MMP-2 observed in cisplatin and H_2O_2 treated oral fibroblasts was merely an effect mediated by the drugs (distinct from inducing senescence), secreted MMP-2 levels were further determined and compared to that of replicative senescent oral fibroblasts. This time the concentrated conditioned media were initially diluted according to the cell number of fibroblasts, to normalize for the amount of secreted soluble factors, using dd H_2O before loading them into respective wells for performing gelatin zymography. It was observed that both cisplatin and H_2O_2 induced premature senescent oral fibroblasts secreted 2.2-times and 2.0-times more MMP-2 than presenescent control fibroblasts, respectively ($n=5$, $p<0.05$) and in a similar manner replicative senescent oral fibroblasts secreted 2.6-times more MMP-2 than control fibroblasts ($n=5$, $p<0.05$) (figure 3.1.2.3.A).

All samples produced gelatinolytic bands at 72 kDa, indicating that the pre-form of MMP-2 is the predominant protein secreted by senescent fibroblasts. Dilution of conditioned media to soluble factors caused only the replicative senescent oral fibroblasts to produce gelatinolytic bands at 130 kDa and 60 kDa, suggesting that these cells secreted more of either MMP-2 dimers or NLP-MMP-9 and mature MMP-2 than stress-induced premature senescent fibroblasts as shown before in figure 3.1.2.3.A.

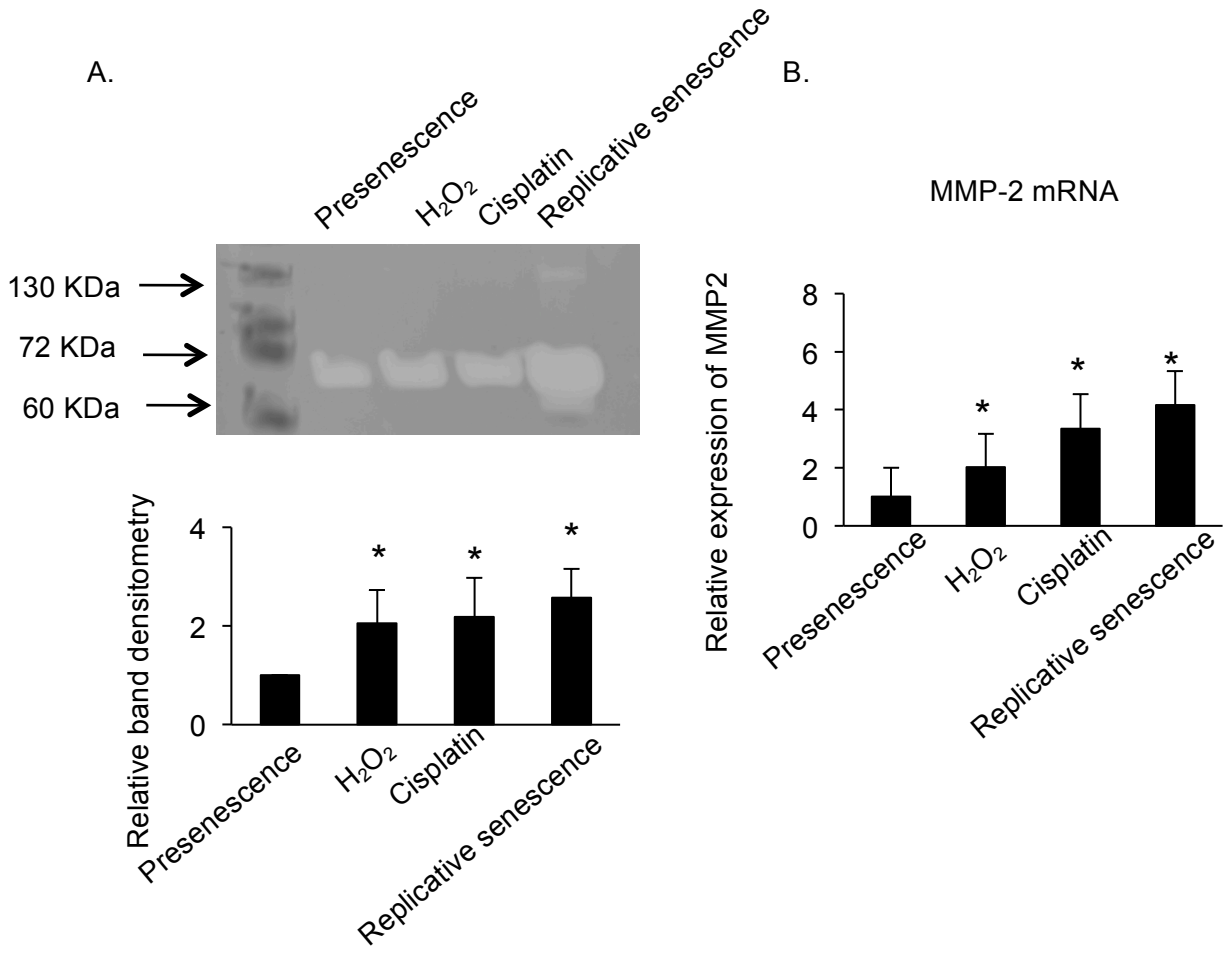

Figure 3.1.2.3: Senescent oral fibroblasts synthesize and secrete MMP-2. Conditioned media were collected from senescent and presenescent oral fibroblasts at specified time-points as described in methods and concentrated using spin columns. The concentrated conditioned media were then diluted according to cell density with distilled water and equal volumes of conditioned media were loaded into protein gel (A). Increasing thickness and lighter bands represent greater amount of secreted MMP-2 as illustrated by band densitometry, N=5 (A). qRT-PCR showed elevated transcripts of MMP-2 mRNA in senescent oral fibroblasts than presenescent control, N=5 in triplicate (B). Data represents mean + SEM of fold change as measured from ΔΔCt normalized to U6 endogenous control (B). *$p<0.05$, one-way ANOVA with post-hoc correction by Dunn's method.

As measurement of relative band density does not reflect the actual quantity of secreted protein due to band saturating effect (as observed in replicative senescent cells) and fail to demarcate pre-synthesized sequestered proteins from newly synthesized proteins by cells upon attainment of senescence, qRT-PCR was performed to determine MMP-2 transcript levels in both senescent and presenescent control fibroblasts. It was observed that in contrast to presenescent control both H_2O_2 and cisplatin induced premature senescent oral fibroblasts expressed significantly more MMP-2 mRNA which were 2-fold and 3-fold higher than control, respectively. Replicative senescent oral fibroblasts also expressed 4-fold higher MMP-2 mRNA than control fibroblasts ($n=5$, $p<0.05$).

Therefore in agreement with previous groups (Davalos *et al*., 2010; Liu and Hornsby, 2007b; Copper *et al*., 2008b) it was confirmed that senescent oral fibroblasts were metabolically active and capable of actively transcribing and secreting proteins (under this circumstances MMP-2 and possibly MMP-9), which may reprogram and remodel the surrounding tissue microenvironment to either suppress or promote tumour formation.

Senescent cells secrete over forty different pro-inflammatory proteins (Coppe *et al*., 2008b) however their type and function varies according to the context of tissue and the inciting stimuli. Until now no group has reported about the secretome developed by human primary oral fibroblasts subjected to cisplatin treatment. In order to determine the secretome of cisplatin induced premature senescent oral fibroblasts the cells were treated with cisplatin for 24 h (described in section 2.2). Untreated presenescent cells were used as control. Analysis of conditioned media using human cytokine array 6 (section 2.15) showed that in contrast to presenescent control, cisplatin-induced premature senescent oral fibroblasts secreted more pro-inflammatory cytokines such as IL-6, MCP-1, MCP-2, IL-4, growth factors such as IGFBP-1, -2, and -4, angiogenin, cytokines belonging to the TGFβ superfamily which were crucial during embryonic

development such as BMP-4 and -6 (Storer *et al*., 2013) and many more contributing to 35% (21 out of 60) of the secreted factors (figure 3.1.2.4). Similarly secretion of pro-fibrotic cytokines such as TGF-β_1, TGF-β_3 and PDGF-BB and pro-proliferative and pro-angiogenic cytokine SDF-1 (Begley *et al*., 2005) were reduced in cisplatin-induced premature senescent oral fibroblasts in contrast to presenescent control contributing to about 12% of the secreted cytokines (figure 3.1.2.4). More than 50% of the secreted cytokines remained unaltered between presenescent control and cisplatin-induced premature senescent oral fibroblasts. These included the pro-inflammatory cytokines IL-1 α and IL-1 β; established to have roles in reinforcement of cellular senescence and SASP (Acosta *et al*., 2013), anti-inflammatory cytokines such as IL-1ra and IL-10, and growth factors such as FGF-7 known to mediate pro-tumourigenic cross-talk between senescent prostatic epithelial cells and neighbouring fibroblasts (Castro *et al*., 2004) and many more (figure 3.1.2.4).

Some variations in the secreted level of cytokines from those reported by previous research groups may be explained by the effect of oxygen saturation on SASP. All the experiments in this thesis were carried out at 20% oxygen saturation whereas those reported by some authors were carried out at either physiological oxygen saturation, which is 3% (Coppe *et al*., 2008b; Acosta *et al*., 2013) or under hypoxic state (Taddei *et al*., 2014). Other factors, which plausibly influenced SASP development in this study include the type of tissue used (gingival fibroblasts), the choice of chemotherapy for senescence induction (cisplatin) and lastly the time-point at which SASP was measured (day 15 post-treatment). Otherwise all other findings corroborated with those that had been previously reported (reviewed by Davalos *et al*., 2010).

Two cytokines, IL-6 and MCP-1, which were up-regulated in the cytokine array were selected for further validation. Many research groups have used elevated secretion of IL-6 by senescent cells as a marker of SASP (Acosta *et al*., 2008; Castro *et al*., 2004;

Bhaumik *et al*., 2009). To confirm that the increased secretion of IL-6 observed in cisplatin treated oral fibroblasts was due to establishment of senescence and SASP, the expression of IL-6 were determined in different modes of senescent oral fibroblasts at both mRNA and protein level. qRT-PCR demonstrated that both H_2O_2 and cisplatin treated oral fibroblasts expressed significantly more IL-6 transcripts; about 2.7-fold and 2.4-fold higher than control, respectively ($n=3$, $p<0.05$; figure 3.1.2.5.A). In contrast replicative senescent cells expressed lesser amount of IL-6 mRNA which was 0.5-times the value of control cells (figure 3.1.2.5.B).

Alternatively ELISA for human IL-6 demonstrated that conditioned media from all kinds of senescent oral fibroblasts contained significantly higher quantity of IL-6 than control cells ($n=3$, $p<0.05$; figure 3.1.2.5.B). It was observed that both H_2O_2 and cisplatin induced premature senescent oral fibroblasts secreted 2.7-times (1.36 ng/mL) and 2.8 times (1.38 ng/mL) more IL-6 than presenescent control (0.5 ng/mL) (figure 3.1.2.5.B). Although replicative senescent oral fibroblasts had lower levels of IL-6 transcripts, they secreted significantly more IL-6 in to the conditioned media than other mode of senescent oral fibroblasts and was 4-times (2.0 ng/mL) higher than control (figure 3.1.2.5.B).

Similar trends were noticed during comparing expression of MCP-1 between presenescent and senescent oral fibroblasts. Both H_2O_2 and cisplatin induced premature senescent oral fibroblasts expressed 6.6-fold higher MCP-1 mRNA transcripts than presenescent control ($n=5$, $p<0.05$, figure 3.1.2.6.A). Replicative senescent oral fibroblasts had 1.8-fold higher levels of MCP-1 mRNA than controls. Quantification of secreted MCP-1 by human MCP-1 ELISA demonstrated that both H_2O_2 and cisplatin induced premature senescent oral fibroblasts secreted 4.2-times (1.871 ng/mL) more MCP-1 than control fibroblasts. Replicative senescent oral fibroblasts secreted comparatively more MCP-1 about 5.2-times (2.328 ng/mL) higher than control fibroblasts (0.446 ng/mL) ($n=3$, $p<0.05$, figure 3.1.2.6.B).

A.

Presenescence

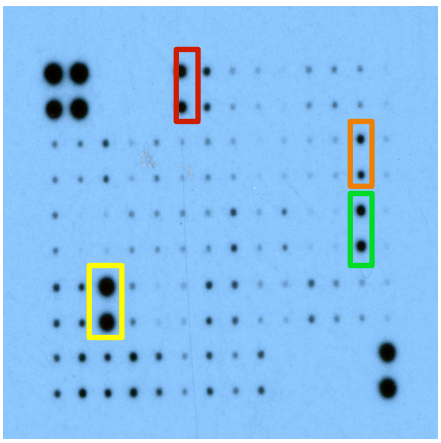

B.

Cisplatin induced premature senescence

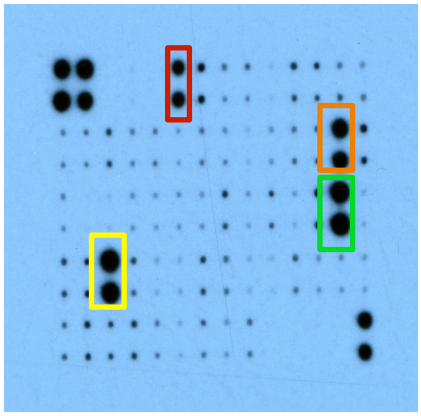

C.

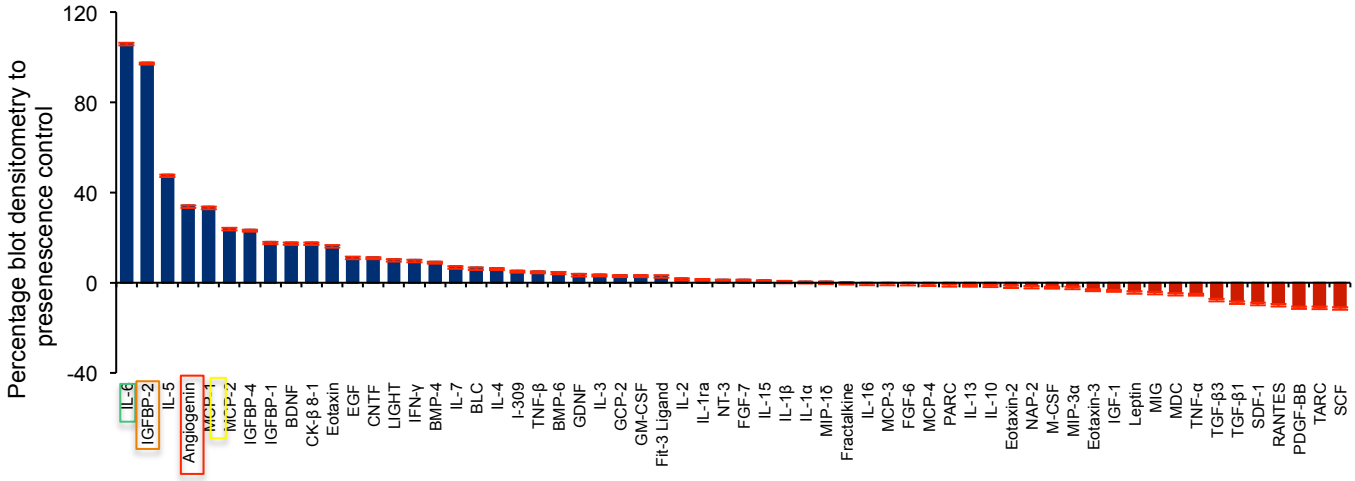

Figure 3.1.2.4: Cytokine secretome profile of cisplatin induced premature senescent oral fibroblasts. Human cytokine antibody array 6 was used to determine and compare the expression of 60 different secreted cytokines in conditioned media derived from cisplatin induced premature senescent oral fibroblasts (B) and control (A). Relative band densitometry illustrates the differences in percentage of secreted cytokine in cisplatin induced premature senescent oral fibroblasts after normalizing the band density to presenescent control (C). IGFBP-2 and angiogenin served as positive controls. N=2, in duplicate.

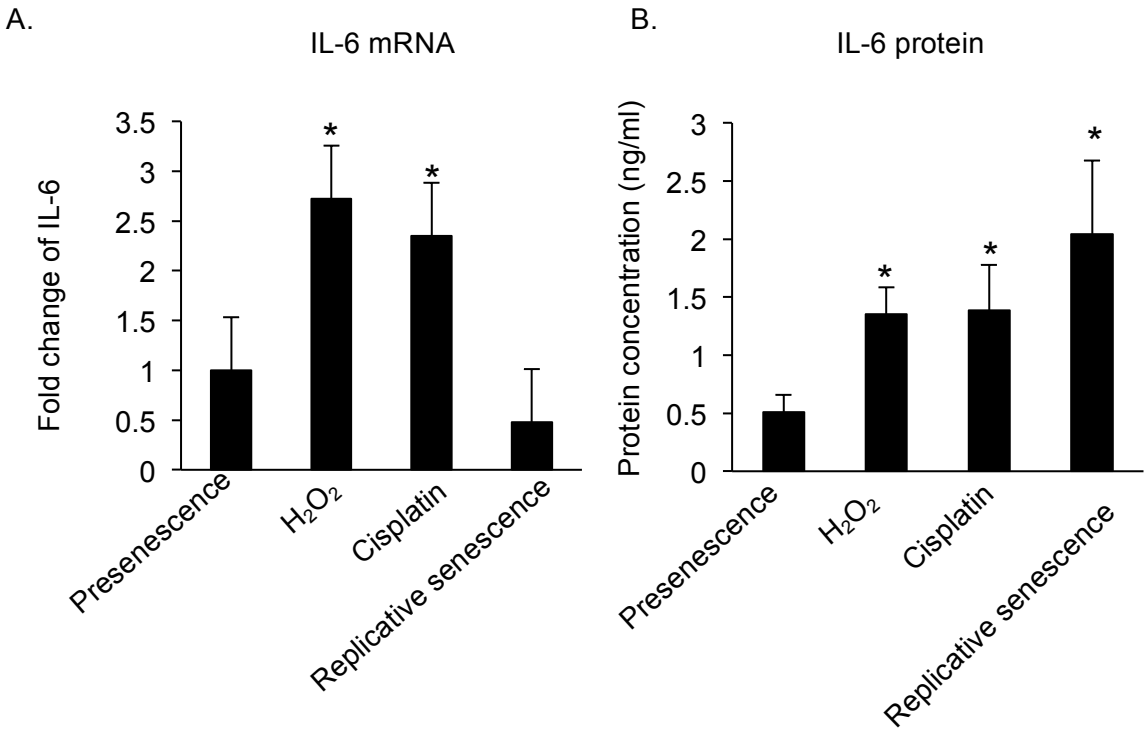

Figure 3.1.2.5: Human senescent oral fibroblasts demonstrate elevated expression of IL-6. qRT-PCR analysis delineated a significant increase and an insignificant decrease in IL-6 mRNA expression in premature senescent and replicative senescent oral fibroblasts than in control cells respectively. The graph represents mean of fold change measured from ΔΔCt + SEM (A). Conditioned media from both senescent and presenescent oral fibroblasts were collected, diluted according to cell density and used to assess the amount of secreted IL-6 by ELISA (B). The graph illustrates a significant increase in IL-6 secretion in senescent fibroblasts relative to control. The data represents mean protein concentration + SEM. N=3, in triplicate, *$p<0.05$, one-way ANOVA with post-hoc correction by Dunn's method.

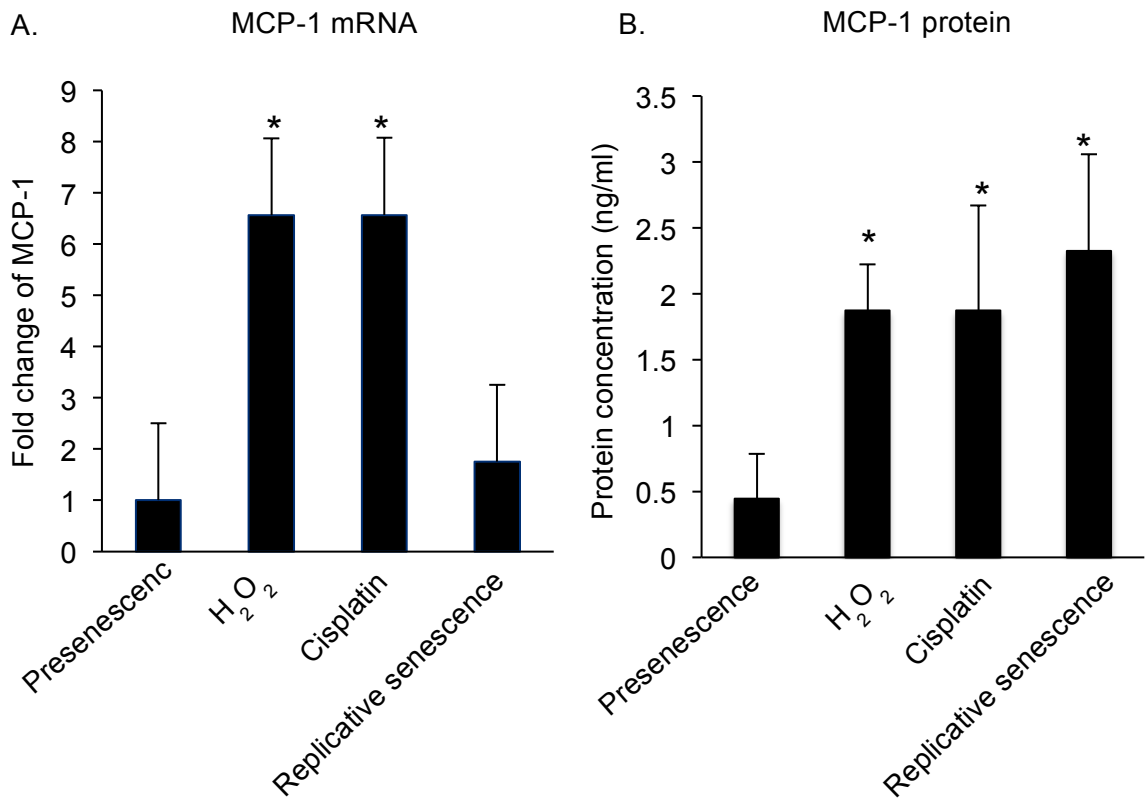

Figure 3.1.2.6: Human senescent oral fibroblasts demonstrate elevated expression of MCP-1. qRT-PCR analysis depicted a significant increase in MCP-1 mRNA expression in premature senescent oral fibroblasts than in control cells. Replicative senescent fibroblasts also demonstrated an increased transcription of MCP-1 but this was insignificant. The graph delineates mean fold change + SEM (A). Conditioned media from both senescent and presenescent oral fibroblasts were collected, diluted according to cell density and used to assess the amount of secreted MCP-1 by ELISA (B). The graph shows a significant increase in MCP-1 secretion by senescent oral fibroblasts relative to control. The data represents mean protein concentration + SEM. N=3, in triplicate. *$p<0.05$, one-way ANOVA with post-hoc correction by Dunn's method.

From these data it is unclear why the IL-6 and MCP-1 mRNA levels in replicative senescent oral fibroblasts does not correspond to protein levels as observed with premature senescent oral fibroblasts. One way of rationalizing this may be due to the fact that replicative senescent oral fibroblasts represent an end stage of senescence fate, a point of no return wherein the mitogenic peptides present in the serum fail to stimulate transcription of these cytokines or else there may be other factors present in these cells which may cause the mRNAs of both IL-6 and MCP-1 to be either rapidly translated or degraded. For instance, gene silencers such as miRNAs can negatively regulate the mRNAs of these cytokines. Moreover it is also possible that these mRNAs are unstable due to increased destructive signalling from AU-rich elements (Brennan and Steitz, 2001). Furthermore recent evidence suggests that senescent cells have deregulated proteasomal degradation of proteins (Chondrogianni *et al*., 2003). Therefore may be in replicative senescent cells the disruption of protein metabolism (in this case IL-6 and MCP-1) plausibly leads to their increased accumulation and secretion despite reduced level of transcription and this may regulate composition of SASP in aged cells.

3.1.3: Conclusion

Here it is shown that primary human oral fibroblasts can undergo premature senescence in response to sub-cytotoxic doses of genotoxic stimuli such as cisplatin and H_2O_2 and by replicative exhaustion. Senescent oral fibroblasts have higher SA-β-Gal activity and elevated levels of CDKIs, p21 and p16, compared to presenescent control cells.

Senescent oral fibroblasts have enlarged nuclei with formation of distinctive heterochromatin and exhibit DDSB. Moreover stress-induced premature senescent oral fibroblasts also gradually develop a pro-inflammatory SASP, a hallmark of senescence. Both H_2O_2 and cisplatin induced premature senescent oral fibroblasts have increased transcripts of IL-6 and MCP-1 that correspond to their high secretory levels. Replicative senescent oral fibroblasts, however, have lower transcript levels of both IL-6 and MCP-1 but secrete more of these proteins into the conditioned media: the reasons for this discrepancy remain to be explicated. All senescent oral fibroblasts secrete significantly more MMP-2 into the conditioned media than young control fibroblasts.

SASP was reported to contribute to the development of late-life cancer and stimulate malignant progression of indolent tumours particularly in cancers of breast and prostate (Castro *et al.*, 2004; Parrinello *et al.*, 2005). The role of SASP in development and progression of head and neck cancer, however, is poorly understood. As a result, next, the effects of SASP of senescent oral fibroblasts in modulating malignant behaviour of oral pre-cancerous and cancerous cell lines were investigated.

Chapter 3.2: SASP mediated cross-talk between oral fibroblasts and oral dysplastic and cancer cells, and monocytes

Hypothesis:

1. Senescent oral fibroblasts develop a pro-tumourigenic SASP by which these cells stimulate proliferation, migration and invasion of oral dysplastic and cancer cell lines *in vitro*.
2. Senescent oral fibroblasts recruit monocytes into the tumour microenvironment and stimulate their polarization.
3. Senescent oral fibroblasts represent a subset of activated fibroblasts and can be reprogrammed by cancer cells to foster tumour progression.

Aims and objectives:

A. Investigation of effects on cancer cells

- To determine the paracrine effect of senescent oral fibroblasts on proliferation and migration of oral dysplastic cell line D20 and OSCC-derived cell lines SCC4 and H357 in 2D *in vitro* assay.
- To determine if senescent oral fibroblasts stimulate invasion of OSCC-derived cell line H357 in 2D and 3D *in vitro* assay and if this is associated with EMT-like changes.

B. Investigation of effect on THP-1 monocytes and macrophages

- To determine if SASP of senescent oral fibroblasts could recruit monocytes.

- To investigate if conditioned media from senescent oral fibroblasts could polarize THP-1 derived macrophages

C. Investigation of the role of MCP-1 in SASP mediated stromal-tumour cross-talk

- To investigate if MCP-1 secreted by senescent oral fibroblasts can stimulate migration and invasion of OSCC cell line H357 in 2D and 3D assay.

D. Investigation of the activated nature of senescent oral fibroblasts

- To examine expression of fibroblast activation marker; α-SMA, in senescent oral fibroblasts.
- To determine if the inflammatory nature of senescent oral fibroblasts could be modulated by cancer cells *in vitro*.

3.2.0: Paracrine effects of SASP

The functional effects of SASP have been studied for many years. While it reinforces senescence in the neighbouring bystander non-senescent homologous population of same cell type, it encourages malignant transformation of surrounding pre-cancerous and less aggressive cancerous cells in paracrine fashion (Kuilman *et al*., 2008; Acosta *et al*., 2013, Wajapeyee *et al*., 2008; Davalos *et al*., 2010). Both senescent and presenescent fibroblasts promote growth and survival of normal epithelial cells to the same extent without any impact on their neoplastic transformation (Krotolica *et al*., 2001, Coppe *et al*., 2008a; Lawrenson *et al*., 2010). Cumulative evidence implies that this growth stimulatory effect of senescent fibroblasts on normal epithelial cells may be a consequence of SASP-mediated alteration of genes regulating normal epithelial differentiation, a common example being the use of irradiated fibroblasts as feeder cells to enhance formation of epithelial sheets by primary keratinocytes (Bisson *et al*., 2013). Further the biological roles of SASP in either tumour suppression or tumour promotion depend on tissue context; that is senescence in epithelial compartment may suppress tumour formation by ceasing multiplication of mutated cells while the same senescent epithelia can reprogram, activate and induce senescence in neighbouring fibroblasts in paracrine manner which subsequently stimulate growth of neighbouring non-senescent epithelia and encourage tumour formation (Castro *et al*., 2003, Castro *et al*., 2004). Furthermore such reciprocal paracrine cross-talk between senescent and non-senescent cell populations are only favoured when cells from two different compartments are involved meaning senescent fibroblasts only stimulate growth of non-senescent epithelia but not fibroblasts and the reverse also holds true (Picard *et al*., 1986; Camps *et al*., 1990).

In this study it was demonstrated in chapter 3.1.1 that cisplatin, a drug routinely used in treatment of solid tumours of head and neck (Huang *et al*., 2011) induced senescence and SASP in human primary oral fibroblasts. Therefore to comprehend the functional

consequences of SASP of oral fibroblasts their effect on proliferation (section 2.18.1.B), migration and invasion (section 2.18.2) of oral precancerous and cancerous cell lines were thoroughly investigated in both 2D and 3D (section 2.18.3.2) *in vitro* assays.

3.2.1: Soluble factors from premature and replicative senescent oral fibroblasts stimulated proliferation and migration of oral dysplasia-derived cell lines *in vitro*

Soluble factors derived from H_2O_2 and cisplatin induced premature senescent oral fibroblasts and replicative senescent oral fibroblasts significantly stimulated proliferation of human oral dysplastic cell line D20 *in vitro* compared to conditioned medium from presenescent fibroblasts and growth factor depleted serum free media controls (n=3, $p<0.001$; figure 3.2.1.A). Among the senescent fibroblasts, conditioned media derived from H_2O_2-treated oral fibroblasts had the greatest impact on enhancing proliferation of D20 cell lines followed by cisplatin-induced premature senescent cells and then replicative senescent cells (n=3, $p<0.001$; figure 3.2.1.A). There was no notable difference in the rate of proliferation of D20 cells in response to conditioned medium from presenescent oral fibroblasts and serum free media, both of which produced minimal growth stimulatory effects (figure 3.2.1.A). There was a dramatic increase in the rate of cell proliferation after addition of conditioned media from senescent fibroblasts both at 24 h and at 48 h (n=3, $p<0.001$; figure 3.2.1.A). Between 48 h and 72 h there was a significant declination in cell proliferation in all samples (n=3, $p=0.028$) implying that this is possibly an intrinsic property of D20 cells rather than an effect of conditioned media. Again at 96 h proliferation was restored and there was a rapid and significant increase in cell proliferation in all samples (n=3, $p=0.002$).

Conditioned media from senescent oral fibroblasts significantly stimulated migration of D20 cells *in vitro* compared to presenescent control cells (n=3, $p<0.05$; figure 3.2.1.B). Pairwise comparison showed H_2O_2-induced premature senescent oral fibroblasts

increased migration of D20 cells by 5.8-fold (n=3, $p<0.05$; figure 3.2.1.B) whereas cisplatin- induced premature senescent oral fibroblasts stimulated migration by 3.4-fold (n=3, $p<0.05$; figure 3.2.1.B) relative to presenescent control. Replicative senescent cells also considerably increased the migration of D20 cells by 3.2-fold compared to presenescent control (n=3, $p<0.05$; figure 3.2.1.B).

There was no significant difference in the stimulatory effect of different types of senescent oral fibroblasts on migration of D20 cells.

In conclusion, both stress-induced premature senescent and replicative senescent oral fibroblasts are liable to promote neoplastic transformation in dysplastic cells by conferring them the advantage to proliferate and migrate and therefore this may influence the early cascade of events which occur at the onset of carcinogenesis.

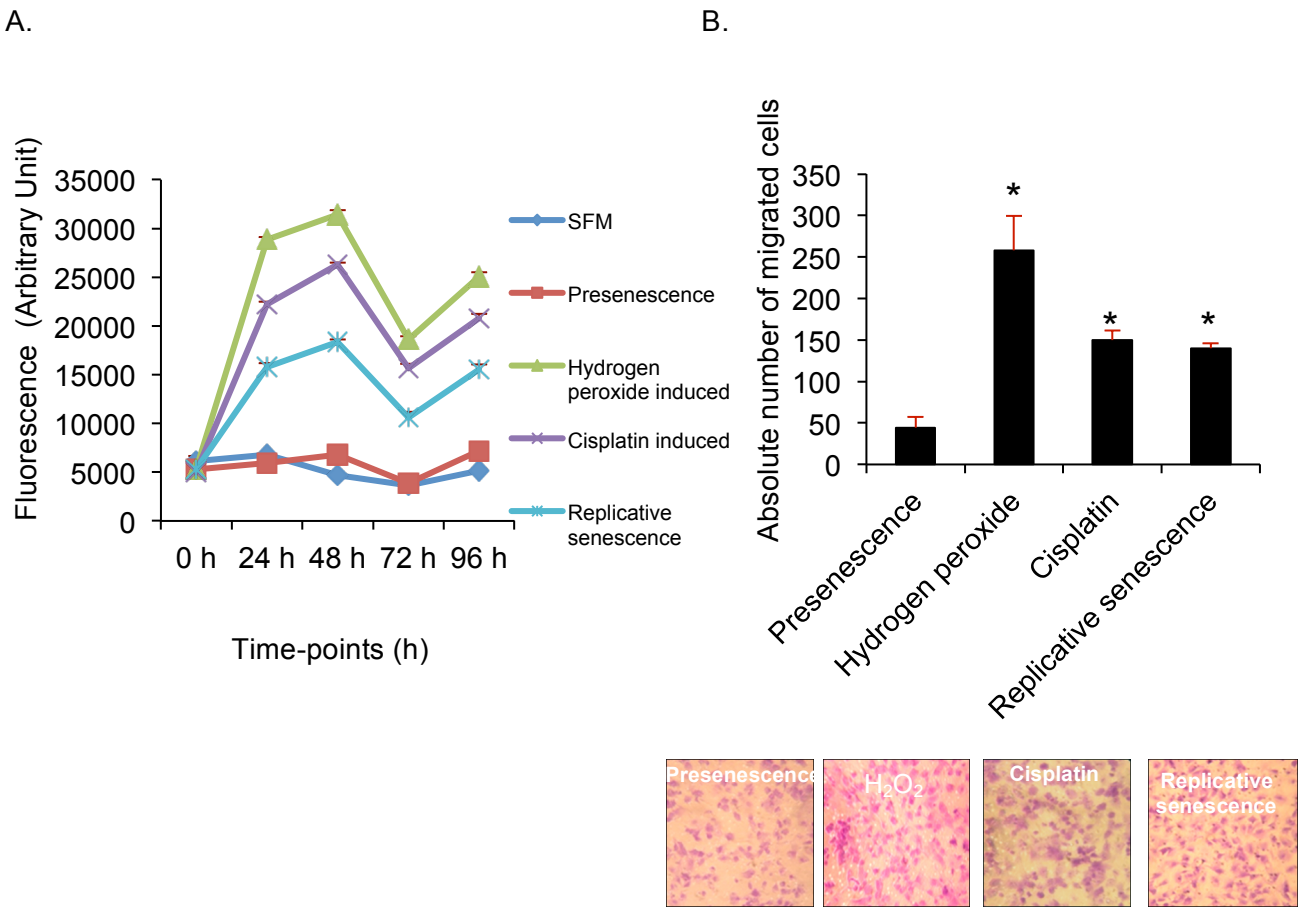

Figure 3.2.1: Human senescent oral fibroblasts stimulate proliferation and migration of preneoplastic cell line: D20 cells, derived from an oral dysplastic lesion, in paracrine fashion *in vitro*. D20 cells were seeded down at 5,000 per well in triplicate in a 96-well plate and serum starved for 24 h. Conditioned media were added after 24 h. Proliferation was measured by CyQuant NF cell proliferation kit. Two-way repeated measure ANOVA was performed with post-hoc Holm-Sidak correction (N=3, in triplicate) (A). 35,000 D20 cells were suspended in 0.1% BSA supplemented DMEM and seeded into the insert of modified Boyden's chamber migration assay and conditioned media to the bottom well. The cells were allowed to migrate for 24 h followed by fixation in 100% methanol and staining with 0.01% crystal violet. Cells from three different fields were counted per transwell as an independent measure of migrated cells. The data represents mean + SEM (B). N=3, in triplicate, *p<0.05, one-way ANOVA with post-hoc correction by Tukey test.

3.2.2: Soluble factors secreted by human senescent oral fibroblasts stimulated proliferation and migration of oral squamous cell carcinoma derived cell line SCC4 in paracrine fashion

To explore if SASP of oral fibroblasts exerted a similar mode of action on oral squamous cell carcinoma (OSCC) derived cell lines *in vitro* the effect of conditioned media of senescent oral fibroblasts on SCC4 cell proliferation and migration were investigated.

The SCC4 cell line was isolated from well-differentiated tongue squamous cell carcinoma of a 55 year old male patient who had prior treatment with methotrexate and radiotherapy (Rheinwald *et al*., 1981). Morphologically these cancer cells appear like normal human keratinocytes and are slow growing but are malignant in the sense that these cells harbor loss of function mutation of *TP53* and *CDKN2A*, form encapsulated tumours in nude mice and resist differentiation upon constraint of anchorage dependent growth (Rheinwald *et al*., 1981; Nichols *et al*., 2012).

It was observed that conditioned media from H_2O_2-induced and replicative senescent oral fibroblasts significantly stimulated proliferation of SCC4 cells compared to presenescent control fibroblasts and serum free media ($n=3$, $p<0.05$; figure 3.2.2.A). Although conditioned medium from cisplatin-treated oral fibroblasts significantly stimulated proliferation of SCC4 cells at different time-points ($n=3$, $p<0.001$; figure 3.2.2.A) however the overall stimulatory effect on SCC4 cell proliferation was insignificant when compared to presenescent control and serum free media. This may be because SCC4 cells were originally extracted from tumours previously treated with neo-adjuvant chemotherapy and possibly these surviving population of cancer cells had been subjected to a senescent microenvironment *in vivo* before they were excised (Rheinwald *et al*., 1981).

As described earlier SCC4 cells yielded non-invasive tumours in nude mice bearing young stroma. Therefore to investigate if co-existence of a senescent stroma, which mimicked the microenvironment from where these cells were extracted, modulated motility of SCC4 cells *in vitro,* 2D transwell migration assays were performed. It was observed that the senescent cells significantly stimulated the migration of SCC4 cells *in vitro* compared to presenescent fibroblasts ($n=3$, $p<0.05$; figure 3.2.2.B). Conditioned medium from replicative senescent oral fibroblasts increased migration of SCC4 cells by 5.2-fold ($n=3$, $p<0.05$), H_2O_2-induced SASP increased migration by 4.5-fold ($n=3$, $p<0.05$) and cisplatin-induced premature senescent oral fibroblasts increased migration by 3.3-fold ($n=3$, $p<0.05$; figure 3.2.2.B) compared to control.

These findings suggest that in contrast to chemotherapy-induced senescence, SASP of replicative senescent and oxidative stress induced premature senescent oral fibroblasts have a more pronounced tumourigenic effect on SCC4 cells, which may result from pre-acclimatization of SCC4 to chemotherapy. Alternatively these results also suggest that age-associated changes in tumour stroma accompanied by generation of ROS may be a substantial threat by which a senescent stroma could predispose development of tumour and chemotherapy resistance at old age.

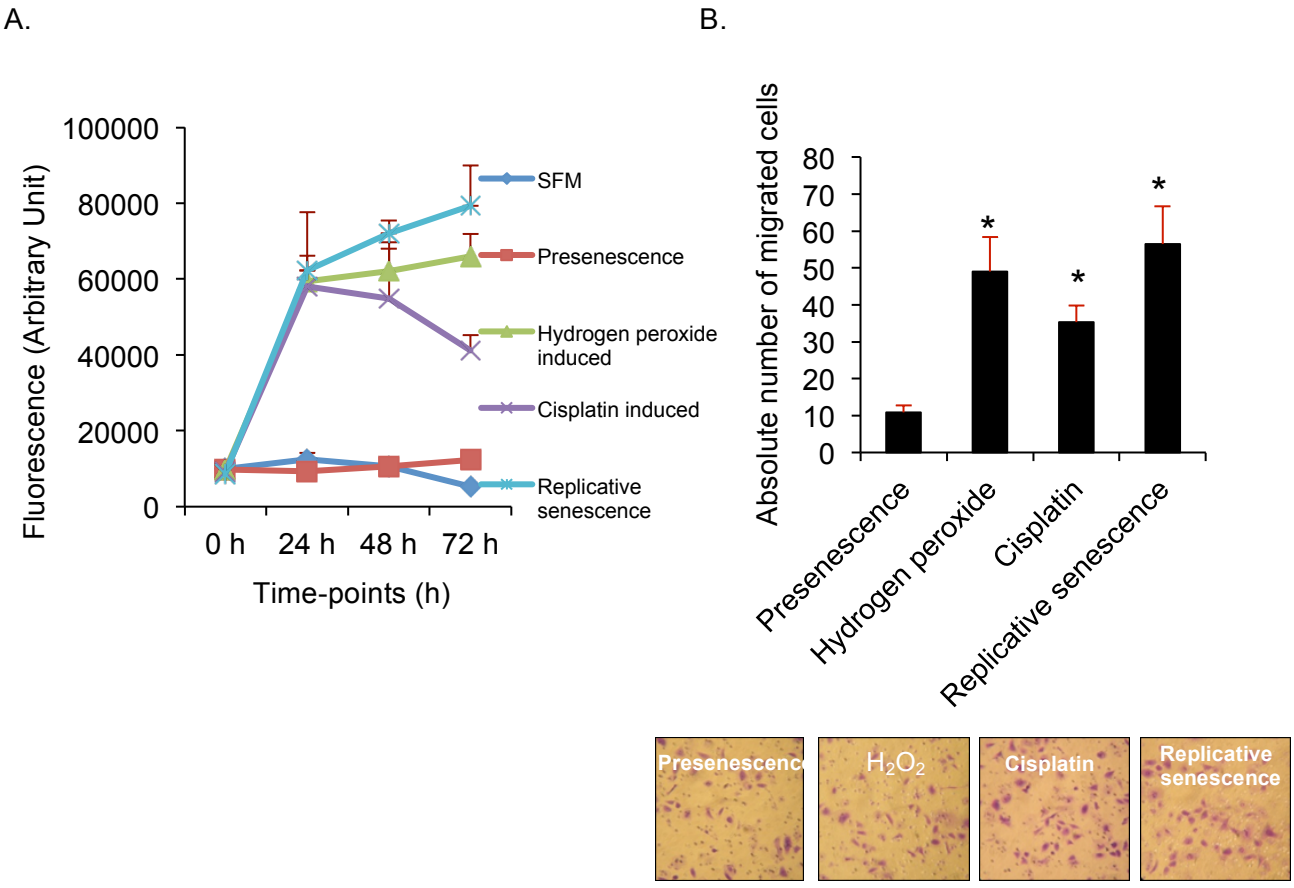

Figure 3.2.2: Human senescent oral fibroblasts stimulate proliferation and migration of oral squamous cell carcinoma derived cell line SCC4 *in vitro* in paracrine manner. SCC4 cells were seeded down at 5,000 per well in triplicate in a 96-well plate and serum starved for 24 h. Conditioned media were added after 24 h. Proliferation were measured by CyQuant NF cell proliferation kit. Two-way repeated measure ANOVA with post-hoc Holm-Sidak corrections, N=3 in triplicate (A). 100,000 SCC4 cells were suspended in 0.1% BSA supplemented DMEM plus F-12 media and seeded into the insert of modified Boyden's chamber migration assay and conditioned media to the bottom well. The cells were allowed to migrate for 24 h followed by fixation in 100% methanol and staining with 0.01% crystal violet. Cells from three different fields were counted per transwell as an independent measure of migrated cells. The data represents mean + SEM (B). N=3, in triplicate, *p<0.05, one-way ANOVA with post-hoc correction by Dunn's method.

3.2.3: Soluble factors from human senescent oral fibroblasts stimulated proliferation and migration of less invasive oral squamous cell carcinoma derived cell line H357 *in vitro* by paracrine action independent of mechanism of senescence induction

Results from previous experiments indicate that in spite of secreting an overlapping subset of SASP factors, the functional consequences of this on neighbouring cells may depend on the nature of the inciting stimuli. This is because even though both stress-induced premature senescent oral fibroblasts and replicative senescent cells secreted approximately same amount of IL-6 and MCP-1 (figure 3.1.2.5.B and figure 3.1.2.6.B) they had variable functional effects on proliferation and migration of D20 and SCC4 cell lines (figure 3.2.2.1 and figure 3.2.2.2). Therefore to evaluate SASP mediated paracrine effects further another, less invasive, oral squamous cell carcinoma derived cell line, H357, was used.

H357 cells were originally extracted from a 74 year old male patient suffering from stage I, well-differentiated squamous cell carcinoma of tongue arising in the floor of the mouth and did not have any prior history of anti-cancer treatment (Prime *et al.*, 1990). These cells are classified as genetically unstable because they harbour mutant forms of *TP53* and *CDKN2A* genes similar to SCC4 cells (Hassona *et al*., 2013; Nichols *et al*., 2012). In addition these cells display mutant H-Ras oncogene with copy number variations resulting from LOH and were previously reported as non-invasive in 3D heterotypic models (Lim *et al*., 2011; Hassona *et al*., 2013). Therefore H357 cells were selected to further investigate the functional consequences of chemotherapy-induced SASP on progression of OSCC including EMT, to exclude the effects of prior exposure to chemotherapy as well as investigating SASP-mediated effects on a different cancer cell line.

As illustrated in figure 3.2.3.A all types of senescent oral fibroblasts significantly stimulated proliferation of H357 cells *in vitro* compared to presenescent control fibroblasts and soluble factor deprived serum free media (n=3, $p<0.05$). There was no obvious difference in the stimulatory effect of presenescent fibroblast from serum free control media on proliferation of H357 cells. Immediately after treatment with conditioned media from senescent fibroblasts the rate of proliferation of H357 cells increased dramatically at both 24 h and 48 h (n=3, $p<0.05$). After 48 h, the rate of cell proliferation increased slowly until about 120 h but remained significantly higher than that observed at the start (n=3, $p<0.001$; figure 3.2.3.A).

Both H_2O_2 and cisplatin induced SASP increased proliferation of H357 cells for the first 72 h, the level of fluorescence remaining relatively higher than that observed with replicative senescent cells (figure 3.2.3.A). At 96 h conditioned media form H_2O_2-treated fibroblasts caused a sharp increase in proliferation of H357 cells whereas those treated with cisplatin caused a gradual increase (figure 3.2.3.A). After 96 h, cisplatin-treated oral fibroblasts stimulated more proliferation of H357 cells than both H_2O_2-induced and replicative senescent oral fibroblasts (figure 3.2.3.A).

In migration assay, cisplatin-induced premature senescent oral fibroblasts significantly stimulated migration of H357 cells by 3.73-fold whereas H_2O_2-induced premature senescent oral fibroblasts stimulated migration by 3.0-fold compared to presenescent control (n=3, $p<0.05$; figure 3.2.3.B). Soluble factors from replicative senescent oral fibroblasts stimulated migration of H357 cells by 3.7-fold (n=3, $p<0.05$) than presenescent control cells (figure 3.2.3.B).

These results therefore suggest that both chemotherapy-induced and age-associated SASP developing in the oral stroma can modify and reprogram the tumourigenic potentials of neighbouring oral cancer cells in non-cell specific manner that had never been exposed to cytotoxic drugs or irradiation and may permeate outgrowths of

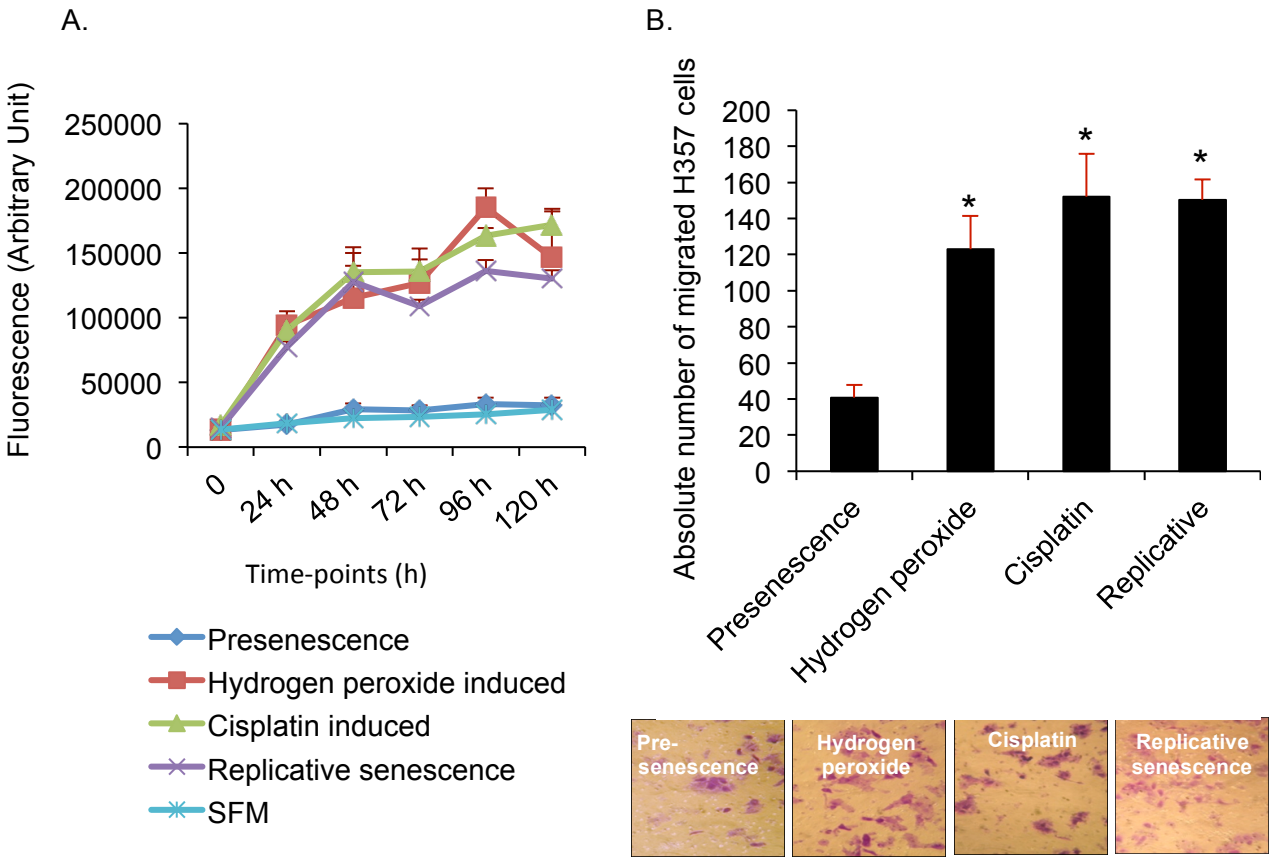

Figure 3.2.3: Human senescent oral fibroblasts stimulate proliferation and migration of H357 cell lines *in vitro* in paracrine manner. H357 cells were seeded down at 2,500 per well in triplicate in a 96-well plate and serum starved for 24 h. Conditioned media were added after 24 h. Proliferation were measured by CyQuant NF cell proliferation kit. Two-way repeated measure ANOVA with post-hoc Holm-Sidak corrections, n=3 in triplicate (A). 100,000 H357 cells were suspended in 0.1% BSA supplemented DMEM and seeded into the insert of modified Boyden's chamber migration assay and conditioned media to the bottom well. The cells were allowed to migrate for 40 h followed by fixation in 100% methanol and staining with 0.01% crystal violet. Cells from three different fields were counted per transwell as an independent measure of migrated cells. The data represents mean + SEM (B). N=3, in triplicate, *p<0.05, one-way ANOVA with post-hoc correction by Dunn's method.

indolent tumours or may even drive the transition of carcinoma in situ into disseminated carcinoma.

3.2.4: Human senescent oral fibroblasts promote invasiveness in non-invasive H357 cells in 2D and 3D *in vitro* assay in paracrine fashion

Tumour metastasis is the primary contributor to mortality from cancer. The process of metastasis can be broadly summarized into three sequential events: invasion, dissemination and distant colonization (Valastyan and Weinberg, 2011).

To acquire an invasive phenotype a cancer cell needs to gain increased motility. It was demonstrated in section 3.2.1, 3.2.2 and 3.2.3 that senescent oral fibroblasts stimulated migration of both oral dysplastic and neoplastic cell lines D20, SCC4 and H357, respectively, *in vitro*. It was also demonstrated in section 3.1.2 that senescent oral fibroblasts synthesized and secreted significant quantities of MMP-2, IL-6 and MCP-1. All these cytokines and matrix degrading proteases have been reported to alter polarization of the initiated cells and facilitate basement membrane disintegration, which ultimately lead to tissue invasion (Valastyan and Weinberg, 2011). Cancer cells can invade and infiltrate into the connective tissue either in small cohesive groups called collective invasion (Hassona *et al*., 2013; Kramer *et al*., 2012) or may invade as single cells involving the intricate play of MMPs, stress fibres, integrins and Rho-ROCK pathways (Valastyan and Weinberg, 2011).

In order to determine the effect of SASP in stimulating invasion of H357 cells, matrigel coated inserts were used in 2D transwell assays. It was observed that conditioned medium from H_2O_2-induced premature senescent oral fibroblasts significantly stimulated invasion of H357 cells by 21.5-fold compared to presenescent control (n=5, $p<0.05$; figure 3.2.4.1). Cisplatin-induced premature senescent oral fibroblasts increased invasion of H357 cells by 6.5-fold relative to control (n=5, $p<0.05$; figure 3.2.4.1), approximately one-third as potent as the effect of H_2O_2-induced senescence.

Replicative senescent oral fibroblasts promoted invasion of H357 cells the least stimulating it by only 6.0-fold compared to control fibroblasts (n=5, $p<0.05$; figure 3.2.4.1). Measurement of invasive index (section 2.18.3.1) showed H357 cells had an invasive index of 7.12-fold, 1.74-fold and 1.63-fold higher in presence of H_2O_2-induced, cisplatin-induced and replicative senescent oral fibroblasts, respectively, compared to control fibroblasts suggesting that in addition to enhancement of motility senescent oral fibroblasts were capable of influencing the invasiveness of H357 cells *in vitro*.

Previous work showed that cancer cells secreted MMPs to favour their invasion and dissemination *in vitro* and *in vivo* (Valastyan and Weinberg, 2011) in cell autonomous manner. However based on above results it can be deduced that the invasion of H357 cells in presence of senescent fibroblasts were predominantly regulated by the abundance of SASP factors in the conditioned media rather than any intrinsic cellular mechanism exhibiting within cancer cells because use of serum free media instead of conditioned media demonstrated no invasion at all. The presence of some invasion in presenescent control as observed in figure 3.2.4.1 can be explained by the fact that these cells too secreted MMP-2 like the senescent fibroblasts but to a lesser extent as showed in section 3.1.2. Further it was observed that invaded H357 cells displayed change of polarity perceived as formation of a lagging edge behind (L) and a leading or invasive edge in front (I) (also appendix 1) of the cell body as illustrated in the bottom panel of figure 3.2.4.1, the arrows indicating the direction of motility.

IL-6 has been described as a potent inducer of EMT, by which cancer cells lose their epithelial polarity and become mesenchymal-like cells to gain motility and acquire resistance to anoikis that help them escape to distant sites (Smith *et al*., 2013). IL-6 was reported to regulate transcriptional factors Twist1 and Snail both of which repress expression of cell adhesion molecules and allows cancer cells to become motile (Smith *et al*., 2013). Therefore based on the current observation and previous findings it was postulated that the invasive phenotype rendered to H357 cells by senescent oral

fibroblasts require additional factors other than MMP-2 that may induce EMT-like changes in these cells (Kramer *et al*., 2012). Further the matrigel used in the study consisted chiefly of collagen type IV and laminin, whereas the basement membrane *in vivo* is a more complex structure comprising of different types of collagens, fibrillins and various connective tissue ingredients. To obtain a definitive understanding of H357 cell invasion a modified 3D organotypic model made from de-epithelialized dermis (DD) was utilized (Colley *et al*., 2011; section 2.18.3.2) onto which H357 cells were co-cultured with either presenescent or cisplatin-induced premature senescent oral fibroblasts. These models carry an intact layer of basement membrane and are therefore better mimics of the *in vivo* tumour microenvironment. DD models produced using replicative senescent oral fibroblasts failed to grow because these cells were unsuccessful in disseminating the dermis (Appendix 13).

Cisplatin-treated oral fibroblasts stimulated more invasion of H357 cells into the dermis of 3D DD models than the untreated control fibroblasts (figure 3.2.4.2). Cisplatin-treated fibroblasts caused H357 cells to invade both as discoid cohesive masses indicative of collective invasion and as single cells resembling mesenchymal invasion possibly resulting from EMT-like changes. In comparison the control fibroblasts only stimulated a few single H357 cells to invade into the dermis (figure 3.2.4.2).

To investigate if cisplatin induced senescence in 3D models, immunohistochemistry was performed for two different biomarkers of senescence: p16 (Pitiyage *et al*., 2011; Waaijer *et al*., 2012) and GLB-1 proteins (Capparelli *et al*., 2012). Previously it was shown that cisplatin induced premature senescent oral fibroblasts expressed significantly more p16 transcripts (figure 3.1.1.8) and demonstrated significantly enhanced SA-β-gal activity in 2D assays. In agreement with previous findings it was ascertained that cisplatin induced premature senescence of human primary oral fibroblasts in 3D DD models and this was visualized by presence of strong positive

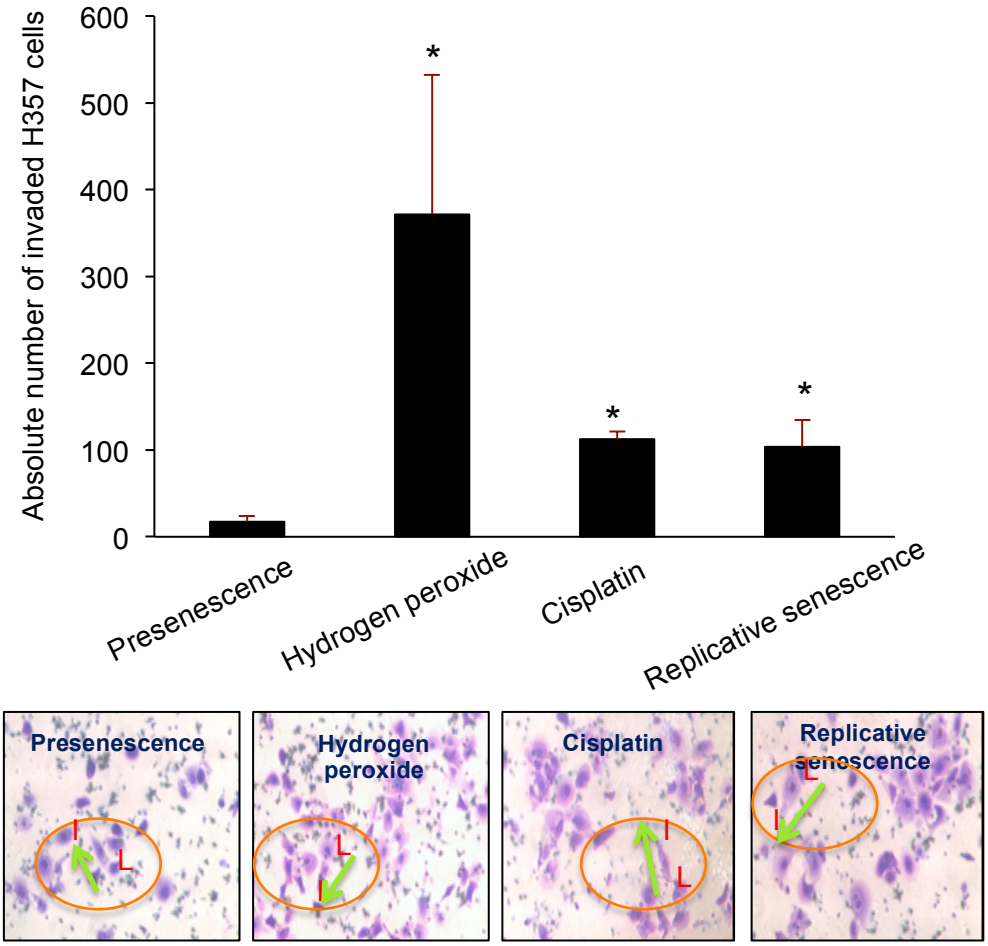

Figure 3.2.4.1: Human senescent oral fibroblasts stimulated directional polarity and invasion of H357 cell lines in 2D *in vitro assay*. 100,000 H357 cells were resuspended in 0.1% BSA supplemented media and seeded onto the matrigel coated insert. Conditioned media were loaded into the bottom well. Invasion was carried out at 37^{o} C for 72 h. After 72 h the non-invading cells from the top chamber were scrapped off, the invaded cells in the bottom chamber were fixed and stained with 0.1% crystal violet. Cells from three different fields were counted as an independent measure of cell invasion at 10X magnification. The data represents mean + SEM. The lower panel portrays photomicrograph of the invaded cells exhibiting directional polarity circled in orange. L represents lagging edge and I represents leading edge, arrow indicates direction of motion. N=3, in triplicate. *p<0.05, one-way ANOVA with post-hoc correction by Dunn's method.

staining for human anti-p16INK4a antibody in cisplatin-treated oral fibroblasts (figure 3.2.4.3.B). The staining was highly specific for fibroblast population and was negative in p16 deficient H357 cells (Hassona *et al*., 2013). Moreover the control presenescent fibroblasts exhibited very weak staining with only 1 or 2 positive cells per field (figure 3.2.4.3.A). To further characterize senescence human anti-GLB-1 antibody was used which detects β-galactosidase expression in human cells. Recently Capparelli *et al.* (2012) demonstrated elevated GLB-1 expression in the senescent population of CAFs in breast cancer specimens. As depicted in figure 3.2.4.3.C and figure 3.2.4.3.D, both H357 cells and oral fibroblasts demonstrated diffuse positive staining for β-galactosidase protein. However it was observed that some β-galactosidase positive cells particularly fibroblasts that were treated with cisplatin demonstrated increased intensity of staining compared to rest of the cells suggesting these are plausibly senescent fibroblasts which theoretically should express more β-galactosidase than the non-senescent cell population. This is because β-galactosidase is a lysosomal enzyme that is expressed by both young and aged cells. Ageing causes cells to accumulate lysosomal mass, which demonstrate residual β-galactosidase activity at sub-optimal pH (Dimri *et al*., 1995; Kurz *et al*., 2000). This is possibly why both cancer cells and young fibroblasts stained mildly for β-galactosidase protein whereas the senescent fibroblasts demonstrated enhanced staining as a manifestation of increased amount of protein. Therefore both of these findings imply that cisplatin-treated oral fibroblasts reached a state of premature senescence in the 3D DD models.

In summary it was shown that chemotherapy-induced premature senescent human primary oral fibroblasts stimulated proliferation, migration and invasion of OSCC derived and premalignant lesion derived cell lines *in vitro* in non-cell specific manner by paracrine action.

H357 cells plus untreated control oral fibroblasts

H357 cells plus cisplatin treated oral fibroblasts

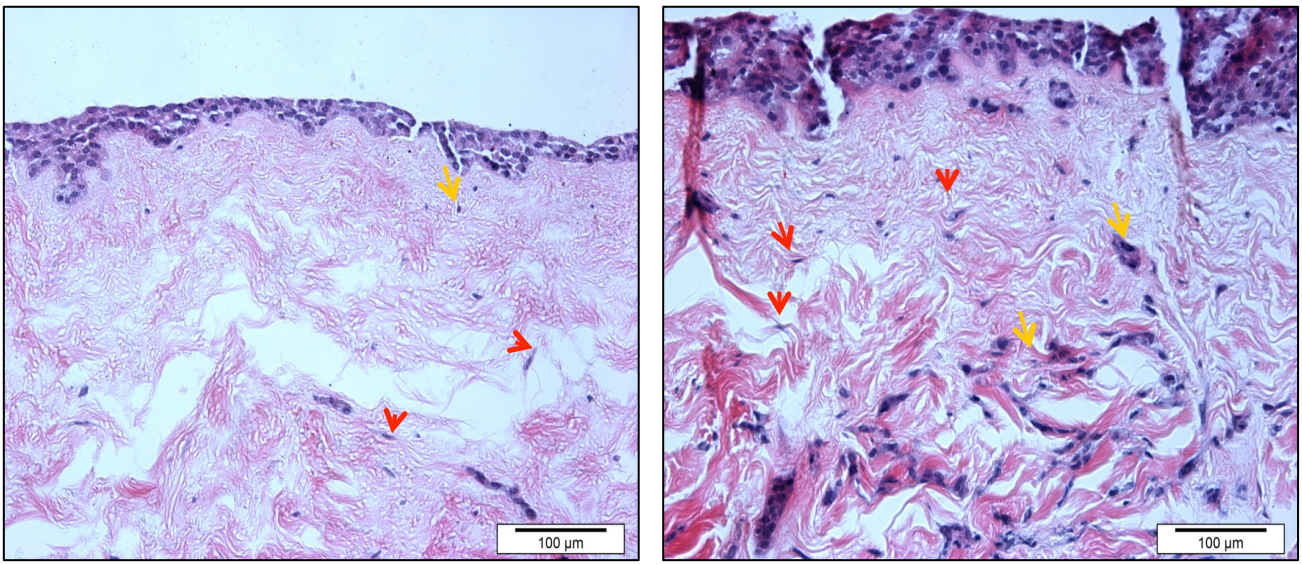

Figure 3.2.4.2: Cisplatin treated oral fibroblasts increased invasiveness of H357 cells in 3D de-epithelialized dermis models. 500,000 oral fibroblasts were seeded down into sterile surgical metallic ring positioned on top of de-epithelialized dermis. The cells were then treated with cisplatin for 24 h. Untreated fibroblasts were used as control. On day 4, 250,000 H357 cells were inoculated onto the models and allowed to grow for 72 h. The models were then transferred onto air-liquid interface and grown for additional period of 21 days. After 3 weeks, the tissues were then formalin fixed and paraffin embedded. Tissue sections were stained with haematoxylin and eosin to assess the depth of invasion of cancer cells. The yellow arrows indicate invading H357 cells whereas the red arrows indicate oral fibroblasts. The photomicrographs were taken at 20X magnification using light microscope. Scale bar = 100 µM.

A.

H357 cells plus normal oral fibroblasts

B.

H357 cells plus cisplatin induced prematurely senescent oral fibroblasts

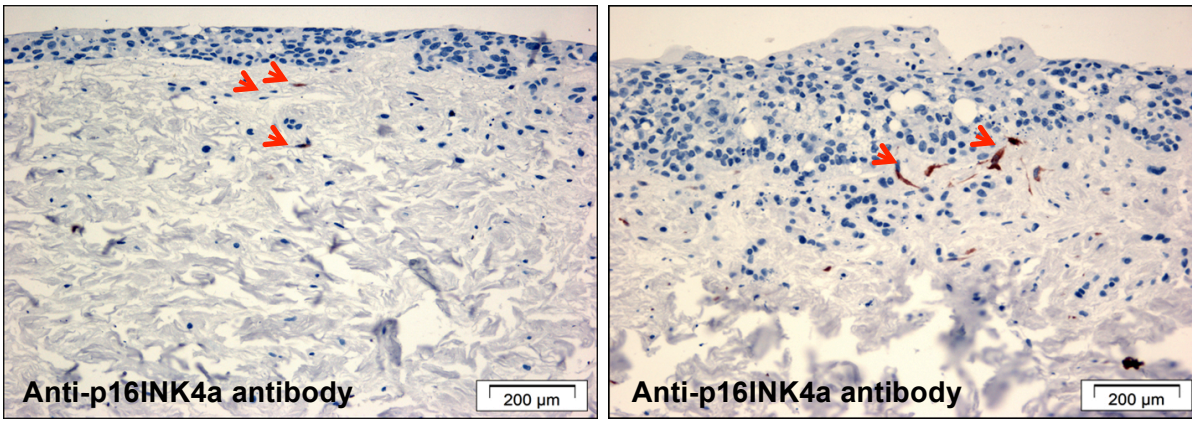

C.

D.

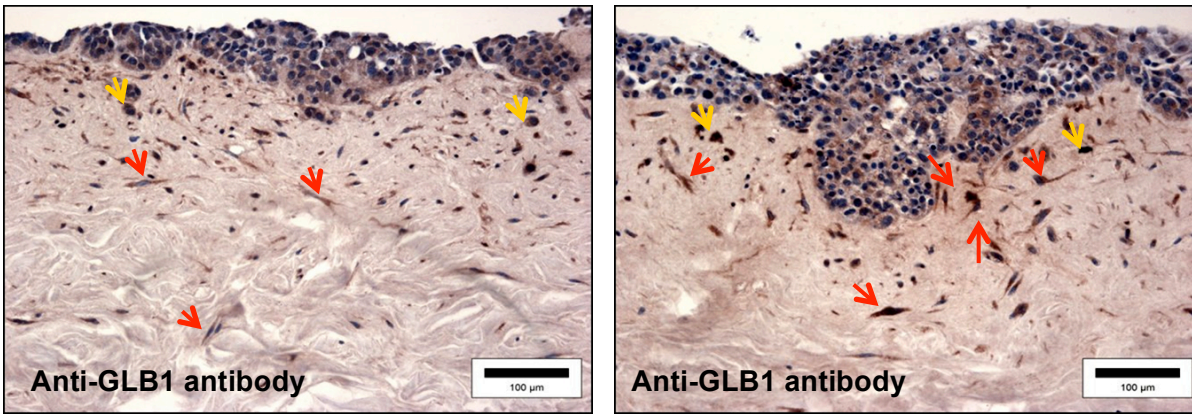

Figure 3.2.4.3: Cisplatin induced senescence of human primary oral fibroblasts in 3D organotypic models. Tissue sections were deparaffinized. Heat mediated antigen retrieval done. Immunohistochemistry for human p16INK4a (A & B) and GLB-1 or β-galactosidase 1 (C & D) proteins were performed. Cisplatin treated oral fibroblasts showed positive staining for p16INKA proteins (B) while control fibroblasts showed very weak or no staining (A). Both H357 cells and oral fibroblasts show basal expression of GLB-1 depicted as diffuse staining (C & D). Some cisplatin treated fibroblasts show increased intensity of staining for GLB-1 (D). Red arrows indicate fibroblasts and yellow arrows indicate cancer cells. The photos were taken at 20X magnification. Scale bar = 200 µM (upper panel) and 100 µM (lower panel).

3.2.5: Senescent oral fibroblasts stimulate invasiveness of OSCC derived cell line H357 *in vitro* via inducing EMT-like changes

The results presented in section 3.2.4 showed that invasive H357 cells displayed change of polarity, lost contact with basement membrane and invaded into the dermis either in groups or as a solitary cell. All these features are reminiscent of EMT-like changes in the cancer cell (Micalizzi *et al*., 2010). One of the hallmarks of EMT is the "cadherin-switching" wherein the epithelial adherence molecule E-cadherin is replaced with the mesenchymal less adherent N-cadherin allowing the cells to become migratory (Micalizzi *et al*., 2010). Mutations such as hypermethylation of the promoter region of E-cadherins and certain growth factors and cytokines can trigger EMT-like changes in non-invasive cancer cells by controlling expression of transcriptional factors (Smith *et al*., 2013). Slug and Twist1 are two such transcriptional factors, which had been reported to provoke EMT in different types of cancer cells such as breast, esophagus, stomach, pancreas and so forth (Jethwa *et al*., 2008; Micalizzi *et al*., 2010). Slug had been reported to be associated with direct transcriptional repression of E-cadherin in both esophageal adenocarcinoma and squamous cell carcinoma and was found to be associated with increasing tumour invasiveness and poor prognosis (Jethwa *et al*., 2008; Uchikado *et al*., 2005). A recent work showed that modulation of Slug expression in tongue squamous cell carcinoma derived cell lines increased their motility by up-regulation of N-cadherin and down-regulation of desmosomal proteins such as plakophilin-2, desmoglein-3 and desmocolin-2 (Katafiasz *et al*., 2011). Moreover another study showed that advanced hypoxic tumours from head and neck cancer patients expressed more Slug and this was associated with poor survival rate (Zhang *et al*., 2013). Conversely Twist1 expression in head and neck cancer was found to be associated with an inflammatory phenotype and with high risk of dissemination to lymph nodes (Ou *et al*., 2008).

Previously it had been shown that SASP stimulated EMT in various cancer cells (reviewed by Davalos *et al*., 2010). Therefore to investigate if soluble factors from cisplatin-induced premature senescent oral fibroblasts stimulated EMT-like changes in H357 cells in 3D organotypic model, immunohistochemistry for Slug and Twist1 were performed.

It was observed that both DD models bearing either presenescent or cisplatin-treated oral fibroblasts expressed Slug in both cancer cells and fibroblasts (figure 3.2.5.A and figure 3.2.5.B). However models comprising of cisplatin-induced premature senescent fibroblasts showed certain areas of intense staining that is absent in the control models, implying that within the entire population of H357 cells there is a specific subpopulation, which increased Slug expression to possibly undergo EMT-like changes (figure 3.2.5.A and figure 3.2.5.B). Unlike Slug, Twist1 expression was confined to only H357 cells in presence of cisplatin-treated oral fibroblasts (figure 3.2.5.C and figure 3.2.5.D). Moreover Twist1 was expressed by only a small group of H357 cells that showed elongated nucleus and were localized invading the stroma beneath the basement membrane (figure 3.2.5.D).

Persistent stimulation of OSCC cells with TGFβ was reported to induce EMT in cancer cells by modulating expression of Slug (Qiao *et al*., 2010). In these models H357 cells were used, previously reported to secrete vast amounts of TGFβ compared to other OSCC cell lines (Fahey *et al*., 1996). However Slug is also expressed by the normal lining epithelium of oesophagus located just above the basement membrane indicating their physiological importance in maintaining tissue homeostasis (Jethwa *et al*., 2008). Perhaps this is why Slug was expressed in both models containing presenescent as well as cisplatin-induced senescent fibroblasts.

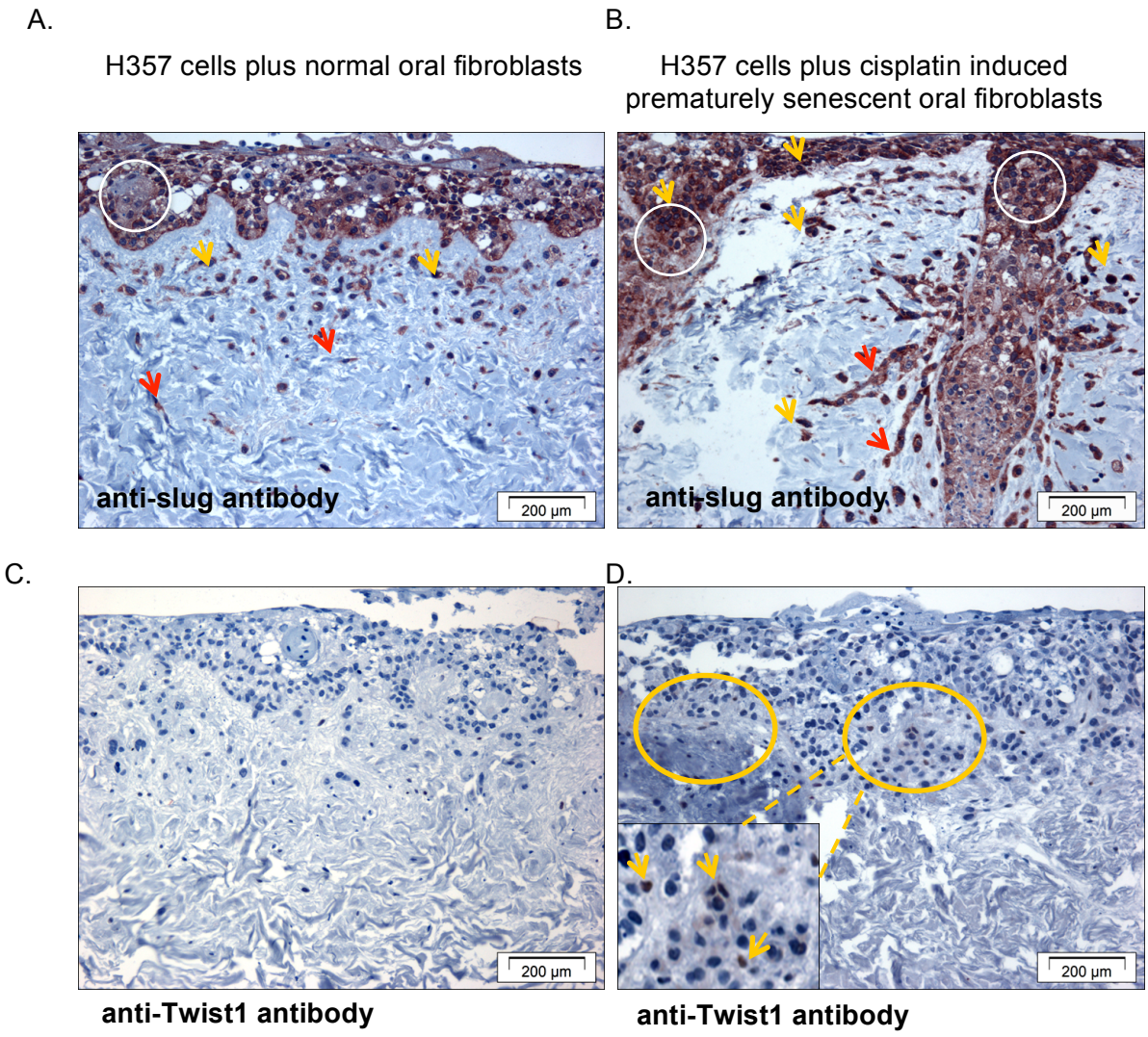

Figure 3.2.5: Cisplatin induced premature senescent oral fibroblasts stimulated invasion of H357 cell line in 3D organotypic models by provoking epithelial to mesenchymal transition (EMT). Specific antibodies to human Slug (A & B) and Twist1 (C & D) were used to detect expression of EMT markers in H357 cells. The white circles represents H357 cells demonstrating more Slug1 proteins in cisplatin treated fibroblast models (B) in comparison to presenescent controls (A). The yellow circle represents H357 cells staining positive for Twist1 (D). The images were taken at 20X magnification. Scale bar = 200 µM. Yellow arrows indicate cancer cells and red arrows indicate fibroblasts.

Staining for Twist 1 was restricted to a fewer cell population of cancer cells but this was characteristic of true EMT occurring in cancer *in vivo* where only a few cells at a time undergo EMT-like changes to escape to distant sites (Micalizzi *et al*., 2010). The staining for Twist1 was only positive in cancer cells in presence of cisplatin-induced premature senescent oral fibroblasts, and not presenescent fibroblasts, indicating that paracrine cross-talk between senescent stroma and cancer cells induced EMT-like changes in H357 cells which facilitated their invasion and migration into the dermis.

These are relatively preliminary observations obtained from DD models (n=3) grown using normal oral fibroblasts from only one patient (DENF008) and therefore requires further validation in more repeats using cells from different patients to eliminate the bias of fibroblast heterogeneity accompanied by independent scoring of staining.

3.2.6: Paracrine effects of MCP-1 on monocyte, macrophages and OSCC cells

During characterization of SASP it was discovered that human senescent oral fibroblasts secreted significantly more MCP-1 compared to young presenescent control fibroblasts (section 3.1.2). MCP-1 is a chemokine which is secreted by not only stromal cells, but also cancer and immune cells (Li *et al*., 2013b). Its primary function is to recruit bone marrow derived monocytes into the tumour microenvironment (reviewed by Sica *et al*., 2008). Macrophages play a pivotal role in chronic inflammation (Sohn *et al*., 2012). Emerging evidence states that gathering of macrophages at sites of chronic disease such as ulcerative colitis can induce senescence in both epithelial cells and stromal fibroblasts via generation of nitric oxide thereby creating a tumour suppressive barrier to prevent neoplastic transformation in epithelial cells (Sohn *et al*., 2012). Conversely infiltration of macrophages at sites of pre-existing tumours is associated with poor prognosis in various cancers including HNSCC (reviewed by Sica *et al*., 2008; Balermpas *et al*., 2014; He *et al*., 2014a).

High levels of MCP-1 are reported in serum of OSCC patients, which corresponds to their elevated expression in tumours (Li *et al*., 2014), but its correlation with prognosis is controversial. Elevated MCP-1 expression in tumour stroma was associated with increased mean survival time in patients suffering from OSCC in contrast to breast cancer patients where this implied poor survival (Ferreira *et al*., 2008; Li *et al*., 2013b). In contrast OSCC with locoregional lymph node metastasis stained positive for MCP-1 and elevated levels of MCP-1 in tumour parenchyma correlated with reduced patient survival (Ferreira *et al*., 2008). Recent evidence indicates that HNSCC demonstrate increased infiltration of macrophages of M2 polarity and this was associated with nodal metastasis and poor prognosis (Balermpas *et al*., 2014; He *et al*., 2014a). Moreover HNSCC that metastasized early recruited more bone marrow derived monocytes into the tissue microenvironment (Balermpas *et al*., 2014). Furthermore infiltrating M2 macrophages in OSCC were found to associate with increasing marker of cancer stem cells (He *et al*., 2014a).

On the other hand less aggressive tumours such as SCC affecting lips also had increased influx of macrophages independent of MCP-1 (Ferreira *et al*., 2008), which possibly represents anti-tumoural resident macrophages (Ginhoux and Jung, 2014). This implies that in OSCC MCP-1 axis possibly determines the nature of body's innate anti-tumour response to cancer cells and may contribute to its progression.

Accumulating evidence indicates that MCP-1 has pleiotropic roles in cancer, therefore, to investigate the potential roles of MCP-1 secreted by senescent fibroblasts on OSCC progression initially the paracrine effects of secreted MCP-1 on recruitment of THP-1 monocytes and effect of SASP on polarization of THP-1 derived macrophages were investigated *in vitro*.

3.2.6.1: Human senescent oral fibroblasts recruit acute monocytic leukaemia derived cell line; THP-1 by secreting MCP-1 and stimulate polarization of THP-1 derived macrophages *in vitro*

In order to examine the effect of conditioned media from senescent oral fibroblasts on monocyte recruitment 2D transwell assays were used. Recombinant human MCP-1 (100 ng) was used as a positive control. In presence of negative IgG control antibody conditioned media from senescent oral fibroblasts significantly stimulated migration of THP-1 cell lines *in vitro* compared to presenescent control (n=3, p=0.007; figure 3.2.6.1). Pairwise comparison showed H_2O_2-induced premature senescent oral fibroblasts stimulated maximum migration of THP-1 cells by 4.2-fold (n=3, $p<0.05$) followed by cisplatin-induced premature senescent fibroblasts which increased migration by 3.03-fold (n=3, $p<0.05$) and then replicative senescent cells which stimulated migration by 2.94-fold (n=3, $p<0.05$) compared to presenescent control fibroblasts.

Addition of anti-MCP-1 antibody (20 μg/mL) remarkably impeded chemotaxis of THP-1 cells *in vitro* (n=3, $p<0.05$; figure 3.2.6.1). Blockade of MCP-1 significantly reduced migration of THP-1 cells to 0.51-times, 0.49-times and 0.47-times in presence of conditioned media derived from presenescent, H_2O_2 and cisplatin induced premature senescent oral fibroblasts, respectively, than their counterpart negative IgG control. However addition of anti-MCP-1 antibody only slightly reduced chemotaxis of THP-1 cells towards conditioned media of replicative senescent oral fibroblasts in comparison to negative IgG control.

Despite causing a significant reduction in migration of THP-1 cell lines following addition of anti-MCP-1 antibody the number of migrated cells remained considerably higher in presence of conditioned media obtained from senescent fibroblasts than presenescent control. This implied senescent oral fibroblasts secreted other

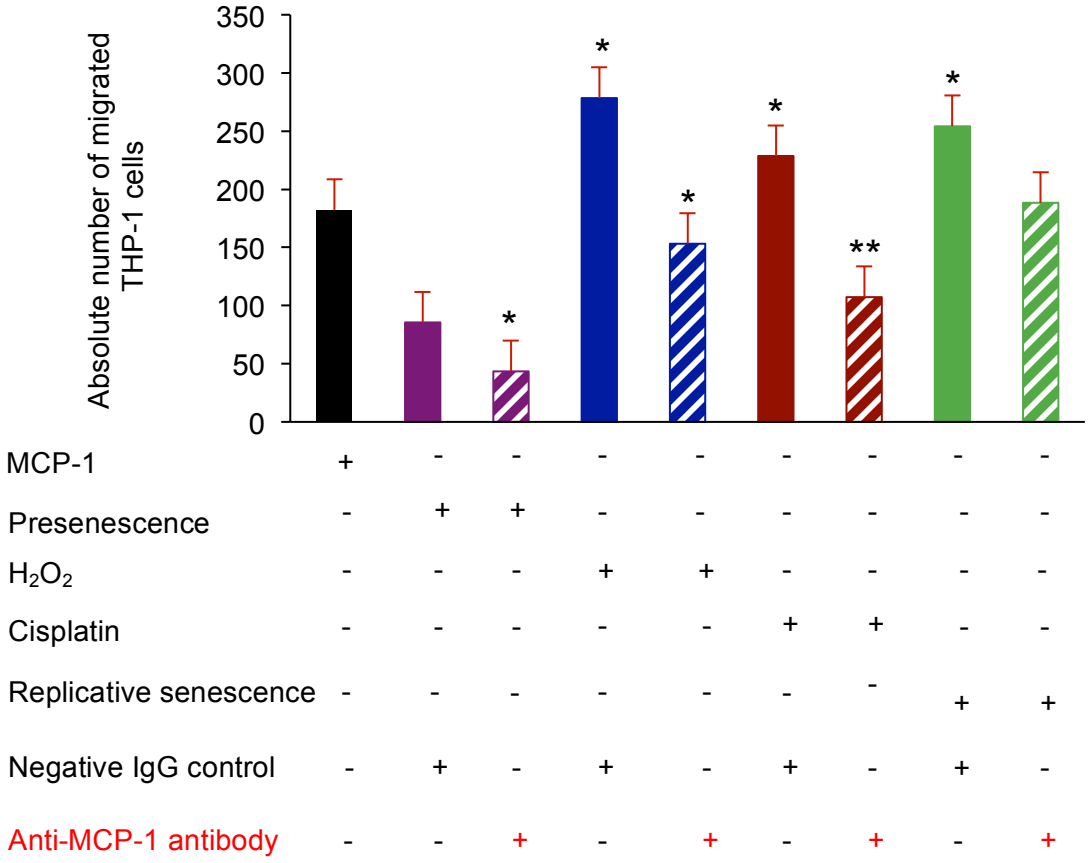

Figure 3.2.6.1: Senescent oral fibroblasts stimulate migration of THP-1 cells *in vitro* in MCP-1 dependent manner. Conditioned media from senescent and presenescent oral fibroblasts with or without anti-MCP-1 antibody were loaded into the bottom chamber of transwell assay. Anti-mouse negative IgG was used as control. 1,00,000 THP-1 cells were suspended in 0.1% BSA containing RPMI and seeded on to the top chamber. Migration was carried out for 4 h. Migration was assessed by taking the mean of summation of cells that migrated to the bottom chamber and those, which remained adhered to the bottom surface of the membrane. The data represents mean + SEM. N=3, in duplicate, *p<0.05, two-way ANOVA with post-hoc correction by Holm-Sidak method.

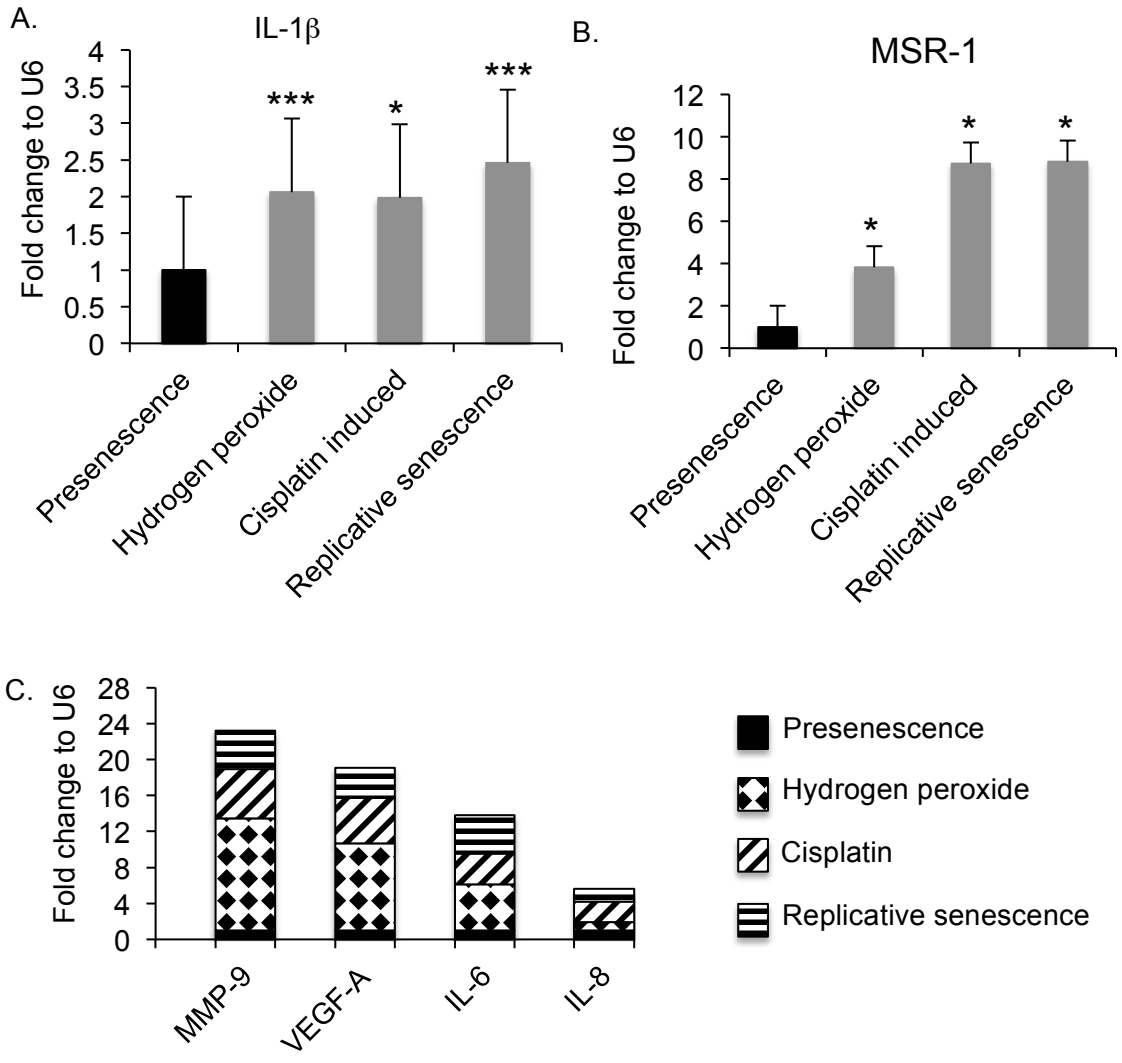

Figure 3.2.6.2: Soluble factors from senescent oral fibroblasts could induce polarization of macrophages *in vitro*. 500,000 THP-1 cells were differentiated in 6-well plates with PMA (200 ng/μL) for 72 h into macrophages. After 5 days of recovery, the differentiated macrophages were then treated with freshly prepared conditioned media from both presenescent and senescent oral fibroblasts for 72 h. RNA was isolated, reverse transcribed and qRT-PCR was performed to screen for markers of macrophage polarization (A and B; N=3), inflammation and angiogenesis (C; N=1). The data is normalized to control fibroblasts and represents mean fold change + SEM. All experiments were done in triplicate. *p<0.05 and ***p<0.001, one-way ANOVA with post-hoc correction by Dunn's method.

chemotactic factors in addition to MCP-1, which stimulated migration of monocytes *in vitro*. This notion also corroborates with the findings of replicative senescent oral fibroblasts in which blockade of MCP-1 appeared to have less reducing effect on monocyte migration.

To understand the significance of monocyte recruitment into the senescent tumour microenvironment it was hypothesized that SASP stimulated polarization of macrophages, by means of which these cells exerted either a pro-inflammatory or an anti-inflammatory response to either promote or regress cancer progression.

To address this THP-1 cells were differentiated *in vitro* using PMA as described in section 2.18.6. These artificially differentiated macrophages were then subjected to conditioned media from senescent and presenescent oral fibroblasts for 72 h. RNA was extracted and qRT-PCR was used to determine expression of various markers of macrophage polarization (Lujambio *et al*., 2013). It was observed that both H_2O_2 and cisplatin induced premature senescent oral fibroblasts significantly stimulated both M1 and M2 polarization demonstrated by increased expression of IL-1β by 2.1-fold (n=3, p=0.0002) and 1.98-fold (n=3, p=0.01), respectively (figure 3.2.6.2.A) and macrophage scavenger receptor-1 (MSR-1) by 3.8-fold (n=3, p=0.01) and 8.7-fold (n=3, p=0.01), respectively (figure 3.2.6.2.B). Presenescent oral fibroblasts appeared to suppress macrophage activation. Replicative senescent oral fibroblasts also significantly stimulated both M1 polarization elevating expression of IL-1β by 2.5-fold (n=3, p<0.001; figure 3.2.6.2.A) and M2 polarization elevating expression of MSR-1 by 8.8-fold (n=3, p=0.02; figure 3.2.6.2.B).

M1 or classical polarization had been linked to the immunosureveillance function of macrophages and is considered to eliminate both senescent cells and tumour cells and thereby reduce tumour burden (Sica *et al*., 2008; Lujambio *et al*., 2013). M2 or altered polarization is mainly observed in tumour associated macrophages wherein these cells

secrete factors like MMP-9 and VEGF and participate in neo-angiogenesis and cancer cell invasion to favour cancer progression (Sica *et al*., 2008).

To investigate the pro-tumourigenic properties of these polarized macrophages further qRT-PCR was performed to determine expression of VEGF-A, MMP-9, IL-6 and IL-8, all of which had been previously reported to promote neo-angiogenesis, tumour growth, invasion and dissemination (Davalos *et al*., 2010; Sica *et al*., 2008). It was found that soluble factors from H_2O_2-induced senescent oral fibroblasts induced relatively more M2-like phenotype in macrophages by elevating expression of MMP-9 by 12.5-fold, VEGF-A by 9.7-fold, IL-6 by 5.2-fold but decreasing expression of IL-8 by 0.9-times than control (figure 3.2.6.2). Cisplatin-induced premature senescent oral fibroblasts also provoked M2-like polarization by stimulating expression of MMP-9 by 5.4-fold, VEGF-A by 5.1-fold, IL-6 by 3.4-fold and IL-8 by 2.3-fold (figure 3.2.6.2) in THP-1 derived macrophages. Similarly replicative senescent oral fibroblasts augmented expression of MMP-9 by 4.3-fold, VEGF-A by 3.3-fold, IL-6 by 4.3-fold and IL-8 by 1.4-fold in THP-1 derived macrophages (figure 3.2.6.2) than presenescent control. From these results therefore it can be deduced that overall senescent oral fibroblasts tend to stimulate a M2-switching in macrophages relative to the young presenescent control.

In summary senescent oral fibroblasts can recruit monocytes *in vitro* and polarize macrophages into M2-phenotype.

3.2.7: Paracrine effect of senescent stroma derived MCP-1 on migration and invasion of OSCC derived cell line H357 in 2D and 3D *in vitro* assay

Recent work showed that high grade tumour cell lines derived from OSCC have elevated levels of MCP-1 which is associated with up-regulation of pro-survival pathways in these cells (Ji *et al*., 2014). Co-culture of OSCC cell lines with CAFs also augmented secretion of MCP-1 by CAFs and this was associated with increased

tumour growth and invasive potential of OSCC cells in both *in vitro* assays and animal models (Li *et al*., 2014). In addition mechanisms intrinsic to CAFs for instance increased expression of galectin-1 was found to regulate myofibroblastic transdifferentiation and MCP-1 expression (Wu *et al*., 2011). Moreover stromal expression of galectin-1 is reported to be important during early events of carcinogenesis in head and neck cancer patients (Chiang *et al*., 2008).

MCP-1 was reported to have no effect on OSCC cell proliferation but rather affected their motility and invasiveness (Wu *et al*., 2011; Li *et al*., 2014). To determine if MCP-1 secreted by senescent oral fibroblasts could modulate invasiveness and spread of OSCC-derived cell H357 *in vitro*, 2D chemotaxis assay was repeated with and without matrigel coated inserts in either presence or absence of anti-MCP-1 antibody (20 μg/mL) in conditioned medium to assess its functional role on cancer cell migration and invasion, respectively.

In agreement with previous findings (figure 3.2.3.B) it was observed that in presence of negative IgG control, soluble factors derived from senescent oral fibroblasts significantly stimulated migration (figure 3.2.7.1) and invasion (figure 3.2.7.2) of H357 cells *in vitro* compared to presenescent control fibroblasts ($n=3$, $p<0.05$). As presented in figure 3.2.7.1 and 3.2.7.2, addition of anti-MCP-1 antibody significantly reduced migration and invasion of H357 cells towards conditioned media of both senescent and presenescent oral fibroblasts ($n=3$, $p<0.05$). Compared to presenescent oral fibroblasts, H_2O_2-induced senescent oral fibroblasts stimulated migration and invasion of H357 cells by 1.76-fold and 3.63-fold, respectively, and this was significantly reduced to 0.46-times and 0.35-times of negative IgG control following addition of anti-MCP-1 antibody ($n=3$, $p<0.05$; figure 3.2.7.1 and 3.2.7.2). Similarly cisplatin-induced premature senescent oral fibroblasts stimulated more migration and invasion of H357 cells *in vitro* by 2.16-fold and 6.30-fold, respectively, relative to presenescent control and this was significantly reduced to 0.38-times and 0.18-times of negative IgG control

by anti-MCP-1-antibody (n=3, $p<0.05$; figure 3.2.7.1 and 3.2.7.2). The migration and invasion of H357 cells were increased by 1.32-fold and 1.29-fold, respectively, by replicative senescent fibroblasts. Blockade of secreted MCP-1 in replicative senescent oral fibroblasts reduced both migration and invasion of H357 cells to 0.56-times (n=3, $p<0.05$; figure 3.2.7.1) and 0.48-times (figure 3.2.7.2) of negative IgG control, respectively. Anti-MCP-1 antibody also reduced migration and invasion of H357 cells by presenescent oral fibroblasts declining it from 1.0 to 0.30-times and 0.51-times of negative IgG control (n=3; figure 3.2.7.1 and 3.2.7.2).

In contrast when invasive index was calculated it was found that in presence of negative control IgG antibody the invasiveness of H357 cells was increased by 2.1-fold and 2.9-fold in presence of H_2O_2 and cisplatin induced premature senescent oral fibroblasts, respectively, compared to presenescent control whereas the invasive index was reduced to 0.96 in presence of replicative senescent oral fibroblasts. Surprisingly addition of anti-MCP-1 antibody decreased the invasive index of H357 cells to 0.94, 0.82 and 0.49 in H_2O_2-induced, cisplatin-induced and replicative senescent oral fibroblasts compared to 1.0 in presenescent control. This result suggested that blockade of MCP-1 to reduce invasion of OSCC may be more promising in disease treatment rather than using it as a prophylactic measure to prevent cancer dissemination at an early stage as determined by the rise in invasive index in the control group following addition of antibody.

To explore this observation further, 3D organotypic model (section 2.18.3.2 and 2.18.4) was used to investigate if blockade of secreted MCP-1 by fibroblasts elicited any change in the invasive potential of H357 cells into the dermis. It was observed that prolonged incubation of models with negative control antibody IgG was toxic to both cancer cells and fibroblasts in this system and therefore these models failed to grow. This was discovered after performing haematoxylin and eosin staining of paraffin embedded sections of models grown for 21 days. No cellular components were

detectable in models treated with negative IgG control (n=2). In contrast the 3D models grew normally after incubation with anti-MCP-1 antibody. It was observed that chronic treatment of 3D models carrying presenescent oral fibroblasts showed increased proliferating, invasive and migratory capacity of H357 cells in comparison to cisplatin-treated oral fibroblasts (figure 3.2.7.3). This observation corroborated with previous finding wherein the invasive index of H357 cells was found decreased in presence of senescent oral fibroblasts in 2D assay after incubation with anti-MCP-1 antibody. These models mimic the real scenario of OSCC invasion *in vivo* and therefore the resemblance in both findings (2D and 3D assays) implied that use of MCP-1 based targeted therapy may be a more complicated approach and depend on the stage and severity of disease.

From figure 3.2.7.3 it can be deduced that blockade of secreted MCP-1 in presenescent fibroblasts attenuated their tumour suppressive effect on H357 cells that was evident in previously grown DD models in absence of antibodies (figure 3.2.4.2). In absence of MCP-1, the H357 cells appear to grow discordantly with irregular deposition of keratins. The basement membrane appears disintegrated which remained intact in DD models containing both presenescent and senescent fibroblasts without antibody treatment (figure 3.2.4.2). Moreover the invasive H357 cells in this model appear more aggressive and invade the dermis irregularly sometimes as single cells or occasionally as elongated cell clusters. These features are reminiscent of a typical anaplastic tumour or a tumour that has progressed to an advanced stage (Kawashiri *et al*., 2009). Based on this observation it may be presumed that blockade of secreted MCP-1 by presenescent fibroblasts disrupted the initiation of a normal desmoplastic response which is frequently used by the body as an initial measure to limit tumour growth and local invasion before the stromal cells become reprogrammed by cancer cells.

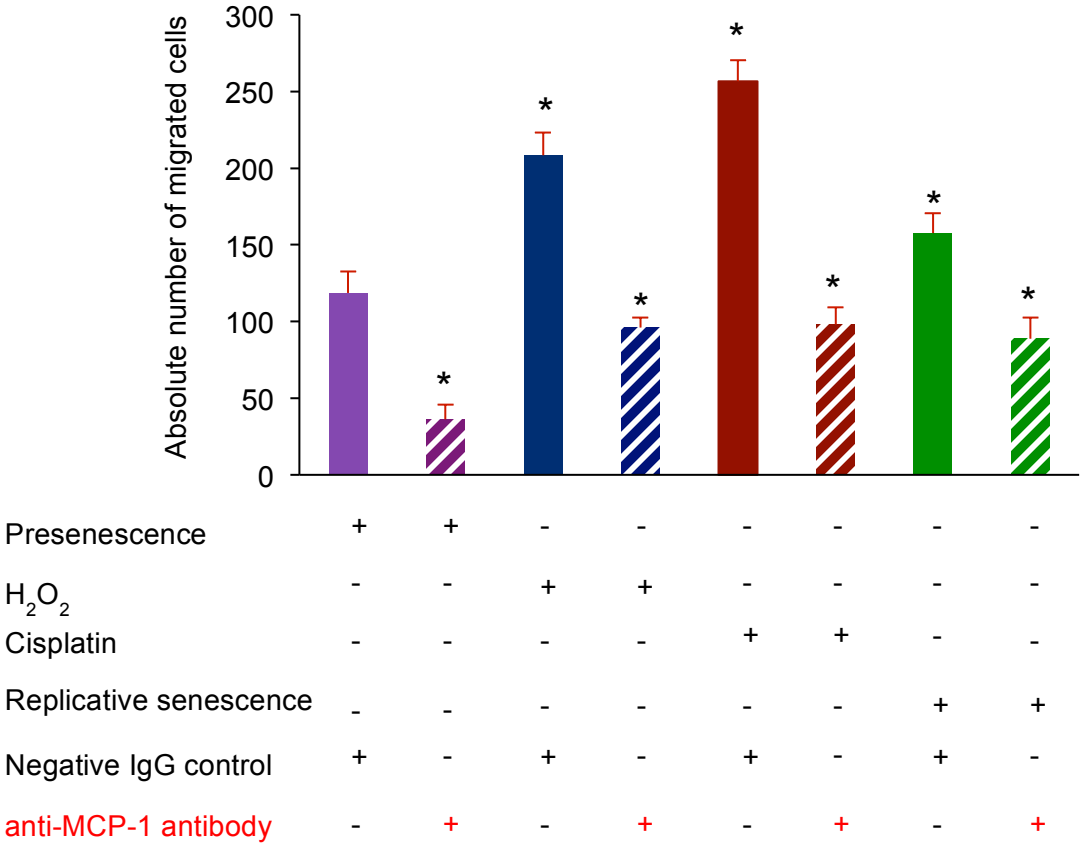

Figure 3.2.7.1: Blockade of secreted MCP-1 in conditioned media of both presenescent and senescent oral fibroblasts reduces migration of H357 cells *in vitro*. 100,000 H357 cells were suspended in 0.1% BSA supplemented DMEM and seeded on to the top chamber of 2D transwell assay. Conditioned media obtained from different senescent oral fibroblasts and presenescent controls were loaded into the bottom chamber in presence and absence of anti-MCP-1 antibody. Isotype IgG2 was used as a negative control. Migration was carried out for 40 h. After completion of migration unmigrated cells were scratched off from the top surface and the migrated cells sticking to the bottom surface were fixed and stained with 0.1% crystal violet. Photomicrographs were taken using light microscope at 10X. Cells from three representative fields were counted as a measure of migration. The data represents mean + SEM. N=3, in duplicate. *$p<0.05$, two-way ANOVA with post-hoc Holm-Sidak corrections.

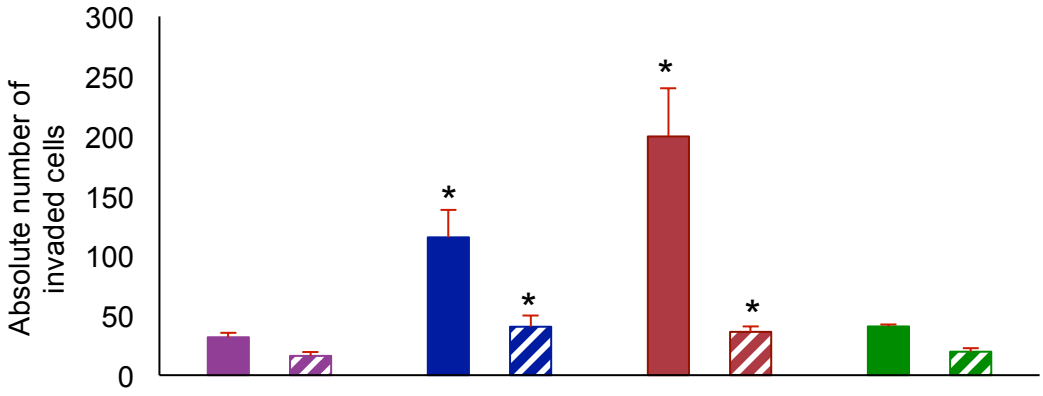

Presenescence	+	+	-	-	-	-	-	-
H_2O_2	-	-	+	+	-	-	-	-
Cisplatin	-	-	-	-	+	+	-	-
Replicative senescence	-	-	-	-	-	-	+	+
Negative IgG control	+	-	+	-	+	-	+	-
anti-MCP-1 antibody	-	+	-	+	-	+	-	+

Figure 3.2.7.2: Blockade of secreted MCP-1 in the conditioned media reduced invasiveness of H357 cells in 2D *in vitro* matrigel bearing transwell assay. 100,000 H357 cells were suspended in 0.1% BSA supplemented DMEM and seeded on to the top chamber of 2D transwell assay which had been coated with matrigel. Conditioned media from different senescent oral fibroblasts and presenescent controls were loaded into the bottom chamber in presence and absence of anti-MCP-1 antibody. Isotype IgG2 was used as a negative control. Invasion was carried out for 72 h. After completion of invasion non-invasive cells were scratched off from the top surface and the invaded cells sticking to the bottom surface were fixed and stained with 0.1% crystal violet. Photomicrographs were taken using light microscope at 10X. Cells from three representative fields were counted as a measure of migration. The data represents mean + SEM. N=3. *$p<0.05$, two-way ANOVA with post-hoc corrections by Holm-Sidak method.

Conversely in models carrying cisplatin-treated fibroblasts addition of anti-MCP-1 antibody appeared to block the pro-tumourigenic inflammatory cues from senescent fibroblasts to adjacent H357 cells and this resulted into a dramatic fall in chiefly proliferative capacity and to a lesser degree invasiveness of H357 cells (figure 3.2.7.3).

MCP-1 had been reported to stimulate phosphorylation of ERK-1, STAT3 and AKT in high-grade OSCC cell lines (Ji *et al*., 2014), which were also reported to remain persistently activated in senescent oral fibroblasts (Jun and Lau, 2010; Mallette *et al*., 2010; Munoz-Espin *et al*., 2013). Therefore it is highly plausible that blocking MCP-1 action may disrupt these pro-survival regulatory loops in senescent fibroblasts and may be to certain extent in cancer cells, which perhaps interferes with their ability to promote tumour progression in these DD models.

Moreover in 3D models co-culture of H357 cells with presenescent oral fibroblasts can be hypothesized to behave as newly formed tumours where cross-talk between both stroma and H357 cells are essential to allow cancer formation. The presenescent fibroblasts here therefore act as naïve fibroblasts, which are yet to differentiate upon signaling from cancer cells. Ongoing work in this lab suggests cancer cells could stimulate an inflammatory phenotype in normal fibroblasts and exaggerate that of senescent fibroblasts (including secretion of MCP-1) (described in section 3.2.9). Therefore if the body utilizes desmoplastic response in an attempt to limit cancer outgrowth, interference of MCP-1 signaling and the inflammatory cascade during fibroblast transdifferentiation may elicit an abnormal response to encourage cancer formation.

On the other hand, previously it was reported that in areas of chronic wounds hyperactivated myofibroblasts underwent senescence as an anti-fibrotic response to reduce the extent of fibrosis (Krizhanovsky *et al*., 2011; Pitiyage *et al*., 2011). Therefore cisplatin treated oral fibroblast models may serve as a model of a late stage oral cancer

H357 cells plus presenescence oral fibroblasts

H357 cells plus cisplatin induced premature senescent oral fibroblasts

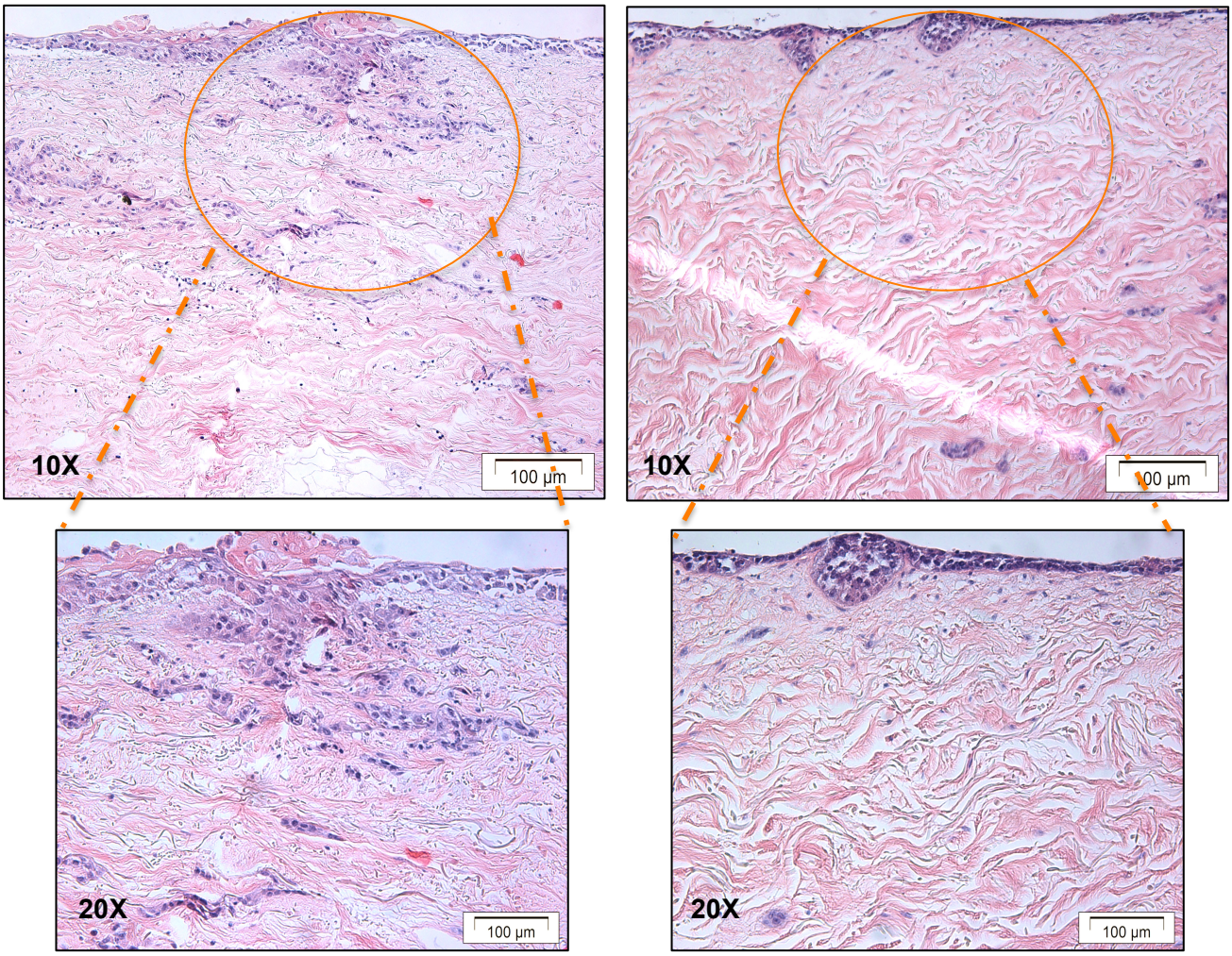

Figure 3.2.7.3: Effect of blockade of secreted MCP-1 by presenescent and cisplatin induced premature senescent oral fibroblasts on invasion of H357 cell lines in 3D organotypic models. Haematoxylin and eosin staining of 3D model sections demonstrate that treatment with anti-MCP-1 antibody accelerated H357 cell proliferation and invasion in presence of presenescent fibroblasts while reduced these effects in presence of cisplatin induced senescent fibroblasts. Photomicrographs were taken at both 10X and 20X by light microscope. Scale bar = 100 µM. N=2.

wherein the fibroblasts had been activated and senesced over time. The lack of selection pressure causes aged or senescent fibroblasts to reinforce cancer growth and hence blockade of MCP-1 in these fibroblasts is blocking the activity of tumour promoting senescent fibroblasts and may be in fact beneficial to cancer treatment.

From these results it can therefore be concluded that MCP-1 based combined chemotherapies may be unsuitable in preventing cancer dissemination at early stages of carcinogenesis as it interferes with normal fibroblast transdifferentiation in diseased state and impedes development of normal desmoplastic reactions. However once cancer is established MCP-1 may serve as a good drug target, especially for treatment of advanced staged tumours, to reduce tumour growth and metastasis. Further very recently it was shown that withdrawal of anti-MCP-1 during cancer treatment increases cancer cell aggressiveness and promotes distant metastasis by a rebound effect (Bonapace *et al.*, 2014). Therefore additional drugs (perhaps IL-6 antagonists; Bonapace *et al.*, 2014) may be necessary to fully block the MCP-1 axis in cancer to minimize drug adverse effects during anti-cancer therapy.

3.2.8: Human senescent oral fibroblasts display a morphology resembling CAFs

As described earlier most genotoxic stmuli induce senescence in human diploid fibroblasts by generation of ROS (Campisi and d'Adda di Fagagna, 2007). A recent study showed that oxidative stress could reprogram normal fibroblasts in to CAFs or myofibroblasts, which facilitated tumour growth and invasion (Toullec *et al*., 2010). Another group demonstrated that a sub-set of CAFs accumulating in GU HNSCC tend to undergo premature senescence (Hassona *et al*., 2013). This senescent sub-population of CAFs, in addition to having the pro-tumourigenic properties of non-senescent CAFs, display a very distinct transcriptome that overlaps with normal senescent fibroblasts. Development of senescence in CAFs in cancer stroma is

reported to reinforce and amplify their tumour promoting capacity and presumably leads to poor prognosis in patients (Hassona *et al*., 2013; Hassona *et al*., 2014). Past reports showed that senescent fibroblasts arise from myofibroblasts in liver diseases (Krizhanovsky *et al*., 2011). The direct link between CAFs or myofibroblasts with senescent fibroblasts is still poorly understood.

To investigate whether senescent oral fibroblasts also had myofibroblastic features both presenescent and senescent oral fibroblasts were examined for expression of α-SMA at both mRNA and protein level. To date α-SMA is the most well characterized biomarker of CAF in addition to many other less specific markers such as vimentin (Kawashiri *et al*., 2009). Usually normal oral fibroblasts stain negative for α-SMA but stain positive for the mesenchymal marker vimentin (Kawashiri *et al*., 2009). In cancer or at sites of wound healing fibroblasts transdifferentiate into myofibroblasts and express α-SMA (Kawashiri *et al*., 2009). Therefore α-SMA was considered to be a suitable marker to investigate myofibroblastic property of senescent fibroblasts. Further the senescent fibroblasts were also screened for another fibroblast activation marker FGF-2, which was also reported to be elevated in senescent fibroblasts (Bavik *et al*., 2006) and in CAFs derived from metastatic OSCC with poor prognosis (Hase *et al*., 2006).

In contrast to presenescent oral fibroblasts, H_2O_2 and cisplatin induced senescent oral fibroblasts displayed increased formation of stress fibers while replicative senescent cells showed increased fluorescence but lack of formation of stress fibers (figure 3.2.8.1.A). This was further validated by western blot and relative band densitometry. It was observed that upon attainment of senescence H_2O_2 and cisplatin treated oral fibroblasts showed significantly increased expression of α-SMA protein compared to presenescent control by 1.4-fold and 1.6-fold, respectively ($n=3$, $p<0.05$; figure 3.2.8.1.B). Western blotting showed a dramatic decrease in α-SMA expression in

replicative senescent oral fibroblasts to 0.11-times of control (n=3, $p<0.05$; figure 3.2.8.1.B). To further determine if this alteration of expression of α-SMA was regulated at transcriptional levels, these cells were screened for α-SMA mRNA by qRT-PCR (figure 3.2.8.1.C). It was observed that both H_2O_2 and cisplatin induced premature senescent oral fibroblasts expressed significantly more α-SMA mRNA which were 3.03-fold and 2.79-fold higher than control, respectively, whereas replicative senescent oral fibroblasts expressed significantly less α-SMA transcripts about 0.32-times of presenescent control fibroblasts (n=5, $p<0.05$).

Screening for FGF-2 by qRT-PCR demonstrated that all types of senescent oral fibroblasts, including replicative senescent oral fibroblasts, expressed remarkably higher amount of FGF-2 mRNA in comparison to presenescent oral fibroblasts (n=4, $p<0.05$; figure 3.2.8.2). H_2O_2 and cisplatin induced premature senescent oral fibroblasts expressed 1.8-fold and 1.6-fold higher FGF-2 mRNA than presenescent control, respectively. Replicative senescent oral fibroblasts also expressed 1.5-fold higher FGF-2 mRNA than presenescent control.

These data suggest that genotoxic stress caused a myofibroblastic transdifferentiation in oral fibroblasts with accompanying senescence fate. However it is still unclear from this work if these cells exhibit both of these phenotypes simultaneously or if myofibroblastic transdifferentiation is a preceding step before fibroblasts reached full senescence. Preliminary time course studies for α-SMA expression using western blot demonstrated no obvious change between presenescent and senescent samples apart from a significant increase at day 15 post-treatment as illustrated in figure 3.2.8.1.B. Replicative senescent cells show a kind of nemosis response characterized by simultaneous presence of inflammatory phenotype and inability to form stress fibers (Rasanen *et al*., 2009), perhaps explaining the reduction in α-SMA observed in these cells. This implies that possibly replicative senescent fibroblasts may contribute to the

small sub-population of CAFs having nemosis response in OSCC patients (Rasanen *et al*., 2009). This is particularly of clinical significance because as α-SMA is a gold standard test for identification of CAFs or myofibroblasts in cancer and healing wounds, an absence of this marker in this sub-population may lead to false negative results as these α-SMA negative CAFs retain their inflammatory character and may contribute to poor disease outcome.

3.2.9: Effect of cancer cell-derived conditioned media on activation of senescent oral fibroblasts

Evidence from 3D organotypic models used in this thesis suggested existence of a possible cross-talk between OSCC derived cell line H357 and both presenescent and cisplatin induced premature senescent oral fibroblasts which plays an essential role in determining the behaviour of cancer cells *in vitro*. Therefore it was hypothesized that soluble factors derived from oral dysplastic cell lines (D20) and OSCC cell lines (H357) can activate senescent and presenescent oral fibroblasts in paracrine fashion.

After confirming senescence in oral fibroblasts they were either treated with conditioned media from H357 or D20 cells for 48 h or left untreated. As illustrated in figure 3.2.9.1 (middle panel) soluble factors from D20 cells failed to either stimulate or inhibit formation of α-SMA positive stress fibers in both presenescent and senescent oral fibroblasts which retained their normal activation phenotype as shown in the upper panel (figure 3.2.9.1). In contrast soluble factors from H357 cells incremented activation of both presenescent and senescent oral fibroblasts *in vitro* seen as enhanced formation of stress fibers accompanied by a more spindly morphology including replicative senescent cells (figure 3.2.9.1, lower panel).

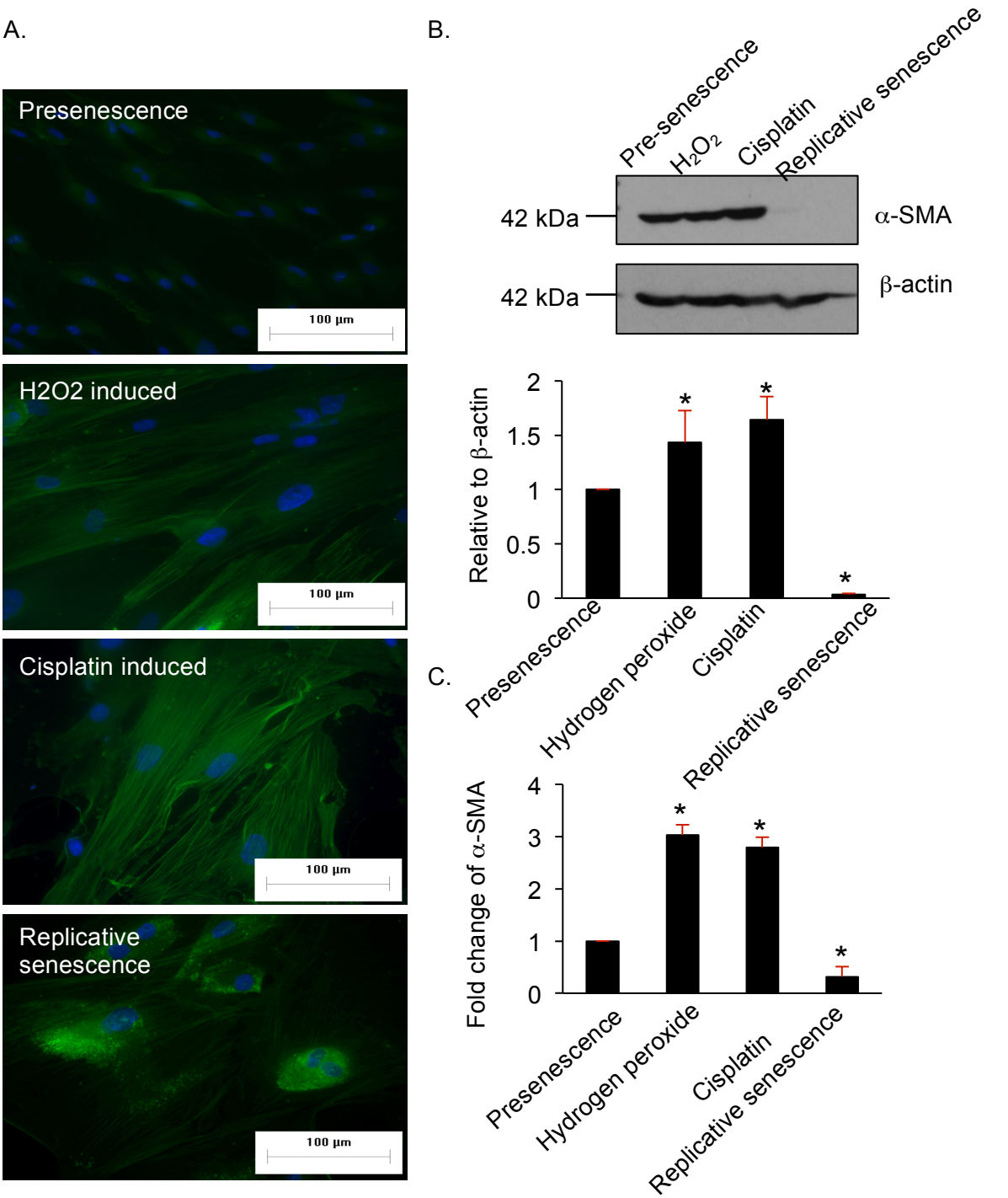

Figure 3.2.8.1: Stress induced senescent oral fibroblasts show elevated expression of α-SMA. Immunofluorescence cytochemistry (A), Western blotting, N=3, *p<0.05, Mann-Whitney U-test (B) and qRT-PCR, N=5, *p<0.05, one-way ANOVA with post-hoc correction by Dunn's method. (C) shows increased formation of α-SMA stress fibers in premature senescent oral fibroblasts than presenescent and replicative senescent oral fibroblasts.

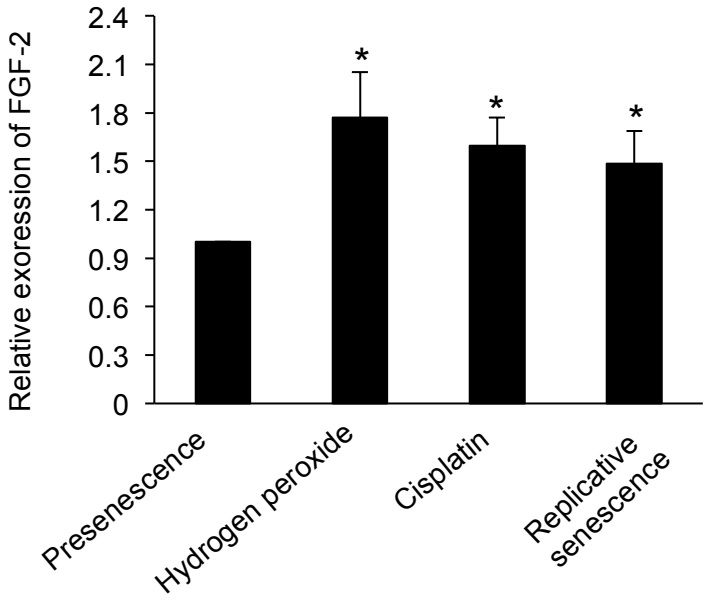

Figure 3.2.8.2: FGF-2 expression is elevated in senescent oral fibroblasts. qRT-PCR demonstrates increased mRNA levels of FGF-2 in both genotoxic stress induced premature and replicative senescent oral fibroblasts compared to presenescent control. ΔΔCt values were used to measure fold change relative to U6 endogenous control. The bars represent mean + SEM. N=4, in triplicate, *$p<0.05$, one-way ANOVA with post-hoc corrections by Dunn's method.

In addition, two of the validated SASP markers IL-6 and MCP-1 mRNA levels were assessed in these fibroblasts to determine the effect of conditioned media of H357 cells on pro-inflammatory nature of senescent fibroblasts. All fibroblasts, both senescent and presenescent, demonstrated a dramatic increase in expression of IL-6, and a smaller increase in MCP-1 mRNA levels as illustrated in figure 3.2.9.2.A and 3.2.9.2.B. Conditioned media from H357 cells increased expression of MCP-1 by 1.33-fold and IL-6 by 227.8-fold in presenescent fibroblasts compared to untreated control. Similarly conditioned media from H357 cells stimulated expression of both MCP-1 and IL-6 in cisplatin-treated oral fibroblasts by 6.57-fold and 510.2-fold than untreated control. Conditioned media from H357 cells also increased expression of IL-6 by 833-fold and MCP-1 by 9-fold in replicative senescent oral fibroblasts than their counterpart untreated control. These are very preliminary data and require further validation.

This pilot data suggests that conditioned media from cancerous cell line H357 but not dysplastic cell lines D20 could reprogram senescent oral fibroblasts into CAFs with exaggerated inflammatory properties and this may contribute to a poorer prognosis in patients. However the length of these experiments was very short while development of cancer is rather a long process. Therefore further time course studies must be carried out before making any further conclusions.

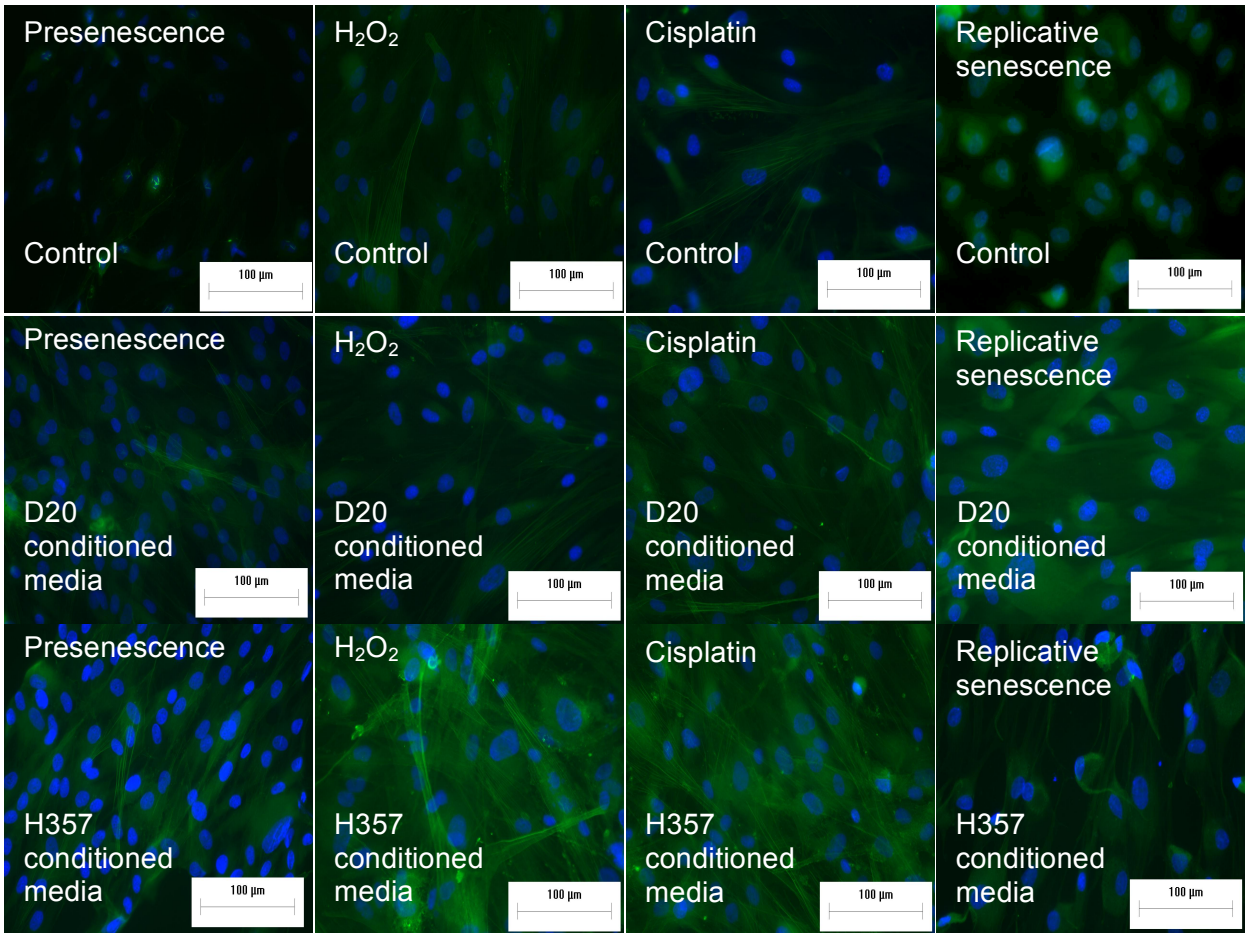

Figure 3.2.9.1: Soluble factors from H357 cells stimulate activation of senescent and presenescent oral fibroblasts *in vitro* by paracrine action. Direct immunofluorescence cytochemistry depicts enhancement in formation of α-SMA stress fibers in senescent fibroblasts upon paracrine stimulation with H357 cells derived conditioned media but not D20 cells. Serum free media was used as control. N=3.

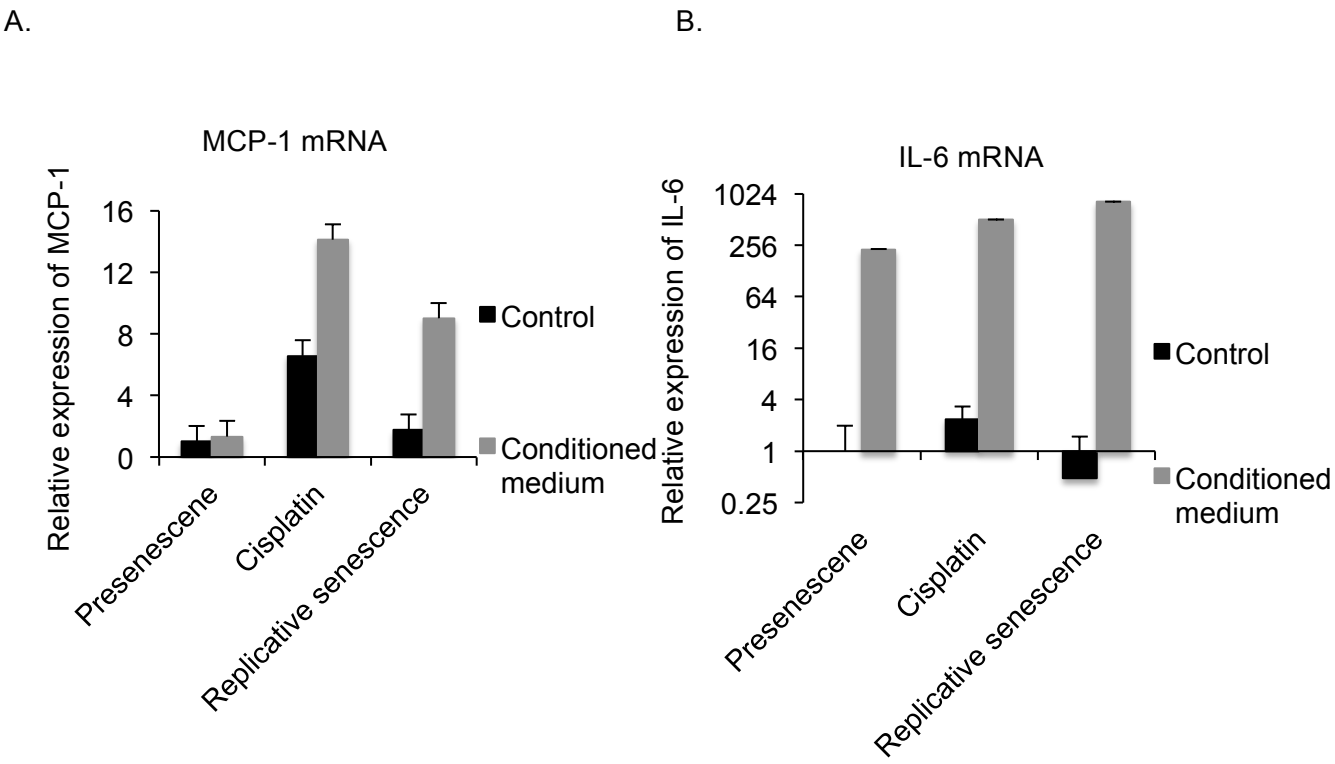

Figure 3.2.9.2: Soluble factors from H357 cells stimulate a pro-inflammatory phenotype in senescent oral fibroblasts. H357 cells stimulated relatively elevated MCP-1 (A) and IL-6 (B) mRNA levels in senescent oral fibroblasts as determined by qRT-PCR. The data represents mean + SEM. N=1, in triplicate.

3.2.10: Conclusion

Overall the data presented in this chapter indicates that senescent oral fibroblasts stimulated proliferation and migration of both oral dysplastic and cancerous cell lines by paracrine action. In addition senescent fibroblasts also induced EMT-like changes in OSCC cell lines, which may have contributed to their invasion in both 2D and 3D *in vitro* assays, which was at least in part dependent on secretion of MCP-1. Further it was shown that blockade of MCP-1 during early tumourigenesis, modeled in an *in vitro* system was detrimental as it increased tumour invasiveness whereas it may be beneficial during late stages of carcinogenesis where (again *in vitro*) it reduced both tumour growth and invasion. Senescent oral fibroblasts can recruit monocytes and stimulate M2 polarization in macrophages, which may further assist in creation of a permissive tumour microenvironment to allow tumour growth and spread. Finally it was shown that senescent oral fibroblasts could represent a subgroup of myofibroblasts or CAFs. Further it was shown by 2D *in vitro* assay that at sites of cancer development, accumulating senescent fibroblasts can be activated into a more inflammatory cell type which may possibly contribute to development of highly aggressive and invasive tumours of head and neck. Moreover chemotherapy-induced senescence causes fibroblasts to acquire similar pro-tumourigenic properties as to that resulting from oxidative stress and replicative senescence. Therefore paracrine effects of these senescent fibroblasts may be an existing mechanism for chemotherapy resistance or formation of new primary tumours or even progression of cancer to a refractory incurable state.

3.3: Role of miRNAs in SASP of human primary oral fibroblasts

Hypothesis:

Human senescent oral fibroblasts express a distinct set of miRNAs which regulate genes that reprogram aged fibroblasts into developing a pro-tumourigenic and pro-inflammatory SASP which can modulate stromal-tumour interactions and contribute to OSCC progression.

Aims and objectives:

- Use comprehensive miRNA profile screening (TaqMan miRNA Tiling Low Density Array) to determine expression of miRNAs in cisplatin-induced premature senescent oral fibroblasts.
- Select and validate candidate miRNA expression in other types of senescent oral fibroblasts by qRT-PCR.
- To determine the functional effects of candidate miRNAs in regulation of SASP in senescent oral fibroblasts.
- To identify and functionally validate miRNA gene targets in senescent oral fibroblasts.
- To determine possible mechanism used by the miRNA gene target(s) to reprogram oral fibroblasts in developing the SASP.

3.3.0: MiRNAs are differentially expressed in stress-induced premature senescent and late-passage oral fibroblasts

Cisplatin induces apoptosis in head and neck cancer cell lines partly by modulating expression of pro-apoptotic and tumour suppressive miRNAs and their processing enzyme DICER1 (Huang *et al*., 2011). Deletion of Dicer in proliferating fibroblasts had been reported to induce premature senescence, emphasizing the possible roles of miRNAs in tumour suppression and senescence (Mudhasani *et al*., 2008; Gomez-Cabello *et al*., 2013). To date several miRNAs have been demonstrated to play a pivotal role in initiating DDR, regulating its downstream kinases, checkpoint proteins and determining cell cycle fate (Hu and Gatti, 2010). Their role in the development of SASP, however, remains unclear.

Since SASP is conserved across species from embryonic life to adult tissues (Munoz-Espin *et al*., 2013) and involves altered expression of hundreds of genes (Bavik *et al*., 2006; Schwarze *et al*., 2005) and comprises of secretion of over 40 different cytokines (reviewed by Davalos *et al*., 2010) some of which had been investigated in section 3.1.2 (figure 3.1.2.4), it is rational to speculate that regulation of SASP may be programmed and this may occur at transcriptional level by epigenetic mechanisms (chromatin remodeling) or at post-transcriptional level by miRNAs. With the exception of miR-146a and miR-210 no other miRNAs had yet been reported to regulate SASP in senescent cells (Bhaumik *et al*., 2009; Taddei *et al*., 2014), and no studies have examined the contribution of miRNAs to SASP-mediated stromal-epithelial interactions. Therefore in order to probe the mechanisms underlying the development of SASP in senescent oral fibroblasts TLDA analysis was performed to obtain a SASP specific miRNA signature from cisplatin-induced premature senescent oral fibroblasts and late-passage oral fibroblasts.

It was observed that in cisplatin-induced premature senescent oral fibroblasts 74 miRNAs were up-regulated and 111 miRNAs were down-regulated in comparison to presenescent control (Appendix 2 & 3).

The top twenty miRNAs up-regulated and down-regulated in cisplatin-treated oral fibroblasts in isolated TLDA platforms comprising human pool A and pool B panels are presented in figure 3.3.1 and figure 3.3.2, respectively. The combined results of the top twenty differentially expressed miRNAs are summarized in figure 3.3.3. Among the up-regulated miRNAs, expression of miR-512-3p, miR-517a, miR-517c, miR-519a, miR-335, miR-146a, miR-137, miR-34a, miR-34c and miR-34a# were significantly increased and among the down-regulated miRNAs expression of miR-1278, miR-130b#, miR-16-1#, miR-643, miR-15#, miR-144#, miR-101# and miR-566 were significantly decreased ($n=3$, $p<0.05$; table 3.1). miR-223 demonstrated the highest and miR-1272 demonstrated the lowest fold change in cisplatin-treated oral fibroblasts (figure 3.3.3). Of these, over-expression of miRNA-34a, miR-146a, miR-335, miR-223 and miR-23a were previously reported in other senescent fibroblasts and human aged tissues (He *et al*., 2007; Hackl *et al*., 2010; Xu *et al*., 2011, Sohn *et al*., 2012, Bonafacio *et al*., 2010; Bhaumik *et al*., 2009).

To ensure that the miRNA signature obtained from cisplatin-induced premature senescent oral fibroblasts were de facto associated with senescence or ageing rather than a cisplatin-specific effect, TLDA was repeated in slowly proliferating late-passage oral fibroblasts obtained from a different patient. These late-passage cells represented aged fibroblasts and showed nearly 60% SA-β-Gal activity (figure 3.3.4.B).

It was observed that in late passage oral fibroblasts out of 754 human miRNAs, 444 were up-regulated and 112 were down-regulated (Appendix 4). Among these, miR-628-5p demonstrated maximum up-regulation and miR-381 demonstrated the most down-

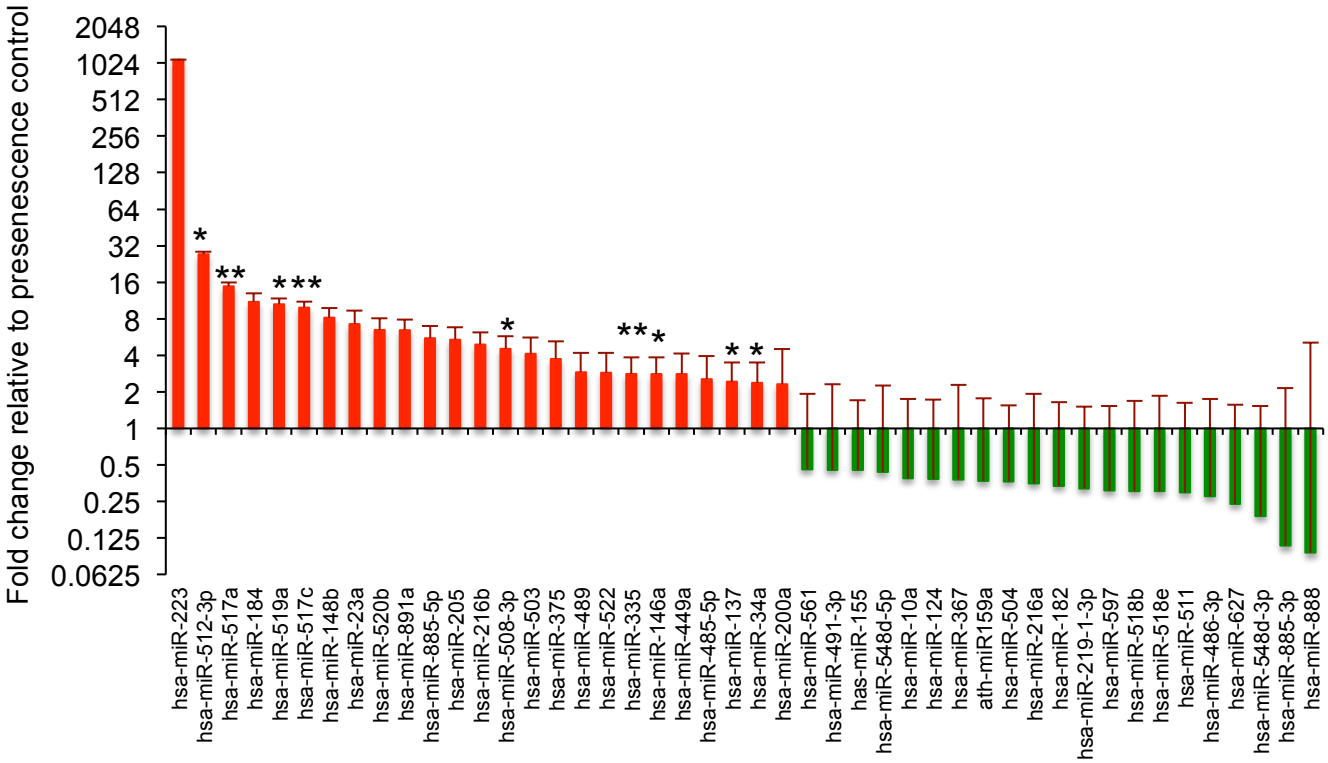

Figure 3.3.1: Differential expression of Pool A miRNA in cisplatin-induced premature senescent oral fibroblasts. TaqMan tiling low density array was used to determine miRNA expression profile in cisplatin-induced premature senescent oral fibroblasts. A cut off point of 34 was applied for Ct. ΔΔCt values were calculated after normalizing the data to U6 endogenous control and presenescent oral fibroblasts. The bars represent mean of fold change + SEM of top 20 up-regulated and down-regulated miRNAs in Pool A card. N=3, *p<0.05, by paired student's t-test.

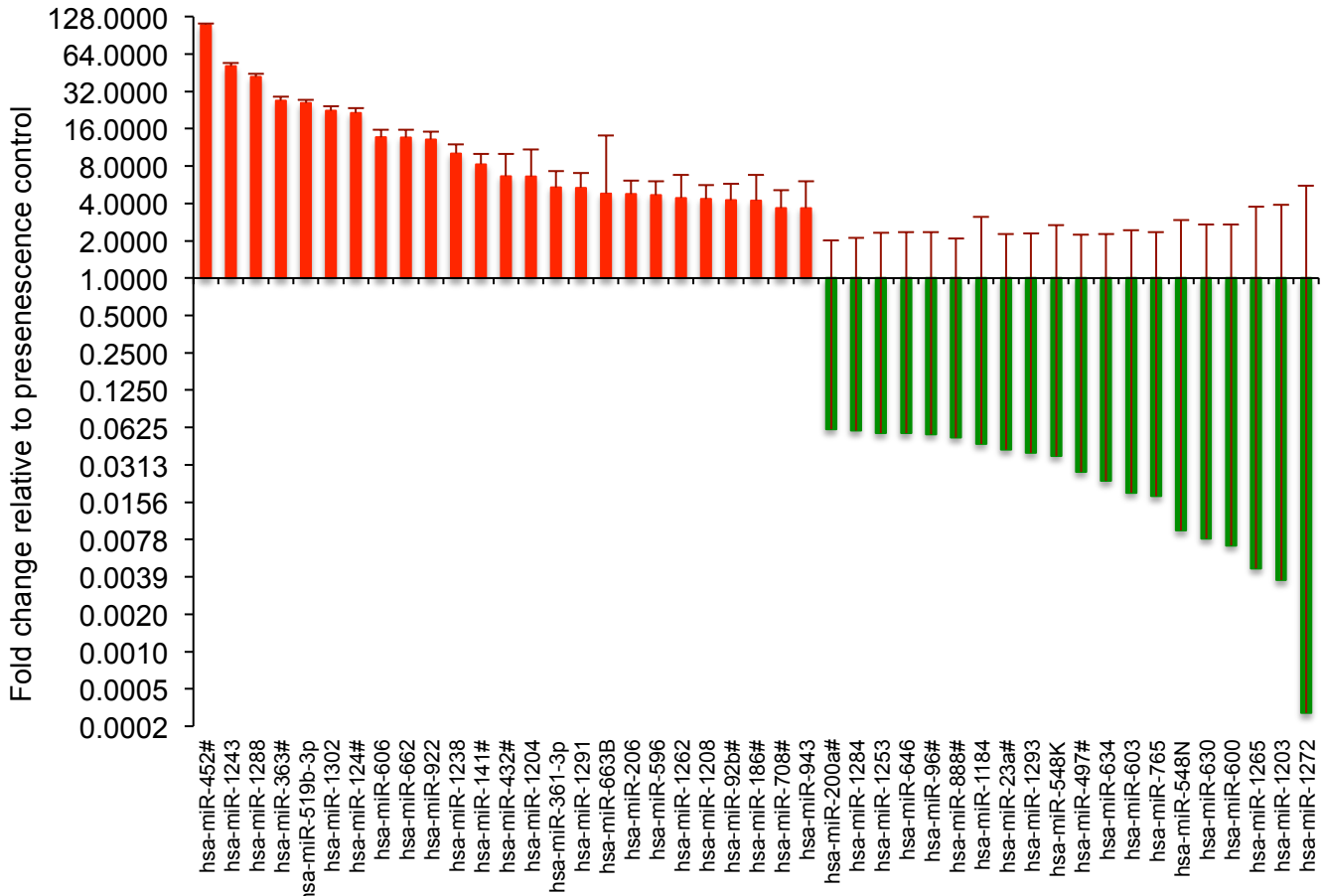

Figure 3.3.2: Differential expression of Pool B miRNA in cisplatin-induced premature senescent oral fibroblasts. TaqMan tiling low density array was used to determine miRNA expression profile in cisplatin-induced premature senescent oral fibroblasts. A cut off point of 34 was applied for Ct. ΔΔCt values were calculated after normalizing the data to U6 endogenous control and presenescent oral fibroblasts. The bars represent mean of fold change + SEM of top 20 up-regulated and down-regulated miRNAs in Pool B card. N=3, *p<0.05, by paired student's t-test.

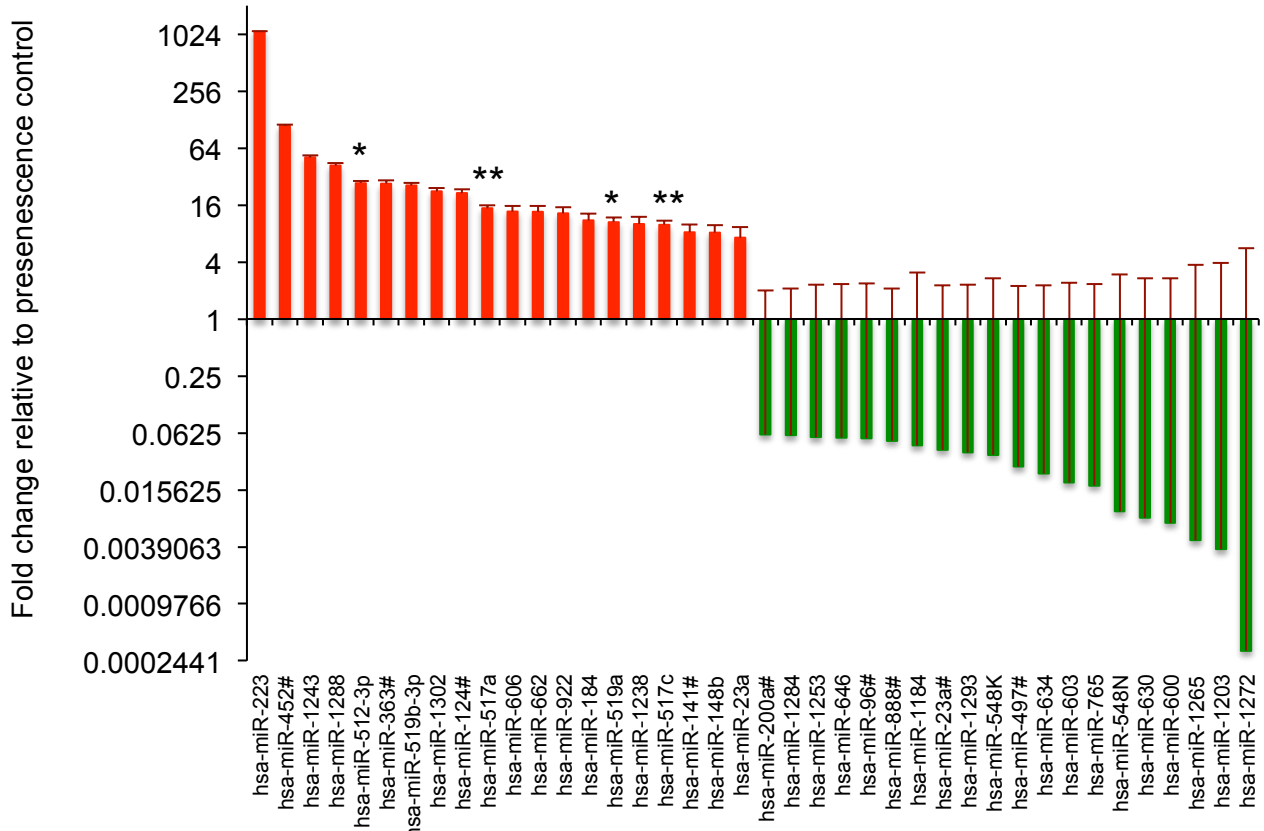

Figure 3.3.3: Top 20 differential expressed miRNA in cisplatin-induced premature senescent oral fibroblasts. The bars represent mean of fold change + SEM of top 20 up-regulated and down-regulated miRNAs from human Pool A and Pool B card. N=3, *p<0.05, by paired student's t-test.

regulation in aged fibroblasts (figure 3.3.4.A). Expression of both of these miRNAs displayed similar pattern in cisplatin-treated oral fibroblasts but were not ranked among the top twenty differentially expressed miRNAs.

In cisplatin-treated oral fibroblasts miR-628-5p was elevated by only 1.8-fold and miR-381 was reduced to only 0.94-times of control cells. The miRNAs which were commonly deranged in both cisplatin-treated and late-passage oral fibroblasts and were included among the top twenty candidates are: miR-23a, miR-137, miR-223, miR-184 and miR-34a (table 3.2). Of these, miR-34a was previously reported to be a direct modulator of TP53 pathway and senescence (He *et al*., 2007) and was increased by 2.4-fold and 2.7-fold in cisplatin-treated and late-passage oral fibroblasts, respectively. Two other miRNAs, which were up-regulated under both conditions but not included within the top twenty range are miR-335 and miR-519a.

Both cisplatin-treated and late-passage oral fibroblasts showed down-regulation of miRNAs belonging to miR-let-7 family (let-7b, let-7d and let-7f) and miR-17 family (miR-17, miR-19a, miR-20b and miR-106a except miR-92, which was down-regulated only in cisplatin-treated cells but remained unaltered upon late-passage) (Dhabi *et al*., 2011; Hackl *et al*., 2010; Faraonio *et al*., 2012) (appendix 2 and 4, table 3.3). It had been proposed in the past that senescent cells exhibited up-regulation of tumour suppressor miRNAs and down-regulation of oncogenic miRNAs that contribute to their tumour suppressive properties in cancer (Hackl *et al*., 2010). In agreement with this theory miR-17-92 cluster was previously reported to function as oncogenic miRNAs in cancer cells (Hackl *et al*., 2010). In contrast let-7 members were classified as tumour suppressor miRNAs in cancer cells (Faraonio *et al*., 2012), which was observed down-regulated in senescent oral fibroblasts in this study, possibly underscoring a distinct mechanism of tumour suppression acting in normal mesenchymal cellular compartments. Expression of two other tumour suppressor miRNAs: miR-15a and miR-

A.

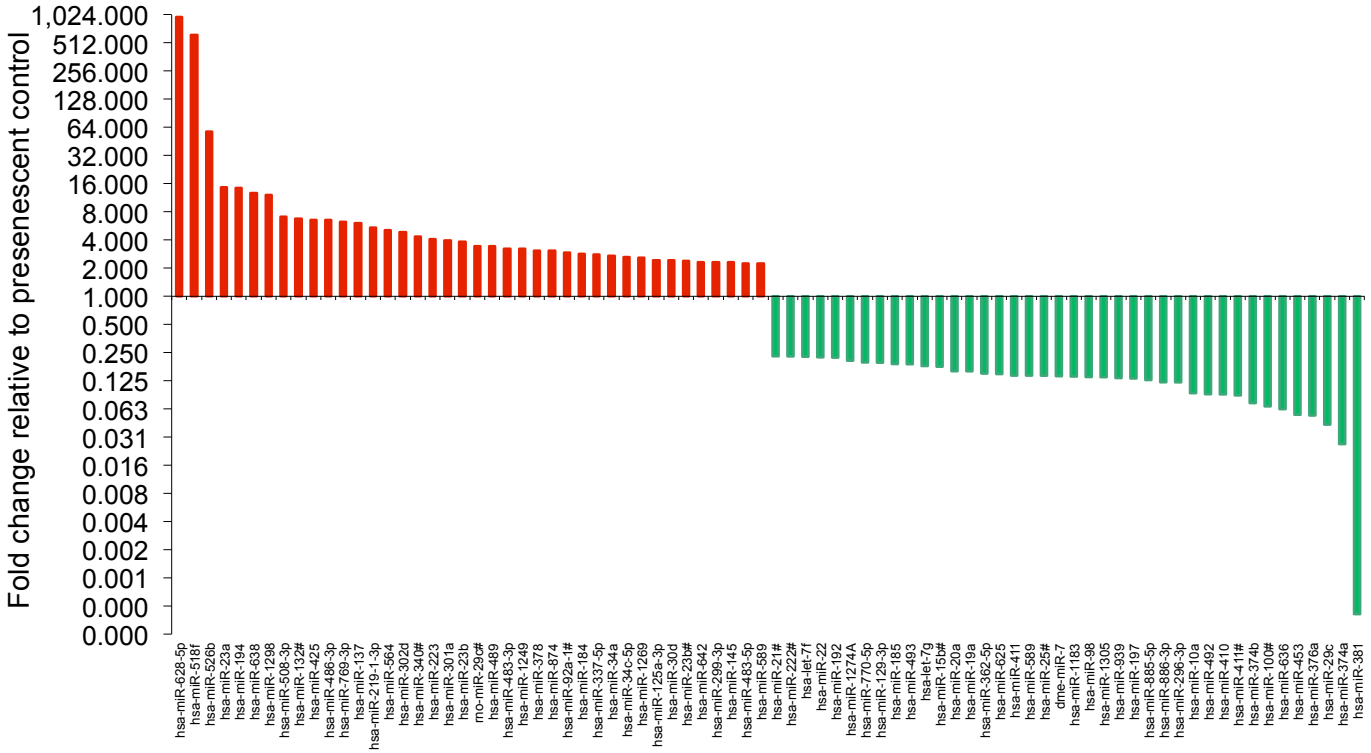

B.

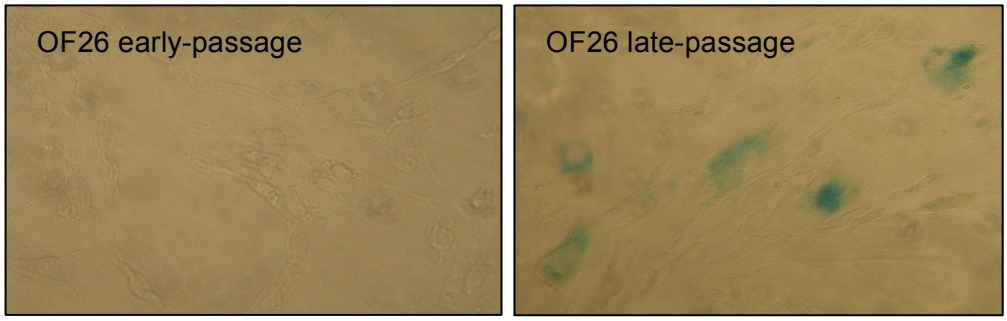

Figure 3.3.4: Differential expression of miRNAs in late passage oral fibroblasts. The bars represent the top 20 up-regulated and down-regulated miRNAs in late passage oral fibroblasts compared to early-passage cells as determined by TaqMan miRNA tiling low density array (A), n=1. Measurement of senescence in late passage-oral fibroblasts demonstrated an increased SA-β-Gal activity compared to early-passage cells visualized by increase in the number of blue stained cells in 96-well microplate (B). N=1.

Derangement	MicroRNA	Fold change	p-Value
Up-regulated	miR-512-3p	27.22	0.028
	miR-517a	14.81	0.002
	miR-517c	9.89	0.008
	miR-519a	10.54	0.02
	miR-335	2.81	0.008
	miR-146a	2.81	0.01
	miR-137	2.43	0.02
	miR-34a	2.37	0.03
	miR-34c	2.00	0.009
	miR-34a#	2.43	0.02
Down-regulated	miR-1278	0.088	0.04
	miR-130b#	0.469	0.04
	miR-16-1#	0.377	0.04
	miR-643	0.347	0.033
	miR-15#	0.332	0.004
	miR-144#	0.252	0.013
	miR-101#	0.249	0.004
	miR-566	0.224	0.025

Table 3.1: List of miRNAs significantly altered in cisplatin-induced premature senescent oral fibroblasts in TaqMan miRNA TLDA. Paired student t-test done to determine changes in miRNA expression that were statistically significant.

Derangement	MicroRNA	Fold change post-cisplatin treatment	Fold change in late-passage
Up-regulated	miR-223	27.22	4.07
	miR-23a	14.81	14.56
	miR-184	9.89	2.84
	miR-137	2.43	6.04
	miR-34a	2.37	2.71

Table 3.2: List of miRNAs altered in both cisplatin-induced premature senescent and late-passage oral fibroblasts in TaqMan miRNA TLDA.

16, reduced in CAFs of prostate cancer (Musumeci *et al*., 2011), were also aberrantly expressed in cisplatin-treated and late-passage oral fibroblasts. In cisplatin-treated oral fibroblasts miR-15a remained unchanged but both miR-16 and miR-15b were reduced to 0.69-times of control fibroblasts. Conversely in late-passage oral fibroblasts expression of miR-15b was unchanged while miR-15a was increased by 2.11-fold and miR-16 was decreased to 0.25-times of control (appendix 2 and 4, table 3.3).

The discrepancies in miRNA expression profile between cisplatin-treated and late-passage oral fibroblasts suggested perhaps there is a difference in regulation of senescence under genotoxic stress from that of the natural process of ageing and perhaps this may underlie the slight disparities in the composition of SASP factors observed in different types of senescent oral fibroblasts and contribute to the variation in their paracrine effects on oral precancerous and cancerous cells (shown in section 3.2).

One of the miRNA identified as modestly down-regulated (0.9-times of control) in cisplatin-induced senescent fibroblasts, miR-145, was previously reported by our group to be diminished in fibroblasts exposed to cigarette smoke condensate (Pal *et al.*, 2013), which may also result in senescence (Coppe *et al*., 2008a). To further probe the

association between miRNA expression profile and the nature of origin of senescent fibroblasts, level of miR-145 were assessed in TLDA and by qRT-PCR in late-passage oral fibroblasts derived from three patients. It was observed according to TLDA miR-145 expression was elevated by 2.3-fold in late-passage oral fibroblasts than early-passage control and was included among the top 20 up-regulated miRNAs in this cell (figure 3.3.4.A). In contrast, validation of miR-145 by qRT-PCR demonstrated a significant decrease in its transcript levels to 0.24-times of control ($n=3$, $p<0.05$, figure 3.3.5.A). Moreover when miR-145 levels were examined in H_2O_2 and cisplatin induced premature senescent oral fibroblasts, it was found significantly reduced to 0.62-times and 0.56-times of control ($n=3$, $p<0.05$, figure 3.3.5.B). Moreover replicative senescent oral fibroblasts generated from the same patient fibroblast used in TLDA (exhibiting 95% SA-β-Gal positivity) also demonstrated a significant decrease in miR-145 levels by 0.8-times of control ($n=3$, $p<0.05$, figure 3.3.5.B). miR-145 was previously reported to decrease in keloid-derived myofibroblasts (activated fibroblasts) that have an increased propensity to senesce (Li *et al*., 2013a; Varmeh *et al*., 2011) and in senescent fibroblasts assessed by deep sequencing (Dhabi *et al*., 2011). Furthermore, we have evidence (Melling *et al*, unpublished data) that miR-145 suppresses the acquisition of a myofibroblastic phenotype in oral fibroblasts. All these findings therefore suggest that miR-145 may participate in emergence of growth arrest state in oral fibroblasts by suppressing pathways, which possibly determines their activation such as the TGF-β pathway (Melling *et al.*, unpublished data), but this requires further investigation.

To further ascertain if the obtained miRNA signature was specific for senescence, expressions of several other candidate miRNAs were examined in the TLDA output. These candidates were a list of miRNAs that had been previously reported to play essential roles in senescence and apoptosis pathway, DDR and SASP development in other systems, to ensure achievement of an indisputable miRNA signature pertaining to SASP of oral fibroblasts.

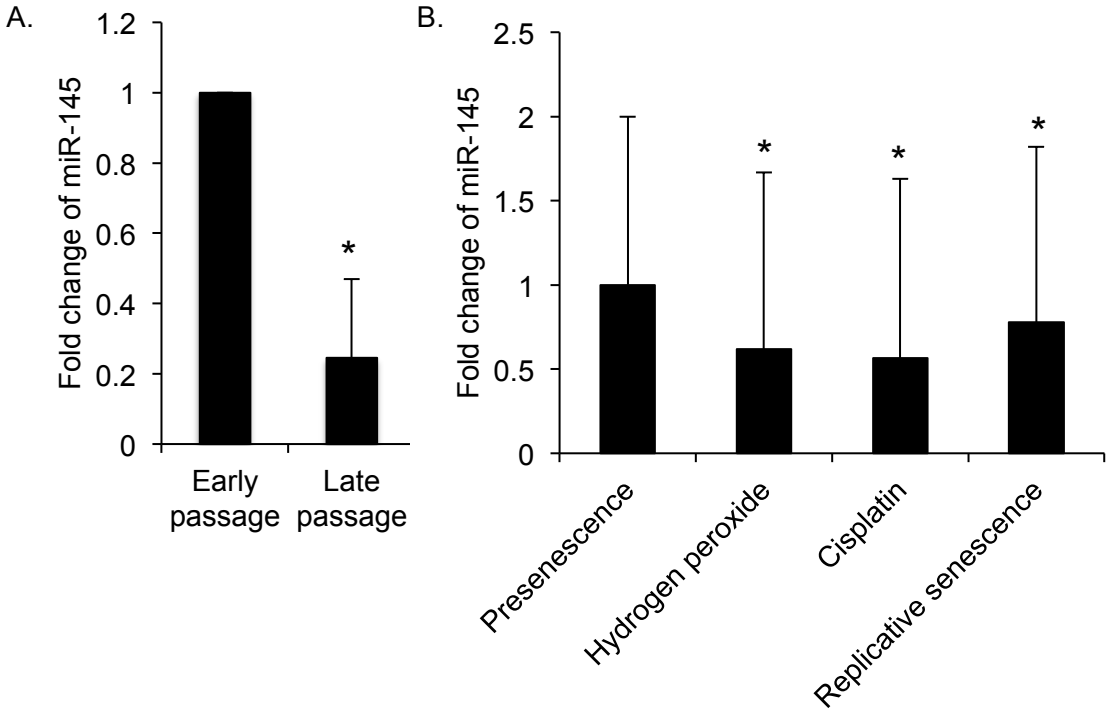

Figure 3.3.5: Expression of miR-145 in late-passage, stress-induced premature senescent and replicative senescent oral fibroblasts. qRT-PCR was used to determine and compare miR-145 mRNA levels among late-passaged, H_2O_2 induced and cisplatin induced premature and replicative senescent oral fibroblasts. RNU48 (A) and U6 (B) were used as the internal control. ΔΔCt was used to calculate fold change compared to control. Bars represent mean of fold change + SEM. N=3, in triplicate. *p<0.05, by paired student's t-test (A) and one-way ANOVA with post-hoc corrections by Dunn's method (B).

One of the hallmarks of senescence is evasion of apoptosis (Reviewed by Campisi and d'Adda di Fagagna, 2007). As a result it was surmised that miRNAs that promoted apoptosis are deregulated in senescent oral fibroblasts. Indeed it was found that miRNAs that regulated apoptosis in head and neck cancer cell lines in response to cisplatin treatment as reported by Huang *et al.* (2011), were inversely expressed in senescent oral fibroblasts in this study. It was observed that pro-apoptotic miRNAs: miR-885-3p and miR-630 which were up-regulated in head and neck cancer cell lines during apoptosis were remarkably reduced to 0.1-times and 0.008-times of control in cisplatin-induced premature senescent oral fibroblasts (appendix 2, table 3.3). Similarly anti-apoptotic miRNAs: miR-519a and miR-181a, that were down-regulated in apoptotic head and neck cancer cells were found elevated in cisplatin-induced senescent oral fibroblasts by 10.5-fold and 1.5-fold, respectively (appendix 2, table 3.3). This implied that possibly the apoptotic machinery is deregulated in premature senescent oral fibroblasts and this allows them to escape apoptosis.

Next, the expression of four miRNAs: miR-26b, miR-210, miR-181a and miR-424 reported to show positive association with p16 expression in senescent cells (Overhoff *et al*., 2013), were examined. In section 3.2.4, it was demonstrated that cisplatin induces expression of p16 in oral fibroblasts. Therefore it is expected that these four miRNAs may also demonstrate a positive association with p16 expression in cisplatin-induced senescent oral fibroblasts. Certainly it was found that except miR-26b, all other miRNAs which increase with p16 expression are up-regulated in cisplatin-treated oral fibroblasts: miR-210 by 1.8-fold, miR-181a by 1.5-fold and miR-424 by 1.2-fold. In contrast only miR-424 was found elevated in late-passage oral fibroblasts by 2.1-fold (appendix 2, table 3.3).

Moreover miRNAs which were previously reported to target *CDKN1A* (encoding p21): miR-106a, miR-93 and miR-20a were found down-regulated in both late-passage and cisplatin-treated oral fibroblasts in concordance with increased expression of p21

mRNA in senescent oral fibroblasts (figure 3.1.1.7) (Gomex-Cabello *et al*., 2013). Furthermore both cisplatin-treated and late-passage oral fibroblasts expressed more DDR associated miRNAs: miR-23b and miR-485-5p (Faraonio *et al*., 2012), which were increased by 2.6-fold and 1.44-fold and 1.5-fold and 3.8-fold, respectively, in comparison to control fibroblasts (appendix 2 and 4, table 3.3).

Among these miRNAs, a higher level of miR-424 was previously reported in CAFs of endometrial cancer (Apprelikova *et al*., 2010) that have myofibroblastic properties. Expression of miR-23b was reported to increase in keloid fibroblasts and predicted to target genes in TGF-β pathway, MAPK pathway and cell cycle (Li *et al*., 2013a). Aberrant expression of these miRNAs along with miR-145 in both late-passage and stress-induced senescent oral fibroblasts suggested that possibly before fibroblasts reached senescence fate they may undergo a preceding myofibroblastic transitory state evidenced by the overlap in deregulation of miRNAs and genes between senescent fibroblasts and myofibroblast-like cells, but this requires further investigation.

Lastly levels of SASP-associated miRNAs were examined in senescent oral fibroblasts. In addition to being a positive regulator of p16 and an inducer of senescence, miR-210 is also linked with the inflammatory SASP of hypoxic senescent stroma in prostate cancer (Taddei *et al*., 2014; Faraonio *et al*., 2012). miR-146a is another inflammatory miRNA that is also associated with SASP of senescent cells wherein it acts as a negative regulator (Bhaumik *et al*., 2009) and is reported to be critical for myofibroblast transdifferentiation because it targets genes acting downstream of TGF-β pathway (Liu *et al*., 2011).

Examination of aged oral fibroblasts for miR-146a expression in TLDA showed it was significantly up-regulated in cisplatin-treated oral fibroblasts by 2.8-fold ($n=3$, $p<0.05$, figure 3.3.1 and 3.3.3) but was down-regulated in late-passage oral fibroblasts to 0.25-times of control. Since the late-passage oral fibroblasts was derived from a different

MicroRNA	Levels	Related pathway	Past evidence
miR-let-7 family (let-7b, let-7d, let-7f)	↓	Tumour suppressor	Faraonio *et al*., 2012
miR-17 family (miR-17, miR-19a, miR-20a, miR-20b, miR-106a)	↓	Oncogenic miR-19a targets PTEN miR-106a, 20a targets p21	Hackl *et al*., 2010; Gomex-Cabello *et al*., 2013
miR-16	↓	Targets FGFR1 and FGF-2	Musumeci *et al*., 2011
miR-15b	↓		
miR-15a	↑		
miR-145	↓	Myofibroblast transdifferentiation	Melling *et al*., unpublished data
miR-885-3p	↓	Pro-apoptotic	Huang et al., 2011
miR-630			
miR-519a	↑	Anti-apoptotic	
miR-181a	↑	Anti-apoptotic Positive association with p16	Huang *et al*., 2011; Overhoff *et al*., 2013
miR-210	↑	Positive association with p16 miR-424 is up-regulated in CAFs miR-210 is associated with SASP	Overhoff *et al*., 2013; Taddei *et al*., 2014
miR-424			
miR-23b	↑	DDR miR-23b targets TGF-β regulated genes	Faraonio *et al*., 2012; Li *et al*., 2013a
miR-485-5p			
miR-146a	↑	SASP associated and targets genes of TGF-β pathway	Bhaumik *et al*., 2009; Liu *et al*., 2011

Table 3.3: Characterisation of senescence-associated miRNA signature in cisplatin-induced premature senescent and late-passage oral fibroblasts.

patient and had less percentage of senescent cells (only 60% SA-β-Gal positive) miR-146a expression was validated by qRT-PCR in different types of senescent oral fibroblasts derived from the same patient used for cisplatin treatment in TLDA that demonstrated more than 80% SA-β-Gal activity. It was observed that miR-146a level was increased by 4.1-fold in both H_2O_2 and cisplatin-induced premature senescent cells and by 4.6-fold in replicative senescent cells ($n=3$, $p<0.05$, figure 3.3.6.A). Moreover ongoing work in this lab shows that indirect co-culture of oral fibroblasts with OSCC cells stimulates miR-146a expression, in keeping with their inflammatory phenotype (also suggested in section 3.2.9).

Most of the miRNAs mentioned above to generate and confirm a SASP-associated miRNA signature in senescent oral fibroblasts had been functionally characterized, albeit in different cell types, by other research groups. Therefore to identify and select a list of entirely novel candidate miRNAs from TLDA output that may play a regulatory role in SASP of oral fibroblasts three criteria were used. First, the miRNAs must show similar expression profile in both cisplatin-treated and late-passage oral fibroblasts. Second, the range of Ct values obtained from real-time PCR must lie between 20 and 30 cycles after using pre-amplified cDNA for amplification. Third, the candidate miRNAs must be computationally predicted, or functionally demonstrated, to target genes that are likely to play a role in cueing stromal-tumour cross-talk. Using these criteria six miRNAs were chosen for further investigations. Apart from miR-146a, which was used as a positive control (as this had been previously characterized in fibroblasts by other groups, Bhaumik *et al.*, 2009), other candidate miRNAs included miR-184, miR-519a, miR-205, miR-335 and miR-148b. Among these miRNAs the TaqMan probe used to validate miR-519a and miR-205 produced abnormal Ct values and amplification plots and were therefore excluded from further study.

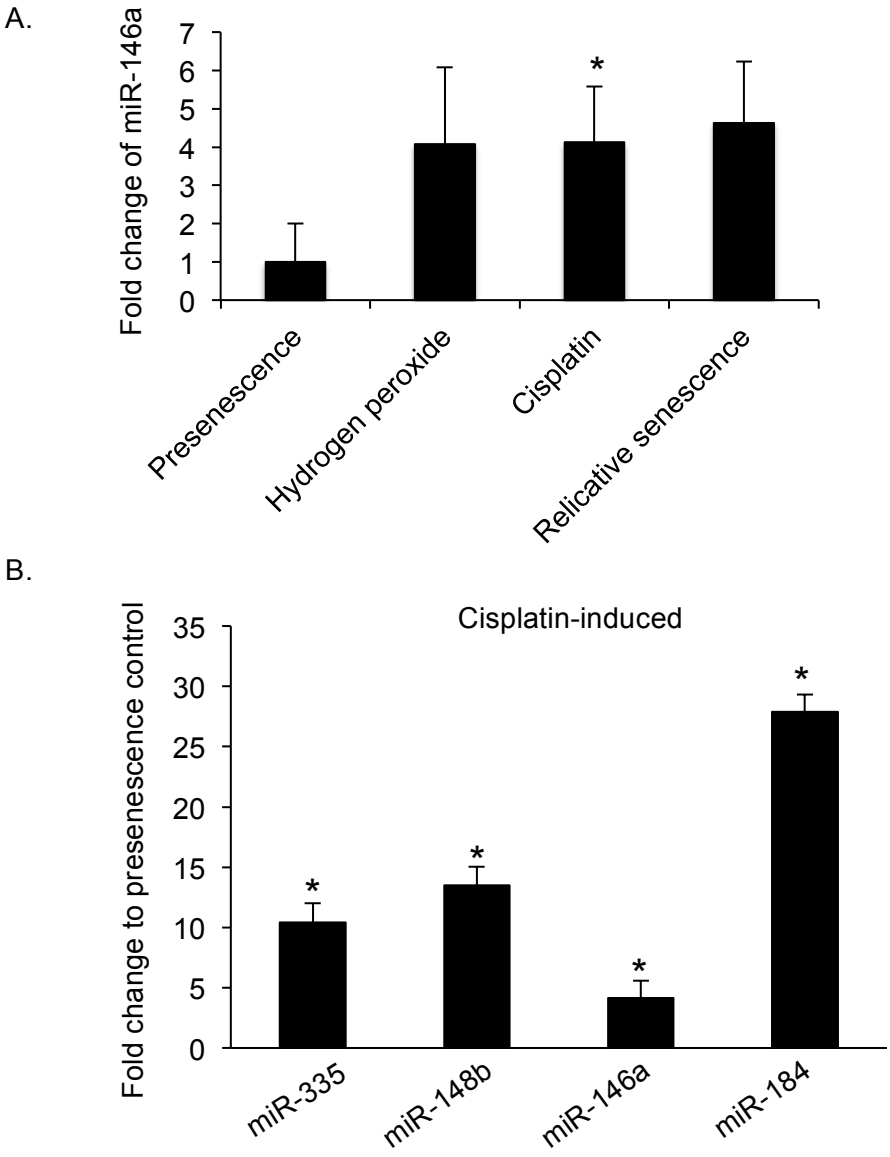

Figure 3.3.6: Validation of candidate miRNAs in senescent oral fibroblasts. qRT-PCR was used to determine mRNA levels of miR-146a in senescent oral fibroblasts (A) and levels of miR-335, miR-148b and miR-184 in cisplatin-induced premature senescent oral fibroblasts (B). U6 was used as the endogenous control. ΔΔCt value was calculated to determine fold expression in comparison to presenescent control. The bars represent mean of fold change + SEM. N=3, in triplicate. *p<0.05, by one-way ANOVA with post-hoc correction by Holm-Sidak method. Paired student's t-test was used for miR-146a validation and Dunn's method based post-hoc correction was used for miR-184 validation.

In cisplatin-treated oral fibroblasts both miR-184 and miR-335 levels were significantly increased by 11.1-fold and 2.8-fold, respectively (n=3, $p<0.05$) while miR-148b was increased by 8.2-fold compared to presenescent control in TLDA (figure 3.3.3). Late-passage oral fibroblasts also had higher levels of miR-184 and miR-335, which were increased by 2.8-fold and 2.1-fold, respectively, in comparison to early-passage cells. In contrast expression of miR-148b was found reduced in late-passage fibroblasts (appendix 4). miR-148b was still chosen for further study because it had good Ct value and previously it was reported that miR-148/-152 family were deregulated in advanced stages of cancer and were associated with development of chemotherapy resistance (Shen *et al*., 2014; Cimino *et al*., 2013).

Freshly prepared samples from three independent experiments were used to validate miRNA expression profile of candidate miRNAs in cisplatin-treated, H_2O_2-treated and replicative senescent oral fibroblasts by qRT-PCR. Cisplatin-treated oral fibroblasts demonstrated a significant increase in expression of miR-335 by 10.4-fold, miR-148b by 13.5-fold and miR-184 by 27.9-fold compared to presenescent oral fibroblasts (n=3, $p<0.05$, figure 3.3.6.B). miR-146a was also significantly elevated but by 4.12-fold only (n=3, $p<0.05$, figure 3.3.6.B). To evaluate if the expression profiles of these miRNAs were associated with SASP development, the transcript levels of each of these candidate miRNAs were measured in cisplatin-treated oral fibroblasts at three different time-points: day 5, day 10 and day 15. It was demonstrated earlier in the study (figure 3.1.2.2) that development of SASP is a gradual process that peaked around day 15, therefore if the selected miRNAs were indeed regulating SASP they must show a similar pattern of expression.

It was observed after cisplatin treatment expression of miR-146a increased gradually from 1.3-fold on day 5 to 2.3-fold on day 10 and reached 10.2-fold on day 15 compared to presenescent control. Two-way repeated measures ANOVA demonstrated that miR-146a transcript levels was significantly higher in oral fibroblasts at day 15 post-

treatment compared to its level on day 5 and day 10 in cisplatin treated cells and untreated controls (n=3, $p<0.05$; figure 3.3.7.A).

Similarly miR-184 transcripts also increased gradually in cisplatin-treated oral fibroblasts rising from 1.6-fold on day 5 to 2.4-fold on day 10, reaching 4.7-fold on day 15 than control cells. The increase was found significantly higher on day 10 and day 15 in cisplatin-treated oral fibroblasts compared to day 5 samples and presenescent control cells (n=3, $p<0.05$; figure 3.3.7.B).

Expression of both miR-335 and miR-148b were also increased progressively in cisplatin-induced premature senescent oral fibroblasts from 1.6-fold and 1.1-fold on day 5 to 4.3-fold and 2.7-fold on day 10 to a maximum level of 8.7-fold and 10.5-fold on day 15, respectively, compared to presenescent control (figure 3.3.8). Two-way repeated measures ANOVA showed transcript levels of both miR-335 and miR-148b in cisplatin-treated oral fibroblasts increased significantly from day 5 to day 10 to day 15 following drug treatment, however, compared to presenescent controls their levels were only significantly higher on day 15 samples post-treatment (n=3, $p<0.05$, figure 3.3.8).

The resemblance in time-course between increase in miRNA expression to that of development of SASP in cisplatin-treated oral fibroblasts (figure 3.1.2.2) suggested that alterations in the levels of these miRNAs may modulate gene expression in senescent oral fibroblasts which can regulate secretion of various factors contributing to SASP of aged fibroblasts.

To further confirm that the changes in expression of the candidate miRNAs in cisplatin-treated oral fibroblasts were an effect of senescence and not a direct effect of chemotherapeutic toxicity, their levels were determined in H_2O_2-induced and replicative senescent oral fibroblasts by qRT-PCR. It was observed that like cisplatin H_2O_2-induced premature senescent oral fibroblasts also showed a dramatic increase in expressions of miR-335 by 3.4-fold, miR-148b by 12.1-fold and miR-184 by 26.5-fold

than presenescent control (n=3, $p<0.05$, figure 3.3.9.A) with miR-146a levels elevated by 4.0 fold. Similarly replicative senescent oral fibroblasts also demonstrated significant up-regulation of both miR-335 and miR-148b by 32.2-fold and by 9.3-fold, respectively (n=3, $p<0.05$) and an insignificant increase in miR-184 expression by 4.2-fold compared to presenescent control (figure 3.3.9.B). miR-146a was increased by 4.63-fold in replicative senescent cells.

Among the candidate miRNAs only miR-335 and miR-148b displayed significant change upon attainment of senescence in oral fibroblasts irrespective of the type of triggering stimuli and were therefore selected for further study.

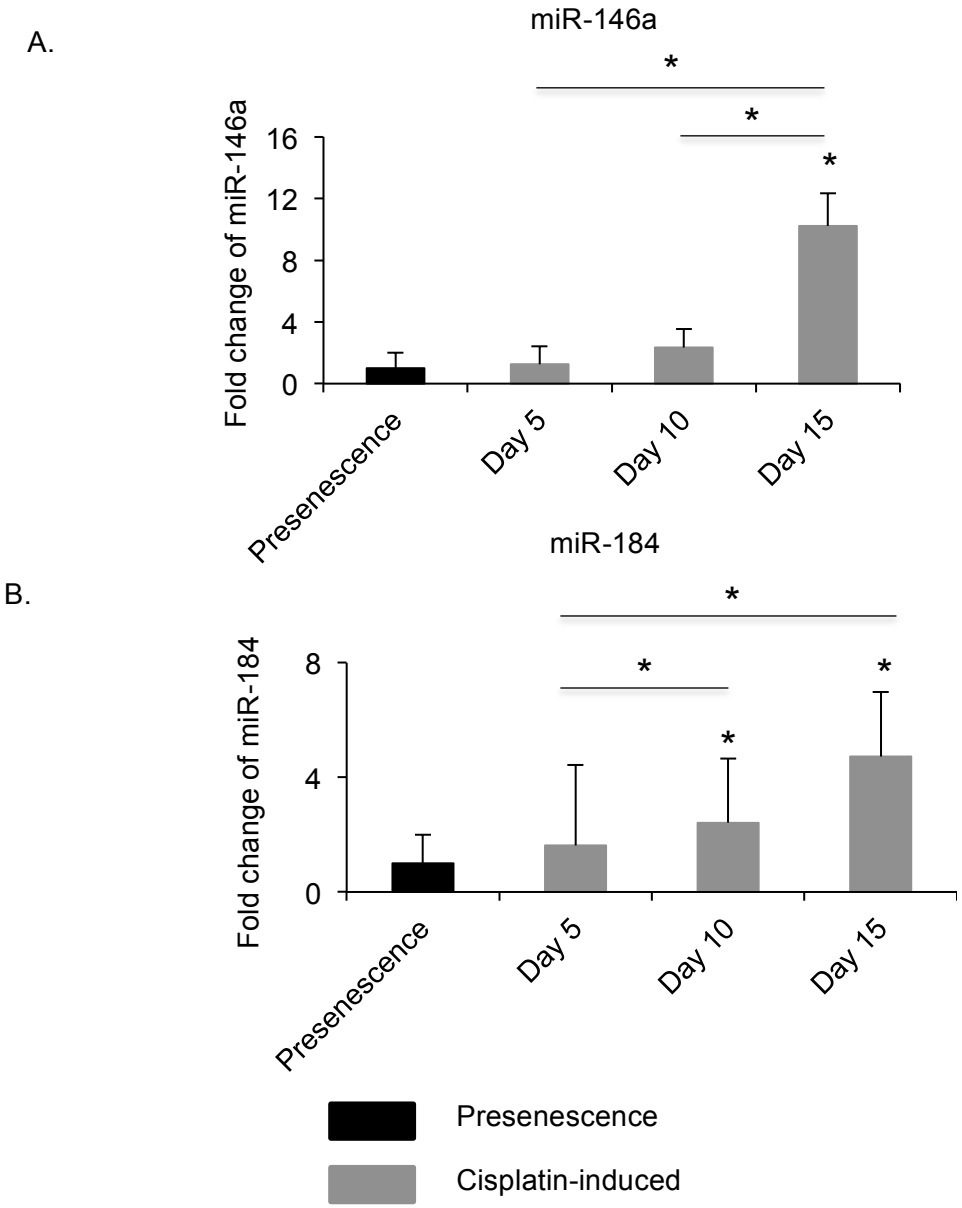

Figure 3.3.7: miR-146a and miR-184 transcripts are gradually elevated in cisplatin-treated oral fibroblasts. qRT-PCR was used to determine expression of miR-146a (A) and miR-184 (B) at different time-points in cisplatin-treated oral fibroblasts compared to control. U6 was used as the endogenous control. ΔΔCt values were calculated to measure fold change. The bars represents mean of fold change + SEM. N=3, in triplicate. *$p<0.05$, two-way repeated measures ANOVA with post-hoc correction by Holm-Sidak method.

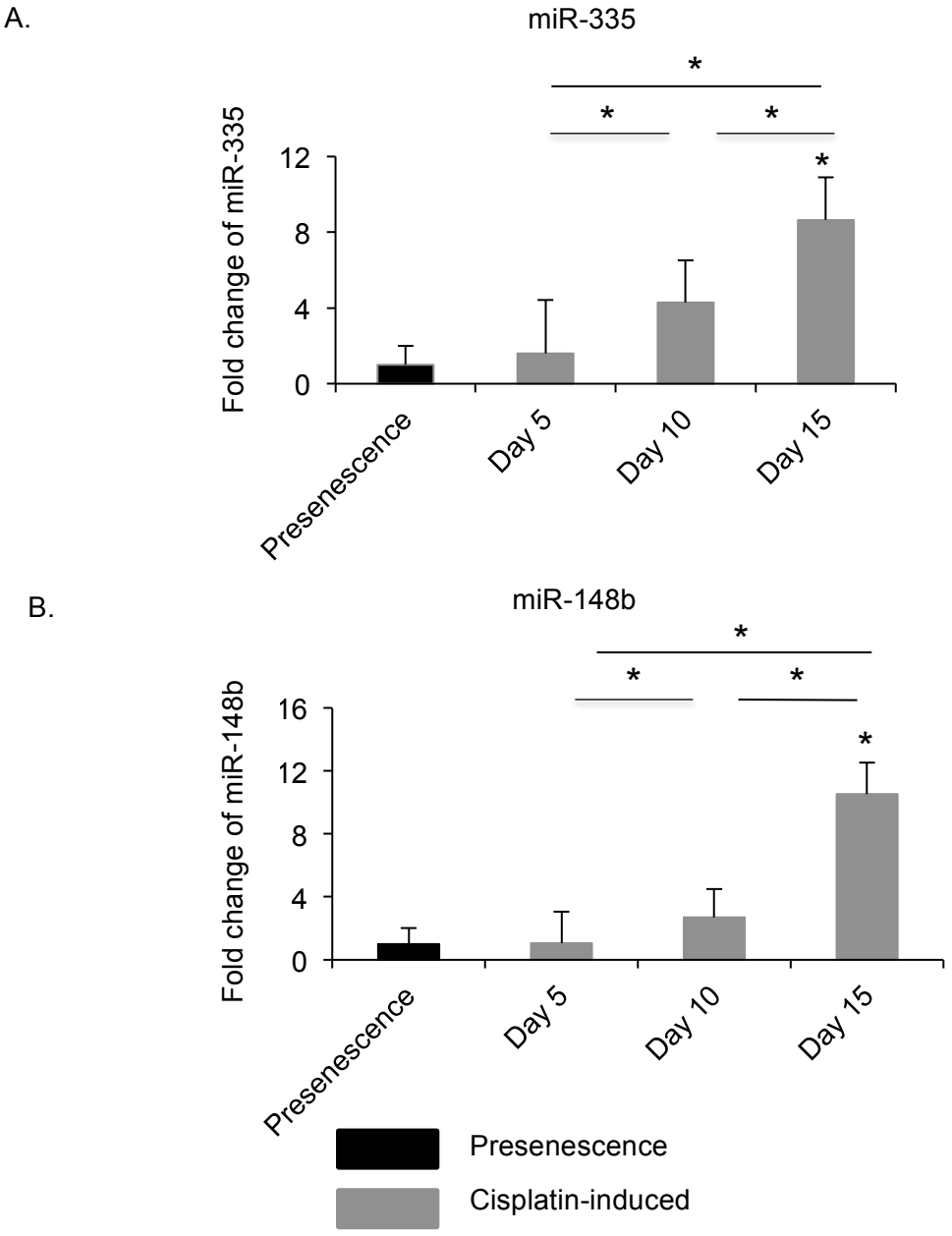

Figure 3.3.8: miR-335 and miR-148b transcripts are gradually elevated in cisplatin-treated oral fibroblasts. qRT-PCR was used to determine expression of miR-335 (A) and miR-148b (B) at different time-points in cisplatin-treated oral fibroblasts compared to control. U6 was used as the endogenous control. ΔΔCt values were calculated to measure fold change. The bars represents mean of fold change + SEM. N=3, in triplicate. *p<0.05, two-way repeated measures ANOVA with post-hoc correction by Holm-Sidak method.

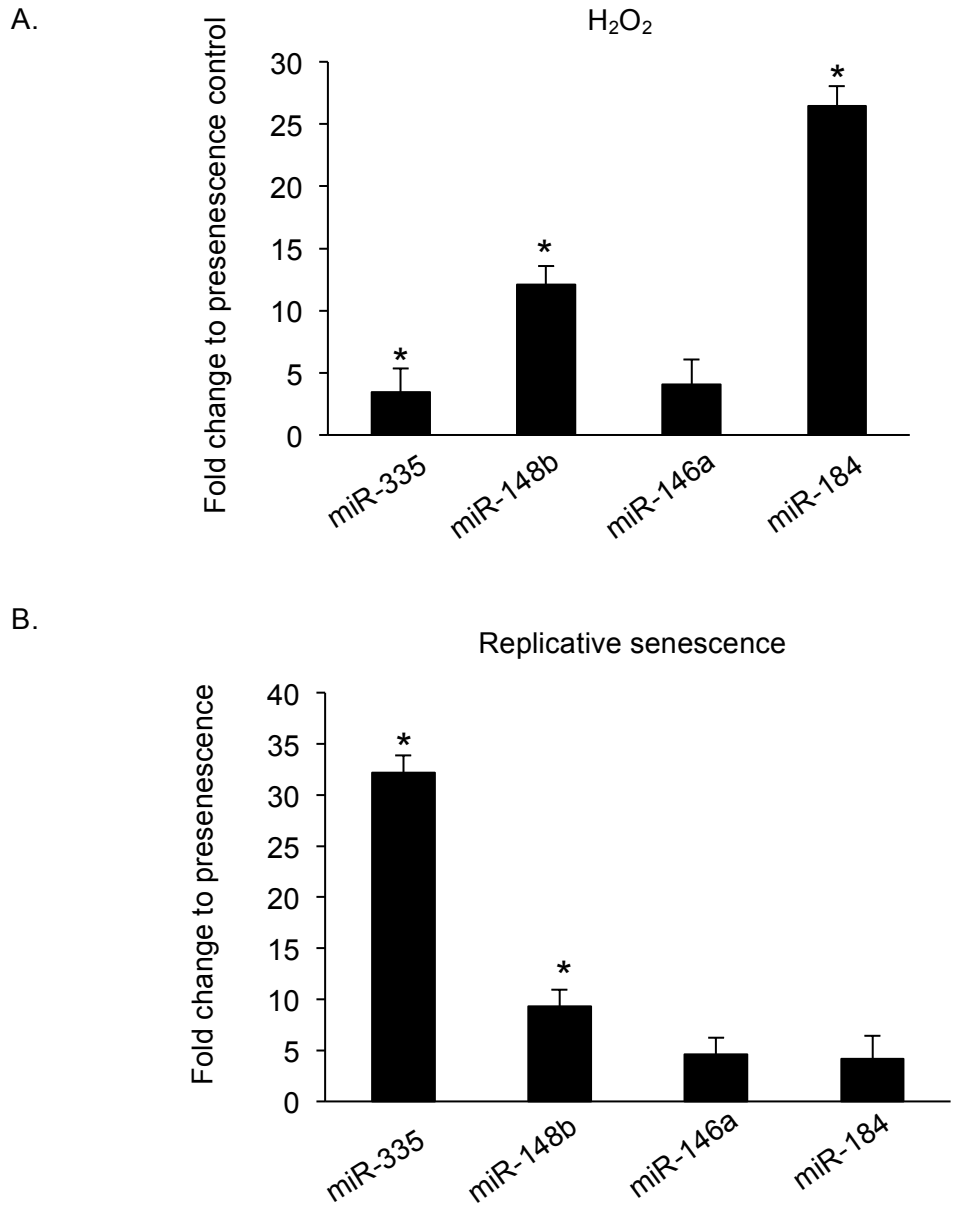

Figure 3.3.9: miR-335 and miR-148b were significantly elevated in H_2O_2-induced and replicative senescent oral fibroblasts. qRT-PCR was used to determine miRNA expression in H_2O_2-treated (A) and replicative senescent oral fibroblasts (B). U6 was used as the endogenous control. ΔΔCt was calculated to determine fold expression to presenescent control fibroblasts. The bars represent mean + SEM. N=3, in triplicate, *p<0.05, by one-way ANOVA with post-hoc correction by Holm-Sidak method. Paired student's t-test was used for miR-146a validation and Dunn's method based post-hoc correction was used for miR-184 validation.

3.3.1: Determination of the role of miR-335 and miR-148b in SASP of oral fibroblasts

miR-335 is a tumour suppressor miRNA whose levels were found increased in aged human tissues and is reported to directly induce senescence in murine and human cells by targeting superoxide dismutase (SOD2) and retinoblastoma protein (RB1) (Bai *et al*., 2011; Scarola *et al*., 2010, Gao *et al*., 2014). In addition miR-335 was found to attenuate osteogenic and chondrogenic differentiation of human mesenchymal stem cells and limit their immunogenic functions by inducing senescence (Tome *et al*., 2014). Recently miR-335 levels were also found raised in serum of invasive breast cancer patients (Shen *et al*., 2014) and in various human cancer cell lines (Scarola *et al*., 2010). All these evidence suggested that the biological functions of miR-335 is not only restricted to regulation of cell proliferation but it may be equally essential in modulating cell differentiation, tissue regeneration, immunosurveillance and tumour suppression.

In contrast miR-148b is a pleiotropic miRNA acting as both an oncomiR and a tumour suppressor that belongs to the miR-148/-152 family of miRNAs along with miR-148a and miR-152, all bearing the same seed sequence to target mRNAs (reviewed by Chen *et al*., 2013). These miRNAs are important modulators of adipogenic, osteogenic and myogenic differentiation and of immunogenic responses (Reviewed by Chen *et al*., 2013). In addition these miRNAs are deregulated in various autoimmune and autoinflammatory diseases such as IgA nephropathy and atherosclerosis (reviewed by Chen *et al*., 2013). Over-expression of miR-148b has been reported to sensitize lymphoma cells to ionizing radiation and breast cancer cells to chemotherapy (Wu *et al*., 2012; Cimino *et al*., 2013). Among these, only miR-152 was reported elevated in senescent cells (Dhabi *et al*., 2011, Xu *et al*., 2011, Wang *et al*., 2011a). Like miR-335, serum miR-148b levels were also highly elevated in patients of breast cancer (Cuk *et al*. 2012, Shen *et al*., 2014) however its levels were dramatically down-regulated in relapsed cases of breast cancer (Cimino *et al*., 2013) and non-small cell lung cancer,

colorectal cancer, gastric, hepatocellular and cholangiocarcinoma and in animal models of OSCC (Liu *et al*., 2014; Zhang *et al*., 2014; Wang *et al*., 2014; reviewed by Chen *et al*., 2013, Yu *et al*., 2009). The source of circulating miRNAs may be complex and is yet to be fully identified.

Until now no reports are available regarding the biological roles of miR-335 and miR-148b in senescent stroma and in modulation of stromal-tumour cross-talk.

3.3.1.1: Stress-induced premature senescent oral fibroblasts have reduced levels of primary miRNA transcripts

To investigate the functional effects of these miRNAs in senescent fibroblasts it was first necessary to understand if the changes in their mature transcript levels were a result of transcriptional up-regulation of pri-miRNA.

It was observed that the transcript levels of both pri-miR-335 and pri-miR-148b were dramatically reduced in stress-induced senescent oral fibroblasts whereas they were significantly elevated in replicative senescent oral fibroblasts. In cisplatin-treated oral fibroblasts the pri-miR-335 and pri-miR-148b were significantly reduced to 0.11-times and 0.29-times of control, respectively (n= 3, $p<0.05$; figure 3.3.10.A and figure 3.3.10.B). In H_2O_2-treated oral fibroblasts the pri-miR-335 and pri-miR-148b were also remarkably reduced to 0.20-times and 0.57-times of control, respectively (n=3, $p<0.05$; figure 3.3.10.A and figure 3.3.10.B). Conversely in replicative senescent oral fibroblasts the level of primary transcripts of miR-335 was significantly increased by 7.4-fold and of miR-148 was increased by 9.2-fold (insignificant) compared to presenescent control (n=3, $p<0.05$; figure 3.3.10.A and 3.3.10.B).

It was described, in section 1.10.1 (figure 1.6), that pri-miRNA transcripts are endogenously processed by DROSHA/DGCR8 to yield pre-miRNAs which are further processed by DICER to form mature miRNA duplexes in cytoplasm during microRNA

biogenesis (Bartel, 2009). The decrease in primary miRNA transcripts therefore implied that either there is a decrease in transcription of primary miRNA transcript or there is an increase in both DROSHA/DGCR8 and DICER activity, which caused the primary miRNA transcript to be rapidly processed into precursor miRNAs and subsequently into mature miRNAs.

In support of the first theory, bioinformatics database mining showed both miR-335 and miR-148b encoding genes were located within introns of MEST and COPZ1 genes in human chromosome 7 and 12, respectively (UCSC browser). As a result it is possible that enhancement in transcriptional activity of either MEST or COPZ1 gene can generate miR-335 and miR-148b in senescent oral fibroblasts via alternative splicing that could bypass DROSHA processing to directly yield mature miRNA duplexes (reviewed by Westholm and Lai, 2011). This can reduce expression of primary miRNA transcripts with concomitant increase in their mature forms.

On the other hand, the second theory may also hold true because it is also possible that before alternative splicing of mRNA, the hairpin miRNAs are cleaved first which will sequentially be processed by conventional microRNA slicer and dicer machinery (Reviewed by Westholm and Lai, 2011). With regard to this it had been reported before that genotoxic stress stimulated enzymatic activity of DICER (Huang *et al*., 2011). Possibly a similar mechanism exists in premature senescent oral fibroblasts which caused a reduction in primary miRNA transcript levels owing to their rapid rate of processing. In replicative senescent oral fibroblasts the sharp increase in levels of both primary miRNA transcript and its mature form imply perhaps in these cells there is increased transcription of both pri-miR-335 and pri-miR-148b with concomitant rise in the enzymatic activity of both DROSHA/DGCR8 and DICER, which may accelerate their processing into mature miRNAs.

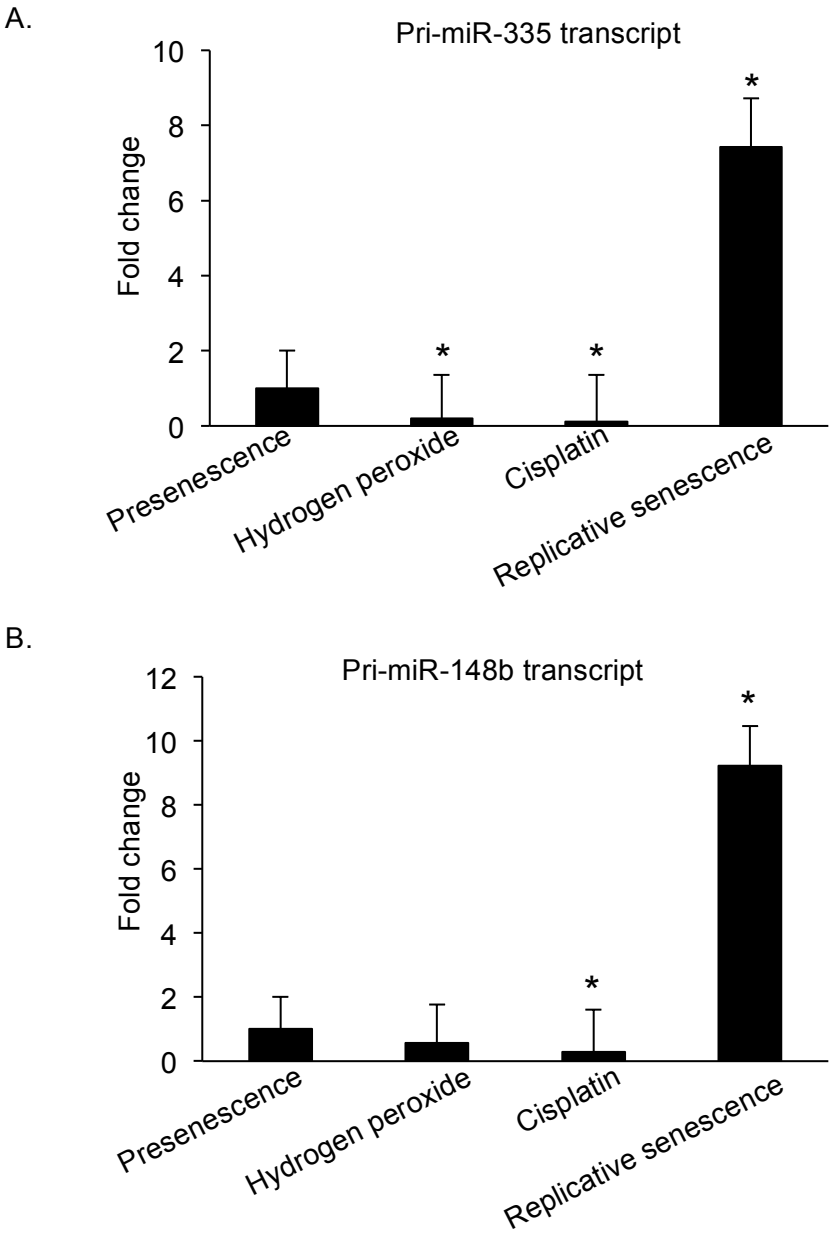

Figure 3.3.10: Senescent oral fibroblasts express less primary miRNA transcripts. qRT-PCR was used to determine expression of human precursor miRNA transcripts for miR-335 (A) and miR-148b (B) in senescent oral fibroblasts. U6 was used as internal control. ΔΔCt was measured to determine fold change to presenescent control. The bars represent mean of fold change + SEM. N=3, in triplicate. *p<0.05, one-way ANOVA with post-hoc corrections by Holm-Sidak method.

3.3.2: Over-expression of miRNAs in senescent oral fibroblasts cause increased synthesis and secretion of SASP factors

To study the functions of miR-335 and miR-148b in SASP, oral fibroblasts were transiently transfected with synthetic human mature miRNA mimics either alone or in combination, or a negative miRNA control precursor. Over-expression of individual miRNAs was validated by qRT-PCR. It was found that oral fibroblasts could be efficiently transfected with miRNA mimics. miR-335 was significantly over-expressed by 34,692-fold and 8,662-fold upon single transfection and co-transfection, respectively, compared to negative control ($n=3$, $p<0.05$, figure 3.3.11.A). miR-148b was also significantly over-expressed by 1,765-fold and 1111-fold in single transfected and co-transfected oral fibroblasts, respectively, compared to negative control ($n=3$, $p<0.05$; figure 3.3.11.B).

Since it had been previously reported that introduction of miR-335 in murine renal mesangial cells or human mesenchymal stem cells induced senescence (Bai *et al*., 2011; Tome *et al*., 2014) the transfected oral fibroblasts were assessed for SA-β-Gal activity. However transient miRNA transfection in oral fibroblasts failed to elicit SA-β-Gal activity. This is probably because these candidate miRNAs were specifically selected for SASP at day 15 post-treatment with genotoxic stimuli and in an established batch of replicative senescent oral fibroblasts in which senescence had been fully induced and developed. Therefore in these cells the candidate miRNAs are probably acting as modulators of SASP rather than participating in senescence induction. Other possibilities for undetectable senescence in miRNA transfected oral fibroblasts may be because miRNA functions are highly tissue specific (Kim *et al.*, 2009) and the duration of transfection was insufficient to induce senescence in young fibroblasts.

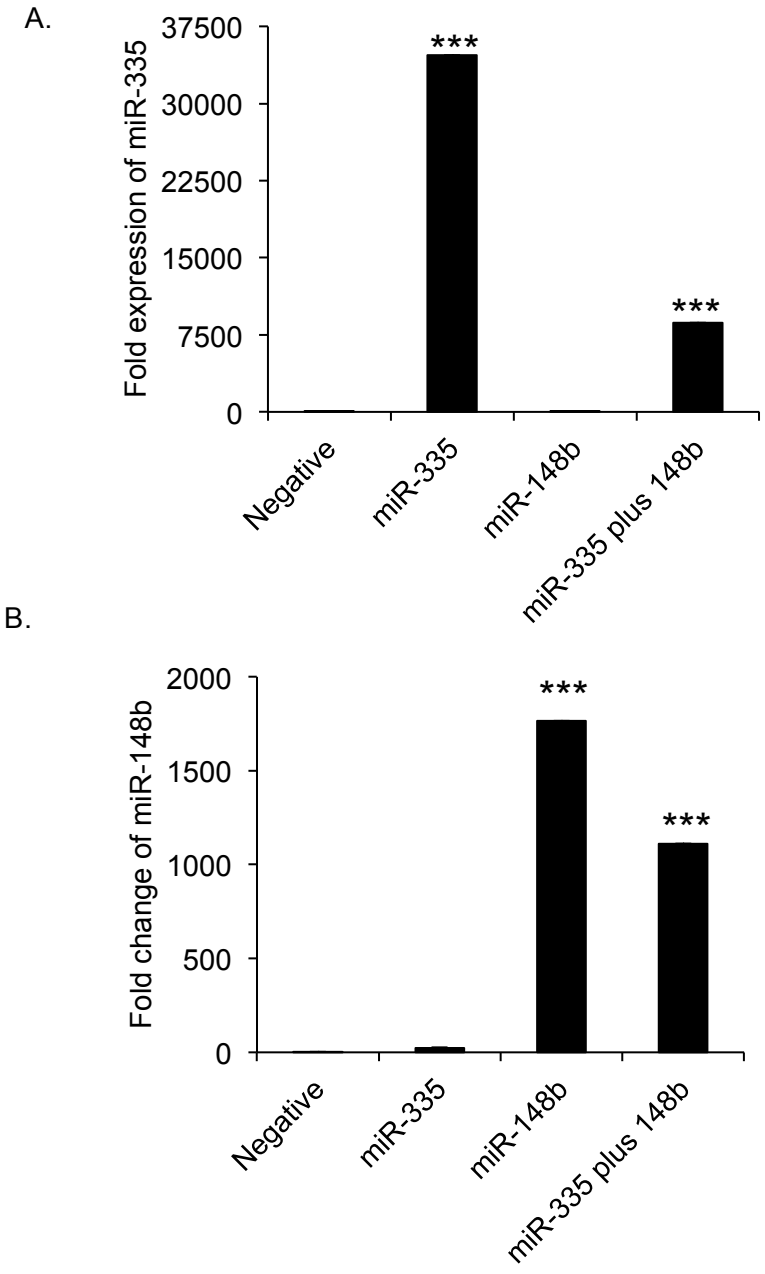

Figure 3.3.11: Validation of miRNA over-expression in human primary oral fibroblasts. Oral fibroblasts were transfected using oligofectamine with mature miRNA mimics at 50 nM. qRT-PCR was used to determine transfection efficiency of miR-335 (A) and miR-148b (B) mimics in human oral fibroblasts. U6 was used as internal control. ΔΔCt was measured to determine fold change to negative control. The bars represent mean of fold change + SEM. N=3, in triplicate. *p<0.05, one-way ANOVA with post-hoc corrections by Tukey test.

Therefore to examine the hypothesis that both miR-335 and miR-148b were associated with SASP the transfected cells were examined for other biomarkers of senescence related to SASP development. The transcriptional activity of TP53, an important mediator of chemotherapy-induced senescence in cancer cells has been implicated in regulation of SASP factor MCP-1 in keratinocyte immune response, induction of miR-335 in DDR associated growth arrest and induction of miR-148b in colorectal cancer cell lines (Hacke *et al*., 2010; Scarola *et al*., 2010, Chang *et al*., 1999a; Wang *et al*., 2014). Oral fibroblasts over-expressing miR-335, miR-148b and both, demonstrated a significant increase in TP53 mRNA by 1.94-fold, 1.50-fold and 1.95-fold, respectively, than negative control (n=3, $p<0.05$; figure 3.3.12.A). To further ascertain the functional activity of *TP53* (Hacke *et al*., 2010; Chang *et al*., 1999a) the transfected cells were assessed for expression of its downstream gene target p21, which was increased in senescent oral fibroblasts. It was found that expression of p21 corresponded to rise in TP53 levels however the change was insignificant in miRNA transfected oral fibroblasts. Over-expression of miR-335 increased p21 by 1.9-fold whereas miR-148b increased it by 1.6-fold compared to negative control (figure 3.3.12.B). In co-transfected cells p21 mRNA was increased by 3-fold (figure 3.3.12.B).

Next, expression of SASP markers MCP-1 and IL-6 were examined in these cells. It was observed over-expression of both miR-335 and miR-148b were associated with a significant increase in MCP-1 mRNA and protein levels in oral fibroblasts (n=3, $p<0.05$). miR-335 increased MCP-1 mRNA and protein by 3.2-fold and 1.60-fold (28.1 ng/mL), respectively, compared to control (figure 3.3.13). miR-148b increased MCP-1 mRNA and protein by 1.7-fold and 1.59-fold (27.9 ng/mL), respectively (figure 3.3.13). Co-transfected oral fibroblasts also demonstrated increased expression of both MCP-1 mRNA and protein by 1.9-fold and 1.71-fold (30 ng/mL), respectively (figure 3.3.13). Control fibroblasts secreted only 17.5 ng of MCP-1.

Conversely miR-335 significantly increased IL-6 transcription by 2.1-fold whereas miR-148b significantly reduced IL-6 transcription to 0.6-times of negative control ($n=3$, $p<0.05$; figure 3.3.14.A). Co-transfected oral fibroblasts also expressed less IL-6 mRNA about 0.7-times of control fibroblasts (figure 3.3.14.A). In contrast although IL-6 secretion was increased in both miR-335 and miR-148b transfected oral fibroblasts their levels were statistically incomparable to negative control fibroblasts. It was observed that miR-335 and miR-148b stimulated IL-6 secretion by 1.5-fold (59 ng/mL) and 1.45-fold (57.7 ng/mL), respectively, compared to control. IL-6 secretion was also increased in co-transfected oral fibroblasts by 1.50 fold (60 ng/mL) (figure 3.3.14.B). Negative control cells secreted 39.8 pg of IL-6 (figure 3.3.14.B).

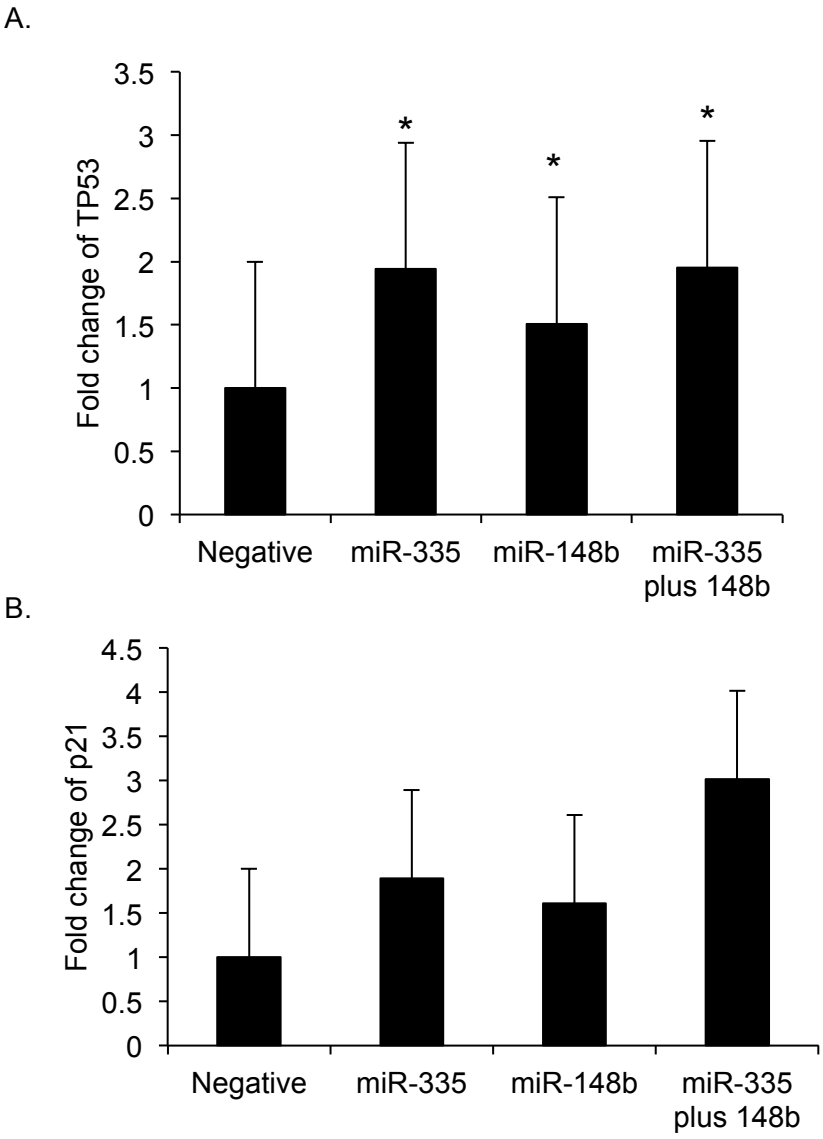

Figure 3.3.12: miR-335 and miR-148b stimulate TP53 activity in oral fibroblasts. Oral fibroblasts were transfected using oligofectamine with mature miRNA mimics at 50 nM. qRT-PCR was used to determine mRNA levels of TP53 (A) and p21/Cip-1 (B). U6 was used as internal control. ΔΔCt was measured to determine fold change to negative control. The bars represent mean of fold change + SEM. N=3, in triplicate. *$p<0.05$, by one-way ANOVA with post-hoc corrections by Dunnett's method.

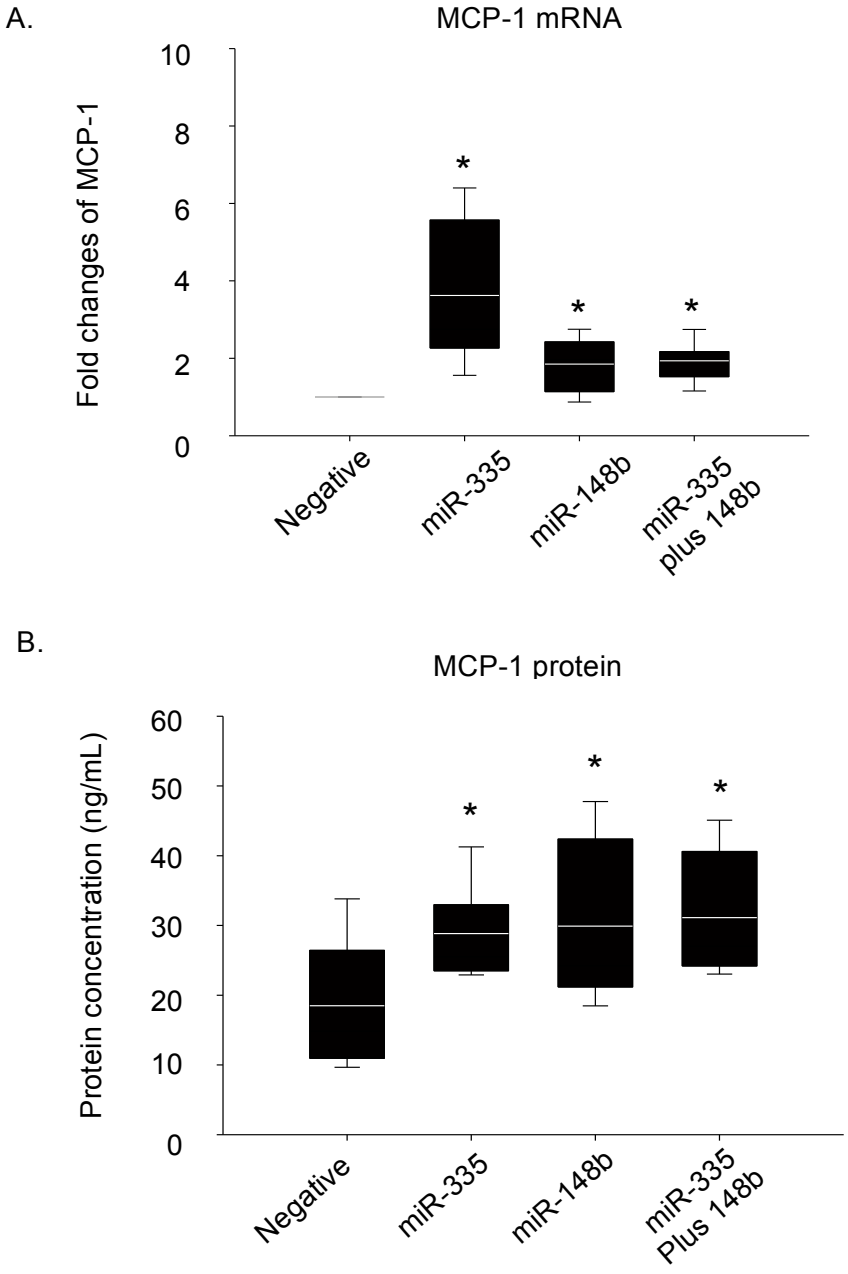

Figure 3.3.13: miR-335 and miR-148b stimulate synthesis and secretion of MCP-1 in oral fibroblasts. Oral fibroblasts were transfected using oligofectamine with mature miRNA mimics at 50 nM. qRT-PCR was used to determine MCP-1 mRNA level (A). U6 was used as internal control. ΔΔCt was measured to determine fold change to negative control. Human MCP-1 ELISA was used to quantify the amount of secreted protein (B). The bars represent mean of fold change + SEM. N=3, in triplicate. *p<0.05, by one-way ANOVA with post-hoc corrections by Holm-Sidak method (A) and Dunnett's method (B).

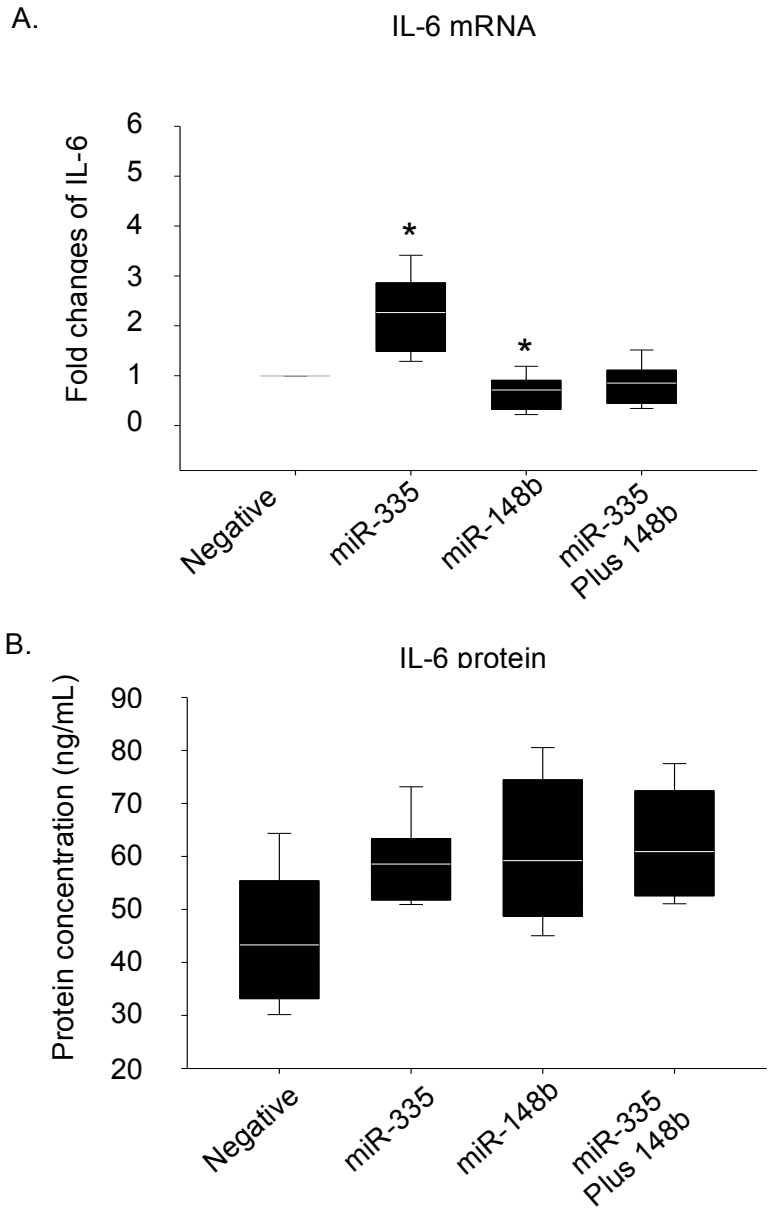

Figure 3.3.14: miR-335 and miR-148b stimulate secretion of IL-6 in oral fibroblasts. Oral fibroblasts were transfected using oligofectamine with mature miRNA mimics at 50 nM. qRT-PCR was used to determine IL-6 mRNA level (A). U6 was used as internal control. ΔΔCt was measured to determine fold change to negative control. Human IL-6 ELISA was used to quantify the amount of secreted protein (B). The bars represent mean of fold change + SEM. N=3, in triplicate, *p<0.05, by one-way ANOVA with post-hoc corrections by Holm-Sidak method (A).

3.3.3: Paracrine effects of miR-335 and miR-148b on OSCC

It was demonstrated in section 3.2 that MCP-1 derived from senescent oral fibroblasts stimulated migration and invasion of OSCC derived cell lines *in vitro*. Further miR-335 and miR-148b identified to be up-regulated in senescent oral fibroblasts stimulated secretion of MCP-1 from oral fibroblasts. Therefore it was hypothesized that over-expression of these two miRNAs in oral fibroblasts may regulate migration and invasion of OSCC in a similar manner to that of senescent oral fibroblasts.

3.3.3.1: Over-expression of miR-335 and miR-148b in oral fibroblasts stimulate migration of OSCC derived cell line H357 cells in 2D assay in MCP-1 dependent manner

At first conditioned media were collected from miRNA transfected oral fibroblasts and their paracrine effect on stimulating migration of H357 cells were determined using 2D transwell assay. It was observed that compared to negative control fibroblasts those over-expressing miR-335 significantly increased the migratory capacity of H357 cells by 1.6-fold ($n=4$, $p<0.05$, figure 3.3.15). Both miR-148b over-expressing and co-transfected oral fibroblasts also significantly stimulated migration of H357 cells by 1.5-fold relative to negative control ($n=4$, $p<0.05$; figure 3.3.15). Next the conditioned media were incubated with either human anti-MCP-1 antibody or isotype IgG control to determine if transfected oral fibroblasts stimulated migration of H357 cells by secreting MCP-1. In presence of isotype IgG control both miR-335 over-expressing and co-transfected oral fibroblasts significantly enhanced the motility of H357 cells by 1.3-fold while miR-148b increased it by 1.6-fold over negative control ($n=3$, $p<0.05$, figure 3.3.16). Blockade of secreted MCP-1 in negative control transfected fibroblasts produced no significant difference in cancer cell migration than their counterpart IgG control. However addition of anti-MCP-1 antibody to conditioned media of miRNA transfected oral fibroblasts dramatically reduced migration of H357 cells *in vitro*

compared to their counterpart IgG control (n=3, $p<0.05$, figure 3.3.16). Anti-MCP-1 antibody reduced migration of H357 cells by 0.6-times, 0.65-times and 0.7-times of IgG control in presence of conditioned media derived from miR-335, miR-148b and co-transfected oral fibroblasts, respectively. The difference in migration of H357 cells in presence of conditioned media derived from negative control and miRNA over-expressing fibroblasts after blockade of MCP-1 secretion were insignificant.

These results therefore suggested that both miR-335 and miR-148b increased secretion of MCP-1 from oral fibroblasts, which eventually stimulated migration of cancer cells *in vitro* implicating their possible regulatory role in SASP of senescent oral fibroblasts.

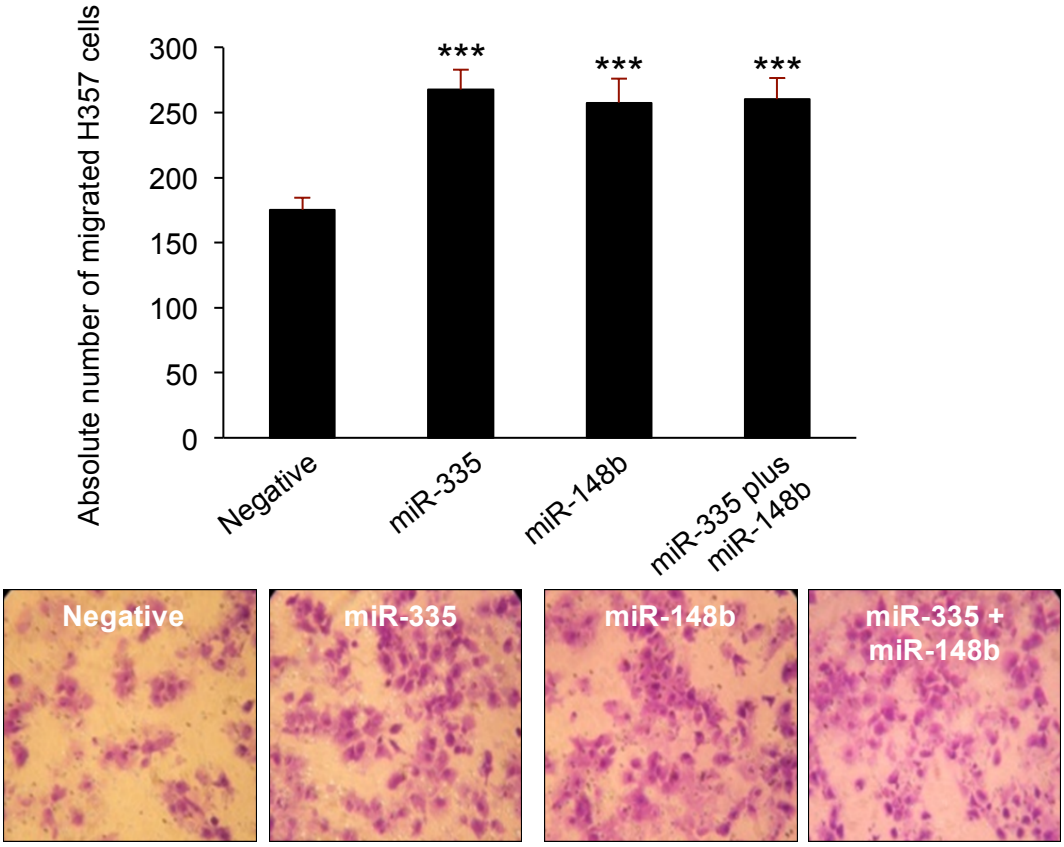

Figure 3.3.15: miR-335 and miR-148b stimulated migration of H357 cell lines *in vitro*. 100,000 H357 cells were seeded down to the top chamber of transwell assay. Conditioned media collected from oral fibroblasts transfected with mature miR-335 and miR-148b mimics and negative control miRNA precursors were pipetted to the bottom chamber. Migration was carried out for 40 h. The cells were fixed and stained with 0.1% crystal violet. Pictures were taken from three separate fields per well at 20X using light microscope as a representative of migrated cells. The bars represent the mean of migrated cells + SEM. N=4, in triplicate. ***p<0.001, pairwise comparison performed with one-way ANOVA with post-hoc corrections by Tukey test.

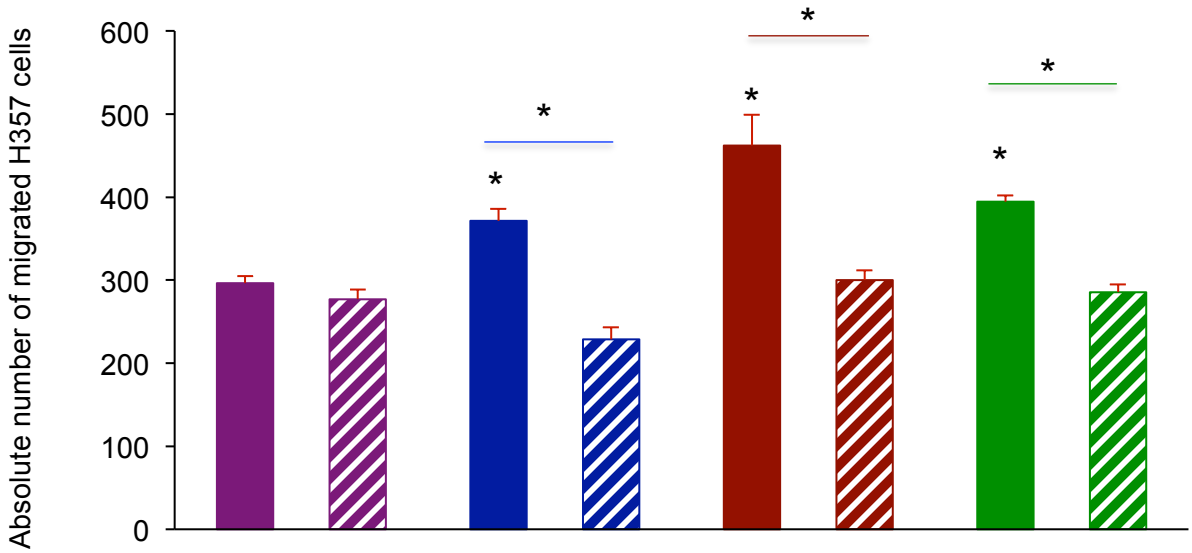

Negative	+	+	-	-	-	-	-	-
miR-335	-	-	+	+	-	-	-	-
miR-148b	-	-	-	-	+	+	-	-
miR-335 plus miR-148b	-	-	-	-	-	-	+	+
Negative IgG control	+	-	+	-	+	-	+	-
anti-MCP-1 antibody	-	+	-	+	-	+	-	+

Figure 3.3.16: MCP-1 secreted by miR-335 and miR-148b over-expressing oral fibroblasts stimulated migration of H357 cell lines *in vitro.* 100,000 cells were seeded on to the top chamber of transwell assay. Conditioned media collected from transfected fibroblasts were added to the bottom chamber in presence and absence of anti-MCP-1 antibody. Isotype IgG was used as control. Migration was carried out for 40 h. The migrated cells were fixed and stained with 0.1% crystal violet. Pictures were taken from three separate fields per well under 20X magnification using light microscope. The bars represent mean of migrated cells + SEM. N=3. *p<0.05, two-way ANOVA with post-hoc corrections by Tukey test.

3.3.3.2: miR-335 and miR-148b reprogram oral fibroblasts to promote invasion of OSCC cell lines *in vitro* in 2D assay

In section 3.2 it was demonstrated that senescent oral fibroblasts promoted invasion of H357 cell lines *in vitro*, at least in part by secreting MCP-1, MMP-2 and inducing EMT-like changes. It was observed that both miR-335 and miR-148b stimulated MMP-2 transcription in oral fibroblasts however the increase was statistically insignificant when compared to negative control (figure 3.3.17.A: lower panel). Further zymography demonstrated no significant difference in the amount of secreted MMP-2 among different types of miRNA transfected fibroblasts (figure 3.3.17.A: upper panel).

Measurement of invasion demonstrated that miRNA transfected oral fibroblasts apparently stimulated invasion of H357 cells in 2D matrigel assay compared to negative control (n=3; figure 3.3.17.B), but this was statistically insignificant. Further measurement of invasive index of H357 cells in presence of conditioned media from miRNA transfected oral fibroblasts showed a rather decrease in the invasive potentials of cancer cells under each conditions compared to negative control (figure 3.3.17.B, left panel). As a result it was concluded that although over-expression of miR-335 and miR-148b in oral fibroblasts appeared to stimulate invasiveness of H357 cells *in vitro*, but this was possibly a superimposition effect produced by their ability to enhance motility of cancer cells and in fact was not true invasion which were brought about by senescent fibroblasts via secretion of MMPs and induction of EMT-like changes in cancer cells.

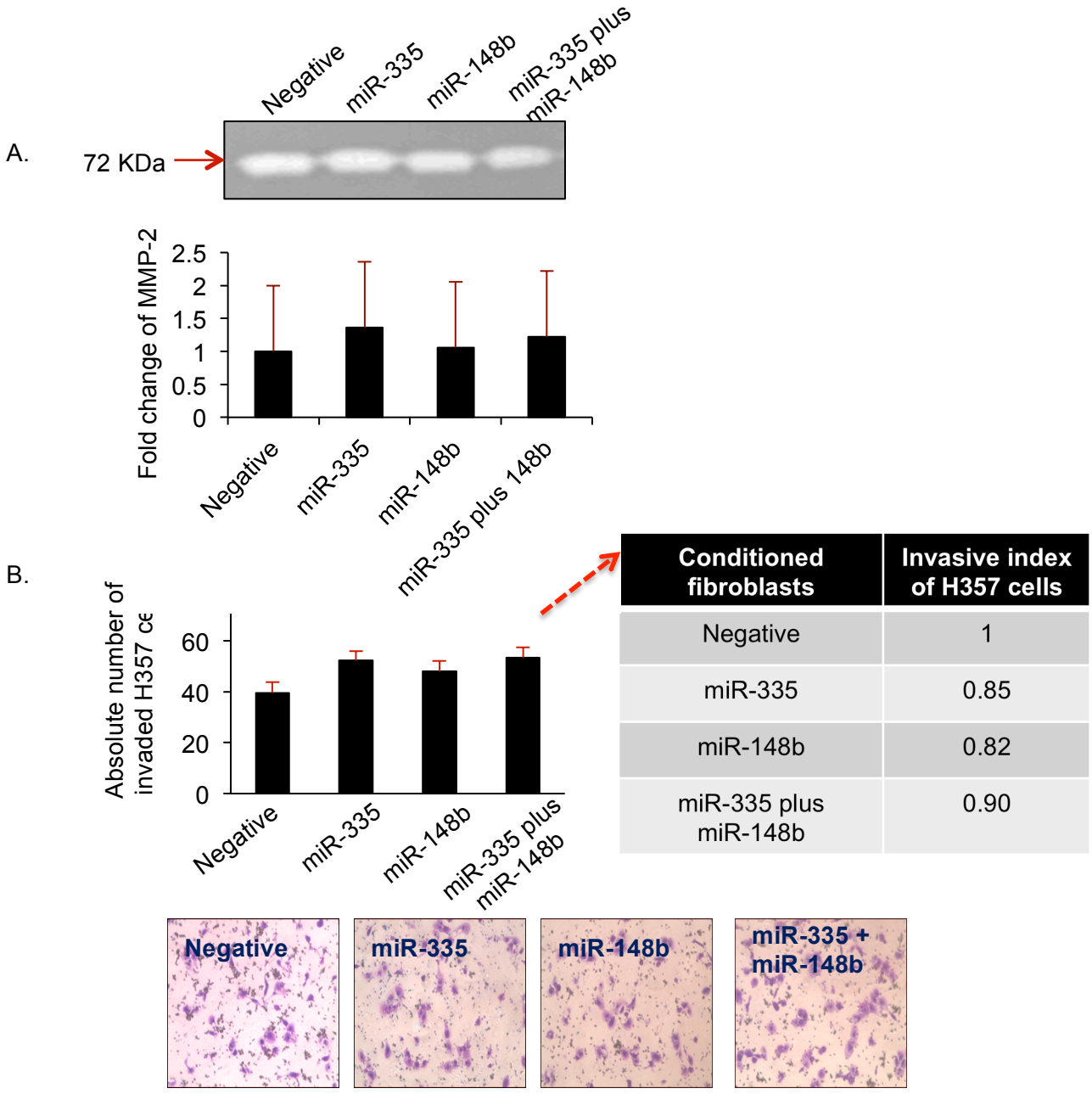

Conditioned fibroblasts	Invasive index of H357 cells
Negative	1
miR-335	0.85
miR-148b	0.82
miR-335 plus miR-148b	0.90

Figure 3.3.17: miR-335 over-expression in oral fibroblasts provoked an apparent increase in H357 cell line invasion *in vitro*. qRT-PCR demonstrated increased synthesis of MMP-2 mRNA in miRNA transfected oral fibroblasts (A, lower panel). miRNA over-expression does not affect the secretory levels of MMP-2 in oral fibroblasts (A, upper panel). Matrigel assay showed miR-335 significantly stimulated invasiveness of H357 cell lines in vitro (B). The bars represent mean + SEM. N=3.

3.3.4: Identification of functional miRNA targets of miR-335 and miR-148b

miRNAs function by binding to complementary 'seed' sequences present predominantly in the 3'UTR of mRNAs to either repress their translation or induce decay. A bioinformatics database, MiRWalk version 2.0, was used to determine putative functional gene targets of miR-335 and miR-148b. This database is a compilation of eight programs that are available online including Targetscan, PITA, PICTAR, miRDB, miRanda, Diana-microT, RNA22 and RNAhybrid used in predicting mRNA targetomes of miRNAs. This in-silico analysis showed that many of the deregulated miRNAs in senescent fibroblasts target the tumour suppressor protein PTEN (figure 3.3.18.A). miR-335 had one and miR-148b had two putative binding sites in the 3'UTR of PTEN mRNA (figure 3.3.18.B).

3.3.4.1: PTEN expression is declined in senescent oral fibroblasts

PTEN has been linked to the aging pathway as it mediates nuclear translocation of FOXO to facilitate expression of genes regulating longevity and senescence (Smith-Vikos and Slack, 2012; Munoz-Espin, 2013). Stromal PTEN is also reported to control mammary gland morphogenesis since birth throughout adult life and during pregnancy (Trimboli *et al*., 2009) and its expression is frequently lost in stroma of breast cancer patients (Perren *et al*., 1999). Further loss of PTEN had been reported in a variety of fibroproliferative disorders (Liu *et al*., 2013, Parapuram *et al*., 2011, Zheng *et al*., 2012). PTEN has long been classified as an important tumour suppressor gene that is a major determinant of cell cycle progression and apoptosis and thus play a pivotal role in regulating sensitivity of cancer cells to cytotoxic therapy (Snietura *et al*., 2012; Bullock *et al*., 2013, Kadera *et al*., 2013). Only recently miRNA mediated loss of PTEN expression in fibroblasts had been linked to emergence of stem cells (He *et al*., 2014b). Moreover growing evidence showed that loss of PTEN could reprogram the stromal

A.

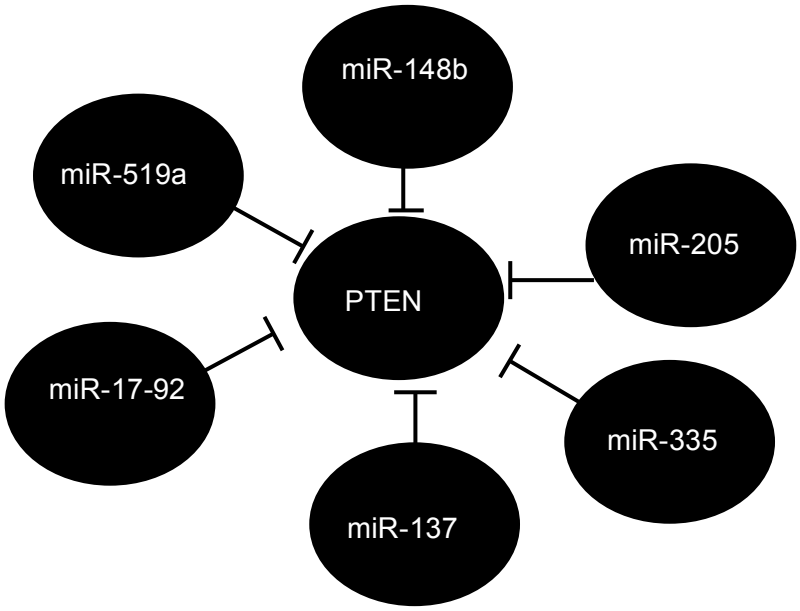

B.

miR- 335

```
2688-2694   5'  CUCCUCUUGA
                   |||||||
            3'  AACGAGAACU
```

miR-148b

```
3154-3158    5' UAUGCACUGA
                  |||||||
             3' CUACGUGACU

2254-2260   5' UUUUGCACUGU
                  |||||||
            3' ACUACGUGACU
```

Figure 3.3.18: Tumour suppressor PTEN is a putative gene target of senescence-associated miRNAs in oral fibroblasts. Examples of miRNAs which are predicted to target PTEN (A). Seed-sequence of miR-335 and miR-148b in 3'UTR of PTEN mRNA (B).

transcriptome profile by modulating expression of miRNAs giving rise to a tumour promoting microenvironment (Bronsiz *et al*., 2011). In light of this, expression of PTEN was first determined in senescent oral fibroblasts by qRT-PCR and western blot. To assess the existence of a possible association between development of SASP and PTEN, its levels were measured at different time-points following induction of senescence. Compared to presenescent oral fibroblasts PTEN mRNA was significantly decreased in cisplatin-treated cells ($n=7$, $p<0.05$, figure 3.3.19.A). Immediately after treatment there was a sharp declination in PTEN mRNA to 0.4-times of control. However on day 10 the mRNA level increased to 0.86-times followed by a decrease on day 15 to 0.61-times of control (figure 3.3.19.A). Relative band densitometry of western blot result showed there was a progressive increase in expression of PTEN protein as young fibroblasts gradually aged with time, from a ratio of 0.52 on day 5 ($n=5$, $p<0.05$) to 0.90 on day 10 to 1.0 on day 15 (figure 3.3.19.B). Cisplatin treatment also increased expression of PTEN protein by 0.60 on day 5, to 0.8 on day 10. However on day 15 the expression of PTEN in cisplatin-treated oral fibroblasts was significantly reduced to 0.75-times of control ($n=5$, $p<0.05$, figure 3.3.19.B).

These observations suggested that PTEN is necessary to induce growth arrest in premature senescent oral fibroblasts in response to cisplatin treatment. It appears that during early stages of senescence induction cisplatin stimulates translation of PTEN mRNA into protein corroborated by the declination in PTEN mRNA and inclination in PTEN protein level on day 5 post-treatment. This is exactly the time-point when fibroblasts display diminished proliferative capacity and senescent cells begin to appear as shown in figure 3.1.1.3 and figure 3.1.1.5 respectively. This is subsequently followed by an accelerated transcription and translation of PTEN, possibly to induce further growth arrest by day 10, when over 90% of cells show positive SA-β-Gal activity. Thereafter there is a decrease in both transcription and translation of PTEN in cisplatin-treated oral fibroblasts possibly because senescence has been established and these

changes also correlate to the increased expression of both miR-335 and miR-148b over-time as determined by qRT-PCR. In addition, this is the time-point when the secretome of senescent oral fibroblasts becomes fully established.

To evaluate that these changes in PTEN expression were actually associated with senescence and SASP both PTEN mRNA and protein levels were also examined in H_2O_2-induced premature and replicative senescent oral fibroblasts. qRT-PCR demonstrated that H_2O_2 and cisplatin-induced premature senescent oral fibroblasts exhibited a significant decrease in PTEN mRNA to 0.4-times and 0.3-times of control ($n=3$, $p<0.05$; figure 3.3.20.A) which corresponded to the decreased protein level by 0.48-times and 0.60-times ($n=9$, $p<0.05$; figure 3.3.20.B), respectively, in comparison to presenescent fibroblasts. Replicative senescent oral fibroblasts expressed lowest amount of PTEN mRNA and protein about 0.20-times ($n=3$, $p<0.05$; figure 3.3.20.A) and 0.24-times ($n=9$, $p<0.05$; figure 3.3.20.B) of control.

As a result it is possible that reduced expression of PTEN in senescent oral fibroblasts may be responsible for maintenance of SASP. Moreover the replicative senescent cells were in fact derived from the presenescent population of fibroblasts that were allowed to age naturally with time. Therefore as discussed before similar to cisplatin, fibroblasts that age naturally also up-regulate PTEN to reach senescence or a state of irreversible growth arrest, after which its level declines possibly owing to diminished PTEN transcription and translation in senescent fibroblasts. However as observed in this study naturally attainment of senescence is a very slow process and is perhaps evolutionary determined to preserve life, sustain cell regenerative capacity and maintain tissue homeostasis and may be accelerated by noxious stimuli like oxidative stress as means of protection against detrimental stimuli. Further when PTEN expression was determined by immunohistochemistry in the 3D organotypic models that had been previously used for assessing invasion of OSCC cells in presence and absence of senescent oral fibroblasts, it was observed that cisplatin-induced premature

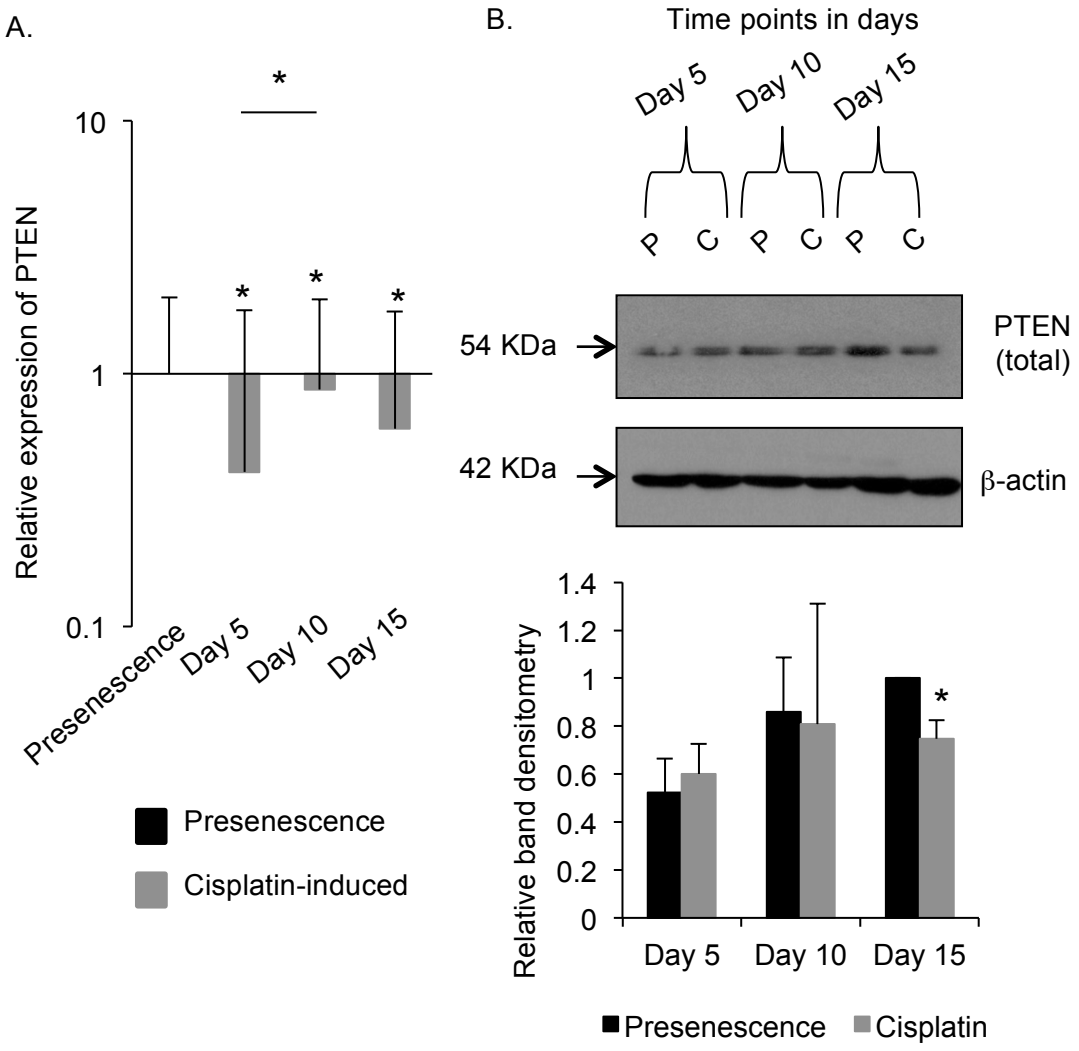

Figure 3.3.19: Determination of PTEN mRNA and protein levels in cisplatin-treated oral fibroblasts at different time-points. qRT-PCR showed that PTEN mRNA levels decrease in cisplatin-treated oral fibroblasts to that of presenescent control, n=7 (A). Western blot (upper panel) and relative band densitometry (lower panel) depicting diminished band intensity of PTEN in oral fibroblasts upon cisplatin treatment, n=5 (B). The bars represent mean+ SEM. "P"= "presenescent". "C"= "cisplatin-treated". *p<0.05, two-way repeated measures ANOVA with post-hoc corrections by Holm-Sidak method (A) and Mann Whitney U-test (B) done.

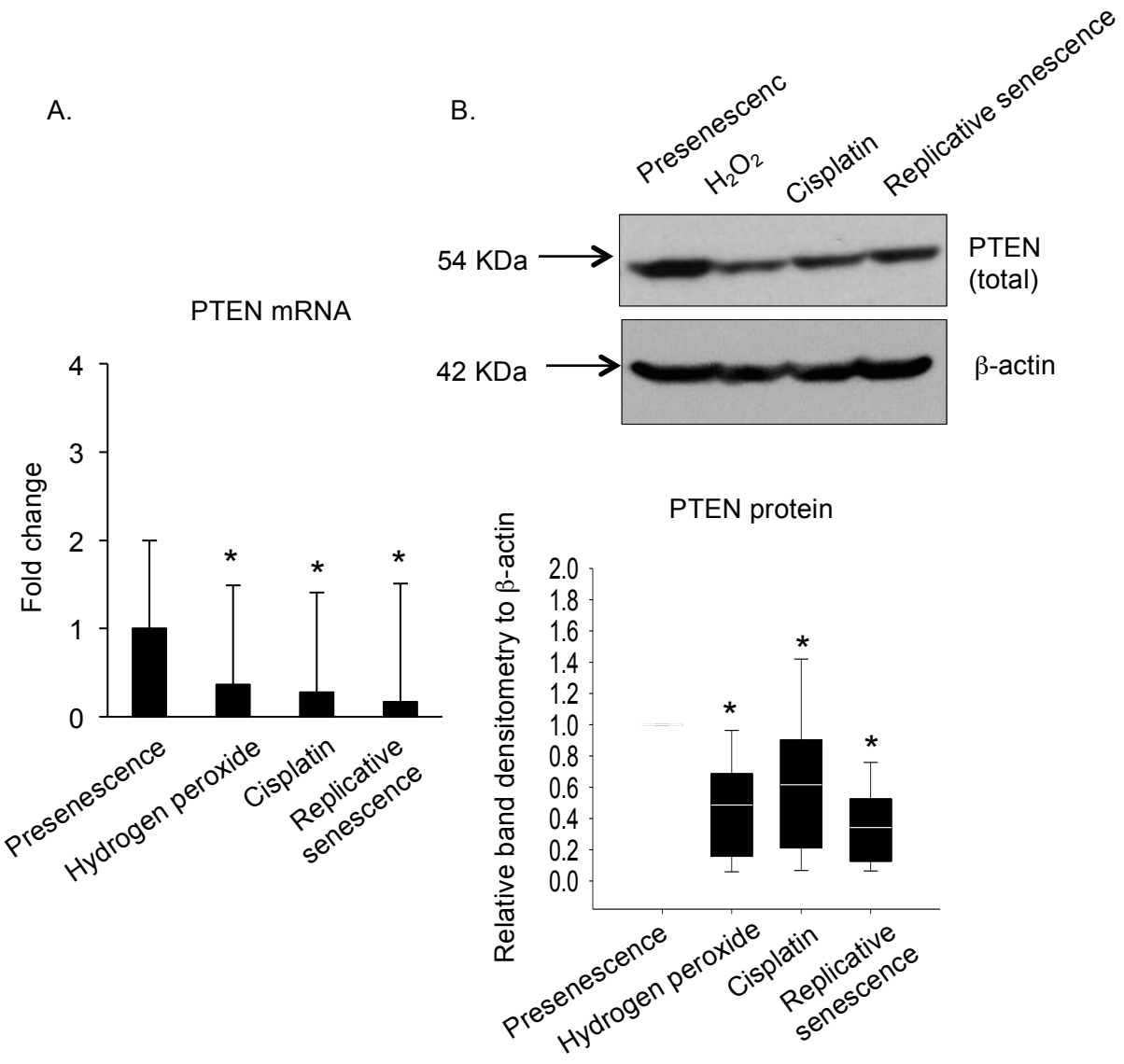

Figure 3.3.20: Determination of PTEN expression in senescent oral fibroblasts. qRT-PCR demonstrated a dramatic decrease in PTEN mRNA level upon attainment of senescence in human primary oral fibroblasts compared to presenescent control, n=3 in triplicate (A). Western blot (upper panel) and relative band densitometry (lower panel) demonstrating a significant decrease in PTEN protein level in senescent oral fibroblasts visible as diminished band intensity, n=9 (B). The bars represent mean + SEM. *$p<0.05$, one-way ANOVA with post-hoc corrections by Dunn's method (A) and Holm-Sidak method (B) done.

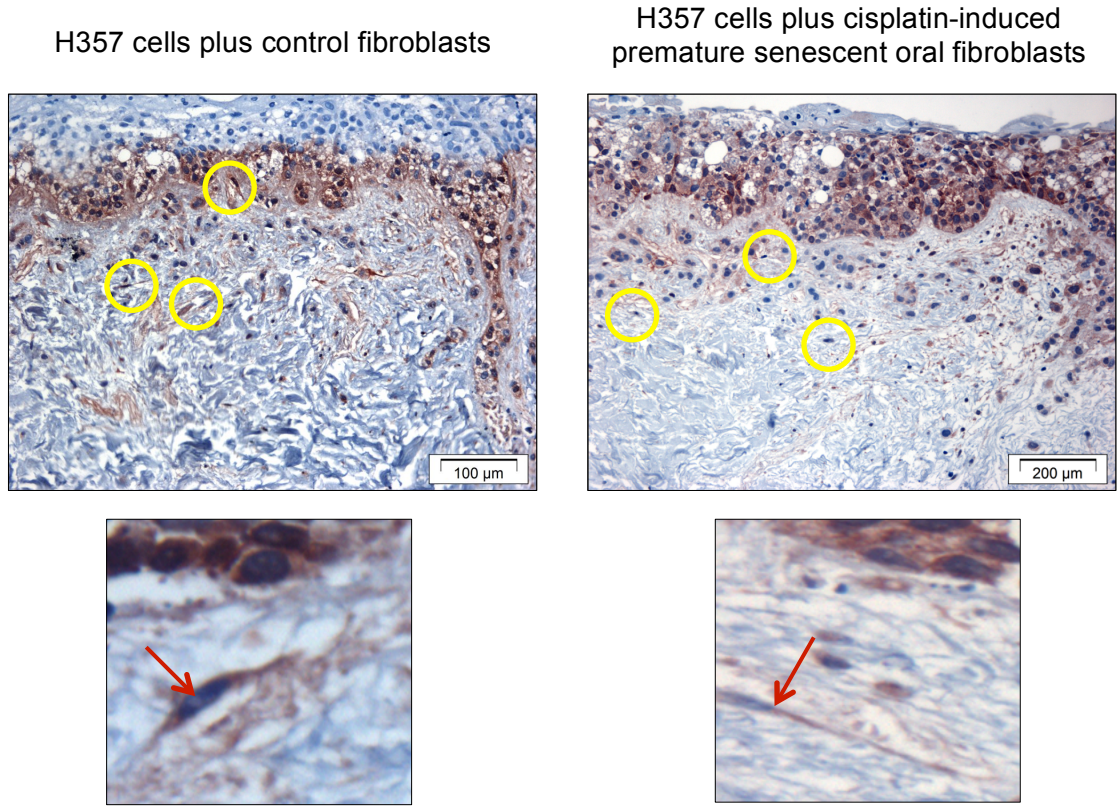

Figure 3.3.21: Immunohistochemistry of PTEN in 3D organotypic models. H357 cells were co-inoculated with either control fibroblasts (left panel) or cisplatin-treated (right panel) oral fibroblasts into human de-epithelialized dermis and grown for a period of 21 days. PTEN immunohistochemistry were performed on paraffin embedded sections of DD models after heat mediated antigen retrieval in citrate buffer. The yellow circles represents fibroblasts which are zoomed at 100X in lower panels wherein the red arrow indicates the intensity of staining in fibroblasts that is greatly diminished in cisplatin-treated cells. Scale bar = 100 μM (left panel) and 200 μM (right panel).

senescent oral fibroblasts showed diminished staining for PTEN protein indicative of its reduced expression (figure 3.3.21, right panel) compared to untreated presenescent fibroblasts (figure 3.3.21, left panel).

3.3.4.2: PTEN is a functional gene target of miR-335 and miR-148b

As stated previously the 3'UTR of PTEN mRNA is predicted to bear complementary seed sequences for miR-335 (one) and miR-148b (two). Therefore PTEN expression was determined in miRNA transfected oral fibroblasts at both mRNA and protein level by qRT-PCR and western blot, respectively.

It was found that although 3'UTR of PTEN had a putative binding site for miR-335, miR-335 transfected oral fibroblasts expressed 1.2-fold more PTEN mRNA and protein than negative control cells (figure 3.3.22). In contrast miR-148b, which have two complementary seed sequences in 3'UTR of PTEN, caused decreased expression of PTEN at both mRNA and protein level by 0.9-times and 0.6-times of control, respectively, in transfected oral fibroblasts (figure 3.3.22). In co-transfected oral fibroblasts expression of both PTEN mRNA and protein were also reduced to 0.9-times and 0.7-times of negative control, respectively (figure 3.3.22). Based on these results it may be concluded that miR-148b regulated PTEN gene expression probably at post-transcriptional levels manifested by the reduction in both PTEN mRNA and protein levels ($n=7$, $p<0.05$; figure 3.3.22.B).

The above results were obtained from oral fibroblasts transfected with 50 nM of miRNAs, which yielded massive over-expression of individual miRNAs exceeding the original fold change that is actually observed in senescent oral fibroblasts. Therefore oral fibroblasts were transfected with lower doses of miRNA mimics commencing from 0.5 nM to 5.0 nm and 50.0 nM and PTEN protein expressions were determined after validation of miRNA over-expression in dose response manner by qRT-PCR (appendix

12). It was observed that compared to negative control both miR-335 and miR-148b caused a gradual decrease in PTEN protein levels as the concentration of the individual miRNAs were increased (n=3). At 0.5 nM concentration the ratio of PTEN protein in both miR-335 and miR-148b transfected oral fibroblasts was 1.3-times higher than negative control and this was reduced by 0.85-times in miR-335 and by 0.91-times in miR-148b transfected oral fibroblasts (n=3, figure 3.3.23) at 5.0 nM concentration. At 50.0 nM concentration in these experiments expression of PTEN protein was found reduced in both miR-335 and miR-148b transfected oral fibroblasts by 0.74-times and 0.85-times of negative control (n=3, figure 3.3.23). In co-transfected oral fibroblasts ratio of PTEN protein was reduced at all range of concentrations by 0.85-times at 0.5 nM, by 0.92-times at 5.0 nM and by 0.72-times at 50.0 nM compared to negative control (n=3, figure 3.3.23).

The dose response effects of individual miRNAs mirrored the changes in PTEN expression over time-points in cisplatin-induced premature senescent oral fibroblasts. As demonstrated earlier both miR-335 and miR-148b levels increase gradually with the attainment of senescence in oral fibroblasts (figure 3.3.8). In contrast the expression of PTEN protein in senescent oral fibroblasts initially increases followed by a significant decrease once senescence is achieved (figure 3.3.19). The decrease of PTEN expression in senescent oral fibroblasts is synchronized with the rising levels of its targeting miRNAs: miR-335 and miR-148b, further substantiating the regulatory effect of these miRNAs on PTEN expression in senescent fibroblasts and in sustaining SASP.

To confirm that PTEN is a direct target of miR-148b, a 1.45 Kbp fragment from its 3'UTR region bearing the complementary seed sequences of both miR-335 and miR-148b, were cloned into a pmiR-reporter vector. Huh-7 cells were used to perform dual luciferase assay (due to the difficulty of performing this assay in primary cells as

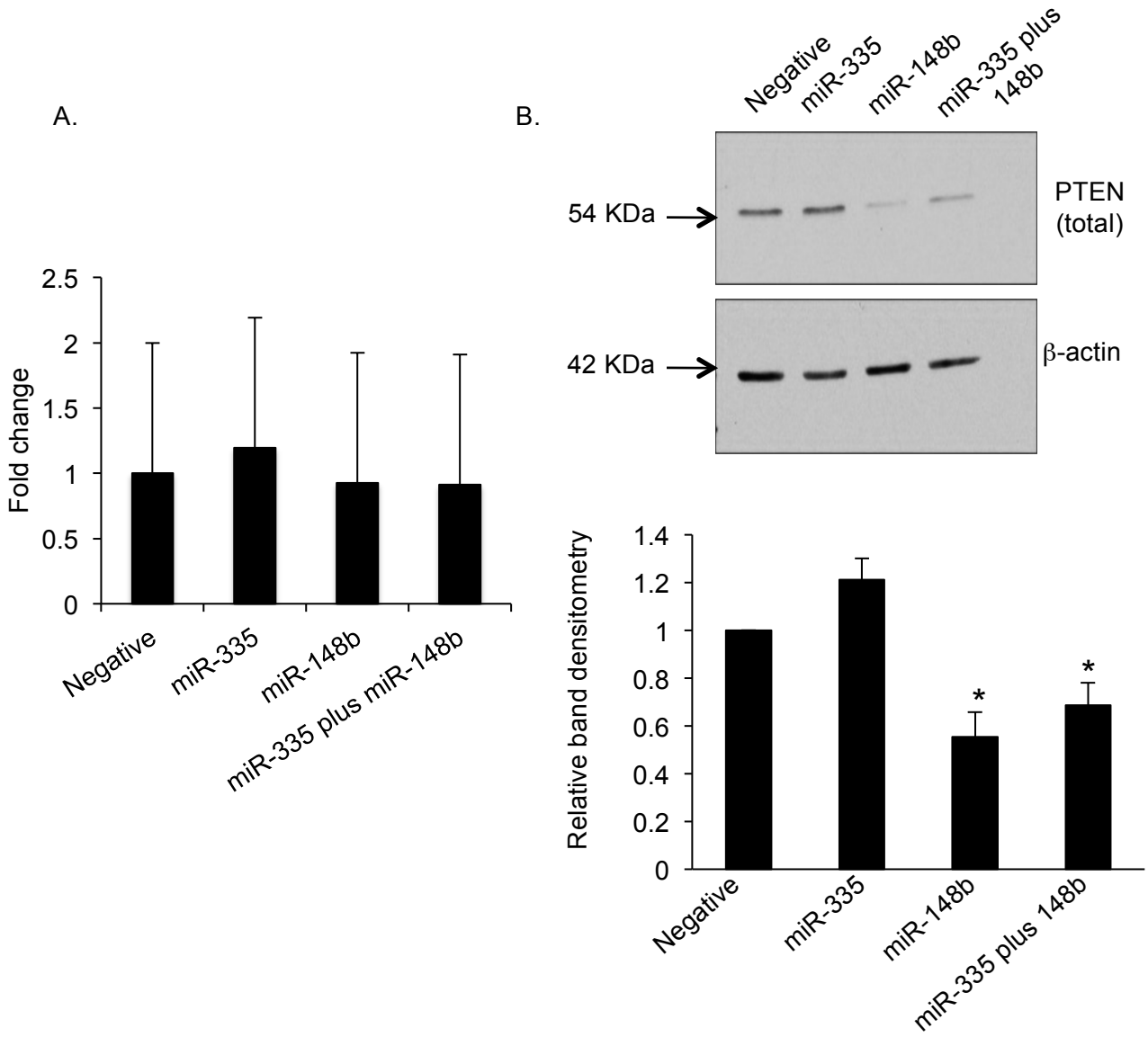

Figure 3.3.22: miR-335 and miR-148b stimulate aberrant expression of PTEN in oral fibroblasts. qRT-PCR showed that miR-335 caused an increase and miR-148b and co-transfection caused a decrease in PTEN mRNA in human primary oral fibroblasts (A). Western blot (upper panel) and relative band densitometry (lower panel) showing that miR-148b caused a dramatic reduction in PTEN protein expression upon both single and dual transfection in oral fibroblasts while miR-335 caused an increase in its protein level (B). The bars represent mean + SEM. N=7. *$p<0.05$, one-way ANOVA with post-hoc corrections by Holm-Sidak method.

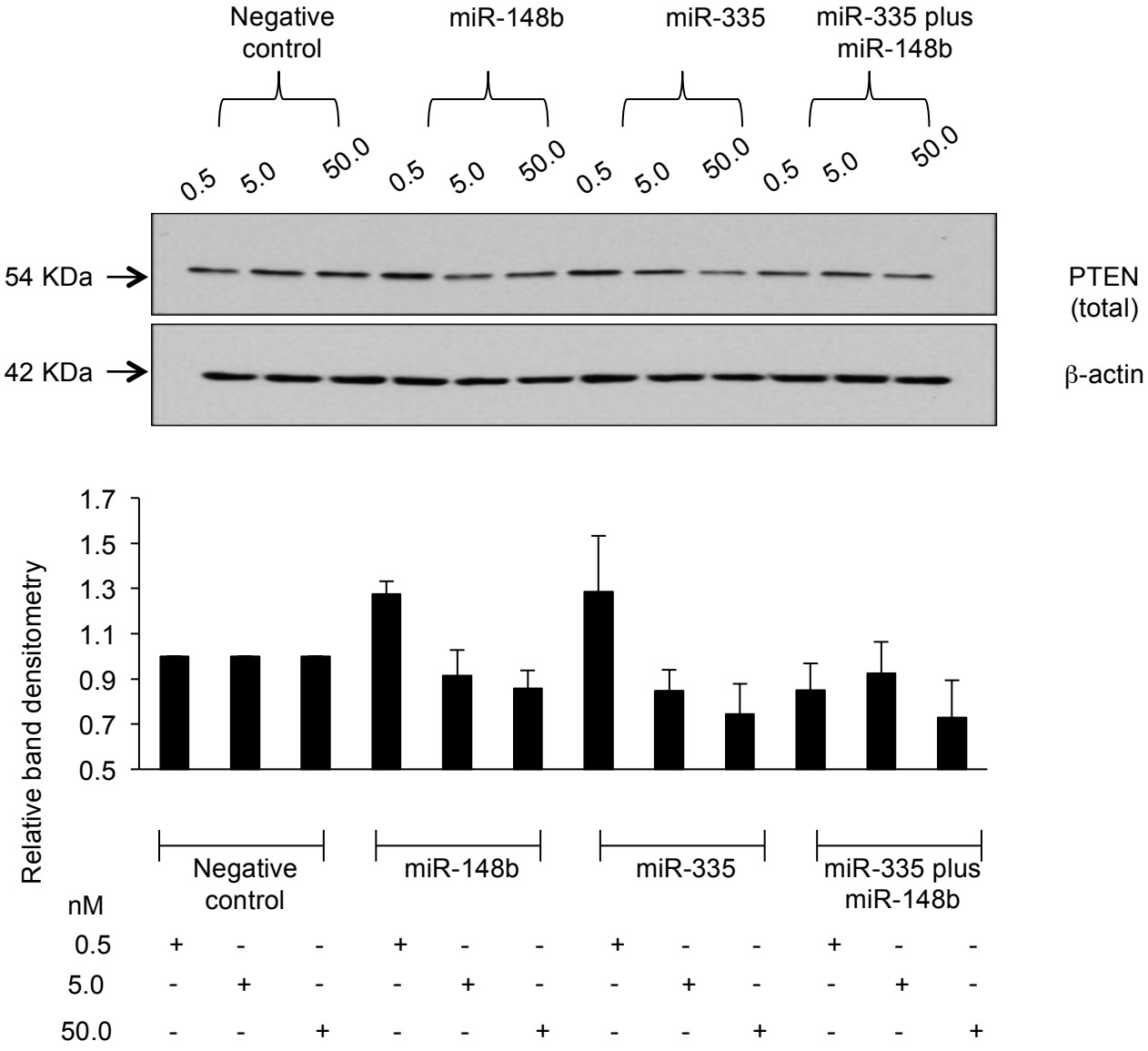

Figure 3.3.23: Dose response effect of miRNA mimics on PTEN protein expression. Western blot (upper panel) and relative band densitometry (lower panel) showed that gradual incrementing of miRNA concentration in oral fibroblasts caused a gradual decrease in PTEN protein expression perceived as reduced band density. N=3.

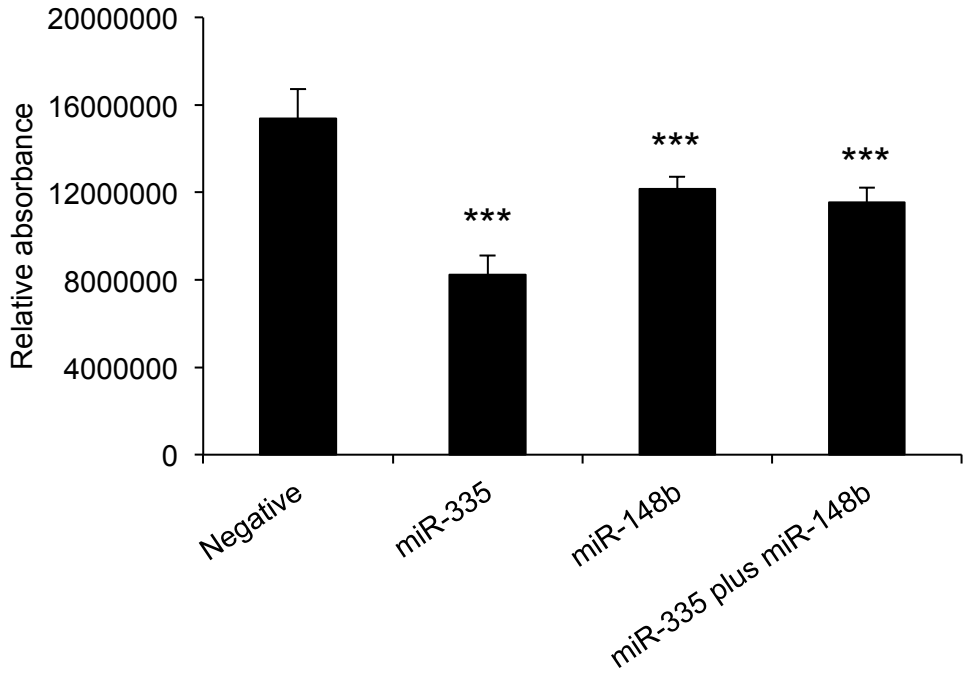

Figure 3.3.24: miR-335 and miR-148b represses PTEN translation. 1.45 Kbp length 3'UTR of PTEN harbouring predicted complementary seed sequences of miR-335 and miR-148b were clones into pmiR-reporter vector. Huh-7 cells were transfected with either miRNA mimics or negative control miRNAs in combination of pmiR-reporter construct containing 3'UTR of PTEN. B-Gal served as the internal control. The graph illustrates normalized data to β-Gal. The bars represent mean + SEM of three independent experiments. N=3, in triplicate. ***p<0.001, by paired student's t-test.

previously determined in the lab) and a β-galactosidase reporter vector was co-transfected to act as an internal control. It was revealed that both miR-335 and miR-148b significantly reduced luminescence from the reporter construct by 0.5-times and 0.8-times of control, respectively (n=3, p<0.001; figure 3.3.24). Further the relative luminescence was also significantly reduced in co-transfected Huh-7 cells by 0.75-times of negative control (n=3, p<0.001; figure 3.3.24). As a result it was concluded that PTEN is a functional gene target of both miR-335 and miR-148b in senescent oral fibroblasts wherein miR-335 repressed PTEN translation and miR-148b caused both translational repression and possibly mRNA decay.

3.3.4.3: Functional effect of PTEN in oral fibroblasts

Loss of PTEN expression in the epithelial compartment had been reported in several cases of inflammatory subtype of OSCC and is linked to development of chemotherapy resistance and presence of cancer stem cells in head and neck cancer patients (Bian *et al*., 2012a). A stromal role of PTEN has only recently emerged in breast cancer and is yet to be determined in OSCC.

In order to evaluate the consequences of PTEN deficiency in oral fibroblasts *PTEN* was transiently knocked down using siRNA. Cy3 labeled negative control siRNA was used to monitor transfection efficiency (figure 3.3.25.A). PTEN siRNA significantly reduced expression of both PTEN mRNA and protein by 0.6-times (n=3, p<0.001; figure 3.3.25.B) and 0.4-times (n=4, p=0.014; figure 3.3.25.C) of control, respectively.

To explore if transient knockdown of PTEN had any effect on the secretory phenotype of oral fibroblasts, the cells were screened for expression of SASP markers: MMP-2 and IL-6 by qRT-PCR. It was found transient knockdown of PTEN had no effect on IL-6 transcription however it significantly increased MMP-2 mRNA by 1.3-fold compared to negative control (n=3, p=0.022; figure 3.3.25.D). Earlier in this section we showed

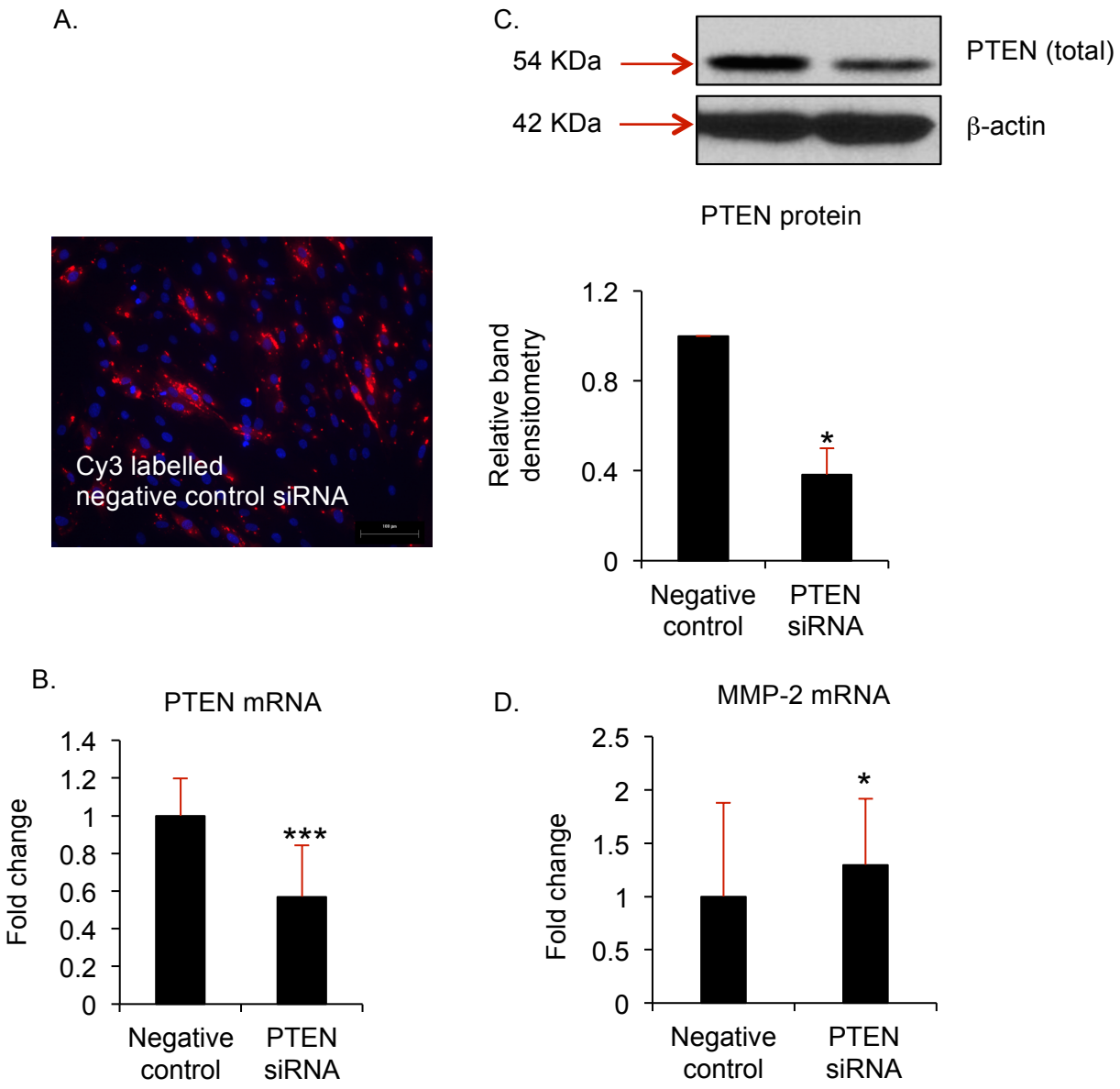

Figure 3.3.25: Determination of knock down efficiency of PTEN in oral fibroblasts. Cy3 labelled negative control siRNA was used to monitor transfer of siRNA into oral fibroblasts (A). qRT-PCR was used to determine decreased PTEN mRNA levels in PTEN siRNA transfected oral fibroblasts, n=3 (B). Western blot (upper panel) and relative band densitometry (lower panel) was done to validate decrease in PTEN protein expression, n=4 (C). MMP-2 mRNA were assessed to determine phenotypic switch in oral fibroblasts following PTEN knock down, n=3 (D). The bars represent mean + SEM of three independent experiments. *$p<0.05$ and ***$p<0.001$, by paired student's t-test.

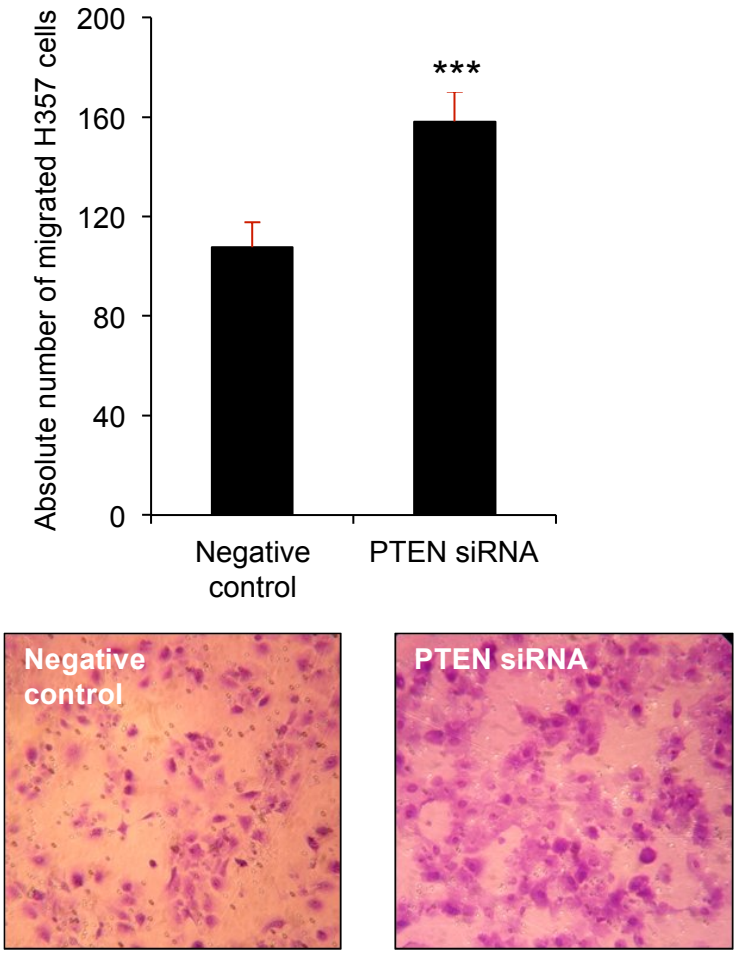

Figure 3.3.26: PTEN deficient oral fibroblasts stimulate migration of H357 cell lines *in vitro*. 100,000 H357 cells were seeded down to the top chamber of the transwell assay. Conditioned media derived from PTEN deficient and negative control oral fibroblasts were loaded to the bottom chamber. Migration was carried out for 40 h. The migrated cells were fixed and stained with 0.1% crystal violet. Pictures were taken under 20X magnification using light microscope from three separate fields per well. The bars represents the mean of migrated cells + SEM of three independent experiments. N=3, in triplicate. ***p<0.001, by paired student's t-test.

cisplatin-treated oral fibroblasts increased invasiveness of H357 cells *in vitro,* which may be partly associated with reduced expression of PTEN. To determine if alteration of PTEN in oral fibroblasts could directly stimulate motility of OSCC cell lines *in vitro*, 2D migration assay was performed. It was observed that conditioned media derived from PTEN deficient oral fibroblasts significantly stimulated the migration of H357 cell lines *in vitro* by 1.5-times to that of negative siRNA control (n=3, p≤0.001; figure 3.3.26). As a result it was clear that diminished expression of PTEN in oral fibroblasts could augment their pro-tumourigenic paracrine effects on cancer cells.

3.3.5: Putative role of PTEN in regulation of SASP in senescent oral fibroblasts

During malignant transformation the cells begin to lose PTEN at an early stage to evade apoptosis (Iliopoulos *et al*., 2010) while according to this study the senescent cells lose PTEN expression at a later stage.

Transient knockdown of PTEN in young oral fibroblasts reproduced the paracrine effect of senescent oral fibroblasts on cancer cells however these cells demonstrated no change in secreted levels of SASP markers primarily MCP-1 and IL-6. Perhaps the pro-tumourigenic properties conferred to fibroblasts by transient knockdown of PTEN may be a direct effect of PTEN deficiency in fibroblasts, which causes them to behave more like cells undergoing either malignant transformation or myofibroblastic transdifferentiation rather than those becoming senescent. This indicated that to study the function of PTEN in senescent oral fibroblasts stable knockdown of the gene was required, however this is not straightforward in primary cells and attempts to do so were precluded by time and resource limitations in this study.

Therefore to associate development of SASP with alterations in PTEN, expression of both MCP-1 and IL-6 were determined at mRNA levels in senescent cells and were

compared to PTEN changes in senescent oral fibroblasts at different time-points (figure 3.3.27). It was observed that MCP-1 mRNA progressively increased in cisplatin-treated oral fibroblasts from 2.0-fold to 4.0-fold to 5.1-fold at day 5 to day 10 to day 15 post-treatment compared to presenescent control (n=7, $p<0.05$, figure 3.3.27.A). IL-6 mRNA was also increased after cisplatin treatment, however the variations in IL-6 transcription was inversely associated with PTEN expression profile (n=3, $p<0.05$; figure 3.3.19 and figure 3.3.27.B). At day 5, when PTEN expression was low, IL-6 mRNA was 1.8-fold higher in cisplatin-treated fibroblasts than control. On day 10 when there was a slight increase in PTEN transcription, IL-6 mRNA declined to 1.1-fold and at day 15 when PTEN expression was reduced the most, IL-6 transcription was increased to 6.3-fold in comparison to control fibroblasts. Previous reports by other groups demonstrated that IL-6 is an important mediator of senescence and aids to reinforce SASP (Kuilman *et al*., 2008). Therefore it is plausible that the reciprocal association between IL-6 and PTEN in senescent oral fibroblasts may synergize in establishing and maintenance of SASP.

3.3.5.1: Senescent oral fibroblasts display elevated COX-2 activity

Cyclooxygenase 2 (COX-2) is an inducible enzyme that is up-regulated during cell injury and is deregulated in cancer including OSCC (Dalwadi *et al*., 2005; Pandey *et al*., 2008; Hinsley *et al*., 2012). IL-6 is a COX-2 dependent cytokine, which activates STAT3 (signal transducer and activator of transcription 3) to regulate transcription of numerous oncogenic signals acting downstream of COX-2 in cancer cells (Dalwadi *et al*., 2005). COX-2 has been reported to be highly up-regulated in senescent cells including fibroblasts (Martien *et al*., 2013). Therefore COX-2 expression was determined in cisplatin-treated fibroblasts at different time-points to evaluate the existence of a positive association with IL-6 expression.

Indeed qRT-PCR showed COX-2 mRNA levels were positively associated with IL-6 mRNA and negatively associated with PTEN mRNA levels in cisplatin-treated oral

A.

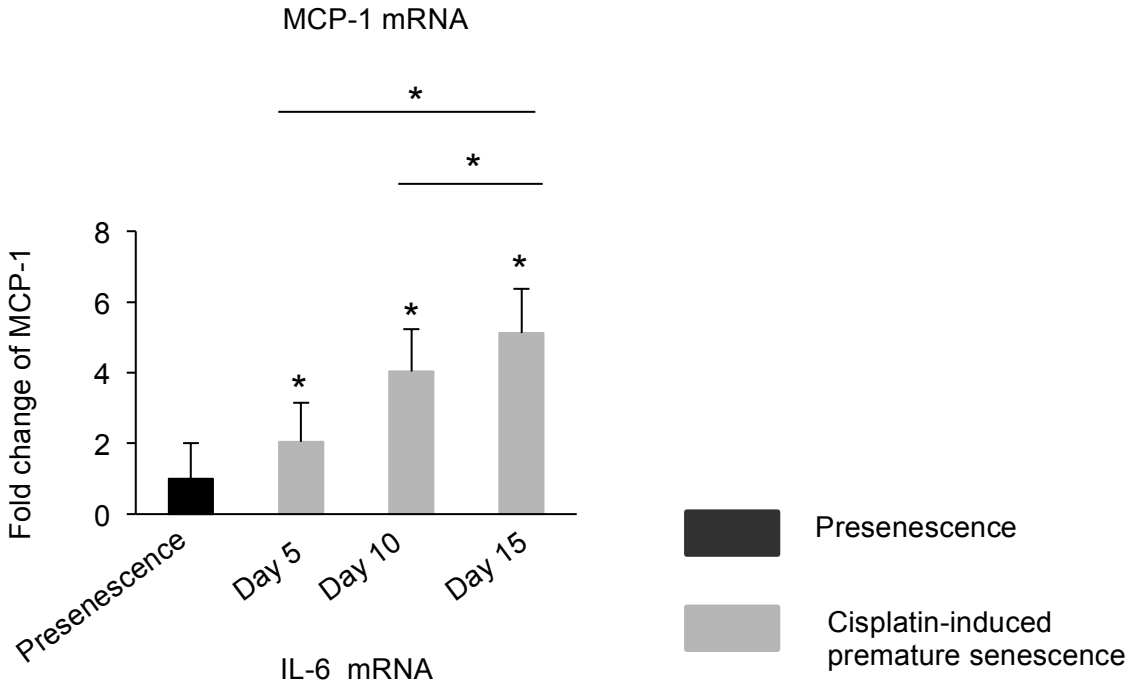

B.

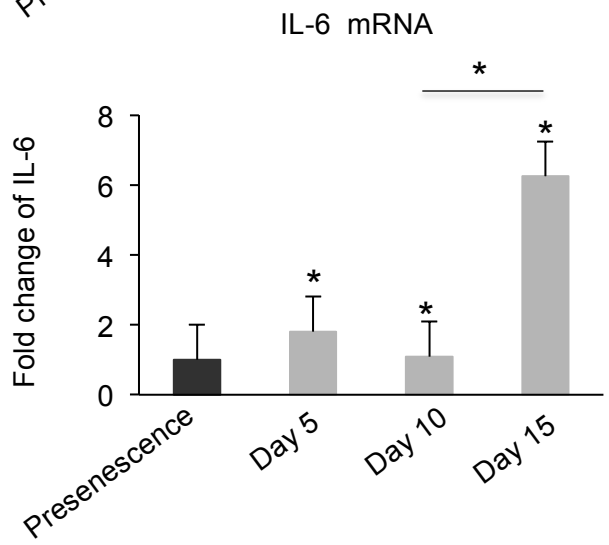

Figure 3.3.27: Increased MCP-1 and IL-6 transcription in cisplatin-induced premature senescent oral fibroblasts. qRT-PCR was performed to determine expression of MCP-1, n=7 (A) and IL-6, n=3 (B) at day 5, day 10 and day 15 following treatment of oral fibroblasts with cisplatin. Day 10 presenescent oral fibroblasts were used as control. The ΔΔCt values were calculated after normalizing the data to U6 internal control. The bars represent mean fold change + SEM. *p<0.05, two-way repeated measures ANOVA with post-hoc corrections by Holm-Sidak method.

fibroblasts. At day 5, COX-2 mRNA was 1.7-fold higher than untreated control which corresponded to the elevated levels of IL-6 mRNA. This was followed by a sharp decline on day 10 to 0.86-times of control corresponding to decreased levels of IL-6 in cisplatin-treated cells. Again on day 15, COX-2 expression was sharply increased to 2.4-fold higher than control, which again corresponded to the increased level of IL-6 mRNA in senescent fibroblasts (figure 3.3.28).

COX-2 expressions were also determined in other types of senescent oral fibroblasts. There was a significant increase in the expression of COX-2 mRNA by 9.2-fold, 5.6-fold and 3.9-fold in H_2O_2 and cisplatin induced premature and replicative senescent oral fibroblasts, respectively, compared to presenescent control ($n=3$, $p<0.05$). These levels also corresponded to the IL-6 mRNA profile in senescent oral fibroblasts as illustrated in figure 3.1.2.5.A. To evaluate the functional effect of COX-2 in development of senescence and SASP both IL-6 and PGE2 (prostaglandin E2), an arachidonic acid metabolite produced by catalytic activity of COX-2 (Krysan *et al*., 2014), were measured in senescent oral fibroblasts that had been either treated with a selective COX-2 inhibitor (celecoxib) or left untreated.

In absence of celecoxib, cisplatin-induced premature senescent oral fibroblasts had 1.8-fold more IL-6 mRNA than presenescent control (figure 3.3.29.A). Blockade of COX-2 activity with celecoxib caused a dramatic reduction in IL-6 transcript levels in both presenescent and cisplatin-treated oral fibroblasts by 0.4-times and 0.6-times of untreated control, respectively. To determine if these changes were also visible at protein level conditioned media derived from celecoxib treated and untreated senescent and presenescent oral fibroblasts were assessed for secreted levels of IL-6. It was found that in absence of celecoxib, cisplatin-treated oral fibroblasts secreted 17.5% more IL-6 than presenescent control fibroblasts ($n=3$, $p<0.05$; figure 3.3.29.B). However after addition of celecoxib, IL-6 secretion was significantly reduced by 15.4% in cisplatin-induced senescent oral fibroblasts than their counterpart untreated control

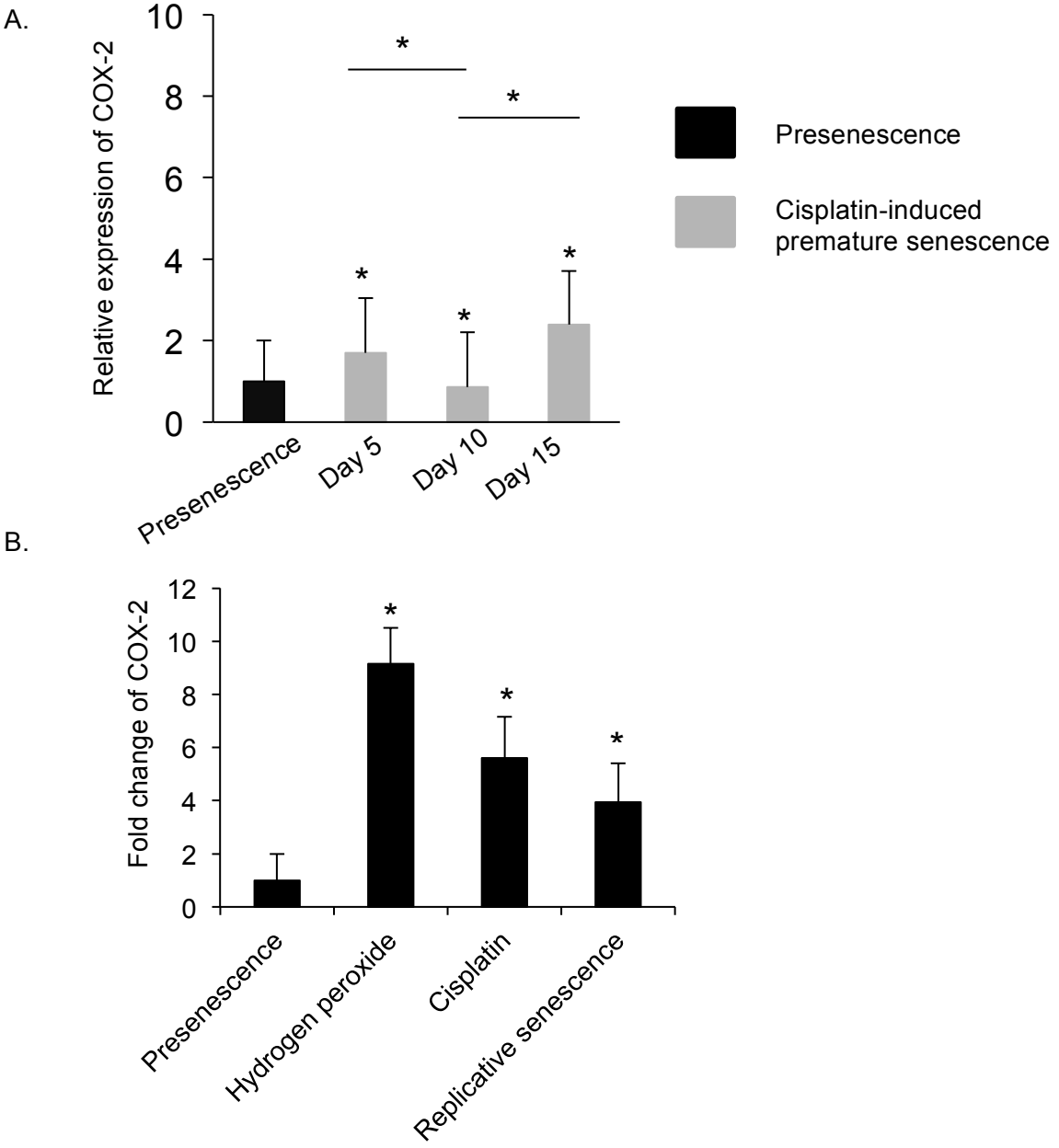

Figure 3.3.28: COX-2 expression is elevated in senescent oral fibroblasts. qRT-PCR was used to determine COX-2 mRNA levels at day 5, day 10 and day 15 in cisplatin-treated oral fibroblasts and compared to day 10 presenescent control (A). COX-2 levels were also determined in other types pf senescent oral fibroblasts (B). ΔΔCt values were measured after normalizing the data to U6 internal control. The bars represents mean + SEM. N=3, in triplicate. *p<0.05. Two-way repeated measures ANOVA with post-hoc corrections by Holm-Sidak method (A) and one-way ANOVA with post-hoc corrections by Dunn's method.

(n=3, $p<0.05$;figure 3.3.29.B). Treatment of presenescent oral fibroblasts with celecoxib also caused 8% reduction in IL-6 secretion. There was no statistical difference in IL-6 secretion between celecoxib treated senescent oral fibroblasts and untreated presenescent control implying that the increased amount of IL-6 secreted by senescent fibroblasts is due to enhanced COX-2 activity. Therefore it appeared that COX-2 activity may be involved in maintenance of SASP.

To further verify the effect of COX-2 activity in senescent oral fibroblasts PGE2 ELISA was performed to determine if senescent cells were secreting PGE2. It was observed that, compared to presenescent fibroblasts, senescent oral fibroblasts secreted significantly more PGE2 (n=3, $p<0.05$, figure 3.3.29.C). Both H_2O_2-induced and replicative senescent oral fibroblasts secreted 1.8-times more PGE2 than presenescent controls. Cisplatin-treated oral fibroblasts secreted 2.2-times more PGE2 than presenescent fibroblasts. Blockade of COX-2 activity in senescent oral fibroblasts caused a substantial decrease in production of PGE2 (n=3, $p<0.05$, figure 3.3.29.C). Celecoxib treatment reduced PGE2 secretion by 0.8-times and 0.6-times in H_2O_2 and cisplatin induced senescent oral fibroblasts, respectively, compared to untreated control. In replicative senescent oral fibroblasts PGE2 secretion was reduced by 0.7-times of untreated control. Inhibition of COX-2 activity also reduced PGE2 secretion in presenescent oral fibroblasts by 0.74-times of its counterpart untreated control.

This evidence implied COX-2 is a functional enzyme in senescent oral fibroblasts and may utilize the functional activity of IL-6 to regulate expression of various secretory factors that contribute to the paracrine effect of SASP. Furthermore, recently it has been reported that PGE2 exerts a pro-fibrotic effect in PTEN deficient murine fibroblasts (Sagana *et al*., 2009). This may further enhance the myofibroblastic property of senescent oral fibroblasts to promote cancer progression.

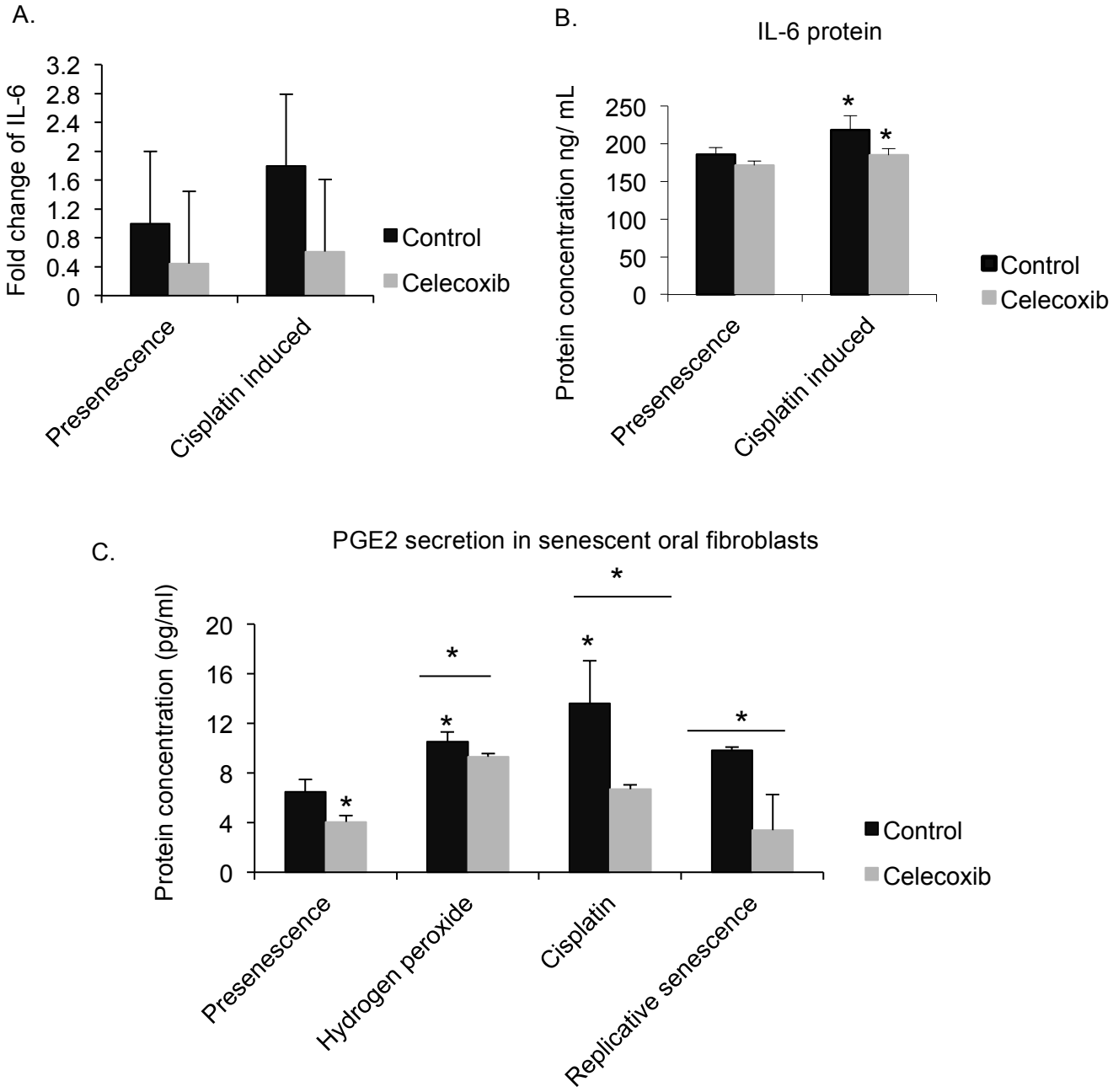

Figure 3.3.29: Senescent oral fibroblasts demonstrated enhanced COX-2 activity. qRT-PCR (A) and IL-6 ELISA (B) were performed to determine changes in expression of IL-6 mRNA and protein in senescent oral fibroblasts after blockade of COX-2 function. The enzymatic activity of COX-2 was further validated by quantifying PGE2 (C) secretion by senescent oral fibroblasts using ELISA in presence and absence of celecoxib. N=3, in triplicate. *p<0.05, two-way ANOVA with post-hoc corrections by Bonferroni t-test.

3.3.5.2: Blockade of COX-2 rescues SASP mediated enhanced migration of OSCC cell lines *in vitro*

After ascertaining that COX-2 was partly responsible for the secretory phenotype of aged oral fibroblasts it was hypothesized that inhibition of COX-2 activity in senescent fibroblasts may impede cancer cell migration *in vitro* thus rescuing the pro-tumourigenic effect of SASP on cancer cells.

Conditioned media was collected from fibroblasts treated or untreated with celecoxib for 48 h to perform migration assay. As previous work from this lab showed celecoxib could directly impede head and neck cancer cell migration *in vitro* (Hinsley *et al*., 2012) a positive control containing 5% serum were run in presence and absence of celecoxib. It was observed that in absence of celecoxib senescent oral fibroblasts significantly stimulated migration of H357 cell lines *in vitro* ($n=3$, $p<0.05$, figure 3.3.30) compared to presenescent control. Treatment with celecoxib dramatically reduced migration of H357 cell lines *in vitro* in both presenescent control and senescent oral fibroblasts ($n=3$, $p<0.05$, figure 3.3.30). There was no difference in migration of H357 cells in presence and absence of celecoxib in positive control wells (Appendix 9, figure 3.3.30).

Cisplatin-treated oral fibroblasts increased migration of H357 cells by 2.4-times than presenescent control and this was significantly reduced by celecoxib to 0.64-times of untreated control. H_2O_2-treated oral fibroblasts also significantly increased migration of H357 cells by 2.9-times compared to presenescent control. This migration was significantly reduced to 0.3-times of untreated control upon celecoxib treatment. Similarly replicative senescent oral fibroblasts stimulated migration of H357 cells by 3.3-fold in contrast to presenescent control and this was dramatically reduced to only 0.54-times of untreated control in presence of celecoxib. Lastly although presenescent oral fibroblasts exerted minimum stimulatory effect on cancer cell migration *in vitro*,

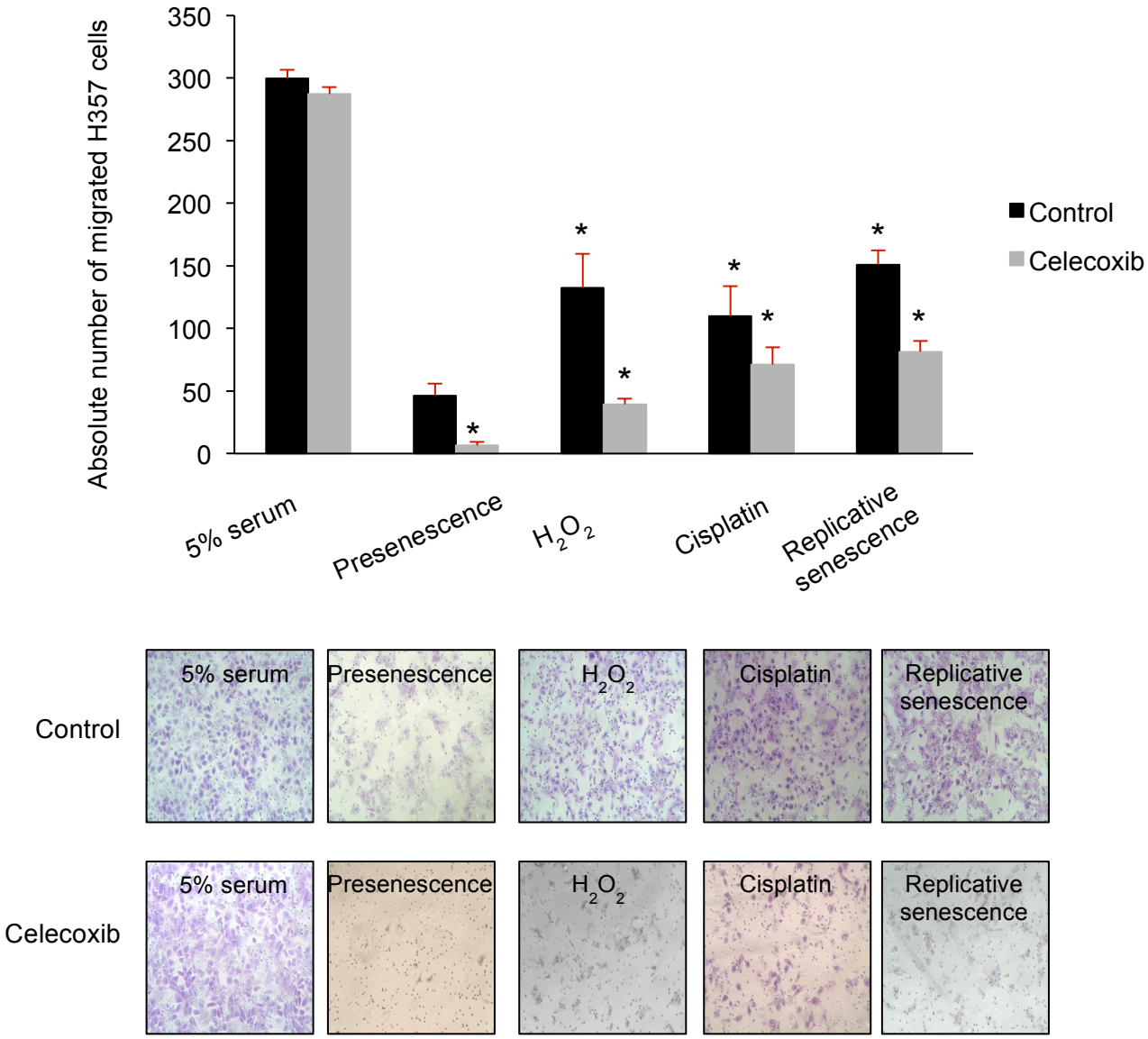

Figure 3.3.30: Blockade of COX-2 activity inhibited stimulatory effect of oral fibroblasts on cancer cell migration. 100,000 H357 cells were seeded down to the top chamber of transell assay. Conditioned media were collected from senescent and presenescent oral fibroblasts-treated or untreated with celecoxib for 48 h and loaded to the bottom chamber. Migration was carried out for 40 h. The migrated cells were fixed and stained with 0.1% crystal violet. Images were taken under 20X magnification using light microscope. The bars represent mean of representative cells + SEM of three independent experiments. N=3, in triplicate. *p<0.05, two-way ANOVA with post-hoc corrections by Bonferroni t-test.

however treatment of these cells with celecoxib completely abolished their stimulatory effect on cancer cells. Previously it had been reported that celecoxib could accelerate the ageing process in dermal fibroblasts independent of its enzymatic activity and via its regulatory effect on caveolin 1 (Lee *et al*., 2012; Kim *et al*., 2008). Therefore SA-β-Gal activity was determined in both presenescent and cisplatin-induced premature senescent oral fibroblasts after celecoxib treatment. These fibroblasts were treated with the same dose of celecoxib utilized by Kim *et al*. (2008) however the duration of treatment was 48 h in contrast to 72 h in the paper. There was no difference between SA-β-Gal activity in presenescent oral fibroblasts treated and untreated with celecoxib. Similarly there was neither an increase nor a decrease in SA-β-gal activity of cisplatin-treated oral fibroblasts after administration of celecoxib (figure 3.3.31.A).

The above observations suggested that celecoxib reduced secretion of soluble factors from senescent oral fibroblasts by a mechanism other than interfering with acquisition of senescence.

It was demonstrated in figure 3.2.7.1 that senescent oral fibroblasts have myofibroblastic properties that were detected by the formation of stress fibers. As mentioned earlier PGE2 is known to exert anti-fibrotic effect in activated fibroblasts carrying normal PTEN (Sagana *et al*., 2009). However in absence of PTEN PGE2 was observed to exaggerate both collagen synthesis and α-SMA expression in activated fibroblasts (Sagana *et al*., 2009). In this thesis it was shown that PTEN expression is reduced in senescent oral fibroblasts. Therefore it was postulated that perhaps increased COX-2 activity stimulated formation of stress fiber in senescent oral fibroblasts depleted of PTEN.

To explore this direct immunofluorescence cytochemistry for α-SMA was carried out in both presenescent and cisplatin-induced premature senescent oral fibroblasts following treatment with celecoxib. Untreated cells were used as controls. Since PGE2 is a

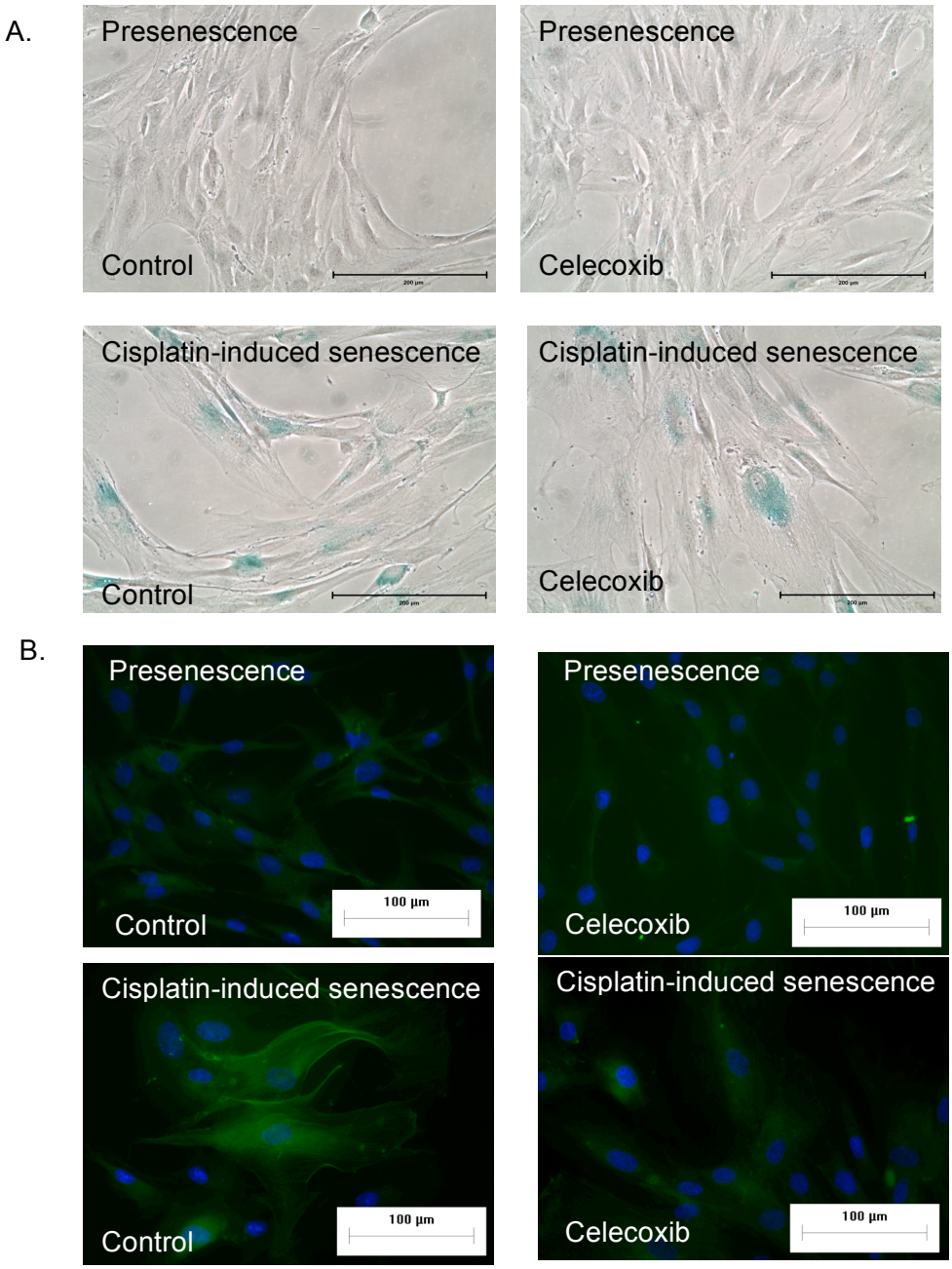

Figure 3.3.31: Celecoxib reduces myofibroblastic phenotype in senescent oral fibroblasts without affecting senescence. SA-β-Gal activity revealed no difference in senescence phenotype between presenescent and senescent oral fibroblasts after celecoxib treatment (A). Direct α-SMA immunofluorescence cytochemistry depicting reduced stress fiber formation in senescent oral fibroblasts after celecoxib treatment (B). N=3.

downstream product of COX-2, inhibition with celecoxib is likely to inhibit action of PGE2 by reducing its secretion (Krysan *et al*. 2014). As expected it was observed that formation of stress fibers in senescent oral fibroblasts were completely abolished upon celecoxib treatment implying that COX-2 regulated the myofibroblastic phenotype of senescent oral fibroblasts possibly in a PGE2/PTEN dependent manner (figure 3.3.31.B).

3.3.5.3: Celecoxib induces PTEN expression in senescent oral fibroblasts by stimulating down-regulation of miR-335 and miR-148b

Recently it was reported that PGE2 conferred chemotherapy resistance to non-small cell lung carcinoma cells by c-Myc dependent up-regulation of oncomiR family of miRNA miR-17-92 cluster which targeted PTEN (Krysan *et al*., 2014). In this study miR-17-92 cluster, however, was found down-regulated in cisplatin-induced senescent oral fibroblasts (appendix 2), however, two tumour suppressor miRNAs miR-335 and miR-148b identified to target PTEN were up-regulated. Both miR-335 and miR-148b were reported to have cMyc binding sites in their promoter region (Iliopoulos *et al*., 2010). Therefore it was hypothesized that blockade of COX-2 will inhibit PGE2 activity in senescent oral fibroblasts and this will increase PTEN expression owing to down-regulation of its targeting miRNAs miR-335 and miR-148b and this would rescue the senescent oral fibroblasts from their myofibroblastic phenotype demonstrated earlier.

In absence of celecoxib, cisplatin-induced premature senescent oral fibroblasts demonstrated reduced expression of PTEN mRNA about 0.76-times of presenescent fibroblasts (figure 3.3.32.A). Treatment with celecoxib, however, remarkably increased PTEN mRNA in cisplatin-treated oral fibroblasts, increasing it by 1.3-times of its original amount whereas it caused a decrease in presenescent control to 0.8-times of untreated control. To further validate these findings western blot was done to detect PTEN at protein level in celecoxib-treated and untreated oral fibroblasts. It was observed that in

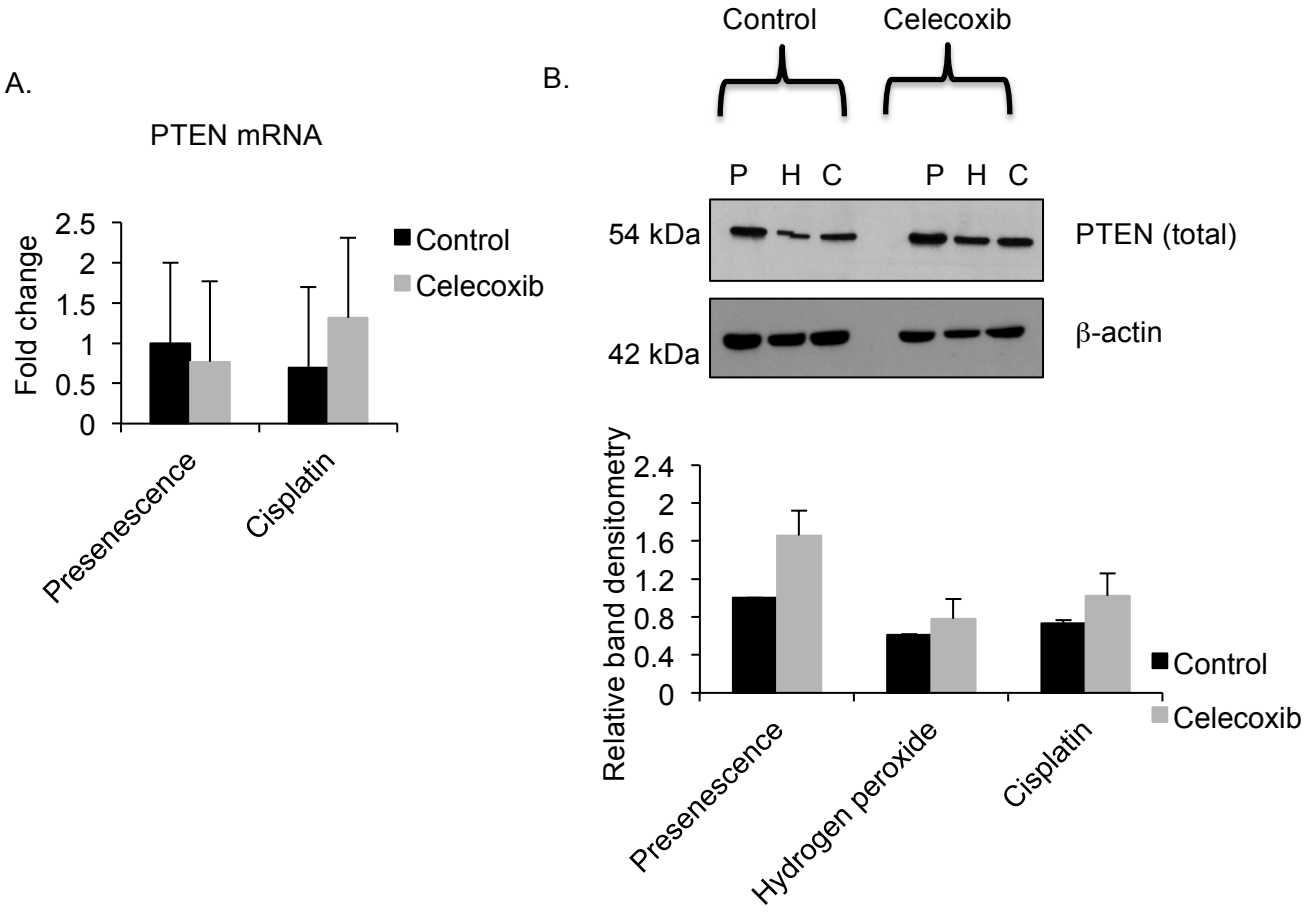

Figure 3.3.32: Celecoxib regulates PTEN transcription and translation in senescent oral fibroblasts. qRT-PCR was used to determine expression of PTEN mRNA in celecoxib-treated presenescent and cisplatin-induced premature senescent oral fibroblasts (A). Untreated cells were used as control (N=1, in triplicate). The mRNA expressions were validated by western blot (B). Cell lysates were collected from celecoxib-treated and untreated presenescent and stress-induced premature senescent oral fibroblasts and proteins were separated by electrophoresis in denaturing gel. The proteins were transferred into nitrocellulose membrane and blocked with total PTEN antibody (1 in 1000, Cell signaling). Relative band densitometry were calculated to quantify changes in PTEN expression. The bars represents mean + SEM of two independent experiments. N=2.

absence of celecoxib treatment the ratio of PTEN protein levels were lower in both H_2O_2 and cisplatin induced premature senescent oral fibroblasts about 0.6-times and 0.7-times of presenescent control, respectively and this was significantly increased upon celecoxib treatment to 0.8 and 1.02 (figure 3.3.32.B). Celecoxib also increased the ratio of PTEN protein in presenescent control increasing it from 1.0 to 1.7 (figure 3.3.32.B). These observations therefore implied celecoxib stimulated the expression of PTEN in senescent oral fibroblasts by blocking COX-2 activity.

3.3.5.4: PTEN deficient senescent oral fibroblasts have increased PI-3-K/AKT and NFκB activity

COX-2 is a downstream target of transcriptional activity of NFκB (Ali *et al*., 2010). Diminished PTEN activity had been reported to enhance NFκB activity via increased phosphorylation of downstream kinase AKT of PI-3-K/AKT pathway (Iliopoulos *et al*., 2010). Furthermore, previously it had been reported that NFκB facilitated development of inflammatory SASP in stress-induced premature senescence (Freund *et al.* 2011 and Bhaumik *et al.* 2009). Therefore, here it was postulated that senescent oral fibroblasts have increased AKT phosphorylation that induced NFκB to stimulate COX-2 expression.

Senescent fibroblasts were therefore screened for phosphorylation status of AKT at both serine-473 (Ou *et al*., 2011) and threonine-308 sites (Ou *et al*., 2011). Western blot revealed loss of PTEN expression in senescent oral fibroblasts are accompanied by enhanced phosphorylation of AKT at both serine-473 and serine-308 sites (figure 3.3.33). Levels of total AKT (pan), however, remained unchanged among senescent and presenescent oral fibroblasts.

To evaluate if this increased AKT activity was associated with increased NFκB activity in senescent oral fibroblasts, oral fibroblasts were transfected with pGL4.32 reporter

vector containing a NFκB response element, along with an internal control vector expressing renilla luciferase (pRL-TK). To exclude the possibility that the rise in NFκB activity was not due to a non-specific effect of growth arrest state quiescent cells were also used as control. It was observed that compared to presenescent control, quiescent cells demonstrated severely diminished NFκB reporter activity which was only 0.11-times of control. In contrast both H_2O_2-induced premature senescent oral fibroblasts and replicative senescent oral fibroblasts demonstrated a dramatic increase in NFκB reporter activity, which were 2.23-fold and 6.94-fold higher than presenescent control fibroblasts, respectively (figure 3.3.34.A). Similarly when miRNA transfected oral fibroblasts were assessed for NFκB activity it was observed that only co-transfected oral fibroblasts demonstrated a significant augmentation of NFκB reporter activity that was 1.9-fold higher than negative control (n=3, $p<0.05$, figure 3.3.34.B). However in miR-335 transfected oral fibroblasts a significant reduction in NFκB activity to 0.8-times of control was observed which corresponded with the increased PTEN protein expression observed in these cells earlier (n=3, $p<0.05$; figure 3.3.34.B).

All these evidence therefore suggested that after attainment of full senescence fate the senescent oral fibroblasts increased expression of miR-335 and miR-148b to silence PTEN. The loss of PTEN possibly withdraws its inhibitory effect on PI-3-K pathway and induces phosphorylation of AKT. The phosphorylated AKT then perhaps stimulates NFκB to stimulate transcription of various genes including COX-2 and IL-6 to reinforce SASP and regulate secretion of factors contributing to SASP such as MCP-1.

3.3.5.5: Celecoxib down-regulates miR-335 and miR-148b in senescent oral fibroblasts

STAT3 is a transcription factor which is reported to be highly up-regulated in cancer cells and during malignant transformation (Iliopoulos *et al*., 2010). Both miR-335 and

miR-148b were reported to have STAT3 binding sites (Iliopoulos *et al*., 2010). It was discovered that during early stages of malignant transformation expression of miR-335 and miR-148b are declined along with other deranged miRNAs with simultaneous elevated STAT3 activity (Iliopoulos *et al*., 2010). However the transcriptional regulatory effect of STAT3 on miR-335 and miR-148b remains to be defined. PGE2 can also mediate miRNA transcription in cancer cells in cMyc dependent manner (Krysan *et al*., 2014). As a result STAT3 mRNA expression was determined in senescent oral fibroblasts by qRT-PCR. It was observed that STAT3 expression was significantly reduced in senescent oral fibroblasts by 0.6-times and by 0.7-times in H_2O_2 and cisplatin treated oral fibroblasts respectively and to 0.4-times in replicative senescent oral fibroblasts compared to control (figure 3.3.35.A). Celecoxib treatment caused an increase in STAT3 expression in presenescent oral fibroblasts but caused a decrease in STAT3 expression in cisplatin-treated oral fibroblasts (figure 3.3.35.B). However to confirm the functional effect of STAT3 it is necessary to study its protein level and phosphorylation status. Therefore further experiments are required before ascertaining the regulatory role of STAT3 in SASP.

Interestingly, celecoxib treatment dramatically reduced miR-335 and miR-148b expression in cisplatin-induced premature senescent oral fibroblasts from 23-times to 0.01-times and from 26-times to 7.44-times, respectively (figure 3.3.35.C). Similar changes were also observed in presenescent oral fibroblasts after celecoxib treatment wherein miR-335 and miR-148b were reduced from 1-times to 0.04-times and 0.038-times, respectively. The decrease in miR-335 and miR-148b levels in both senescent and presenescent oral fibroblasts corresponded to the rise in PTEN protein levels observed in western blot. As a result from these evidence it can now be concluded that COX-2 regulates expression of both miR-335 and miR-148b which down-regulate PTEN expression in senescent oral fibroblasts and stimulate their pro-tumourigenic phenotype.

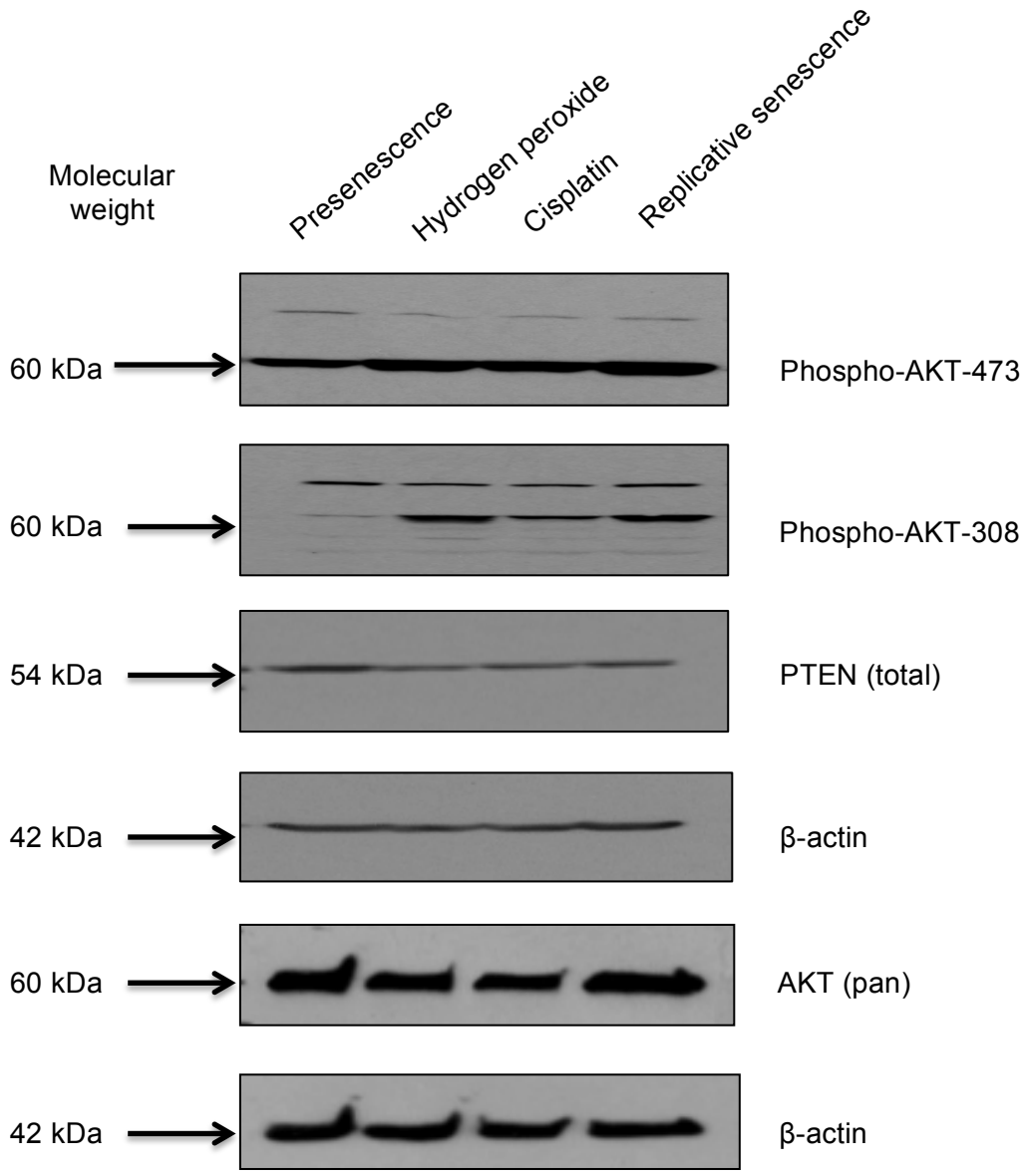

Figure 3.3.33: Increased AKT activity in senescent oral fibroblasts. Western blot was carried out using cell lysates from H_2O_2-induced, cisplatin-induced and replicative senescent oral fibroblasts. The proteins were separated in a denaturing gel by protein gel electrophoresis and transferred onto a nitrocellulose membrane. The membranes were incubated with anti-AKT1 (ser-473), anti-AKT2 (thr-308) and anti-AKT (pan) antibody at dilution of 1 in 1000 for 8 h at 4^{o} C.

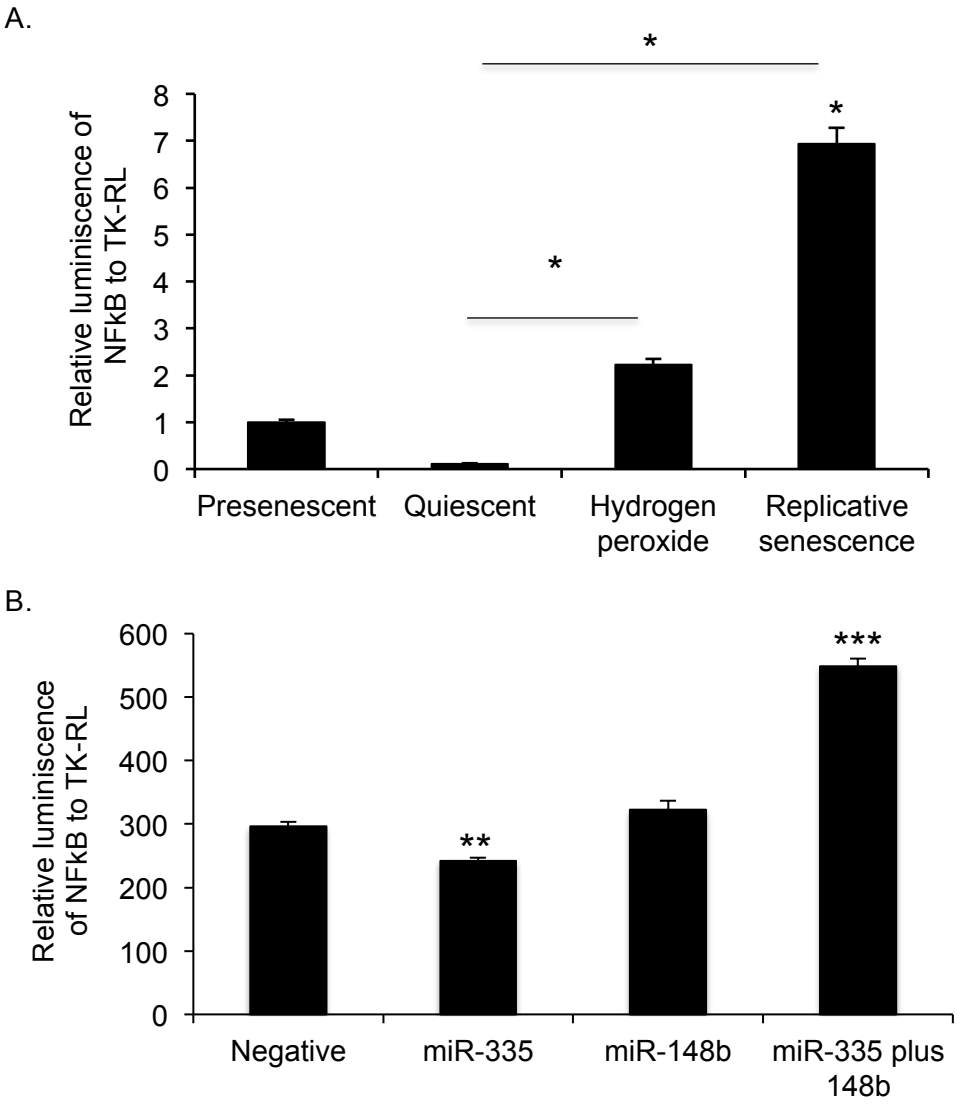

Figure 3.3.34: Senescent and co-transfected oral fibroblasts demonstrate increased NFκB activity. Stress-induced prematurely senescent, replicative senescent, presenescent and quiescent oral fibroblasts (A) and miRNA over-expressing fibroblasts (B) were co-transfected with pGL4.32 carrying NFκB response element and renilla luciferase. Enhancement of luminescence recorded as absorbance by a luminometer**.** The data were normalized to presenescent oral fibroblast. The NFκB activity is measured as mean ± SEM of three independent experiments. N=3, in triplicate. *p<0.05, one-way ANOVA with post-hoc correction by Tukey test (A) and paired student's t-test (B).

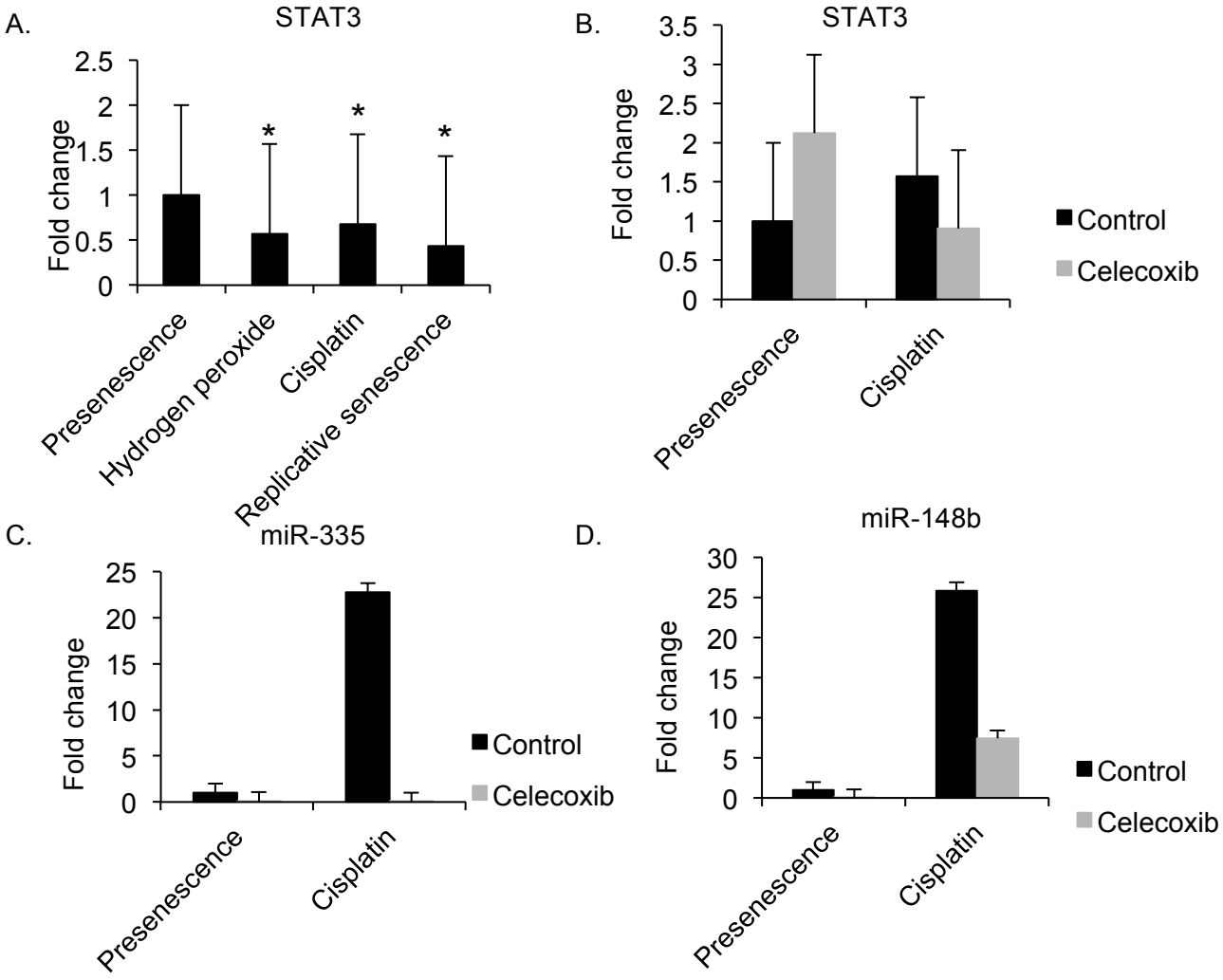

Figure 3.3.35: Celecoxib down-regulates miR-335 and miR-148b expressions in senescent oral fibroblasts. qRT-PCR was used to determine mRNA levels of STAT3 in senescent oral fibroblasts (A) and celecoxib-treated oral fibroblasts (B). Effect of celecoxib in miRNA expression was also evaluated by qRT-PCR for miR-335 (C) and miR-148b (D) expression in presenescent and cisplatin-treated oral fibroblasts. The bars represent fold change + SEM of two independent experiments. *$p<0.05$, one-way ANOVA with post-hoc corrections by Holm-Sidak method (A).

3.3.6: Conclusion

In this section it was demonstrated that miRNAs are aberrantly expressed in cisplatin-induced premature senescent oral fibroblasts among which miR-146a, miR-148b, miR-184 and miR-335 are up-regulated in both stress-induced premature senescent (H_2O_2 and cisplatin induced) and replicative senescent oral fibroblasts. Transient over-expression of miR-335 and miR-148b could reprogram young oral fibroblasts to secrete more MCP-1 and IL-6 and express less PTEN, which contribute to SASP of senescent oral fibroblasts but failed to elicit senescence in these cells. Moreover over-expression of both miR-335 and miR-148b in oral fibroblasts promoted migration of OSCC derived cell line H357 *in vitro* by paracrine mechanism partly dependent on MCP-1. Transient knockdown of PTEN in oral fibroblasts also reprogrammed them to promote cancer cell migration *in vitro* but this was independent of SASP. In depth investigation of the pro-inflammatory phenotype of senescent oral fibroblasts revealed that PTEN expression in senescent oral fibroblasts was regulated by elevated COX-2 activity, which could regulate expression of both miR-335 and miR-148b, possibly via PGE2/cMyc or IL-6/STAT3 axis that need to be further investigated. Blockade of COX-2 activity with celecoxib could rescue the inflammatory phenotype of senescent oral fibroblasts by reducing secretion of both IL-6 and PGE2. Celecoxib also attenuated the active state of senescent oral fibroblasts by diminishing formation of stress fibers and reduced their pro-tumourigenic effect on cancer cells. Both miR-335 and miR-148b induced translational repression of PTEN in senescent oral fibroblasts and in addition miR-148b could possibly stimulate its mRNA decay based on evidence form reduced protein expression in western blot in miR-148b transfected oral fibroblasts. Furthermore, lack of PTEN in senescent oral fibroblasts is associated with increased phosphorylation of AKT and enhanced NFκB activity, which possibly instigates a vicious feedback loop to establish and maintain SASP.

As apprised in introduction of this thesis, naturally occurring CAFs originating from GU OSCC exhibit a gene expression profile characteristic of senescent cells and are reported to contribute to the emergence of highly aggressive tumours with poor prognosis (Kim *et al*., 2011; Hassona *et al*., 2013; Hassona *et al*., 2014). These studies examined the mechanism of development of senescent subpopulation in CAFs and revealed MMP-2 as the chief constituent of SASP that led to tumour invasion (Hassona *et al*., 2013; Hassona *et al*., 2014). It was demonstrated in section 3.1.2 (figure 3.1.2.3) that stress-induced and replicative senescent oral fibroblasts derived from healthy donors secreted more MMP-2 than their younger counterparts. Therefore it was proposed that SASP in senescent CAFs resembled that of artificially induced premature senescent oral fibroblasts and is regulated by alteration in expression of miRNAs targeting PTEN in COX-2 dependent fashion.

Chapter 3.4: Regulation of SASP in senescent CAFs of OSCC

Hypothesis:

1. Cancer associated fibroblasts (CAFs) derived from genetically unstable (GU) OSCC are enriched for a subset of senescent fibroblasts which contribute to their inflammatory secretory phenotype resembling SASP.
2. CAFs of GU OSCC express abnormal levels of miRNAs that target genes contributing to their pro-tumourigenic properties.
3. PTEN is down-regulated in CAFs of GU OSCC and modulation of COX-2 activity in CAFs can regulate PTEN expression and their activated secretory phenotype in a similar manner to stress-induced premature senescent oral fibroblasts.

Aims and objectives:

- To screen CAFs for markers of senescence and SASP.
- To determine that CAFs retained their activated phenotype *in vitro*.
- To determine the consequences of treatment of non-senescent CAFs with cisplatin on their paracrine effects on oral dysplastic and cancer cell lines in 2D and 3D *in vitro* assay.
- To determine miRNA expression profile in CAFs using TaqMan miRNA TLDA and validate expression of candidate miRNAs in CAFs by qRT-PCR.
- To determine expression of PTEN in CAFs
- To determine if alteration of COX-2 activity modulates PTEN protein in CAFs and attenuated the activated phenotype of CAFs *in vitro*.

3.4.0: SASP in OSCC derived CAFs

To understand SASP in CAFs of OSCC initially CAFs derived from both GS and GU OSCC were examined for markers of both senescence and SASP, with and without cisplatin treatment. Thereafter SASP in senescent-CAFs was thoroughly investigated focusing primarily on its regulatory mechanism.

3.4.1: Cisplatin stimulates premature senescence in CAFs derived from GS OSCC but reinforces senescence in CAFs derived from GU OSCC

Measurement of SA-β-Gal activity demonstrated that CAFs derived from GS OSCC (BICR69 and BICR70) stained negative for this senescence marker, however, after cisplatin treatment they gradually accumulated blue cells suggesting that cisplatin induced premature senescence in these cells (figure 3.4.1, left panel). In contrast, CAFs derived from GU OSCC (BICR31, BICR63 and BICR18) demonstrated SA-β-Gal activity, manifested by the increased number of blue cells compared to those derived from GS tumours and the level of staining was enhanced upon cisplatin treatment (figure 3.4.1, right panel) indicating that chemotherapy amplified the senescent phenotype of these cells.

To ensure that these CAFs retained their myofibroblastic phenotype *in vitro* direct immunofluorescence for α-SMA was carried out. It was observed that CAFs of both origins retained expression of α-SMA despite of being cultured in 2D indicative of their sustained active phenotype (figure 3.4.2). After cisplatin treatment there was a remarkable increase in stress fiber formation in CAFs: BICR69 and BICR70 whereas visibly there was no difference in α-SMA expression among CAFs: BICR31, BICR63 and BICR18, before and after cisplatin treatment (figure 3.4.2).

These results therefore suggest that CAFs derived from GU OSCC are enriched for a sub-population of senescent cells and are comparatively more active than non-

senescent CAFs derived from GS OSCC. Moreover cisplatin can trigger senescence in CAFs from GS OSCC and exaggerate their active phenotype causing them to behave like CAFs of GU OSCC. Next these CAFs were evaluated for expression of SASP markers that were previously used in the study to characterize SASP of stress-induced and replicative senescent oral fibroblasts and the existence of any correlation with their senescent nature were determined.

3.4.2: CAFs derived from GU OSCC secrete more MCP-1 and IL-6

It was shown in section 3.1.2 that stress-induced and replicative senescent oral fibroblasts secreted more inflammatory cytokines than their counterpart presenescent control. To determine if senescent CAFs displayed similar features they were screened for expression of SASP markers; MCP-1 and IL-6, at both mRNA and protein level. qRT-PCR demonstrated CAFs derived from GU OSCC expressed significantly more MCP-1 mRNA, about 20-times higher than normal human oral fibroblasts; NHOF. CAFs of GS OSCC expressed a significantly lower amount of MCP-1 mRNA than CAFs of GU OSCC and was about 0.66-times of NHOF ($n=2$, $p<0.05$; figure 3.4.3.A). Quantification of secreted MCP-1 by ELISA demonstrated that CAFs of GU OSCC secreted significantly more MCP-1 than CAFs of GS OSCC and NHOF (GU CAFs, $n=3$; GS CAFs, $n=2$; NHOF, $n=3$; $p<0.05$; figure 3.4.3.B). CAFs of GU OSCC secreted 6.9-times and CAFs of GS OSCC secreted only 1.2-times more MCP-1 than NHOF and this corresponded to the differences in their transcripts level (figure 3.4.3.B).

Conversely, both CAFs of GU and GS OSCC showed elevated level of IL-6 transcripts, about 1.6-times and 3.2-times higher than NHOF, respectively, however these increase were statistically insignificant (figure 3.4.4.A). At protein level only CAFs derived from

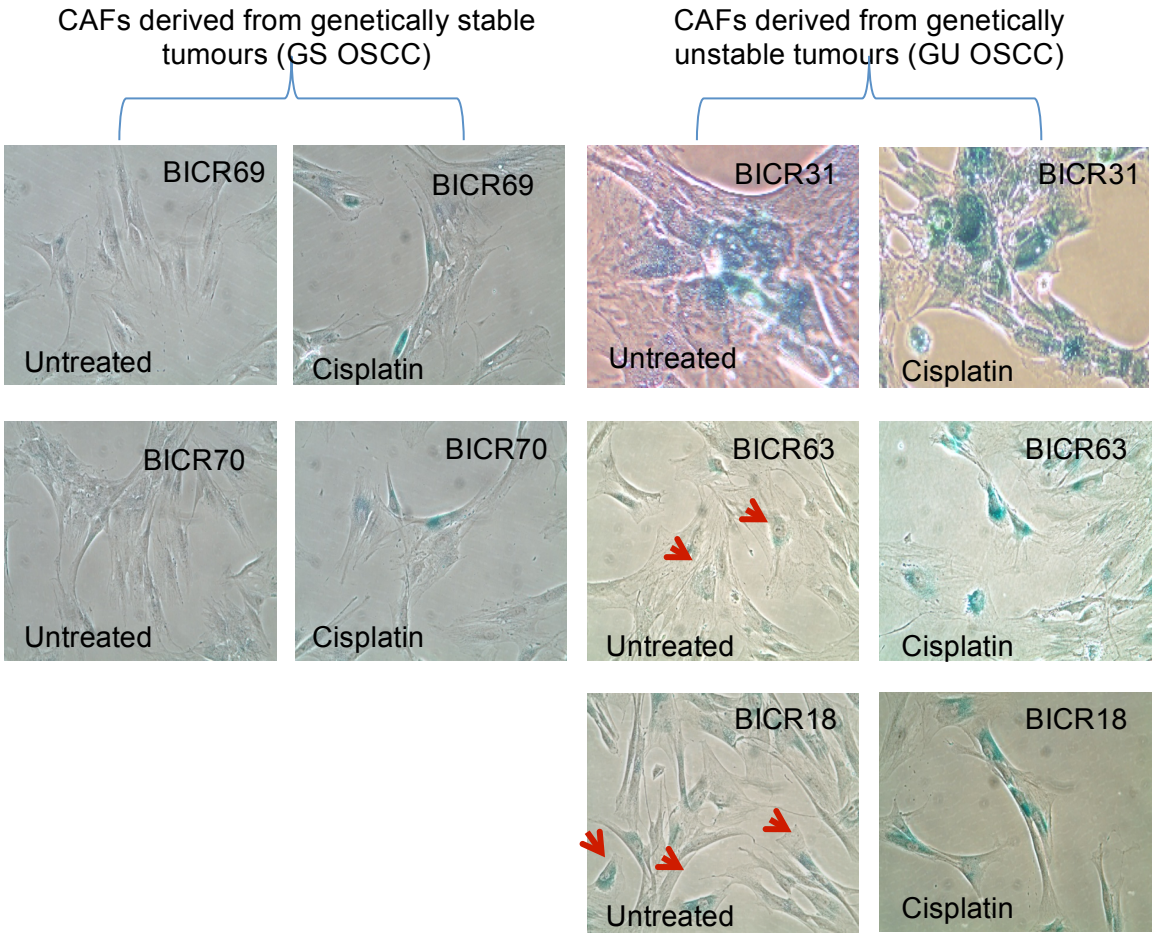

Figure 3.4.1: CAFs of GU tumours display more SA-β-Gal activity than those from GS OSCC. SA-β-Gal activity was measured in CAFs of both GS and GU OSCC treated and untreated with cisplatin. Senescence was confirmed by appearance of blue precipitate in perinuclear area of cells. The red arrows indicated blue senescent cell in untreated CAFs of GU OSCC. The photographs were taken under 20X magnification under light microscope.

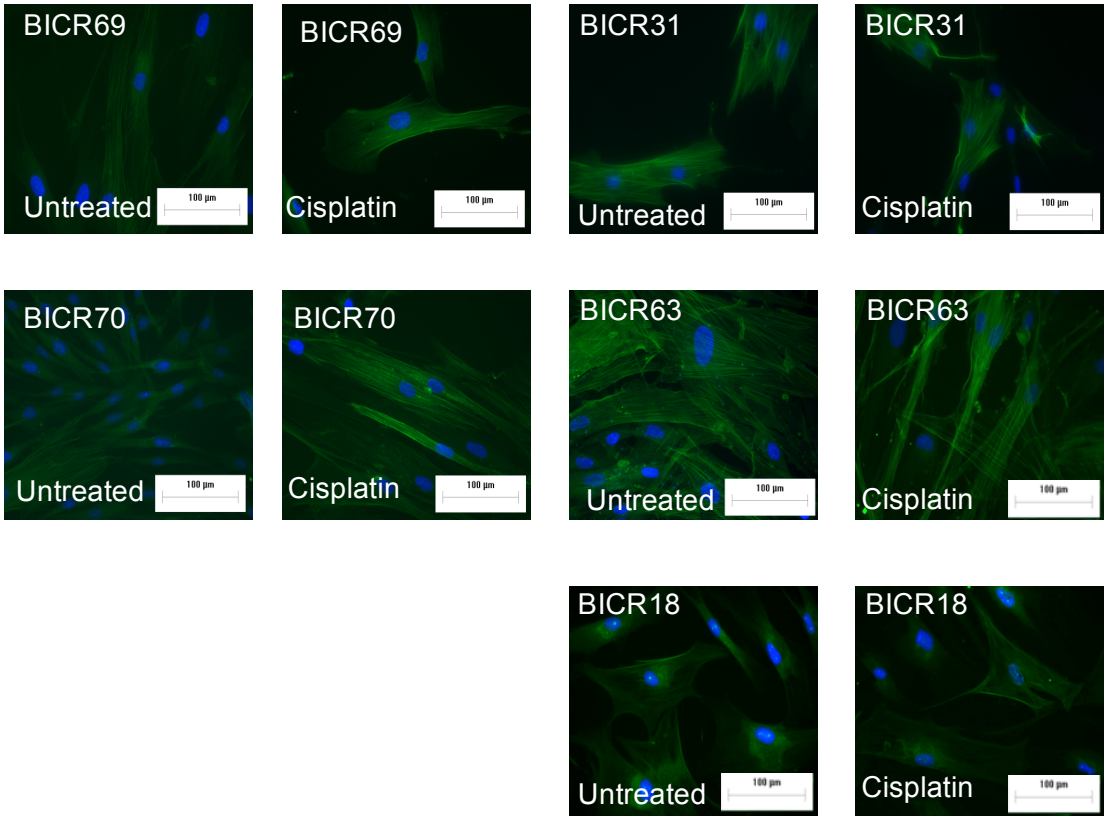

Figure 3.4.2: CAFs of GU OSCC display increased formation of stress fibers despite treatment with cisplatin. CAFs of GS (left panel) and GU (right panel) OSCC were either treated with cisplatin or left untreated. After confirming attainment of senescence the cells were seeded down at a density of 50,000 on sterile glass cover slips and direct immunofluorescence cytochemistry for α-SMA was done. Activated fibroblasts demonstrated enhanced fluorescence and formation of elongated green stress fibers. The photographs were taken at 20X magnification using fluorescence microscope. Scale bar = 100 μM.

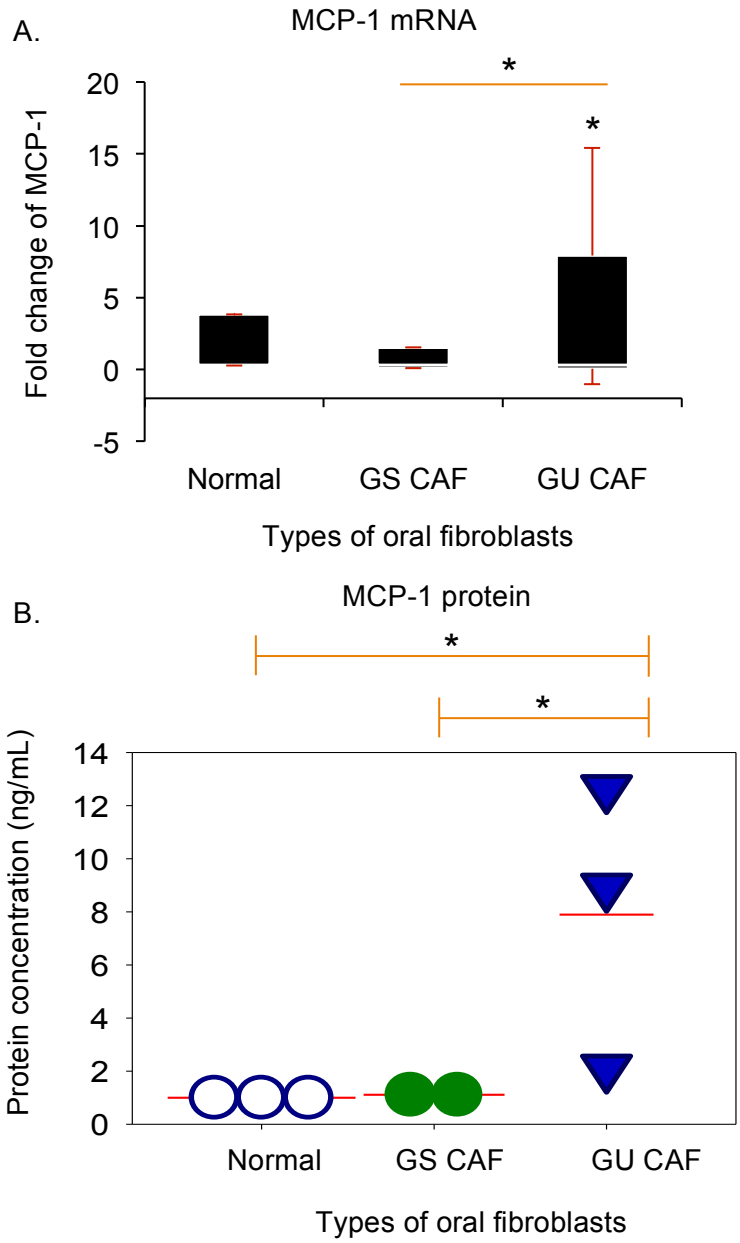

Figure 3.4.3: MCP-1 expression is elevated in CAFs of GU OSCC. MCP-1 transcription and secretion is dramatically increased in CAFs of GU OSCC than those of GS OSCC and normal fibroblasts as determined by qRT-PCR (A) and human MCP-1 ELISA (B). The density plot represents mean of triplicate (denoted by red line) of different patients (denoted by round or triangular objects) in individual group. N=3 (GU CAFs) and N=2 (GS CAFs), in triplicate. *p<0.05, one-way ANOVA with post-hoc correactions by Dunn's method.

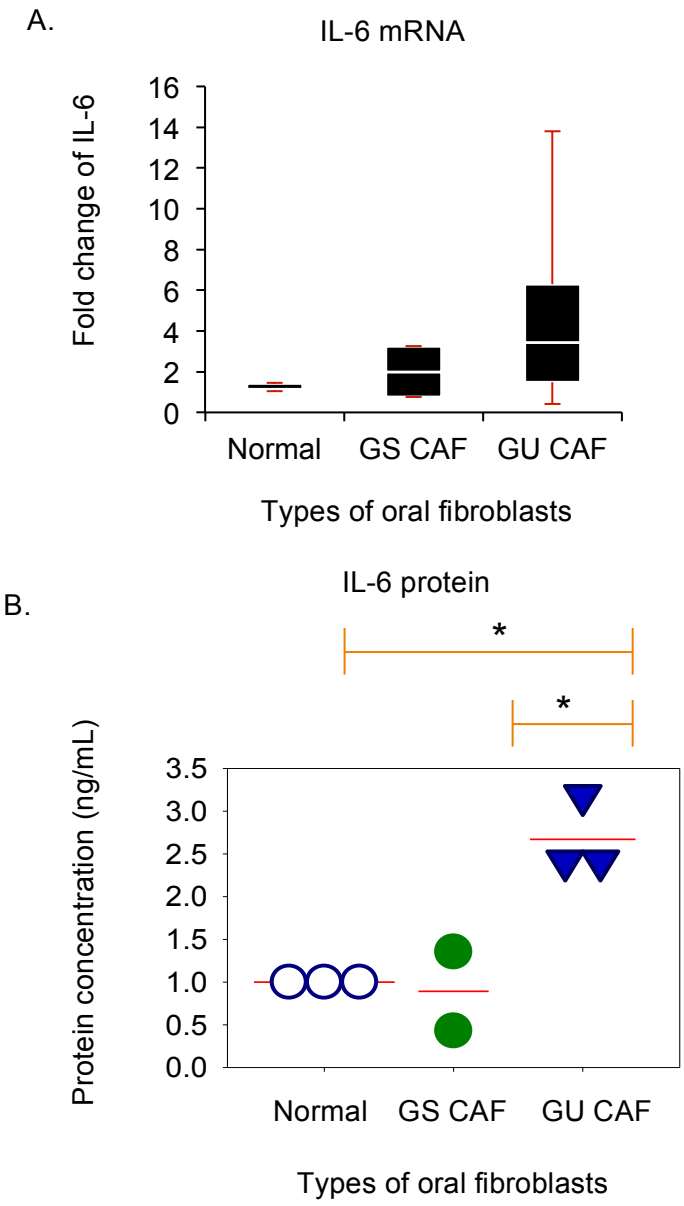

Figure 3.4.4: IL-6 expression is elevated in CAFs of GU OSCC. IL-6 transcription and secretion is increased in CAFs of GU OSCC than those of GS OSCC and normal fibroblasts as determined by qRT-PCR (A) and human IL-6 ELISA (B). The density plot represents mean of triplicate (denoted by red line) of different patients (denoted by round or triangular objects) in individual group. N=3 (GU CAFs) and N=2 (GS CAFs), in triplicate. *p<0.05, one-way ANOVA with post-hoc correactions by Dunn's method (A) and by Holm-Sidak method (B).

GU OSCC secreted significantly more IL-6 (2.7-times) than NHOF whereas CAFs of GS OSCC secreted similar amount of IL-6 to that of NHOF (about 0.9-times of control) (GU CAFs, n=3; $p<0.05$; GS CAFs, n=2; $p<0.05$). From this evidence it may be concluded that GU CAFs synthesized and secreted more MCP-1 and IL-6 relative to non-senescent CAFs of GS OSCC and NHOF. This difference in secretory activity between CAFs of GU and GS OSCC may result from existence of SASP within its senescent subset.

To ensure that SASP of CAFs of GU OSCC was functional and could reproduce the pro-tumourigenic effects of stress-induced premature senescent oral fibroblasts the paracrine effects of both types of CAFs on proliferation, migration and invasion of oral dysplastic and cancerous cell lines were investigated.

3.4.3: Paracrine effect of CAFs on proliferation and migration of oral dysplastic cell lines

CAFs derived from GS OSCC were induced to senesce by treatment with cisplatin to mimic secretory phenotype of senescent-CAFs of GU OSCC. Serum starved D20 cells were treated with conditioned media from both untreated non-senescent and cisplatin-induced senescent CAFs of GS OSCC. Serum free media and conditioned media derived from NHOF were used as controls. In contrast to serum free media and conditioned media derived from NHOF and non-senescent CAFs, conditioned media derived from cisplatin-induced senescent CAFs, both BICR69 (figure 3.4.5.A) and BICR70 (figure 3.4.5.B), significantly stimulated proliferation of the oral dysplasia-derived cell line, D20, from 0 h to 96 h.

In migration assay, conditioned media from senescent CAFs of GU OSCC (BICR18, BICR63, BICR31) significantly stimulated migration of D20 cells *in vitro* compared to both NHOF and CAFs derived from GS tumours (GU CAFs, n=3; $p<0.05$; GS CAFs,

n=2; p<0.05) irrespective of cisplatin treatment (figure 3.4.5.C). In absence of cisplatin treatment there was no significant difference in stimulatory effect of CAFs of GS OSCC (BICR69 and BICR70) from NHOF on migration of dysplastic cells. However after induction of senescence with cisplatin both CAFs of GS OSCC and cisplatin-induced premature senescent-NHOF dramatically enhanced migration of D20 cells compared to their non-senescent counterparts except BICR70, which increased migration but the stimulatory effect remained much lower than NHOF. There was no significant difference between stimulatory effect of senescent CAFs from GS tumours and senescent normal fibroblasts.

Compared to NHOF non-senescent CAFs from GS OSCC stimulated migration of D20 cells by 1.3-times (BICR69) and 0.4-times (BICR70) and this increased to 2.1-times and 0.7-times, respectively, after cisplatin treatment (figure 3.4.5.C). Cisplatin-induced premature senescent-NHOF stimulated 1.9-times more migration of D20 cells than non-senescent-NHOF. CAFs from GU OSCC, which contained a senescent sub-population (section 3.4.1) significantly stimulated migration of D20 cells by 1.5-times (BICR31), 3.6-times (BICR63) and 6.7-times (BICR18) compared to non-senescent-NHOF and these stimulatory effect was further augmented by cisplatin treatment to 3.6-times, 6.3-times and 14.0-times, respectively (figure 3.4.5.C).

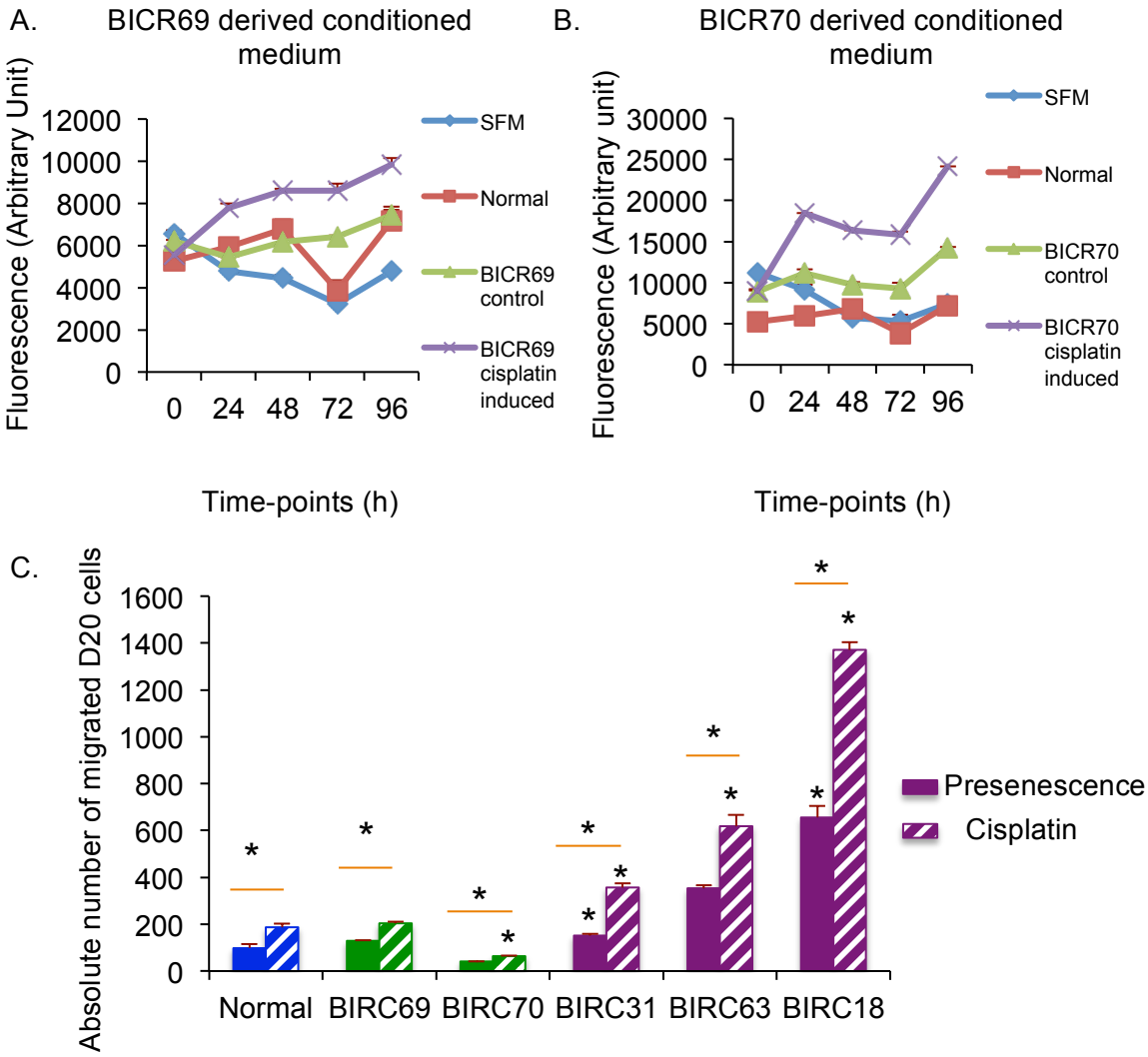

Figure 3.4.5: Senescent CAFs from GS OSCC stimulated proliferation and migration of D20 cells *in vitro* in a similar manner to CAFs of GU OSCC. CyQuant NF cell proliferation assay was used to determine the rate of proliferation of D20 cells in presence of conditioned media derived from both senescent and non-senescent BICR69 (A) and BICR70 (B) fibroblasts. Transwell assay was used to determine and compare the stimulatory effect of senescent and non-senescent CAFs on D20 cell migration (C). The bars represent mean + SEM. *p<0.05, two-way repeated measures ANOVA with post-hoc corrections by Holm-Sidak method (A) and two-way ANOVA with post-hoc corrections by Bonferroni t-test (B).

3.4.4: Paracrine effects of CAFs on proliferation and migration of OSCC derived cell line SCC4

In section 3.2.2 it was shown that cisplatin-induced senescent NHOFs had less stimulatory effect on proliferation and migration of SCC4 cells compared to oxidative stress-induced and replicative senescent NHOFs, probably due to prior adaptation in a tumour microenvironment exposed to anti-cancer drugs. To understand if cisplatin-induced senescent-CAFs behaved similar to that of senescent-NHOF their effects on proliferation and migration of SCC4 cells were investigated.

It was observed addition of conditioned media from cisplatin-induced senescent-CAFs of GS OSCC (BICR69 and BICR70) significantly stimulated proliferation of SCC4 cells compared to their non-senescent counterparts and NHOFs (figure 3.4.6.A and B). Two-way repetitive measure ANOVA showed for the first 48 h, conditioned media from both senescent-BICR69 and senescent-BICR70 significantly stimulated proliferation of SCC4 cells. At 72 h, senescent-CAFs stimulated proliferation of D20 cells but this effect was insignificant compared to previous time-points. There was no significant difference in rate of proliferation of SCC4 in presence of conditioned media from non-senescent-BICR69, non-senescent-NHOF and serum free media. In contrast conditioned media from non-senescent BICR70 also significantly stimulated proliferation of SCC4 cells at 48 h than non-senescent-NHOF and serum free media.

2D transwell assay demonstrated conditioned media from CAFs of GU tumours significantly stimulated migration of SCC4 cells than CAFs of GS OSCC and non-senescent-NHOF; and this effect was magnified dramatically by cisplatin treatment (figure 3.4.6.C). There was no significant difference in migration of SCC4 cells towards conditioned media of non-senescent-NHOF and non-senescent-CAFs of GS OSCC. Induction of senescence in both NHOF and CAFs of GS OSCC remarkably increased their stimulatory effect on SCC4 migration in comparison to their non-senescent

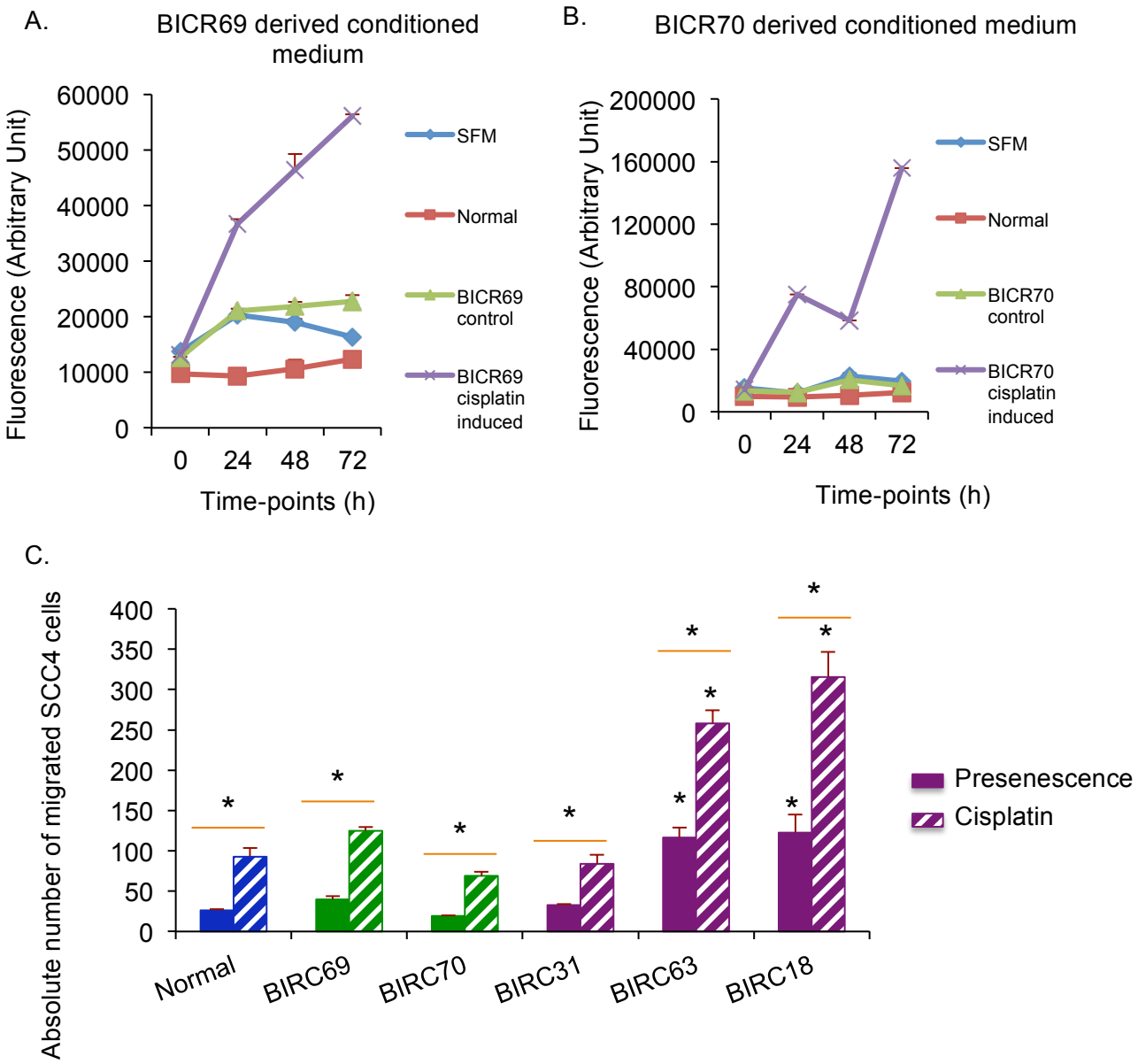

Figure 3.4.6: Senescent CAFs from GS OSCC stimulated proliferation and migration of SCC4 cells *in vitro* in a similar fashion to CAFs of GU OSCC. CyQuant NF cell proliferation assay was used to measure the rate of proliferation of SCC4 cells in presence of conditioned media derived from both senescent and non-senescent CAFs BICR69 (A) and BICR70 (B). Transwell assay was used to determine and compare the potentials of senescent and non-senescent CAFs from GS and GU OSCC on migration of SCC4 cells *in vitro* (C). The bars represent mean + SEM. *p<0.05, two-way repeated measures ANOVA with post-hoc corrections by Holm-Sidak method (A) and two-way ANOVA with post-hoc corrections by Bonferroni t-test (B).

counterparts. Non-senescent BICR69 and BICR70 stimulated SCC4 migration by 1.5-times and 0.74-times, respectively, compared to non-senescent-NHOFs and this was dramatically increased to 4.8-times and 2.63-times after cisplatin treatment. Statistically the stimulatory effects of senescent-CAFs of GS OSCC were incomparable to the stimulatory effect of cisplatin-induced premature senescent-NHOFs, which increased SCC4 migration by 3.5-times. BICR31, BICR63 and BICR18 significantly stimulated SCC4 migration by 1.3-times, 4.4-times and 4.7-times, respectively, than non-senescent-NHOFs and this was significantly increased to 3.2-times, 10-times and 12-times, respectively, after cisplatin treatment.

3.4.5: Paracrine effects of CAFs on proliferation and migration of OSCC derived cell line H357

In section 3.2.3 and 3.2.4, it was shown stress-induced senescent oral fibroblasts significantly stimulated proliferation, migration and invasion of H357 cells *in vitro*. Moreover Hassona and group (2013) demonstrated that CAFs of GU OSCC amplified the invasive phenotype of H357 cells in 3D organotypic models. To explore this further and to determine if chemotherapy treatment could alter the tumour promoting properties of CAFs, cisplatin was used again to induce senescence in CAFs: BICR69 and BICR70, derived from GS OSCC. Two-way repeated measure ANOVA showed that H357 cells treated with conditioned media from cisplatin-induced senescent BICR69 (figure 3.4.7.A) and BICR70 (figure 3.4.7.B) demonstrated a significant increase in the rate of proliferation of H357 cells from time-point 0 h to 96 h compared to their non-senescent counterparts, non-senescent-NHOFs and serum free media. There was negligible difference in the stimulatory effect between non-senescent-CAFs and non-senescent-NHOF in the rate of proliferation of H357 cells.

For migration assay only conditioned media of CAF BICR70 from GS OSCC was used

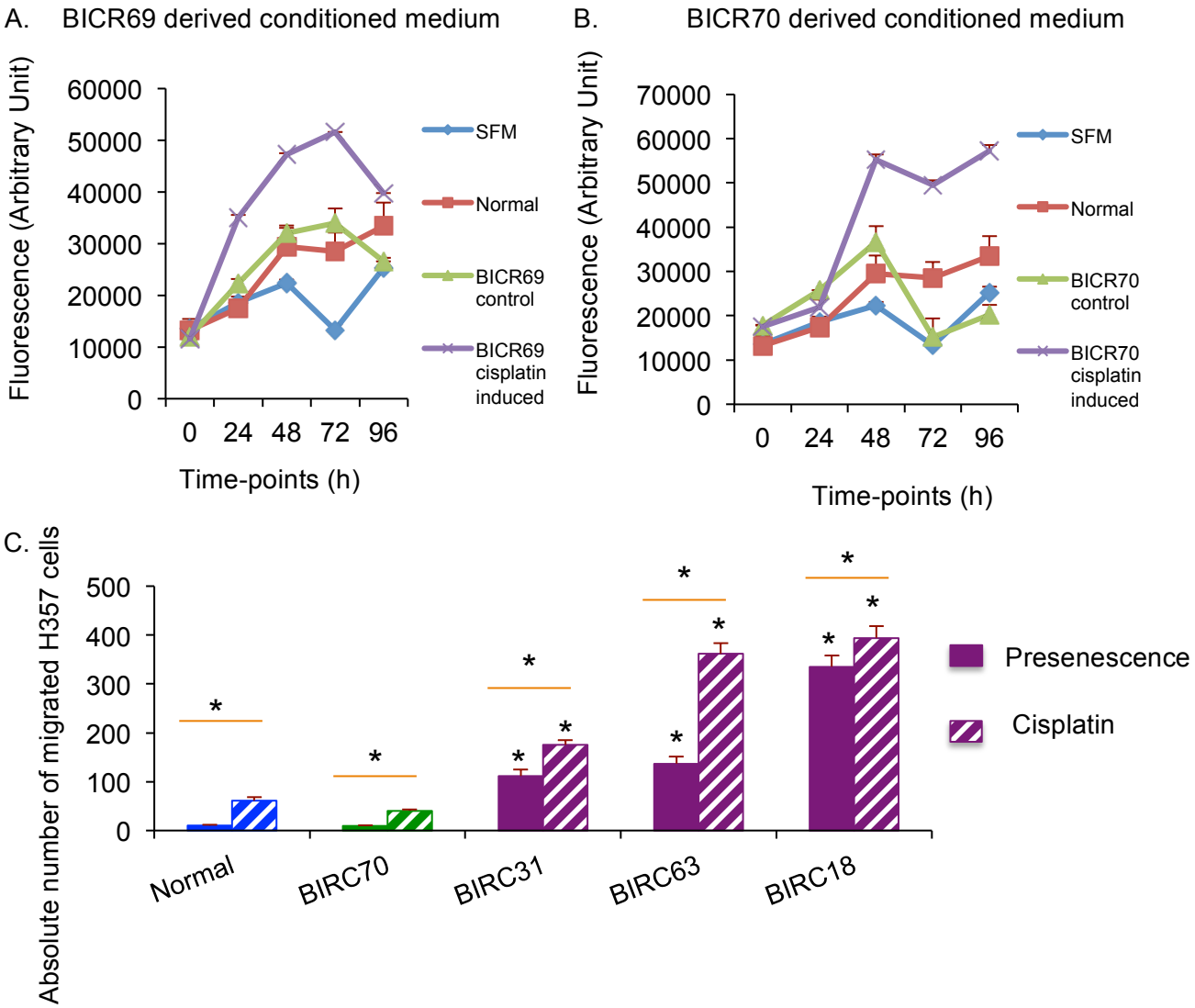

Figure 3.4.7: Senescent CAFs from GS OSCC stimulated proliferation and migration of H357 cells in vitro in a similar fashion to CAFs of GU OSCC. CyQuant NF cell proliferation assay was used to measure the rate of proliferation of H357 cells in presence of conditioned media derived from both senescent and non-senescent CAFs BICR69 (A) and BICR70 (B). Transwell assay was used to determine and compare the capacity of senescent and non-senescent CAFs from GS and GU OSCC to stimulate migration of H357 cells in vitro (C). The bars represent mean + SEM. *p<0.05, two-way repeated measures ANOVA with post-hoc corrections by Holm-Sidak method (A) and two-way ANOVA with post-hoc corrections by Bonferroni t-test (B).

to compare their stimulatory effect with senescent CAFs from GU OSCC and NHOF. It was observed that conditioned media from CAFs of GU OSCC (BICR31, BICR63 and BICR18) significantly stimulated migration of H357 cells *in vitro* by more than 11-times, 13-times and 33-times, respectively, compared to non-senescent-NHOFs (figure 3.4.7.C). Treatment of these CAFs with cisplatin further incremented their stimulatory effects in promoting migration of H357 cells to more than 17-times, 36-times and 39-times, respectively. There was no difference in the stimulatory effect between non-senescent-BICR70 and non-senescent-NHOF on H357 cell migration. However induction of senescence with cisplatin in both of these cells significantly increased migration of H357 cells by more than 4.0-times and 6.0-times, respectively, compared to their non-senescent counterparts (figure 3.4.7.C).

These functional assays suggested presence of senescent population in CAFs is necessary for exerting their pro-tumourigenic effect on neighbouring cancer cells that lead to tumour progression. It is also apparent that senescent fibroblasts co-evolve in a subset of CAFs with the advancement of tumour stage, which subsequently synergize with other stromal components to support growth and invasion of adjacent cancer cells as demonstrated by Hassona *et al*. (2013). Further the functional effects of non-senescent-CAFs and non-senescent-NHOFs on OSCC cells were indistinguishable implying that perhaps these CAFs represented a subset of good CAFs and their existence in tumour microenvironment may be beneficial as they behaved in similar fashion to the resting fibroblasts and lacked the pro-tumourigenic properties of aggressive CAFs. Alternatively CAFs of GS OSCC can be rapidly reprogrammed into tumour promoting fibroblasts as observed in cisplatin treated cells, which may be taken into consideration during administration of chemotherapy to such patients.

3.4.6: CAFs from GS and GU OSCC stimulate invasiveness of H357 cell lines in 3D organotypic models

It was recently published that CAFs from GU OSCC secreted more MMP-2 than those from GS OSCC (Hassona *et al*., 2014). Consequently it was hypothesized that like stress-induced premature senescent-NHOFs CAFs from GU OSCC can stimulate invasiveness of OSCC cell lines *in vitro* by secreting MMP-2 and inducing EMT-like changes. Therefore gelatin zymography was carried out to ascertain secretion of MMP-2 by CAFs. It was observed that compared to normal oral fibroblasts CAFs from both GS and GU OSCC secreted 2.2-times more MMP-2, as assessed by the increased density of gelatinolytic bands in zymogram ($p<0.05$; figure 3.4.8).

Next 3D organotypic models were used to co-culture H357 cells in presence of NHOFs, CAFs from GS (BICR69 and BICR70) and from GU (BICR63) tumours that were either untreated or treated with cisplatin for 24 h for senescence induction (method section 2.18.3.2, figure 3.4.9). Senescence was confirmed by increased expression of p16 in fibroblasts as determined by immunohistochemistry (figure 3.4.10). The number of H357 cells that invaded into the dermis was quantified by counting the total number of cancer cells present in the dermis (figure 3.4.11). It was observed that irrespective of origin, CAFs from both GS and GU OSCC increased invasion of H357 cells into the dermis than non-senescent-NHOFs (figure 3.4.9 and figure 3.4.11). Both BICR69 and BICR70 cells stimulated twice as much invasion of H357 cells than non-senescent-NHOFs (figure 3.4.11) whereas BICR63 increased invasiveness by 1.5-times to that of non-senescent-NHOFs.

When p16 expression was examined to assess fibroblast senescence it was observed that both BICR69 and BICR63 cells contained p16 positive fibroblasts visible as dark brown nuclear and cytoplasmic staining that were absent in non-senescent-NHOF controls and BICR70 cells (figure 3.4.10). However when BICR69 CAFs were tested in

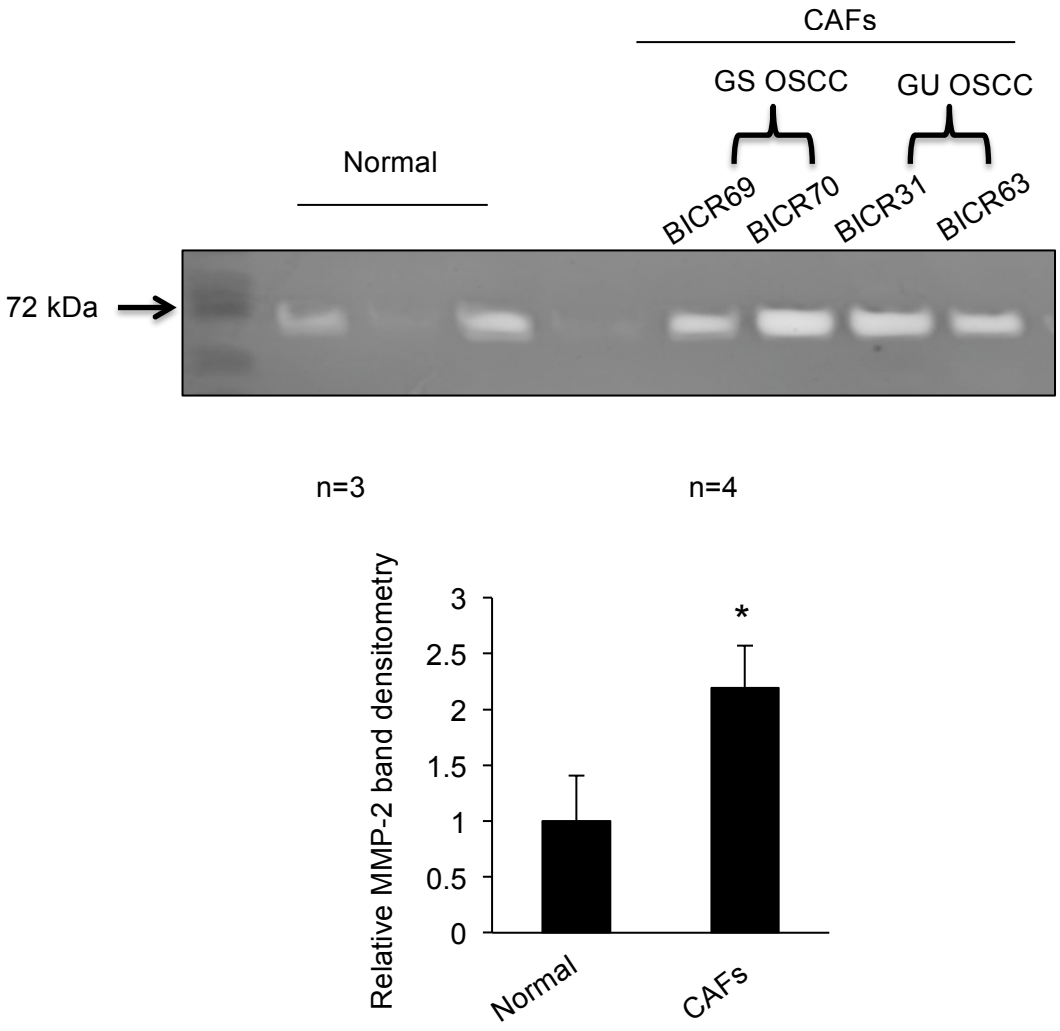

Figure 3.4.8: CAFs from both GS and GU OSCC secrete more MMP-2 than normal oral fibroblasts irrespective of senescence. MMP-2 zymography was carried out using concentrated conditioned media from 2 CAFs of GS (BICR69 and BICR70) tumour and 2 CAFs from GU (BICR31 and BICR63) tumours and 3 normal oral fibroblasts. Commassie staining of gel demonstrates formation of thickened and intensified gelatinolytic bands by CAFs vs normal fibroblasts. The bars represent mean of relative band densitometry of CAF vs normal + SEM. *$p<0.05$, by paired student's t-test.

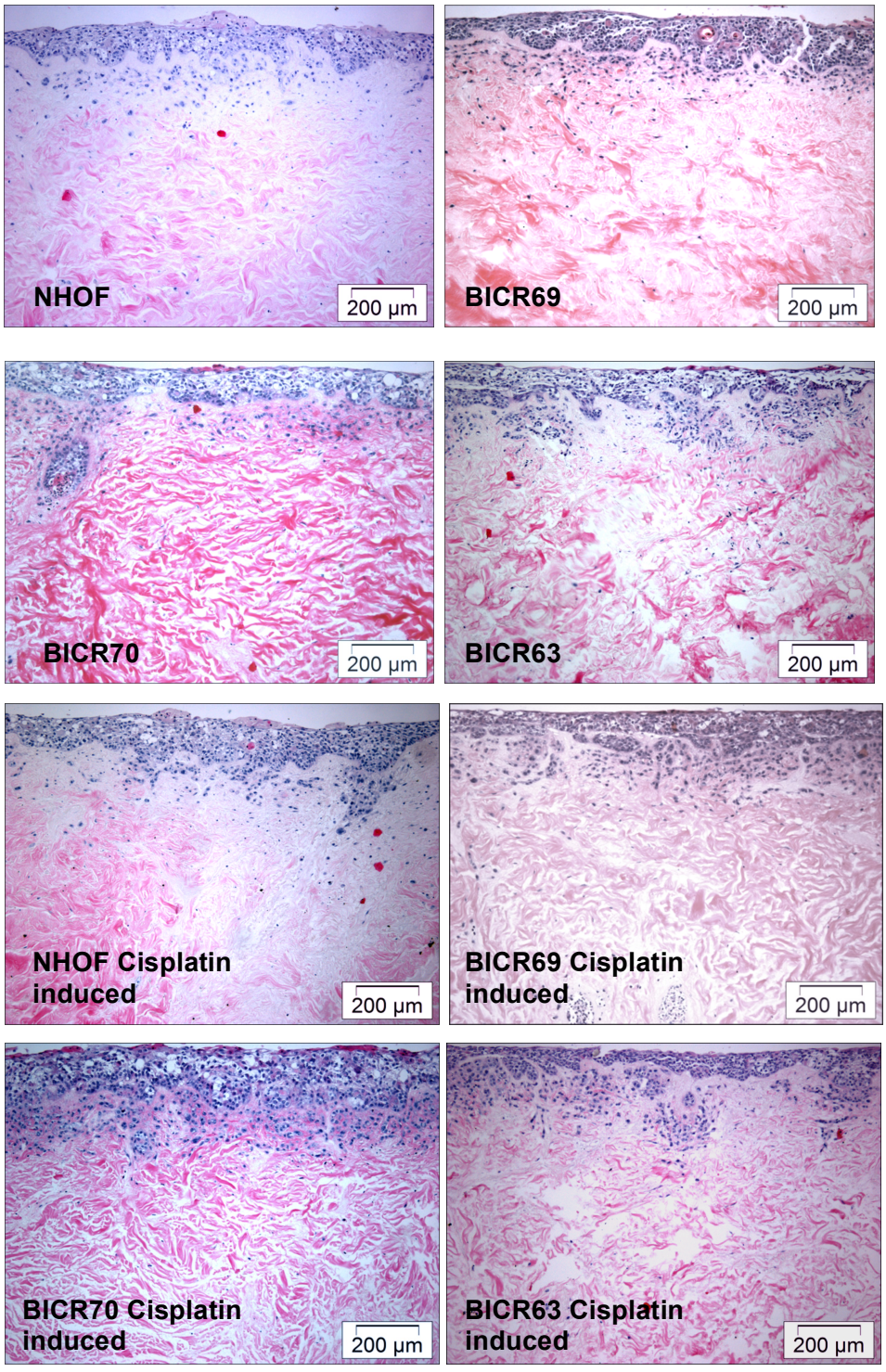

Figure 3.4.9: Determination of invasion of H357 cells by senescent CAFs of GU and GS OSCC. 3D organotypic model was used to grow H357 cells in presence of normal fibroblasts and CAFs from GS (left panel) and GU (right panel) OSCC without (upper panel) and with cisplatin treatment (lower panel). The photographs represent haematoxylin and eosin staining of paraffin embedded sections. Scale bar = 200 µm.

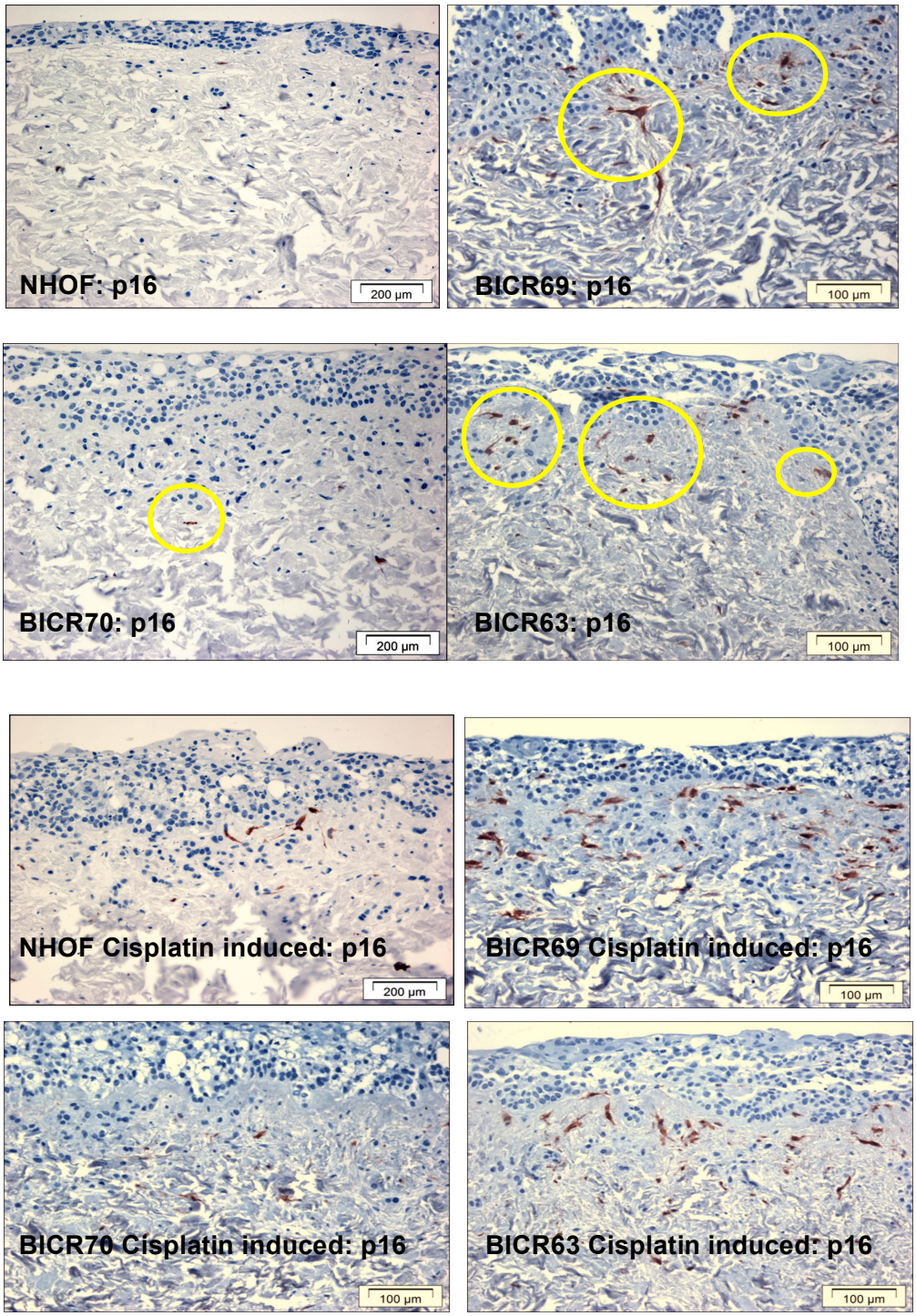

Figure 3.4.10: Determination of senescence in CAFs of GU and GS OSCC. Immunohistochemistry for p16 was carried out of paraffin embedded sections of 3D models to determine senescence in normal fibroblasts (NHOF) and CAFs from GS (BIRC69, BICR70) and GU (BICR63) OSCC without (upper panel) and with cisplatin treatment (lower panel). The photographs were captured at 20X. Scale bar = 200 µm.

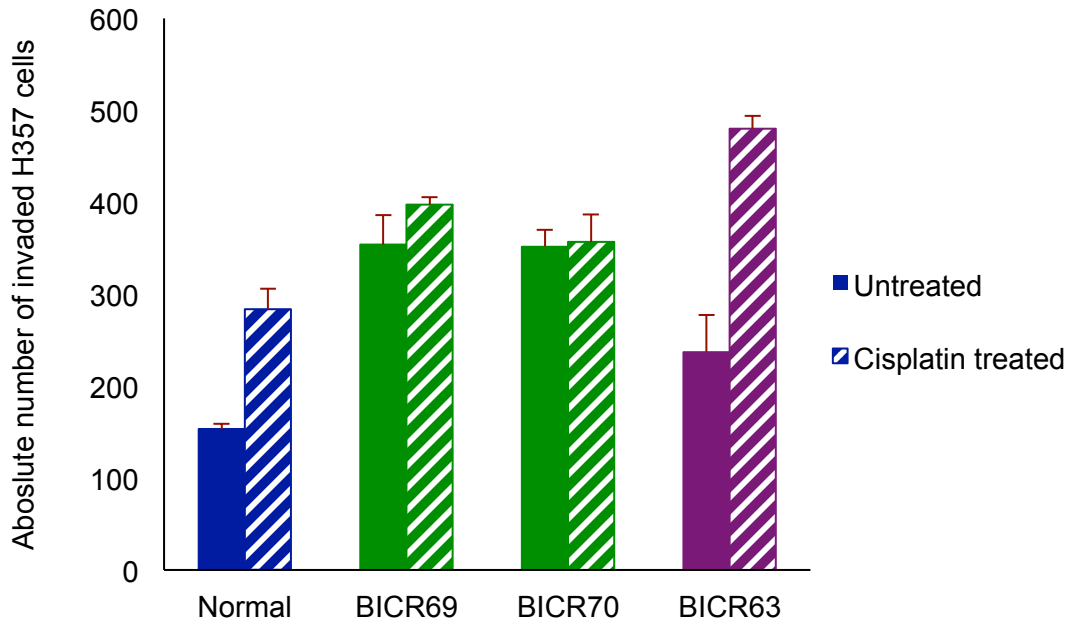

Figure 3.4.11: CAFs stimulated more invasion of H357 cells in 3D organotypic models than normal oral fibroblasts and induction of senescence in CAFs further stimulated their pro-invasive property. Quantification of the absolute number of invaded H357 cells in 3D organotypic models by counting cells at X2 magnification using Image J software. The bars represent mean + SEM of two independent fields of haematoxylin and eosin stained paraffin embedded sections of the DD models.

2D cultures (in the absence of cancer cells) they demonstrated no SA-β-Gal activity (figure 3.4.1). Therefore development of senescence during co-culture with GU OSCC derived cancer cell line H357 implied that cues from cancer cells (Hassona *et al*., 2013) or possibly alteration in matrix components (Jun and Lau, 2010; Suwan *et al*., 2009) caused a sub-population of BICR69 to senesce prematurely and evolve into a more pro-tumourigenic cell-type that fostered tumour growth and invasion in these models (figure 3.4.9 and figure 3.4.10, right upper panel).

Conversely treatment of BICR69 with cisplatin further increased accumulation of p16 positive fibroblasts (figure 3.4.10, right lower panel) which encouraged even more invasion of H357 cells in to the dermis about 2.4-times higher than their counterpart untreated control fibroblasts (figure 3.4.11). Similarly cisplatin treatment also increased the number of p16 positive cells in BICR70 models. However upon induction of senescence these fibroblasts failed to increase invasion of H357 cells over that induced by their untreated counterparts but caused more invasion of cancer cells than non-senescent-NHOFs. Cisplatin also triggered premature senescence in NHOFs visualized by the increased number of p16 positive cells (figure 3.4.10, left lower panel) and caused 1.7-times more invasion of H357 cells than non-senescent-NHOFs (figure 3.4.11).

Incorporation of BICR63 fibroblasts into DD models stimulated invasiveness of H357 cells into dermis but to a lesser extent than both BICR69 and BICR70 cells. This is possibly because BICR63 cells contained a subset of non-migratory senescent cell population that failed to disperse as effectively into the dermis as CAFs of GS tumours post-inoculation. This is manifested by the pattern of p16 staining in fibroblasts, which were limited to only the papillary dermis region in BICR63 CAFs whereas in BICR69 and BICR70 the staining extended throughout dermis. Other factors that determined their pro-invasive nature such as the ability to secrete MMP-2 and induce EMT-like changes in cancer cells, were found similar to that of CAFs of GS OSCC (figure 3.4.8

and section 3.4.7). However upon cisplatin treatment BICR63 fibroblasts demonstrated an even greater expression of p16 indicative of reinforcement of senescence (figure 3.4.10, right lower panel) and this increased invasiveness of H357 cells by nearly 3-times compared to non-senescent-NHOFs and by 2-times compared to their untreated counterparts (figure 3.4.11).

3.4.7 CAFs from both GS and GU tumours induce EMT-like changes in H357 cells in 3D organotypic models

It was presented in figure 3.2.5 that *in vitro* induction of senescence in NHOFs stimulated EMT-like changes in H357 cell lines in 3D models that may be partly responsible for their increased invasiveness into the dermis. To understand if this was a natural event in carcinogenesis immunohistochemistry for Slug and Twist1 were performed in 3D models carrying both senescent and non-senescent CAFs in presence and absence of cisplatin treatment.

It was observed that in absence of cisplatin treatment only 3D models carrying H357 cells in presence of BICR63 (GU OSCC) expressed more Slug, in both cytoplasm and nucleus, in the entire layer of epidermis composed of cancer cells (figure 3.4.12). In contrast although BICR69 cells demonstrated similar pattern of p16 expression as that of BICR63 in 3D models without cisplatin treatment, these cells failed to augment Slug expression in all layers of cancer cells. Rather Slug expressions in H357 cells in this model were similar to those in models containing non-senescent-NHOFs and non-senescent-BICR70 CAFs with distinctive faint staining predominately localized to the cytoplasm of cancer cells (figure 3.4.12). In models carrying cisplatin treated CAFs and NHOFs the intensity of staining for Slug protein was remarkably enhanced and was observed expressed by both cancer cells and fibroblasts confined to both nucleus and cytoplasm (figure 3.4.12).

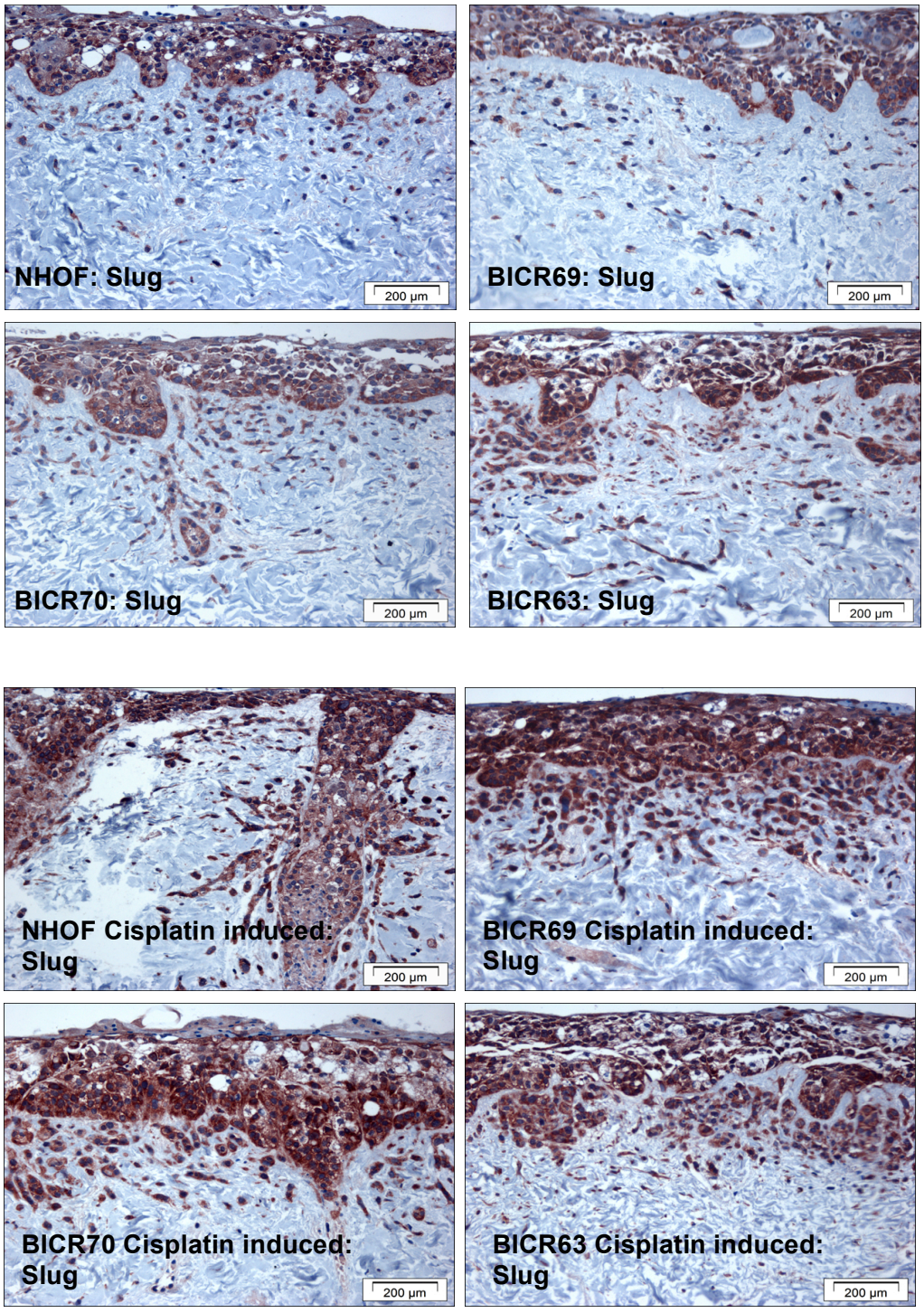

Figure 3.4.12: GU CAF and senescent stroma increase Slug expression in 3D models. Immunohistochemistry for Slug was carried out to determine EMT changes in H357 cells in presence of CAFs from GS (BICR69, BICR70) and GU (BICR63) OSCC without (upper panel) and with cisplatin treatment (lower panel) of paraffin embedded sections of 3D models. The photographs were captured at 20X. Scale bar = 200 µm.

Twist1 expression was absent in both fibroblasts and H357 cells in 3D models carrying non-senescent-NHOF controls (figure 3.4.13, left upper panel). However in models carrying CAFs: BICR69, BICR70 and BICR63 without cisplatin treatment, some cancer cells and few fibroblasts expressed Twist1 (figure 3.4.13, upper panel).

Visibly it was impossible to distinguish expression of Twist1 in different CAF models. 3D models carrying cisplatin-induced senescent fibroblasts (NHOF, BICR69 and BICR70) showed a mild increase in the number of Twist1 positive cells. However there was no visible difference in Twist1 expression in BICR63 containing models in presence of cisplatin treated and untreated CAFs (figure 3.4.3, bottom panel).

Only a subset of H357 cells stained positive for Twist1 in 3D models and this was positively associated with the presence of CAFs and premature senescent oral fibroblasts implying that Twist1 was induced in cancer cells by transdifferentiated fibroblasts.

Alternatively Slug expression is retained by H357 cells in presence of both normal fibroblasts and non-senescent CAFs and is augmented by accumulation of senescent fibroblasts. Slug is expressed by normal keratinocytes in the basal and suprabasal lining of oesophagus (Jethwa *et al*., 2008) perhaps contributing to the physiological epithelial migratory activity to compensate for regular epithelial loss from desquamation. In these models BICR63 stimulated the most Slug expression in H357 cells, which demonstrated epithelial atrophy possibly due to diminished proliferation or increased invasion into the dermis and possibly due to erosion from DD surface. The epithelial atrophy may send “epithelial loss” signals to CAFs, which eventually stimulates Slug expression to replenish the layer of lost keratinocytes. Conversely Twist1 expression is low in normal keratinocytes, increases during metaplasia and disappears once cancer

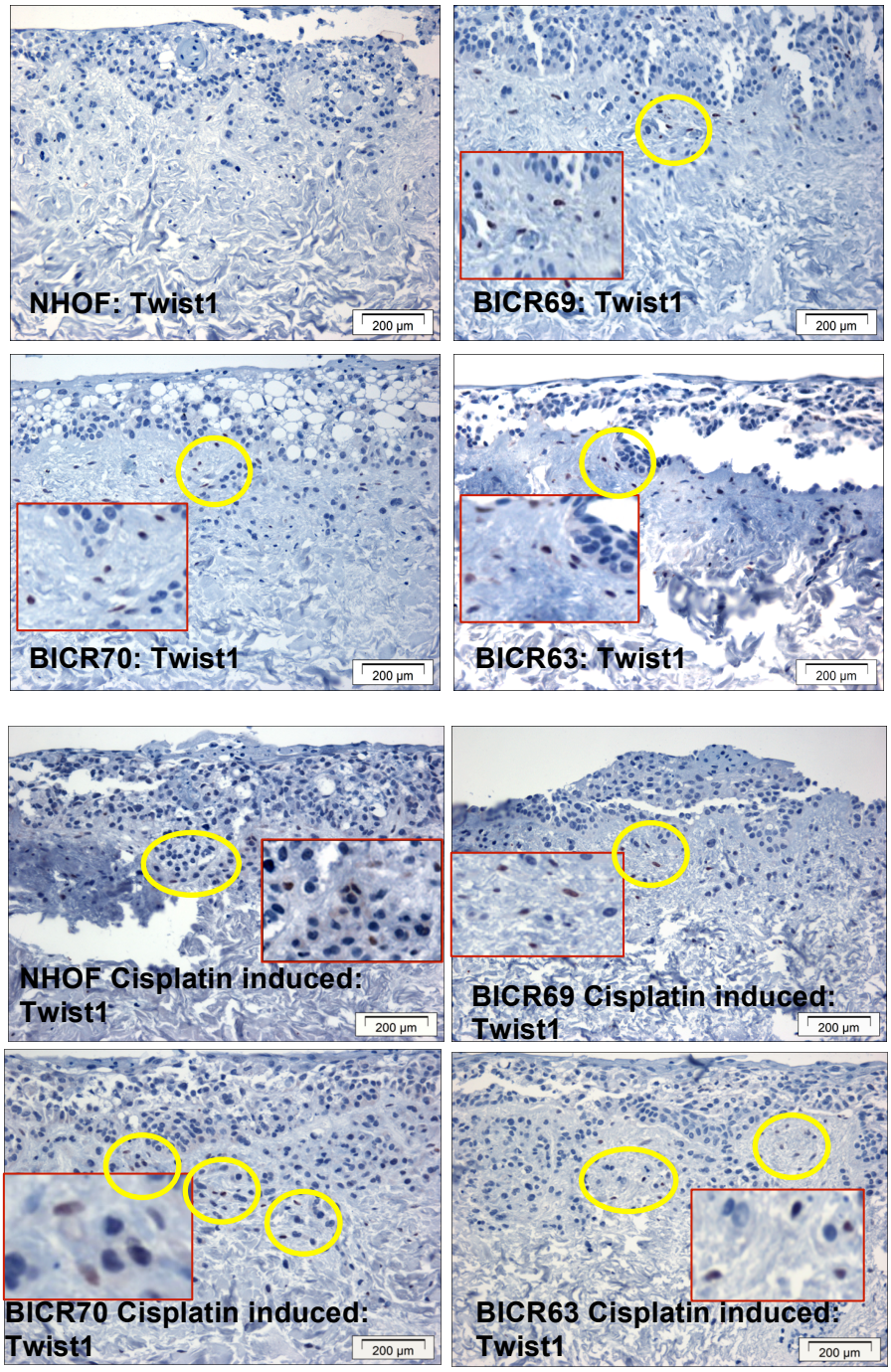

Figure 3.4.13: CAFs increase Twist1 expression in 3D models. Immunohistochemistry for Twist1 was carried out to determine EMT changes in H357 cells in presence of normal fibroblasts (NHOF), CAFs from GS (BICR69, BICR70) and GU (BICR63) OSCC without (upper panel) and with cisplatin treatment (lower panel) of paraffin embedded sections of 3D models. The photographs were captured at 20X. Scale bar = 200 μm.

is established (Jethwa *et al*., 2008). This suggests that Twist1 may be an important regulator of cellular differentiation and perhaps cells acquire resistance to stressful conditions by increasing expression of Twist1.

It had been reported that during early embryonic life developing tissues up-regulate Twist to evade senescence and apoptosis and acquire motility to resist cellular death by anoikis (reviewed by Micalizzi *et al*., 2010). However during embryogenesis all developing tissues have a definite cell fate that is lost upon neoplastic transformation by accumulation of genetic abnormalities and due to persistent stimulation by oncogenic signals from neighbouring cells (reviewed by Micalizzi *et al*., 2010). The appearance of Twist1 in a number of H357 cells in DD models therefore suggests that the senescent fibroblasts and CAFs are reactivating the embryonic program in cancer cells but with an indefinite fate ultimately leading into cancer progression.

Storer *et al*. (2013) showed senescent embryonic tissues guided migration and limb development in animal models by secreting FGFs (Storer *et al*., 2013) and in this thesis FGF-2 transcripts were found elevated in senescent oral fibroblasts. In addition FGF was also reported to stimulate Snail expression in embryonic tissue (reviewed by Micalizzi *et al*., 2010).

Increased expression of both Slug and Twist1 in H357 cells were found positively associated with presence of senescent fibroblasts and CAFs, and their increased invasiveness. Twist1 was recently reported to be re-expressed by disseminating cancer cells (Casas *et al*., 2011) and required Slug to carry out its action. Moreover emerging evidence suggests that STAT3 dependent expression of Twist1 in head and neck cancer cell lines is associated with their increasing stemness (Smith *et al*., 2013) wherein it inhibits PTEN expression in differentiated sub-population of cancer stem cells enabling them to evade apoptosis (Yin *et al*., 2010). STAT3 is a downstream target of IL-6 (Iliopoulos *et al*., 2010). In this study IL-6 was found highly elevated in

both senescent CAFs and stress-induced senescent-NHOFs. Therefore it is possible that both senescent-CAFs and cisplatin-induced premature senescent oral fibroblasts secrete IL-6, which possibly binds to IL-6 receptors on H357 cells in paracrine manner and possibly stimulates STAT3 mediated Twist1 expression in certain cancer cells and and it is conceivable that this contributes to the development of a subset of cancer stem cells in patients with old age. Further work is required to test this hypothesis.

The pro-invasive potential of both non-senescent BICR69 and BICR70 CAFs of GS OSCC in 3D models also suggests that presence of senescent fibroblasts is not the sole determinant of cancer cell invasiveness and is theoretically reasonable because development of senescent stroma is a late event and by this time some cancer cells had already initiated the process of invasion and metastasis. Therefore senescent stroma is probably expected to support the progression of an already established tumour along with the non-senescent CAFs. A minimal level of Twist1 expression was also observed in CAFs in these 3D models. Stromal Twist1 had been linked to diagnosis of advanced cancer stage (Smith *et al*., 2013).

All these functional studies therefore supported the hypothesis that senescent CAFs of GU OSCC were phenotypically similar to stress-induced premature senescent oral fibroblasts. Therefore next it was postulated that, like stress-induced senescent oral fibroblasts, miRNAs may be also aberrantly expressed in senescent CAFs and this may regulate gene expression that can modulate SASP.

3.4.8 miRNAs are differentially expressed in CAFs of GU OSCC

Aberrant expression of miRNAs in CAFs had been reported in various cancers as that of breast, prostate, colon and many more (reviewed in Li *et al*., 2012). To date no one has yet characterized miRNA expression profile in CAFs derived from head and neck cancer patients with particular focus on their roles on senescence and SASP. In the previous section it was shown that miRNAs are deregulated in stress-induced and

replicative senescent oral fibroblasts derived from healthy volunteers. To explore if senescent-CAFs demonstrated a similar miRNA expression profile to stress-induced premature senescent oral fibroblasts TaqMan miRNA TLDA was carried out in CAFs of GU OSCC (BICR3, BICR31 and BICR63) that are enriched for a population of senescent fibroblasts and compared to normal young fibroblasts obtained from healthy donors. BICR18 was not used in TLDA because this CAF was derived from a lymph node with metastatic deposit and therefore may display phenotypic differences.

After normalizing the data to young fibroblasts it was observed that 536 miRNAs were up-regulated and 20 miRNAs were down-regulated in CAFs of GU OSCC (Appendix 5 & 6). Among the up-regulated miRNAs, 44 miRNA from human pool A were significantly increased in all CAFs of GU OSCC (figure 3.4.14). MiR-324-5p showed the greatest fold change and was significantly up-regulated by more than 13.0-fold relative to control. MiR-618 showed the least fold change of 0.44-times of control (figure 3.4.14). Some of the other miRNAs that were significantly up-regulated in human pool A panel are miR-500, miR-423-5p, miR-193b, miR-10a, miR-138, miR-152, miR-92a, miR-320, miR-331-3p, miR-103 and miR-197.

The miRNAs that are most differentially expressed in CAFs of GU OSCC from human pool B panel is represented in figure 3.4.15. Among these miR-1247 and miR-517* demonstrated the maximum and minimum fold change of 19767-fold and 0.02-times of control, respectively. Other up-regulated miRNAs include miR-34b and miR-10b*.

The summary of top 20 up-regulated and down-regulated miRNAs from both pool A and pool B panel is shown in figure 3.4.16.

Interestingly the expression of miRNAs in senescent-CAFs of GU OSCC was very distinct from miRNA profile of stress-induced senescent-NHOF. However certain miRNAs biologically important for ageing were found conserved in these cells. For instance, like stress-induced senescent-NHOFs CAFs of GU tumours demonstrated

increased expression of miR-34 family: miR-34a by 8-fold, miR-34b by 558-fold and miR-34c by 23.5-fold, all of which are transcribed following activation of TP53 (He *et al*., 2007). Again, miRNAs positively regulated with p16 expressions were also elevated in CAFs (Overhoff *et al*. 2013). These included up-regulation of miR-210 by 13.8-fold, miR-181a by 15.8-fold, miR-26b by 6-fold and miR-424 by 33.6-fold. Interestingly miRNAs targeting p21 were found up-regulated in CAFs in contrast to stress-induced and replicative senescent oral fibroblasts (Gomez-Cabello *et al*., 2013). Expression of miR-106a was increased by 4.8-fold, miR-93 by 3.9-fold and miR-20a by 5.4-fold compared to control fibroblasts, and all these miRNAs were members of oncogenic miR-17-92 cluster.

On the other hand inflammatory miRNAs that were reported to induce senescence in fibroblasts *in vitro* and in epithelial cells *in vivo* (Sohn *et al*., 2012) were found up-regulated in both CAFs of GU OSCC and stress-induced senescent-NHOFs. miR-146a was up-regulated by 4.6-fold, miR-17 by 4.3-fold, miR-126 by 6.7-fold, miR-21a by 18-fold and miR-23b by 16-fold. However among these miRNAs the oncogenic miRNAs such as miR-17 and miR-21a were unchanged in cisplatin-induced premature senescent and late-passage oral fibroblasts implying the critical role of cues from neighbouring cells such as cancer cells and immune cells in determining the senescence fate and perhaps the activation profile of CAFs under pathological conditions and this may define the functional changes in miRNAs and subsequent gene expression in these cells.

Again, miR-145 and miR-143, two well characterized tumour suppressor miRNAs were up-regulated in senescent CAFs of GU OSCC however decreased upon stress-induced senescence. miR-145 was increased by 7.8-fold whereas miR-143 was increased by 12-fold. Activated HSCs and tumour stroma of gastric cancer have elevated levels of this cluster (Chen *et al*., 2011; Naito *et al*., 2014a) and therefore alteration of this miRNA may also indicate the mode of origin of CAFs in cancer. TGF-β is presumed to

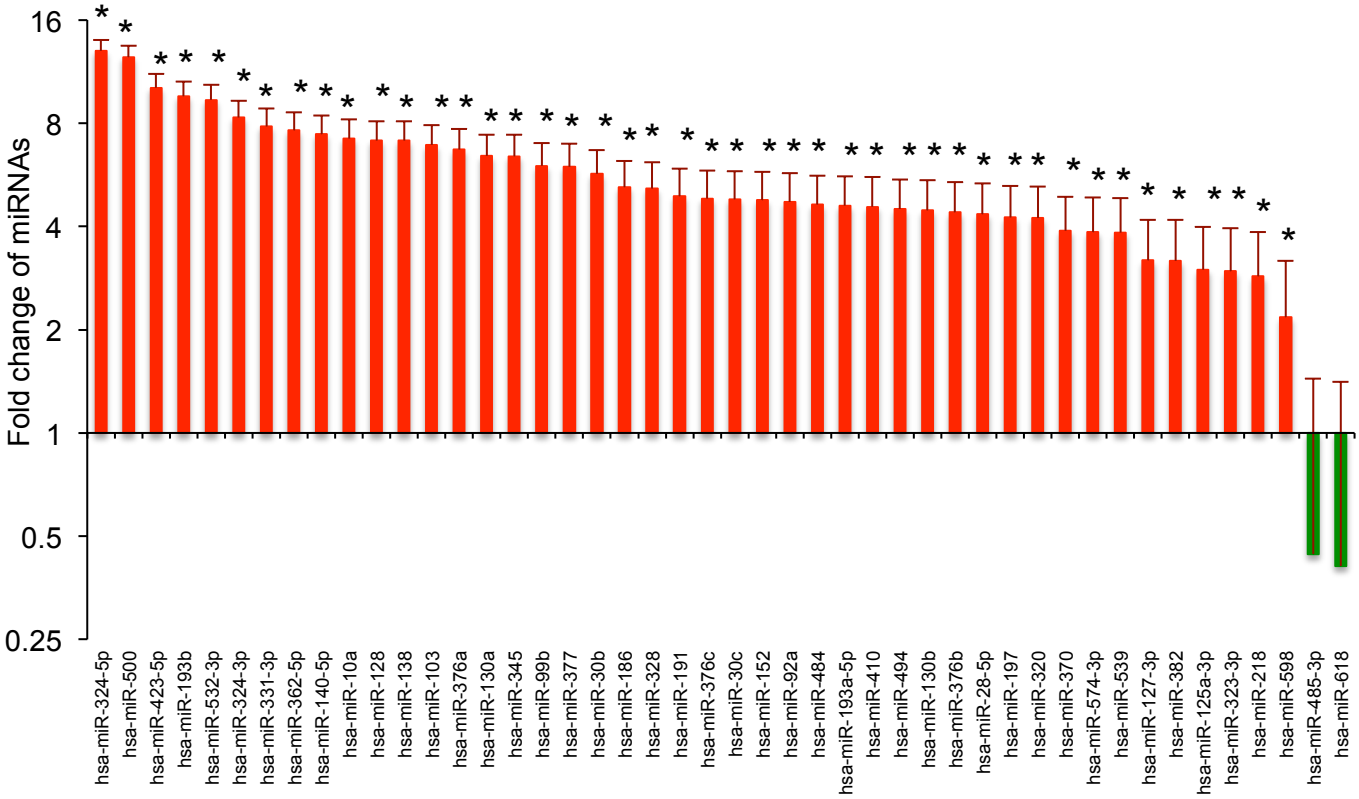

Figure 3.4.14: Differentially expressed miRNAs in human pool A panel by CAFs of GU OSCC. RNA from GU OSCC derived CAFs and normal fibroblasts were reverse transcribed using megaplex reverse transcription. The cDNA were then pre-amplified using specific human pool A pre-amp primers and hybridized against specific human miRNA probes on 384-well bearing microfluidic cards in qRT-PCR. The Ct values were normalized to U6 internal control and ΔΔ Ct values were calculated after normalizing the data to normal young fibroblasts using Data Assist software. The bars represent mean of times change + SEM of three independent patient samples. *p<0.05, by paired student's t-test.

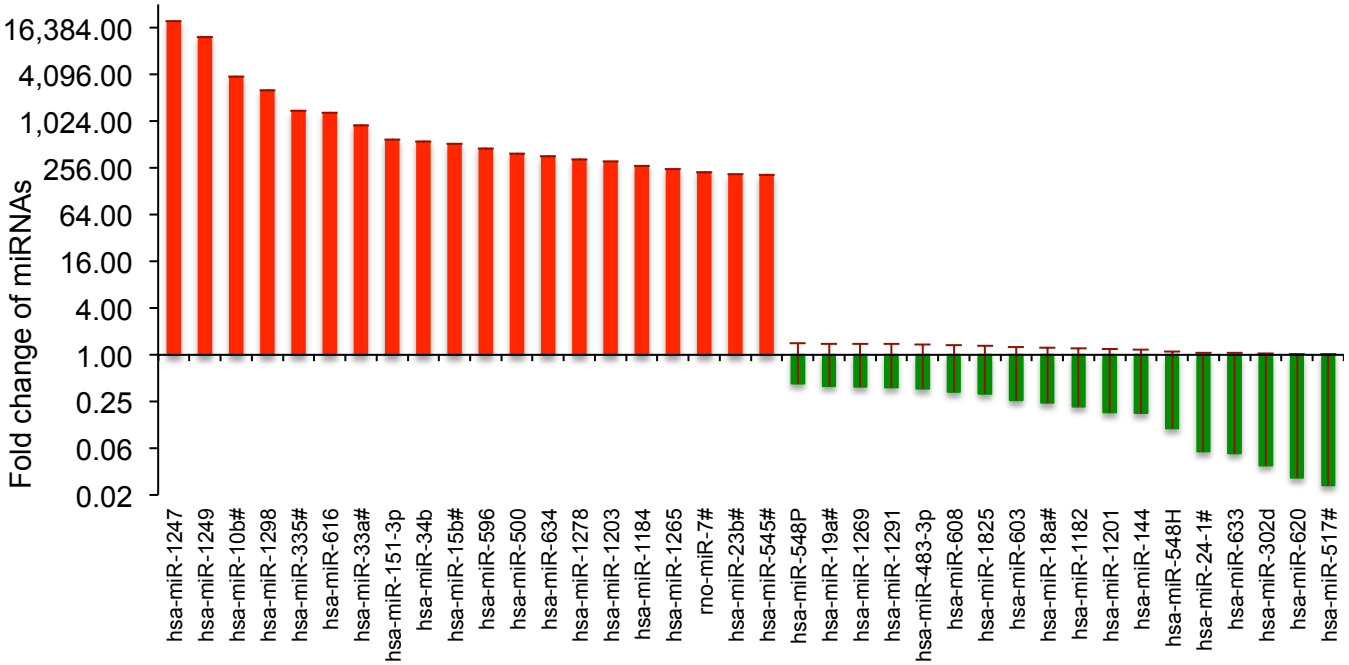

Figure 3.4.15: Differentially expressed miRNAs in human pool B panel by CAFs of GU OSCC. RNA was reverse transcribed using megaplex reverse transcription. The cDNA were then pre-amplified using specific human pool B pre-amp primers and hybridized against probes specific to human pool B miRNAs on 384-well bearing microfluidic cards by qRT-PCR. The Ct values were normalized to U6 internal control. ΔΔCt values were calculated after normalizing the data to normal young fibroblasts. The bars represent mean of times change + SEM of three independent patient samples.

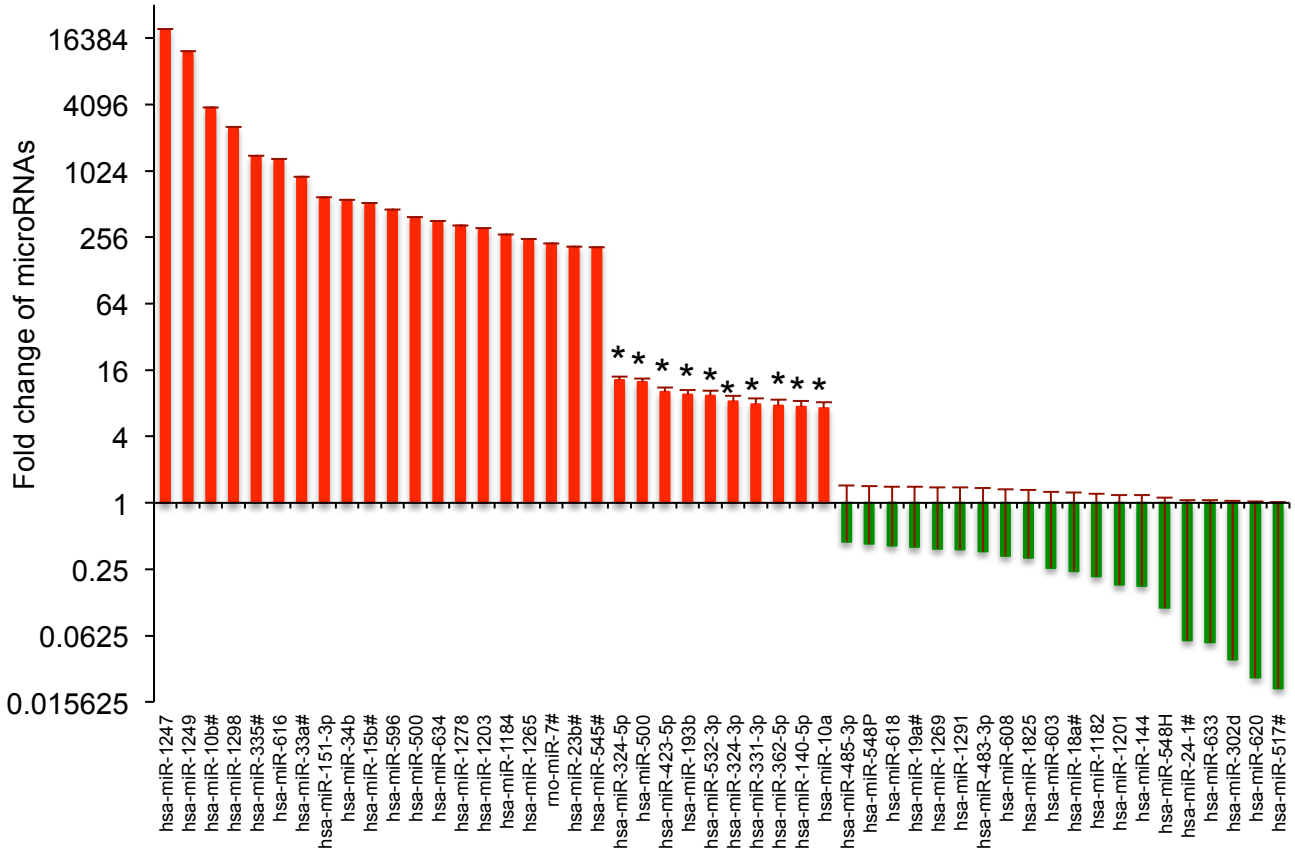

Figure 3.4.16: Summary of top 20 up-regulated and down-regulated miRNAs in CAFs of GU OSCC. TaqMan miRNA tiling low density array (TLDA) were hybridized with pre-amplified cDNA from CAFs of GU OSCC and normal young fibroblasts from healthy donors using pool A and pool B specific forward and reverse primers to mature miRNAs. ΔΔ Ct were calculated after normalizing the data to U6 internal control and to normal fibroblast controls. The bars represent the mean of times change + SEM of three independent patients samples. *p<0.05, by paired student's t-test.

activate this cluster in stromal fibroblasts of gastric cancer and possibly in head and neck cancer (Naito *et al*., 2014a; Naito *et al*., 2014b; Abidin *et al*., unpublished). Indeed CAFs of GU OSCC were shown to senesce by chronic stimulation with TGF-β from OSCC cells (Hassona *et al*., 2013) and perhaps this is why they showed increased expression of both miR-143 and miR-145.

CAFs of GU OSCC also expressed miRNAs that were inversely associated with that of senescent fibroblasts obtained from healthy subjects. The oncogenic miRNA family miR-17-92, which is commonly down-regulated in senescent fibroblasts and aged human tissues (Hackl *et al*., 2010; Faraonio *et al*., 2012) and observed down regulated in cisplatin-induced premature senescent oral fibroblasts were found up-regulated in CAFs of GU OSCC. However in contrast to cisplatin-induced senescent oral fibroblasts, CAFs of GU OSCC expressed more of tumour suppressor miRNAs belonging to let-7 family (Dhabi *et al*., 2011).

Therefore CAFs of GU OSCC express miRNAs that are deregulated in both myofibroblasts of cancer and in senescent fibroblasts of ageing. To evaluate if these CAFs showed same trend in alterations of miRNAs to that of senescent oral fibroblasts the fold change of miR-335 and miR-148b were assessed. It was found that miR-335 was significantly increased in CAFs by 13-fold and miR-148b was increased by 2.7-fold in comparison to normal fibroblasts in TLDA output. These changes were then further validated by qRT-PCR in all the CAF samples from GU OSCC including BICR18 derived from nodal metastasis and those from GS tumours.

3.4.8.1: miR-335 and miR-148b expressions are elevated in CAFs of both GS and GU OSCC

CAFs of GU OSCC were initially selected for validation of expression of miR-335 and miR-148b because they were enriched for senescent fibroblasts and subsequently these candidate miRNAs were also validated in CAFs of GS OSCC. qRT-PCR demonstrated that CAFs of GU OSCC expressed significantly more miR-335 and miR-148b which were elevated by 104-fold and 122-fold, respectively, in comparison to young fibroblasts from healthy donors (figure 3.4.17). Surprisingly expression of miR-335 and miR-148b were also remarkably elevated in CAFs from GS OSCC by 337-fold and 770-fold of control, respectively (figure 3.4.17). Moreover CAFs of GS OSCC expressed significantly more miR-335 than CAFs of GU OSCC.

The expressions of each of these miRNAs in individual CAFs are demonstrated in figure 3.4.18. qRT-PCR showed BICR31, BICR63 and BICR18 derived from GU OSCC had elevated levels of miR-335 by 60-fold, 270-fold and 27-fold than control, respectively. In contrast BICR3 expressed less miR-335 about 0.5-times of young fibroblasts (figure 3.4.18.A). miR-335 expression was increased in BICR69 and BICR70 (of GS OSCC) by 153-fold and 619-fold, respectively, compared to young normal fibroblasts (figure 3.4.18.A).

Expression of miR-148b was also increased in CAFs of GU OSCC, by 63-fold, 26-fold, 333-fold and 413-fold in BICR3, BICR31, BICR63 and BICR18, respectively, than young normal fibroblasts (figure 3.4.18.B). Both BICR69 and BICR70 also had increased expression of miR-148b, about 58-fold and 3193-fold higher than control, respectively (figure 3.4.18.B).

To evaluate if the increase in expression of miR-335 and miR-148b were a consequence of stimulated transcriptional activity by endogenous signals, the CAFs were screened for expression of oncogenic transcription factor STAT3 and primary

miRNA transcripts for miR-335 and miR-148b by qRT-PCR. STAT3 up-regulation had been reported during malignant transformation in mammary epithelial cells wherein it induces transcription of miR-21 and miR-181b to silence tumour suppressor protein PTEN and cylindromatosis respectively (Iliopoulos *et al*., 2010). Hyperactivity of IL-6 could also induce STAT3 (Iliopoulos *et al*., 2010).

CAFs of GU OSCC had higher levels of miR-21 than normal fibroblasts and secreted significantly more IL-6. It was found that, unlike stress-induced senescent oral fibroblasts STAT3 mRNA levels were remarkably increased in both CAFs of GS and GU OSCC. Expression of STAT3 mRNA was 8-fold higher in both BICR69 and BICR63 than normal fibroblasts. BICR70 and BICR18 expressed 7-fold and 3-fold more STAT3 mRNA than normal fibroblasts, respectively (figure 3.4.19.A). However this is only pilot data and the protein levels of its phosphorylated form need to be determined before giving any concluding remarks.

The levels of both pri-miR-335 and pri-miR-148b transcripts were decreased in both CAFs irrespective of their origin and senescent oral fibroblasts (figure 3.4.19.B & C). In BICR69 and BICR70 pri-miR-335 expression was decreased to 0.01-times of control. Its level was further declined in BICR63 and BICR18 to 0.008-times and 0.002-times of control, respectively. Expression of pri-miR-148b was reduced by 0.01-times in BICR69, 0.015-times in BICR70, 0.017-times in BICR63 and 0.004-times in BICR18 than control.

From the levels of primary miRNA transcript it can be deduced that the increased expression of mature miRNAs in CAFs did not ensue from increased transcription of their primary miRNA transcripts but rather from increased rate of processing of primary miRNA transcripts to mature miRNA probably by enhanced DICER1 activity. Conversely as mentioned in the previous chapter the increased level of their mature forms may also result from increased alternative splicing of mRNAs (MEST and COPZ1) within which they are located.

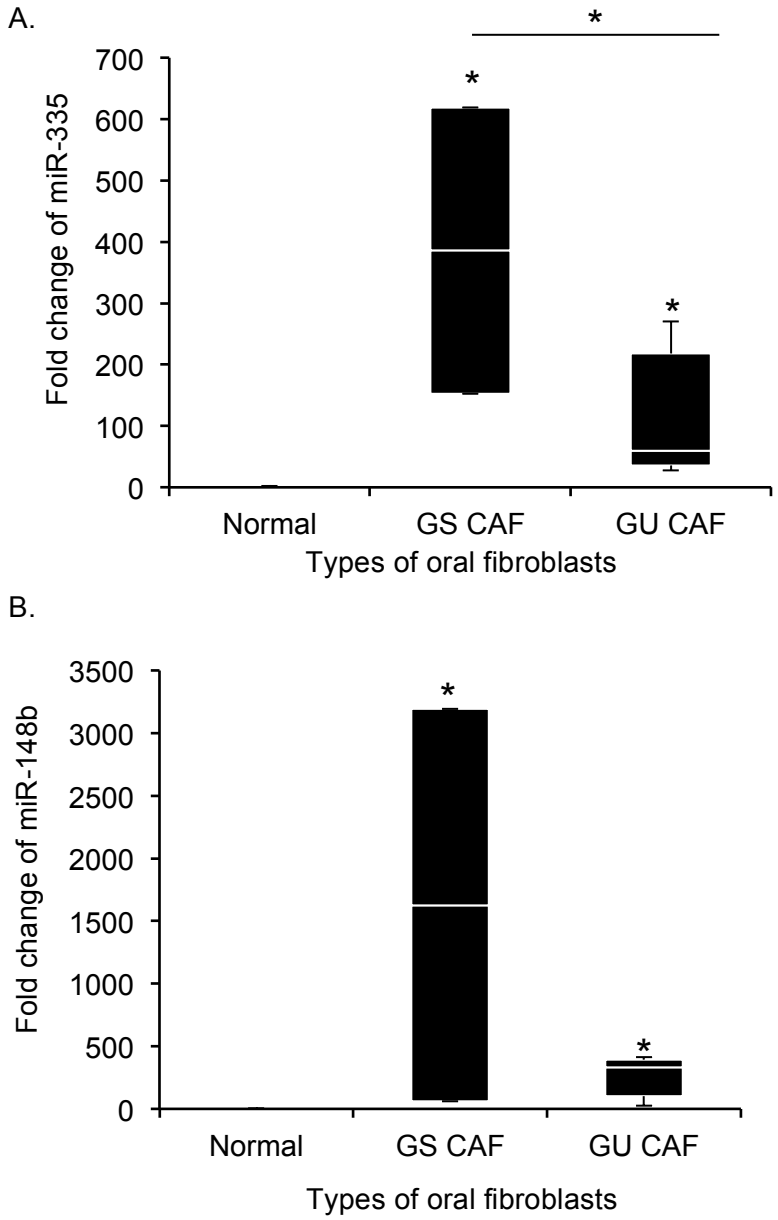

Figure 3.4.17: miR-335 and miR-148b levels are elevated in CAFs of GS and GU OSCC. The box plot represents the mean of times change ± SEM of miR-335 (A) and miR-148b (B) after categorizing the CAFs into two groups based on the type of OSCC: GS and GU. *p<0.05, one-way ANOVA with post-hoc corrections by Holm-Sidak method.

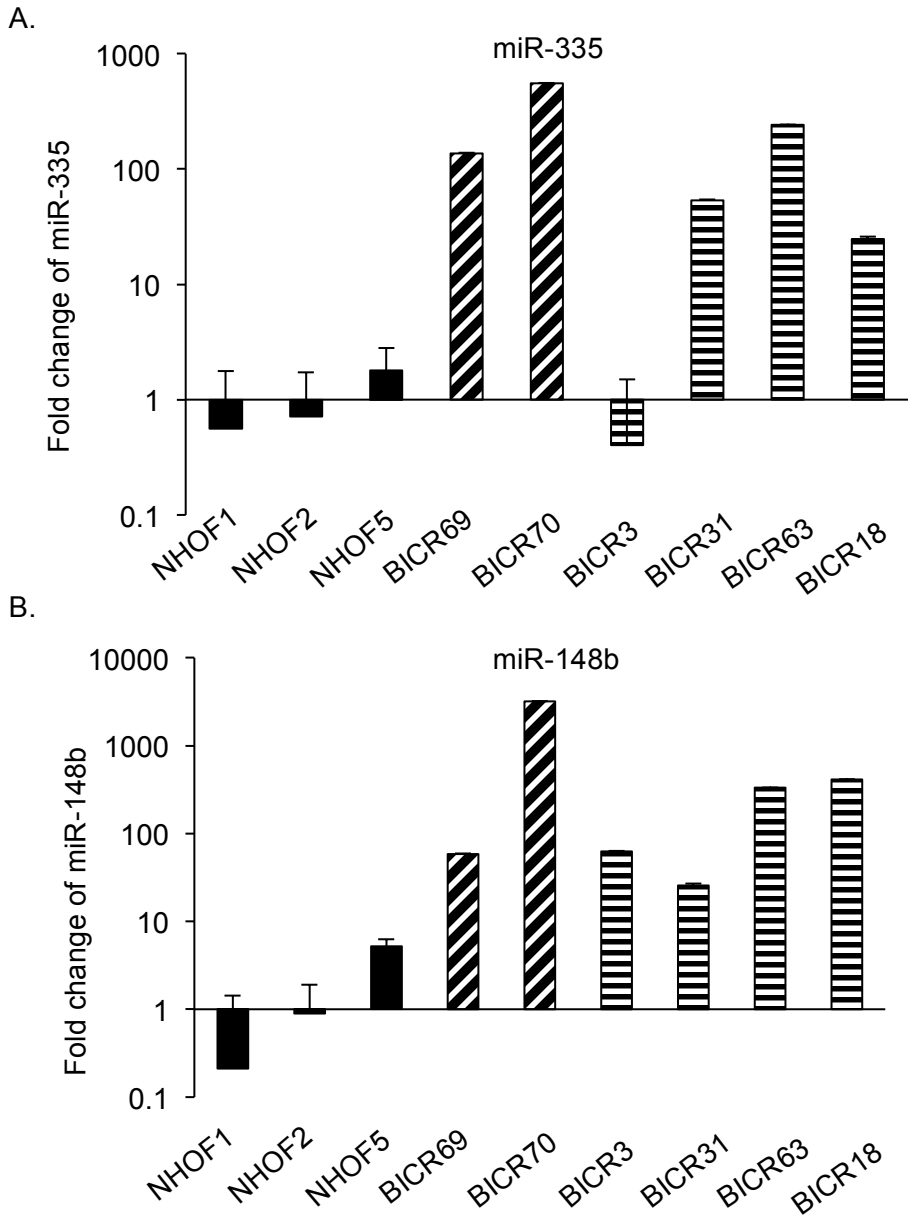

Figure 3.4.18: Validation of miR-335 and miR-148b in CAFs and normal oral fibroblasts by qRT-PCR. miR-335 (A) and miR-148b (B) levels were determined by qRT-PCR. The ΔΔCt were normalized to U6 endogenous control and young normal fibroblasts. The bars represent mean times change + SEM.

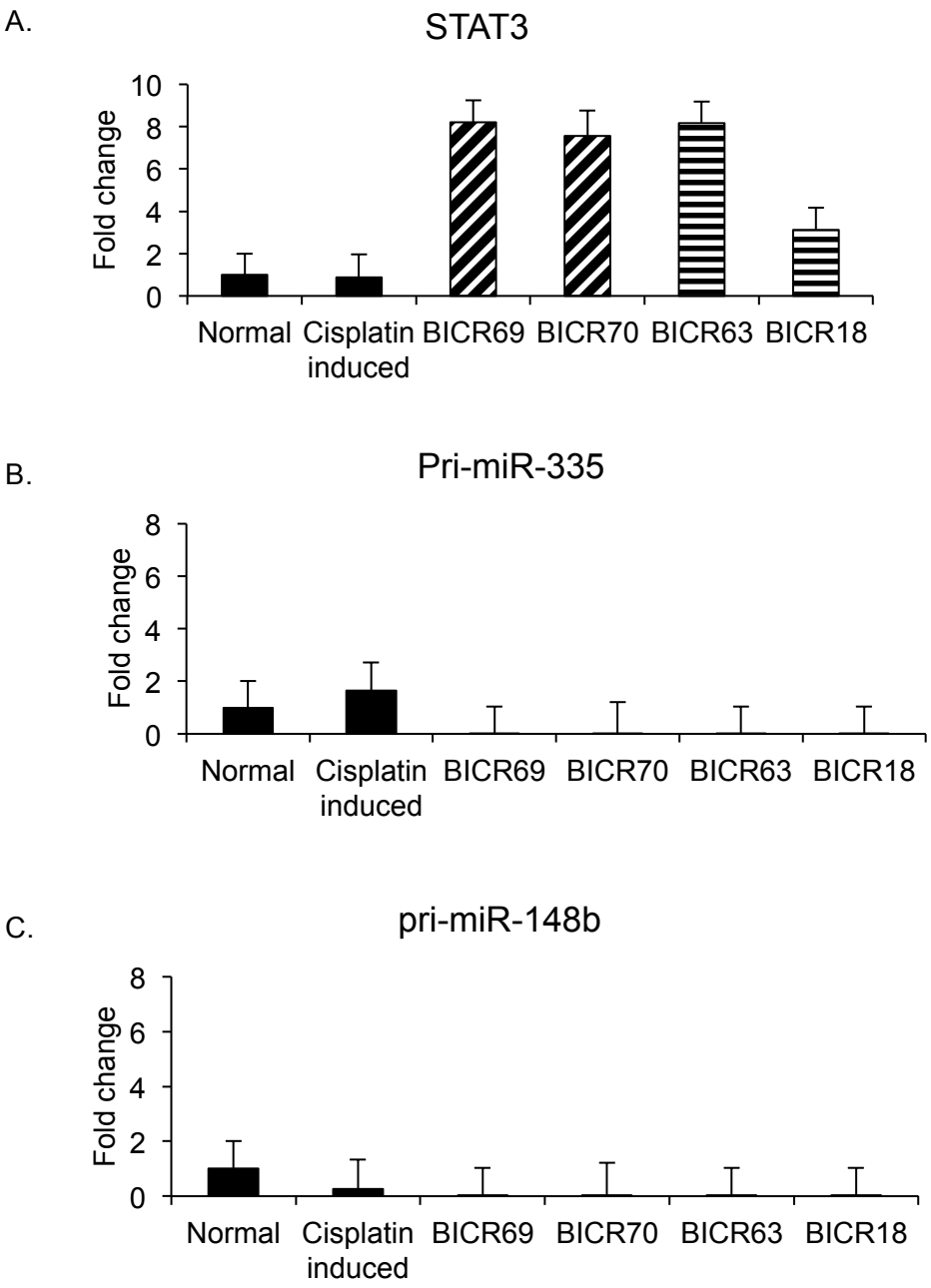

Figure 3.4.19: Elevated expression of STAT3 and reduced expression of primary-miRNA transcripts in CAFs. qRT-PCR was used to determine expressions of STAT3 (A) and primary microRNA transcripts: pri-miR-335 (B) and pri-miR-148b (C). ΔΔCt values were calculated after normalizing the Ct values to U6 endogenous control and normal non-senescent oral fibroblasts. The bars represent mean of times change + SEM.

The discrepancy in expression of miRNAs between senescent-CAFs and stress-induced senescent oral fibroblasts indicate that although both these cells share the same senescence fate and produce the same SASP the stimuli triggering this response is distinct and is predetermined by the diseased state and possibly evolutionarily conserved. This is chiefly because senescent-CAFs predominately express miRNAs that regulate genes in response to cues from both cancer cells and other cell types of the tumour microenvironment and is possibly assocated with CAF heterogeneity. In contrast, stress-induced senescent normal fibroblasts express primarily tumour suppressor miRNAs, possibly because they were extracted from healthy tissue. Intriguingly, miRNAs deregulated in both senescent-CAFs and senescent-NHOFs target the same set of genes.

Since both senescent CAFs and stress-induced senescent NHOFs yielded the same SASP it was postulated that similar set of genes regulated their secretome. As a result the expression of PTEN in CAFs was determined and compared to normal oral fibroblasts.

3.4.9: CAFs of GU OSCC express less PTEN

PTEN was observed down-regulated in both stress-induced senescent and replicative senescent oral fibroblasts. Therefore both non-senescent CAFs and senescent CAFs were assessed for expression of PTEN.

qRT-PCR showed expression of PTEN mRNA was significantly reduced by 0.14-times in non-senescent-CAFs of GS OSCC than non-senescent-NHOFs ($p<0.05$; figure 3.4.20. B). CAFs of GU OSCC also expressed less PTEN mRNA about 0.75-times of control but this decrease was statistically incomparable to non-senescent control fibroblasts.

Western blot demonstrated CAFs of GU OSCC expressed less PTEN protein than non-senescent-CAFs of GS OSCC and non-senescent-NHOFs observed as reduced band intensity (figure 3.4.20.A). Quantification of protein by relative band densitometry revealed that PTEN protein was significantly reduced in CAFs of GU OSCC to 0.76-times of control than both non-senescent-NHOFs and non-senescent-CAFs of GS tumours ($n=4$, $p<0.05$, figure 3.4.20.C).

However in contrast to western blot immunohistochemistry of PTEN in paraffin embedded blocks of 3D models showed that PTEN expression were relatively faint in all CAFs (BICR69, BICR70 and BICR63) when compared to non-senescent-NHOFs (figure 3.4.21). Further immunohistochemistry of PTEN on tissue sections derived from post-radiotherapy patients demonstrated reduced expression of PTEN in fibrotic areas corresponding to increased expressions of α-SMA whereas normal expression was retained in keratinocytes (figure 3.4.22).

These results imply that perhaps reduced PTEN expression in CAFs of GU OSCC regulate their pro-tumourigenic secretome. Meanwhile CAFs of GS OSCC appears to be either at a phase of initiating senescence as most of its mRNA are being rapidly translated into PTEN protein as observed during the early stages of senescence in premature senescent oral fibroblasts or are up-regulating miR-335 and miR-148b to repress PTEN translation in an attempt to evolve into a more pro-tumourigenic fibroblast. The latter reason is corroborated by evidence from 3D models in which PTEN expression was observed reduced in all CAFs further underscoring its potential role in regulating fibroblast secretome and thereby stromal-tumour cross-talk. Furthermore loss of PTEN expression in fibrotic stroma of post-radiotherapy specimens may also predict clinical outcomes after anti-cancer treatment but requires more repeat.

To determine if PTEN expression in senescent-CAFs is also modulated by COX-2 activity as in senescent-NHOFs, the amount of secreted PGE2 was measured.

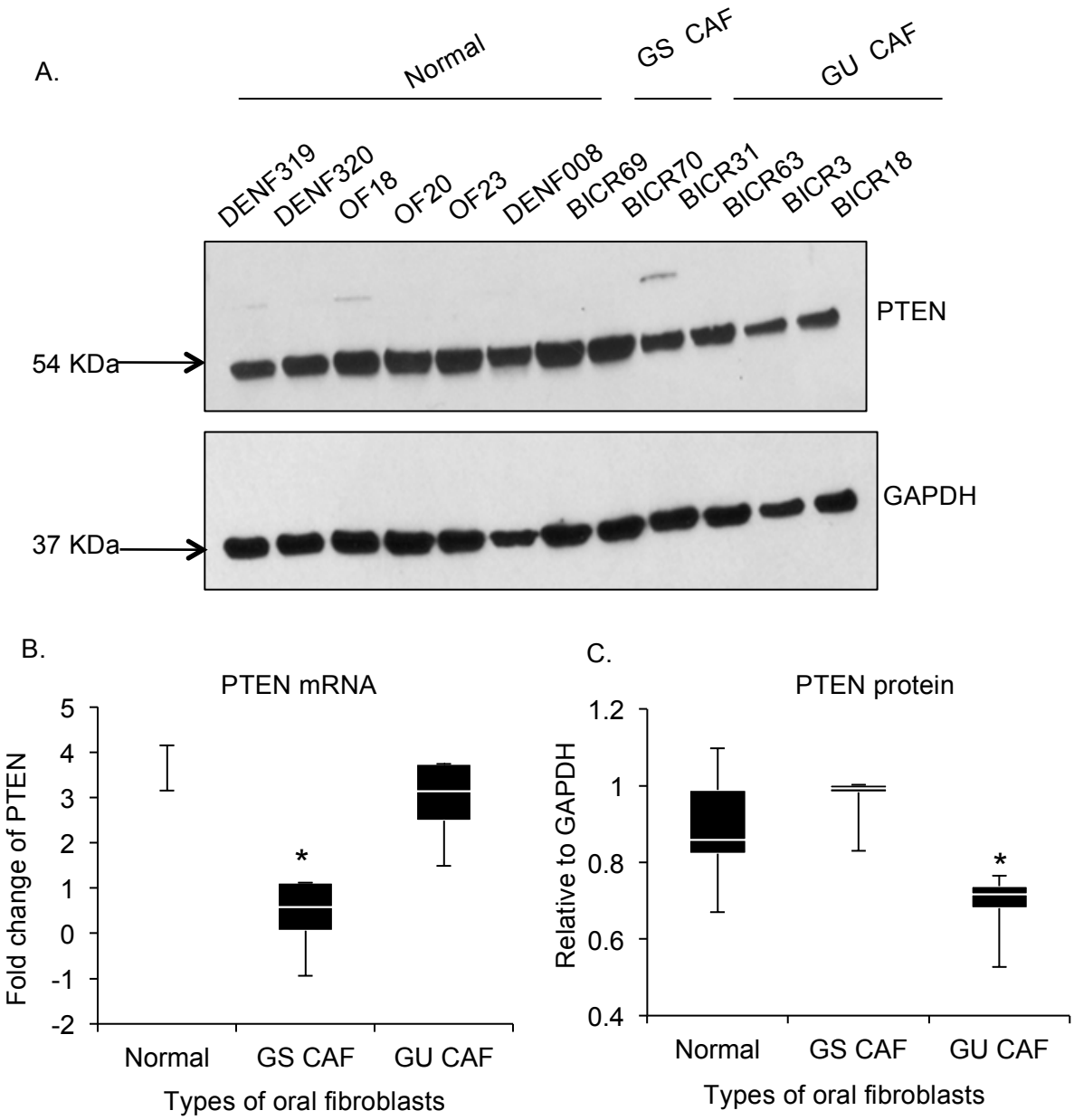

Figure 3.4.20: PTEN expression is deranged in CAFs. PTEN expressions were detected and compared at both protein and mRNA levels by western blot (A) and qRT-PCR (B) respectively in CAFs of GS and GU OSCC. Young fibroblasts from healthy donors were used as control. Proteins were further quantified using relative band densitometry (C) . The box plots represent mean ± SEM. N=2 (GS CAFs) and N=4 (GU CAFs). *p<0.05, one-way ANOVA with post-hoc corrections by Dunn's method (A) and Holm-Sidak method (B).

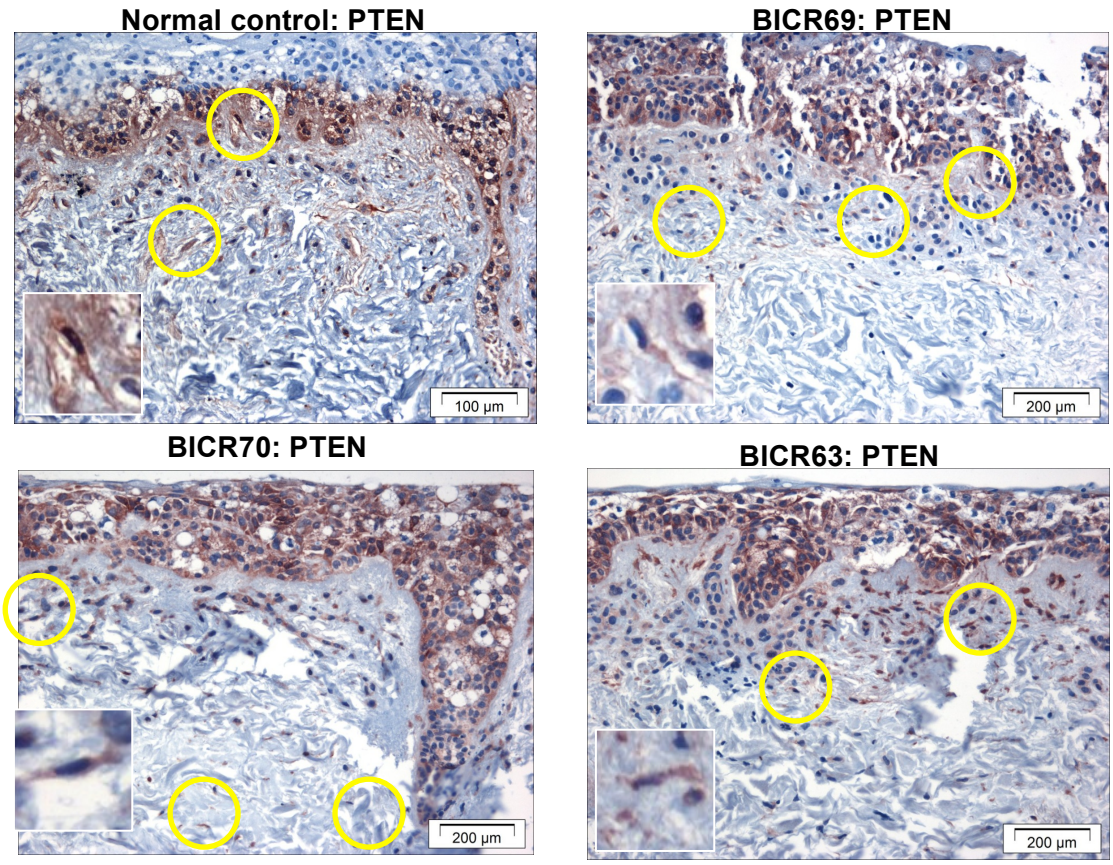

Figure 3.4.21: PTEN expression is reduced in CAFs in 3D organotypic models. Immunohistochemistry was performed to determine expression of PTEN in CAFs and H357 cells in paraffin embedded sections of 3D models and compared to that of normal fibroblasts. Heat mediated antigen retrieval was done in citrate buffer at pH=6.0. The yellow circles enclose the areas where fibroblasts are seen in models and a zoomed section demonstrating the pattern of staining of individual fibroblast is represented in the box located in bottom left corner of each image. The photomicrographs were captured at 20X using light microscope. Scale bar = 200 µM.

Post-irradiation: Archival tissue

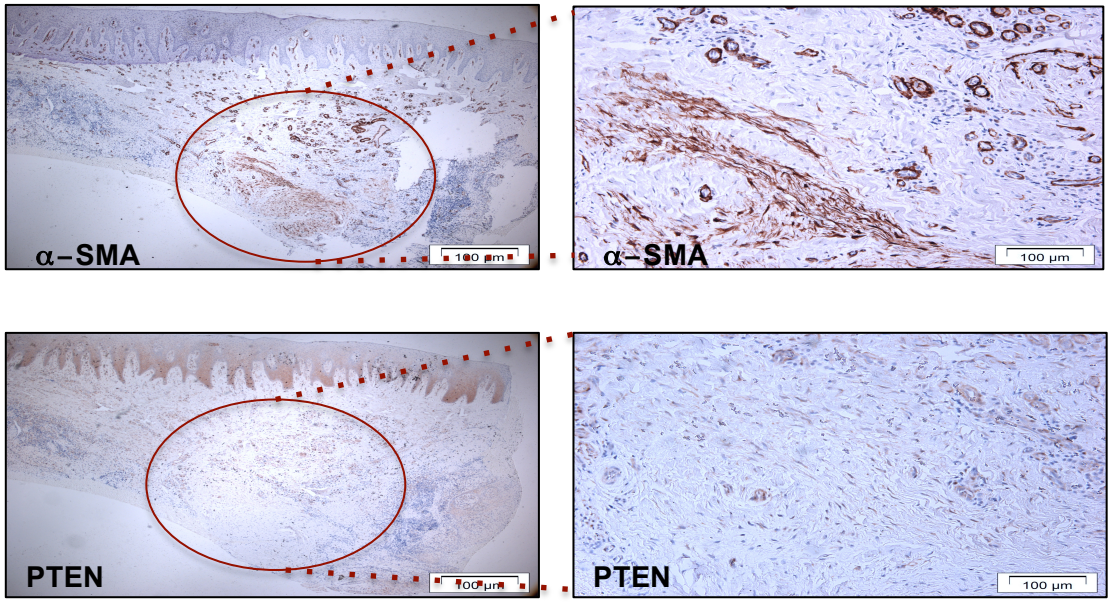

Figure 3.4.22: PTEN expression is reduced in fibrotic stroma after radiotherapy. PTEN immunohistochemistry demonstrated a reciprocal relationship between PTEN and α-SMA expression in activated fibroblasts following radiotherapy. The red circle enclosed an area of fibrotic stroma. The photomicrographs were captured at 4X and 10X. Scale bar = 200 μM.

3.4.10: The pro-tumourigenic effects of CAFs depend on elevated cyclooxygenase activity

The pro-tumourigenic properties of stress-induced premature senescent oral fibroblasts were observed to depend on elevated COX-2 activity and down-regulation of PTEN protein. To determine if similar trend was mirrored in CAFs, conditioned media derived from CAFs of GU OSCC before and after cisplatin treatment were investigated for PGE2 secretion, as a functional determinant of COX-2 activity. It was found that CAFs of GU OSCC secreted significantly more PGE2 than both normal non-senescent and senescent fibroblasts (figure 3.4.23). Compared to non-senescent-NHOFs, CAFs of GU OSCC (BICR31, BICR63 and BICR18) secreted 4.4-times more PGE2 whereas cisplatin-induced premature senescent-NHOFs secreted 2-times more PGE2 ($n=3$, $p<0.05$). Cisplatin treatment further amplified secretion of PGE2 in CAFs by 5.5-times of non-senescent-NHOFs ($n=3$, $p<0.05$).

To evaluate that this increased secretion was in fact due to raised COX-2 catalytic activity, celecoxib was used to selectively block COX-2 function in both non-senescent-NHOFs and CAFs (figure 3.4.24). It was found that celecoxib reduced PGE2 secretion in both CAFs and NHOFs declining it by 0.34-times and 0.71-times of untreated counterparts, respectively. However the secretion of PGE2 in CAFs still remained 33% higher than non-senescent-NHOFs even after celecoxib blockade indicating the requirement of higher dose of celecoxib to completely block COX-2 activity in CAFs.

To explore if PGE2 secreted by CAFs exerted a paracrine effect on OSCC cell lines *in vitro*, celecoxib was used to block COX-2 activity in CAFs and the conditioned medium was collected to perform migration assay (figure 3.4.25). In absence of celecoxib treatment CAFs of GU OSCC stimulated H357 cell migration by more than 9-times than non-senescent-NHOFs *in vitro*. However diminished secretion of PGE2 by CAFs following blockade of COX-2 activity significantly reduced migration of H357 cells by 27%

of untreated controls, however this remained significantly higher than non-senescent-NHOFs. This may be partly due to incomplete blockade of COX-2 activity in CAFs as observed in ELISA or because CAFs secreted additional factors other than PGE2, which are also chemotactic for cancer cells.

To ensure if the reduced motility of cancer cells in the presence of celecoxib was caused by diminished activity of CAFs, direct immunofluorescence for α-SMA was carried out in CAFs of GU OSCC in presence and absence of celecoxib. It was observed that blockade of COX-2 activity caused a dramatic decrease in stress fiber formation in CAFs in comparison to non-senescent-NHOF controls (figure 3.4.26).

It was observed before that blockade of COX-2 activity in stress-induced premature senescent-NHOFs was associated with increased PTEN expression with subsequent decrease in their pro-tumourigenic properties. Therefore PTEN expression was determined in late passage CAFs of GS OSCC (replicative senescent CAFs) and early-passage CAFs of GU OSCC, before and after celecoxib treatment, by western blot (figure 3.4.27.A). As expected, it was confirmed that in absence of celecoxib treatment PTEN expression was relatively low in senescent-CAFs of both GS and GU OSCC compared to non-senescent-NHOF controls. After celecoxib treatment there was a dramatic increase in PTEN expression in both normal fibroblasts and in CAFs implying that COX-2 activity is functionally conserved in CAFs.

To quantitate the changes in PTEN protein expression after celecoxib treatment relative band densitometry was done. It was observed that PTEN expression was reduced by 51% in senescent-CAFs compared to non-senescent-NHOFs (n=3, p=0.008; figure 3.4.27.B). Celecoxib treatment significantly increased PTEN expression in senescent-CAFs by 33.5% of their untreated counterparts (n=3, p=0.03; figure 3.4.27.B), although the increase remained 15% below the level of non-senescent-NHOFs. Statistically there was no significant difference in PTEN expression between

non-senescent-NHOFs before and after celecoxib treatment, and between non-senescent-NHOFs and senescent-CAFs after celecoxib treatment.

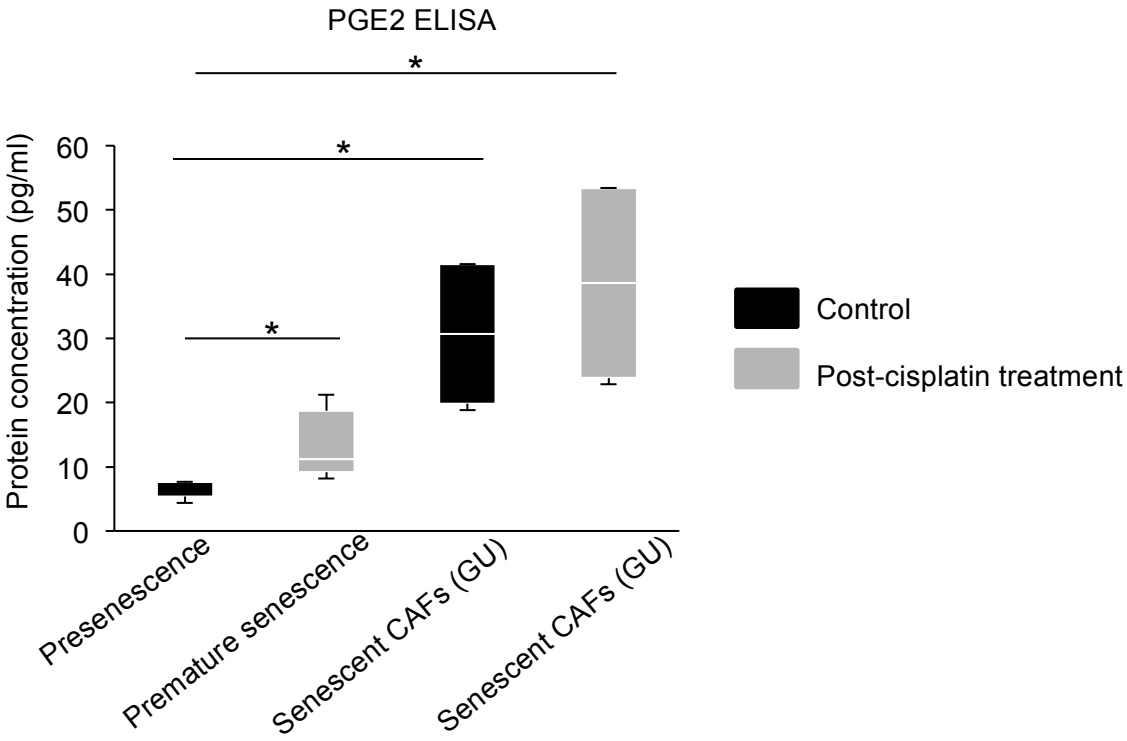

Figure 3.4.23: PGE2 secretion is increased in CAFs of GU OSCC. PGE2 ELISA was carried out using conditioned media from CAFs of GU OSCC with and without treatment with cisplatin. Normal non-senescent and senescent oral fibroblasts were used as control. The box-plot illustrates the mean of protein concentration ± SEM of three independent experiments. *p<0.05, by paired student's t-test.

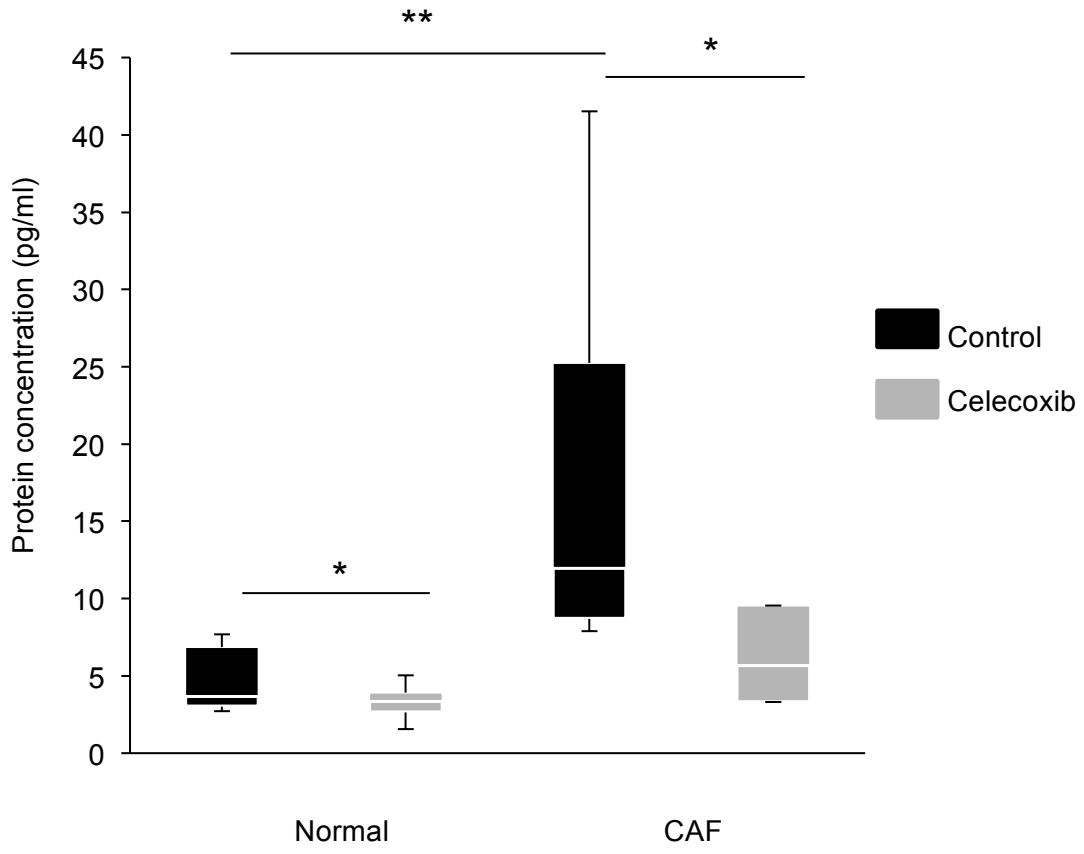

Figure 3.4.24: Blockade of COX-2 activity diminishes PGE2 secretion in CAFs. PGE2 ELISA was performed to determine COX-2 activity in CAFs and normal oral fibroblasts by selectively inhibiting COX-2 function using celecoxib. The box-plot represents mean of protein concentration ± SEM of three independent experiments. *p<0.05 and **p<0.01, two-way ANOVA with post-hoc corrections by Bonferroni t-test.

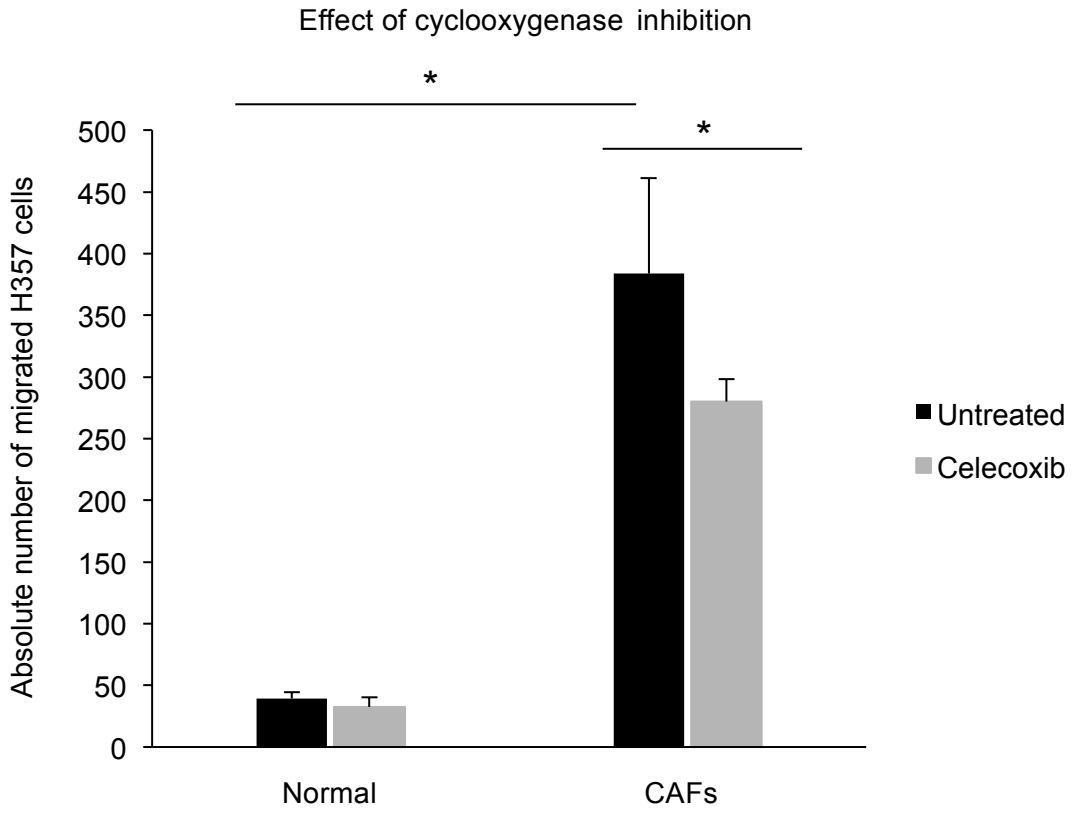

Figure 3.4.25: Blockade of COX-2 activity in CAFs reduces migration of H357 cell lines *in vitro*. 2D transwell assay was used to measure migration of H357 cells towards conditioned media of normal oral fibroblasts and CAFs before and after inhibiting COX-2 activity in fibroblasts for 48 h. Migration was carried out for 40 h. The migrated cells were fixed and stained with 0.1% crystal violet. Pictures were taken from three independent fields per well at 10X using light microscope. The cells were counted and averaged to give a representative number of migrated cells under each condition. The bars represent mean + SEM. *$p<0.05$, two-way ANOVA with post-hoc corrections by Tukey test.

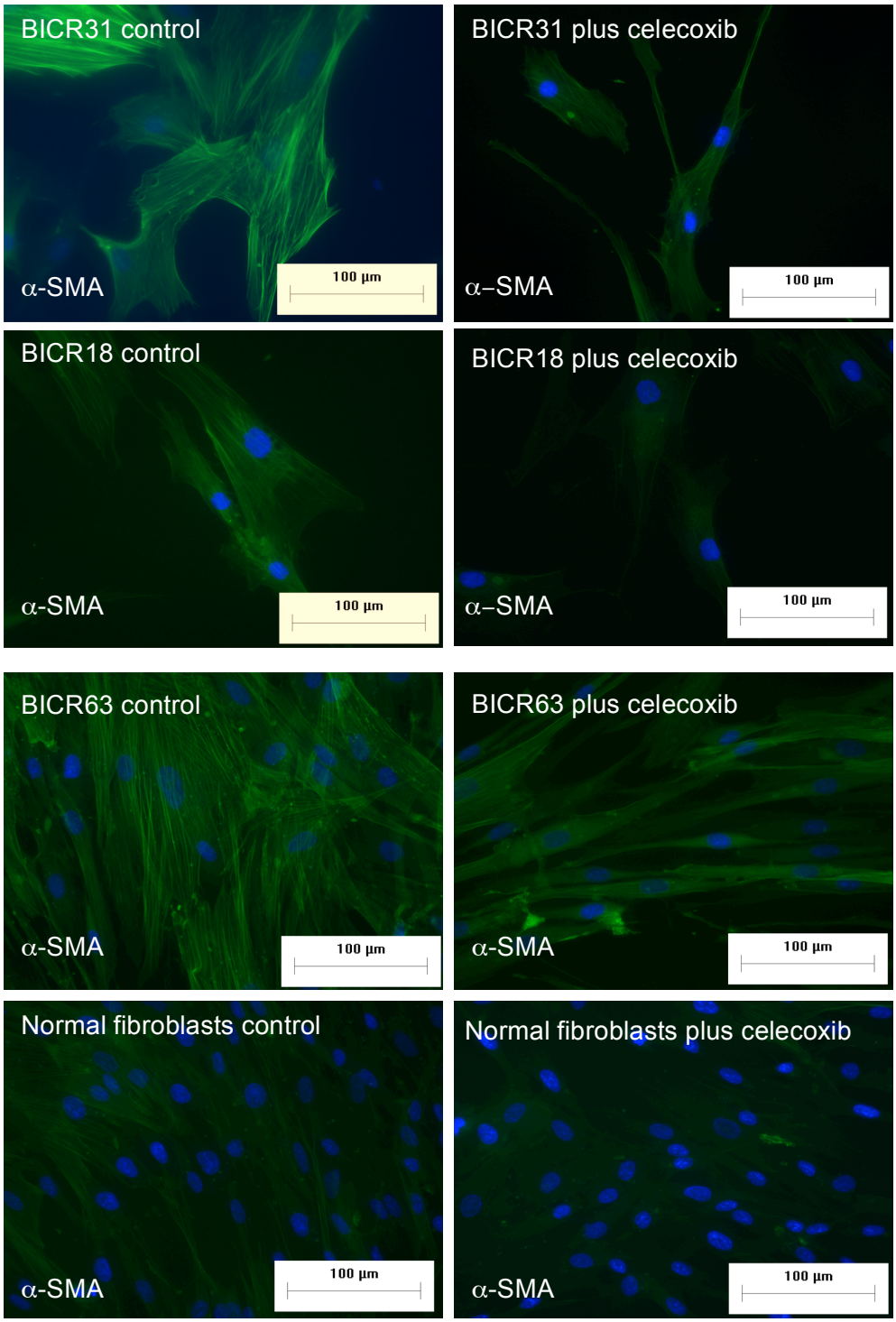

Figure 3.4.26: Reduced COX-2 activity in CAFs diminishes their myofibroblastic potential. Direct immunofluorescence for α-SMA was carried out in CAFs and normal oral fibroblasts after treating them with celecoxib. Untreated cells were used as control. The images were taken at 20X using fluorescence microscope. Scale bar = 100 µM.

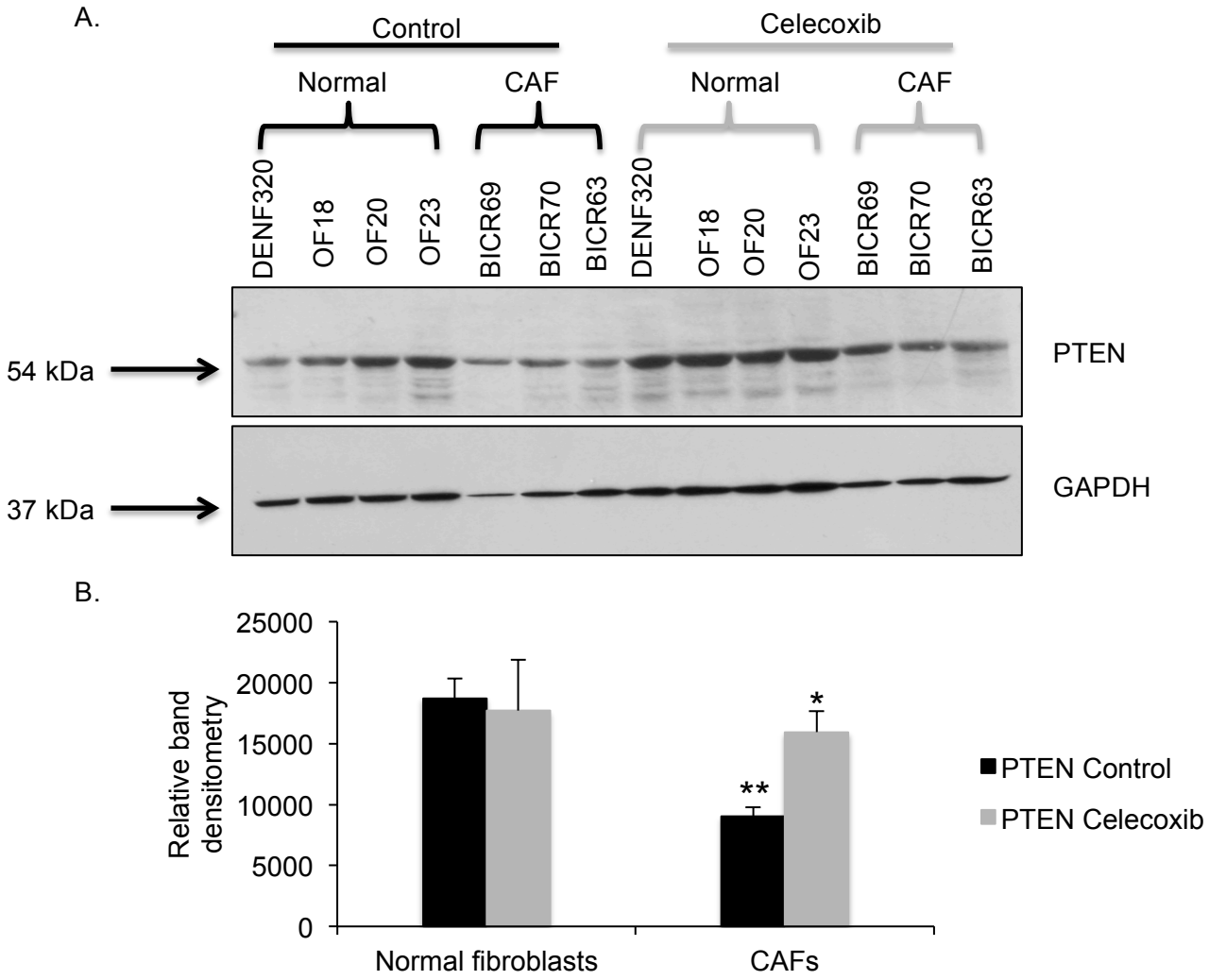

Figure 3.4.27: Celecoxib induces PTEN expression in CAFs of GS and GU OSCC. PTEN expression was determined by western blot in normal oral fibroblasts, late passage (P-10) CAFs of GS OSCC and early-passage (P-8) CAF of GU OSCC before and after treatment with celecoxib (A). Relative band densitometry was performed to obtain a relative quantification of PTEN to GAPDH internal control (B). The bars represent mean + SEM. Paired student's t-test was used to determine statistical significance. *p<0.05 and **<0.01.

3.4.11: Conclusion

In summay this section shows CAFs from GU OSCC are enriched for a sub-population of senescent fibroblasts compared to CAFs of GS OSCC. Cisplatin treatment induced premature senescence in CAFs of GS OSCC and amplified the senescence fate in those of GU OSCC. Premature senescent CAFs of GS OSCC are phenotypically similar to stress-induced premature senescent-NHOFs in 2D monoculture models however they behave more like CAFs of GU OSCC in 3D co-culture models. CAFs of GU OSCC have a more aggressive SASP than stress-induced premature senescent oral fibroblasts, which is exaggerated by cisplatin treatment.

Both premature senescent CAFs of GS OSCC and senescent-CAFs of GU OSCC stimulate migration and invasion of OSCC derived cell line H357 cells in 2D and 3D *in vitro* assay partly by secreting higher amounts of MMP-2 and partly by inducing EMT-like changes. CAFs of GU OSCC express some miRNAs that are common to stress-induced premature senescent oral fibroblasts but in addition they also display a miRNA signature specific to CAFs reported in other cancers. Similar to stress-induced premature senescent oral fibroblasts CAFs also demonstrated increased COX-2 activity and this was not restricted to only those of GU OSCC. PTEN expression was decreased in early-passage CAFs of GU OSCC and late-passage CAFs of GS OSCC. Further an association between increased COX-2 activity and reduced PTEN expression was found conserved in both normal fibroblasts and CAFs. CAFs also demonstrated elevated miR-335 and miR-148b transcript levels that were shown to negatively regulate PTEN in stress-induced and replicative senescent oral fibroblasts. However miRNA mediated post-transcriptional regulation of PTEN may be different in CAFs, because CAFs of GU OSCC express several oncogenic miRNAs such as miR-19a (He *et al*., 2014b), miR-21 (Liu *et al*., 2013; Iliopoulos *et al*., 2010) and miR-106 (Yang *et al*., 2014) all of which had been previously reported to target PTEN in CAFs of breast and gastric cancer or targeted PTEN during malignant transformation of cells.

Therefore understanding miRNA expression profiles in CAFs may assist in predicting pathways, which are commonly deregulated in aged CAFs in comparison to aged normal fibroblasts and this may help to identify novel therapeutic targets to implement cancer treatment.

4.0: Discussion

Cancer had been long recognized as a disease wherein the embryonic program is reactivated but is beyond control. Both senescence and apoptosis purportedly evolved as means of suppressing the cell autonomous growth of cancer cells. But cancer is also stimulated in non-cell autonomous manner by establishment of reciprocal cross-talk between cancer cells and surrounding stroma which encompasses immune cells, fibroblasts, vessels, lymphatics, ECM proteins and resident and circulating progenitor cells. The mechanism that reprograms the repressive stroma into encouraging malignant transformation and metastasis is only emerging. Recent discoveries using stromal markers (including senescent CAFs) to predict clinical outcome in HNSCC patients signifies the importance of tumour microenvironment in disease progression (Marsh *et al*., 2011; Lim *et al*., 2011), compelling to fully understand the molecular mechanisms regulating stromal fibroblast behaviour in cancer. In this thesis genotoxic agents: cisplatin and H_2O_2, and replicative exhaustion, were utilized to induce senescence (ageing) in human primary oral fibroblasts to model the features of ageing stroma in oral cavity and unveil the existence of a possible mechanism that subsidized development of cancer and chemotherapy resistance in HNSCC, in elderly patients.

This is the first study to report genotoxic stress provoked by cisplatin induced premature senescence in human primary oral fibroblasts by modulating expression of the tumour suppressor protein PTEN that synergizes with both TP53 and p16 pathways to stimulate irreversible growth arrest, a phenomenon also found conserved in other modes of senescence such as replicative and oxidative stress induced senescence. This study also confirms that senescent human oral fibroblasts develop a pro-inflammatory SASP and demonstrate differential expression of microRNAs. Further loss of PTEN expression was found to be critical in sustaining SASP in senescent oral fibroblasts, attributing to their CAF-like behaviour in tumour microenvironment and is

found functionally conserved in a bona fide population of senescent-CAFs derived from OSCC patients. Lastly, PTEN expression in senescent oral fibroblasts was found regulated at cellular level by COX-2 activity and at post-transcriptional levels by miR-335 and miR-148b.

4.1: Genotoxic stress and replicative exhaustion induced senescence and a pro-inflammatory and a pro-tumourigenic SASP, in human primary oral fibroblasts associated with differential expression of miRNAs

Treatment of human primary oral fibroblasts with sub-cytotoxic doses of cisplatin and H_2O_2 induced persistent DDR that culminated into irreversible growth arrest or premature senescence manifested by increased SA-β-Gal activity, enhanced expression of CDKI: p21 and p16, and secretion of various pro-inflammatory cytokines contributing to SASP. These markers were also expressed by replicative senescent oral fibroblasts. Among SASP factors increased secretion of MCP-1, IL-6, Endothelin I (Appendix 8), PGE2A and MMP-2 were found conserved in all modes of senescent oral fibroblasts. Elevated levels of these cytokines were not restricted to only protein level but also observed at transcriptional level, implying that senescent cells actively transcribed these mRNAs that were eventually translated into the respective cytokines. Investigating their functional effects revealed that soluble factors of SASP stimulated proliferation and migration of both oral dysplastic and cancer cell lines *in vitro* in paracrine fashion. In addition senescent oral fibroblasts were observed to enforce EMT-like changes in OSCC derived cell line H357 and stimulated their invasion in both 2D and 3D *in vitro* assays. In correspondence to this, EMT associated transcription factors, Slug and Twist1, were found elevated within certain subsets of H357 cells in presence of senescent oral fibroblasts in 3D models. Furthermore dermal invasion of H357 cells is additionally encouraged by increased secretion of both MMP-2 and MCP-1 by senescent oral fibroblasts. These observations suggested that in addition to

developing a pro-inflammatory SASP senescent oral fibroblasts also developed a CAF-like pro-tumourigenic phenotype that could possibly subsidize tumour progression *in vivo*.

The senescent oral fibroblasts also showed heterochromatin formation possibly due to depletion of laminin B from nuclear membrane (Shah *et al*., 2013). This was supported by analysis of certain SASP factors from cytokine array in UCSC browser, which verified that most of the genes deregulated in cisplatin-induced senescent oral fibroblasts were clustered within a specified region of the same chromosomes. For instance: MCP-1, MCP-3, IGFBP4, Eotaxin-1 are clustered in chromosome 17; IL-6, PDGFA, Eotaxin-2, Eotaxin-3, Twist1, IGFBP-1 and IGFBP-3 are clustered in chromosome 7; IL-8 and FGF-2 are clustered in chromosome 4; and angiogenin and BMP-4 are clustered in chromosome 14. The exact allocation of senescence associated heterchromatic foci are yet to be elucidated. Recently it was discovered that miRNAs can be recruited into the heterochromatin of senescent cells wherein it acts with E2F/RB1 repressor complex to silence promoter activity of multiple gene targets thus expanding their gene repression capacity (Benhamed *et al*., 2012). Therefore a similar mechanism may exist in senescent oral fibroblasts by which the deregulated miRNAs act in concert to regulate expression of multiple SASP factors and their subsequent functions in ageing. In order to acquire a comprehensive understanding of the regulatory mechanism of SASP, the miRNA expression profile of human senescent oral fibroblasts were thoroughly investigated.

Consistent with previous reports expression of senescence-associated miRNAs such as miR-34 family (He *et al*., 2007), miR-210 (Overhoff *et al*., 2013) and miR-146a (Bhaumik *et al*., 2009) were found elevated whereas miR-17-92 cluster and miR-145 were found reduced in both cisplatin-treated and late passage oral fibroblasts (Hackl *et al*., 2010; Dhabi *et al*., 2011). Other miRNAs that were specifically elevated in both late-passage and cisplatin-induced premature senescent oral fibroblasts were miR-137,

miR-184, miR-23, miR-223a and miR-335. Several miRNAs deranged in senescent oral fibroblasts also overlapped with miRNAs associated with DDR (Faraonio *et al*., 2012) emphasizing the convergence of commonly activated pathways linking ageing to DNA damage.

Among the candidate miRNAs, only miR-335 and miR-148b demonstrated time dependent up-regulation in senescent oral fibroblasts that corresponded to the development of SASP. Both these candidate miRNAs were previously reported to disappear in immortalized epithelium during malignant transformation underscoring their tumour suppressive function (Iliopoulos *et al*., 2010). Furthermore miR-335 and miR-152 of miR-148/152 family were also reported to be over-expressed in senescent cells (Scarola *et al*., 2010; Wang *et al*., 2011b). Therefore both miR-335 and miR-148b were selected for further investigation to identify any possible association between these two candidate miRNAs and SASP development in senescent oral fibroblasts.

It was found that senescent oral fibroblasts expressed significantly more mature miR-335 and miR-148b, compared to young fibroblasts. This suggested that certain types of intracellular signals prevailing in senescent cells are causing active transcription of these miRNAs. However the levels of their pri-miRNA transcript were found remarkably reduced in stress-induced premature senescent oral fibroblasts, indicating that in chronically active senescent cells the rate of miRNA processing exceeded the rate of pri-miRNA transcription possibly by sustained activation of miRNA processing enzymes; DICER and DROSHA/DGCR8 (Bartel, 2009, Huang *et al*., 2011) that produced increased amount of mature miRNAs. Conversely in-silico analysis confirmed that both of these candidate miRNAs were transcribed within introns of mRNA coding genes MEST and COPZ1 and therefore the mature forms of both miR-335 and miR-148b can also result from accelerated alternative splicing of these mRNAs in senescent fibroblasts with concomitant decrease in the levels of pri-miRNA transcripts. In replicative senescent oral fibroblasts expression of both pri-miRNA transcripts and

mature miRNAs were markedly elevated than controls. This implied that in these cells both the rate of pri-miRNA transcription and its subsequent processing into mature miRNAs were increased. The progressive increase in mature forms of the candidate miRNAs in senescent oral fibroblasts suggested that presence of both of these miRNAs were necessary for biological functions of senescent cells and possibly they are involved in regulating genes controlling fibroblast secretome.

Functional studies showed transient over-expression of either miR-335 or miR-148b, individually or in combination, failed to induce senescence in oral fibroblasts as determined by negative staining for SA-β-Gal activity instead increased expression of both these miRNAs were positively associated with phenotypic features of SASP. Over-expression of both miR-335 and miR-148b (particularly the former) were associated with activation of TP53 pathway wherein both induced transcription of p21. Both these miRNAs also simultaneously stimulated secretion of MCP-1 and IL-6 from oral fibroblasts compared to negative control suggesting their critical role in SASP regulation. It is unclear why these miRNAs were ineffective in stimulating senescence in oral fibroblasts especially miR-335, which was previously reported to provoke senescence in murine mesangial cells by targeting SOD2 and human cancer cell lines by targeting RB1 via maintaining a pool of ROS and exaggerating function of TP53, respectively (Scarola *et al*., 2012; Bai *et al*., 2011). This is notably due to the short duration (only 3 days) of over-expression of these miRNAs that were unsuccessful in provoking senescence in oral fibroblasts, which usually required a lag period of 4-7 days in stress-induced senescent oral fibroblasts. Another possibility is both these candidate miRNAs were selected at a time-point (day 15 post-treatment) when senescence was established and SASP was reinforced and maintained in oral fibroblasts. In agreement with this, it was found that over-expression of both miR-335 and miR-148b could reprogram oral fibroblasts to secrete soluble factors, which

stimulated migration of OSCC cells *in vitro* in paracrine fashion similar to senescent oral fibroblasts.

Target analysis using bioinformatics database mining predicted tumour suppressor PTEN as a functional gene target of both miR-335 and miR-148b. Recently loss of PTEN in CAFs of breast cancer patients were reported to stimulate loss of tumour suppressor miRNAs and activation of oncogenic transcriptional factors such as Ets2, controlling gene expression that reprogrammed the entire mammary tumour microenvironment to foster neoplastic growth (Bronisz *et al*., 2012). As a result before, validating PTEN as a target of miR-335 and miR-148b, senescent oral fibroblasts were first investigated for markers of myofibroblast, PTEN expression and its possible function.

4.2: Senescent oral fibroblasts show both myofibroblast-like properties and nemosis response *in vitro*

The persistent inflammatory phenotype of senescent oral fibroblasts similar to CAFs evinced that these cells may phenotypically demonstrate myofibroblast-like properties. Indeed except replicative senescent oral fibroblasts both cisplatin and H_2O_2 induced premature senescent oral fibroblasts displayed formation of conspicuous stress fibers of α-SMA indicative of their hyper-activated phenotype compared to young control fibroblasts. In contrast replicative senescent oral fibroblasts manifested intense fluorescence for α-SMA but were deficient in stress fiber formation. Further measurement of α-SMA expression at different time-points in cisplatin-induced senescent oral fibroblasts confirmed that its level was only elevated during the end-stage of senescence fate compared to presenescent fibroblasts. Based on this evidence it was concluded that stress-induced senescent oral fibroblasts possibly sustained their persistent activated pro-inflammatory phenotype by terminally differentiating into myofibroblast-like cells. However this notion contradicted with the

activated inflammatory phenotype of replicative senescent oral fibroblasts that exhibited all hallmarks of senescence but failed to form stress fibers. This prompted to investigate if cues from surrounding epithelial cells or cancer cells could stimulate formation or enhance the distribution of pre-existing stress fibers in senescent oral fibroblasts that presumably mirrored part of the conditions *in vivo*. Interestingly it was discovered that although senescent oral fibroblasts could stimulate malignant transition in oral dysplastic cells but cues from these cells had no stimulatory effect on myofibroblast-like transdifferentiation in senescent fibroblasts. In contrast soluble factors from cancer cells rearranged the orientation of pre-existing stress fibers as well as stimulated formation of new actin filaments in premature senescent oral fibroblasts imparting them a more contractile phenotype. The replicative senescent oral fibroblasts also demonstrated enhanced contractile phenotype but were incapable of forming stress fibers. Further analysis of SASP markers by qRT-PCR revealed that cues from cancer cells exaggerated the inflammatory response in both presenescent and senescent oral fibroblasts. Therefore it was reasoned that phenotypically replicative senescent oral fibroblasts represented a distinct population of cells within senescent fibroblasts. Elevated levels of inflammatory enzyme COX-2, a marker of nemosis response (Rasanen *et al.*, 2009), in senescent oral fibroblasts suggested that perhaps the replicative senescent oral fibroblasts demonstrated nemosis wherein they displayed all features of inflammation but were unable to form stress fibers *in vitro*.

As a result it was concluded that activation of stress-induced senescent oral fibroblasts were associated with myofibroblast-like phenotype whereas of replicative senescent oral fibroblasts were associated with nemosis response.

To date several pathways had been investigated in association with the activation of CAFs and myofibroblast-like cells in OSCC, however the mechanism that regulated activation of senescent oral fibroblasts leading into SASP is poorly understood. Since PTEN was identified as a putative target of several of the up-regulated miRNAs

including miR-335 and miR-148b in senescent oral fibroblasts and had been previously reported to regulate fibroblast secretome (Trimboli *et al*., 2009) its role was thoroughly investigated in SASP of senescent oral fibroblasts.

4.3: Senescent oral fibroblasts sustain SASP by down-regulating expression of PTEN and up-regulating expression of COX-2

During the early stages of senescence development, the rise in PTEN expression in cisplatin-treated oral fibroblasts synchronized with enhanced TP53 activity determined by increased transcription of p21 and accumulation of senescent cells. However once senescence was established the declination in PTEN expression was associated with elevated COX-2 activity and senescence-associated miRNAs. This suggested PTEN has dual purposes in senescent fibroblasts. Its initial inclination following cisplatin treatment may be associated with sustained inhibition of phosphatidylinositide-3-kinase (PI-3-K) pathway that allows fibroblasts to escape from the growth stimulating effect of mitogenic peptides present in the external milieu allowing cells to reach irreversible growth arrest at M1 phase (Wright *et al*., 1989). Alternatively its down-regulation at the terminal phase of senescence may reinforce and maintain a state of growth arrest in oral fibroblasts. This theory is supported by data from our collaborators who showed that down-regulation of PTEN in irradiation-induced senescent oral fibroblasts was associated with enhanced NOX-4 activity which maintained both senescence and their myofibroblast-like behaviour via generation of ROS (Mellone *et al*., submitted).

The connection between loss of PTEN expression in senescent oral fibroblasts with development of SASP was derived from several observations in this study. Firstly, all senescent oral fibroblasts in 2D monocultures displaying inflammatory phenotype were deprived of PTEN. Secondly, down-regulation of PTEN in cisplatin-treated oral fibroblasts was associated with increased invasiveness of cancer cells in 3D models in paracrine manner. Thirdly, transient knockdown of PTEN in young oral fibroblasts was

observed to reprogram them to stimulate migration of H357 cells in 2D assays. Although all forms of senescent oral fibroblasts expressed less PTEN and secreted more SASP factors than controls, transient knockdown of PTEN in young fibroblasts were unfruitful in eliciting an inflammatory response *in vitro*. In addition, transient knockdown of PTEN also failed to stimulate senescence in young fibroblasts. It was thought that this may probably result from the short duration of PTEN knockout that was insufficient to bring about changes in gene expression related to SASP in oral fibroblasts (in this case MCP-1 and IL-6 levels). Moreover the pro-tumourigenic properties conferred to the young fibroblasts possibly resulted from the direct effect of PTEN loss commonly occurring during fibroblast transactivation as observed in chronic inflammatory diseases (Parapuram *et al*., 2011).

This study also confirmed that decreased expression of PTEN in senescent oral fibroblasts was associated with increased phosphorylation of AKT at both serine 473 and threonine 308. Previous work showed that PTEN suppressed NFκB activation by constraining AKT mediated activation of IKK (Iliopoulos *et al*., 2010), critical in establishment of inflammatory SASP, regulating expression of various cytokines including IL-6, IL-8, MCP-1 as well as SASP-associated miRNAs such as miR-146a (Bhaumik *et al*., 2009; Koide *et al*., 2007). In the present study elevated NFκB activity was recorded in both stress-induced senescent and late passage oral fibroblasts, which corroborated with anti-inflammatory role of PTEN in aged cells. As a result decreased expression of PTEN in senescent oral fibroblasts was assumed to instigate a vicious inflammatory loop via perpetuating activation of NFκB. However what causes senescent oral fibroblasts to selectively lose PTEN expression remains to be determined. Therefore PTEN expression was thoroughly investigated in senescent oral fibroblasts at both mRNA and protein levels with simultaneous investigation of SASP factors.

When PTEN mRNA levels were determined in senescent oral fibroblasts it was found inconsistent but reduced at most times. The variability in PTEN mRNA at different time-points and the gradual fall in its protein level suggested that PTEN was strictly regulated at post-transcriptional levels that prevented its mRNA from being translated into proteins in senescent cells. Alternatively the reciprocal relation in pattern of PTEN transcription to IL-6 mRNA suggested that the pro-inflammatory cytokines were perhaps negatively regulating PTEN. This result prompted the suggestion that factors regulating IL-6 expression may be indirectly or directly regulating PTEN expression in senescent fibroblasts. In line with this it was discovered that senescent oral fibroblasts demonstrated elevated levels of COX-2 mRNA with simultaneous increase in PGE2 secretion. COX-2 mRNA demonstrated the same transcriptional trend as IL-6 mRNA and was negatively associated with PTEN expression. IL-6 is one of the several gene targets of COX-2 in HNSCC (Dalwadi *et al*., 2005) and PGE2 was reported to stimulate NFκB transcriptional activity to exert the pro-inflammatory effect of COX-2 (Poligone and Baldwin, 2001). Moreover another group reported that in PTEN deficient fibroblasts PGE2 exerted a pro-fibrotic effect increasing expression of both collagen and α-SMA which was rescued by restoration of PTEN (Sagana *et al*., 2009). As a result to ensure the regulatory role of COX-2 in SASP, a selective COX-2 inhibitor, celecoxib was used to inhibit its action in senescent oral fibroblasts. Indeed celecoxib remarkably reduced secretion of PGE2 from PTEN deficient senescent oral fibroblasts. This was accompanied by attenuation in stress fiber formation in senescent fibroblasts indicative of their diminished activated state. Moreover assessment of SASP marker IL-6 (gene target of COX-2) in celecoxib treated senescent oral fibroblasts demonstrated a significant decrease. Inhibition of COX-2 in senescent oral fibroblasts also impeded their stimulatory effect on cancer cell migration by paracrine action. To verify if this attenuated inflammatory state of senescent oral fibroblasts following COX-2 inhibition was associated with alteration in PTEN, its levels were assessed in senescent

fibroblasts both before and after celecoxib treatment. Surprisingly blockade of COX-2 was accompanied by restoration of PTEN expression in senescent oral fibroblasts. All these findings inferred that elevated COX-2 activity in senescent oral fibroblasts was negatively regulating PTEN expression while simultaneously stimulating transcriptional activity of NFκB to sustain the pro-inflammatory SASP, which ultimately promoted proliferation, migration and invasion of cancer cells. Recently it was reported that administration of chemotherapy in bladder carcinoma induces release of PGE2 from apoptotic cells, which then stimulates proliferation of neighbouring surviving cancer cells and enrich for a population of cancer stem cells (Kurtova *et al*., 2014). Therefore it is conceivable that increased secretion of PGE2 by senescent fibroblasts may also select for a population of initiated cancer cell or stem-like cell to cause formation of new tumours or chemotherapy resistance.

4.4: COX-2 can modulate composition of inflammatory miRNAs in senescent oral fibroblasts and thereby regulate expression of PTEN by miR-335 and miR-148b induced silencing complex

Enhancement of PTEN expression in celecoxib treated senescent oral fibroblasts with concomitant attenuation of SASP signified COX-2 activity was critical in regulating PTEN and therefore fibroblast secretome. To explore the mechanism of how COX-2 regulated PTEN protein levels in senescent oral fibroblasts, it was postulated that up-regulation of COX-2 in senescent fibroblasts elicited changes in expression of specific microRNAs, which regulated genes (in this case PTEN) at post-transcriptional levels.

In agreement with this hypothesis it is shown for the first time that both miR-335 and miR-148b repressed translation of luciferase when a short fragment of PTEN 3'UTR bearing the seed sequences of these candidate miRNAs were cloned into the pmiR-Reporter vector. Moreover it may be assumed that in addition miR-148b also induced PTEN mRNA decay manifested by absence or diminished intensity of PTEN band in

western blot while miR-335 invariably increased band intensity suggesting miR-335 perhaps indirectly stimulated PTEN expression in senescent oral fibroblasts despite of causing translational repression. The efficiency of miRISC is ostensibly determined by the presence of two complementary seed sequences for miR-148b compared to only one for miR-335 in 3'UTR of PTEN. However the increase in PTEN protein level following miR-335 over-expression may be indirectly associated with activation of TP53 (observed during the early stages of senescence development in oral fibroblasts) which was significantly increased by only miR-335 although miR-148b also stimulated an increase but to a lesser degree. This also highlights the possibility that long term over-expression of miR-335 in oral fibroblasts may in fact induce senescence indirectly via activating TP53 dependent DDR signaling pathway. In contrast co-transfection with miR-335 and miR-148b stimulated both translational repression and mRNA decay of PTEN. Measuring NFκB activity showed it was stimulated only in co-transfected oral fibroblasts compared to cells carrying single miRNA transfection and was inversely associated with PTEN protein expression in miR-335 transfected cells.

On the other hand COX-2 mRNA levels remained unchanged in all miRNA transfected oral fibroblasts pinpointing miR-335 and miR-148b did not regulate COX-2 expression in senescent cells. This instigated investigation of whether COX-2 activity actually regulated miR-335 and miR-148b levels in senescent oral fibroblasts. It was discovered that upon blockade of COX-2 activity by celecoxib in senescent fibroblasts, the levels of both miR-335 and miR-148b were reduced which corresponded to enhanced expression of both PTEN mRNA and protein in senescent cells.

4.5: Paracrine role of MCP-1 in senescent microenvironment

Next the research was further extended to study the paracrine effects of MCP-1. It was found that MCP-1 from senescent oral fibroblasts recruited THP-1 monocytes *in vitro*. In addition SASP factors were found to stimulate both M1 and M2 switching in THP-1

derived differentiated macrophages, associated with tumour aggression (Sica *et al*., 2008). Very recent evidence showed activation of TP53 following DDR causes tissue macrophage to polarize into anti-tumourigenic M1 phenotype which can phagocytose senesced cells and eliminate them from the tumour vicinity within liver (Lujambio *et al*. 2013). In the present study MCP-1 expression was positively associated with both miR-335 over-expression (miRNA previously reported to be regulated by TP53; Scarola *et al*., 2010) and elevated TP53 activity (Hacke *et al*., 2010) in senescent oral fibroblasts but based on *in vitro* data it is impossible to predict the exact consequences of macrophage polarization in ageing stroma of oral cancer. Moreover *in vivo* the tumour microenvironment also contains resident macrophage progenitor cells which display different immunoreactivity than circulating monocytes due to their embryonic memory and origin from a different lineage (Ginhoux and Jung, 2014). Furthermore more recent works showed that senescence occurred during early embryogenesis where senescent embryonic tissues guided organ growth and development and controlled tissue involution and once their role were complete senescent cells were successfully eliminated by foetal macrophages and NK cells (Storer *et al*., 2013; Munoz-Espin *et al*., 2013). The liver is infact colonized by both foetal macrophages arising from yolk sac and haemapoetic stem cells (Ginhoux and Jung, 2014). As a result it is possible for macrophages present in liver to eliminate senescent cells owing to their embryonic memory which may be ineffective in tissue microenvironement of head and neck region. On the otherhand, the excessive secretion of cytokines such as IL-6 and lower amount of IL-2 by senescent oral fibroblasts as determind by the human cytokine array, could potentiate development of immunosenescence (Vredevoe *et al*., 2004). As a result the pilot data from this study suggests senescent oral fibroblasts can recruit circulating monocytes into the tumour microenvironment and stimulate their polarization. Their functional consequences in tumour microenvironment are currently being investigated by another member of the group in this laboratory.

MCP-1 from CAFs was also reported to stimulate migration of OSCC cells (Wu *et al*., 2011). In agreement with above, this thesis shows for the first time MCP-1 from senescent oral fibroblasts stimulated invasion and migration of OSCC-derived cell lines in both 2D and 3D *in vitro* assay. Interestingly, consistent with observations made by Li and group (2013) it was found that blockade of secreted MCP-1 in normal oral fibroblasts in 3D models markedly accelerated invasiveness of H357 cells. This is possibly associated with blockade of trasdifferentiation of resting fibroblast into myofibroblast via MCP-1/CCL2 and CCR2 interaction (Murray *et al*., 2008) or due to rebound IL-6 secretion by activated fibroblast after MCP-1 discontinuation (Bonapace *et al*., 2014). MCP-1 was shown to induce expression of TGFβR2 and procollagen I and III in myofibroblasts and help in establishment of vicious positive feedback loop in chronic inflammatory disorders (Murray *et al*., 2008). As a result loss of MCP-1 action on resting fibroblasts may inhibit their tumour suppressive function, preventing them to deposit collagen around cancer cells to limit their invasion. It is also possible that blockade of secreted MCP-1 during early stages of cancer progression is insufficient to halt cancer dissemination. Since the young fibroblasts retain expression of other functional receptors than TGFβR2, cancer cells can use them to their advantage in favour of non-cell autonomous growth before they became fully cell-autonomous. Moreover it had been reported in the past that the amount of collagen content gradually decreases from healthy oral mucosa to grade 4C OSCC underscoring their importance in limiting tumour invasion and is found to be reexpressed during advanced stage of cancer possibly assisting cancer cells to colonize and form micro or macro- metastasis (Kawashiri *et al*., 2009). Senescent fibroblasts represents a population of aged but activated fibroblasts which predominately stimuated cancer cell migration and invasion via secreted factors and inducing EMT-like changes. Senescent fibroblasts tend to show selective sensitivity to only certain signals possibly owing to receptor desensitization and thus cancer cells fail to use senescent fibroblasts

to their advantage in absence of MCP-1 signalling. MCP-1 is recently reported to stimulate IL-6 secretion by breast cancer stroma (Bonapace *et al*., 2014). This evidence further implies that blockade of MCP-1 perhaps interrupt the entire secretory loop of SASP in senescent oral fibroblasts and the paracrine cross-talk between senescent stroma and cancer cells. This is probably why blockade of MCP-1 was successful in reducing the invasiveness of OSCC cell lines co-cultured with senescent oral fibroblasts in 3D models but was unsuccessful in reducing cancer cell invasiveness in presence of young resting fibroblasts wherein addition of anti-MCP-1 antibody rather worsened the invasiveness of cancer cells.

4.6: Senescent-CAFs derived from OSCC exhibit a similar regulatory mechanism of SASP to that of normal senescent oral fibroblasts

This work was further expanded into studying senescent-CAFs derived from patients suffering HNSCC to identify a possible similarity or dissimilarity between artificially aged models and naturally aged CAFs. As expected senescent-CAFs also expressed less PTEN than non-senescent-CAFs and normal oral fibroblasts. These cells also demonstrated deregulation of miRNAs. Interestingly the miRNAs that are abnormally expressed in senescent CAFs overlapped with both oncogenic miRNAs commonly deranged in fibroblasts associated with cancer and tumour suppressor miRNAs elevated in normal senescent oral fibroblasts (Appendix 5 & 6). Both miR-335 and miR-148b were elevated in senescent-CAFs. These two tumour suppressor miRNAs were also dramatically elevated in non-senescent-CAFs to even greater extent than senescent-CAFs that exerted reduced pro-tumourigenic effect on cancer cells in indirect co-culture studies. These two miRNAs have regulatory roles in modulating cell differentiation (Tome *et al*., 2014; reviewed by Chen *et al*., 2013) and possibly repress genes that regulate myofibroblastic transdifferentiation in non-senescent-CAFs.

The senescent-CAFs also secreted more IL-6 and MCP-1 than non-senescent-CAFs and normal younger fibroblasts. The senescent-CAFs (BICR63) demonstrated reduced migratory capacity into the dermis in 3D models compared to non-senescent-CAFs and normal fibroblasts and treatment with cisplatin amplified their senescence response and pro-tumourigenic properties. Both senescent and non-senescent CAFs demonstrated elevated COX-2 activity and it was found like stress-induced senescent oral fibroblasts inhibition of COX-2 activity in CAFs attenuated their activated phenotype and stimulated PTEN expression subsequently declining their pro-tumourigenic character.

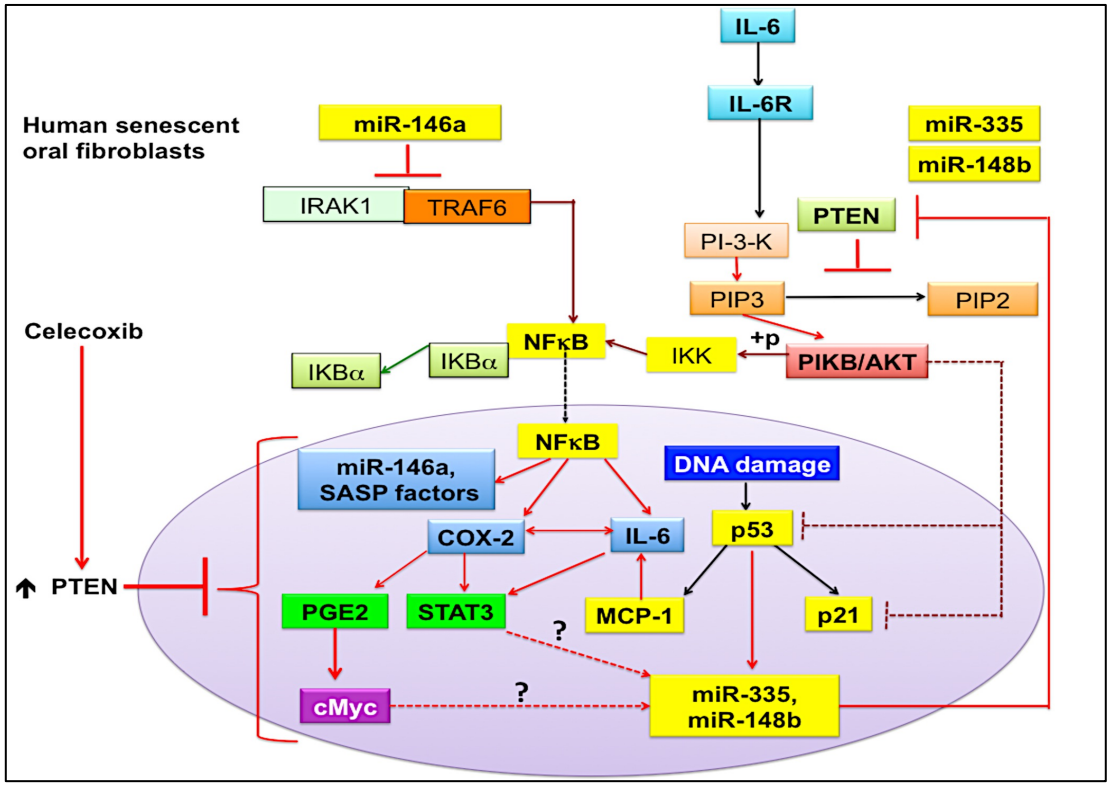

Figure 4.1: Proposed model for miRNA-mediated regulation of SASP in human oral fibroblasts. COX-2 expressions are elevated in senescent oral fibroblasts that up-regulates inflammatory and DDR associated miRNAs, miR-335 and miR-148b, to silence PTEN and remove its anti-inflammatory suppressive effect on NFκB activity. Selective COX-2 inhibtior can rescue SASP of oral fibroblasts by inducing PTEN.

4.7: Conclusion

To summarize this thesis showed genotoxic stress and natural process of ageing initiate DDR in human primary oral fibroblasts, which culminate by reaching irreversible growth arrest or senescence. This is associated with formation of heterochromatin, which possibly leads into active transcription of several SASP factors such as IL-6, MCP-1, and COX-2 and produced alteration in the levels of miRNAs. However the senescent fibroblasts use ingenious maneuvers to regulate this diverse range of gene expression to survive and escape apoptosis. Both miR-335 and miR-148b genes possess binding sites for transcriptional factor STAT3 that is another COX-2 gene target and cMyc that can be induced by PGE2 (Dalwadi *et al*., 2005; Iliopoulos *et al*., 2010; Krysan *et al*., 2014). As a result it is possible COX-2 directly stimulates expression of STAT3 and indirectly stimulates expression of cMyc, to enhance transcription of miR-335 and miR-148b in senescent oral fibroblasts. These miRNAs then represses PTEN expression and withdraws its inhibitory effect on NFκB action. COX-2 metabolite PGE2 also stimulates NFκB activity. The enhanced NFκB activity then leads into transcription of various pro-inflammatory genes contributing to SASP. Again the hyperactivity of NFκB is fine tuned by elevated levels of anti-inflammatory miRNA miR-146a (this study and Bhaumik *et al*., 2009) ensuring efficient regulation of SASP in senescent cells. A probable model for COX-2/miRNA/PTEN mediated SASP regulation in human senescent oral fibroblasts is illustrated in figure 4.1.

As a result accumulating senescent fibroblasts maintain a vicious regulatory loop for secretion of SASP factors which subsequently act on neighbouring cancer cells to promote their survival, proliferation, invasion and migration to distant site or even initiate or select for a population of cancer stem cells leading into development of new tumours, cancer recurrences and chemotherapy failure at old age. All these observations are also mirrored in senescent-CAFs of HNSCC patients. Further this study shows for the first time that chemotherapeutic drugs (cisplatin) could induce

senescence in non-senescent-CAFs and amplify the senescence phenotype of senescent-CAFs in tumour microenvironment. This finding is of great clinical significance because during administration of chemotherapies, most anti-cancer drugs exert cytotoxic effect on cancer cells by either inducing senescence or apoptosis and in doing so they are likely to stimulate senescence of fibroblasts in the tumour microenvironment generating the so called desmoplastic stroma in post-chemotherapy patients. Endurance of this newly activated stroma (possibly due to immunosenescence) is likely to superimpose with pre-existing reactive stroma of the tumour to create a more susceptible niche to foster growth of new tumours and promote their metastasis, thus contributing to emergence of chemotherapy resistance in cancer patients.

5: Future work

Firstly, site directed mutagenesis would be used to determine if the candidate miRNAs specifically repressed translation of PTEN in the reporter assay described herein. Secondly anti-miRs will be used to knock down these miRNAs in normal fibroblasts to evaluate if these could rescue SASP. Thirdly PTEN will be over-expressed in normal oral fibroblasts to the time-point when SASP is established, to understand if re-introduction of PTEN to senescent oral fibroblasts could rescue cells from developing pro-inflammatory SASP. Fourthly, senescent cells will be examined for expression of phosphorylated STAT3 protein (and also cMyc) to identify a possible mechanism for regulation of SASP-associated miRNAs. Finally human archival tissue sections from pre- and post-chemotherapy patients will be assessed for expression of PTEN and COX-2 to investigate if PTEN expression in tumour stroma following chemotherapy could be used to predict clinical outcomes in head and neck cancer patients.

6: References

1. Acosta J. C., O'Loghlen A., Banito A., Guijarro M. V., Augert A., *et al*. (2008). Chemokine signaling via the CXCR2 receptor reinforces senescence. Cell. 133(6): 1006-18.
2. Acosta J. C., Banito A., Wuestefeld T., Georgilis A., Janich P., *et al*. (2013). A complex secretory program orchestrated by the inflammasome controls paracrine senescence. Nat Cell Biol. 15(8): 978-90.
3. Al-Ansari M. M., Hendrayani S. F., Shehata A. I. and Aboussekhra A. (2013). P16(INK4a) represses the paracrine tumor-promoting effects of breast stromal fibroblasts. Oncogene. 32(18):2356-64.
4. Alcorta D. A., Xiong Y., Phelps S., Hannon G., Beach D., *et al*. (1996). Involvement of the cyclin-dependent kinase inhibitor p16 (INK4a) in replicative senescence of normal human fibroblasts. Proc Natl Acad Sci U S A, 93, 13742-7.
5. American cancer society. Cancer facts & figures 2014. Atlanta: American caner society; 2014.
6. Apprelikova O., Yu X., Palla J., Wei B. R., John S., *et al*. (2010). The role of miR-31 and its target gene SATB2 in cancer-associated fibroblasts. Cell Cycle. United States.
7. Ali S., Ahmad A., Banerjee S., Padhye S., Dominiak K., *et al*. (2010). Gemcitabine sensitivity can be induced in pancreatic cancer cells through modulation of miR-200 and miR-21 expression by curcumin or its analogue CDF. Cancer Res. 70 (9): 3606-3617.
8. Bai X-Y., Ma Y., Ding R., Fu B., Shi S., *et al*. (2011). miR-335 and miR-34 promote renal senescence by suppressing mitochondrial antioxidative enzymes. J Am Soc Nephrol. 22: 1252-1261.
9. Balermpas P., Rodel F., Liberz R., Oppermann J., Wagenblast J., *et al*. (2014). Heand and neck cancer relapse after chemotherapy correlates with CD163+ macrophages in primary tumour and CD11b+ myeloid cells in recurrences. Br J Cancer. 111(8):1509-18.
10. Barcellos-Hoff M. H. and Ravani S. A. (2000). Irradiated mammary gland stroma promotes the expression of tumorigenic potential by unirradiated epithelial cells. Cancer Res. 60:1254-1260.
11. Bartel D. P. (2009). MicroRNAs: Genomics, Biogenesis, Mechanism, and Function(Review). Cell .116,281-297.

12. Bavik C., Coleman I., Dean J. P., Knudsen B., Plymate S., *et al*. (2006). The gene expression program of prostate fibroblast senescence modulates neoplastic epithelial cell proliferation through paracrine mechanisms. Cancer Research, 66, 794-802.
13. Bartkova J., Horejsi Z., Koed K., Kramer A., Tort F., *et al*. (2005). DNA damage response as a candidate anti-cancer barrier in early human tumorigenesis. Nature. 434:864-70.
14. Begley L., Monteleon C., Shah R. B., Macdonald J. W., and Macoska J. A. (2005). CXCL12 overexpression and secretion by aging fibroblasts enhance human prostate epithelial proliferation in vitro. Aging Cell. England.
15. Benhamed M., Herbig U., Ye T., Dejean A., and Bischof O. (2012). Senescence is an endogenous trigger for microRNA-directed transcriptional gene silencing in human cells. Nat Cell Biol. 14(3):266-75.
16. Bennett D. C. and Medrano E. E. (2002). Molecular regulation of melanocyte senescence. Pigment Cell Res. 15(4): 242-50.
17. Bhaumik D., Scott G. K., Schokrpur S., Patil C. K., Orjalo A. V., *et al*. (2009). MicroRNAs miR-146a/b negatively modulate the senescence-associated inflammatory mediators IL-6 and IL-8. Aging (Albany NY), 1, 402-11.
18. Bian Y., Hall B., Sun Z-J., Molinolo A., Chen W., *et al*. (2012a). Loss of TGF-β signaling and PTEN promotes head and neck squamous cell carcinoma through senescence evasion and cancer-related inflammation. Oncogene. 31: 3322-3332.
19. Bian E-B., Huang C., Ma T-T, Tao H., Zhang H., *et al*. (2012b). DNMT1-mediated PTEN hypermethylation confers hepatic stellate cell activation and liver fibrogenesis in rats. Toxicology and Applied Pharmacology. 264:13-22.
20. Bianchi-Frias D, Vakar-Lopez F, Coleman IM, Plymate SR, Reed MJ, *et al*. (2010) The Effects of Aging on the Molecular and Cellular Composition of the Prostate Microenvironment. PLoS ONE 5(9): e12501. doi:10.1371/journal.pone.0012501
21. Binet R., Ythier D., Robles A. I., Collado M., Larrieu D., *et al*. (2009). WNT16B is a new marker of cellular senescence that regulates p53 activity and the phosphoinositide 3-kinase/AKT pathway. Cancer Res. 69(24):9183-91.
22. Bishop N. A., and Guarente L. (2007). Two neurons mediate diet-restriction-induced longevity in *C. elegans*. Nature. 447(7144): 545-549.
23. Bisson F., Rochefort E., Lavoie A., Larouche D., Zaniolo K., *et al*. (2013). Irradiated human dermal fibroblasts are as efficient as mouse fibroblasts as a

feeder layer to improve human epidermal cell culture life span. Int J Mol Sci. 14(3): 4684-704.

24. Bonapace L., coissieux M-M., Wyckoff J., Mertz K. D., Varga Z., *et al*. (2014). Cessation of CCL-2 inhibition accelerates breast cancer metastasis by promoting angiogenesis. Nature. 515 (7525): 130-3.
25. Bonifacio LN, Jarstfer MB (2010) MiRNA Profile Associated with Replicative Senescence, Extended Cell Culture, and Ectopic Telomerase Expression in Human Foreskin Fibroblasts. PLoS ONE 5(9): e12519. doi:10.1371/journal.pone.0012519.
26. Brennan C. M. and Steitz J. A. (2001). HuR and mRNA stability. Cell Mol Life Sci. 58(2):266-77. Review.
27. Bronisz A., Godlewski J., Wallace J. A., Merchant A. S., Nowicki M. O., *et al*. (2012). Reprogramming of the tumour microenvironment by stromal PTEN-regulated miR-320. Nat Cell Biol. 14(2):159-167.
28. Bullock M. D., Pickard K. M., Nielsen B. S., Sayan A. E., Jenei V., *et al*. (2013). Pleiotropic actions of miR-21 highlight the critical role of deregulated stromal microRNAs during colorectal cancer progression. Cell Death and Disease. 4: e684.
29. Cahu J., Bustany S. and Sola B. (2012). Senescence-associated secretory phenotype favors the emergence of cancer stem-like cells. Cell death and disease. 3,e466.
30. Camps J. L., Chang S. M., Hsu T. C., Freeman M. R., Hong S. J., *et al*. (1990). Fibroblast-mediated acceleration of human epithelial tumor growth in vivo. Proc Natl Acad Sci U S A, 87, 75-9.
31. Campisi J. and D'Adda di Fagagna F. (2007). Cellular senescence: when bad things happen to good cells. Nat Rev Mol Cell Biol. England.
32. Cancer Research UK, Oral cancer statistics, November, 2014
33. Cancer Research UK, Oral cancer statistics, September, 2014
34. Casas E., Kim J., Bendesky A., Ohno-Machado L., Wolfe C. J., *et al*. (2011). Snail2 is an essential mediator of Twist1-induced epithelial-mesenchymal transition and metastasis. Cancer Res. 71(1):245-254.
35. Castro P., Giri D., Lamb D. J., and Ittmann M. (2003). Cellular senescence in the pathogenesis of benign prostatic hyperplasia. Prostate, 55, 30-8.
36. Castro P., Xia C., Gomez L., Lamb D. J., and Ittmann M. (2004). Interleukin-8 expression is increased in senescent prostatic epithelial cells and promotes the development of benign prostatic hyperplasia. Prostate, 60, 153-9.

37. Chang B. D., Broude E. V., Dokmanovic M., Zhu H., Ruth A., *et al*. (1999). A senescence-like phenotype distinguishes tumor cells that undergo terminal proliferation arrest after exposure to anticancer agents. Cancer Res, 59, 3761-7.
38. Chang B-D., Watanabe K., Broude E. V., Fang J., Poole J. C., *et al*. (2000). Effects of $p21^{Waf1/Cip1/Sdi1}$ on cellular gene expression: Implications for carcinogenesis, senescence, and age-related diseases. PNAS. 97(8): 4291-4296.
39. Chaudhary M., Gadbail A. R., Vidhale G., Mankar Gadbali M.P., Gondivkar S. M., *et al*. (2012). Comparison of myofibroblasts expression in oral squamous cell carcinoma, verrucous carcinoma, high risk epithelial dysplasia, low risk epithelial dysplasia and normal oral mucosa. Heand Neck Pathol. 6(3):305-13.
40. Chen Q. and Ames B. N. (1994). Senescence-like growth arrest induced by hydrogen peroxide in human diploid fibroblast F65 cells. Proceedings of the National Academy of Sciences of the United States of America, 91, 4130-4.
41. Chen Q., Fischer A., Reagan J. D., Yan L. J., and Ames B. N. (1995). Oxidative DNA damage and senescence of human diploid fibroblast cells. Proceedings of the National Academy of Sciences of the United States of America, 92, 4337-41.
42. Chen Y., Song Y-X. and Wang Z-N. (2013). The MicroRNA-148/152 Family: Multi-faceted Players. Molecular Cancer. 12(43): 1-8.
43. Chesnoy S. and Huang L. (2000). Structure and function of lipid-DNA complexes for gene delivery. Annu. Rev. Biophys. Biomol. Struct. 29:27-47.
44. Chiang W-F., Liu S-Y., Fang L-Y., Lin C-N., Wu M-H., *et al*. (2008). Overexpression of galectin-1 at the tumor invasion front is associated with poor prognosis in early-stage oral squamous cell carcinoma. Oral Oncology. 44: 325-334.
45. Chien Y., Scuoppo C., Wang X., Fang X., Balgley B., *et al*. (2011). Control of the senescence-associated secretory phenotype by NFkB promotes senescence and enhances chemosensitivity. Genes & Development. 25:2125-2136.
46. Choi J., Shendrik I., Peacocke M., Peehl D., Buttyan R., *et al*. (2000). Expression of senescence-associated beta-galactosidase in enlarged prostates from men with benign prostatic hyperplasia. Urology. United States.
47. Chondrogianni N., Stratford F. L. L., Trougako I. P., Friguet B., Rivett A. J., *et al*. (2003). Central role of the proteasome in senescence and survival of human fibroblasts: Induction of a senescence-like phenotype upon its inhibition and resistance to stress upon its activation. J. Biol. Chem. 278:28026-28037.

48. Cichon A., Pickard A., McDade S. S., Sharpe D. J., Moran M., *et al*. (2013). AKT in stromal fibroblasts control invasion of epithelial cells. Oncotarget. 4:1103-1116.
49. Cimino D., De Pitta C., Orso F., Zampini M., Casara S., *et al*. (2013). miR-148b is a major coordinator of breast cancer progression in relapse-associated microRNA signature by targeting ITGA5, ROCK1,PIK3CA, NRAS and CSF1. FASEB J. 27 (3). 1223-35.
50. Colley H. E., Hearnden V., Jones A. V., Weinreb P. H., Violette S. M., *et al*. (2011). Development of tissue-engineered models of oral dysplasia and early invasive oral squamous cell carcinoma. British Journal of Cancer. 105: 1582-1592.
51. Coppe J. P., Kauser K., Campisi J., and Beausejour C. M. (2006). Secretion of vascular endothelial growth factor by primary human fibroblasts at senescence. J Biol Chem. United States.
52. Coppe J. P., Boysen M., Sun C. H., Wong B. J., Kang M. K., *et al*. (2008a). A role for fibroblasts in mediating the effects of tobacco-induced epithelial cell growth and invasion. Mol Cancer Res. United States.
53. Coppe J. P., Patil C. K., Rodier F., Sun Y., Munoz D. P., *et al*. (2008b). Senescence-associated secretory phenotypes reveal cell-nonautonomous functions of oncogenic RAS and the p53 tumor suppressor. PLoS Biol. United States.
54. Coppe J. P., Patil C. K., Rodier F., Krtolica A., Beausejour C. M., *et al*. (2010). A human-like senescence-associated secretory phenotype is conserved in mouse cells dependent on physiological oxygen. PLoS One, 5, e9188.
55. Coppe J. P., Rodier F., Patil C. K., Freund A., Desprez P. Y., *et al*. (2011). Tumor suppressor and aging biomarker p16(INK4a) induces cellular senescence without the associated inflammatory secretory phenotype. J Biol Chem. United States.
56. Costea D.E., Hills A., Osman H.A., *et al*. (2013). Identification of two distinct carcinoma-associated fibroblast subtypes with differential tumour-promoting abilities in oral squamous cell carcinoma. Cancer Research.
57. Cuk K., Zucknick M., Heil J., Madhavan D., Schott S., *et al*. (2012). Circulating microRNAs in plasma as early detection markers for breast cancer. Int J Cancer. 132(7):1602-12.
58. da Costa A. A., D'Almeida Costa F., Ribeiro A. R., Guimaraes A. P., Chinen L. T., *et al*. (2014). Low PTEN expression is associated with worse overall survival

in head and neck squamous cell carcinoma patients treated with chemotherapy cetuximab. Int J Clin Oncol.

59. Dalwadi H., Krysan K., Heuze-Vourc'h N., Dohadwala M., Elashoff D., *et al*. (2005). Cyclooxygenase-2-Dependent Activation of Signal Transducer and Activator of Transcription 3 by Interleukin-6 in Non-Small Cell Lung Cancer. Clin Cancer Res. 11(21):7624-7682.
60. Daigneault M., Preston J. A., Marriott H. M., Whyte M. K. B. and Dockrell D. H. (2010). The identification of markers of macrophage differentiation in PMA-stimulated THP-1 cells and monocyte-derived macrophages. PLoS ONE. 5(1):e8668.
61. Davalos A. R., Coppe J. P., Campisi J., and Desprez P. Y. (2010). Senescent cells as a source of inflammatory factors for tumor progression. Cancer Metastasis Rev, 29, 273-83.
62. De-Assis E. M., Pimenta L. G. G. S., Costea-e-Silva E., Souza P. E. A. and Horta M. C. R. (2012). Stromal myofibroblasts in oral leukoplakia and oral squamous cell carcinoma. Med Oral Patol Oral Cir Bucal. 17(5):e733-e738.
63. Dhabi J. M., Atamna H., Boffelli D., Magis W., Spindler S. R., *et al*. (2011). Deep sequencing reveals novel microRNAs and regulation of microRNA expression during cell senescence. PLoS One. United States.
64. Dilley T. K., Bowden G. T. and Chen Q. M. (2003). Novel mechanisms of sublethal oxidant toxicity: induction of premature senescence in human fibroblasts confers tumor promoter activity. Exp Cell Res. 290(1):38-48.
65. Dimri G. P., Lee X., Basile G., Acosta M., Scott G., *et al*. (1995). A biomarker that identifies senescent human cells in culture and in aging skin in vivo. Proc Natl Acad Sci U S A, 92, 9363-7.
66. di Val Cervo P. R., Lena A. M., Nicoloso M., Rossi S., Mancini M., *et al*. (2012). P63-microRNA feedback in keratinocyte senescence. PNAS. 109(4): 1133-1138.
67. Elenbaas B. and Weinberg R. A. (2001). Heterotypic signaling between epithelial tumor cells and fibroblasts in carcinoma formation. Experimental Cell Research. 264: 169-184.
68. Ehrlich H. P. (1988). The modulation of contraction of fibroblast populated collagen lattices by types I, II and III collagen. Tissue Cell. 20(1):47-50.
69. Elbashir S. M., Lendeckel W. and Tuschl T. (2001). RNA interference is mediated by 21-and 22-nucleotide RNAs. Genes and Development. 15: 188-200.

70. Eulalio A., Behm-Ansmant I., Schweizer D., *et al*. (2007). P-body formation is a consequence, not the cause, of RNA-mediated gene silencing. Molecular and Cellular Biology. 27:3970-3981.
71. Ewald J., Desotelle J., Almassi N., and Jarrard D. (2008). Drug-induced senescence bystander proliferation in prostate cancer cells in vitro and in vivo. Br J Cancer. England.
72. Fabian M. R., Sonenberg N., and Filipowicz W. (2010). Regulation of mRNA translation and stability by microRNAs. The Annual Review of Biochemistry.79, 351-379.
73. Fahey M. S., Paterson I. C., Stone A., Collier A. J., Heung Y. L. M., *et al*. (1996). Dysregulation of autocrine TGF-β isoform production and ligand responses in human tumour-derived and Ha-ras-transfected keratinocytes and fibroblasts. British Journal of Cancer. 74:1074-1080.
74. Faraonio R., Salerno P., Passaro F., Sedia C., Iaccio A., *et al*. (2012). A set of miRNAs participates in the cellular senescence program in human diploid fibroblasts. Cell death and differentiation. 19:713-721.
75. Farr A. and Roman A. (1992). A pitfall of using a second plasmid to determine transfection efficiency. Nucleic Acids Res. 20: 920.
76. Ferreira F. O., Ribeiro F. L., Batista A. C., Leles C. R., de Cassia Goncalves Alencar R., *et al*. (2008). Association of CCL2 with lymph node metastasis and macrophage infiltration in oral cavity and lip squamous cell carcinoma. Tumour Biol. 29 (2):114-21.
77. Franks T. M and Lykke-Andersen J. (2008). The control of mRNA decapping and P-body formation. Mol Cell. 32(5):605-615.
78. Freund A., Patil C. K., and Campisi J. (2011). p38MAPK is a novel DNA damage response-independent regulator of the senescence-associated secretory phenotype. EMBO J. England.
79. Friedman D. B., and Johnson T. E. (1988). A mutation in the age-1 gene in *Caenorhabditis elegans* lengthens life and reduces hermaphrodite fertility. Genetics. 118:75-86.
80. Gao Y., Zeng F., Wu J. Y., Li H. Y. Fan J. J. (2014). miR-335 inhibits migration of breast cancer cells through targeting oncoprotein c-Met. Tumour Biol.
81. Giannoni E., Bianchini F., Masieri L., *et al*. (2010). Reciprocal activation of cancer cells and cancer-associated fibroblasts stimulates epithelial-mesenchymal transition and cancer stemness. Cancer Res. 70 (17):6945-6956.

82. Ginhoux F., and Jung S. (2014). Monocytes and macrophages: Developmental pathways and tissue homeostasis. Nature Reviews. 14:392-404.
83. Gomez-Cabello D., Adrados I., Gamarra D., Kobayashi H., Takatsu Y., *et al*. (2013). DGCR8-mediated disruption of miRNA biogenesis induces cellular senescence in primary fibroblasts. Aging Cell. 12: 923-931.
84. Gorgoulis V. G., Vassiliou L. V., Karakaidos P., Zacharatos P., Kotsinas A., *et al*. (2005). Activation of the DNA damage checkpoint and genomic instability in human precancerous lesions. Nature. 434:907-13.
85. Greene S. B., Gunaratne P. H., Hammond S. M. and Rosen J. M. (2010). A putative role for microRNA-205 in mammary epithelial cell progenitors. Journal of Cell Science. 123(4): 606-618.
86. Guo G. E., Ma L. W., Jiang B., Yi J., Tong T. J., *et al*. (2010). Hydrogen peroxide induces p16(INK4a) through AUF1-dependent manner. J Cell Biochem. 109(5): 1000-5.
87. Hacke K., Rincon-Orozco B., Buchwalter G., Siehler S. Y., Wasylyk B., *et al*. (2010). Regulation of MCP-1 chemokine transcription by p53. Molecular Cancer. 9:82.
88. Hackl M., Brunner S., Fortschegger K., Schreiner C., Micutkova L., *et al*., (2010). miR-17, miR-19b, miR-20a, and ,iR-106a are down-regulated in human aging. Aging Cell. 9:291-296.
89. Hartog C. M., Wermelt J. A., Sommerfeld C. O., Eichler W., Dalhoff K., *et al*. (2003). Pulmonary matrix metalloproteinase excess in hospital-acquired pneumonia. Am J Respir Crit Care Med. United States.
90. Hase T., Kawashiri S., Tanaka A., Nozaki S., Noguchi N., *et al*. (2006). Correlation of basic fibroblast growth factor expression with the invasion and the prognosis of oral squamous cell carcinoma. J Oral Pathol. 35(3):136-9.
91. Hassona Y., Cirillo N., Lim K.P., Herman A., Mellone M., *et al*. (2013). Progression of genotype-specific oral cancer leads to senescence of cancer-associated fibroblasts and is mediated by oxidative stress and TGF-b. Carcinogenesis.
92. Hassona Y., Cirillo N., Heesom K., Parkinson E. K. and Prime S. S. (2014). Senescent cancer-associated fibroblasts secrete active MMP-2 that promotes keratinocyte dis-cohesion and invasion. Br J Cancer. 111(6):1230-7.
93. Hayflick L. (1995). The limited in vitro lifetime of human diploid cell strains. Exp Cell Res, 37, 614-36.
94. Hayward S. W., Wang Y., Cao M., *et al*. (2001). Malignant transformation in

nontumorigenic human prostatic epithelial cell line. Cancer Res. 61:8135-8142.

95. He X., He L. and Hannon G. J. (2007). The Guardian's Little Helper: MicroRNAs in the p53 tumour suppressor network. Cancer Res. 67:11099-11101.
96. He K-F., Zhang L., Huang C-F., Ma S-R., Wang Y-F., *et al*. (2014a). CD163+ tumour-associated macrophages correlated with poor prognosis and cancer stem cells in oral squamous cell carcinoma. BioMed Research International. 1-9.
97. He X, Cao Y, Wang L, Han Y, Zhong X, *et al*. (2014b) Human Fibroblast Reprogramming to Pluripotent Stem Cells Regulated by the miR19a/b-PTEN Axis. PLoS ONE 9(4): e95213.
98. Hedback N., Jensen D. H., Specht L., Fiehn A-M. K., Therkildsen M. H., *et al*. (2014). MiR-21 expression in the tumor stroma of oral squamous cell carcinoma: An independent biomarker of disease free survival. PLoS ONE. 9 (4):e95193.
99. Hinsley E. E., Hunt S., Hunter K. D., Whawell S. A. and Lambert D. W. (2012). Endothelin-1 stimulates motility of head and neck squamous cell carcinoma cells by promoting stromal-epithelial interactions. Int J Cancer. 130(1):40-7.
100. Huang Y., Chuang A., Hao H., Talbot C., Sen T., *et al*. (2011). Phospho-ΔNp63α is a key regulator of the cisplatin-induced microRNAome in cancer cells. Cell Death Differ. 18(7):1220-30.
101. Humphreys D. T., Westman B. J., Martin D. I. K., *et al*. (2005). MicroRNAs control translation initiation by inhibiting eukaryotic initiation factor 4E/cap and poly(A) tail function. PNAS. 102: 16961-16966.
102. Iliopoulos D., Jaeger S. A., Hirsch H. A., Bulyk M. L. and Struhl K. (2010). STAT3 activation of miR-21 and miR-181b-1 via PTEN and CYCLD are part of the epigenetic switch linking inflammation to cancer. Mol Cell. 39 (4): 493-506.
103. Jethwa P., Naqvi M., Hardy R. G., Hotchin N. A., Roberts S., *et al*. (2008). Overexpression of Slug is associated with malignant progression of esophageal adenocarcinoma. World J Gastroenterol. 14(7):1044-1052.
104. Ji W-T., Chen H-R., Lin C-H., Lee J-W., Lee C-C., *et al*. (2014). Monocyte chemotactic protein 1 (MCP-1) modulates pro-survival signaling to promotes progression of head and neck squamous cell carcinoma. PLoS ONE. 9(2):e88952.
105. Jin Y., Chen D., Cabay R. J., Wang A., Crowe D. L., *et al*. (2013). Role of microRNA-138 as a Potential Tumor Suppressor in Head and Neck Squamous Cell Carcinoma. Int Rev Cell Mol Biol. 303:357-385.
106. Jun J. I., and Lau L. F. (2010). The matricellular protein CCN1 induces

fibroblast senescence and restricts fibrosis in cutaneous wound healing. Nat Cell Biol. 12, 676-85.

107. Kadera BE, Li L, Toste PA, Wu N, Adams C, *et al*. (2013) MicroRNA-21 in Pancreatic Ductal Adenocarcinoma Tumor-Associated Fibroblasts Promotes Metastasis. PLoS ONE 8(8): e71978. doi:10.1371/journal.pone.0071978

108. Kalluri R. and Zeisberg M. (2006). Fibroblasts in cancer. Nature Reviews. 6:392-401.

109. Kang J., Chen W., Xia J., Li Y., Yang B., *et al*. (2008). Extracellular matrix secreted by senescent fibroblasts induced by UVB promotes cell proliferation in HaCaT cells through PI3K/AKT and ERK signaling pathways. Int J Mol Med, 21, 777-84.

110. Kato M., Putta S., Wang M., Yuan H., Lanting L., *et al*. (2009). TGF-β activates Akt kinase via a microRNA-dependent amplifying circuit targeting PTEN. Nat Cell Biol. 11 (7):881-889.

111. Kawashiri S., Tanaka A., Noguchi N., Hase T., Nakaya H., *et al*. (2009). Significance of stromal desmoplasia and myofibroblast appearance at the invasive front in squamous cell carcinoma of the oral cavity. Head Neck. 10: 1346-53.

112. Kenyon C. J. (2010). The genetics of ageing. Nature. 464 (7288):504-512.

113. Kim S. R., Jung H. P., Mi E. L., Jeong S. P., Sang C. P. *et al*. (2008). Selective COX-2 inhibitors modulate cellular senescence in human dermal fibroblasts in a catalytic activity-independent manner. Mechanisms of Ageing and Development. 129: 706-713.

114. Kim V. N., Han J., and Siomi M. C. (2009). Biogenesis of small RNAs in animals.Nature Reviews, Molecular Cell Biology.10, 126-139.

115. Kim H. J., Ham S. A., Kim M. Y., Hwang J. S., Lee H., *et al*. (2011). PPARδ coordinates angiotensin II-induced senescence in vascular smooth muscle cells through PTEN-mediated inhibition of superoxide generation. J Biol Chem. 286(52):44585-93.

116. Koide S., Okazaki M., Tamura M., Ozumi K., Takatsu H., *et al*. (2007). PTEN reduces cuff-induced neointima formation and pro-inflammatory cytokines. Am J Physiol Heart Circ Physiol. 292:H2824-H2831.

117. Kojima Y., Acar A., Eaton E. N., Mellody K. T., Scheel C., *et al*. (2010). Autocrine TGF-β and stromal cell-derived factor-1 (SDF-1) signaling drives the evolution of tumor-promoting mammary stromal myofibroblasts. PNAS. 107(46):

20009-20014.

118. Kortlever R. M., Higgins P. J. and Bernards R. (2006). Plasminogen activator inhibitor -1 is a critical downstream target of p53 in the induction of replicative senescence. Nat Cell Biol. 8(8):877-884.

119. Krizhanovsky V., Yon M., Dickins R. A., Hearn S., Simon J., *et al*. (2008). Senescence of activated stellate cells limits liver fibrosis. Cell. United States.

120. Krtolica A., Parrinello S., Lockett S., Desprez P. Y., and Campisi J. (2001). Senescent fibroblasts promote epithelial cell growth and tumorigenesis: a link between cancer and aging. Proc Natl Acad Sci U S A. United States.

121. Kurose K., Gilley K., Matsumoto S., Watson P. H., Zhou X-P., *et al*. (2002). Frequent somatic mutations in *PTEN* and TP53 are mutually exclusive in the stroma of breast carcinomas. Nature Genetics. 32: 355-357.

122. Kurtova A. V., Xiao J., Mo Q., Pazhanisamy S., Krasnow R., *et al*. (2014). Blocking PGE2-induced tumour repopulation abrogates bladder cancer chemoresistance. Nature. 517(7533):209-13.

123. Kurz D. J., Decary S., Hong Y. and Erusalimsky J. D. (2000). Senescence-associated (beta)-galactosidase reflects an increase in lysosomal mass during replicative ageing of human endothelial cells. J Cell Sci. 113(Pt 20):3613-22.

124. Krishna D. R., Sperker B., Fritz P. and Klotz U (1999). Does pH 6 beta-galactosidase activity indicate cell senescence? Mech Ageing Dev. 109(2):113-23.

125. Krysan K., Kusko R., Grogan T., O'Hearn J., Reckamp K. L., *et al*. (2014). PGE2-driven expression of c-Myc and OncomiR-17-92 contributes to apoptosis resistance in NSCLC. Mol Cancer Res. 12(5): 765-774.

126. Kuilman T., Michaloglou C., Vredeveld L. C., Douma S., van Doom R., *et al*. (2008). Oncogene-induced senescence relayed by an interleukin-dependent inflammatory network. Cell. 133(6):1019-31.

127. Laberge R. M., Awad P., Campisi J., and Desprez P. Y. (2012). Epithelial-mesenchymal transition induced by senescent fibroblasts. Cancer Microenviron, 5, 39-44.

128. Lakowski B., and Hekimi S. (1996). Determination of life-span in *Caenorhabditis elegans* by four clock genes. Science. 272 (5264): 1010-3.

129. Lawrenson K., Grun B., Benjamin E., Jacobs I. J., Dafou D., *et al*. (2010). Senescent fibroblasts promote neoplastic transformation of partially

transformed ovarian epithelial cells in a three-dimensional model of early stage ovarian cancer. Neoplasia, 12, 317-25.

130. Lee B. Y., Han J. A., Im J. S., Morrone A., Johung K., *et al*. (2006). Senescene-associated beta-galactosidase is lysosomal beta-galactosidase. Aging Cell. 5(2):187-95.

131. Lee J-J, Kim B. B., Park M-J., Lee Y-S., Kim Y-N., *et al*. (2011). PTEN status switches cell fate between premature senescence and apoptosis in glioma exposed to ionizing radiation. Cell Death and Differntiation. 18: 667-677.

132. Lee M. E., Kim S. R., Lee S., Jung Y-J., Choi S., S, *et al*. (2012). Cyclooxygenase-2 inhibitors modulate skin aging in a catalytic activity-independent manner. Experimental and Molecular Medicine. 44 (9):536-544.

133. Li G., Robinson G. W., Lesche R., Martinez-Diaz H., Jiang Z., *et al*. (2002). Conditional loss of PTEN leads to precocious development and neoplasia in the mammary gland. Development. 129: 4159-4170.

134. Li X., Wu Z., Fu X. and Han W. (2012). A microRNA component of the neoplastic microenvironment: Microregulators with far-reaching impact. BioMed Research International. 2013: 1-7.

135. Li C., Bai Y., Liu H., Zuo X., Yao H. *et al*. (2013a). Comparative study of microRNA profiling in keloid fibroblast and annotation of differential expressed microRNAs. Acta Biochim Biophys. 45:692-699.

136. Li M., Knight D. A., Snyder L. A., Smyth M. J. and Stewart T. J. (2013b). A role for CCL2 in both tumor progression and Immunosurveillance. Oncoimmunology. 2(7):e25474.

137. Li X., Xu Q., Wu Y., Li J., Tang D. *et al*. (2014). A CCL2/ROS autoregulation loop is critical for cancer-associated fibroblasts-enhanced tumor growth of oral squamous cell carcinoma. Carcinogenesis. 35(6): 1362-1370.

138. Lim K. P., Cirillo N., Hassona Y., Wei W., Thurlow J. K. , *et al*. (2011). Fibroblast gene expression profile reflects the stage of tumour progression in oral squamous cell carcinoma. J Pathol. 223(4):459-69.

139. Liu D., and Hornsby P. J. (2007a). Fibroblast stimulation of blood vessel development and cancer cell invasion in a subrenal capsule xenograft model: stress-induced premature senescence does not increase effect. Neoplasia, 9, 418-26.

140. Liu D., and Hornsby P. J. (2007b). Senescent human fibroblasts increase the early growth of xenograft tumors via matrix metalloproteinase secretion. Cancer Res. United States.

141. Liu Z., Lu C. L., Cui L. P., Hu Y. L., Yu Q., *et al*. (2012). MicroRNA-146a modulates TGF-beta1-induced phenotypic differentiation in human dermal fibroblasts by targeting SMAD4. Arch Dermatol Res, 304, 195-202.

142. Liu Y., Wang X., Yang D., Xiao Z. and Chen X. (2013). MicroRNA-21 affects proliferation and apoptosis by regulating expression of PTEN in human keloid fibroblasts. Plastic and reconstructive surgery. 134 (4): 561e-573e.

143. Liu G. L., Liu X., Lv X.B., Wang X. P., Fang X. S., *et al*. (2014). miR-148b functions as a tumor suppressor in non-small cell lung cancer by targeting carcinoembryonic antigen (CEA). Int J Clin Exp Med. 15(7): 1990-9.

144. Lujambio A., Akkari L., Simon J., Grace D., Tschaharganeh D. F., *et al*. (2013). Non-cell-autonomous tumour suppression by p53. Cell. 153(2): 449-60.

145. Maes O. C., Sarojini H., and Wang E. (2009). Stepwise up-regulation of microRNA expression levels from replicating to reversible and irreversible growth arrest states in WI-38 human fibroblasts. J Cell Physiol, 221, 109-19.

146. Maffini M. V., Soto A. M., Calabro J. M., Ucci A. A. and Sonnenschein C. (2003). The stroma as a crucial target in rat mammary gland carcinogenesis. Journal of Cell Science. 117(8):1495-1502.

147. Mallette F. A., Calabrese V., Ilangumaran S. and Ferbeyre G. (2010). SOCS1, a novel interaction partner of p53 controlling oncogene-induced senescence. Aging. 2(7):445-52.

148. Mancini M., Saintigny G., Mahe C., Annicchiarico-Petruzzalli M., Melino G. *et al*. (2012). MicroRNA-152 and -181a participate in human dermal fibroblasts senescence acting on cell adhesion and remodeling of the extracellular matrix. Aging. 4 (11): 843-853.

149. Marsh D., Suchak K., Moutasim K. A., Vallath S., Hopper C., *et al*. (2011). Stromal features are predictive of disease mortality in oral cancer patients. J Pathol. 223(4):470-81.

150. Martein S., Pluquet O., Vercamer C., Malaquin N., Martin N., *et al*. (2013). Cellular senescence involves an intracrine prostaglandin E2 pathway in human fibroblasts. Biochimica et Biophysica Acta. 1831: 1217-1227.

151. Micalizzi D. S., Farabaugh S. M. and Ford H. L. (2010). Epithelial-mesenchymal transition in cancer: Parallels between normal development and tumour progression. J Mammary Gland Biol Neoplasia. 15:117-134.

152. Morreau H., Galjart N. J., Gillemans N., Willemsen R., van der Horst G. T., *et al*. (1989). Alternative splicing of beta-galactosidase mRNA generates the classic lysosomal enzyme and a beta-galactosidase-related protein. J Biol

Chem. 264(34): 20655-63.

153. Mudhasani R., Zhu Z. Q., Hutvagner G., Eischen C. M., Lyle S., *et al*. (2008). Loss of miRNA biogenesis induces p19(Arf)-p53 signaling and senescence inprimary cells. J Cell Biol. 181:1055-1063.

154. Munoz-Espin D., Canamero M., Maraver A., Gomez-Lopez G., Contreras J., *et al*. (2013). Programmed cell senescence during mammalian embryonic development. Cell. 155(5):1104-18.

155. Murphy C. T., McCarroll S. A., Bargmann C. I., Fraser A., Kamath R. S. *et al*. (2003). Genes that act downstream of DAF-16 to influence the life span of *Caenorhabditis elegans*. Nature. 424(6946):277-83.

156. Murray L. A., Argentieri R. L., Farrell F. X., Bracht M., Sheng H., *et al*. (2008). Hyper-responsiveness of IPF/UIP fibroblasts: Interplay between TGFβ1, IL-13 and CCL2. The International Journal of Biochemistry and Cell Biology. 40: 2174-2182.

157. Musumeci M., Coppola V., Addario A., Patrizii M., Maugeri-Sacca M., *et al*. (2011). Control of tumor and microenvironment cross-talk by miR-15a and miR-16 in prostate cancer. Oncogene. 30 (14): 4231-42.

158. Naito Y., Sakamoto N., Oue N., Yashiro M., Sentani K., *et al*. (2014a). MicroRNA-143 regulates collagen type III expression in stromal fibroblasts of scirrhous type gastric cancer. Cancer Sci. 105(2):228-35.

159. Naito Y., Yasuno K., Tagawa H., Sakamoto N., Oue N., *et al*. (2014b). MicroRNA-145 is a potential prognostic factor of scirrhous type gastric cancer. Oncol Rep. 32(4):1720-6.

160. Nichols A. C., Yoo J., Palma D. A., Fung K., Franklin J. H., *et al*. (2012). Frequent mutatios in TP53 and CDKN2A found by next-generation sequencing of head and neck cancer cell lines. 138(8):732-739.

161. Ohuchida K., Mizumoto K., Murakami M., Qian L. W., Sato N., *et al*. (2004). Radiation to stromal fibroblasts increases invasiveness of pancreatic cancer cells through tumor-stromal interactions. Cancer Res, 64, 3215-22.

162. Olumi A. F., Grossfeld G. D., Hayward S. W., Carroll P. R., Tlsty T. D., *et al*. (1999). Carcinoma-associated fibroblasts direct tumor progression of initiated human prostatic epithelium. Cancer Res, 59, 5002-11.

163. Orimo A., Gupta P. B., Sgroi D. C., Arenzana-Seisdedos F., Delaunay T., *et al*. (2005). Stromal fibroblasts present in invasive human breast carcinomas promote tumor growth and angiogenesis through elevated SDF-1/CXCL12 secretion. Cell. United States.

164. Orimo A., and Weinberg R. A. (2006). Stromal fibroblasts in cancer: a novel tumor-promoting cell type. Cell Cycle. United States.

165. Overhoff M. G., Garbe J. C., Koh J., Stampfer M. R., Beach D. H., *et al*. (2013). Cellular senescence mediated by $p16^{INK4a}$ –coupled miRNA pathway. Nucleic Acids Research. 42(3):1606-1618.

166. Ou D. L., Chien H. F., Chen C. L., Lin T. C., Lin L. I. (2008). Role of Twist in head and neck carcinoma with lymph node metastasis. Anticancer Res. 28 (2B): 1355-9.

167. Ou Y. H., Torres M., Ram R., Formstecher E., Roland C., *et al*. (2011). TBK1 directly engages Akt/PKB survival signaling to support oncogenic transformation. Mol Cell. 41 (4): 458-70.

168. Pal A., Melling G., Hinsley E. E., Kabir T. D., Colley H. E., *et al*. (2012). Cigarette smoke condensate promotes pro-tumourigenic stromal-epithelial interactions by suppressing miR-145. J Oral Pathol Med. 42 (4): 309-14.

169. Pandey M., Prakash O., Santhi W. S., Soumithran C. S. and Pillai R. M. (2008). Overexpression of COX-2 gene in oral cancer is independent of stage of disease and degree of differentiation. Int. J. Oral Maxillofac. Surg. 37: 379-383.

170. Paradis V., Youssef N., Dargere D., Ba N., Bonvoust F., *et al*. (2001). Replicative senescence in normal liver, chronic hepatitis C, and hepatocellular carcinomas. Hum Pathol. United States: 2001 by W.B. Saunders Company.

171. Parapuram S.K., Shi-wen X., Elliott C., Welch I.D., Jones H., *et al*. (2011). Loss of PTEN expression by dermal fibroblasts causes skin fibrosis. Journal of Investigative Dermatology. 131: 1996-2003.

172. Park S. I., Liao J., Berry J. E., Li X., Koh A. J., *et al*. (2012). Cyclophosphamide creates a receptive microenvironment for prostate cancer skeletal metastasis. Cancer Res. 72(10):2522-32.

173. Parrinello S., Coppe J. P., Krtolica A., and Campisi J. (2005). Stromal-epithelial interactions in aging and cancer: senescent fibroblasts alter epithelial cell differentiation. J Cell Sci. England.

174. Pazolli E., Luo X., Brehm S., Carbery K., Chung J. K., *et al*. (2009). Senescent stromal-derived osteopontin promotes preneoplastic cell growth. Cancer Res. United States.

175. Pazolli E., Alspach E., Milczarek A., Prior J., Piwnica-Worms D., *et al*. (2012). Chromatin remodeling underlies the senescence-associated secretory

phenotype of tumor stromal fibroblasts that supports cancer progression. Cancer Res. 72(9): 2251-2261.

176. Peng Q, Zhao L, Hou Y, Sun Y, Wang L, *et al*. (2013) Biological Characteristics and Genetic Heterogeneity between Carcinoma-Associated Fibroblasts and Their Paired Normal Fibroblasts in Human Breast Cancer. PLoS ONE 8(4): e60321. doi:10.1371/journal.pone.0060321

177. Perren A., Weng L-P., Boag A. H., Ziebold U., Thakore K., *et al*. (1999). Immunohistochemistry evidence of loss of PTEN expression in primary ductal adenocarcinomas of the breast. Am. J. Pathol. 155(4):1253-1260.

178. Poligone B. and Baldwin A. S. (2001). Positive and negative regulation of NFκB by COX-2. The Journal of Biological Chemistry. 276(42): 38658-38664.

179. Picard O., Rolland Y., and Poupon M. F. (1986). Fibroblast-dependent tumorigenicity of cells in nude mice: implication for implantation of metastases. Cancer Res, 46, 3290-4.

180. Pitiyage G. N., Slijepcevic P., Garbani A., Chianea Y. G., Lim K. P., *et al*. (2011). Senescent mesenchymal cells accumulate in human fibrosis by a telomere-independent mechanism and ameliorate fibrosis through matrix metalloproteinases. J Pathol, 223, 604-17.

181. Prime S. S., Nixon S. V., Crane I. J., Stone A., Matthews J. B. *et al*. (1990). The behaviour of human oral squamous cell carcinoma in cell culture. J Pathol. 160 (3):259-269.

182. Qiao B., Johnson N. W. and Gao J. (2010). Epithelial-mesenchymal transition in oral squamous cell carcinoma triggered by transforming growth factor-β1 is Snail family-dependent and correlates with matrix metalloproteinase-2 and -9 expressions. International Journal of Oncology. 37:663-668.

183. Ramos D.M., Chen B. L., Boylen K., Stern M., Kramer R. H., *et al*. (1997). Stromal fibroblasts influence oral squamous-cell carcinoma cell interactions with tenascin-C. Int. J. Cancer. 72: 369-376.

184. Rasanen K., Virtanen I., Salmenpera P., Grenman R. and Vaheri A. (2009). Differences in the nemosis response of normal and cancer-associated fibroblasts from patients with oral squamous cell carcinoma. PLoS One. 4(9): e6879.

185. Roberson R. S., Kussick S. J., Vallieres E., Chen S. Y., and Wu D. Y. (2005). Escape from therapy-induced accelerated cellular senescence in p53-null lung cancer cells and in human lung cancers. Cancer Res. 65(7):2795-803.

186. Rodier F., Coppe J. P., Patil C. K., Hoeijmakers W. A., Munoz D. P., *et al*. (2009). Persistent DNA damage signalling triggers senescence-associated inflammatory cytokine secretion. Nat Cell Biol. 11(8):973-9.

187. Roninson I. B. (2002). Oncogenic functions of tumour suppressor p21(Waf1/Cip1/Sdi1): association with cell senescence and tumour-promoting activities of stromal fibroblasts. Cancer Lett. 179(1):1-14.

188. Rheinwald J. G. and Beckett M. A. (1981). Tumorigenic keratinocyte lines requiring anchorage and fibroblast support cultured from human squamous cell carcinomas. Cancer Res. 41: 1657-1663.

189. Sagana R. L., Yan M., Cornett A. M., Tsui J. L., Stephenson D. A., *et al*. (2009). Phosphatase and tensin homologue on chromosome 10 (PTEN) directs prostaglandin E2-mediated fibroblast response via regulation of E prostanoid 2 receptor expression. J Biol Chem. 284 (47): 32264-71.

190. Scarola M., Schoeftner S., Schneider C. and Benetti R. (2010). miR-335 directly targets Rb1 (pRb/p105) in a proximal connection to p53-dependent stress response. Cancer Res. 70 (17):6925-33.

191. SCHWARZE, S. R., FU, V. X., DESOTELLE, J. A., KENOWSKI, M. L. & JARRARD, D. F. (2005). The identification of senescence-specific genes during the induction of senescence in prostate cancer cells. Neoplasia, 7, 816-23.

192. Schor S. L., Schor A. M., Grey A. M. and Rushton G. (1988). Foetal and cancer patient fibroblasts produce an autocrine migration-stimulating factor not made by normal adult cells. J Cell Sci. 90(Pt 3): 391-0.

193. Shah P. P., Donahue G., Otte G. L., Capell B. C., Nelson D. M., *et al*. (2013). Lamin B1 depletion in senescent cells triggers large-scale changes in gene expression and chromatin landscape. Genes & Development. 27:1787-1799.

194. Shen J., Hu Q., Schrauder M., Yan L., Wang D., *et al*. (2014). Circulating miR-148b and miR-133a as biomarkers for breast cancer detection. Oncotarget. 5(14):5284-94.

195. Siddik Z. H. (2003). Cisplatin: mode of cytotoxic action and molecular basis of resistance. Oncogene. 22: 7265-7279.

196. Sica A., Larghi P., Mancino A., Rubino L., Porta C., *et al*. (2008). Macrophage polarization in tumour progression. Seminars in Cancer Biology. 18(5): 349-355.

197. Smith-Vikos T. and Slack F. J. (2012). MicroRNAs and their roles in aging. J Cell Sci. 125(Pt 1):7-17.

198. Smith A., Teknos T. N. and Pan Q. (2013). Epithelial to messenchymal transition in head and neck squamous cell carcinoma. Oral Oncol. 49(4):287-292.

199. Snietura M, Jaworska M, Mlynarczyk-Liszka J, Goraj-Zajac A, Piglowski W, *et al*. (2012) PTEN as a Prognostic and Predictive Marker in Postoperative Radiotherapy for Squamous Cell Cancer of the Head and Neck. PLoS ONE 7(3): e33396. doi:10.1371/journal.pone.0033396

200. Sohn JJ, Schetter AJ, Yfantis HG, Ridnour LA, Horikawa I, *et al*. (2012) Macrophages, Nitric Oxide and microRNAs Are Associated with DNA Damage Response Pathway and Senescence in Inflammatory Bowel Disease. PLoS ONE 7(9): e44156. doi:10.1371/journal.pone.0044156

201. Storer M., Mas A., Robert-Moreno A., Pecoraro M., Ortells M. C., *et al*. (2013). Senescence is a developmental mechanism that contributes to embryonic growth and patterning. Cell. 155(5): 1119-30.

202. Sugimoto H., Mundel T. M., Kieran M. W., and Kalluri R. (2006). Identification of fibroblast heterogeneity in the tumor microenvironment. Cancer Biol Ther. 5(12): 1640-6.

203. Sun F., Fu H., Liu Q., Tie Y., Zhu J., *et al*. (2008). Downregulation of CCND1 and CDK6 by miR-34a induces cell cycle arrest. FEBS Lett. 582:1564-1568.

204. Sun Y., Campisi J., Higano C., Beer T. M., Porter P., *et al*. (2012). Treatment-induced damage to the tmor microenvironment promotes prostrate cancer therapy resistance through WNT16B. Nature Medicine. 18: 1359-1368.

205. Suwan K., Choocheep K., Hatano S., Kongtawelert P., Kimata K., *et al*. (2009). Versican/PG-M assembles hyaluronan into extracellular matrix and inhibits CD44-mediated signaling toward premature senescence in embryonic fibroblasts. J Biol Chem. 284(13):8596-604.

206. Taddei M. L., Cavallini L., Comito G., Giannoni E., Folini M., *et al*. (2014). Senescent stroma promotes prostrate cancer progression: The role of miR-210. Mol Oncol. 8(8): 1729-46.

207. Takeuchi S., Takahashi A., Motoi N., Yoshimoto S., Tajima T., *et al*. (2010). Intrinsic cooperation between p16INK4a and p21Waf1/Cip1 in the onset of cellular senescence and tumor suppression in vivo. Cancer Res. 70(22):9381-90.

208. Te Poele R. H., Okorokov A. L., Jardine L., Cummings J., and Joel S. P. (2002). DNA damage is able to induce senescence in tumor cells in vitro and in

vivo. Cancer Res, 62, 1876-83.

209. Tissenbaum H. A., and Ruvkun G. (1998). An insulin-like signaling pathway affects both longevity and reproduction in *Caenorhabditis elegans*. Genetics. 148(2): 703-17.

210. Tome M., Sepulveda J. C., Delgado M., Andrades J. A., Campisi J., *et al*. (2014). miR-335 correlates with senescence/aging in human messenchymal stem cells and inhibits their therapeutic actions through AP-1 activity. Stem Cells. 32 (8): 2229-44.

211. Togo S., Polanska U. M., Horimoto Y. and Orimo A. (2013). Carcinoma-associated fibroblasts are a promising therapeutic target. Cancers (Basel). 5(1): 149-69.

212. Trimboli A.J., Fulkino K., de Bruin A., Wei G., Shen L., *et al*. (2008). Direct evidence for epithelial-messenchymal transitions in breast cancer. Cancer Res: 37:899-905.

213. Trimboli A.J., Cantemir-Stone C. Z., Li F., Wallace J. A., Merchant A., *et al*. (2009). Pten in stromal fibroblasts suppresses mammary epithelial tumours. Nature. 461(7267):1084-1091.

214. Ucar A., Vafaizadeh V., Jarry H., Fiedler J., Klemmt P. A., *et al*. (2010). miR-212 and miR-132 are required for epithelial stromal interactions necessary for mouse mammary gland development. Nat Genet. 42(12):1101-1108.

215. Varmeh S., Egia A., Mcgrouther D., Tahan S. R., Bayat A., *et al*. (2011). Cellular senescence as a possible mechanism for halting progression of keloid lesions. Genes Cancer. United States.

216. Vredevoe D. L., Widawski M., Fonarow G. C., Hamilton M., Martinez-Maza O., *et al*. (2004). Interleukin-6 (IL-6) expression and natural killer (NK) cell dysfunction and anergy in heart failure. Am J Cardiol. 93:1007-1011.

217. Wallace J.A., Li F., Leone G., *et al*. (2011). Pten in the breast tumour microenvironment: Modeling tumour-stroma coevolution. Cancer Res. 71:1203-1207.

218. Wajapeyee N., Serra R. W., Zhu X., Mahalingam M. and Green M. R. (2008). Oncogenic BRAF induces senescence and apoptosis through pathways mediated by the secreted protein IGFBP7. Cell. 132(3):363-74.

219. Wang M., Cheng Z., Tian T., Chen J., Dou F., *et al*. (2011a). Differential expression of oncogenic miRNAs in proliferating and senescent human fibroblasts. Mol Cell Biochem. 352:271-279.

220. Wang Y., Scheiber M. N., Neumann C., Calin G. A., and Zhou D.

(2011b). MicroRNA regulation of ionizing radiation-induced premature senescence. Int J Radiat Oncol Biol Phys. United States: 2011 Elsevier Inc.

221. Wang C., Bian Z. and Zhang J. G. (2011c). miR-29b regulates migration of human breast cancer cells. Mol Cell Biochem. 353(1-2):197-207.

222. Wang G., Cao X., Lai S., Luo X., Feng Y., *et al*. (2014). Altered p53 regulation of miR-148b and p55PIK contributes to tumor progression in colorectal cancer. Oncogene.

223. Waaijer M. E., Parish W. E., Strongitharm B. H., van Heemst D., Slagboom P. E., *et al*. (2012). The number of p16INK4a positive cells in human skin reflects biological age. Aging Cell. 11 (4): 722-5.

224. Wei J., Feng L., Li Z., Xu G. and Fan X. (2013). MicroRNA-21 activates hepatic stellate cells via PTEN/AKT signaling. Biomedicine & Pharmacotherapy. 67: 387-392.

225. West M. D., Pereira-Smith O. M. and Smith J. R. (1989). Replicative senescence of human skin fibroblasts correlates with a loss of regulation and overexpression of collagenase activity. Experimental Cell Research. 184: 138-147.

226. Westholm J. O. and Lai E. C. (2011). Mirtrons: microRNA biogenesis via splicing. Biochimie. 93(11): 1897-1904.

227. White E. S., Atrasz R. G., Hu B., Phan S. H., Stambolic V., *et al*. (2006). Negative regulation of myofibroblast differentiation by PTEN (Phosphatase and Tensin homolog deleted on chromosome 10). Am J Respir Crit Care Med. 173: 112-121.

228. Wiemann S. U., Satyanarayana A., Tsahuridu M., Tillmann H. L., Zender L., *et al*. (2002). Hepatocyte telomere shortening and senescence are general markers of human liver cirrhosis. The FASEB Journal. 16:935-942.

229. Wright W. E. , Pereira-Smith O. M. and Shay J. W. (1989). Reversible cellular senescence: Implications for immortalization of normal human diploid fibroblasts. Molecular and cellular biology.9: 3088-3092.

230. Wu L., Fan J. and Belasco J. G. (2006). MicroRNAs direct rapid deadenylation of mRNA. PNAS. 103, 4034-4039.

231. Wu M-H., Hong H-C., Hong T-M., Chiang W-F., Jin Y-T., *et al*. (2011). Targeting Galectin-1 in carcinoma-associated fibroblasts inhibits oral squamous cell carcinoma mestastasis by downregulating MCP-1/CCL2 expression. Clin Cancer Res. 17(6): 1306-1316.

232. Wu Y., Liu G. L., Liu S. H., Wang C. X., Xu Y. L., *et al*. (2012).

MicroRNA-148b enhances the radiosensitivity of non-Hodgkin's Lymphoma cells by promoting radiation-induced apoptosis. J Radiat Res. 53: 516-525.

233. Wutzl A., Ploder O., Kermer C., Millesi W., Ewers R., *et al*. (2007). Mortality and causes of death after multimodality treatment for advanced oral and oropharyngeal cancer. J Oral Maxillofac Surg. 65:255-260.

234. Xu D., Takeshita F., Hino Y., Fukunaga S., Kudo Y., *et al*. (2011). miR-22 represses cancer progression by inducing cellular senescence. J. Cell Biol. 193:409-424.

235. Yanagi S., Kishimoto H., Kawahara K., Sasaki T., Sasaki M., *et al*. (2007). Pten controls lung morphogenesis, bronchoalveolar stem cells, and onset of lung adenocarcinomas in mice. J. Clin. Invest. 117:2929-2940.

236. Yao Q., Cao S., Li C., Mengesha A., Kong B., *et al*. (2011). Micro-RNA 21 regulates TGF-β-induced myofibroblast differentiation by targeting PDCD4 in tumor-stroma interaction. Int. J. Cancer. 128. 1783-1792.

237. Yang T-S., Yang X-H., Chen X., Wang X-D., Hua J., *et al*. (2014). MicroRNA-106b in cancer-associated fibroblasts from gastric cancer promotes cell migration and invasion by targeting PTEN. FEBS Letters. 588. 2162-2169.

238. Yin G., Chen R., Alvero A. B., Hu H-H., Holmberg J., *et al*. (2010). TWISTing stemness, inflammation, and proliferation of epithelial ovarian cancer cells through MIR199A2/214. Oncogene. 29(24):3545-3553.

239. Ying H., Elpek K. G., Vinjamoori A., Zimmerman S. M., Chu G. C., *et al*. (2011). Pten is a major tumour suppresspr in pancreatic ductal adenocarcinoma and regulates an NF-kB-cytokine network. Cancer Disco. 1(2):158-169.

240. Yu T., Wang X. Y., Gong R. G., Li A., Yang S., *et al*. (2009). The expression profile of microRNAs in a model of 7,12-dimethyl-benz[a]anthracene-induced oral carcinogenesis in Syrian hamster. J Exp Clin Cancer Res. 28:64.

241. Zhang J., Cheng Q., Zhou Y., Wang Y., and Chen X. (2013). Slug is a key mediator of hypoxia induced cadherin switch in HNSCC: correlations with poor prognosis. Oral Oncol. 49 (11): 1043-50.

242. Zhang Z., Zheng W. and Hai J. (2014). MicroRNA-148b expression is decreased in hepatocellular carcinoma and associated with prognosis. Med Oncol. 31(6):984.

243. Genome.ucsc.edu (Last accessed on 15/01/2015).

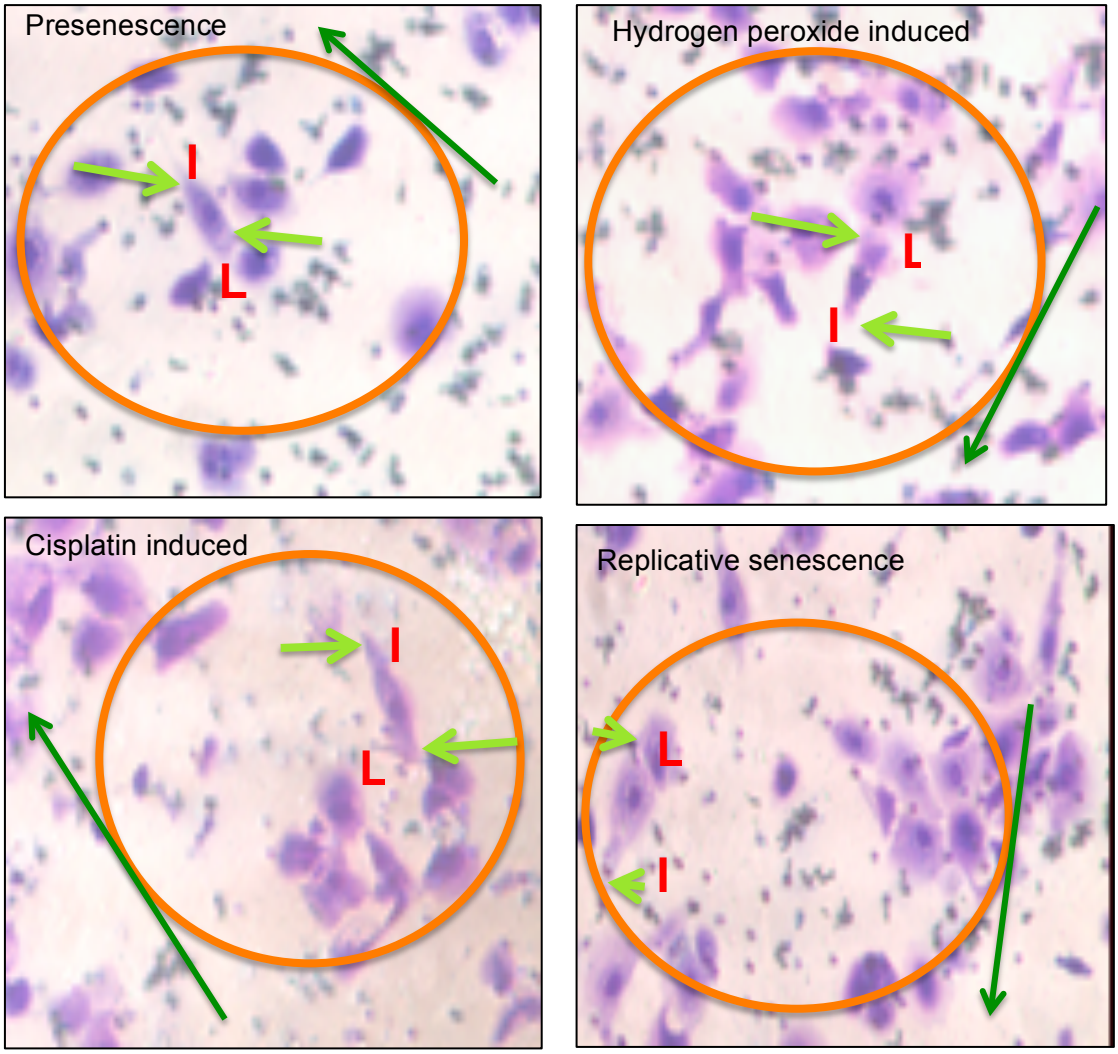

Appendix 1: Magnified images of invasive H357 cells towards conditioned media of senescent and presenescent oral fibroblasts. L indicates lagging edge and I indicates invasive edge. The dark green arrow shows direction of motion. Light green arrows mark the edges of the invaded H357 cells denoting change in polarity.

Appendix 2: miRNA deregulated in pool A in Cisplatin induced premature senescent oral fibroblasts

miRNA Pool A	Fold Change	miRNA Pool A	Fold Change
hsa-miR-363-4378090	2.0273	hsa-miR-329-4373191	1.2839
hsa-miR-544-4395376	2.0067	hsa-miR-331-3p-4373046	1.2763
hsa-miR-34c-5p-4373036	2.0002	hsa-miR-152-4395170	1.2757
hsa-miR-519d-4395514	1.9974	hsa-miR-186-4395396	1.2723
hsa-miR-520e-4373255	1.9614	hsa-miR-339-3p-4395295	1.2624
hsa-miR-372-4373029	1.906	hsa-miR-324-5p-4373052	1.2619
hsa-miR-491-5p-4381053	1.8603	hsa-miR-337-5p-4395267	1.2491
hsa-miR-628-5p-4395544	1.848	hsa-miR-219-5p-4373080	1.2482
hsa-miR-210-4373089	1.7576	hsa-miR-21-4373090	1.2451
hsa-miR-302c-4378072	1.7482	hsa-miR-30c-4373060	1.2415
hsa-miR-422a-4395408	1.6683	hsa-let-7g-4395393	1.2387
hsa-miR-185-4395382	1.6427	hsa-miR-424-4373201	1.2302
hsa-miR-369-5p-4373195	1.6249	hsa-miR-299-3p-4373189	1.2195
hsa-miR-127-5p-4395340	1.6158	hsa-miR-150-4373127	1.2132
hsa-miR-134-4373299	1.613	hsa-miR-323-3p-4395338	1.2098
hsa-miR-215-4373084	1.5954	hsa-miR-574-3p-4395460	1.2019
hsa-miR-373-4378073	1.5954	hsa-miR-672-4395438	1.2018
hsa-miR-708-4395452	1.5942	hsa-miR-362-3p-4395228	1.1982
RNU44-4373384	1.588	hsa-miR-340-4395369	1.1917
hsa-miR-539-4378103	1.5727	hsa-miR-889-4395313	1.1841
hsa-miR-655-4381015	1.5434	hsa-miR-545-4395378	1.1824
hsa-miR-181a-4373117	1.5367	hsa-miR-532-5p-4380928	1.1809
hsa-miR-29b-4373288	1.5279	hsa-miR-523-4395497	1.1809
hsa-miR-95-4373011	1.5178	hsa-miR-302a-4378070	1.1805
hsa-miR-136-4373173	1.5109	hsa-miR-616-4395525	1.179

hsa-miR-299-5p-4373188	1.489	hsa-miR-379-4373349	1.1784
hsa-let-7c-4373167	1.4842	hsa-miR-433-4373205	1.1632
hsa-miR-449b-4381011	1.4821	hsa-miR-135a-4373140	1.1621
hsa-miR-154-4373270	1.4779	hsa-miR-1-4395333	1.1599
hsa-miR-126-4395339	1.471	hsa-miR-105-4395278	1.1599
hsa-miR-494-4395476	1.4632	hsa-miR-122-4395356	1.1599
hsa-miR-23b-4373073	1.4577	hsa-miR-133b-4395358	1.1599
hsa-miR-29c-4395171	1.4474	hsa-miR-142-5p-4395359	1.1599
hsa-miR-196b-4395326	1.4419	hsa-miR-147-4373131	1.1599
hsa-miR-409-5p-4395442	1.429	hsa-miR-147b-4395373	1.1599
hsa-miR-9-4373285	1.424	hsa-miR-153-4373305	1.1599
hsa-miR-328-4373049	1.4171	hsa-miR-183-4395380	1.1599
hsa-miR-365-4373194	1.4071	hsa-miR-187-4373307	1.1599
hsa-miR-548a-3p-4380948	1.3937	hsa-miR-188-3p-4395217	1.1599
hsa-let-7a-4373169	1.3923	hsa-miR-208-4373091	1.1599
hsa-miR-29a-4395223	1.3911	hsa-miR-208b-4395401	1.1599
hsa-miR-217-4395448	1.3699	hsa-miR-211-4373088	1.1599
hsa-miR-191-4395410	1.3529	hsa-miR-219-2-3p-4395501	1.1599
hsa-miR-411-4381013	1.3517	hsa-miR-220b-4395317	1.1599
hsa-miR-139-5p-4395400	1.349	hsa-miR-220c-4395322	1.1599
hsa-miR-222-4395387	1.347	hsa-miR-298-4395301	1.1599
hsa-miR-127-3p-4373147	1.3422	hsa-miR-325-4373051	1.1599
RNU48-4373383	1.3401	hsa-miR-326-4373050	1.1599
hsa-miR-374b-4381045	1.3378	hsa-miR-346-4373038	1.1599
hsa-miR-493-4395475	1.3029	hsa-miR-371-3p-4395235	1.1599
hsa-miR-487b-4378102	1.2943	hsa-miR-384-4373017	1.1599
hsa-miR-412-4373199	1.1599	hsa-miR-876-3p-4395336	1.1599
hsa-miR-448-4373206	1.1599	hsa-miR-876-5p-4395316	1.1599
hsa-miR-450b-3p-4395319	1.1599	hsa-miR-887-4395485	1.1599
hsa-miR-492-4373217	1.1599	hsa-miR-891b-4395321	1.1599

hsa-miR-499-3p-4395538	1.1599	hsa-miR-892a-4395306	1.1599
hsa-miR-499-5p-4381047	1.1599	hsa-miR-96-4373372	1.1599
hsa-miR-501-3p-4395546	1.1599	hsa-miR-125b-4373148	1.1594
hsa-miR-506-4373231	1.1599	hsa-miR-370-4395386	1.1585
hsa-miR-507-4373232	1.1599	hsa-miR-140-3p-4395345	1.1522
hsa-miR-508-5p-4395203	1.1599	hsa-miR-485-3p-4378095	1.1516
hsa-miR-509-3-5p-4395266	1.1599	hsa-miR-376a-4373026	1.1499
hsa-miR-509-5p-4395346	1.1599	hsa-miR-425-4380926	1.1456
hsa-miR-510-4395352	1.1599	hsa-miR-431-4395173	1.1266
hsa-miR-512-5p-4373238	1.1599	hsa-miR-221-4373077	1.1186
hsa-miR-513-5p-4395201	1.1599	hsa-miR-140-5p-4373374	1.1185
hsa-miR-515-3p-4395480	1.1599	hsa-miR-454-4395434	1.1181
hsa-miR-515-5p-4373242	1.1599	hsa-miR-532-3p-4395466	1.1179
hsa-miR-516a-5p-4395527	1.1599	hsa-miR-30b-4373290	1.1135
hsa-miR-516b-4395172	1.1599	hsa-miR-27b-4373068	1.1134
hsa-miR-518a-3p-4395508	1.1599	hsa-miR-149-4395366	1.1127
hsa-miR-518a-5p-4395507	1.1599	hsa-miR-660-4380925	1.1116
hsa-miR-518c-4395512	1.1599	hsa-miR-369-3p-4373032	1.1054
hsa-miR-518d-5p-4395500	1.1599	hsa-miR-15a-4373123	1.1008
hsa-miR-519c-3p-4373251	1.1599	hsa-miR-193a-3p-4395361	1.1008
hsa-miR-519e-4395481	1.1599	hsa-miR-200c-4395411	1.1008
hsa-miR-520a-3p-4373268	1.1599	hsa-miR-218-4373081	1.0982
hsa-miR-520a-5p-4378085	1.1599	hsa-miR-24-4373072	1.0976
hsa-miR-520d-5p-4395504	1.1599	hsa-miR-548b-5p-4395519	1.0966
hsa-miR-520f-4373256	1.1599	hsa-miR-203-4373095	1.0897
hsa-miR-520g-4373257	1.1599	hsa-miR-542-3p-4378101	1.082
hsa-miR-521-4373259	1.1599	hsa-miR-99a-4373008	1.0794
hsa-miR-524-5p-4395174	1.1599	hsa-miR-139-3p-4395424	1.0789
hsa-miR-525-3p-4395496	1.1599	hsa-miR-451-4373360	1.0769
hsa-miR-525-5p-4378088	1.1599	hsa-miR-197-4373102	1.0736

hsa-miR-526b-4395493	1.1599	hsa-miR-194-4373106	1.0708
hsa-miR-548a-5p-4395523	1.1599	hsa-miR-452-4395440	1.0679
hsa-miR-548b-3p-4380951	1.1599	hsa-miR-28-5p-4373067	1.0677
hsa-miR-548c-3p-4380993	1.1599	hsa-miR-345-4395297	1.0664
hsa-miR-556-3p-4395456	1.1599	hsa-miR-103-4373158	1.0631
hsa-miR-556-5p-4395455	1.1599	hsa-miR-429-4373203	1.0593
hsa-miR-582-3p-4395510	1.1599	hsa-miR-130b-4373144	1.0548
hsa-miR-582-5p-4395175	1.1599	hsa-miR-590-5p-4395176	1.0545
hsa-miR-624-4395541	1.1599	hsa-miR-107-4373154	1.0534
hsa-miR-651-4381007	1.1599	hsa-miR-410-4378093	1.0495
hsa-miR-653-4395403	1.1599	hsa-miR-455-3p-4395355	1.0491
hsa-miR-674-4395193	1.1599	hsa-miR-542-5p-4395351	1.0415
hsa-miR-871-4395465	1.1599	hsa-miR-190-4373110	1.041
hsa-miR-872-4395375	1.1599	hsa-miR-143-4395360	1.0392
hsa-miR-873-4395467	1.1599	hsa-miR-193a-5p-4395392	1.0369
hsa-miR-874-4395379	1.1599	hsa-miR-192-4373108	1.0365
hsa-miR-875-3p-4395315	1.1599	hsa-miR-484-4381032	1.0348
hsa-miR-455-5p-4378098	1.0252	hsa-miR-423-5p-4395451	0.909
hsa-miR-26b-4395167	1.0189	hsa-miR-125a-5p-4395309	0.8933
hsa-miR-551b-4380945	1.0187	hsa-miR-671-3p-4395433	0.892
hsa-miR-886-5p-4395304	1.0181	hsa-miR-212-4373087	0.8883
hsa-miR-31-4395390	1.016	hsa-miR-500-4395539	0.8874
hsa-miR-204-4373094	1.0125	hsa-miR-99b-4373007	0.8841
hsa-miR-324-3p-4395272	1.0102	hsa-miR-214-4395417	0.883
hsa-miR-615-5p-4395464	1.0093	hsa-miR-495-4381078	0.875
hsa-miR-636-4395199	1.0084	hsa-miR-382-4373019	0.8669
hsa-miR-26a-4395166	1.0068	hsa-miR-25-4373071	0.8648
hsa-miR-450a-4395414	1.0056	hsa-miR-758-4395180	0.8475
MammU6-4395470	1	hsa-miR-320-4395388	0.8459
hsa-miR-28-3p-4395557	0.9983	hsa-miR-501-5p-4373226	0.84

hsa-miR-361-5p-4373035	0.9931	hsa-miR-146b-5p-4373178	0.8336
hsa-miR-193b-4395478	0.9929	hsa-let-7f-4373164	0.8332
hsa-miR-199a-5p-4373272	0.9863	hsa-miR-744-4395435	0.8312
hsa-miR-100-4373160	0.9828	hsa-miR-195-4373105	0.8216
hsa-miR-27a-4373287	0.9792	hsa-miR-32-4395220	0.8158
hsa-miR-502-3p-4395194	0.9768	hsa-miR-488-4395468	0.8139
hsa-miR-130a-4373145	0.9759	hsa-miR-302b-4378071	0.8106
hsa-miR-200b-4395362	0.9757	hsa-miR-19b-4373098	0.8038
hsa-miR-518f-4395499	0.9735	hsa-miR-106b-4373155	0.8022
hsa-miR-129-3p-4373297	0.9727	hsa-miR-598-4395179	0.8007
hsa-miR-296-5p-4373066	0.9704	hsa-let-7d-4395394	0.7968
hsa-miR-181c-4373115	0.9674	hsa-miR-135b-4395372	0.7959
hsa-miR-654-3p-4395350	0.9662	hsa-miR-342-3p-4395371	0.7864
hsa-let-7e-4395517	0.9646	hsa-miR-518d-3p-4373248	0.7834
hsa-miR-376c-4395233	0.9621	hsa-miR-362-5p-4378092	0.7775
hsa-miR-330-3p-4373047	0.9611	hsa-miR-338-3p-4395363	0.7692
hsa-miR-145-4395389	0.9589	hsa-miR-615-3p-4386777	0.7647
hsa-miR-142-3p-4373136	0.9588	hsa-let-7b-4395446	0.7591
hsa-miR-101-4395364	0.9583	hsa-miR-579-4395509	0.7518
hsa-miR-339-5p-4395368	0.9546	hsa-miR-301b-4395503	0.7421
hsa-miR-132-4373143	0.9528	hsa-miR-224-4395210	0.7397
hsa-miR-331-5p-4395344	0.9519	hsa-miR-17-4395419	0.7393
hsa-miR-374a-4373028	0.9467	hsa-miR-92a-4395169	0.7361
hsa-miR-129-5p-4373171	0.9443	hsa-miR-652-4395463	0.7296
hsa-miR-502-5p-4373227	0.9407	hsa-miR-589-4395520	0.7183
hsa-miR-890-4395320	0.9397	hsa-miR-125a-3p-4395310	0.7178
hsa-miR-381-4373020	0.935	hsa-miR-198-4395384	0.7108
hsa-miR-98-4373009	0.9346	hsa-miR-106a-4395280	0.7086
hsa-miR-886-3p-4395305	0.9332	hsa-miR-376b-4373196	0.7082
hsa-miR-138-4395395	0.9321	hsa-miR-496-4386771	0.7032

hsa-miR-450b-5p-4395318	0.9321	hsa-miR-16-4373121	0.6982
hsa-miR-517b-4373244	0.9251	hsa-miR-15b-4373122	0.6806
hsa-miR-128-4395327	0.9224	hsa-miR-301a-4373064	0.6805
hsa-miR-487a-4378097	0.9199	hsa-miR-220-4373078	0.6792
hsa-miR-141-4373137	0.9196	hsa-miR-505-4395200	0.6782
hsa-miR-22-4373079	0.9185	hsa-miR-199b-5p-4373100	0.6617
hsa-miR-199a-3p-4395415	0.9176	hsa-miR-570-4395458	0.6597
hsa-miR-33b-4395196	0.911	hsa-miR-618-4380996	0.5932
hsa-miR-625-4395542	0.6596	hsa-miR-20b-4373263	0.5896
hsa-miR-19a-4373099	0.6531	hsa-miR-576-3p-4395462	0.5888
hsa-miR-453-4395429	0.639	hsa-miR-296-3p-4395212	0.5809
hsa-miR-93-4373302	0.639	hsa-miR-576-5p-4395461	0.5784
hsa-miR-377-4373025	0.6345	hsa-miR-642-4380995	0.5745
hsa-miR-10b-4395329	0.631	hsa-miR-330-5p-4395341	0.5737
hsa-miR-383-4373018	0.6271	hsa-miR-18b-4395328	0.5576
hsa-miR-146b-3p-4395472	0.6156	hsa-miR-490-3p-4373215	0.5432
hsa-miR-18a-4395533	0.613	hsa-miR-380-4373022	0.5424
hsa-miR-483-5p-4395449	0.6088	hsa-miR-548c-5p-4395540	0.5385
hsa-miR-20a-4373286	0.5992	hsa-miR-342-5p-4395258	0.5313
hsa-miR-629-4395547	0.5938	hsa-miR-202-4395474	0.5

Appendix 3: miRNAs deregulated in pool B in cisplatin induced premature senescent oral fibroblasts

miRNA	Fold change	miRNA	Fold change
hsa-miR-620-002672	2.7048	hsa-miR-1283-002890	1.4196
hsa-miR-638-001582	2.6772	hsa-miR-571-001613	1.4065
hsa-miR-149#-002164	2.6618	RNU48-001006	1.4027
hsa-miR-548G-002879	2.6555	hsa-miR-320B-002844	1.3784
hsa-miR-892b-002214	2.5427	hsa-miR-213-000516	1.3726
hsa-miR-378-002243	2.4595	hsa-miR-1271-002779	1.366
hsa-miR-34a#-002316	2.4309	hsa-miR-30a-3p-000416	1.3381
hsa-miR-1290-002863	2.3486	hsa-miR-30e-3p-000422	1.3367
hsa-miR-520h-001170	2.1763	hsa-miR-1247-002893	1.336
hsa-miR-377#-002128	2.1313	hsa-miR-505#-002087	1.3291
hsa-miR-664-002897	2.0564	hsa-miR-589-001543	1.3156
hsa-miR-1197-002810	2.0094	hsa-miR-126#-000451	1.3143
hsa-miR-668-001992	1.9777	hsa-miR-23b#-002126	1.3018
hsa-miR-548E-002881	1.9761	hsa-miR-1267-002885	1.2988
hsa-miR-1274A-002883	1.9666	hsa-miR-769-5p-001998	1.2982
RNU44-001094	1.9591	hsa-miR-650-001603	1.2946
hsa-miR-148a#-002134	1.9056	hsa-miR-105#-002168	1.2729
hsa-miR-1254-002818	1.8874	hsa-miR-106a#-002170	1.2729
hsa-miR-1179-002776	1.8782	hsa-miR-1178-002777	1.2729
hsa-miR-34b-000427	1.8736	hsa-miR-1200-002829	1.2729
hsa-let-7c#-002405	1.8551	hsa-miR-1205-002778	1.2729
hsa-miR-592-001546	1.852	hsa-miR-1206-002878	1.2729
hsa-miR-1248-002870	1.8505	hsa-miR-1224-3P-002752	1.2729
hsa-miR-613-001586	1.8323	hsa-miR-1250-002887	1.2729
hsa-miR-520c-3p-002400	1.8298	hsa-miR-1251-002820	1.2729
hsa-miR-1296-002908	1.8286	hsa-miR-1255A-002805	1.2729

hsa-miR-34b-002102	1.8229	hsa-miR-1257-002910	1.2729
hsa-miR-1269-002789	1.8053	hsa-miR-1263-002784	1.2729
hsa-miR-30c-1#-002108	1.7803	hsa-miR-1286-002773	1.2729
hsa-miR-1225-3P-002766	1.7185	hsa-miR-1304-002874	1.2729
hsa-miR-1201-002781	1.7098	hsa-miR-138-2#-002144	1.2729
hsa-miR-624-001557	1.6622	hsa-miR-182#-000483	1.2729
hsa-miR-99a#-002141	1.6597	hsa-miR-1826-002873	1.2729
hsa-miR-24-1#-002440	1.6044	hsa-miR-185#-002104	1.2729
hsa-miR-1825-002907	1.5992	hsa-miR-18b#-002310	1.2729
hsa-miR-1301-002827	1.5848	hsa-miR-194#-002379	1.2729
hsa-miR-409-3p-002332	1.5496	hsa-miR-196a#-002336	1.2729
hsa-miR-148b#-002160	1.5367	hsa-miR-200b#-002274	1.2729
hsa-miR-7-2#-002314	1.5292	hsa-miR-200c#-002286	1.2729
hsa-miR-376a#-002127	1.5273	hsa-miR-20b#-002311	1.2729
hsa-miR-30a-5p-000417	1.5011	hsa-miR-218-1#-002094	1.2729
hsa-miR-500-001046	1.4891	hsa-miR-223#-002098	1.2729
hsa-miR-378-000567	1.4813	hsa-miR-302b#-002119	1.2729
hsa-miR-154#-000478	1.4678	hsa-miR-302c#-000534	1.2729
hsa-miR-99b#-002196	1.4544	hsa-miR-302d#-002120	1.2729
hsa-miR-1305-002867	1.4356	hsa-miR-30b#-002129	1.2729
hsa-miR-577-002675	1.4261	hsa-miR-30c-2#-002110	1.2729
hsa-miR-33a#-002136	1.4206	hsa-miR-367#-002121	1.2729
hsa-miR-513B-002757	1.2729	hsa-miR-935-002178	1.2729
hsa-miR-513C-002756	1.2729	hsa-miR-936-002179	1.2729
hsa-miR-517#-001113	1.2729	hsa-miR-31#-002113	1.2628
hsa-miR-518c#-001158	1.2729	hsa-miR-425#-002302	1.2549
hsa-miR-518e#-002371	1.2729	hsa-miR-221#-002096	1.2541
hsa-miR-518f#-002387	1.2729	hsa-miR-545#-002266	1.2486
hsa-miR-519e#-001166	1.2729	hsa-miR-192#-002272	1.2422
hsa-miR-548M-002775	1.2729	hsa-miR-584-001624	1.229

hsa-miR-552-001520	1.2729	hsa-miR-30d-000420	1.2282
hsa-miR-553-001521	1.2729	hsa-miR-1227-002769	1.2085
hsa-miR-554-001522	1.2729	hsa-miR-744#-002325	1.2022
hsa-miR-555-001523	1.2729	hsa-miR-20a#-002437	1.1964
hsa-miR-557-001525	1.2729	hsa-miR-22#-002301	1.1897
hsa-miR-558-001526	1.2729	hsa-miR-432-001026	1.1878
hsa-miR-559-001527	1.2729	hsa-miR-628-3p-002434	1.1869
hsa-miR-562-001529	1.2729	hsa-miR-1274B-002884	1.1712
hsa-miR-563-001530	1.2729	hsa-miR-374b#-002391	1.1712
hsa-miR-569-001536	1.2729	hsa-miR-1233-002768	1.1611
hsa-miR-575-001617	1.2729	hsa-miR-551a-001519	1.1585
hsa-miR-578-001619	1.2729	hsa-miR-564-001531	1.1578
hsa-miR-583-001623	1.2729	hsa-miR-136#-002100	1.145
hsa-miR-588-001542	1.2729	hsa-miR-340#-002259	1.1356
hsa-miR-593-001547	1.2729	hsa-let-7f-2#-002418	1.1262
hsa-miR-593-002411	1.2729	hsa-miR-145#-002149	1.0985
hsa-miR-595-001987	1.2729	hsa-miR-411#-002238	1.0958
hsa-miR-599-001554	1.2729	hsa-miR-1303-002792	1.095
hsa-miR-617-001591	1.2729	hsa-miR-337-3p-002157	1.0932
hsa-miR-621-001598	1.2729	hsa-miR-767-5p-001993	1.0905
hsa-miR-622-001553	1.2729	hsa-miR-605-001568	1.0823
hsa-miR-623-001555	1.2729	hsa-miR-26b#-002444	1.0716
hsa-miR-626-001559	1.2729	hsa-miR-581-001622	1.0715
hsa-miR-631-001564	1.2729	hsa-miR-1282-002803	1.0531
hsa-miR-637-001581	1.2729	hsa-let-7i#-002172	1.0457
hsa-miR-640-001584	1.2729	hsa-miR-222#-002097	1.04
hsa-miR-647-001600	1.2729	hsa-miR-590-3P-002677	1.0389
hsa-miR-648-001601	1.2729	hsa-miR-769-3p-002003	1.0214
hsa-miR-649-001602	1.2729	hsa-miR-656-001510	1.0163
hsa-miR-657-001512	1.2729	hsa-miR-614-001587	1.0078

hsa-miR-658-001513	1.2729	U6 snRNA-001973	1
hsa-miR-675-002005	1.2729	hsa-miR-488-001106	0.9996
hsa-miR-767-3p-001995	1.2729	hsa-miR-720-002895	0.9815
hsa-miR-802-002004	1.2729	hsa-miR-616-001589	0.9761
hsa-miR-920-002150	1.2729	hsa-miR-191#-002678	0.9716
hsa-miR-921-002151	1.2729	hsa-miR-93#-002139	0.9712
hsa-miR-924-002154	1.2729	hsa-miR-374a#-002125	0.9679
hsa-miR-92a-2#-002138	1.2729	hsa-miR-32#-002111	0.9637
hsa-miR-933-002176	1.2729	hsa-miR-591-001545	0.961
hsa-miR-934-002177	1.2729	hsa-miR-629-001562	0.9599
hsa-miR-543-002376	0.9592	rno-miR-7#-001338	0.6493
hsa-miR-659-001514	0.9592	hsa-miR-497-001043	0.6446
hsa-miR-550-002410	0.9564	hsa-miR-183#-002270	0.6435
hsa-miR-151-5P-002642	0.9506	hsa-miR-548L-002904	0.6293
hsa-miR-21#-002438	0.9472	hsa-miR-302d-000535	0.6291
hsa-miR-1275-002840	0.9399	hsa-miR-17#-002421	0.6248
hsa-miR-18a#-002423	0.9354	hsa-miR-550-001544	0.6195
rno-miR-29c#-001818	0.9236	hsa-miR-625#-002432	0.6171
hsa-miR-1260-002896	0.9205	hsa-let-7a#-002307	0.6168
hsa-miR-572-001614	0.9201	hsa-miR-1228#-002763	0.6101
hsa-miR-587-001540	0.9156	hsa-miR-195#-002107	0.606
hsa-miR-766-001986	0.9077	hsa-miR-942-002187	0.5979
hsa-miR-1244-002791	0.9025	hsa-miR-609-001573	0.5938
hsa-miR-770-5p-002002	0.8968	hsa-miR-27a#-002445	0.582
hsa-miR-601-001558	0.8877	hsa-miR-29b-1#-002165	0.5818
hsa-miR-941-002183	0.8836	hsa-miR-875-5p-002203	0.5718
hsa-miR-520D-3P-002743	0.8812	hsa-miR-338-5P-002658	0.5539
mmu-let-7d#-001178	0.8735	hsa-miR-661-001606	0.5396
hsa-miR-100#-002142	0.8718	hsa-miR-1292-002824	0.5305
hsa-miR-335#-002185	0.871	dme-miR-7-000268	0.5106

hsa-miR-155#-002287	0.8698	hsa-miR-1300-002902	0.5099
hsa-miR-1180-002847	0.8508	hsa-miR-645-001597	0.5067
hsa-miR-181a-2#-002317	0.8348	hsa-miR-10b#-002315	0.4779
hsa-miR-1236-002761	0.8343	hsa-miR-125b-2#-002158	0.4744
hsa-miR-193b#-002366	0.83	hsa-miR-130b#-002114	0.4686
hsa-miR-29a#-002447	0.8296	hsa-miR-30d#-002305	0.468
hsa-miR-549-001511	0.8281	hsa-let-7f-1#-002417	0.4674
hsa-miR-19b-1#-002425	0.8046	hsa-miR-122#-002130	0.4592
hsa-let-7e#-002407	0.801	hsa-miR-573-001615	0.4586
hsa-miR-641-001585	0.798	hsa-miR-608-001571	0.4583
hsa-miR-214#-002293	0.7919	hsa-miR-19a#-002424	0.4567
hsa-let-7g#-002118	0.7871	hsa-miR-1249-002868	0.4553
hsa-miR-24-2#-002441	0.7837	hsa-miR-607-001570	0.4513
hsa-miR-125b-1#-002378	0.7808	hsa-miR-151-3p-002254	0.4396
hsa-miR-218-2#-002294	0.7763	hsa-miR-1270-002807	0.4174
hsa-miR-424#-002309	0.7761	hsa-miR-1183-002841	0.396
hsa-miR-302a#-002381	0.7372	hsa-miR-16-1#-002420	0.3767
hsa-miR-454#-001996	0.7325	hsa-miR-567-001534	0.3757
hsa-miR-1226#-002758	0.7245	hsa-miR-586-001539	0.3686
hsa-miR-27b#-002174	0.7234	hsa-miR-643-001594	0.3468
hsa-miR-26a-2#-002115	0.7056	hsa-miR-580-001621	0.3432
hsa-miR-190b-002263	0.7023	hsa-miR-551b#-002346	0.3413
hsa-miR-33a-002135	0.6904	hsa-miR-26a-1#-002443	0.334
hsa-miR-380-5p-000570	0.6853	hsa-miR-15a#-002419	0.3316
hsa-miR-92a-1#-002137	0.6781	hsa-miR-548H-002816	0.3263
hsa-miR-29b-2#-002166	0.678	hsa-miR-1324-002815	0.3249
hsa-miR-633-001574	0.6731	hsa-let-7b#-002404	0.3217
hsa-miR-106b#-002380	0.6544	hsa-miR-1276-002843	0.3028
hsa-miR-516-3p-001149	0.2953	hsa-miR-1289-002871	0.2567
hsa-miR-541#-002200	0.2929	hsa-miR-483-3p-002339	0.2548

hsa-miR-944-002189	0.2912	hsa-miR-939-002182	0.2535
hsa-miR-129#-002298	0.2826	hsa-miR-144#-002148	0.252
hsa-miR-15b#-002173	0.2795	hsa-miR-101#-002143	0.2489
hsa-miR-548J-002783	0.2787	hsa-miR-1298-002861	0.2428
hsa-miR-585-001625	0.2743	hsa-miR-1255B-002801	0.2361
hsa-miR-132#-002132	0.2708	hsa-miR-25#-002442	0.2361
hsa-miR-16-2#-002171	0.2667	hsa-miR-1294-002785	0.2323
hsa-miR-566-001533	0.2241	ath-miR159a-000338	0.1158
hsa-miR-143#-002146	0.2053	hsa-miR-431#-002312	0.115
hsa-miR-639-001583	0.1859	hsa-miR-1285-002822	0.1003
hsa-miR-1256-002850	0.1827	hsa-miR-1278-002851	0.089
hsa-miR-1259-002796	0.1666	hsa-miR-146a#-002163	0.0873
hsa-miR-10a#-002288	0.1658	hsa-miR-1245-002823	0.0855
hsa-miR-144-002676	0.1451	hsa-miR-937-002180	0.0848
hsa-miR-181c#-002333	0.1429	hsa-miR-665-002681	0.0769
hsa-miR-1264-002799	0.1396	hsa-miR-1182-002830	0.0768
hsa-miR-644-001596	0.1386	hsa-miR-135b#-002159	0.0749
hsa-miR-130a#-002131	0.1184	hsa-miR-635-001578	0.0671
hsa-miR-524-001173	0.1168	hsa-miR-548I-002909	0.0635
hsa-miR-548P-002798	0.1163	hsa-miR-202#-002362	0.0616

Appendix 4: Deregulated miRNAs in late-passage oral fibroblasts

miRNA	Fold change	miRNA	Fold change
hsa-miR-519a-4395526	2.2236	hsa-miR-1256-002850	2.1174
hsa-miR-107-4373154	2.1958	hsa-miR-1257-002910	2.1174
hsa-miR-203-4373095	2.1779	hsa-miR-1259-002796	2.1174
hsa-miR-221#-002096	2.1689	hsa-miR-1263-002784	2.1174
ath-miR159a-000338	2.1174	hsa-miR-1264-002799	2.1174
ath-miR159a-4373390	2.1174	hsa-miR-1265-002790	2.1174
hsa-let-7a#-002307	2.1174	hsa-miR-127-5p-4395340	2.1174
hsa-let-7f-1#-002417	2.1174	hsa-miR-1272-002845	2.1174
hsa-let-7f-2#-002418	2.1174	hsa-miR-1278-002851	2.1174
hsa-let-7g#-002118	2.1174	hsa-miR-1283-002890	2.1174
hsa-miR-1-4395333	2.1174	hsa-miR-1284-002903	2.1174
hsa-miR-101#-002143	2.1174	hsa-miR-1286-002773	2.1174
hsa-miR-101-4395364	2.1174	hsa-miR-1288-002832	2.1174
hsa-miR-105#-002168	2.1174	hsa-miR-1289-002871	2.1174
hsa-miR-105-4395278	2.1174	hsa-miR-129#-002298	2.1174
hsa-miR-106a#-002170	2.1174	hsa-miR-129-5p-4373171	2.1174
hsa-miR-10a#-002288	2.1174	hsa-miR-1293-002905	2.1174
hsa-miR-10b#-002315	2.1174	hsa-miR-1294-002785	2.1174
hsa-miR-10b-4395329	2.1174	hsa-miR-1302-002901	2.1174
hsa-miR-1178-002777	2.1174	hsa-miR-1304-002874	2.1174
hsa-miR-1179-002776	2.1174	hsa-miR-130a#-002131	2.1174
hsa-miR-1182-002830	2.1174	hsa-miR-1324-002815	2.1174
hsa-miR-1184-002842	2.1174	hsa-miR-133a-4395357	2.1174
hsa-miR-1200-002829	2.1174	hsa-miR-133b-4395358	2.1174
hsa-miR-1203-002877	2.1174	hsa-miR-135a-4373140	2.1174
hsa-miR-1204-002872	2.1174	hsa-miR-135b#-002159	2.1174
hsa-miR-1205-002778	2.1174	hsa-miR-136-4373173	2.1174

hsa-miR-1206-002878	2.1174	hsa-miR-138-2#-002144	2.1174
hsa-miR-1208-002880	2.1174	hsa-miR-139-3p-4395424	2.1174
hsa-miR-122#-002130	2.1174	hsa-miR-141#-002145	2.1174
hsa-miR-122-4395356	2.1174	hsa-miR-141-4373137	2.1174
hsa-miR-1224-3P-002752	2.1174	hsa-miR-142-3p-4373136	2.1174
hsa-miR-1225-3P-002766	2.1174	hsa-miR-142-5p-4395359	2.1174
hsa-miR-1228#-002763	2.1174	hsa-miR-143#-002146	2.1174
hsa-miR-1236-002761	2.1174	hsa-miR-144#-002148	2.1174
hsa-miR-1238-002927	2.1174	hsa-miR-144-002676	2.1174
hsa-miR-124#-002197	2.1174	hsa-miR-146a#-002163	2.1174
hsa-miR-124-4373295	2.1174	hsa-miR-147-4373131	2.1174
hsa-miR-1243-002854	2.1174	hsa-miR-147b-4395373	2.1174
hsa-miR-1245-002823	2.1174	hsa-miR-148a#-002134	2.1174
hsa-miR-1248-002870	2.1174	hsa-miR-153-4373305	2.1174
hsa-miR-1250-002887	2.1174	hsa-miR-154-4373270	2.1174
hsa-miR-1251-002820	2.1174	hsa-miR-155#-002287	2.1174
hsa-miR-1252-002860	2.1174	hsa-miR-15a-4373123	2.1174
hsa-miR-1253-002894	2.1174	hsa-miR-16-1#-002420	2.1174
hsa-miR-1255A-002805	2.1174	hsa-miR-16-2#-002171	2.1174
hsa-miR-17#-002421	2.1174	hsa-miR-302b#-002119	2.1174
hsa-miR-181c#-002333	2.1174	hsa-miR-302b-4378071	2.1174
hsa-miR-182#-000483	2.1174	hsa-miR-302c#-000534	2.1174
hsa-miR-182-4395445	2.1174	hsa-miR-302c-4378072	2.1174
hsa-miR-1826-002873	2.1174	hsa-miR-302d#-002120	2.1174
hsa-miR-183-4395380	2.1174	hsa-miR-30b#-002129	2.1174
hsa-miR-185#-002104	2.1174	hsa-miR-30c-1#-002108	2.1174
hsa-miR-186#-002105	2.1174	hsa-miR-30c-2#-002110	2.1174
hsa-miR-187-4373307	2.1174	hsa-miR-32#-002111	2.1174
hsa-miR-188-3p-4395217	2.1174	hsa-miR-32-4395220	2.1174
hsa-miR-18b#-002310	2.1174	hsa-miR-325-4373051	2.1174

hsa-miR-193a-3p-4395361	2.1174	hsa-miR-326-4373050	2.1174
hsa-miR-194#-002379	2.1174	hsa-miR-330-5p-4395341	2.1174
hsa-miR-195#-002107	2.1174	hsa-miR-335-4373045	2.1174
hsa-miR-196a#-002336	2.1174	hsa-miR-338-3p-4395363	2.1174
hsa-miR-196b-4395326	2.1174	hsa-miR-33a-002135	2.1174
hsa-miR-19a#-002424	2.1174	hsa-miR-33b-4395196	2.1174
hsa-miR-200a#-001011	2.1174	hsa-miR-346-4373038	2.1174
hsa-miR-200a-4378069	2.1174	hsa-miR-361-3p-002116	2.1174
hsa-miR-200b#-002274	2.1174	hsa-miR-362-3p-4395228	2.1174
hsa-miR-200b-4395362	2.1174	hsa-miR-363#-001283	2.1174
hsa-miR-200c#-002286	2.1174	hsa-miR-363-4378090	2.1174
hsa-miR-202#-002362	2.1174	hsa-miR-367#-002121	2.1174
hsa-miR-205-4373093	2.1174	hsa-miR-367-4373034	2.1174
hsa-miR-206-000510	2.1174	hsa-miR-369-5p-4373195	2.1174
hsa-miR-208-4373091	2.1174	hsa-miR-371-3p-4395235	2.1174
hsa-miR-208b-4395401	2.1174	hsa-miR-372-4373029	2.1174
hsa-miR-20a#-002437	2.1174	hsa-miR-373-4378073	2.1174
hsa-miR-20b#-002311	2.1174	hsa-miR-374a#-002125	2.1174
hsa-miR-211-4373088	2.1174	hsa-miR-374b#-002391	2.1174
hsa-miR-215-4373084	2.1174	hsa-miR-375-4373027	2.1174
hsa-miR-216a-4395331	2.1174	hsa-miR-376a#-002127	2.1174
hsa-miR-216b-4395437	2.1174	hsa-miR-376b-4373196	2.1174
hsa-miR-217-4395448	2.1174	hsa-miR-377-4373025	2.1174
hsa-miR-218-1#-002094	2.1174	hsa-miR-380-4373022	2.1174
hsa-miR-218-2#-002294	2.1174	hsa-miR-384-4373017	2.1174
hsa-miR-219-2-3p-4395501	2.1174	hsa-miR-412-4373199	2.1174
hsa-miR-219-5p-4373080	2.1174	hsa-miR-424-4373201	2.1174
hsa-miR-220-4373078	2.1174	hsa-miR-429-4373203	2.1174
hsa-miR-220b-4395317	2.1174	hsa-miR-431#-002312	2.1174
hsa-miR-220c-4395322	2.1174	hsa-miR-448-4373206	2.1174

hsa-miR-223#-002098	2.1174	hsa-miR-449b-4381011	2.1174
hsa-miR-24-1#-002440	2.1174	hsa-miR-450b-3p-4395319	2.1174
hsa-miR-26a-2#-002115	2.1174	hsa-miR-450b-5p-4395318	2.1174
hsa-miR-298-4395301	2.1174	hsa-miR-451-4373360	2.1174
hsa-miR-301b-4395503	2.1174	hsa-miR-452#-002330	2.1174
hsa-miR-302a#-002381	2.1174	hsa-miR-454#-001996	2.1174
hsa-miR-302a-4378070	2.1174	hsa-miR-488-001106	2.1174
hsa-miR-488-4395468	2.1174	hsa-miR-520d-5p-4395504	2.1174
hsa-miR-491-3p-4395471	2.1174	hsa-miR-520e-4373255	2.1174
hsa-miR-497#-002368	2.1174	hsa-miR-520f-4373256	2.1174
hsa-miR-499-3p-4395538	2.1174	hsa-miR-520g-4373257	2.1174
hsa-miR-499-5p-4381047	2.1174	hsa-miR-520h-001170	2.1174
hsa-miR-501-3p-4395546	2.1174	hsa-miR-521-4373259	2.1174
hsa-miR-503-4373228	2.1174	hsa-miR-522-4395524	2.1174
hsa-miR-504-4395195	2.1174	hsa-miR-523-4395497	2.1174
hsa-miR-506-4373231	2.1174	hsa-miR-524-001173	2.1174
hsa-miR-507-4373232	2.1174	hsa-miR-524-5p-4395174	2.1174
hsa-miR-508-5p-4395203	2.1174	hsa-miR-525-3p-4395496	2.1174
hsa-miR-509-3-5p-4395266	2.1174	hsa-miR-525-5p-4378088	2.1174
hsa-miR-509-5p-4395346	2.1174	hsa-miR-541#-002200	2.1174
hsa-miR-510-4395352	2.1174	hsa-miR-541-4395312	2.1174
hsa-miR-511-4373236	2.1174	hsa-miR-544-4395376	2.1174
hsa-miR-512-3p-4381034	2.1174	hsa-miR-545#-002266	2.1174
hsa-miR-512-5p-4373238	2.1174	hsa-miR-545-4395378	2.1174
hsa-miR-513-5p-4395201	2.1174	hsa-miR-548a-3p-4380948	2.1174
hsa-miR-513B-002757	2.1174	hsa-miR-548a-5p-4395523	2.1174
hsa-miR-513C-002756	2.1174	hsa-miR-548b-3p-4380951	2.1174
hsa-miR-515-3p-4395480	2.1174	hsa-miR-548b-5p-4395519	2.1174
hsa-miR-515-5p-4373242	2.1174	hsa-miR-548c-3p-4380993	2.1174
hsa-miR-516a-5p-4395527	2.1174	hsa-miR-548c-5p-4395540	2.1174

hsa-miR-516b-4395172	2.1174	hsa-miR-548d-3p-4381008	2.1174
hsa-miR-517#-001113	2.1174	hsa-miR-548d-5p-4395348	2.1174
hsa-miR-517a-4395513	2.1174	hsa-miR-548E-002881	2.1174
hsa-miR-517b-4373244	2.1174	hsa-miR-548G-002879	2.1174
hsa-miR-517c-4373264	2.1174	hsa-miR-548I-002909	2.1174
hsa-miR-518a-3p-4395508	2.1174	hsa-miR-548J-002783	2.1174
hsa-miR-518a-5p-4395507	2.1174	hsa-miR-548K-002819	2.1174
hsa-miR-518b-4373246	2.1174	hsa-miR-548M-002775	2.1174
hsa-miR-518c#-001158	2.1174	hsa-miR-548N-002888	2.1174
hsa-miR-518c-4395512	2.1174	hsa-miR-548P-002798	2.1174
hsa-miR-518d-3p-4373248	2.1174	hsa-miR-549-001511	2.1174
hsa-miR-518d-5p-4395500	2.1174	hsa-miR-551a-001519	2.1174
hsa-miR-518e#-002371	2.1174	hsa-miR-551b-4380945	2.1174
hsa-miR-518e-4395506	2.1174	hsa-miR-552-001520	2.1174
hsa-miR-518f#-002387	2.1174	hsa-miR-553-001521	2.1174
hsa-miR-519b-3p-002384	2.1174	hsa-miR-554-001522	2.1174
hsa-miR-519c-3p-4373251	2.1174	hsa-miR-555-001523	2.1174
hsa-miR-519d-4395514	2.1174	hsa-miR-556-3p-4395456	2.1174
hsa-miR-519e#-001166	2.1174	hsa-miR-556-5p-4395455	2.1174
hsa-miR-519e-4395481	2.1174	hsa-miR-557-001525	2.1174
hsa-miR-520a-3p-4373268	2.1174	hsa-miR-558-001526	2.1174
hsa-miR-520a-5p-4378085	2.1174	hsa-miR-559-001527	2.1174
hsa-miR-520b-4373252	2.1174	hsa-miR-561-4380938	2.1174
hsa-miR-520c-3p-002400	2.1174	hsa-miR-562-001529	2.1174
hsa-miR-520D-3P-002743	2.1174	hsa-miR-563-001530	2.1174
hsa-miR-566-001533	2.1174	hsa-miR-628-3p-002434	2.1174
hsa-miR-567-001534	2.1174	hsa-miR-630-001563	2.1174
hsa-miR-569-001536	2.1174	hsa-miR-631-001564	2.1174
hsa-miR-570-4395458	2.1174	hsa-miR-633-001574	2.1174
hsa-miR-571-001613	2.1174	hsa-miR-634-001576	2.1174

hsa-miR-573-001615	2.1174	hsa-miR-635-001578	2.1174
hsa-miR-575-001617	2.1174	hsa-miR-637-001581	2.1174
hsa-miR-576-3p-4395462	2.1174	hsa-miR-639-001583	2.1174
hsa-miR-577-002675	2.1174	hsa-miR-640-001584	2.1174
hsa-miR-578-001619	2.1174	hsa-miR-641-001585	2.1174
hsa-miR-580-001621	2.1174	hsa-miR-644-001596	2.1174
hsa-miR-581-001622	2.1174	hsa-miR-646-001599	2.1174
hsa-miR-582-3p-4395510	2.1174	hsa-miR-647-001600	2.1174
hsa-miR-582-5p-4395175	2.1174	hsa-miR-648-001601	2.1174
hsa-miR-583-001623	2.1174	hsa-miR-649-001602	2.1174
hsa-miR-585-001625	2.1174	hsa-miR-650-001603	2.1174
hsa-miR-586-001539	2.1174	hsa-miR-651-4381007	2.1174
hsa-miR-587-001540	2.1174	hsa-miR-653-4395403	2.1174
hsa-miR-588-001542	2.1174	hsa-miR-656-001510	2.1174
hsa-miR-590-3P-002677	2.1174	hsa-miR-657-001512	2.1174
hsa-miR-591-001545	2.1174	hsa-miR-658-001513	2.1174
hsa-miR-592-001546	2.1174	hsa-miR-659-001514	2.1174
hsa-miR-593-001547	2.1174	hsa-miR-665-002681	2.1174
hsa-miR-593-002411	2.1174	hsa-miR-672-4395438	2.1174
hsa-miR-595-001987	2.1174	hsa-miR-674-4395193	2.1174
hsa-miR-596-001550	2.1174	hsa-miR-675-002005	2.1174
hsa-miR-599-001554	2.1174	hsa-miR-7-2#-002314	2.1174
hsa-miR-600-001556	2.1174	hsa-miR-708#-002342	2.1174
hsa-miR-603-001566	2.1174	hsa-miR-765-002643	2.1174
hsa-miR-604-001567	2.1174	hsa-miR-767-3p-001995	2.1174
hsa-miR-605-001568	2.1174	hsa-miR-767-5p-001993	2.1174
hsa-miR-606-001569	2.1174	hsa-miR-802-002004	2.1174
hsa-miR-607-001570	2.1174	hsa-miR-871-4395465	2.1174
hsa-miR-608-001571	2.1174	hsa-miR-872-4395375	2.1174
hsa-miR-609-001573	2.1174	hsa-miR-873-4395467	2.1174

hsa-miR-613-001586	2.1174	hsa-miR-875-3p-4395315	2.1174
hsa-miR-614-001587	2.1174	hsa-miR-876-3p-4395336	2.1174
hsa-miR-615-3p-4386777	2.1174	hsa-miR-876-5p-4395316	2.1174
hsa-miR-615-5p-4395464	2.1174	hsa-miR-885-3p-4395483	2.1174
hsa-miR-616-001589	2.1174	hsa-miR-887-4395485	2.1174
hsa-miR-617-001591	2.1174	hsa-miR-888#-002213	2.1174
hsa-miR-620-002672	2.1174	hsa-miR-888-4395323	2.1174
hsa-miR-621-001598	2.1174	hsa-miR-890-4395320	2.1174
hsa-miR-622-001553	2.1174	hsa-miR-891a-4395302	2.1174
hsa-miR-623-001555	2.1174	hsa-miR-891b-4395321	2.1174
hsa-miR-624-4395541	2.1174	hsa-miR-892a-4395306	2.1174
hsa-miR-626-001559	2.1174	hsa-miR-892b-002214	2.1174
hsa-miR-627-4380967	2.1174	hsa-miR-9#-002231	2.1174
hsa-miR-9-4373285	2.1174	hsa-miR-431-4395173	1.4496
hsa-miR-920-002150	2.1174	hsa-miR-136#-002100	1.4108
hsa-miR-921-002151	2.1174	U6 snRNA-001973	1.4075
hsa-miR-922-002152	2.1174	hsa-miR-624-001557	1.4017
hsa-miR-924-002154	2.1174	hsa-miR-299-5p-4373188	1.3976
hsa-miR-92a-2#-002138	2.1174	hsa-miR-154#-000478	1.3925
hsa-miR-92b#-002343	2.1174	hsa-miR-661-001606	1.3904
hsa-miR-933-002176	2.1174	hsa-miR-1300-002902	1.3451
hsa-miR-934-002177	2.1174	hsa-miR-337-3p-002157	1.3418
hsa-miR-935-002178	2.1174	hsa-miR-1201-002781	1.3341
hsa-miR-936-002179	2.1174	hsa-miR-550-002410	1.3312
hsa-miR-937-002180	2.1174	hsa-miR-214-4395417	1.3261
hsa-miR-938-002181	2.1174	hsa-miR-27b-4373068	1.3137
hsa-miR-943-002188	2.1174	hsa-miR-222-4395387	1.3111
hsa-miR-944-002189	2.1174	hsa-miR-26b#-002444	1.311
hsa-miR-95-4373011	2.1174	hsa-miR-139-5p-4395400	1.3024
hsa-miR-96#-002140	2.1174	hsa-miR-449a-4373207	1.2941

hsa-miR-96-4373372	2.1174	hsa-miR-338-5P-002658	1.2913
mmu-let-7d#-001178	2.1174	hsa-miR-1825-002907	1.288
hsa-miR-1276-002843	2.1165	hsa-miR-99a#-002141	1.2768
hsa-miR-34b-000427	2.0761	hsa-miR-151-5P-002642	1.2704
hsa-miR-190b-002263	2.0737	hsa-miR-490-3p-4373215	1.2659
hsa-miR-146b-3p-4395472	2.0699	hsa-miR-30c-4373060	1.2528
hsa-miR-1292-002824	2.022	hsa-miR-18b-4395328	1.25
hsa-miR-132-4373143	1.9902	hsa-miR-149#-002164	1.2377
hsa-miR-643-001594	1.9766	hsa-miR-572-001614	1.2295
hsa-miR-342-5p-4395258	1.9667	hsa-miR-128-4395327	1.191
hsa-miR-383-4373018	1.9526	RNU44-001094	1.1843
hsa-miR-548H-002816	1.9145	hsa-miR-576-5p-4395461	1.1811
hsa-let-7i#-002172	1.8488	hsa-miR-369-3p-4373032	1.1719
hsa-miR-30a-5p-000417	1.7995	hsa-miR-1197-002810	1.1707
hsa-miR-29b-2#-002166	1.746	hsa-miR-183#-002270	1.1548
hsa-miR-342-3p-4395371	1.7297	hsa-miR-331-3p-4373046	1.1477
hsa-miR-320B-002844	1.7214	RNU44-4373384	1.1351
hsa-miR-30d#-002305	1.6733	hsa-miR-27a#-002445	1.1336
hsa-miR-193b#-002366	1.6707	hsa-miR-15b-4373122	1.0926
hsa-miR-500-001046	1.6445	hsa-miR-126#-000451	1.0909
hsa-miR-224-4395210	1.6284	hsa-miR-212-4373087	1.0863
hsa-miR-548L-002904	1.5904	hsa-miR-34a#-002316	1.0857
hsa-miR-135b-4395372	1.58	hsa-miR-15a#-002419	1.0831
hsa-miR-662-001607	1.568	hsa-miR-24-4373072	1.0767
hsa-miR-744#-002325	1.5194	hsa-miR-92a-4395169	1.0728
hsa-miR-1247-002893	1.4693	hsa-miR-1291-002838	1.0727
hsa-miR-501-5p-4373226	1.4657	hsa-miR-1255B-002801	1.0722
hsa-miR-324-5p-4373052	1.4605	hsa-miR-328-4373049	1.0532
hsa-miR-340-4395369	1.4545	hsa-miR-21-4373090	1.0524
hsa-miR-502-5p-4373227	1.4507	hsa-miR-452-4395440	1.0466

hsa-miR-485-5p-4373212	1.4498	hsa-miR-455-3p-4395355	1.0437
hsa-miR-335#-002185	1.0388	hsa-miR-323-3p-4395338	0.8129
hsa-miR-654-5p-4381014	1.0355	hsa-miR-505#-002087	0.8047
hsa-miR-590-5p-4395176	1.028	hsa-miR-598-4395179	0.7984
hsa-miR-1180-002847	1.026	hsa-miR-125a-5p-4395309	0.7979
hsa-let-7e#-002407	1.0237	hsa-miR-29a-4395223	0.7922
hsa-miR-889-4395313	1.0236	hsa-miR-1270-002807	0.7909
hsa-miR-720-002895	1.0221	hsa-miR-758-4395180	0.7898
hsa-miR-432-001026	1.0169	hsa-miR-1267-002885	0.7815
hsa-miR-579-4395509	1.001	hsa-miR-766-001986	0.7786
hsa-miR-29b-4373288	1.0006	hsa-miR-668-001992	0.7769
hsa-miR-199a-3p-4395415	0.9989	hsa-miR-660-4380925	0.7765
hsa-miR-486-5p-4378096	0.9874	hsa-miR-148a-4373130	0.7727
hsa-miR-99b-4373007	0.9824	hsa-miR-664-002897	0.7703
hsa-miR-27a-4373287	0.9744	hsa-miR-25-4373071	0.7697
hsa-miR-663B-002857	0.9739	hsa-miR-505-4395200	0.7641
hsa-miR-30b-4373290	0.9708	hsa-miR-1227-002769	0.7631
hsa-miR-18a-4395533	0.9688	hsa-miR-152-4395170	0.7628
hsa-miR-192#-002272	0.9626	hsa-miR-1262-002852	0.7617
RNU48-001006	0.9582	hsa-miR-487b-4378102	0.7568
hsa-miR-654-3p-4395350	0.958	hsa-miR-496-4386771	0.7567
hsa-miR-30e-3p-000422	0.943	hsa-miR-1275-002840	0.7413
hsa-miR-148b#-002160	0.939	hsa-miR-19b-4373098	0.7405
hsa-miR-551b#-002346	0.9281	hsa-miR-769-5p-001998	0.7391
hsa-miR-30a-3p-000416	0.9242	hsa-miR-409-3p-002332	0.733
hsa-miR-1282-002803	0.9213	hsa-miR-23a#-002439	0.7257
hsa-miR-127-3p-4373147	0.9198	hsa-miR-1290-002863	0.7234
hsa-miR-204-4373094	0.9173	hsa-miR-487a-4378097	0.7188
hsa-miR-1301-002827	0.9105	MammU6-4395470	0.7105
hsa-miR-409-5p-4395442	0.9032	hsa-miR-379-4373349	0.7102

hsa-miR-214#-002293	0.8964	hsa-miR-433-4373205	0.7052
hsa-miR-1260-002896	0.8855	hsa-miR-601-001558	0.6896
hsa-miR-516-3p-001149	0.8847	hsa-miR-140-5p-4373374	0.6866
hsa-miR-31-4395390	0.881	hsa-miR-93#-002139	0.6852
hsa-miR-181a-2#-002317	0.8797	hsa-miR-193a-5p-4395392	0.6841
hsa-miR-193b-4395478	0.8773	hsa-miR-140-3p-4395345	0.682
hsa-miR-199a-5p-4373272	0.873	hsa-miR-423-5p-4395451	0.6804
hsa-miR-574-3p-4395460	0.8478	hsa-miR-218-4373081	0.6795
hsa-miR-450a-4395414	0.8454	hsa-miR-148b-4373129	0.6635
hsa-miR-210-4373089	0.8411	hsa-miR-28-3p-4395557	0.6603
hsa-miR-34b-002102	0.8409	hsa-miR-190-4373110	0.6591
hsa-miR-378-000567	0.8386	hsa-let-7b-4395446	0.6586
hsa-miR-151-3p-002254	0.8379	hsa-miR-31#-002113	0.6523
hsa-miR-125b-4373148	0.8261	hsa-miR-380-5p-000570	0.6461
hsa-miR-645-001597	0.8252	hsa-miR-324-3p-4395272	0.642
hsa-miR-103-4373158	0.8219	hsa-miR-22#-002301	0.64
hsa-miR-125b-1#-002378	0.8169	hsa-miR-942-002187	0.6275
hsa-miR-1285-002822	0.8147	hsa-miR-532-5p-4380928	0.6247
hsa-miR-199b-5p-4373100	0.8137	hsa-miR-100-4373160	0.621
hsa-miR-455-5p-4378098	0.612	hsa-miR-330-3p-4373047	0.4712
hsa-miR-502-3p-4395194	0.595	hsa-miR-130b-4373144	0.4711
hsa-miR-1244-002791	0.5942	hsa-miR-29a#-002447	0.4711
hsa-miR-146b-5p-4373178	0.592	hsa-let-7a-4373169	0.4688
hsa-miR-584-001624	0.5864	hsa-miR-26a-4395166	0.4658
hsa-miR-744-4395435	0.5844	has-miR-155-4395459	0.4651
hsa-miR-200c-4395411	0.5829	hsa-miR-106b#-002380	0.4613
hsa-miR-484-4381032	0.5781	hsa-miR-29b-1#-002165	0.4602
hsa-miR-1254-002818	0.5764	hsa-miR-532-3p-4395466	0.457
hsa-miR-126-4395339	0.5747	hsa-miR-1271-002779	0.4369
hsa-miR-370-4395386	0.5728	hsa-miR-542-3p-4378101	0.4356

hsa-let-7c#-002405	0.5682	hsa-miR-671-3p-4395433	0.435
hsa-miR-382-4373019	0.5681	hsa-miR-202-4395474	0.4319
hsa-miR-221-4373077	0.5678	hsa-miR-339-3p-4395295	0.4303
hsa-miR-296-5p-4373066	0.567	hsa-miR-26b-4395167	0.4259
hsa-miR-491-5p-4381053	0.5652	hsa-miR-454-4395434	0.4237
hsa-miR-329-4373191	0.5505	hsa-miR-191#-002678	0.4236
hsa-miR-1274B-002884	0.5481	hsa-miR-875-5p-002203	0.4185
hsa-miR-138-4395395	0.5472	hsa-miR-150-4373127	0.4162
hsa-miR-497-001043	0.5471	hsa-miR-93-4373302	0.4152
hsa-miR-629-4395547	0.5464	hsa-miR-616-4395525	0.4029
hsa-miR-543-002376	0.5417	hsa-miR-130b#-002114	0.3982
hsa-miR-99b#-002196	0.5404	hsa-miR-432#-001027	0.3934
hsa-miR-550-001544	0.535	hsa-miR-618-4380996	0.3838
hsa-miR-345-4395297	0.5319	hsa-miR-26a-1#-002443	0.3742
hsa-miR-331-5p-4395344	0.5311	hsa-miR-20b-4373263	0.3737
hsa-miR-655-4381015	0.5291	hsa-miR-27b#-002174	0.3717
hsa-miR-186-4395396	0.5267	hsa-let-7b#-002404	0.368
hsa-miR-422a-4395408	0.52	hsa-miR-542-5p-4395351	0.368
hsa-miR-99a-4373008	0.518	hsa-miR-125b-2#-002158	0.3666
hsa-miR-1233-002768	0.5159	hsa-miR-629-001562	0.3637
hsa-miR-106b-4373155	0.5137	rno-miR-7#-001338	0.3584
hsa-miR-145#-002149	0.5117	hsa-miR-495-4381078	0.3524
hsa-let-7c-4373167	0.5103	hsa-miR-376c-4395233	0.3474
hsa-miR-28-5p-4373067	0.5086	hsa-miR-494-4395476	0.3452
hsa-miR-539-4378103	0.5035	hsa-miR-130a-4373145	0.3377
hsa-miR-143-4395360	0.5026	hsa-miR-149-4395366	0.3365
hsa-miR-198-4395384	0.5012	hsa-miR-625#-002432	0.3361
hsa-miR-181a-4373117	0.4995	hsa-miR-361-5p-4373035	0.3335
hsa-miR-424#-002309	0.4894	hsa-let-7e-4395517	0.3277
hsa-miR-213-000516	0.4866	hsa-miR-1226#-002758	0.3239

hsa-miR-1296-002908	0.4859	hsa-miR-365-4373194	0.3229
hsa-miR-500-4395539	0.482	hsa-miR-17-4395419	0.3224
hsa-miR-485-3p-4378095	0.4816	hsa-miR-33a#-002136	0.3195
hsa-miR-134-4373299	0.4802	hsa-let-7d-4395394	0.3052
hsa-miR-652-4395463	0.4778	hsa-miR-886-5p-4395304	0.2966
hsa-miR-195-4373105	0.4764	hsa-miR-181c-4373115	0.2942
hsa-miR-941-002183	0.473	RNU48-4373383	0.2897
hsa-miR-191-4395410	0.2874	hsa-miR-146a-4373132	0.2569
hsa-miR-18a#-002423	0.2856	hsa-miR-16-4373121	0.2568
hsa-miR-425#-002302	0.2836	hsa-miR-19b-1#-002425	0.2544
hsa-miR-708-4395452	0.2785	hsa-miR-339-5p-4395368	0.2528
hsa-miR-24-2#-002441	0.2743	hsa-miR-377#-002128	0.2509
hsa-miR-106a-4395280	0.2711	hsa-miR-320-4395388	0.2499
hsa-miR-597-4380960	0.2611	hsa-miR-1303-002792	0.2464

Appendix 5: Deregulated miRNAs in CAFs of GU OSCC in human Pool A

miRNA	Fold change	miRNA	Fold change
hsa-miR-518d-5p-4395500	96.9194	hsa-miR-23a-4373074	8.1608
hsa-miR-22-4373079	50.311	hsa-miR-34a-4395168	8.0328
hsa-miR-133a-4395357	41.0442	hsa-miR-145-4395389	7.9743
hsa-miR-424-4373201	33.6259	hsa-miR-361-5p-4373035	7.8792
hsa-miR-362-3p-4395228	33.4375	hsa-miR-199a-3p-4395415	7.8392
hsa-miR-502-3p-4395194	33.0905	hsa-miR-125b-4373148	7.7441
hsa-miR-660-4380925	32.9392	hsa-miR-199b-5p-4373100	7.5259
hsa-miR-203-4373095	31.7956	hsa-miR-381-4373020	7.496
hsa-miR-101-4395364	31.7396	hsa-miR-199a-5p-4373272	7.2778
hsa-miR-181c-4373115	30.7453	hsa-miR-140-3p-4395345	7.17
hsa-miR-522-4395524	27.1162	hsa-miR-200c-4395411	6.953
hsa-miR-503-4373228	25.4357	hsa-miR-425-4380926	6.8041
hsa-miR-34c-5p-4373036	23.5443	hsa-miR-27a-4373287	6.7619
hsa-let-7c-4373167	21.6266	hsa-miR-490-3p-4373215	6.7522
hsa-miR-496-4386771	20.658	hsa-miR-629-4395547	6.7497
hsa-miR-204-4373094	19.2454	hsa-miR-126-4395339	6.6491
hsa-miR-542-3p-4378101	18.6858	hsa-miR-501-5p-4373226	6.6451
hsa-miR-9-4373285	17.6364	hsa-miR-146a-4373132	6.5728
hsa-miR-21-4373090	17.5497	hsa-miR-26a-4395166	6.5186
hsa-miR-502-5p-4373227	17.4139	hsa-miR-28-3p-4395557	6.4396
hsa-miR-532-5p-4380928	16.3899	hsa-miR-299-5p-4373188	6.3918
hsa-miR-23b-4373073	15.8634	hsa-miR-127-5p-4395340	6.3603
hsa-miR-181a-4373117	15.7465	hsa-miR-365-4373194	6.3497
hsa-miR-146b-5p-4373178	15.006	hsa-miR-29b-4373288	6.2665
hsa-miR-337-5p-4395267	14.5399	hsa-miR-885-3p-4395483	6.2532
hsa-miR-142-3p-4373136	13.9163	hsa-miR-100-4373160	6.1512
hsa-miR-210-4373089	13.8281	hsa-miR-214-4395417	6.0828

hsa-miR-137-4373301	13.2145	hsa-miR-26b-4395167	6.0369
hsa-miR-185-4395382	13.0136	hsa-miR-99a-4373008	5.8783
hsa-miR-198-4395384	13.0133	hsa-miR-19b-4373098	5.7726
hsa-miR-335-4373045	12.9837	hsa-miR-25-4373071	5.6207
hsa-miR-652-4395463	12.2794	hsa-miR-342-3p-4395371	5.6163
hsa-miR-192-4373108	12.076	hsa-let-7e-4395517	5.612
hsa-miR-143-4395360	11.9921	hsa-miR-654-3p-4395350	5.5811
hsa-miR-450a-4395414	11.7134	hsa-miR-32-4395220	5.5536
hsa-miR-331-5p-4395344	10.8592	hsa-miR-422a-4395408	5.533
hsa-miR-184-4373113	10.2865	hsa-miR-301b-4395503	5.4075
hsa-miR-106b-4373155	9.7765	hsa-miR-20a-4373286	5.3774
hsa-miR-27b-4373068	9.6622	hsa-miR-374b-4381045	5.3336
hsa-miR-511-4373236	9.5552	hsa-miR-889-4395313	5.333
hsa-miR-651-4381007	9.2495	hsa-miR-590-5p-4395176	5.2839
hsa-miR-340-4395369	9.1528	hsa-miR-744-4395435	5.2746
hsa-miR-374a-4373028	8.909	hsa-miR-411-4381013	5.2699
hsa-miR-455-5p-4378098	5.2427	hsa-miR-890-4395320	3.3778
hsa-miR-134-4373299	5.234	hsa-miR-654-5p-4381014	3.3373
hsa-miR-369-3p-4373032	5.1954	hsa-miR-886-3p-4395305	3.2494
hsa-miR-98-4373009	5.1818	hsa-miR-135b-4395372	3.2436
hsa-let-7g-4395393	5.1536	hsa-miR-125a-5p-4395309	3.1142
hsa-miR-579-4395509	5.0699	hsa-miR-190-4373110	3.0376
hsa-miR-505-4395200	5.0694	hsa-miR-708-4395452	2.9492
hsa-let-7a-4373169	5.0556	hsa-miR-452-4395440	2.8971
hsa-miR-31-4395390	5.0379	hsa-miR-148a-4373130	2.8189
hsa-miR-520a-3p-4373268	5.0329	hsa-miR-642-4380995	2.7939
hsa-miR-221-4373077	4.8592	hsa-miR-339-3p-4395295	2.7157
hsa-miR-655-4381015	4.8046	hsa-miR-148b-4373129	2.6732
hsa-miR-106a-4395280	4.8004	hsa-miR-149-4395366	2.6376
hsa-miR-15a-4373123	4.7776	hsa-miR-597-4380960	2.4837

hsa-miR-379-4373349	4.6801	hsa-miR-409-5p-4395442	2.4836
hsa-let-7b-4395446	4.6592	hsa-miR-95-4373011	2.4601
hsa-miR-491-5p-4381053	4.6162	hsa-miR-139-5p-4395400	2.4432
hsa-miR-132-4373143	4.5776	hsa-miR-493-4395475	2.4404
hsa-miR-223-4395406	4.5637	hsa-miR-302c-4378072	2.4331
hsa-miR-495-4381078	4.5079	hsa-miR-339-5p-4395368	2.4185
hsa-miR-29a-4395223	4.4729	hsa-miR-636-4395199	2.418
hsa-miR-195-4373105	4.2926	hsa-miR-628-5p-4395544	2.3293
hsa-miR-29c-4395171	4.2884	hsa-miR-16-4373121	2.3146
hsa-miR-17-4395419	4.2812	hsa-miR-487a-4378097	2.1821
hsa-miR-19a-4373099	4.2378	hsa-miR-431-4395173	2.1445
hsa-miR-329-4373191	4.192	hsa-miR-576-3p-4395462	2.1154
hsa-miR-20b-4373263	4.1836	hsa-miR-367-4373034	2.092
hsa-miR-486-5p-4378096	4.1775	hsa-miR-454-4395434	2.092
hsa-miR-18a-4395533	4.0688	hsa-miR-758-4395180	1.9714
hsa-miR-455-3p-4395355	3.9712	has-miR-155-4395459	1.9415
hsa-miR-93-4373302	3.9397	hsa-miR-542-5p-4395351	1.8968
hsa-miR-487b-4378102	3.8991	hsa-miR-296-5p-4373066	1.7779
hsa-miR-107-4373154	3.8469	hsa-miR-330-3p-4373047	1.7651
hsa-miR-129-3p-4373297	3.8248	hsa-miR-433-4373205	1.6518
hsa-miR-15b-4373122	3.82	hsa-miR-886-5p-4395304	1.6245
hsa-miR-301a-4373064	3.7957	hsa-miR-302a-4378070	1.5258
hsa-miR-200b-4395362	3.783	RNU48-4373383	1.4985
hsa-let-7d-4395394	3.7685	hsa-miR-523-4395497	1.4935
hsa-miR-24-4373072	3.7204	RNU44-4373384	1.4538
hsa-miR-194-4373106	3.6926	hsa-miR-383-4373018	1.3819
hsa-let-7f-4373164	3.6605	hsa-miR-224-4395210	1.3791
hsa-miR-671-3p-4395433	3.6254	hsa-miR-483-5p-4395449	1.3497
hsa-miR-202-4395474	3.555	MammU6-4395470	1
hsa-miR-212-4373087	3.5093	hsa-miR-518b-4373246	0.9648

hsa-miR-222-4395387	3.4274	hsa-miR-888-4395323	0.9531
hsa-miR-627-4380967	0.7469	hsa-miR-150-4373127	0.5004
hsa-miR-302b-4378071	0.7318	hsa-miR-485-3p-4378095	0.443
hsa-miR-520e-4373255	0.696	hsa-miR-618-4380996	0.409
hsa-miR-515-3p-4395480	0.6802		

Appendix 6: Deregulated miRNAs in CAFs of GU OSCC in human pool B

miRNA	Fold change	miRNA	Fold change
hsa-miR-941-002183	204.3365	hsa-miR-516-3p-001149	27.4043
hsa-miR-765-002643	181.1082	hsa-miR-659-001514	27.0183
hsa-miR-1283-002890	158.8126	rno-miR-29c#-001818	26.6856
hsa-miR-206-000510	158.5523	hsa-miR-424#-002309	25.7597
hsa-miR-497#-002368	153.7945	hsa-miR-186#-002105	25.6371
hsa-miR-378-000567	144.4758	hsa-miR-361-3p-002116	25.2248
hsa-miR-33a-002135	137.4333	hsa-miR-106b#-002380	24.3526
hsa-miR-92a-1#-002137	137.2074	hsa-miR-578-001619	23.7451
hsa-miR-1294-002785	124.1416	hsa-miR-1178-002777	23.5636
hsa-miR-1243-002854	112.743	hsa-miR-1293-002905	23.158
hsa-miR-650-001603	96.0804	hsa-miR-1233-002768	21.3057
hsa-miR-630-001563	93.0228	hsa-miR-1248-002870	21.2815
hsa-miR-766-001986	91.677	hsa-miR-181c#-002333	21.2088
hsa-miR-1288-002832	82.5381	hsa-miR-888#-002213	21.0114
hsa-miR-99a#-002141	75.7578	hsa-miR-664-002897	20.9636
hsa-miR-550-001544	72.9208	hsa-miR-380-5p-000570	20.6336
hsa-miR-1253-002894	71.8564	hsa-miR-222#-002097	20.4816
hsa-miR-26a-1#-002443	71.6134	hsa-miR-505#-002087	20.1038
hsa-miR-744#-002325	71.4784	hsa-miR-520c-3p-002400	19.2109
hsa-let-7c#-002405	71.2403	hsa-miR-1284-002903	18.947
hsa-miR-200c#-002286	71.1372	hsa-miR-30a-5p-000417	18.6596
hsa-miR-320B-002844	64.8835	hsa-miR-25#-002442	18.4091
hsa-miR-641-001585	54.6647	hsa-miR-1228#-002763	18.1762
hsa-miR-1204-002872	54.1216	hsa-miR-638-001582	17.8076
hsa-miR-939-002182	48.9847	hsa-miR-125b-2#-002158	17.8
hsa-miR-213-000516	48.2222	hsa-miR-628-3p-002434	16.9144
hsa-miR-1179-002776	46.7899	hsa-miR-1245-002823	16.79

hsa-miR-221#-002096	42.7966	hsa-miR-16-2#-002171	16.4551
hsa-miR-609-001573	39.7896	hsa-miR-93#-002139	16.3183
hsa-miR-378-002243	37.494	hsa-miR-181a-2#-002317	16.0159
hsa-miR-30d#-002305	36.9543	hsa-miR-218-2#-002294	15.8301
hsa-miR-30d-000420	34.9349	hsa-miR-643-001594	15.585
hsa-miR-548L-002904	34.7771	hsa-miR-21#-002438	15.4455
hsa-miR-376a#-002127	34.348	hsa-miR-214#-002293	15.3012
hsa-miR-497-001043	32.9667	hsa-miR-920-002150	15.1643
hsa-miR-661-001606	30.7817	hsa-miR-606-001569	14.6222
hsa-miR-34b-002102	30.4502	hsa-let-7f-1#-002417	14.3766
hsa-miR-1208-002880	29.8992	hsa-miR-30a-3p-000416	14.1047
hsa-miR-1197-002810	29.884	hsa-miR-592-001546	13.9807
hsa-miR-1264-002799	28.7913	hsa-miR-149#-002164	13.9155
hsa-miR-575-001617	27.4567	hsa-miR-136#-002100	13.7406
hsa-miR-146a#-002163	13.5909	hsa-miR-658-001513	8.5289
hsa-miR-377#-002128	13.2956	hsa-miR-657-001512	8.5289
hsa-miR-604-001567	12.9967	hsa-miR-649-001602	8.5289
hsa-miR-769-5p-001998	12.8165	hsa-miR-648-001601	8.5289
hsa-miR-452#-002330	12.7953	hsa-miR-647-001600	8.5289
hsa-miR-656-001510	12.6009	hsa-miR-646-001599	8.5289
hsa-miR-1255A-002805	12.4454	hsa-miR-644-001596	8.5289
hsa-miR-572-001614	12.3284	hsa-miR-640-001584	8.5289
hsa-miR-27a#-002445	12.0942	hsa-miR-639-001583	8.5289
hsa-miR-1225-3P-002766	11.7112	hsa-miR-637-001581	8.5289
hsa-miR-1324-002815	11.6876	hsa-miR-635-001578	8.5289
hsa-miR-549-001511	11.6045	hsa-miR-631-001564	8.5289
hsa-miR-340#-002259	11.5064	hsa-miR-626-001559	8.5289
hsa-let-7b#-002404	11.4573	hsa-miR-622-001553	8.5289
hsa-miR-10a#-002288	11.4202	hsa-miR-621-001598	8.5289
hsa-miR-202#-002362	10.7234	hsa-miR-614-001587	8.5289

hsa-miR-1238-002927	10.026	hsa-miR-613-001586	8.5289
hsa-miR-30e-3p-000422	10.0094	hsa-miR-607-001570	8.5289
hsa-miR-130b#-002114	9.9208	hsa-miR-605-001568	8.5289
hsa-miR-1274A-002883	9.911	hsa-miR-600-001556	8.5289
hsa-miR-668-001992	9.7533	hsa-miR-599-001554	8.5289
hsa-miR-585-001625	9.2266	hsa-miR-595-001987	8.5289
hsa-miR-31#-002113	8.9137	hsa-miR-593-001547	8.5289
hsa-miR-193b#-002366	8.8438	hsa-miR-591-001545	8.5289
hsa-let-7a#-002307	8.7302	hsa-miR-588-001542	8.5289
hsa-miR-593-002411	8.6911	hsa-miR-587-001540	8.5289
hsa-miR-148b#-002160	8.6286	hsa-miR-586-001539	8.5289
hsa-miR-617-001591	8.6017	hsa-miR-584-001624	8.5289
mmu-let-7d#-001178	8.5289	hsa-miR-583-001623	8.5289
hsa-miR-96#-002140	8.5289	hsa-miR-581-001622	8.5289
hsa-miR-944-002189	8.5289	hsa-miR-580-001621	8.5289
hsa-miR-943-002188	8.5289	hsa-miR-569-001536	8.5289
hsa-miR-937-002180	8.5289	hsa-miR-567-001534	8.5289
hsa-miR-936-002179	8.5289	hsa-miR-566-001533	8.5289
hsa-miR-935-002178	8.5289	hsa-miR-563-001530	8.5289
hsa-miR-934-002177	8.5289	hsa-miR-562-001529	8.5289
hsa-miR-933-002176	8.5289	hsa-miR-559-001527	8.5289
hsa-miR-92a-2#-002138	8.5289	hsa-miR-558-001526	8.5289
hsa-miR-924-002154	8.5289	hsa-miR-557-001525	8.5289
hsa-miR-922-002152	8.5289	hsa-miR-555-001523	8.5289
hsa-miR-892b-002214	8.5289	hsa-miR-554-001522	8.5289
hsa-miR-802-002004	8.5289	hsa-miR-553-001521	8.5289
hsa-miR-769-3p-002003	8.5289	hsa-miR-552-001520	8.5289
hsa-miR-767-5p-001993	8.5289	hsa-miR-551b#-002346	8.5289
hsa-miR-767-3p-001995	8.5289	hsa-miR-551a-001519	8.5289
hsa-miR-708#-002342	8.5289	hsa-miR-550-002410	8.5289

hsa-miR-665-002681	8.5289	hsa-miR-548K-002819	8.5289
hsa-miR-662-001607	8.5289	hsa-miR-548I-002909	8.5289
hsa-miR-541#-002200	8.5289	hsa-miR-1250-002887	8.5289
hsa-miR-524-001173	8.5289	hsa-miR-124#-002197	8.5289
hsa-miR-520h-001170	8.5289	hsa-miR-1236-002761	8.5289
hsa-miR-519e#-001166	8.5289	hsa-miR-1224-3P-002752	8.5289
hsa-miR-518f#-002387	8.5289	hsa-miR-1205-002778	8.5289
hsa-miR-518e#-002371	8.5289	hsa-miR-1200-002829	8.5289
hsa-miR-518c#-001158	8.5289	hsa-miR-106a#-002170	8.5289
hsa-miR-513C-002756	8.5289	hsa-miR-105#-002168	8.5289
hsa-miR-513B-002757	8.5289	hsa-miR-101#-002143	8.5289
hsa-miR-488-001106	8.5289	hsa-let-7g#-002118	8.5289
hsa-miR-431#-002312	8.5289	hsa-miR-151-5P-002642	8.394
hsa-miR-367#-002121	8.5289	hsa-miR-564-001531	8.378
hsa-miR-32#-002111	8.5289	hsa-miR-34a#-002316	8.3733
hsa-miR-30c-2#-002110	8.5289	hsa-miR-22#-002301	8.3414
hsa-miR-30c-1#-002108	8.5289	hsa-miR-1271-002779	8.2775
hsa-miR-30b#-002129	8.5289	hsa-miR-938-002181	8.0726
hsa-miR-302d#-002120	8.5289	hsa-miR-29b-1#-002165	8.0344
hsa-miR-302c#-000534	8.5289	hsa-miR-7-2#-002314	7.6777
hsa-miR-302b#-002119	8.5289	hsa-miR-1296-002908	7.6704
hsa-miR-302a#-002381	8.5289	hsa-miR-144#-002148	7.6345
hsa-miR-223#-002098	8.5289	hsa-miR-1255B-002801	7.6255
hsa-miR-218-1#-002094	8.5289	hsa-miR-363#-001283	7.5163
hsa-miR-20b#-002311	8.5289	hsa-miR-1256-002850	7.4017
hsa-miR-200b#-002274	8.5289	hsa-miR-92b#-002343	7.3751
hsa-miR-200a#-001011	8.5289	hsa-miR-454#-001996	7.0242
hsa-miR-196a#-002336	8.5289	hsa-miR-675-002005	6.6316
hsa-miR-195#-002107	8.5289	hsa-miR-141#-002145	6.5407
hsa-miR-194#-002379	8.5289	hsa-miR-663B-002857	6.3409

hsa-miR-192#-002272	8.5289	hsa-miR-29a#-002447	6.3167
hsa-miR-18b#-002310	8.5289	hsa-miR-145#-002149	6.297
hsa-miR-185#-002104	8.5289	hsa-miR-155#-002287	6.2347
hsa-miR-1826-002873	8.5289	hsa-miR-432#-001027	6.1733
hsa-miR-182#-000483	8.5289	hsa-let-7f-2#-002418	5.9915
hsa-miR-148a#-002134	8.5289	hsa-miR-625#-002432	5.9664
hsa-miR-143#-002146	8.5289	hsa-miR-548J-002783	5.6575
hsa-miR-138-2#-002144	8.5289	hsa-miR-624-001557	5.5963
hsa-miR-135b#-002159	8.5289	hsa-miR-26a-2#-002115	5.5638
hsa-miR-132#-002132	8.5289	hsa-miR-571-001613	5.5611
hsa-miR-130a#-002131	8.5289	hsa-miR-27b#-002174	5.5234
hsa-miR-1292-002824	8.5289	hsa-miR-191#-002678	5.2472
hsa-miR-129#-002298	8.5289	hsa-miR-15a#-002419	5.1052
hsa-miR-1289-002871	8.5289	hsa-miR-374a#-002125	5.0497
hsa-miR-1286-002773	8.5289	hsa-let-7i#-002172	5.0431
hsa-miR-1272-002845	8.5289	hsa-miR-875-5p-002203	4.9598
hsa-miR-1263-002784	8.5289	hsa-miR-26b#-002444	4.8616
hsa-miR-1259-002796	8.5289	hsa-miR-122#-002130	4.661
hsa-miR-1257-002910	8.5289	hsa-miR-1300-002902	4.6542
hsa-miR-1251-002820	8.5289	hsa-miR-432-001026	4.6499
hsa-miR-1282-002803	4.5907	hsa-miR-1262-002852	1.503
hsa-miR-548N-002888	4.5463	hsa-miR-601-001558	1.4772
hsa-miR-1290-002863	4.5032	hsa-miR-1227-002769	1.4528
hsa-miR-590-3P-002677	4.4819	hsa-miR-17#-002421	1.4093
hsa-let-7e#-002407	4.4181	hsa-miR-1304-002874	1.3882
dme-miR-7-000268	4.4132	hsa-miR-374b#-002391	1.3647
hsa-miR-24-2#-002441	4.389	hsa-miR-548E-002881	1.3082
hsa-miR-29b-2#-002166	4.3446	hsa-miR-1206-002878	1.2697
hsa-miR-154#-000478	4.2175	hsa-miR-1244-002791	1.1792
hsa-miR-645-001597	4.09	RNU44-001094	1.132

hsa-miR-19b-1#-002425	3.992	hsa-miR-190b-002263	1.1218
hsa-miR-100#-002142	3.9879	U6 snRNA-001973	1
hsa-miR-99b#-002196	3.754	hsa-miR-1301-002827	0.9488
hsa-miR-770-5p-002002	3.6818	hsa-miR-1260-002896	0.8635
hsa-miR-20a#-002437	3.6506	RNU48-001006	0.8279
hsa-miR-425#-002302	3.5856	hsa-miR-1302-002901	0.8221
hsa-miR-1267-002885	3.5376	hsa-miR-623-001555	0.7574
hsa-miR-720-002895	3.4822	hsa-miR-573-001615	0.7246
hsa-miR-519b-3p-002384	3.3902	hsa-miR-520D-3P-002743	0.6935
hsa-miR-577-002675	3.3788	hsa-miR-1252-002860	0.6892
hsa-miR-126#-000451	3.3772	hsa-miR-1303-002792	0.6636
hsa-miR-1183-002841	3.2754	hsa-miR-589-001543	2.2851
hsa-miR-1285-002822	3.2604	hsa-miR-409-3p-002332	2.2498
hsa-miR-1226#-002758	3.2309	hsa-miR-337-3p-002157	2.0466
hsa-miR-1270-002807	3.1999	hsa-miR-1276-002843	2.0445
hsa-miR-411#-002238	3.1976	hsa-miR-543-002376	1.992
hsa-miR-1275-002840	3.066	hsa-miR-629-001562	1.9471
hsa-miR-183#-002270	3.0084	hsa-miR-548G-002879	1.9373
hsa-miR-1274B-002884	2.8127	hsa-miR-338-5P-002658	1.7768
hsa-miR-921-002151	2.7973	hsa-miR-9#-002231	1.7362
hsa-miR-125b-1#-002378	2.7005	hsa-miR-16-1#-002420	1.723
hsa-miR-1180-002847	2.5527	hsa-miR-1305-002867	1.6802
hsa-miR-942-002187	2.5419	hsa-miR-1254-002818	1.5329
hsa-miR-548M-002775	2.3973	hsa-miR-23a#-002439	1.5196
ath-miR159a-000338	2.3583		

Appendix 7: Melt Curves or primer dissociation curves of SYBR green primers

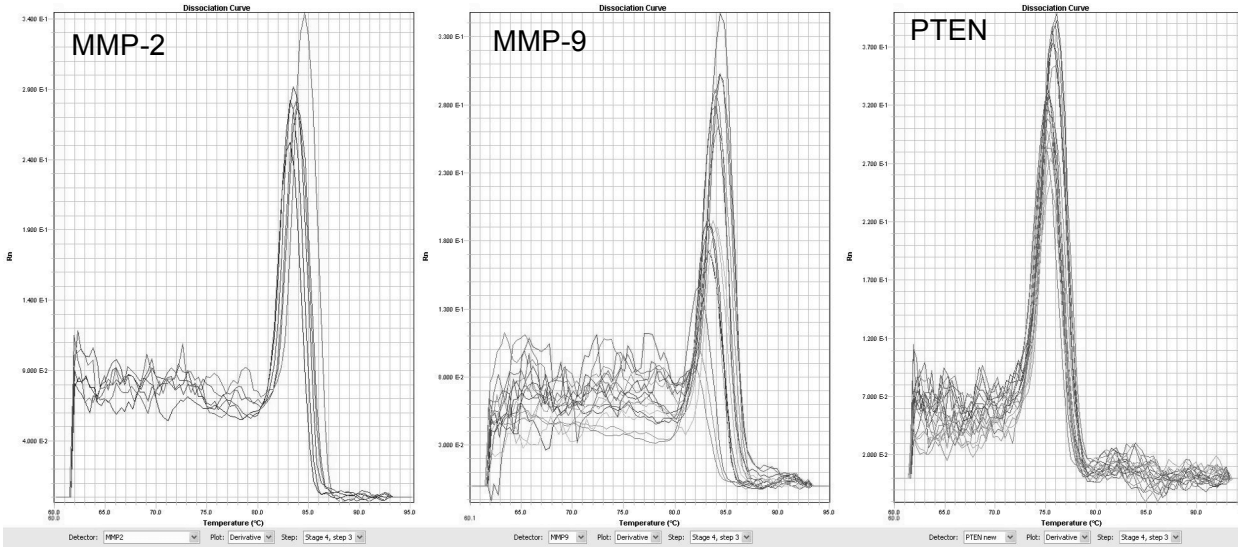

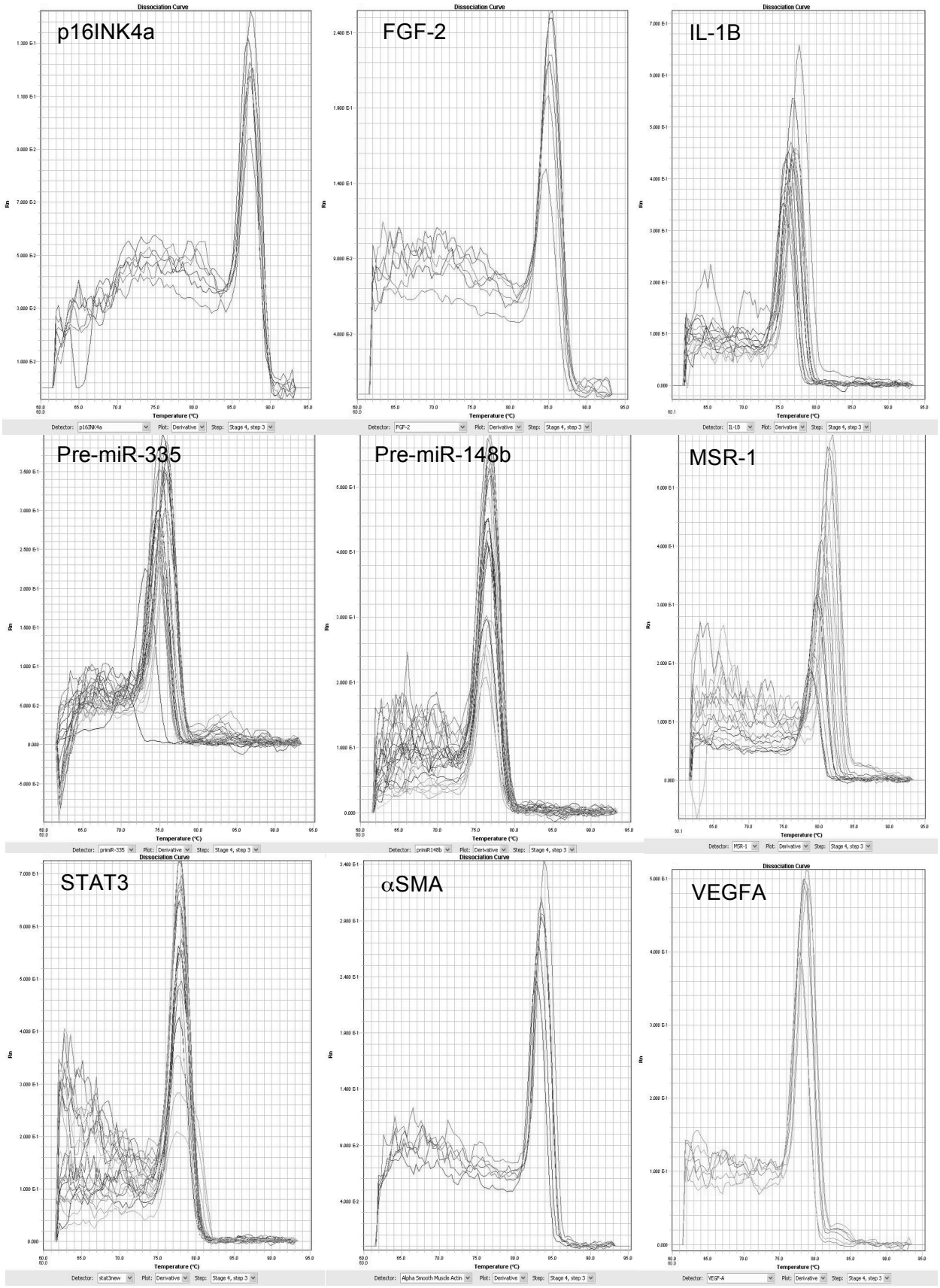
p16INK4a
FGF-2
IL-1B
Pre-miR-335
Pre-miR-148b
MSR-1
STAT3
αSMA
VEGFA
Dissociation Curve
Rn
Temperature (°C)

A. Human Endothelin I ELISA

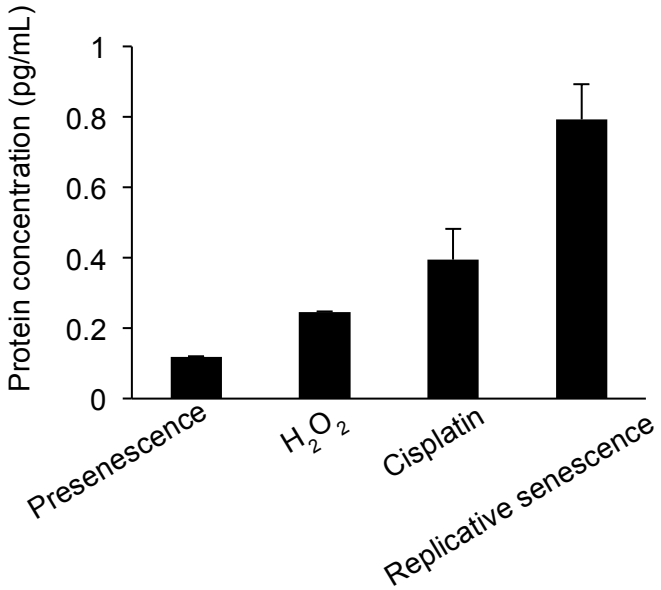

B.

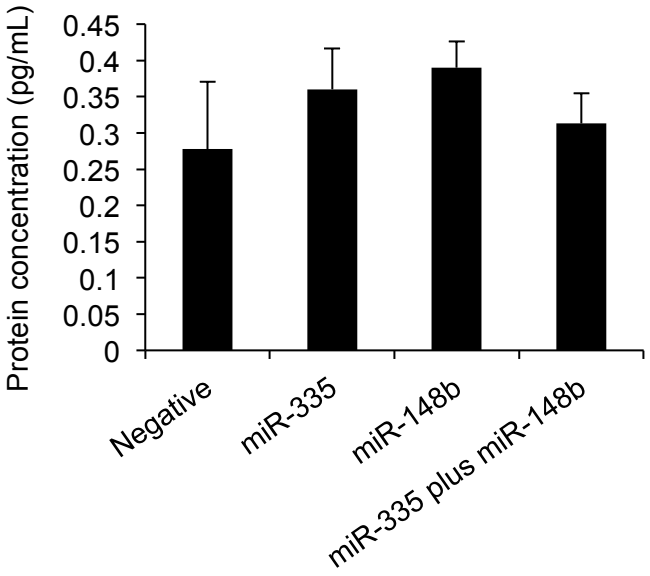

Appendix 8: Human Endothelin 1 ELISA. Secretion of human endothelin I into conditioned media by senescent human oral fibroblasts (A) and miRNA transfected oral fibroblasts (B) were determined using ELISA. The bars represent mean + SEM.

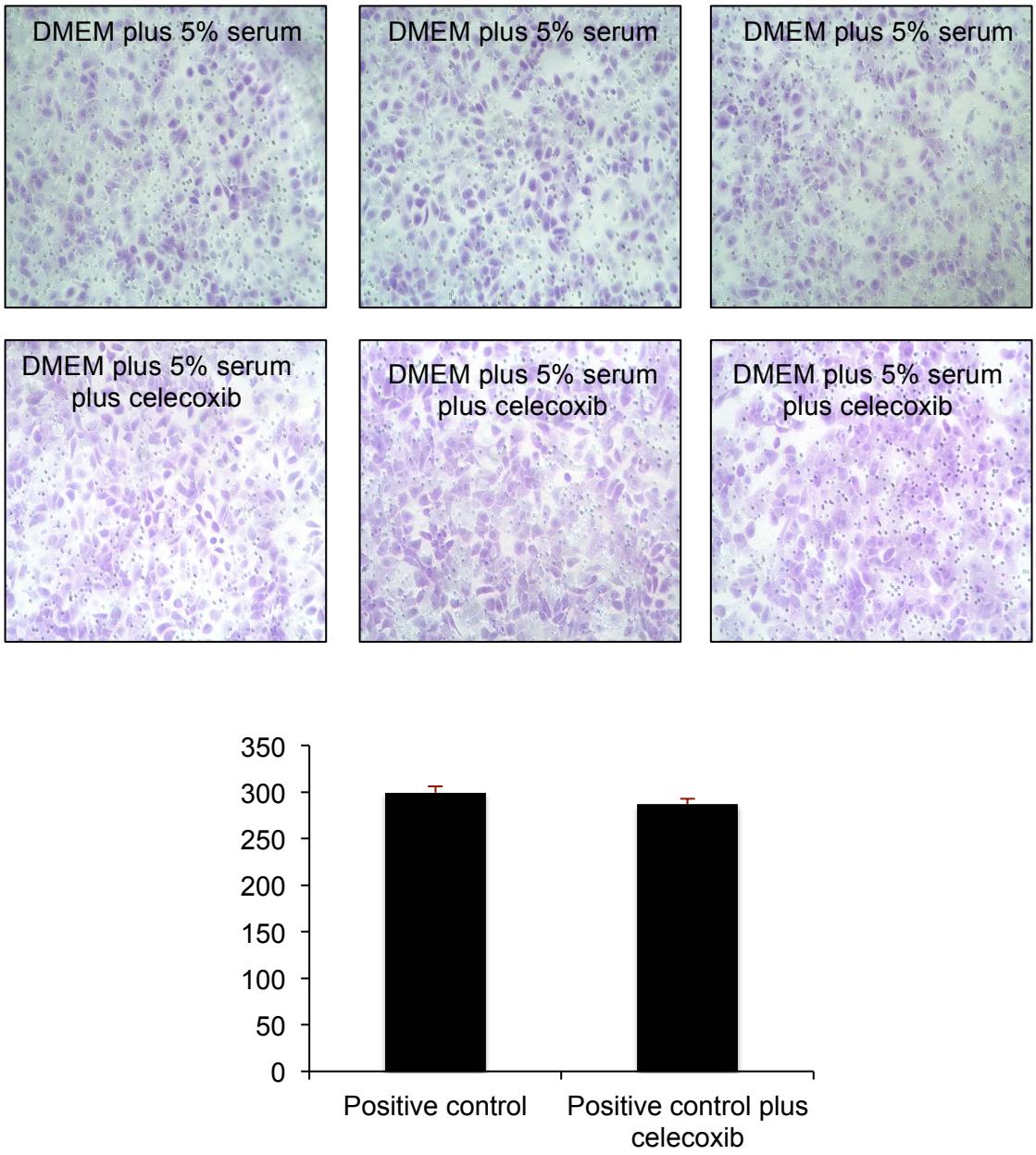

Appendix 9: Differences in H357 migration in positive control in response to celecoxib (DMEM plus 5% serum) before and after treatment with celecoxib. N=3, p=0.33. *p<0.05.

A.

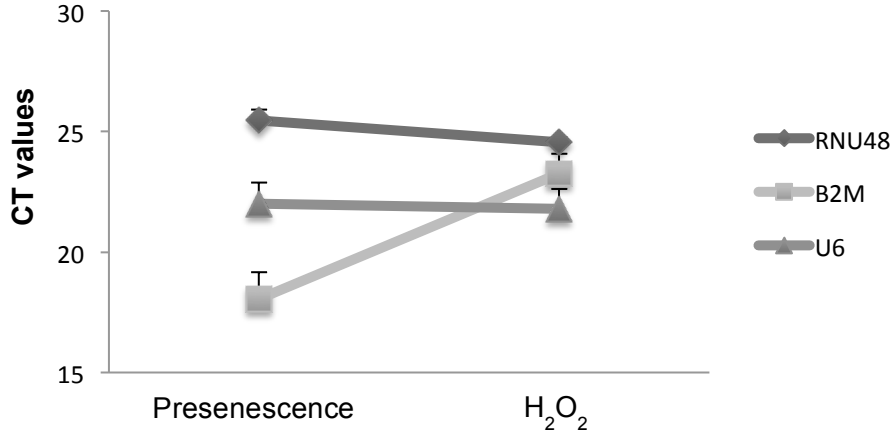

B.

Standard deviation	RNU48	B2M	U6
Experiment 1	0.572217386	3.292605119	0.43113189
Experiment 2	0.451038383	2.130606565	0.126223223
Experiment 3			0.561001286

C.

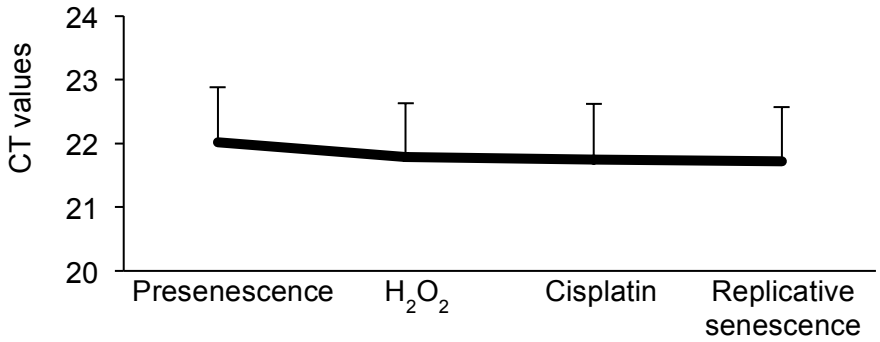

Appendix 10 : Determination of CT values of internal controls in senescent and presenescent oral fibroblasts. qRT-PCR was done to determine the standard deviation of CT values of three different internal controls (B2M, RNU48 and U6) in hydrogen peroxide induced premature senescent and presenescent oral fibroblasts (A and B). Validation of deviation of CT values of U6 in all samples by qRT-PCR (C). The lines represent mean of CT values + SEM.

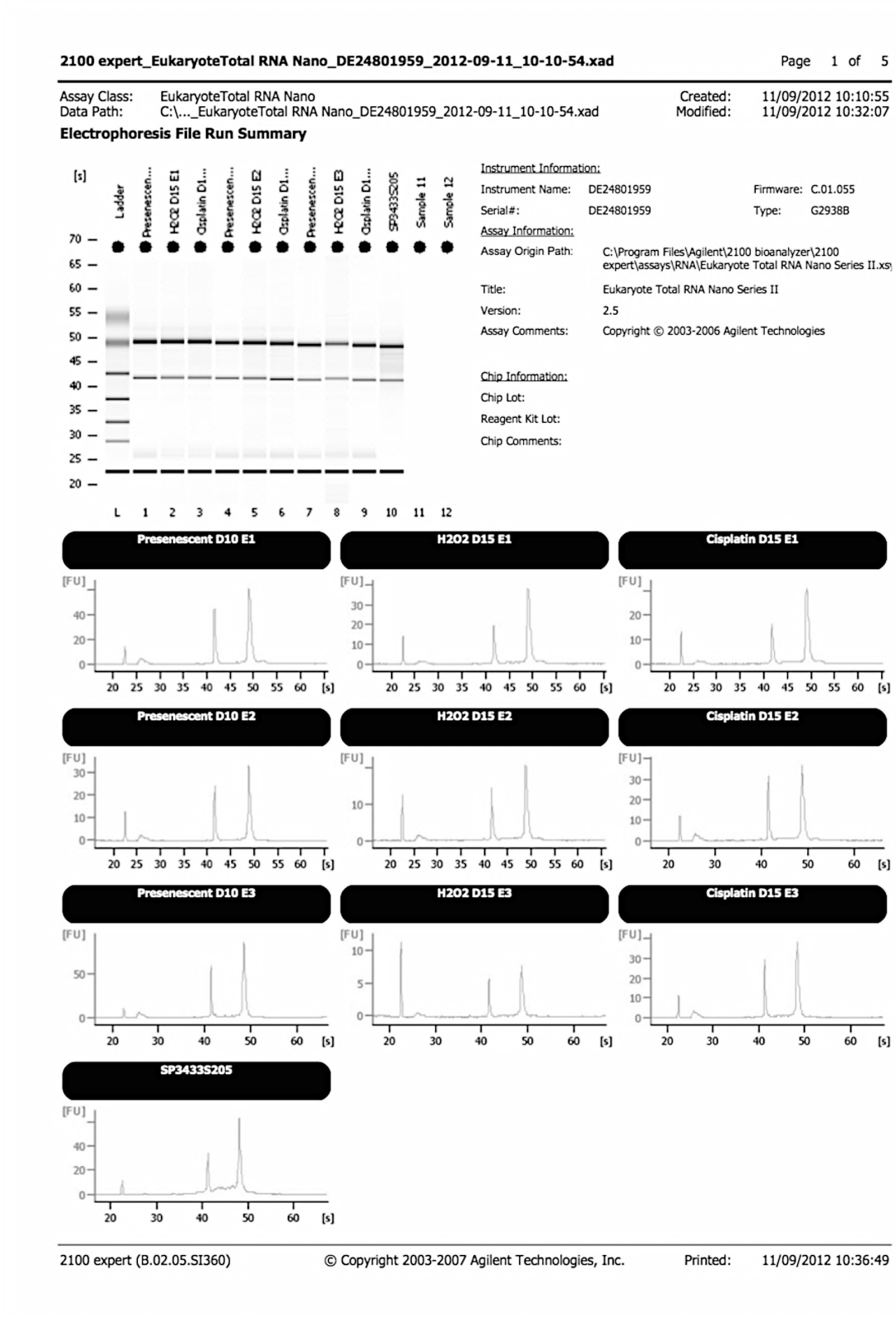

Appendix 11A: Electropherogram summary of RNA integrity using bioanalyzer

2100 expert_EukaryoteTotal RNA Nano_DE24801959_2012-09-11_10-10-54.xad Page 3 of 5

Assay Class: EukaryoteTotal RNA Nano
Data Path: C:\..._EukaryoteTotal RNA Nano_DE24801959_2012-09-11_10-10-54.xad

Created: 11/09/2012 10:10:55
Modified: 11/09/2012 10:32:07

Electropherogram Summary

Ladder

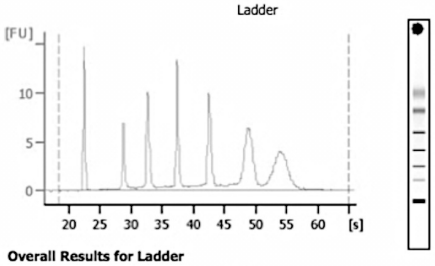

Overall Results for Ladder

RNA Area:	118.2
RNA Concentration:	150 ng/µl
Result Flagging Color:	
Result Flagging Label:	

Presenescent D10 E1

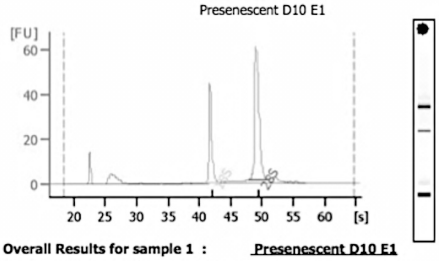

Overall Results for sample 1 : Presenescent D10 E1

RNA Area:	209.4
RNA Concentration:	266 ng/µl
rRNA Ratio [28s / 18s]:	2.1
RNA Integrity Number (RIN):	10.0 (B.02.05)
Result Flagging Color:	
Result Flagging Label:	

Fragment table for sample 1 : Presenescent D10 E1

Name	Start Time [s]	End Time [s]	Area	% of total Area
18S	40.87	43.22	48.2	23.0
28S	47.82	51.06	100.1	47.8

H2O2 D15 E1

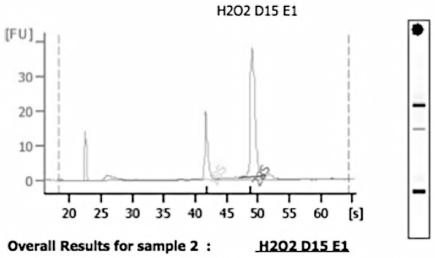

Overall Results for sample 2 : H2O2 D15 E1

RNA Area:	112.9
RNA Concentration:	143 ng/µl
rRNA Ratio [28s / 18s]:	2.5
RNA Integrity Number (RIN):	10.0 (B.02.05)
Result Flagging Color:	
Result Flagging Label:	

Fragment table for sample 2 : H2O2 D15 E1

Name	Start Time [s]	End Time [s]	Area	% of total Area
18S	40.88	43.04	24.1	21.3
28S	46.92	50.94	61.0	54.0

Cisplatin D15 E1

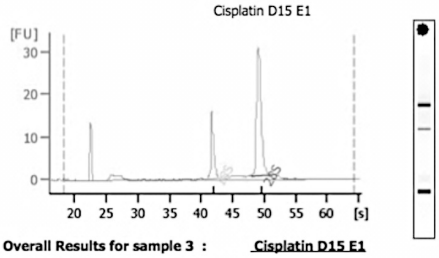

Overall Results for sample 3 : Cisplatin D15 E1

RNA Area:	96.1
RNA Concentration:	122 ng/µl
rRNA Ratio [28s / 18s]:	2.4
RNA Integrity Number (RIN):	10.0 (B.02.05)
Result Flagging Color:	
Result Flagging Label:	

Fragment table for sample 3 : Cisplatin D15 E1

Name	Start Time [s]	End Time [s]	Area	% of total Area
18S	40.66	43.41	20.3	21.2
28S	47.99	51.16	48.8	50.8

2100 expert (B.02.05.SI360) Printed: 11/09/2012 10:36:49

Appendix 11B: Electropherogram summary of RNA integrity using bioanalyzer

2100 expert_EukaryoteTotal RNA Nano_DE24801959_2012-09-11_10-10-54.xad Page 4 of 5

Assay Class: EukaryoteTotal RNA Nano Created: 11/09/2012 10:10:55
Data Path: C:\..._EukaryoteTotal RNA Nano_DE24801959_2012-09-11_10-10-54.xad Modified: 11/09/2012 10:32:07

Electropherogram Summary Continued ...

Presenescent D10 E2

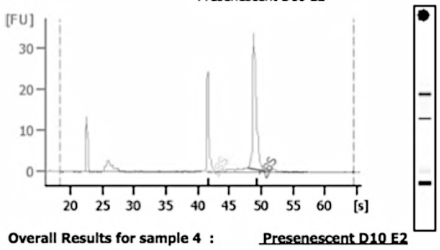

Overall Results for sample 4 : Presenescent D10 E2

RNA Area:	85.8
RNA Concentration:	109 ng/µl
rRNA Ratio [28s / 18s]:	2.1
RNA Integrity Number (RIN):	10.0 (B.02.05)
Result Flagging Color:	
Result Flagging Label:	

Fragment table for sample 4 : Presenescent D10 E2

Name	Start Time [s]	End Time [s]	Area	% of total Area
18S	40.73	42.89	20.7	24.1
28S	47.86	50.63	42.9	50.0

H2O2 D15 E2

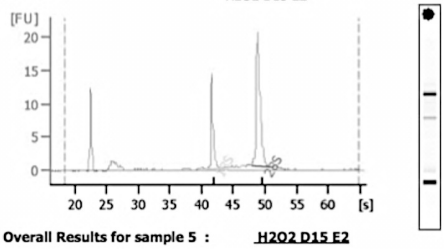

Overall Results for sample 5 : H2O2 D15 E2

RNA Area:	63.3
RNA Concentration:	80 ng/µl
rRNA Ratio [28s / 18s]:	2.1
RNA Integrity Number (RIN):	10.0 (B.02.05)
Result Flagging Color:	
Result Flagging Label:	

Fragment table for sample 5 : H2O2 D15 E2

Name	Start Time [s]	End Time [s]	Area	% of total Area
18S	40.72	43.02	13.7	21.7
28S	47.82	51.07	28.2	44.6

Cisplatin D15 E2

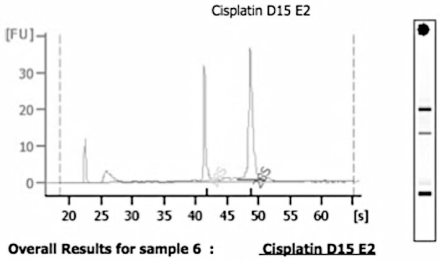

Overall Results for sample 6 : Cisplatin D15 E2

RNA Area:	123.7
RNA Concentration:	157 ng/µl
rRNA Ratio [28s / 18s]:	1.9
RNA Integrity Number (RIN):	10.0 (B.02.05)
Result Flagging Color:	
Result Flagging Label:	

Fragment table for sample 6 : Cisplatin D15 E2

Name	Start Time [s]	End Time [s]	Area	% of total Area
18S	40.60	42.97	27.4	22.2
28S	46.65	50.91	53.3	43.1

Presenescent D10 E3

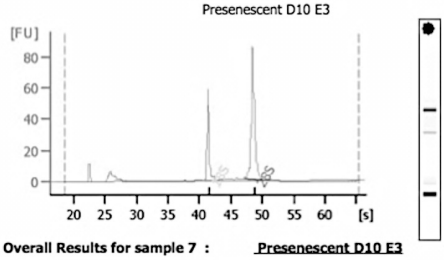

Overall Results for sample 7 : Presenescent D10 E3

RNA Area:	220.6
RNA Concentration:	280 ng/µl
rRNA Ratio [28s / 18s]:	2.2
RNA Integrity Number (RIN):	10.0 (B.02.05)
Result Flagging Color:	
Result Flagging Label:	

Fragment table for sample 7 : Presenescent D10 E3

Name	Start Time [s]	End Time [s]	Area	% of total Area
18S	40.54	42.77	50.7	23.0
28S	47.04	50.60	110.8	50.2

2100 expert (B.02.05.SI360) Printed: 11/09/2012 10:36:49

Appendix 11C: Electropherogram summary of RNA integrity using bioanalyzer

Assay Class: EukaryoteTotal RNA Nano
Data Path: C:\..._EukaryoteTotal RNA Nano_DE24801959_2012-09-11_10-10-54.xad

Created: 11/09/2012 10:10:55
Modified: 11/09/2012 10:32:07

Electropherogram Summary Continued ...

H2O2 D15 E3

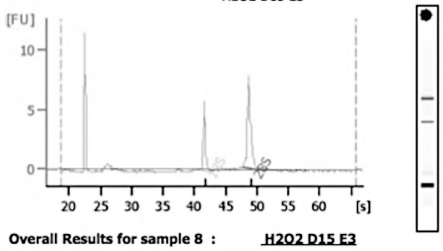

Cisplatin D15 E3

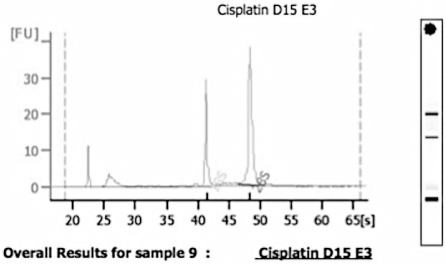

Overall Results for sample 8 : H2O2 D15 E3

RNA Area:	17.8
RNA Concentration:	23 ng/µl
rRNA Ratio [28s / 18s]:	1.9
RNA Integrity Number (RIN):	10.0 (B.02.05)
Result Flagging Color:	
Result Flagging Label:	

Fragment table for sample 8 : H2O2 D15 E3

Name	Start Time [s]	End Time [s]	Area	% of total Area
18S	40.99	42.85	5.2	29.3
28S	47.72	50.59	9.7	54.3

Overall Results for sample 9 : Cisplatin D15 E3

RNA Area:	110.1
RNA Concentration:	140 ng/µl
rRNA Ratio [28s / 18s]:	2.1
RNA Integrity Number (RIN):	10.0 (B.02.05)
Result Flagging Color:	
Result Flagging Label:	

Fragment table for sample 9 : Cisplatin D15 E3

Name	Start Time [s]	End Time [s]	Area	% of total Area
18S	40.54	42.70	24.8	22.5
28S	46.39	50.37	52.1	47.3

Appendix 11D: Electropherogram summary of RNA integrity using bioanalyzer

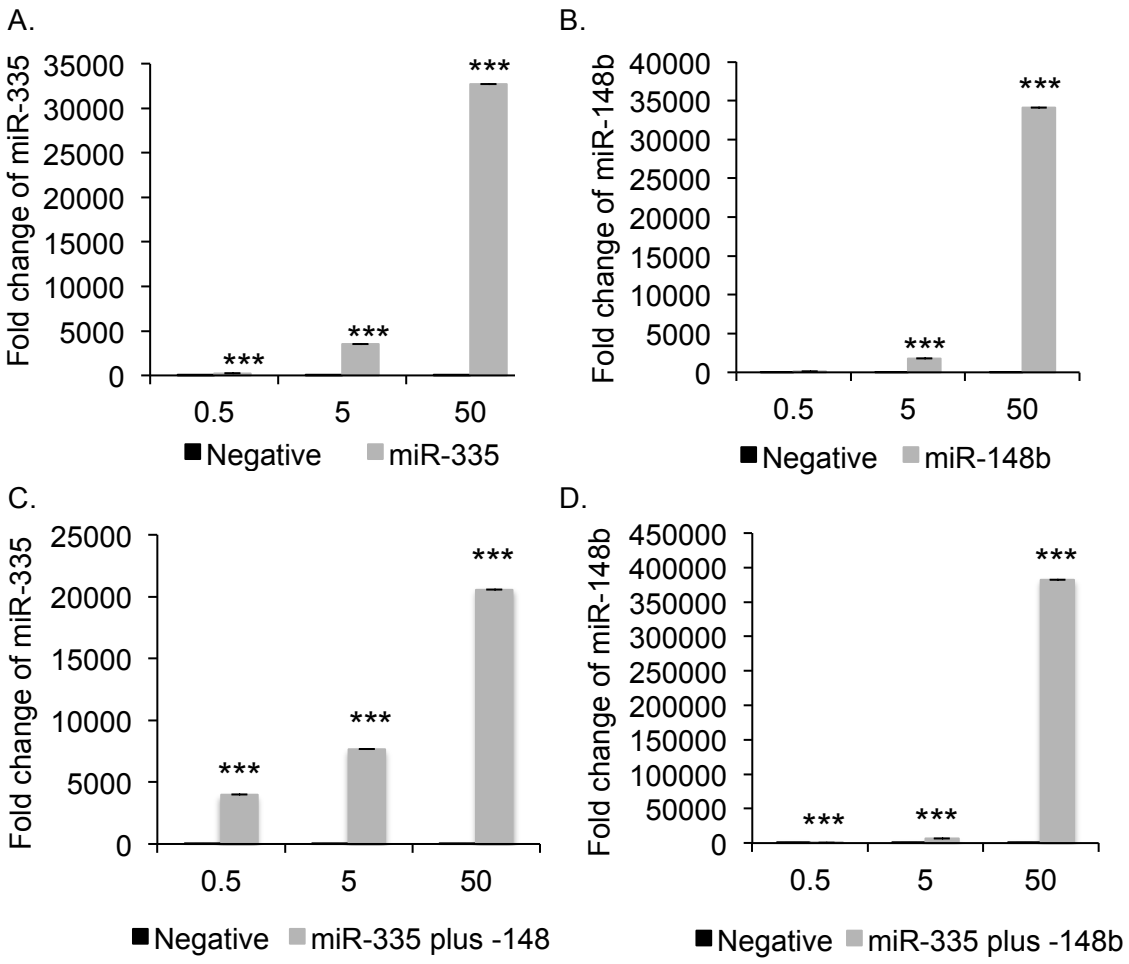

Appendix 12: Validation of dose response effect of miRNA over-expression in transfected primary oral fibroblasts. qRT-PCR performed to determine transcript levels of miRNA-335 in miR-335 transfected (A) and co-transfected oral fibroblasts (C) and miR-148b in miR-148b transfected (B) and co-transfected oral fibroblasts (D) following transfection with incrementing doses of pre-miRNA precursors. ***p<0.001, two-way repeated measures ANOVA with post-hoc corrections by Tukey test.

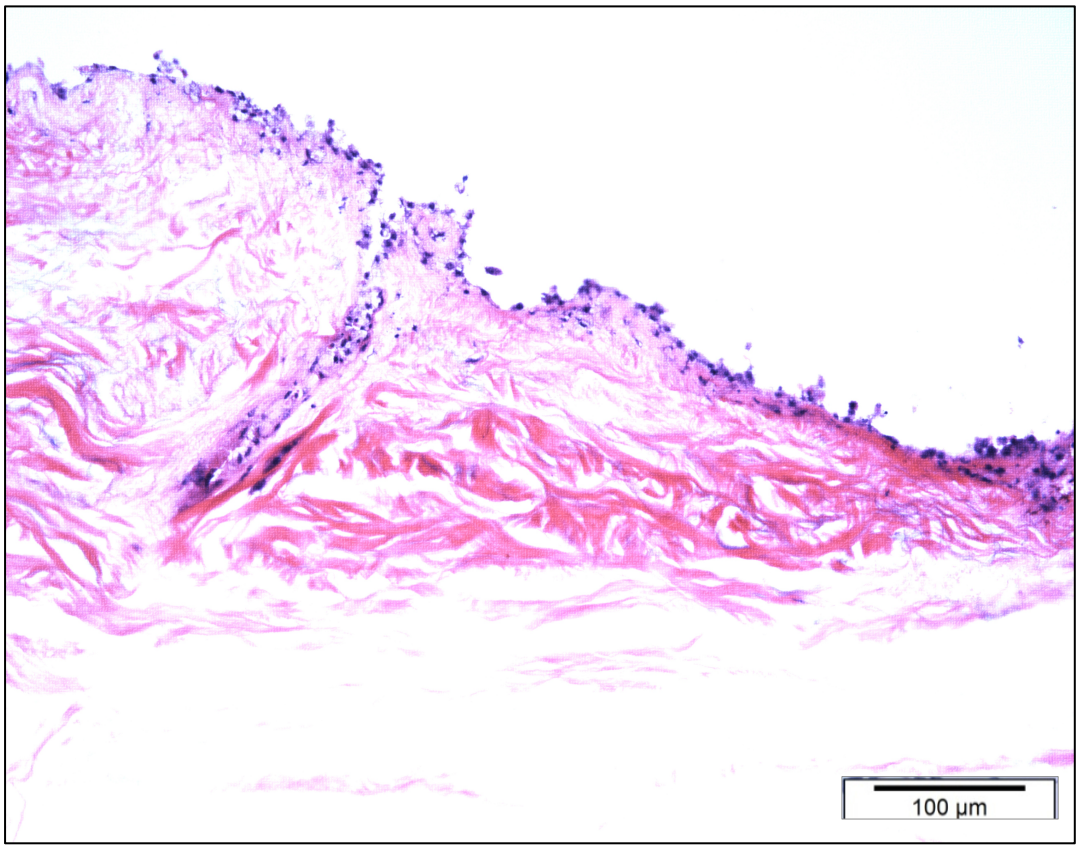

Appendix 13: Development of 3D organotypic model using replicative senescent oral fibroblasts. Replicative senescent oral fibroblasts failed to efficiently disseminate into the dermis like presenescent oral fibroblasts and therefore development of 3D organotypic models using human de-epithelialized dermis was unsuccessful.